JOINT EUROPEAN TORUS JET

JET JOINT UNDERTAKING

PROGRESS REPORT 1992

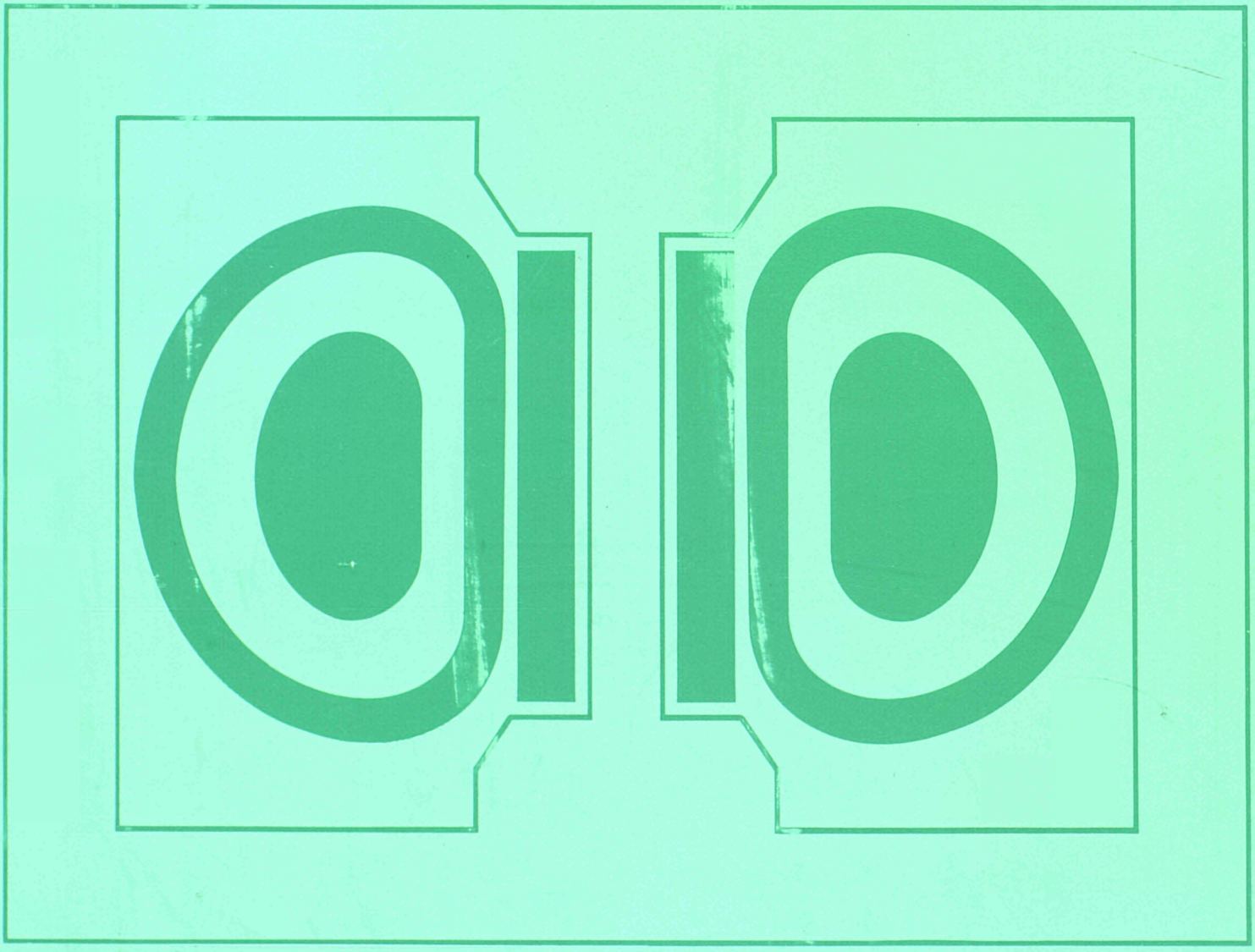

EUR 15081-EN-C
EUR-JET-PR10

JET JOINT UNDERTAKING

PROGRESS REPORT 1992

April 1993

This document is intended for information only and should not be used as a technical reference.

EUR15081 EN (EUR-JET-PR10) April 1993.
Editorial work on this report was carried out by B.E.Keen.
The preparation for publication was undertaken by
JET Publications Group, JET Joint Undertaking, Abingdon, UK.

Catalogue number : CD-NB-15081-EN-C for the Report EUR 15081

Printed in England

Contents

Foreword and Overview

This is the tenth JET Progress Report, which provides an overview summary and puts into context scientific and technical advances made on JET during 1992. This Report provides a more detailed account of JET's progress than that contained in the JET Annual Report. It is aimed not only at specialists and experts engaged in nuclear fusion and plasma physics, but also at a more general scientific community. To meet these general aims, the Report contains a brief summary of the background to the Project, and describes the basic objectives of JET and the principal design aspects of the machine. In addition, the Project Team structure is included as it is within this structure that activities and responsibilities for machine operation are carried out and the scientific programme is executed.

At the beginning of 1992, JET was still in the midst of an experimental campaign which had started in June 1991. This campaign finished in February 1992, and the machine entered a long shutdown to undertake major modifications and changes for operation of the Pumped Divertor Phase of JET . This overview summarizes the final experiments during that experimental campaign and the shutdown activities during 1992. In addition, it outlines preparations for the continuing shutdown activities which will take until the end of 1993 and reviews subsequent programme options. Finally, it sets out changes in senior management at JET during 1992.

The 1991 experimental programme encompassed several objectives, all of which were successfully accomplished. Amongst the major achievements were: the first demonstration of the use of tritium in a tokamak and the production of 1.7MW of fusion power; the demonstration of high current (2MA) AC operation of the tokamak; the detailed comparison of carbon and beryllium as divertor target materials and an extensive exploration of divertor physics; and the attainment of long pulse operation in both L- (60s) and H-modes (18s). In addition, a wide range of tokamak physics issues were addressed, covering fundamental processes influencing energy and particle transport.

The two-months experimental campaign at the beginning of 1992 essentially sought to extend and complete the experimental investigations addressed during 1991. The major themes of the programme were to advance understanding in several key areas of tokamak physics (such as energy and particle transport, impurity production and transport and H-mode physics); to improve fusion performance; and to address issues central to the pumped divertor and other items relevant to Next Step devices.

Of particular note is the study of 7MA plasmas. These were first produced several years ago, but recent improvements in the design of the vessel protection tiles and advances in disruption control have increased the safety margin for high current operation and allowed more extensive experimentation at 7MA. As a result, of the fifty 7MA pulses in 1992, there was only one disruption, despite additional heating powers of up to ~28 MW. This demonstrates significantly higher reliability than usual in other less technically demanding programmes and reflects the learning process on this scenario over the years, care in preparation, and perhaps significantly, a diagnostic effort organised primarily for 'plasma safety' during the experiments.

The flat-top duration of 7MA plasmas was also extended to nearly 9s, by employing lower hybrid current drive (LHCD) and additional heating to reduce flux consumption. Energy confinement of these discharges was good, with

total stored energies of up to 12MJ achieved (close to the highest H-mode value of 12.7MJ).

Power handling was the major problem during 7MA experiments. The plasma position could not be optimized to share power between the upper beryllium and lower carbon limiters (since the plasma-wall clearance at the top and bottom of the vessel was insufficient), and substantial melting of the beryllium limiter occurred in high power experiments. As a result, plasma purity was relatively poor, plasma density was high and the ion temperature was low. Therefore, the best value of the fusion triple product produced at 7MA was $n_i(0)T_i(0)\tau_E = 1 \times 10^{20} m^{-3} keVs$, substantially below the best values achieved in 3MA hot-ion H-mode plasmas.

Establishing acceptable ripple in the toroidal magnetic field is fundamental to the design of a tokamak reactor. By operating JET with 16 (rather than 32) toroidal field coils, it was possible to study the effect of ripple on plasma parameters. In L-mode plasmas with NB injection, a loss of stored energy of about 30% was observed. In H-mode plasmas with NB injection, it was found that, in the high-ripple case, no ELM-free H-mode could be sustained. With ICRF heating in high ripple L-mode plasmas, a severe reduction of heating efficiency and a loss of fast minority particles were observed. These findings confirmed that high ripple cannot be tolerated in any future tokamak reactor.

Considerable efforts were made during the campaign to establish an experimental database for the validation of the modelling of the plasma edge and divertor region. Detailed studies were undertaken on, for example, impurity retention in the divertor, the effects of the ion ∇B-drift direction and the relative merits of carbon and beryllium as divertor target materials. A key experiment was the attempt to establish a 'gas target' or radiative divertor plasma. The need for such an approach arises from the excessively high power densities, much higher than $10 MWm^{-2}$, to which divertor targets in ITER will be exposed unless a substantial fraction of the power is distributed over a large surface area by atomic processes, such as charge-exchanged neutral losses and radiation.

The most successful attempts to establish a radiative divertor utilized the beryllium target in a single-null X-point configuration. In most experiments, a pre-programmed gas-puff was applied at the start of additional heating and was increased with heating power. Quasi-steady state operation was demonstrated at powers of up to 22MW and for pulse lengths of up to 4s. In a more advanced scenario, feedback control of the gas target regime was achieved using thermal radiation from the divertor target to determine the gas-puff rate. The demonstration of this regime is of major significance for the development of reactor-relevant scenarios.

The experimental campaign finished in February 1992, completing Phase III of the planned operation programme on Full Power Optimization Studies. With this, the stage had then been reached where two of the main objectives set out in the original JET design had been fulfilled - that is demonstrating effective heating methods in near reactor conditions, and the scaling of plasma behaviour as parameters approached the reactor range. The pursuit of the other major objectives - of studying plasma wall interactions in near reactor conditions and studying alpha-particle production, confinement and consequent plasma heating - were well advanced.

The analysis of JET data obtained during the 1991/92 experimental campaign continued during 1992. In particular, analysis of high performance discharges obtained during the first tritium experiments was completed. The overall picture was unchanged and confirmed that hot-ion H-mode plasmas yielded the highest neutron yield of $4.3 \times 10^{16} s^{-1}$, corresponding to a fusion product $n_i(0)T_i(0)\tau_E \sim 10^{21} m^{-3} keVs$ and $Q_{DT} = 1.14$.

The 1991/92 campaign made significant progress in determining the conditions required in a reactor. JET results have been outstanding, advancing knowledge of tokamak physics and improving technological capabilities. However, high performance has only been achieved in a transient manner. The behaviour confirmed that the control of the heat and particle flux to the first wall and the resultant impurity influxes to the plasma is one of the most important problems currently facing the development of fusion as a viable energy source. The new phase of JET, based on the installation of a pumped divertor, is designed to address this problem and to develop techniques for its satisfactory resolution. The main objective of this plan is to establish the effective control of plasma impurities in operating conditions close to those of the Next Step.

In February 1992, JET completed its experimental campaign in the machine's original configuration. The machine then entered a major shutdown, which is the longest and most complex shutdown yet undertaken by JET. It is expected to be completed by the end of 1993 and will lead to a totally transformed interior of the JET vessel. The shutdown is being undertaken in three stages and involves the exchange of two Toroidal Field (TF) coils and

the installation of the components of the pumped divertor and its associated system modifications. These included: a lower divertor structure with Mark I carbon fibre composite (CFC) target plates (inertially-cooled); four internal divertor coils and associated power supplies; pumping chamber and cryopump; poloidal limiters; new ICRF antennae and modified protections; full lower hybrid current drive system with modified launcher, grill and protections; divertor diagnostics and internal saddle coils for disruption control.

Stage 1 involved the removal of components and beryllium decontamination of the vacuum vessel for installation of the divertor coils. During this stage, it was intended to replace a TF coil which had been found in 1990 to have a fault, but was not serious enough to prevent operation during 1990 and 1991. The coil was replaced and the change was completed by June. Subsequently, a further less severe fault in an adjacent coil became apparent and, in view of the difficulty of changing a TF coil once the divertor coils were installed, it was prudent to replace this second coil, while the opportunity still existed. The change was successfully completed by August 1992. The consequential delay in the shutdown was limited to eight weeks, by intensive working and by drawing on previous experience.

In late October, work began on Stage 2 of the shutdown with the fabrication of the divertor coils and cases. The assembly of the four divertor coils and casings inside the vacuum vessel was in progress at the end of 1992. It is believed to be the first time that full manufacture and assembly of coils has been undertaken in such a confined space, and the work is being done to demanding standards to ensure the highest reliability during subsequent operations.

In parallel with the in-vessel work, which constitutes the critical path for the divertor shutdown, many ex-vessel activities were carried out. Intensive design and procurement activities for the pumped divertor components to be installed in the third phase of the shutdown have continued. The complexity of the new configuration has required close attention to the sequence in which components are installed and means that it is important for all components to be ready for installation in accordance with the shutdown schedule. Testing and training on mock-ups has taken place to ensure efficient completion.

Preparations for the full D-T phase of operations have also continued. The installation of the systems in the Active Gas Handling building has been completed. The function of these systems is to collect exhaust gases from the torus, to remove impurities and to separate pure deuterium and tritium so that it can be stored for re-injection through neutral beam, pellet or torus gas introduction systems, as required. Significant progress in commissioning was made in Exhaust Detritiation, Gas Chromatography and the Analytical Laboratory. In addition, a series of tests and modifications to improve the performance of the Cryodistillation System were carried out.

Following completion of the shutdown, the first operating period will focus initially on establishing reliable operation in the new configuration. Subsequently, attention will be devoted to the study of the pumped divertor in controlling impurities, plasma density and exhaust, and power loading on the target plates. Preparations for D-T operations will also continue during this period, including finalisation of remote handling tests and commissioning of the Active Gas Handling System with tritium gas. A second tritium experiment is being considered as a possible option at a time, yet to be determined, when divertor operation has been well-established. The information derived from preliminary tritium experiments provide a safer approach to the full D-T phase and aid optimisation of active handling and waste management arrangements. On present plans, the final Phase of full D-T operation should start at the end of 1995, subject to approval by the JET Council and to the necessary official consents.

1992 was also a year of change in senior management at JET. In July 1992, the ITER Engineering Design Activity (EDA) agreement was signed by the four parties (European Community, Japan, United States and the Russian Federation). In September, the ITER Council nominated Dr P-H. Rebut (the then Director of JET) as the inaugural Director of ITER and Dr M. Huguet (former Associate Director of JET and Head of Machine and Development Department) as a Deputy Director of ITER and Head of the Co-centre at Naka, Japan. In October 1992, I was nominated by the JET Council to the position of Acting Director of JET. Subsequently, in February 1993, I was appointed Director of JET, when Dr Rebut formally took up his post as Director of ITER. In addition, JET has provided three Division Heads to ITER, as well as other staff. Whilst we are reluctant to lose the services of such high calibre staff, we have to accept that JET is a natural source of expertise and experience for the Next Step. We can be proud that JET personnel are filling such a high proportion of senior posts in ITER.

JET made impressive advances during 1992, in spite of severe budgeting constraints. However, the Project must

continue to achieve economies where possible during the coming years to ensure successful completion of the programme. It has already been necessary to restrict the scope of the programme, to reduce staffing levels and to intensify economies in operational expenditure. In October 1992, I informed the JET Council that I wished to assess the existing scientific Programme and discuss it with the JET Scientific Council. The JET Council supported a review within the existing statutory conditions and noted my intention to clarify the major options, objectives, schedules and decision points. The proposals emerging from this review will be presented to the JET Scientific Council and the JET Council during the first half of 1993. However, it is already clear that, JET must continue along the path towards simulating the operation of a fusion reactor and in making unique and essential contributions to the ITER EDA.

JET's exceptional achievements reflect the continuous cooperation and assistance received from the Associated Laboratories and from the Commission of the European Communities. I am confident that with the continued dedication of the staff and the support and guidance of the JET Council, JET Scientific Council and the JET Executive Committee, the Project will meet the challenges ahead and continue to make substantial contributions of crucial information that will ensure fusion is an important source of energy for future generations.

Dr. M. Keilhacker
Director
April 1993

Introduction, Background and Report Summary

Introduction

JET Progress Reports are aimed both at specialists in plasma physics and nuclear fusion research and at the more general scientific community. This contrasts with the JET Annual Reports, which provide overview descriptions of the scientific, technical and administrative status of the JET programme, and is directed at the average member of the public.

To meet these general aims, the Progress Report contains a brief summary of the background to the Project, describes the basic objectives of JET and sets out the principal design aspects of the machine. In addition, the Project Team structure is detailed, since it is within this framework that machine activities and responsibilities are organized and the scientific programme is executed.

The main part of the 1992 Report provides overview summaries of scientific and technical advances made during the year, supplemented by detailed cross-references to the more important JET scientific and technical articles produced during the year. The final part of the Report briefly sets out developments underway to further improve JET's performance and plans for future experiments through to its foreseen completion.

Background

Objectives of JET

The Joint European Torus (JET) is the largest single project of the nuclear fusion research programme of the European Atomic Energy Community (EURATOM). The project was designed with the essential objectives of obtaining and studying plasma in conditions and with dimensions approaching those needed in a fusion reactor. These studies are aimed at defining the parameters, the size and working conditions of a tokamak reactor. The realisation of this objective involves four main areas of work:

(i) the scaling of plasma behaviour as parameters approach the reactor range;
(ii) the plasma-wall interaction in these conditions;
(iii) the study of plasma heating; and
(iv) the study of alpha-particle production, confinement and consequent plasma heating.

Two of the key technological issues in the subsequent development of a fusion reactor are faced for the first time in JET. These are the use of tritium and the application of remote maintenance and repair techniques. The physics basis of the post-JET programme will be greatly strengthened if other fusion experiments currently in progress are successful. The way should then be clear to concentrate on the engineering and technical problems involved in progressing from an advanced experimental device like JET to a prototype power reactor.

Basic JET Design

To meet these overall aims, the basic JET apparatus was designed as a large tokamak device with overall dimensions of about 15m in diameter and 12m in height. A diagram of the apparatus is shown in Fig.1 and its principal parameters are given in Table I. At the heart of the machine, there is a toroidal vacuum vessel of major radius 2.96m having a D-shaped cross-section 2.5m wide by 4.2m high. During operation of the machine, a small quantity of gas (hydrogen, deuterium or tritium) is introduced into the vacuum chamber and is heated by passing a large current through the gas. Originally, the machine was designed to carry 4.8MA, but has already been modified to achieve 7MA. This current is produced by transformer action using the massive eight-limbed magnetic circuit, which dominates the

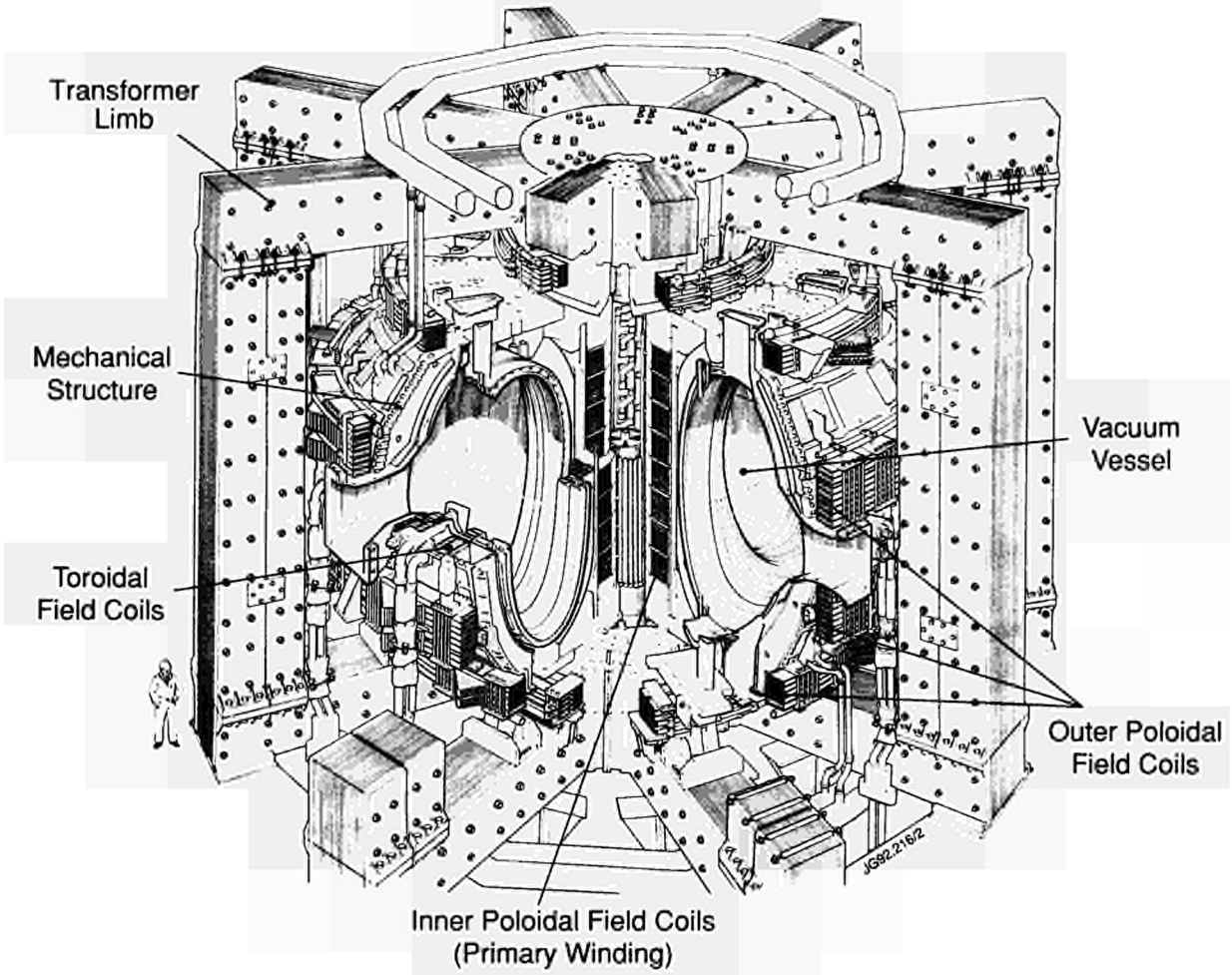

Fig.1: Diagram of the JET Tokamak.

Table I
Principal Parameters

Parameter	*Value*
Plasma minor radius (horizontal), a	1.25m
Plasma minor radius (vertical), b	2.10m
Plasma major radius, R_0	2.96m
Plasma aspect ratio, R_0/a	2.37
Plasma elongation ratio, ε=b/a	1.68
Flat top pulse length	60s
Toroidal magnetic field (plasma centre)	3.45T
Plasma current, D-shaped plasma	7.0MA
Volts-seconds available	54Vs
Toroidal field peak power	380MW
Poloidal field peak power	300MW
Additional heating power (into torus)	~50MW
Weight of vacuum vessel	108t
Weight of toroidal field coils	364t
Weight of iron core	2800t

apparatus (see Fig.1). A set of coils around the centre limb of the magnetic circuit forms the primary winding of the transformer with the plasma acting as the single turn secondary. Additional heating of the plasma is provided by the propagation and absorbtion of high power radio frequency waves in the plasma and by the injection of beams of energetic neutral atoms into the torus.

The plasma is confined away from the walls of the vacuum vessel by a complex system of magnetic fields, in which the main component, the toroidal field, is provided by 32 D-shaped coils surrounding the vacuum vessel. This field, coupled with that produced by the current flowing through the plasma, forms the basic magnetic field for the tokamak confinement system, which provides a full design field at the plasma centre of 3.45T. The poloidal coils, positioned around the outside of the vacuum vessel, shape and position the plasma in operation.

Initial experiments have been undertaken using hydrogen and deuterium plasmas, but in the later stages of the

operation, it is planned to operate with deuterium-tritium plasmas, so that fusion reactions can occur to produce significant α-particle heating in the plasma.

In order to reach conditions close to those relevant to a fusion reactor, a plasma density of ~$10^{20}m^{-3}$ at a temperature of 10-20keV would be needed. Even with a current of up to 7MA in JET, this would be inadequate to provide the temperature required using ohmic heating alone. Consequently, additional heating is required and two main systems are being used at JET, as follows:

- Injection into the plasma of highly energetic neutral atoms (Neutral Injection Heating);
- Coupling of high power electromagnetic radiation to the plasma (Radio Frequency (RF) Heating).

Project Team Structure

The Project structure adopted, for management purposes, is divided into four Departments (see Table II):

- Machine and Development Department;
- Experimental and Theory Department;
- Heating and Operations Department;
- Administration Department.

In addition, some scientific and technical duties are carried out within the Directorate and in the Coordinating Staff Unit.

The main duties of the Administration Department have been described in previous JET Annual Reports. This Report concentrates on progress made in the scientific and technical areas during 1992. To aid this description, the functions of these Departments are described below.

Machine and Development Department

The Machine and Development Department is responsible for the performance capacity of the machine as well as equipment for the active phase, together with enhancements directly related to it (excluding heating) and the integration of any new elements on to the machine. In addition, the Department is responsible for machine services. The Department contains three Divisions:

(a) *Magnet and Power Supplies Division* is responsible for the design, construction, installation, operation and maintenance of the tokamak electromagnetic system and of plasma control. The area of responsibility encompasses the toroidal, poloidal and divertor magnets,

Table II
JET Departmental and Divisional Structure

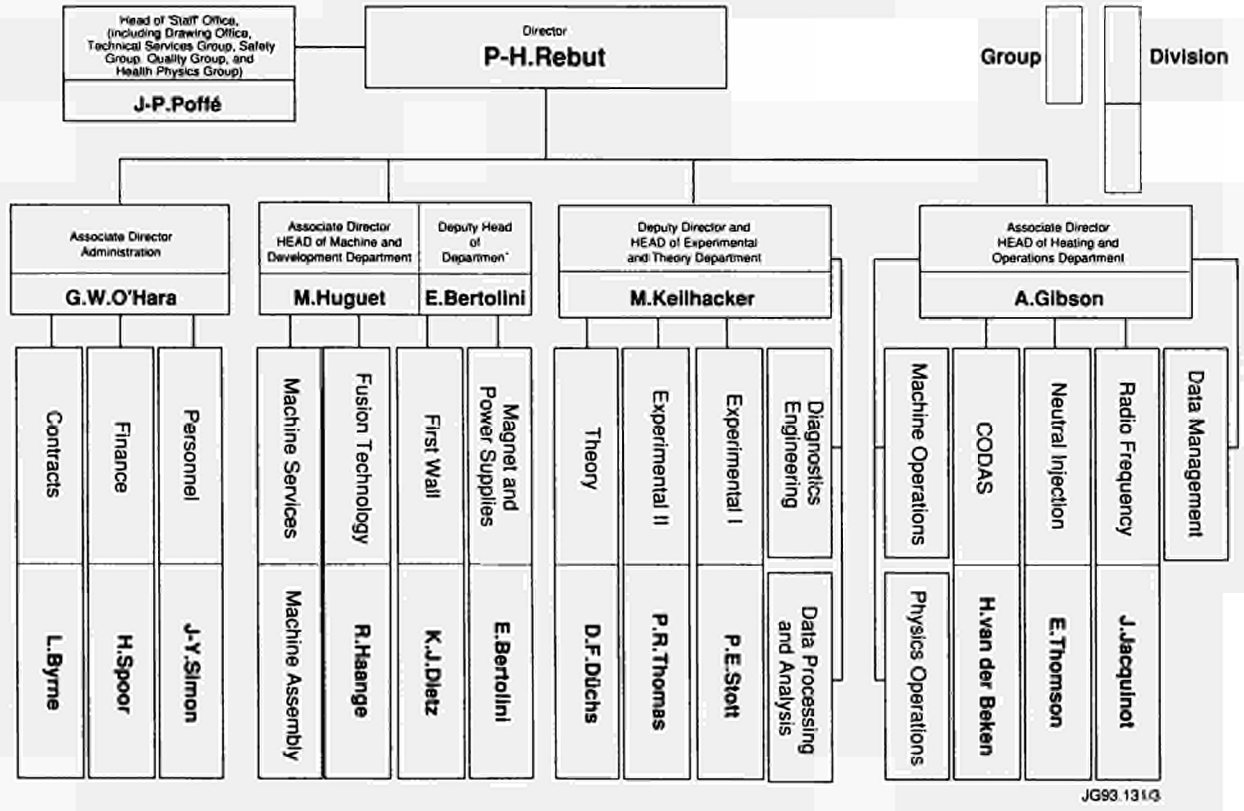

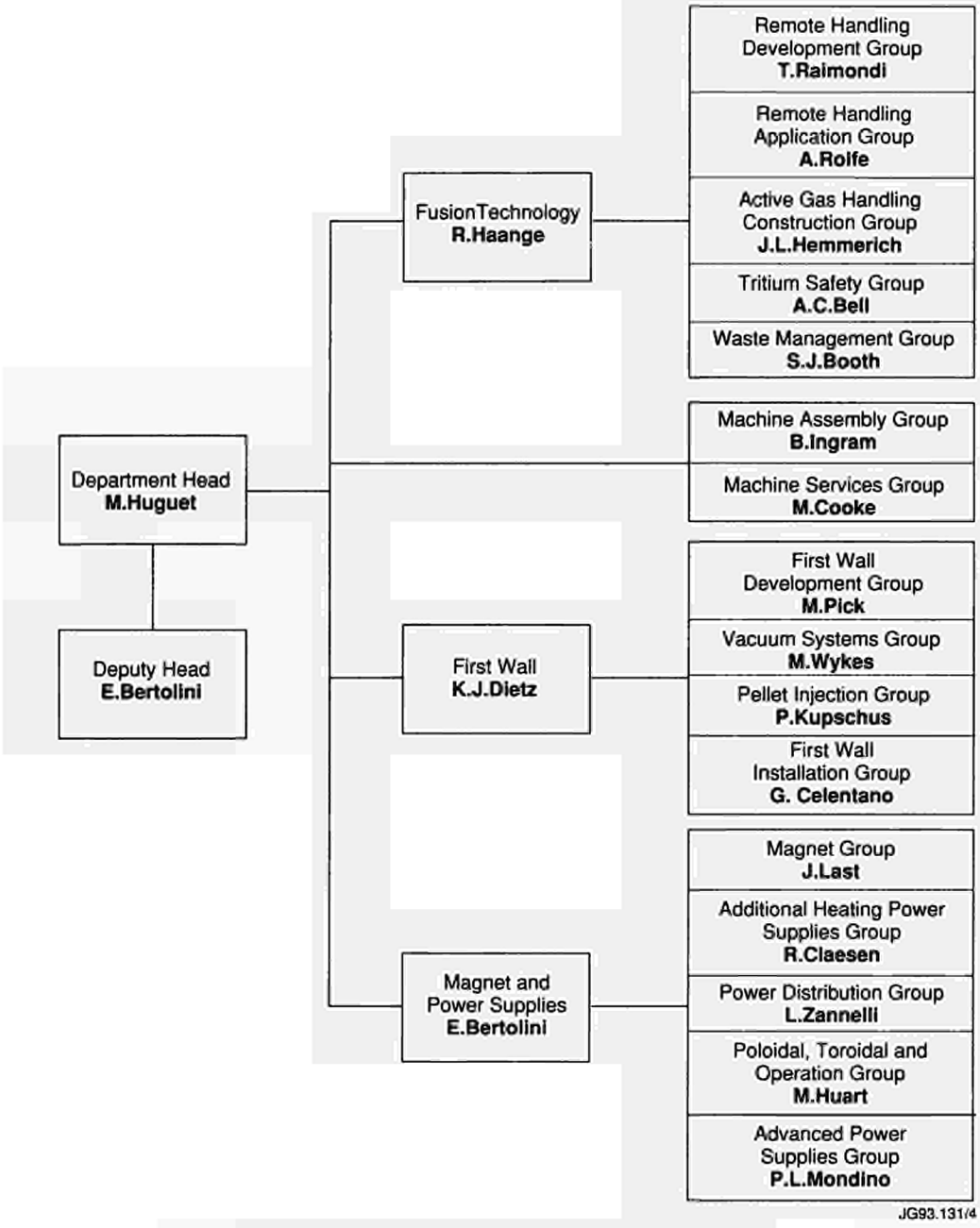

Fig.2: Machine and Development Department, Group Structure (December 1992)

mechanical structure, methods for controlling plasma position and shape and all power supply equipment needed for magnets, plasma control, additional heating and auxiliaries;

(b) *First Wall Division*, which is responsible for the vital area of plasma wall interactions. Its main tasks include the provision and maintenance inside the vacuum vessel of conditions leading to high quality plasma discharges. The Division develops, designs, procures and installs the first wall systems and its components, such as limiters, wall protections and internal pumping devices. The area of responsibility encompasses the vacuum vessel as a whole, together with its associated systems, such as pumping, bakeout and gas introduction;

(c) *Fusion Technology Division*, which is responsible for the design and development of remote handling methods and tools to cope with the requirements of the JET device, and for maintenance, inspection and repairs. Tasks also include the design and construction of facilities for handling tritium and waste management.

The Structure of the Machine and Development Department to Group Leader level is shown in Fig.2 and the list of staff within the Department is shown in Fig.3.

MACHINE AND DEVELOPMENT DEPARTMENT

Head of Department: M. Huguet
Deputy Head of Department: E. Bertolini

D. Carre
Mrs. H. Marriott
B. Ingram
S. McLaughlin
C. Sborchia
R.A.S. Smith

MAGNET AND POWER SUPPLIES DIVISION

Head: E. Bertolini

P. Barabaschi
P. Bertoldi
T. Bonicelli
D. Chiron
R. Claesen
E. Daly
N. Dolgetta
P. Doyle
H. T. Fielding
C. Folco
M. Garibba
J. Goff
D. Halliwell
M. Huart
F. Jensen
J. R. Last
H. McBryan
J. McKivett
V. Marchese
G. Marcon
L. Mears
P. Mondino
G. Murphy
P. Noll
R. Ostrom
P. Presle
A. Santagiustina
G. Sannazzaro
S. Shaw
M. Tabellini
A. Tesini
S. Turley
J. van Veen
C. R. Wilson
G. C. Wilson
L. Zannelli

FUSION TECHNOLOGY DIVISION

Head: R. Haange

A. C. Bell
G. Benali
S. J. Booth
P. Boucquey
P. Brown
T. Businaro
C. J. Caldwell-Nichols
Mrs. J. Campbell
P. Chuilon
Miss. L. Cotmore
R. Cusack
C. Davies
F. Delvart
L. Galbiati
A. Galetsas
J. L. Hemmerich
M. Irving
Mrs. M. E. Jones
L. P. D. F. Jones
J. F. Jaeger
J. F. Junger
R. Lässer
M. Laveyry
Miss. J. Lech
A. Loving
J. Lupo
J. Mart
P. Milverton
G. Newbert
A. Nowak
S. Puppin
T. Raimondi
J. Salanave
K. D. Walker

FIRST WALL DIVISION

Head: K. J. Dietz

W. P. Bailey
S. Bryan
H. Buttgereit
G. Celentano
Mrs. D. Cranmer
E. Deksnis
C. Froger
M. Gadeberg
N. Green
D. Holland
F. Hurd
Mrs. I. Hyde
G. Israel
H. Jensen
P. Kupschus
E. Martin
T. Martin
B. Macklin
A. Miller
J. Orchard
A. Peacock
R. Pearce
M. Pick
L. Rossi
S. Scott
T. Szabo
M. Watson
T. Winkel
M. Wykes

Fig.3: Project Team Staff in the Machine and Development Department (December 1992)

JG93.131/5

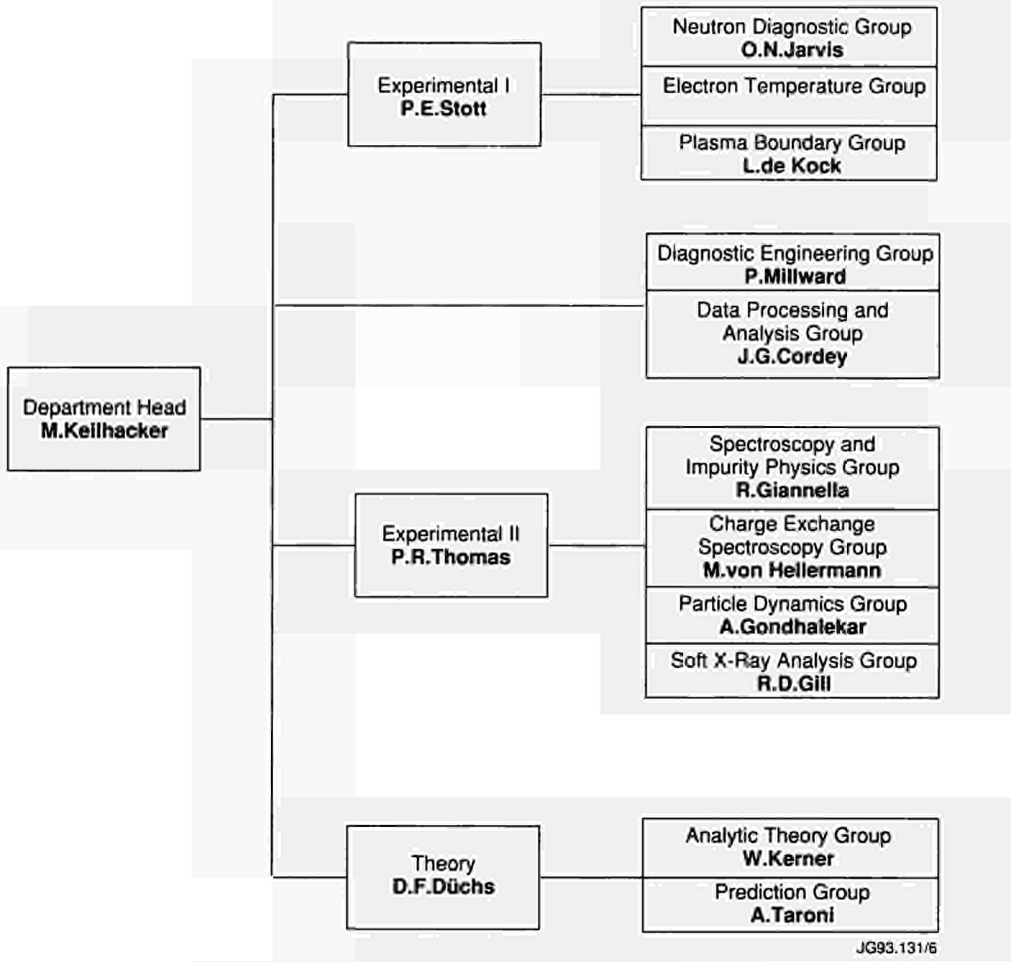

Fig.4: Experimental and Theory Department, Group Structure (December 1992)

Experimental and Theory Department

The main functions of the Department relate to the measurement and validation of plasma parameters and to the theory of tokamak physics. The main tasks are:

- to conceive and define a set of coherent measurements;
- to be responsible for the construction of necessary diagnostics;
- to be responsible for the operation of the diagnostics and the quality of measurements and the definition of the plasma parameters;
- to follow the theory of tokamak physics;
- to play a major role in interpretation of data.

The Department contains two Groups (Diagnostics Engineering Group and Data Processing and Analysis Group) and three Divisions:

(a) *Experimental Division 1 (ED1)*, which is responsible for specification, procurement and operation of about half the JET diagnostic systems. ED1 undertakes electrical measurements, electron temperature measurements, surface and limiter physics and neutron diagnostics;

(b) *Experimental Division 2 (ED2)*, which is responsible for specification, procurement and operation of the other half of the JET diagnostic systems. ED2 undertakes all spectroscopic diagnostics, bolometry, interferometry, the soft X-ray array and neutral particle analysis;

(c) *Theory Division*, which is responsible for prediction by computer simulation of JET performance, interpretation of JET data and the application of analytic plasma theory to gain an understanding of JET physics.

The structure of the Experimental and Theory Department to Group Leader level is shown in Fig.4 and the list of staff in the Department is shown in Fig.5.

Heating and Operations Department

Heating and Operations Department is responsible for heating the plasma, the organisation of experimental data, and the day-to-day operation of the machine. The main functions of the Department are:

- heating the plasma and analysis of its effects;

EXPERIMENTAL AND THEORY DEPARTMENT

Head of Department: M. Keilhacker

B. Balet
M. Barnes
K. Blackler
J. Christiansen
J. G. Cordey
C. J. Hancock
J. P. Jéral
P. Millward
D. O'Brien
R. Oord
J. Reid
Miss K. Slavin
Mrs. P. Stubberfield
K. Thomsen
Mrs. R. Thormaehlen
A. Tiscornia
E. van der Goot
G. Vlases
D. Ward
J. Wesson
C. H. Wilson
D. Wilson

EXPERIMENTAL DIVISION I

Head: P. E. Stott

S. Ali-Arshad
Miss. N. Avery
D. Bartlett
H. Bindslev
B. W. Brown
D. Campbell
S. Clement
E. Clipsham
J. P. Coad
A. E. Costley
J. Ehrenberg
L. de Kock
J. Fessey
C. Gowers
Mrs. M. Harper
P. J. Harbour
M. Hone
J. Hoekzema
I. Hurdle
O. N. Jarvis
B. Laundy
M. Loughlin
F. B. Marcus
G. Matthews
G. Neill
P. Nielsen
H. Oosterbeek
R. Prentice
P. Roberts
G. Sadler
B. Schunke
A. C. C. Sips
A. Stevens
D. Summers
P. van Belle
J. Vince

EXPERIMENTAL DIVISION II

Head: P. R. Thomas

B. Alper
Mrs. K. Bell
G. Braithwaite
J. L. Bonnerue
S. Corti
G. B. Denne-Hinnov
A. Edwards
Mrs. A. Flowers
R. Giannella
R. Gill
A. Gondhalekar
N. Gottardi
L. D. Horton
H. Jäckel
G. Janeschitz
R. König
G. Magyar
P. Morgan
H. Morsi
C. Nicholson
R. Reichle
J. O'Rourke
J. Ryan
M. Stamp
S. A. Staunton-Lambert
M. von Hellermann
B. Viaccoz

THEORY DIVISION

Head: D. F. Düchs

W. Core
L. G. Eriksson
A. Galway
W. Kerner
F. Porcelli
M. Ottaviani
R. Simonini
E. Springmann
A. Taroni
F. Tibone
W. Zwingmann

Fig.5: Project Team Staff in Experimental and Theory Department (December 1992)

JG93.131/7

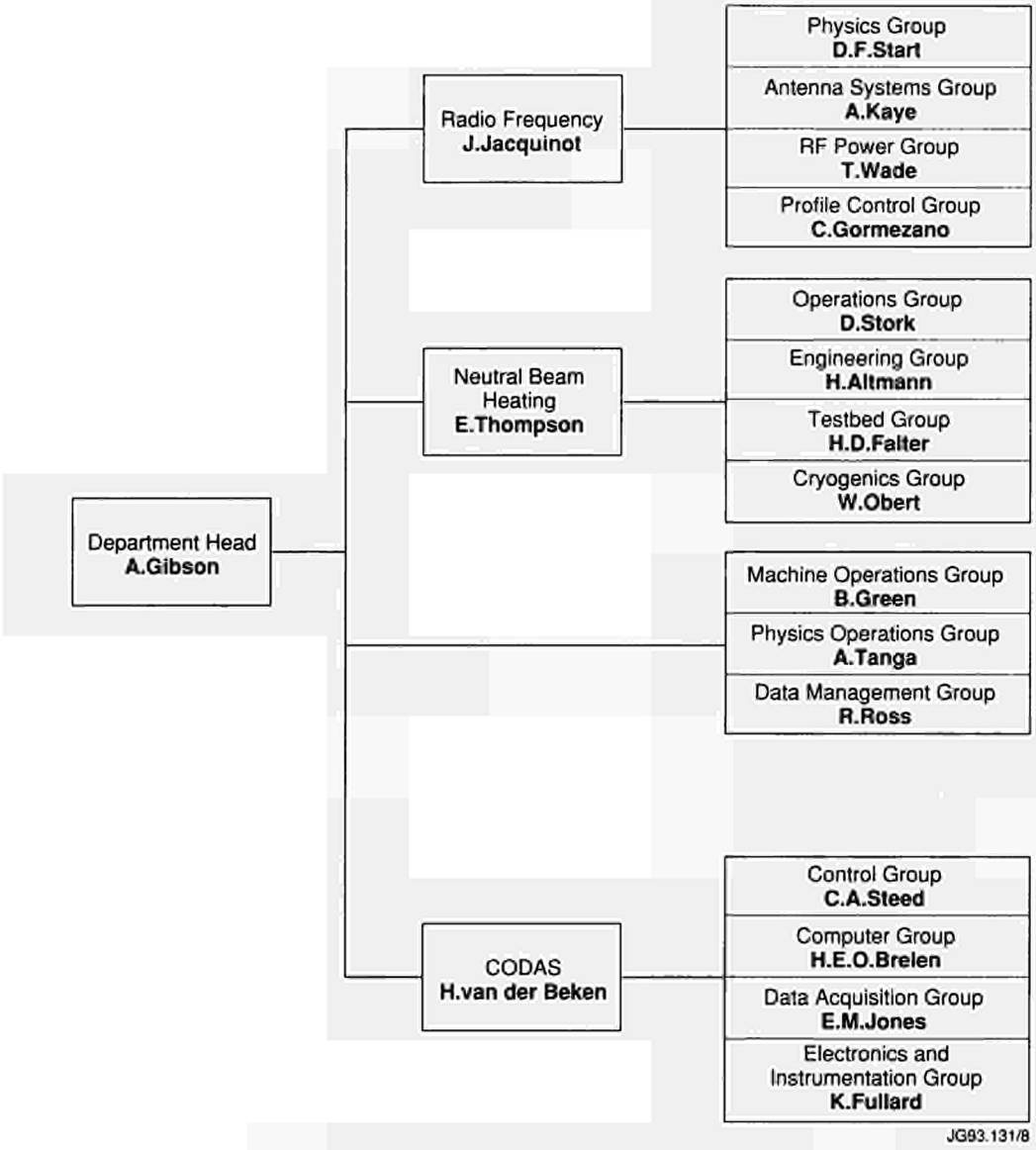

Fig.6: Heating and Operations Department, Group Structure (December 1992)

- centralising the interpretation of experimental results and investigating their coherence;
- organising data acquisition and computers;
- preparing and co-ordinating operation of the machine across the different Departments.

The Department is composed of three groups (Machine Operations Group, Physics Operation Group, and Data Management Group) and three Divisions:

(a) *Control and Data Acquisition System Division (CODAS)*, which is responsible for the implementation, upgrading and operation of computer-based control and data acquisition systems for JET;

(b) *Neutral Beam Heating Division*, which is responsible for construction, installation, commissioning and operation of the neutral injection system, including development towards full power operation. It also participates in studies of physics of neutral beam heating;

(c) *Radio Frequency Heating Division*, which is responsible for the design, construction, commissioning and operating the RF heating system during the different stages of its development to full power. The Division also participates in studies of the physics of RF heating.

The structure of the Heating and Theory Department to Group Leader level is shown in Fig.6, and the list of staff in the Department is shown in Fig.7.

In addition, all Divisions are involved in:

- execution of the experimental programme;
- interpretation of results in collaboration with other Divisions and Departments;
- making proposals for future experiments.

PLASMA HEATING AND OPERATION DEPARTMENT

Head of Department: A. Gibson

K. Adams
M. J. Bolton
S. Cooper
T. Dale
P. Gaze
B. Green
R. Greenfield
J. Hocking
J. How
M. Hughes
M. Johnson
P. J. Lomas
Mrs. P. Longworth
C. Lowry
M. Macrae
R. C. Meadows
C. Rayner
B. S. Regan
Mrs. J. Roberts
R. T. Ross
P. Sagar
G. Saibene
Miss. D. Samuel
R. Sartori
P. Smeulders
W. Smith
A. Tanga
K. A. Taylor
B. Tubbing
M. Wallwork
J. M. Watt
B. Workman

NEUTRAL BEAM HEATING DIVISION

Head: E. Thompson

H. Altmann
A. Bickley
A. Browne
C. D. Challis
D. Cooper
J. F. Davies
A. Dines
H. P. L. de Esch
D. Ewers
H. Falter
Mrs. S. Humphreys
D. Hurford
J. Z. Jensen
T. T. C. Jones
F. Long
J. G. Lundqvist
D. Martin
P. Massmann
C. Mayaux
Mrs. D. Noyes
W. Obert
S. Papastergiou
A. J. Parfitt
D. Raisbeck
D. Stork
L. Svensson
J. Waterhouse

RADIO FREQUENCY HEATING DIVISION

Head: J. Jacquinot

V. Bhatnagar
S. C. Booth
G. Bosia
M. Brandon
H. Brinkschulte
M. Brusati
M. Bures
Miss. M. Casson
G. Cottrell
P. Crawley
T. Dobbing
D. T. Edwards
A. Franklin
P. Finberg
M. Gammelin
B. Glossop
C. Gormezano
R. Horn
G. Jessop
A. Kaye
M. Lennholm
P. Murray
J. Plancoulaine
F. Rimini
P. Schild
M. Schmid
Miss. V. Shaw
A. Sibley
D. Start
C. Steele
T. Wade
C. Walker

CONTROL AND DATA ACQUISITION SYSTEMS DIVISION

Head: H. van der Beken

M. B. Baronian
Mrs. A. M. Bellido
M. J. M. Botman
H. E. O. Brelen
W. J. Brewerton
T. Budd
P. J. Card
J. J. Davis
S. Dmitrenko
S. E. Dorling
K. Fullard
E. M. Jones
F. J. Junique
N. G. Kidd
J. G. Krom
C. Perry
C. A. Steed
C. Terella
G. Wolfers
I. D. Young

Fig.7: Project Team Staff in Plasma Heating and Operation Department (December 1992)

JG93.131/9

Directorate

A scientific and a technical group, (Scientific Assistants to the Director and Technical Assistant to the Director (including Publications Group)), report directly to the Director:

- Scientific Assistants to the Director, who assist and advise the Director on scientific aspects of JET operation and future development;
- Technical Assistant to the Director, who assists and advises the Director on organizational and technical matters related to JET operation and future development. He also acts as JET Publications Officer, and is Leader of the Publications Group.

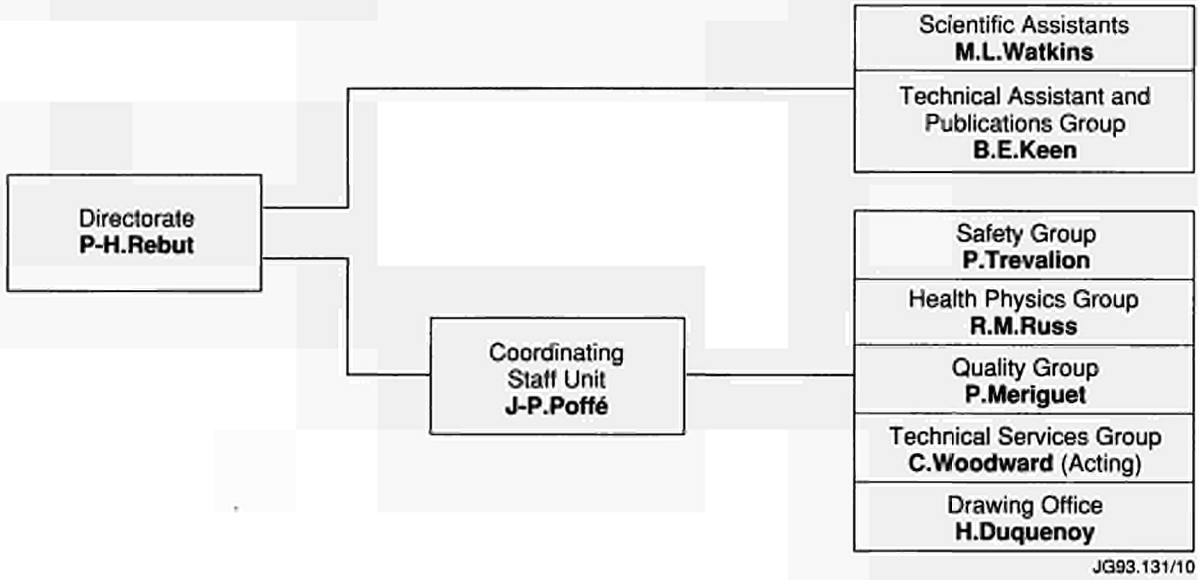

Fig.8: Directorate and Coordinating Staff Unit, Group Structure (December 1992)

DIRECTORATE AND COORDINATING STAFF UNIT

Director: Dr. P-H. Rebut

DIRECTORATE

D. Boucher	D. Gambier	T. O'Hanlon
Mrs. M. Deitrich	Miss. C. Hampson	Mrs. J. Talbot
M. Drew	J. McMahon	M. L. Watkins

COORDINATING STAFF UNIT

Head: J-P. Poffé

Ms. L. Ashby	A. Gibson	H. Panissie
M. Axton	A. Girard	B. Patel
P. Barker	J. A. Green	Mrs. J. Reid
J. Banham	M. Guillet	R. M. Russ
P. Burton	A. D. Haigh	K. Sandland
C. Callaghan	H. D. Jones	P. Schofield
D. Campling	R. Litchfield	M. Scotcher
G. Dalle-Carbonare	Miss. K. Luker	P. Trevalion
N. Davies	P. Meriguet	C. Woodward
H. Duqenoy		

Fig.9: Project Team Staff in Directorate and Coordinating Staff Unit (December 1992)

JG93.131/11

Coordinating Staff Unit

The Coordinating Staff Unit is responsible for the provision of engineering services to the Project and for the implementation of specific coordinating tasks at the Project level.

It comprises five Groups:

- Safety Group;
- Health Physics Group;
- Quality Group;
- Technical Services Group;
- Drawing Office.

The structure of the Directorate and Coordinating Staff Unit to Group Leader level is shown in Fig.8 and the list of staff in these areas is shown in Fig.9.

Report Summary

The first section of this Report provides a brief introduction and background information relevant to the Report. The second and third sections set out an overview of progress on JET during 1992 and with a survey of scientific and technical achievements during 1992 sets these advances in their general context. This summary is specifically cross-referenced to reports and articles prepared and presented by JET staff during 1992. The full list of articles is given in Appendix II, and copies can be obtained by application to JET Publications Office.

The fourth section is devoted to future plans and certain developments which might enable enhancements of the machine to further improve its overall performance. Some attention has been devoted to methods of surmounting certain limitations and these are detailed in this section.

The Appendices contain a list of work topics which have been carried out under Task Agreements with various Association Laboratories. In addition, a full list is included of all Articles, Reports and Conference papers published by JET authors in 1992.

Technical Achievements during 1992

Introduction

On 21st February 1992, JET completed its planned phase of Full Power Optimization Studies in the machine's original configuration. The machine then entered a major shutdown, which is expected to be completed by the end of 1993. This shutdown was intended to change a toroidal field (TF) coil in Octant No:4 and then to install the components of the pumped divertor and its associated system modifications. These included:

- lower divertor structure with Mark I CFC target plates (inertially cooled);
- four internal divertor coils and power supplies;
- pumping chamber and cryopump;
- poloidal limiters;
- new ICRF antennae (A2) and modified protections;
- full lower hybrid current drive (LHCD) system with modified launcher (L1), grill and protections;
- divertor diagnostics;
- disruption control system using internal saddle coils.

The shutdown is being undertaken in three major stages:

- Stage 1 involves the removal of components and the preparation of the vacuum vessel for installation of the divertor coils;
- Stage 2 involves the assembly of the four divertor coils and casings inside the vacuum vessel;
- Stage 3 involves the installation of the Mark I inertially-cooled divertor, cryopump, RF antennae, limiters and saddle coils.

During the first stage of the shutdown, it was intended to replace one faulty toroidal field (TF) coil (No:4.2). When this had been completed, further checks revealed a smaller fault in a neighbouring coil (No:4.3). It was considered prudent to remove and replace this coil, in view of its future inaccessibility. The consequential increase in the shutdown was limited to eight weeks by intensive working and by drawing on experience gained in replacing previous coils.

In late October, work began on Stage 2 of the shutdown with the fabrication of the coil cases. The assembly of the four divertor coils and casings inside the vacuum vessel was in progress at the end of 1992. It is believed to be the first time that full manufacture and assembly of coils has been undertaken in such a confined space, and the work is being done to demanding standards to ensure the highest reliability during subsequent operations.

Intensive design and procurement activities for the pumped divertor components to be installed in the third phase of the shutdown have continued. The complexity of the new configuration has required close attention to the sequence in which components are installed and means that it is important for all components to be ready for installation in accordance with the shutdown schedule.

At the end of the shutdown, JET will be in a position to begin its programme of operations to demonstrate effective methods of power exhaust and impurity control in operational conditions close to those envisaged for ITER, before the final phase of full D-T operations.

The following sections detail the technical achievements made during 1992.

Torus Systems

At the end of February 1992, the experimental phase concluded as planned and the longest and most complex shutdown yet undertaken by JET was started (see Fig.10). This shutdown period will be used to install all the new components of the pumped divertor and will lead to a totally transformed interior of the JET vessel. The shutdown is

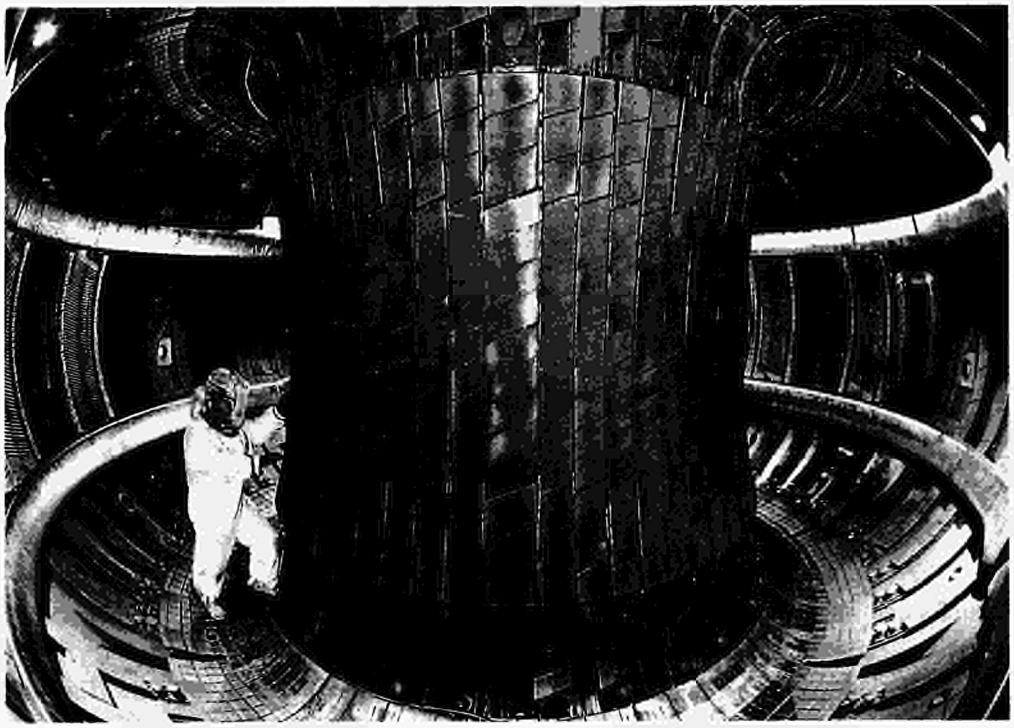

Fig.10: The interior of the vacuum vessel at the start of the Divertor Shutdown.

planned for completion by the end of 1993. The most critical part of the work is that within the vacuum vessel itself. Here, the confined space, the high quality and high accuracy requirements, and the safety restrictions when working in a beryllium, tritium and a radiation environment, means that all the work must be optimized. Each work package must be studied, recorded, practised, planned and organised in minute detail. The components and jigs must be well designed and the tools well tried, effective and easy to use.

The Divertor Shutdown

The shutdown has been divided into three stages. First Wall Division is charged with the task of preparing and managing Stages 1 and 3 and with assisting Magnet and Power Supplies Division with Stage 2. The three stages are:

Stage 1: Preparation of the vacuum vessel for the coil installation;

Stage 2: Manufacture and assembly of the four divertor coils and casings inside the vacuum vessel (Magnet and Power Supplies Division);

Stage 3: Installation and alignment of all new divertor and first wall components and diagnostic systems.

Stage 1

This Stage included the following activities:

- Removal of all Beryllium and Carbon tiles;
- Removal of all in-vessel components;
- Strip out all welded bosses and supports;
- Exchange of TF Coil at Octant No: 4 (carried out twice);
- In-vessel decontamination;
- Installation of all welded bosses, blocks and plates for coils support, baffle and lower saddle coil;
- Installation of lower saddle coil crossover bar;
- Installation of equipment necessary for the coil build including temporary coil supports, load bearing floor and arched beams for roof lifting points.

About 30 tonnes of components were removed from the vacuum vessel.

Vessel Strip-Out

In the pumped divertor arrangement, only a small number of the existing in-vessel components will be re-used. As a consequence, the first task was a careful removal of all the tiles, the beryllium evaporators, the Lower Hybrid Current Drive Launcher, the Radio Frequency antennae, the upper and lower belt limiters and dump plates as well as many in-vessel diagnostic systems (see Fig.11). Finally, all the welded bosses used to attach these components to the vessel wall were carefully removed (see Fig.12). This work was carried out in fully pressurised suits, due to the beryllium and tritium residues.

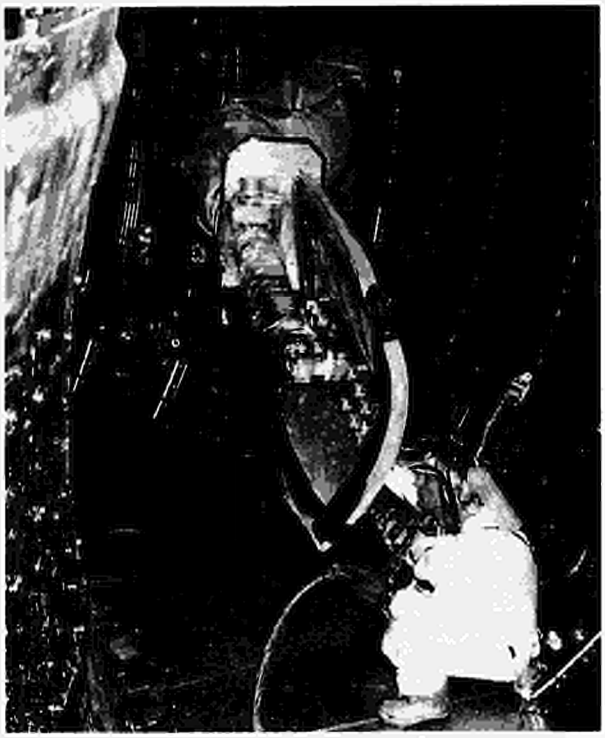

Fig.11: The Remote Handling Boom being used to remove large components from the vacuum vessel.

TF Coil Exchange

The changing of a TF coil required a significant amount of in-vessel work. This involved cutting and removing sections of upper and lower inner restraint rings, cutting and removing a number of horizontal and vertical ports, and cutting joints between adjacent octants. When the coil was changed, all components had to be refurbished or renewed and then re-welded back in position and leak checked. At the end of this rewelding, it was discovered that an adjacent TF coil was also faulty and it was prudent to change it at this time. The whole process was then repeated.

Vessel Decontamination

After many years of operation, the JET vacuum vessel wall had been covered in layers of carbon, beryllium, and metal from accidental melting of components. This layer contained tritium from D-D reactions and, in particular, from the recently performed Preliminary Tritium Experiment (PTE). The layer had to be removed before any new attachments could be welded onto the vessel wall. It was clear from the outset that to maintain the proposed timetable, it was necessary to clean the vessel of beryllium and tritium to a level at which it was not necessary for in-vessel workers to wear air-suits. Although no such cleaning exercise had been carried out previously (nor was it known to have been done elsewhere), the shutdown plans did envisage such a cleaning.

Fig.12: Removing redundant bosses welded to the vacuum vessel wall.

Many techniques were studied for effectiveness, their safety aspects and their possible effect on future plasma operations. Some were tried out in mock-up experiments. The method selected consisted of water blasting the vessel at high pressure with boron carbide abrasive grit (Fig.13). This method proved highly effective, fast, and had the added advantage that any residual material was not expected to be detrimental to operations. The cleaning was accomplished in three weeks (Fig.14) and resulted in a vessel in which the airborne beryllium levels and tritium levels were so low or below the limits of detection that in-vessel work could be performed without requiring respiratory protection.

Installations Prior to Coil Build

Before the divertor coils could be built, a number of components needed to be installed. These included the divertor coil

Fig.13: Cleaning the vacuum vessel walls.

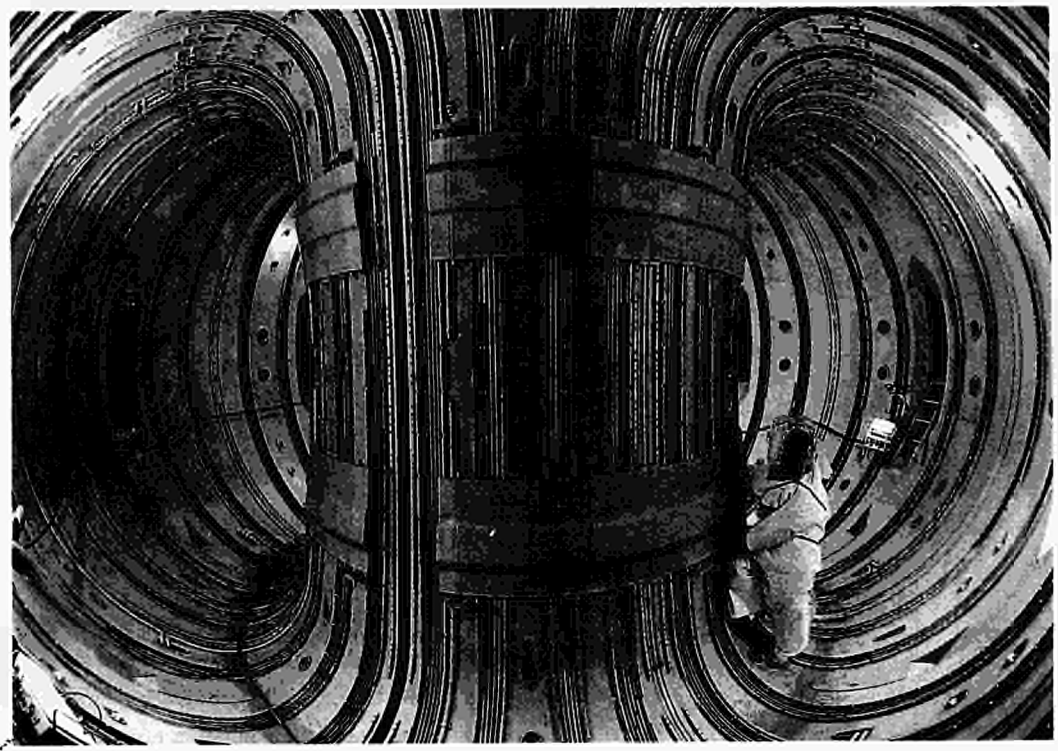

Fig.14: The interior of the vacuum vessel after decontamination. The sections of ring removed are where one joint is prepared ready for an octant removal.

supports, the cryopump baffle supports, the lower sections of the saddle coils and their supports, temporary supports for the coils during their build, arched beams attached to welded bosses on top of the vessel for lifting the coils and load bearing floors.

Many of the bosses and supports had to be positioned to a very high accuracy (± 1 mm) and to do this, a previously designed and manufactured special master survey ring was installed and used (Fig.15). The variation in profile and position of the vacuum vessel also meant that each block had to be profile machined to suit. The blocks were carefully welded to the wall to ensure alignment. Using highly trained and well practised staff, this work was completed very satisfactorily.

Shutdown Summary

A total of 172 days had been planned for the Stage 1 work in the initial plans. These plans, detailed about one year before work began, were based on optimistic but realistic estimates of the length of time required for each work package put together in such a way as to optimise progress. The plans took into account, in addition to the actual installation work required for each job, the relationship of one job compared to all others (i.e. interfaces), the number of people involved in each job and the location of the work within the vessel, the safety related aspects of the procedures and the work load on individual staff members.

Stage 1 of the shutdown ended on 26 October 1992. About 30 tonnes of components had been removed from the vessel. Over 13,000 man-hours of effort was spent inside the vessel of which over 5000 man-hours were in air-suits. Except for the seven weeks additional time taken to change the second TF coil, Stage 1 was completed according to schedule.

Stage 3

Stage 3 is scheduled to start in May 1993. The detailed day-to-day plans are now being finalised. This stage includes the following activities in sequence:

- Fit coil clamps and links;
- Fit coil diagnostics and gas introduction system;
- Set coil position;
- Mark out and weld fixing bosses on inner and outer wall for antennae and limiters. Fit saddle coil feedthroughs;
- Fit upper dump plates and upper saddle coils;
- Install the cryopump and baffles;
- Rails for divertor modules;
- Install lower cooling pipework;
- Install lower saddle coils;

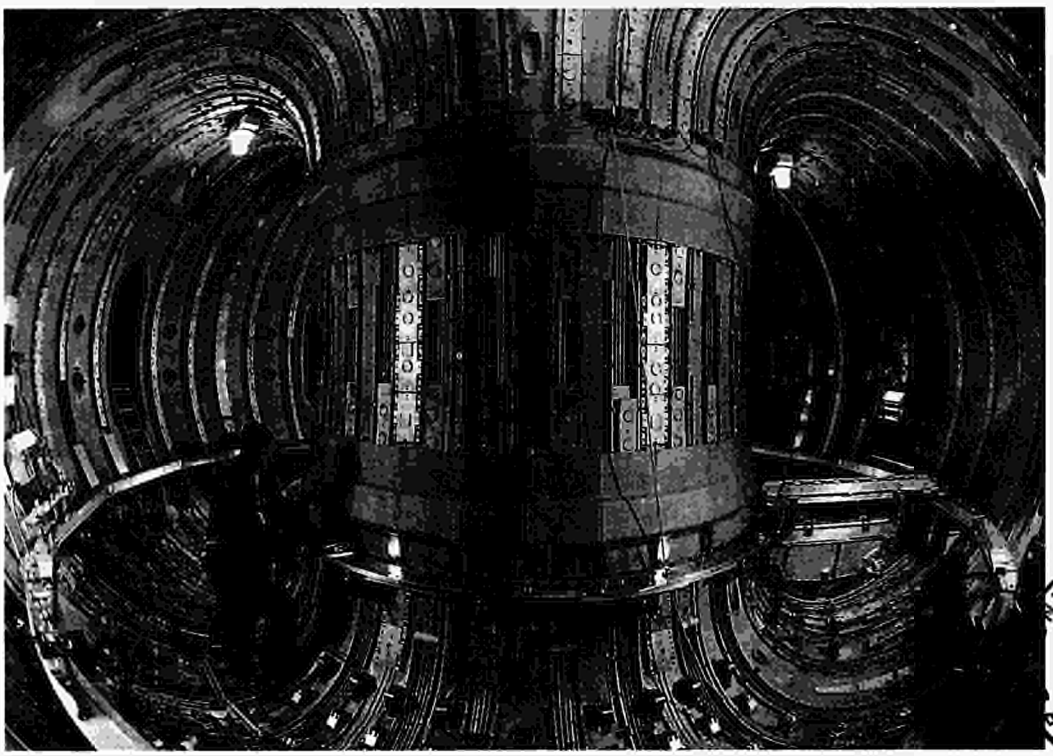

Fig.15: All divertor coil supports are fully welded in a position defined by the two survey and positioning rings shown.

- Install RF antennae and poloidal limiters;
- Install inner wall guard limiters;
- Fit graphite and beryllium tiles in the upper half of the vessel;
- Install LHCD system at Octant No: 3;
- Install target plate modules, flexible hoses and electrical breaks;
- Install remaining tiles at the bottom of the vessel and diagnostics;
- Remove all equipment;
- Fit local protection;
- Final clean and inspection;
- Diagnostics check.

At the completion of Stage 3, about 50 tonnes of new components and tiles will have been installed inside the vessel. Stage 3 will be carried out almost entirely in Class O (i.e. no requirement for respiratory protection), and has been estimated to take about eight months (about. 22,000 man-hours). The refurbishment and resetting of the vessel supports and dampers is also part of Stage 3.

New In-Vessel Components

The in-vessel shutdown work was accompanied by a large effort devoted to the design, procurement and preparation of many in-vessel components as well as jigs and fixtures.

The upper dump plates will be re-installed, mainly as vessel protection during vertical instabilities. A clean-up procedure was developed and tested, allowing components which had previously been in the vessel and which were covered in beryllium as well as being contaminated with tritium to be decontaminated to such an extent that they can be re-classified as clean. This procedure involves wet grit blasting of the components with boron carbide grit. It proved so successful that even the graphite tiles could be cleaned leaving them free of beryllium and tritium.

The saddle coils, designed to prevent MHD instabilities, were modified for the divertor configuration and have been partially installed in the vessel. Sixteen inner-wall guard limiters are being manufactured. The carbon fibre reinforced graphite tiles which cover these limiters have been designed not only to protect or guard the inner wall but also to allow plasma start-up and ramp-down.

The twelve poloidal limiters on the outer wall, which are also in the manufacturing stage, will carry graphite tiles. Most of the tiles will be the original belt limiter tiles, re-machined with a new profile. This limiter system, which is primarily intended to protect the adjacent antennae, will also be used for plasma start up and ramp-down. The most vulnerable areas of the limiters will be equipped with new tiles made of fibre reinforced graphite tiles.

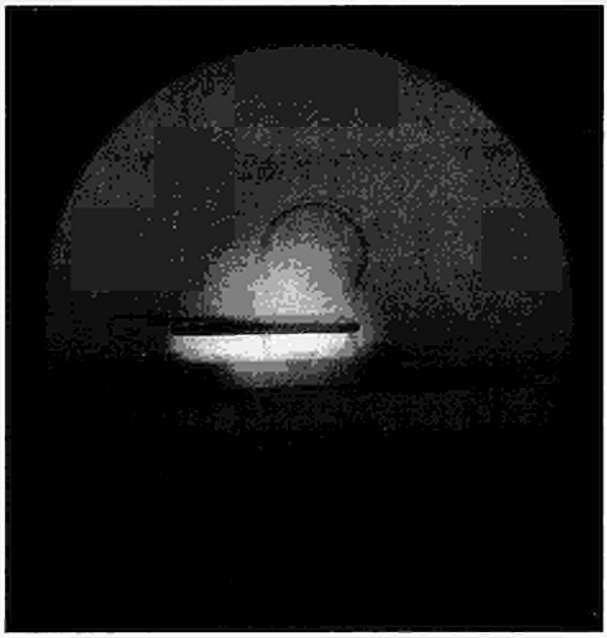

Fig.16: New GDC electrode system under test.

A detailed analysis has been undertaken on the final alignment precision of the target tiles which must be achieved and the procedures to achieve it. The analysis takes into account all of the manufacturing and expected installation tolerances, which influence the position of the tiles as well as all the expected plasma configurations and sweeping scenarios and ultimately also the design of the tiles themselves which depends on the results of the former. Two sets of tiles are being manufactured, one set of beryllium tiles and one set of fibre reinforced graphite tiles.

The graphite tiles are manufactured from material which is the result of an extensive tender action from companies in Europe, the USA and Japan. The companies sent samples which were then subjected to extensive high heat flux tests in the NB Testbed. The objective was to find the most competitive material with a high thermal conductivity, strong enough to withstand the thermal and mechanical stresses and with a delivery time of about six months. The tender was won by a European company, and has led to developments in several companies to produce new and very interesting materials which could be of significant importance to fusion research in the future.

Eight new gas introduction modules are being built to inject gas into the torus, four at the top of the machine and four into the divertor region where a distribution network of pipes gives 24 gas injection points. The gas introduction modules (GIMs) incorporate fast acting piezo-valves which, by design modification and rigorous quality assurance, have been made tritium compatible.

The beryllium evaporators have been modified to fit into the divertor configuration and are now undergoing functional tests and conditioning, prior to insertion in the machine at the end of the shutdown, to be used as part of the vessel conditioning programme.

To clean the first wall of the vacuum chamber during operation, JET (and most other tokamaks) has used an RF assisted DC discharge. However, the electrodes have been large and water cooled, occupying two of the main vertical ports. These have only been capable of providing power at 10A, 400V, requiring several days of cleaning after each shutdown. In response to pressure to move to smaller ports, KFA-Julich, Germany have developed a more solid, compact inertially cooled electrode, capable of running at 20A. JET has now designed four of these electrodes to be installed equispaced on the upper wall, giving a capability of 80A, or 8 times the previous cleaning capability, without water cooling (Fig.16).

Vessel Supports

During the last operational period, a study of the signal trends from the displacement transducers installed on the inertia brakes implied that some of the brakes, having been previously locked, were slipping during the pre-load phase of vessel heat up. Thus, some of the brakes may not have been sufficiently pre-loaded to close the gap between the drum and stator and establish an adequate contact force. Subsequent analysis indicated that the thermal finger device may be operating at the limit of its frictional capability.

A development programme is being conducted to augment the frictional capability of the brakes by using a high performance friction material between the thermal finger and the brake drum with a view to having upgraded brakes installed for the next operating period.

Vacuum System

The main work on the vacuum system has been concerned with clean-up of equipment contaminated during the PTE and with tasks related to the Divertor Shutdown. The temporary Gas Collection System used to cryopump torus exhaust gases during the PTE has been decontaminated to a level, whereby it could be completely dismantled and removed to allow the installation of the cryosupply for the Divertor cryopump. The Rotary High Vacuum Valves (RHVV) were removed from the torus as part of the shutdown programme and the RHVV at Octant No: 8, which had experienced high tritium exposures during the PTE, was found to exhibit high

internal surface contamination (measured specific surface activity of up to 8000 Bq/cm^2). This RHVV is being decontaminated by hand swabbing and high pressure water jetting and the results obtained to date indicate that the valve will be decontaminable to a level where it can be refurbished and reinstalled in the torus, without health physics constraints from a radiological standpoint. The Octant No: 4 RHVV will be decontaminated in the same way, in due course.

During the shutdown, much effort has been expended to ensure that the many new vacuum welds being performed are leak tight to UHV requirements ($< 10^{-9}$ mbℓ s^{-1}). This was particularly important for certain welds, for example those at the small circular ports at the bottom of the vacuum vessel, which will become inaccessible following installation of the divertor coils and target plates. To enhance the leak tightness validation of these welds, it was deemed prudent to perform in-situ leak tests at a temperature above that at which small leaks could be blocked by water films (>120°C). To this end, a copper heater block incorporating electric cartridge heaters was designed to encompass the standard small circular port weldments. The heater was used inside evacuated pumping probes and operating weld temperatures of 150°C were typically achieved. Using this device, welds which were leak tight at room temperature were found to leak at >150°C.

Control and instrumentation

Over forty electrical cubicles are used for the vacuum control, instrumentation, vessel conditioning and gas introduction. During the last period of machine operations, some reliability problems were experienced with these cubicles, partly due to the age of equipment. During this shutdown, an extensive programme of preventative maintenance has been started to help ensure the future high reliability of these essential systems.

The first production versions of the remote radiation hard residual gas analyzer (RGA), developed in a collaborative programme with industry, has been installed. The quadrupole head has been installed on a small vacuum system in the Torus Hall to allow extensive testing and the development of the CODAS communications protocol. Preparations are continuing for the installation of four more of the new RGAs before the end of the shutdown.

The control cubicle for the new divertor gas introduction system has been designed and is in the process of being built. This cubicle will facilitate the sequencing for the safe control of the ten piezo-valve based gas introduction modules, as well as providing a control and instrumentation interface to CODAS.

Pellet Injection

After only a short period of operation following the PTE the repetitive pellet launcher, built by Oak Ridge National Laboratory (ORNL) was de-commissioned and returned to ORNL for refurbishment and further use on D-IIID in San Diego, USA. This device had been jointly operated by the partners of the JET-USDoE (Department of Energy) Pellet Agreement under the umbrella of the EC-USDoE Agreement on Collaborative Fusion Research. The tritium assessment made prior to the PTE for the use of the ORNL launcher following the PTE was fully vindicated by subsequent measurements. The Pellet Agreement was concluded at the end of 1992 although both partners have exchanged letters of intent for extending the collaboration.

For the next operational period in 1994, two pellet launching devices are now foreseen. The first device is a high-speed (4kms^{-1}) single-shot pneumatic launchers (formerly dubbed PROTOTYPE launcher relating to a now cancelled advanced pellet launcher), employing two-stage gun drivers and delivering pellets through the pellet injector box (PIB) vacuum interface to the torus. There will be two of these high speed launchers. The second device is a new mechanical pellet centrifuge, an expansion of the ASDEX Upgrade centrifuge (IPP Garching, Germany) whose advice is provided under a contract with JET. These devices will be reported further in the Development and Future Plans section of the report.

The first part of the pellet injection work in the Torus Hall was concerned with adaptation of the PIB system to the new plasma centre, which will move to ~300 mm above midplane due to the incorporation of the divertor into the torus. This will allow central deposition of high-speed pellets. This is of particular importance for the generation of PEP mode plasmas. Both the PIB and the two-stage gun supporting steelwork in the Torus Hall were raised by 300mm. In addition, the pellet injection port on the flange cover of the main horizontal port at Octant No: 2 was modified in conjunction with bolometer and soft-X-ray diagnostics to accommodate the change. The first measures are now virtually completed. However, the flange and related modifications are still being worked on. Welding on the flange cover has been successfully carried out and has passed the hot leak test; the cover will be welded into the main port early in 1993.

and the PIB valve and bellows are presently under modification. The LHe system for the injector supply is being modified for additional LN_2 cooling in line with improved LHe economy featuring a new LN_2 cooled LHe cryoline from the LHe cryoplant. The LHe valve box has been disassembled to incorporate the necessary changes. The in-flight pellet photography for the high-speed pellets is being improved to alleviate short-comings regarding optical adjustment and temperature control (vicinity to the PIB cryopump).

The second part of work concerned preparations for the new pellet centrifuge. Apart from providing an access port in the main horizontal port flange, the centrifuge will need service connections to the West Wing where its gas supplies, electrical control, and data acquisition cubicles are located: The main cabling has been pulled and terminated in a new junction box in the Torus Hall as well as in the local electrical cubicle in the West Wing. Also gas supply and larger diameter lines (corrugated, 60mm ID, pre-fabricated and pre-tested in one length of about 70m) for pumping of deuterium and helium are about to be delivered and installed.

Power Supplies and Magnet Systems

The JET electromagnetic system is made up of toroidal and poloidal coils with their mechanical structure. Its purpose is to establish, maintain and control the tokamak magnetic configuration (Fig.17). It includes the toroidal coils, which establish the toroidal magnetic field, the poloidal coils P1, acting as primary windings of the tokamak transformer, and coils P2, P3, and P4 to control plasma radial position, vertical position and shape. Towards the end of 1992, the installation of the divertor coils D1, D2, D3 and D4 had started. These coils will become part of the poloidal system and, in conjunction with the existing coils, will permit establishment and control of the new divertor magnetic configuration. To perform their functions, these coils must be energised by suitable DC power supplies, whose voltages and currents are controlled in real time by the plasma position and current control (PPCC) system. Other DC power supplies energise the neutral beam injectors (NB) and the ion cyclotron radio frequency (ICRF) system for plasma heating, and the lower hybrid current drive (LHCD) system for plasma current profile control.

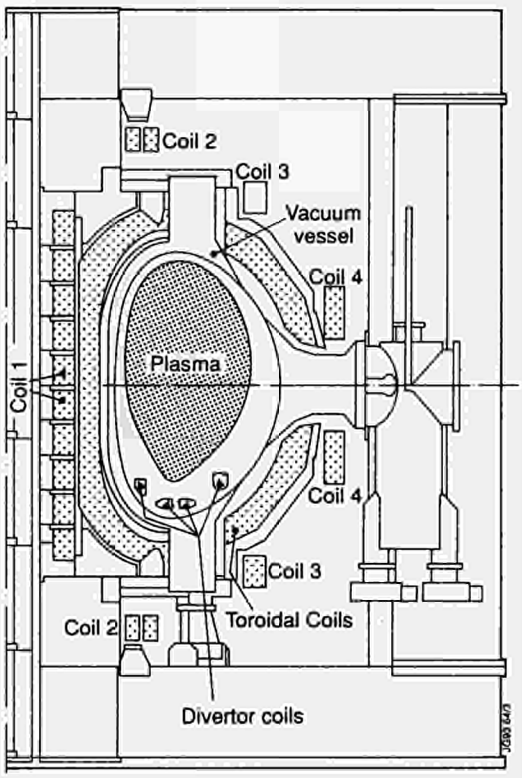

Fig 17: Cross-section of JET showing toroidal, poloidal and divertor coils

The total installed DC power exceeds 1500 MVA, capable of delivering a peak power above 1000 MW and an energy per pulse above 10,000 MJ. More than half of the power and of the energy is taken directly from the UK National Grid at 400kV and the rest is provided by two vertical shaft flywheel generators. Consequently a major feature of JET is the 400kV-36kV distribution system. Auxiliary power is supplied by the 20 MVA, 11kV/3.6kV/415V distribution system.

JET development, an essential part of the scientific programme towards enhanced plasma performance, calls for continuous modification and upgrading of the electromagnetic system, of the plasma control and of the additional heating power supplies. The main objective of 1992 was the major upgrading of the electromagnetic system to greatly extend the operating range of JET in the magnetic limiter configuration. This includes, in addition to the new four divertor coils, four DC power supplies to energise the coils, the fast radial field amplifiers (FRFA) for the vertical stabilisation of divertor plasmas, and a completely new PPCC system.

Magnet System

The magnetic system remained unchanged up to the end of operation in February 1992.

Toroidal Field (TF) Coils

A fault was discovered in Coil No:4.2 in 1990 but, as the fault was of relatively high resistance, operation continued through 1990 and 1991 using the maximum toroidal field in a limited number of plasma discharges. Coil No: 4.2 was replaced by a spare in the shutdown. The change was completed by June.

When the machine was re-assembled after the replacement of Coil No: 4.2, the impedance of all the 32 TF coils was re-checked over a wide range of frequencies (from 20Hz to 50kHz). At this stage, a further small fault in Coil No: 4.3 became apparent.

This fault was far less severe than the faults discovered in Coils No:3.1 and No:4.2. Therefore, it was likely to have no operational consequences during the next few years, if ever. However, in view of the difficulty of changing a TF coil once the divertor coils were installed, it was decided that it would be prudent to replace Coil No:4.3, while the opportunity still existed. The change was completed by August 1992. After Coil No: 4.3 was replaced, the impedance measurement was repeated and no further detectable faults were found.

Fault Detection Problems

The fault in Coil No:4.3 was masked by the fault in Coil No:4.2 and the fault in Coil No:4.2 was previously masked by the fault in Coil No:3.1 (a coil that was replaced in early 1990). This was due to a combination of unfortunate factors:

a) Each fault was approximately an order of magnitude less severe than the previous one;
b) The faults were in nearby coils (four coils between Coil No:3.1 and Coil No:4.2, and none between Coil No:4.2 to Coil No:4.3) and the measured impedance was affected by magnetic coupling with other closed conducting loops, in particular nearby coils with short-circuits. Thus, it was difficult to distinguish between a fault and the effect of an adjacent coil.

Diagnosis of Faulty Coils

Coil No:4.2 was known to have had an internal coolant leak and the approximate location of the fault was also known. Therefore it was assumed that water from this leak caused faults in a similar way to Coil No:3.1. The change to freon coolant came too late to prevent the initiation of the fault and did not prevent the fault developing.

The fault in Coil No:4.3, being less severe, was harder to localise and a coolant leak has not yet been detected. Thus the diagnosis of Coils No:4.2 and No:4.3 is at an early stage. The fact that Coils No:4.2 and No:4.3 were adjacent is not believed to be significant but the fact that they were the 22nd and 23rd in the production series may be relevant. A full investigation of all these factors is planned.

Status of the Installed TF Coils

As the faults have become successively less severe, detection methods had to become more sensitive. However, there are no detection methods capable of detecting the evolution of a fault for an interturn resistance decaying from 10^4-$10^5\Omega$ down to values comparable with the resistance of one copper turn (~80μΩ). This can be expressed in terms of fault resistance and measurement frequency. Higher frequencies are needed to measure higher fault resistances. Table. III lists fault resistances and measurement frequencies for the three faulty coils.

Table. III

Coil Number	Fault resistance	Measurement frequency to detect fault (Hz)
3.1	20μΩ to 80μΩ	DC*
4.2	250μΩ to 3000μΩ	50Hz
4.3	0.5Ω to 1Ω	3kHz

*ie, detectable by resistance measurements

The frequency that can be used is limited by resonances to about 15kHz. This allows 5 to 10Ω faults to be detected.

Measurements made after the replacement of the last coil show no abnormalities in the full set of 32 TF coils. Therefore, if there are any interturn faults, their resistance is higher than 5Ω. At this level, they would have no effect on operation; indeed, like Coil No:4.3, they should not be detectable during operation. The only question is whether these faults could develop to dangerous or inconvenient levels. As the faults are believed to have been initiated by conduction through water and as it is now two years since the coil coolant was changed to an insulating fluid, this seems unlikely.

Visual inspection showed that delamination of the epoxy glass ground insulation which surrounds each coil seems to be a more widespread problem than was thought previously. For instance, the removal of Octant No:4 revealed that not only were Coils No:4.2 and No:4.3 delaminated over a wide area but so were Coils No:4.4 and No:5.1. (Note that the ground insulation itself is in good condition but is detached internally from the copper conductors).

Even coil production Coil No:1, which has replaced the faulty Coil 4.3, showed delamination of the ground insulation, in spite of the fact this coil had never been used. This suggests that delamination might be present on several coils that could not be inspected and also that it seems to be independent of the presence of electrical faults or coolant leaks. The presence of delamination in combination with a water leak could nevertheless have made the initiation of electrical faults easier in the past.

The use of freon as a coolant should now prevent insulation failures if new leaks develop. The delamination of the ground insulation is not a cause for concern in itself, since it does not have any mechanical purpose, other than transmitting compressive loads, and, from the electrical point of view, the insulation is not impaired.

Divertor Coils

The copper conductor bars are pre-formed into half or third turns at the manufacturer's factory and then brazed together to form a coil in the vacuum vessel. The coil will then be assembled in its Inconel case and impregnated with epoxy resin.

Work at the Factory

Equipment design and procurement

The following equipment was designed and manufactured or procured for use at the Factory (F) and/or at JET (J):

a) two inspection benches for formed conductors (which were also used for conductor end machining) (F);
b) machine tool to produce a chamfer on conductors (F);
c) coil assembly tables for pre-assembly tests at the factory and final assembly at JET of Coil D1, D2/D3 and D4, in aluminium alloy detachable parts for easy insertion into the JET vacuum vessel (F, J);
d) brazing equipment (power supply, clamping tool, stretching tool) (F, J);
e) lifting equipment (F, J).

The brazing equipment was designed, procured and used for qualifying the brazing process as well as for brazing part of the coil terminals at the factory. The power supply (50kW, 10-30kHz) feeds a water cooled induction coil through a 15m long cable. The brazing jig aligns the two conductor's ends and keeps them compressed throughout the brazing cycle. It is hydraulically operated using demineralised water, since oil is not permitted in-vessel. The stretching tool is also hydraulic and is used to stretch the joint after brazing (80MPa), thus recovering some of the material properties after annealing. Both tools can accommodate straight and curved conductors.

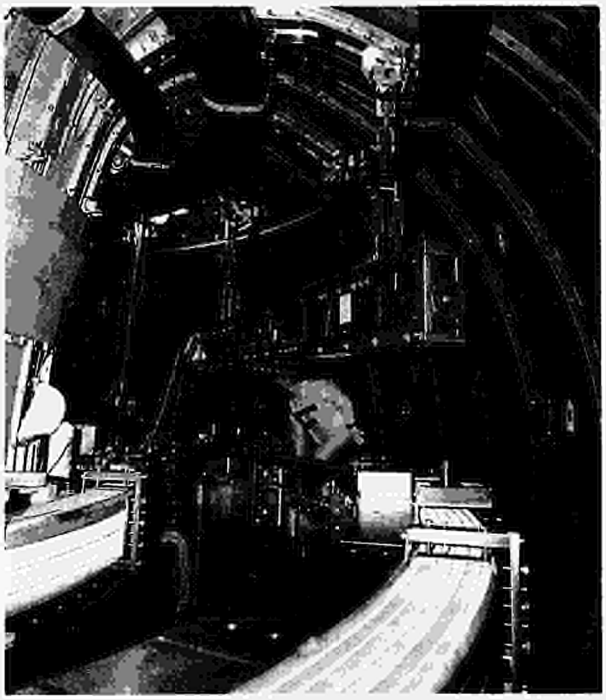

Fig 18: Motorised lifting beam used during the manufacturing process of the divertor coils inside the JET vacuum vessel

The lifting beams (three per coil) were designed and built for use in the vacuum vessel and were tested in lifting trials at the factory and at JET (Fig.18). The lifting beams are mounted above or below the coil and suspended from special "arched beams" in the vessel. A single motorised lead screw drives two nuts coupled to a set of pulleys, which wind in or out the amount of rope necessary for lifting or lowering. This system will be used at JET for lifting coils during ground insulation application, for electrical/hydraulic terminals brazing/welding, for fine positioning of coils during insertion into the cases and for lowering the coils into their final position.

Pre-production tests

Copper brazing: the copper brazing process was qualified by making test brazes on short bars. Each sample was subjected to dimensional and visual inspection (internally with an endoscope) and hardness, dye penetrant, helium leak, hydraulic pressure and X-ray tests. Selected samples were subjected to static tensile, fatigue, macro examination and guided bend tests. All samples passed the tests. Interpretation of radiographs was difficult but was aided by calibration joints with sample defects. Two separate regions of the joint (with different maximum acceptable defect size) were established. A joint re-

brazing process was also qualified for use in case a joint failed tests during production, using the same tests as the first braze.

Copper/Stainless steel brazing: Joints between the copper conductor and the stainless steel cooling pipes were made by brazing. These joints were brazed in air using induction heating and brazing alloy rings to fill the joint gap. After extensive trials a satisfactory brazing technique was established and all the prescribed pre-production tests were passed successfully.

Stainless steel welding: Welding of the water cooling pipes is by a conventional TIG process. However access for some of the welds is difficult. The manual welding process was therefore simulated using a model of the coil, in the most complex situation. This model was also used to qualify the welder.

Electrical insulation: Both the interturn and the ground insulation passed mechanical tests (interlaminar tensile, shear and fatigue shear) and electrical tests (breakdown).

Impregnation: Impregnation tests to show that the epoxy resin (in the conditions to be used at JET) flows freely through the tight glass/Kapton coupled tape insulation system proved successful. A preliminary test was done using a straight model coil. A second model representing 1/8 of Coil No: D2, including the case, was also produced using the same impregnation equipment and process as that for JET. The model was cut after impregnation and examined (visually and macrographically). Irradiation tests of the divertor coils electrical insulation system showed that a significant amount of gas develops as a consequence of the radiation damage to the epoxy resin. This gas can be pumped out of the cases provided that a minimum gap is left between epoxy and case. This is possible if release agent is applied to inner side of the case, as this prevents the cured resin sticking to the case.

Trials and staff training inside the vessel model: All major operations were rehearsed at the factory using a full size model of the JET vacuum vessel. This included assembly of the coil tables and conductor handling exercises, lifting trials and brazing in different situations. Most coil installation related problems were anticipated and solved while the workers selected for work at JET were trained.

Manufacture

Conductor bars were procured and formed using a combination of tools: bending machine to form the conductors to the required radius, joggling machine to form the vertical transitions and cross-bow for the radial transitions; Special pieces (terminals, water connections, joggles) were manufactured from special copper sections by a sequence of machining, forming and re-machining.

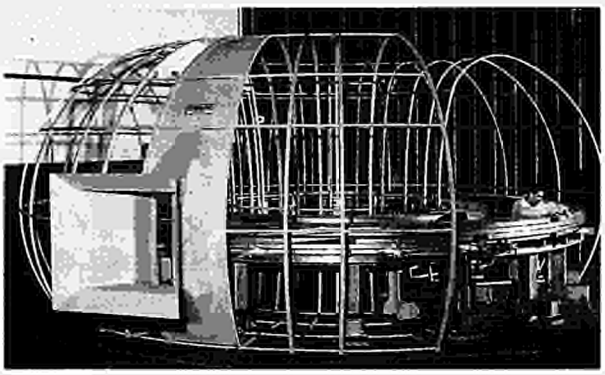

Fig.19: Pre-assembly of the Divertor Coils No:D2 and No:D3 on the assembly tables in the factory

All 220 formed pieces (of which 50% are standard conductors and 50% are specially shaped pieces) were checked using special inspection devices. The conductors were then pre-assembled into coils (Fig.19) on the same tables which are being used inside the JET vessel, to check dimensions and fit.

After degreasing, the conductors were treated with primer and insulated with dry glass and Kapton, except at the ends. Other work included machining of glass reinforced epoxy blocks for filling gaps between turns and between assembled coil and its case and manufacture of cooling pipes.

Work at JET

The coil contractor started work at JET in October and in-vessel in November. At the end of 1992, brazing of Coils D1 and D4 was half completed (Fig..20). Installation of impregnation equipment had started.

Fig.20: Coil No:D1 and Coil No:D4 copper bar conductor being brazed inside the JET vacuum vessel

Assembly sequence

The outline assembly sequence was as follows:

a) Assembly of three coil cases (for Coils No:D1, No:D2 and No:D4) from pre-formed quarters, top parts (lid) stored close to the vessel ceiling and bottom parts (gutter) stored below the vessel temporary floor;
b) Assembly of Coils No:D1 and No:D4 in parallel, electrical insulation application, insertion into cases and lid welding, tests and resin vacuum impregnation;
c) Assembly of Coils No:D2 and No:D3 in casing and parallel and electrical insulation application;
d) Assembly of case for Coil No:D3;
e) Insertion of Coils No:D2 and No:D3 in the casing and resin vacuum impregnation.

Preparation

Before start of coil work, the coil assembly tables were introduced into the vacuum vessel and assembled. Special arched beams shaped to follow the contour of the vessel ceiling with machined fixing point for lifting equipment were also installed in the vessel and proof tested.

Copper conductor insertion

Each copper conductor bar, weighing 70-90kg, is introduced into the vessel by hand and turned over for final positioning onto the assembly table using ropes and pulleys.

Copper conductor brazing

The brazing process was controlled by two parameters: joint temperature, using a thermocouple in proximity of the joint, and time. The heating time was kept short to minimise the extent of the copper annealed zone. The power supply, situated outside the vessel, was controlled by the brazer (inside the vessel) through a control panel with a start and stop button. The shape of the induction coil for copper joints brazing was optimised and fitted with steel laminations to obtain uniform heating of the copper cross-section. A special induction coil was used for brazing chamfered cross-sections. Before brazing, the conductor ends were carefully cleaned and silver coated. The silphos brazing shim (a copper/phosphorus/silver alloy) was also cleaned using an ultrasonic bath. After brazing and stretching, the copper joint was inspected visually, helium leak tested and X-rayed.

Resin impregnation

The resin impregnation equipment consists of resin mixer, pipework, resin expansion tank, vacuum pumping system, temperature and vacuum gauges. The impregnation process included the following steps:

a) Coil heating (using a 2000A, 30V DC power supply) and vacuum pumping to drive moisture out of electrical insulation,
b) Leak testing of coil case,
c) Leak testing of impregnation pipework and connections,
d) Vacuum impregnation,
e) Curing.

The vacuum impregnation was carried out with the coils near their final position. When the filling process is complete, a pressure of about 300mbar was applied to the resin. Special clamps limited case deformation to 1mm generally and less in areas where the dimensional interface with other divertor components was critical. Thermal insulation was applied around the coils during the impregnation and the curing cycle to reduce thermal losses and minimise electric heating power requirements. To avoid resin spillages inside the vacuum vessel the resin in the pipes must be fully cured before pipework disassembly. Special supports are provided to allow coil thermal expansion during heating cycle.

Status

The assembly work in the vessel started in November with Coils No:D1 and No:D4. Some difficulties were encountered in brazing the copper bars in the vessel, which was disappointing since the results of the prefabrication tests in factory were excellent. The main reason for the relatively high failure rate (~20% as compared to 3% in the prefabrication tests) was found to be due mainly to the brazing jig that did not exert the right pressure on the silphos (brazing material) sheet in the joint. At the end of the year, brazing of Coils No:D1 and No:D4 was half completed.

Divertor Busbars

Busbars from the four divertor coils pass through the Torus Hall pit, across the Basement ceiling to the J1 North Wing and power supply area. Busbars in the Torus Hall and Basement are of water-cooled copper, because of the restricted space available. The basic design of the water-cooled busbars (copper cross-section, insulation and support system) is the same as for the poloidal busbars already installed in the basement.

A contract for manufacture and installation of the water cooled busbar system (including insulated bars, support structure and enclosure) was placed at the beginning of 1992. Manufacture of the insulated busbars was almost

completed during 1992 and the support structure will be manufactured in early 1993. Installation will be in mid-1993.

New Coil Protection System

Principle

A new protection and fault detection system based on a circuit simulation run in real time is being installed. As the poloidal and divertor coils are magnetically coupled, the system must include all the coils. The TF coils are not electrically coupled and can be treated in the same way but separately. In either case, the computed currents are compared with the measured currents. A large difference would indicate a possible fault and would terminate the pulse.

The motivation for new coil protection systems comes mainly from the divertor coils but also from the fact that existing systems do not detect open circuit faults. Existing fault detection systems include:

a) voltage comparison between TF coils and P1 coils to detect short circuits (relies on having many identical coils or pairs of coils);
b) ampere-turn measurement on TF and outer PF coils to detect shorted turns (space needed for Rogowski coil measuring ampere-turns).

Neither of these detection methods are feasible for the divertor coils, because all four are different and there is no space to install ampere-turn detectors.

In addition to the circuit simulation the protection system will also:

a) make real time computations of forces and stresses in the coils;
b) check current and voltage levels and coil heating effects.

If acceptable values for any of these parameters are exceeded, the pulse will be terminated.

Implementation

Circuits

The circuit solver can work in two ways. Either:

a) take measured currents and compute the voltages, or,
b) take measured voltages and compute the currents.

The second option has been chosen since it is basically an integration process, which automatically reduces noise. In either case, all currents and voltages have to be measured and fed to the processor, either for computation or comparison.

The poloidal system now has eight and eventually will have 12 coupled circuits. There will be 23 coils, sub-coils or electromagnetic elements.

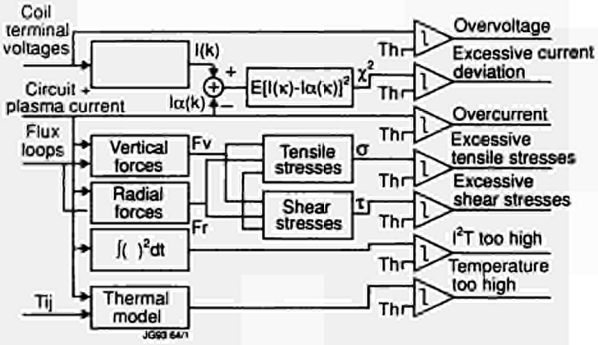

Fig.21: Block diagram of the new coil protection system

The circuit equations are of the form $V = RI + L(dI/dt)$ which can be changed to $dI/dt = (V - RI)/L$ for integration. For numerical integration a time step of 10ms is proposed, as the shortest circuit time constant is about 140ms.

Several difficulties can be overcome, namely:

a) the plasma is a non-linear element but its current and fluxes can be measured directly rather than calculated;
b) the non-linearity of the magnetic circuit can be overcome by a direct measurement of the flux in the iron;
c) the vacuum vessel has a short time constant and will be ignored.

The protection system can provide protection against mechanical or thermal overstressing of the coils. If the calculated stresses exceed a safe value the pulse will be stopped.

Transducers

The new protection system requires voltage and current measurements for each circuit and will be provided with an independent set of transducers. Some existing redundant transducers will be used and new ones will be procured.

Processor

A fully digital implementation of the algorithms is proposed using a digital signal processor similar to that proposed for the PPCC system. A block diagram of the protection system is shown in Fig.21.

Most of the coil protection system hardware has been defined and the procurement of transducers is underway. A programme has been written for convenient off-line calculation or check of model parameters with JET data. Simulations of the circuit behaviour were carried out and compared with JET pulse data for a preliminary verification of the circuit validation routine.

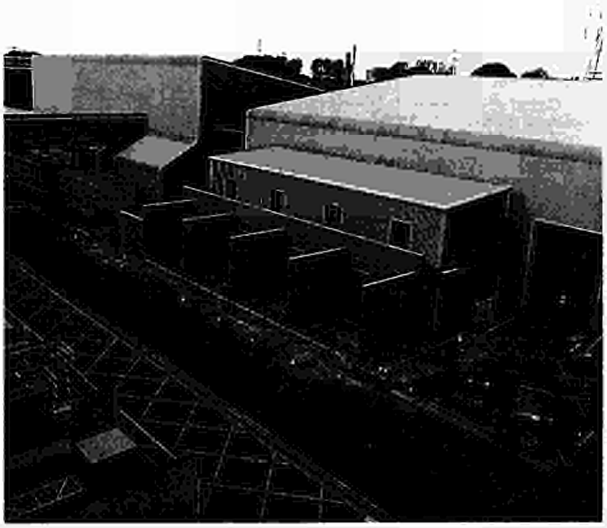

Fig.22: PDFA power supplies building

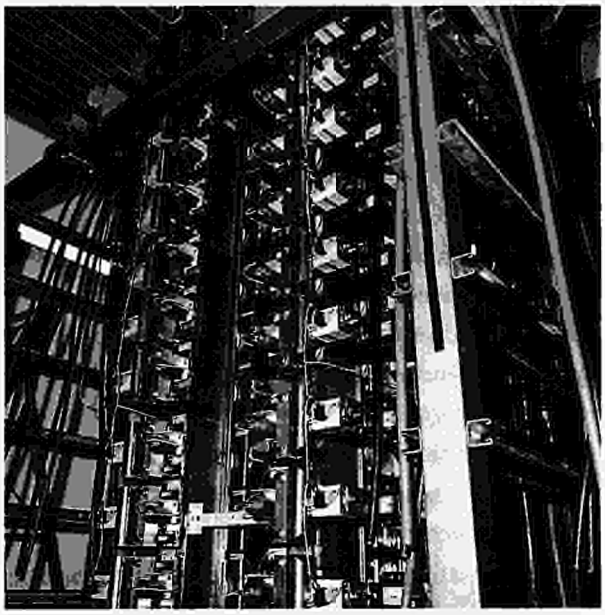

Fig.23: Installation of the thyristor rectifiers for the PDFA

Magnet Power Supplies

The toroidal field power supplies consist of a flywheel generator diode rectifier, (rated 67kA DC, 9kV no-load voltage, 2600MJ delivered energy) and of two transformer - thyristor rectifiers, supplied directly from the 36kV distribution, (each rated 67kA, DC 2kV open circuit). These three power supplies are connected in series (67kA DC, 13kV open circuit).

The poloidal field power supplies consist of a flywheel-generator-diode rectifier (identical to the toroidal field supplies), a DC switching network and a transformer-thyristor PVFA 5-6; rated 2.8kV DC no-load voltage, 35kA DC. This establishes and sustains current, up to 7MA, in the plasma ring. In addition, the poloidal field power supplies include the amplifiers to control the position of the plasma ring: PRFA 1-2 + PRFA 3-4 rated ±5.2kV DC (no-load), ±3kA DC, for the control of the vertical position, PVFA 3-4 and PVFB, rated 12kV at 1kA, 4.7kV at 6kA, 2.3kV at 25kA for the control of the radial position and PVFA 1, rated 1.4kV DC (no-load), 40kA DC for the control of the plasma shape. A new power supply system is now needed to supply the four divertor coils.

Poloidal Divertor Field Amplifiers (PDFA)

The four divertor power supplies, PDFA1-4 are independent and each consists of two transformers within the same tank, each feeding a rectifier module consisting of six full thyristor bridges connected in parallel. Each single thyristor bridge is connected directly to the transformer output by means of individual three-phase AC cables to improve the current sharing. Each rectifier module has a DC choke to limit the asymmetrical components of the DC current in the case of a DC short circuit. The two modules are normally parallel connected but can be re-configured in series by means of bolted busbar links.

The ratings of PDFA1 and PDFA4 are 500V, 40kA for 20s while PDFA2 and PDFA3 are 650V/550V, 40kA for 20s, every 10 minutes. The dual voltage rating of PDFA2 and PDFA3 is achieved by means of a tapping winding and a two step manual tap changer. The power supplies have been designed to withstand the anticipated peak short circuit current of 172kA. The insulation level is 20kV rms 50Hz, 1 minute for the transformer, AC cables and DC busbar and 10kV rms 50Hz, 1 minute for the rectifier modules. The PDFA power supplies are housed in a new building (Building J31) consisting of a shelter (insulated and heated) for the rectifiers, controls and of an enclosure (non-heated) for the DC busbars, DC chokes and earthing switches. The new building, situated close to the Generator Building J3, was designed to match architecturally with the surrounding buildings (Fig.22). The contract for the design, manufacture, installation and testing of the four power supplies together with the Building J31 was placed in July 1992.

During 1992, the design was completed, the building and services were erected and commissioned, the transformers and three rectifiers (Fig.23) were installed as well as the AC cables. The rectifier unit of PDFA4 was completed in factory in preparation for the factory type tests to take place in January 1993. The commissioning on site of the other units will start in March 1993.

Air Cooled DC Busbars for Divertor Power Supplies

The divertor power supplies are connected to the water cooled busbars of the divertor coils in Building J1 by means of four pairs of air-cooled aluminium busbars. The routing of this new busbar system crosses several buildings on a route length of about 110m; the Generator Building J3 (where the dummy load will be located), the static unit building J4 and the Additional Heating Building J1H together with two busbar bridges. In view of the many restrictions along route, a compact design was chosen with a busbar extrusion of rectangular box section together with insulated clamps to withstand the peak fault current of 172kA. The detailed design of the route together with the required steelwork support was made prior to issuing the call for tender. The call for tender was issued in March 1992 to nine companies.

After technical evaluation, the contract was placed in July 1992. By the end of 1992, the design calculation and detailed drawings were completed, the thermal type test on a sample of busbar and flexible was completed and the mechanical and electrical type testing of the insulated clamps and post insulators was also satisfactorily completed. The busbar extrusions were received and the clamps plus post insulators were released for manufacture. Manufacture of the busbar will start in January 1993 after satisfactory completion of the weld qualifications.

Fast Radial Field Amplifiers

The existing Poloidal Radial Field Amplifier (PRFA) would not have the level of power nor the speed to control plasma vertical position in the new divertor configuration. The new system is a set of four power supplies, each capable of 2.5kV, 2.5kA, rise time 0.5ms. The concept is based on an H-bridge in which each arm consists of two Gate Turn Off (GTO) thyristors connected in parallel (Fig.24). The civil work for the PRFA started in January and was completed in May. Factory tests on the first sub-unit started in February, power tests on dummy load, including the tests foreseen in the contract, started in June and were concluded successfully by August. Tests have been carried out on the so-called Stage 3 configuration. Two invertors were connected in parallel, supplied by the same convertor; since the current in each invertor is halved, its switching frequency can be increased, with the same junction temperature. The tests have shown that the switching frequency can be increased by 25%. Installation

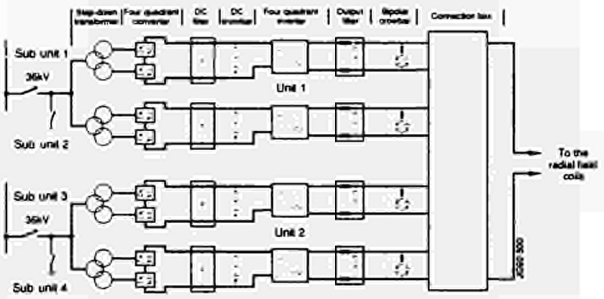

Fig.24: Schematic of the GTO invertor for the FRFA

at the JET site started in May; two shelters were delivered in August, and the following three arrived on site at the end of September, since then the installation work has continued and has been completed by the end of December. Commissioning on site started in September, and at the end of the year has reached the stage by which the signal commissioning has been completed.

Disruption Feedback Amplifier System (DFAS)

The purpose of the amplifier is to supply the eight saddle coils due to be installed inside the vacuum vessel during the shutdown, to allow control of m=1, n=2, MHD instabilities. The basic component is the Insulated Gate Bipolar Transistor (IGBT). The system consists of four amplifiers, each capable of 1.5kV, output frequency 0-10kHz and a current of 3kA (0-1kHz) and 3kA/f(kHz) (1-10kHz). By the end of 1991, the integrated tests, performed on site on Amplifier 3, were successfully completed (Stage 2), this amplifier was built at first and was equipped with the 1000V IGBT and with the modified prototype cards.

The final version of the printed circuit boards (PCB) was only available in April, therefore also the second and the third amplifiers were tested with the prototype cards that were progressively swapped with the final PCBs. By the end of June, all four amplifiers passed the completion tests as foreseen in the contract, individually on the dummy load. Moreover, all four amplifiers were tested simultaneously to verify as far as possible, their immunity to mutually induced noise.

During the long period of commissioning on site (from September 1991 to June 1992), it became progressively clear that two components, the shunts and the filter resistors did not meet specifications. After several technical discussions, it was agreed that the shunts would be replaced and the insulation level of the filter resistor would be reduced by a factor two by reconnecting the filter resistors.

Plasma Control

For pumped divertor operation, a new plasma position and current control system (PPCC) is being developed. It is based on a multi-DSP system (fast floating point digital signal processors) housed in a VME-crate (Versa Module Europe). The DSPs chosen are of type TMS320C40, running at 40MHz. This system replaces the previous CAMAC based integer arithmetic microprocessor system and will provide the enhanced processing power needed for the plasma boundary identification in real time and for all control functions.

Magnetic signal processing

The previous magnetic signals used for control will be supplemented by various new magnetic signals obtained from inside the torus. New general purpose acquisition modules being developed by CODAS provide integration, isolation, A/D conversion, corrections and real-time access from shared memory. Every 2ms, all magnetic signals required for plasma control will be transmitted digitally to the PPCC. In addition, the four divertor coil current signals are needed for the derivation of control quantities such as plasma current and plasma boundary shape variables.

Analysis has shown that the plasma current and the position of the plasma current centroid can be obtained with sufficient precision, with the previously applied method of linear magnetic signal combination (representing contour integrals), corrected by the contribution of divertor coil currents. For the control of the X-point position and of gaps between the plasma boundary and internal structures (RF antennae, etc.), a real time version of the XLOC boundary identification algorithm has been developed and optimised. This code uses various magnetic signals from sensors located near to the plasma, in addition to the existing pick-up coil and saddle loop signals. The execution time on a DSP selected for PPCC is <1ms, which is sufficient for shape feedback control.

Plasma current and shape control

Nine poloidal field (PF) circuits are available for plasma control, excluding the vertical stabilisation, which are strongly coupled magnetically. Therefore, a decoupling control algorithm is being implemented for feedback control of the plasma current and of a limited number of geometrical plasma boundary quantities, for example plasma/structure gaps and X-point position. The algorithm uses a reduced parameter model of JET established with the PROTEUS equilibrium code. It involves multiplications of preloaded system matrices with the errors of variables to be controlled (gaps, currents). The knowledge of internal plasma parameters (beta, ℓ_i) is not needed. At the start of operation, most currents will be pre-programmed proportional to the plasma current. With experience, the number of gap feedback loops can be increased. In any case, the feedback control of shape variables can be supported by feed-forward control of PF currents based on an estimate of the required currents.

Various simulations have been performed, which indicate that the system behaviour upon setpoint changes does not depend crucially on the correctness of the applied model. Therefore, modifications of the control matrix during a pulse can be avoided or kept minimal.

Vertical stabilisation

The divertor plasma is more difficult to stabilise than the previous X-point plasmas. A new fast radial field amplifier (FRFA) has been installed to provide the required increased performance. The stabilisation principle is similar to that applied previously: the stabilisation uses feedback of the vertical speed of the plasma current centroid (weighed with I_p), the average FRFA current is maintained at zero by current feedback with a PI controller.

The new system uses direct analogue signal transmission to PPCC, independent of other systems. The derivation of the displacement signal is more complex than previously. It includes corrections for current changes in the divertor coils, transmitted from new sensors at D-coil busbars, and also a correction due to plasma current changes at a displaced position Z_p, where Z_p is transmitted from the shape control part of PPCC. These signal handling and controller functions will now be performed by a DSP, providing a higher degree of flexibility than the previous analogue system.

The system has been simulated taking into account the particular characteristics of the FRFA and using a simplified model of the plasma and the JET apparatus. In particular, the response on small and large amplitude perturbations was examined. Results and further analysis will be used to prepare the commissioning without and with plasma. A block diagram of the new PPCC system is shown in Fig.25.

General Electromagnetic Analysis

2D-Code

The interactive 2D equilibrium evolution code has been enhanced to include halo currents using adjustable current profile parameters. This serves to improve the estimate of

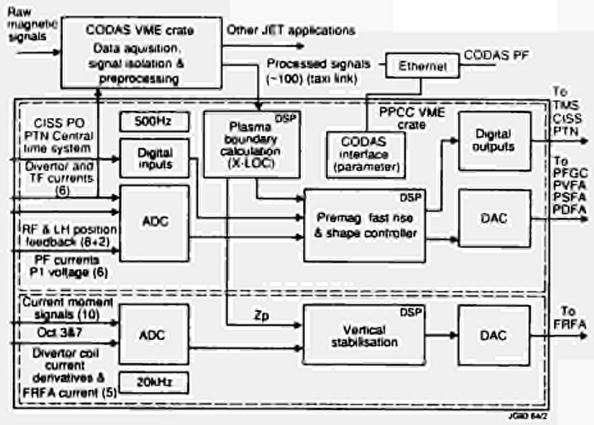

Fig.25: Block diagram of the new PPCC system

forces on internal structures expected during disruptions and vertical displacements of the divertor plasma. A case matched to a JET disruption and an example of a displaced divertor model plasma have been performed. The code was also used in support of a magnetic analysis of ITER.

Forces at Divertor Elements

The assessment of forces expected during disruptions and vertical instabilities of the divertor plasma have been continued. These checks included a re-assessment of forces at the cryopump, an estimate of forces at interior ducts for diagnostics and to the assessment of currents and forces which may result from isolation faults at the internal disruption control coils. This latter examination was instigated by the report of an isolation breakdown observed in ASDEX-U. Subsequently, some coil supports were strengthened.

Additional Heating Power Supplies

During 1991, the additional heating power supplies reached their final configuration. Upgrading and modifications aimed at increased reliability have been undertaken during 1992.

Radio Frequency (ICRF) Power Supplies

At the beginning of the shutdown, the RF power supplies were re-arranged in line with the re-grouping of RF generators. After this work was completed, a general re-commissioning of the power supplies was necessary. This work had to be done as a priority, as even during the shutdown, RF power supply for the testbed was used on a regular basis.

Lower Hybrid (LHCD) Power Supplies

All the Lower Hybrid power supplies have now been operated with the klystrons as load, although not all at the full nominal power. Some minor design changes were carried out to the power supplies after these tests. During the last operating period, the Lower Hybrid Power Supplies used in operation were most reliable. Major maintenance was carried out on the thyristor modules and other components of the power supplies. Near the end of the year, the calibration of the power supplies was checked and found to be within the original specifications of 1%.

Neutral Beam Power Supplies

During the last operating period, the reliability of the Neutral Beam Power Supplies was over 90%. However, to improve the reliability even further several modifications were implemented during this shutdown.

During the last operating period, the largest number of faults was due to the power supply switching off at the beginning of a pulse without indication of the reason. A measuring campaign was set up at the start of the shutdown to try to find this fault. It was tracked down to an asynchronous transmission fault internally inside the protection system. A design change was implemented on all the modules; in addition, the same modification was instituted on the PINI testbed to gain experience under normal operating conditions.

In the past, it has been observed that faults were becoming more frequent as the ambient temperature increased. Tests showed that even at 20°C, the temperature inside a protection system could be as high as 40°C. So to improve the reliability, cooling units were installed on the protection systems.

On the outdoor thyristor rectifiers, all units have been cleaned and overhauled. Since arcing caused by condensation was one of the problems during the last operating period, anti condensation heaters have been installed on all units.

Neutral Beam Testbed Power Supplies

Major re-wiring has been carried out to the testbed protection system. This made this system similar identical to the power supplies of Octant No:4 and Octant No:8 systems. Proposed modifications and improvements can therefore be tested on the power supplies in the testbed before they are implemented on the Octant No:4 and Octant No:8 power supplies.

Power Distribution

Most of the activities during 1992 have been directed and focussed on the preparation of the electrical facilities neces-

sary for shutdown work in-vessel and ex-vessel, and on the execution of the general shutdown work and electrical services related to the new installations.

Extension of 36kV and 415V Distribution

During the year, two new contracts were placed. The first one was to extend the 36kV busbar system with two additional circuit breakers needed to power the PDFA system. Design work and HV cubicle fabrication were completed during 1992 while overall erection on site will be completed by mid-1993. The second contract was to extend the 415V system with a new TA9 substation and further systems for Diagnostic Roof Laboratory, J2 Building, FRFA, PDFA and cooling pumps.

Reactive Power Compensation

A major fault developed at the end of 1992 on two damping resistors of the reactive power compensation system during operation; the fault was only detected during a maintenance period in January.

An investigation was started to find the causes of the fault and to make the necessary modifications. Analysis was carried out with computer models, and the design of the damping resistor has been improved using outdoor insulators with larger creepage distance. A better design has also been adopted for the neutral resistors of the three 400kV/36KA transformers. Moreover, arresters will be added in parallel to the neutral resistors to prevent dangerous over-voltages to the 36kV transformer starpoint.

Stage 2 (two units of 50MVAR each) was released in December 1991, its construction was delayed because of the fault reported above. In May, it was decided to reduce Stage 2 from two to one 50MVAR Unit (Stage 2a). Construction of the equipment started in June, some components have already been delivered and the others are ready for shipment.

Service, Construction and Installation Work

The following tasks were undertaken during 1992:

- design, manufacture and installation of the special safety electrical services to be utilised for the divertor coil construction;
- rearrangement of the J2 415V power distribution which included the removal of a rotating 180kVA UPS and the installation of a 300kVA static UPS to serve the relocated IBM computer and the new JET UNIX computer;
- removal of 18km of redundant cables from machine to create room for the new divertor diagnostic cabling;
- pellet injection centrifuge instrumentation link which included design of new cable route and pulling, terminating and testing of about 140 multicore cables;
- design for routing in basement of Pellet Injection gas pipe and cryoline for divertor coils; procurement and installation of steelwork for both systems;
- electrical services for FRFA system including design, fabrication and installation of two 36kV disconnector cubicles, 36kV and 415V cables and terminations;
- removal of about 1000 machine jumper cables to be re-installed at the end of shutdown;
- design and supervision for the electrical services in PDFA building;
- air cooled PDFA busbar routing design including building modifications and busbar steel supports;
- design for gas introduction pipe link from Building J25 to JET machine and for a variety of modifications and/or enhancements to ensure reliability of Building J25 services;
- electrical services for PDFA system at 36kV and 415V.

The overall performance has required 60,000 skilled man-hours of effort supported by 12,000 hours of design work and 10,000 hours of technical assistance.

Electricity Supply

Electricity supply is provided by means of three separate contracts.

Southern Electric

This contract is for the supply at 11kV of all auxiliary power required by JET. This is supplemented by a small contract with AEA Culham, to supply JET's rented building.

Following negotiations with Southern Electric, a reduction from 10MVA to 5MVA in the reserved available capacity was agreed, and it was also agreed that the reduced charges could be applied retrospectively. Southern Electric pointed out however, that increasing this available capacity back to 10MVA could not be guaranteed even if a considerable period of notice was given. This matter is still under consideration.

National Grid

This contract is for the use of the 400kV grid to supply all JET's major pulsed loads.

Table. IV
Electricity expenditure for 1992

Invoices	Units (kWh)	ECU/Unit	Cost (ECU)
Culham supply	2,362,360	0,0556	131,421
Southern Electric	24,351,570	0,0562	1,369,408
National Power (pulsed line)	3,947,200	0,2504	988,725
National Grid Connection	-	-	121,974
National Grid Consultancy	-	-	-
(1 ECU - 0.76£)		TOTAL	2,611,528

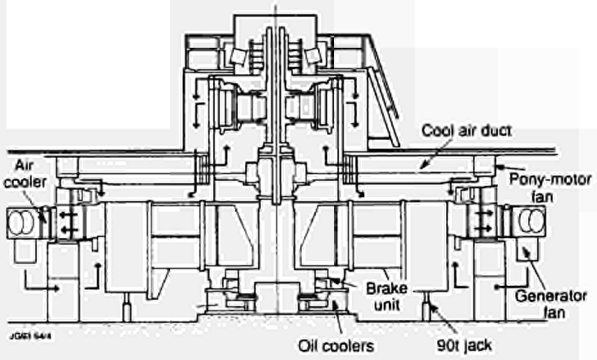

Fig 26: Stator and rotor of the toroidal flywheel generator

National Power

This contract is for the supply of electric power to JET from National Power power stations through the 400kV grid. After prolonged negotiations, an acceptable contractual definition was agreed and JET is now awaiting the final version of the contract for signature.

The actual expenditure for electricity are shown in Table.IV. The cost trend is typical of a year mostly dedicated to shutdown activities.

Maintenance Operation and Other Studies

Following two months operation in 1992, each power supply underwent an extended overhaul including some upgrading and a number of small but significant modifications.

Maintenance and Overhaul

As many of the magnet power supplies had been operating for nearly ten years, several key parts of the equipment were selected to carry out an extensive examination in addition to the scheduled maintenance.

Flywheel Generator

The stator and rotor of the toroidal flywheel generator were chosen for close examination (Fig.26) of the larger energy delivered during operation.

The detailed inspection took three months to complete and did not reveal any weakness in the design or construction of this pulse generator. This applies to both stator and rotor. In addition, the scheduled maintenance was carried out on both generators; the low friction pads between the rotor rim and rotor spider was removed, examined and replaced. All bearing pads were removed for inspection, the thrust bearing pads being examined ultrasonically.

Pulsed Transformer

Two pulsed transformers with the largest pulse duty were examined; one uses the foil winding type and the other the layer winding type for the LV winding.

The transformer of PVFA1 was dismantled and inspected. The whole transformer was found to be in good condition. It was further concluded that examination of the other transformers of the same construction was not necessary. The excitation transformer of the toroidal generator was dismantled and inspected. The transformer was found in very good condition and no loss of coil clamp pressure was found (layer winding).

Site Earthing Mat

An important task was to check the integrity of the earth mat on the JET site. Some three hundred connections were checked. Only one connection was found to be completely open, which was next to the excavation for the transformer pens for the new divertor power supplies.

Bi-Directional Transformer

During the three weeks outage on the 400kV line, requested by National Grid, which took place in July/August, the 30kVA Bi-directional Transformer has been successfully brought into operation for the first time. This transformer supplies a load at 36kV, when fed at 11kV and vice-versa. The transformer has enabled the resuming of the essential 36kV supply for the NB Testbed, from the 11kV line.

Power Supply Upgrading

In view of the unique opportunity given by this long shutdown to install the pump divertor, many projects for upgrading or enhancing the magnet power supplies were selected, namely; upgrade of the amplifiers PVFA 3-4, PVFA 5-6 to

40kA (PVFA 1-2 was already upgraded), new measurement and protection cubicle for the ohmic heating circuit, modification of the toroidal field circuit for imbalance current, upgrade of the auxiliary distribution for the ohmic heating circuit, etc. Design for most of these activities has taken place in 1992 and implementation has already started.

Neutral Beam Heating System

In common with the experimental programme, neutral beam (NB) operation was limited to the first two months of 1992, followed by the start of the major shutdown to install the pumped divertor. Analysis of injector operation over the duration of the 1991-92 experimental campaign revealed that the high availability and reliability were maintained and in some cases improved upon. The use of high power beams of ^{3}He, ^{4}He and H, in addition to D made significant contributions to the overall experimental programme. The planned improvements and modifications of the injection systems for execution during the shutdown are underway and proceeding satisfactorily.

The NB Testbed has continued with its active programme of testing high heat flux elements and materials for the Mark I divertor (inertially cooled). Various graphites and carbon fibre composites (CFCs) have been tested to enable the most appropriate material to be selected. The planned major upgrade of the cryoplant is continuing and contracts for an additional helium liquifier and enhanced liquid nitrogen system have been placed. More detailed activities appear in the following paragraphs.

Operations Activities

Summary of Operation in 1992

The range of plasma currents over which injection has been performed was extended in 1992, with routine injection being achieved at the 15-16MW level into 7MA plasmas and also into 1.5MA plasmas. 7MA operation at was a severe test of the stray-field compensation system and its ability to cancel the substantial stray poloidal field which exists at these high plasma currents. Correct and trouble-free alignment of the neutral beams was maintained successfully throughout this programme. The injection experiments at low plasma currents and toroidal fields (1.5MA, 0.9T) were instrumental in achieving a toroidal plasma beta (β_T) which exceeded the Troyon limit by ~ 20%.

The short operation period enabled further characterisation of the performance of the two so-called "high current" PINIs which were installed on the beamline for the preliminary tritium experiment (PTE) in 1991. One of the PINIs achieved its design current of close to 60A, while the other PINI delivered a current ~15% below the design figure. The reason for this is not clear, but it is suspected that the tolerance required for the reduced grid-spacing had not been maintained. This will be evaluated when the system is dismounted during the shutdown.

System Reliability and Availability

During the brief operation period, the injectors were operated in D, ^{3}He and ^{4}He. Operation in the heavier helium isotope was restricted to short pulses and powers of less than 7MW for experimental purposes, in order to study the transport of thermalised He^{++}. The power injected in D and ^{3}He was not restricted and attained 16 and 13.5MW levels, respectively. The high levels of ***reliability*** (defined as the energy injected during the pulse as a fraction of the energy requested prior to the pulse) attained in 1991 were also maintained at over 90% in 1992.

In addition, the ***availability*** of the injectors (which quantifies the percentage of time that a given injector is available for use during tokamak operations) has also been maintained at a high level. Since each injector contains eight beams, it is possible to have partial availability (eg. only 6 out of 8 PINIs available). Consequently, the availability of the system (SA) is defined as

$$SA = [(TS - (TD + FD \times FS))/TS] \times 100\%$$

where TS = total duration of operational shift, TD = total time for which 100% of the injector is not available, FS is the fraction of the injector not available for a time FD.

Figure.27 shows results of an analysis of availability for each injector from 1987 to the present. After the first year of operation, availability has been ~80-90%. The reductions in availability of the Octant No:8 injector at various times reflects its use to bring into operation various new configurations - notably 140kV and He injection. It is significant that the subsequent corresponding changes to the Octant No: 4 injector were incorporated with little or no loss in availability due to the experience gained on the first systems.

Shutdown Activities

During the shutdown, the major upgrades/improvements to control and instrumentation subsystems will concen-

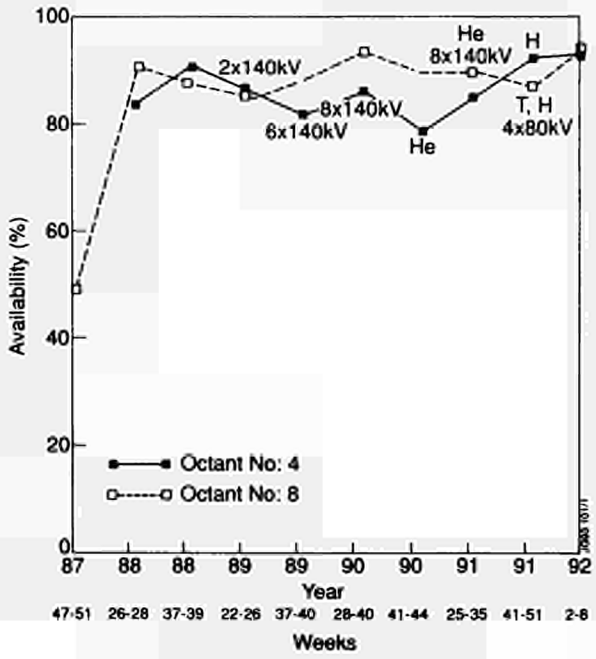

Fig.27: Analysis of injector availability

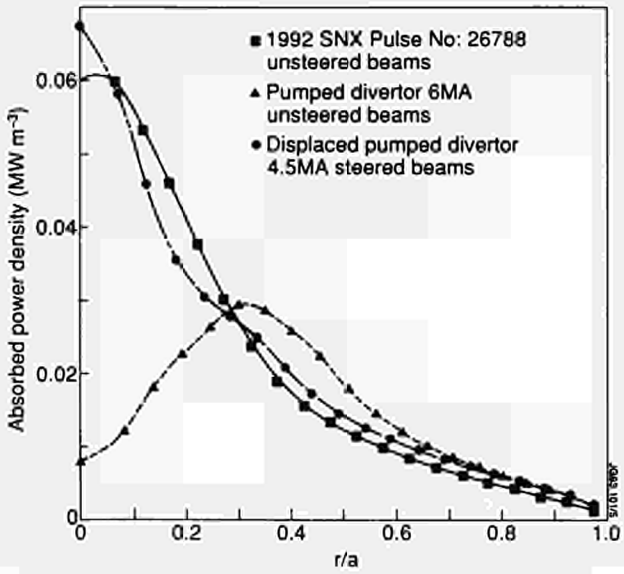

Fig.28: Absorbed power density as a function of normalised plasma radius for 1MW of 140kV beams

trate on providing simpler and/or more fail-safe operation for future operation with tritium injection. Experience gained during the PTE has proved to be highly valuable in highlighting some of these requirements, which include:

- upgrade of the fast shutter control system;
- modifications to the gas introduction system to enable improved accounting of the total amount of gas introduced into the injectors;
- the installation of absolute manometers for pressure measurements (which require the development of remote readout electronics for the D-T phase).

A "HAZOP" study of the beamlines has been initiated to analyse failure probabilities during the final D-T phase of operation. These probabilities, weighted with any associated potential tritium release, will be used to determine whether or not further modifications to part of the injector control system, beamline components or modes of operation will require re-assessment and/or modification.

Finally, remotely controlled steering of all 16 PINIs will be available for the next experimental campaign in order to re-aim the beams. This is required to give optimum power deposition in the upwardly shifted plasma equilibria which will be characteristic of the new phase of JET. Figure.28 shows the results of computations of the power deposition profile with and without re-steering for a high performance NB heated plasma. Figure.29 shows the more significant corresponding values of integrated power deposition profile. The beamline thermocouple instrumentation data collection and analysis system is being enhanced to handle the additional instrumentation required to diagnose and ensure safe operation of the re-aimed beams in the new configuration.

Studies of NB Configurations for the Next Phase of Operation

Following an extensive study of injection scenarios using the various combinations of PINI configurations available, it has been decided to equip one injector with eight PINIs in

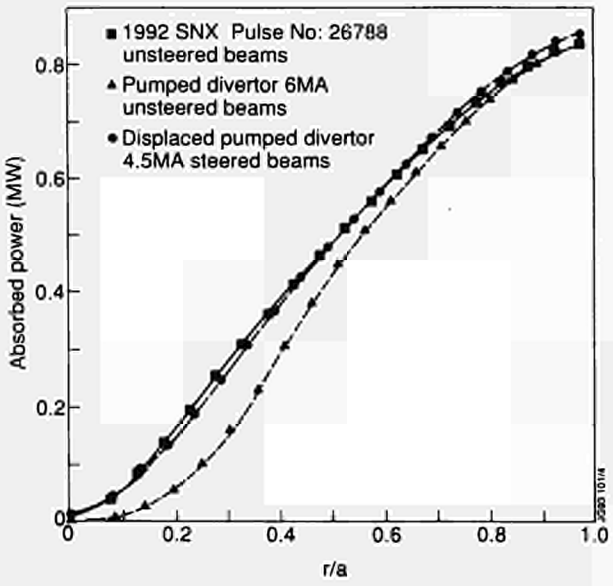

Fig.29: Absorbed power as a function of normalised plasma radius for 1MW of 140kV beams

Table V

Expected power to JET from each Injector for differing beam species available.

Beam Species (each Box)	Injection Voltage (kV)	Power to JET (MW)	
T	150	11	24
D	80	13	
D	140	7	20
D	80	13	
H	115	3	10
H	70	7	
^{3}He	155	7.5	17.5
	85	10	
^{4}He	120	6	18
	85	12	

Note: Differing values of injection voltages for various species result from maximum values of current from HV and magnet power supplies

the 140/160kV configuration and the other with eight 80kV "high current" PINIs first developed to give increased D^0 power for the PTE. Not only should this configuration result in 20-24MW for D-T operation (should it be decided to carry out a PTE II), it should also provide very significant power levels in H, D, ^{3}He and ^{4}He.

The predicted maximum values of injected power which will be available are summarised in Table.V. In all cases, the expected power is in excess of that available during the previous campaign and in addition to studies of high fusion performance plasmas, it will allow studies of H-mode physics and further confinement studies as a function of atomic mass to be carried out in the absence of neutron generation.

Engineering Activities

The main engineering activities during 1992 have been in the following areas.

Modifications and Upgrades to the Injectors

The third (spare) Central Support Column (CSC), which carries the majority of the beamline components (deflection magnet, ion dumps and beamline calorimeter) has been brought up to its full specification with the installation of improved Full Energy Ion Dumps, electrical feedthroughs and water drainage system. This CSC will replace that in the Octant No: 8 injector which was used for the PTE and will now become the spare CSC.

Modifications are being carried out to enable the re-aiming of the beams for the new phase of JET. These include PINI steering mechanisms and bellows, re-alignment of neutralisers and the provision of additional thermocouple instrumentation of the calorimeter.

Both of the Mark II Duct Liners have been prepared for installation during 1993 and the Mark I versions have been removed using full Be and T_2 contamination compatible procedures, although subsequent measurements indicated that the T_2 contamination level was negligible.

As part of the preparations for full D-T operation, the Neutral Injector Box (NIB) Scrapers are being modified to be cooled by the NIB water cooling loop as opposed to the poloidal coil loop used to date. This, in conjunction with improvements to the NIB cooling water system, will provide enhanced safety in the event of component failure.

Components for the Pumped Divertor (PD)

Although contractual difficulties were experienced in the manufacture of the pumped divertor cryopump, these have now been resolved satisfactorily. Considerable progress has been achieved with respect to the major technological developments and production is now well in hand to enable installation as planned. The manufacture of water cooled baffles is proceeding satisfactorily and modules are being delivered to the firm responsible for assembly into larger units prior to installation in the torus.

Satisfactory progress has been made with the manufacture of hypervapotron elements for the water-cooled divertor target plates. Further manufacture has been halted pending a review of the total divertor programme at JET.

Further delays have been encountered with the manufacturing contract for the LHCD cryopump. These have now been resolved and delivery is scheduled for early 1993.

Development of Brazing Beryllium to Hypervapotrons

Water-cooled hypervapotrons clad with Be to form the plasma facing surface are a possible candidate for divertor target plates capable of steady state operation. It has been demonstrated using mechanical shear testing of relatively small samples, that induction brazing results in a stronger and more reliable joint (compared to that obtained using

vacuum-oven brazing) of Be to the CuCrZr alloy used to manufacture hypervapotrons. This has been confirmed by high heat flux tests in the NB Testbed.

The limiting value of heat flux as evidenced by failure of the brazed joint and subsequent melting of the Be has been measured for three values of thickness of the Be tiles. The limiting values of power density obtained were 14.5, 17.0 and 15.0MWm^{-2} for 1.5, 2.0 and 3.0mm thick tiles, respectively.

Metallurgical studies show the presence of a brittle Cu-Be intermetallic layer within the joint. Attempts to prevent intermetallic formation using a layer of silver on the Be have been unsuccessful so far, due to the difficulty of obtaining a sufficiently adherent silver layer. Nevertheless, the bond strengths obtained to date are sufficiently interesting, provided that sufficient reliability can be demonstrated, to make the present technique a viable candidate for use as divertor target plates.

Neutral Beam Testbed

High Heat Flux Tests

A considerable fraction of the 1992 programme was devoted to high heat flux studies of carbon fibre composites (CFCs). An extensive series of tests was carried out using 13 samples of CFC material from seven manufacturers to determine experimentally the most cost-effective material for the Mark I divertor, which will use the thermal capacity of the CFC to absorb the incident power during a pulse. The surface temperature of the samples was measured as a function of time for incident heat fluxes in the range 5-20MWm^{-2} for pulse lengths up to 5s. Subsequent analysis of the data enabled the most suitable material to be selected, in terms of the combination of thermal conductivity, specific heat and density. All samples withstood the tests without mechanical damage, including the additional tests of the most interesting samples at power density of up to 80MWm^{-2} for ≤0.5s.

In addition to studies of CFC for pulsed power loads, tests have also been carried out, in co-operation with NET, to assess the use of these materials for steady-state operation in, for example, a water cooled divertor. Samples of CFC blocks brazed onto copper and also TZM cooling water pipes have been tested to power densities of up to 30 MWm^{-2} for pulse lengths of 2s and 18MWm^{-2} for 9s. The tests of the first three samples provided by NET showed considerable variation in surface temperature along a given element. Presumably, this was due to variation in heat transfer due to imperfections in the braze, although variations in thermal conductivity of the CFC could not be excluded. Further tests of this technology will be carried out in future.

Finally, tests of high heat flux elements undertaken for ENEA, Italy, as part of a proposal for a "drive-in" target neutron source have been completed successfully. In addition to the high heat flux aspects of this contract, neutron diagnostics were used to measure the transient behaviour and equilibrium concentration of implanted deuterons in a titanium surface layer bonded to the front surface of the panels.

Implantation by Beams and Isotopic Exchange

Studies of the exchange of hydrogen isotopes implanted in surfaces were initiated in 1991 to provide information for the PTE. The experimental results gave essential information regarding the procedures necessary to convert the injector operation from deuterium to tritium and the equally important subject of the removal of implanted tritium from injector components. Further experiments have been carried out to develop models of the exchange process and gain an understanding of the underlying physics for application to future tritium experiments, which will use much larger quantities of tritium.

The original work [2] showed that the implantation could be described by the so-called local mixing model. However, this model should only be applicable for copper close to ambient temperatures, whereas in these experiments the surface temperature of the copper reached ~650K. It would then have been expected that diffusion would lead to a relatively rapid release of the implanted material.

An experiment was carried out using neutron measurements from D-D reactions between incident beam atoms and implanted particles, to monitor the density of implanted species:

(a) The testbed beam calorimeter was saturated with implanted deuterium by bombardment with a beam of pure deuterium (saturation of the neutron yield being used to indicate that the implanted atom density reached its equilibrium value);

(b) The pure deuterium beam was changed to H_2 with 2% D_2 added to enable the depletion of the pre-implanted D_2 by the H_2 beam to be monitored via the neutron yield;

(c) The beam was changed back to 100% D_2 and the panel re-implanted with D_2.

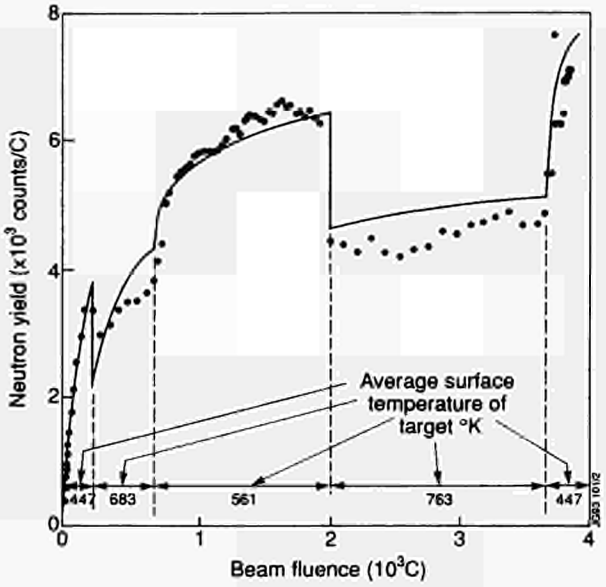

Fig.30: Measured neutron yield as a function of the fluence of the implanting beam of deuterium. The solid curve is the result of computer modelling

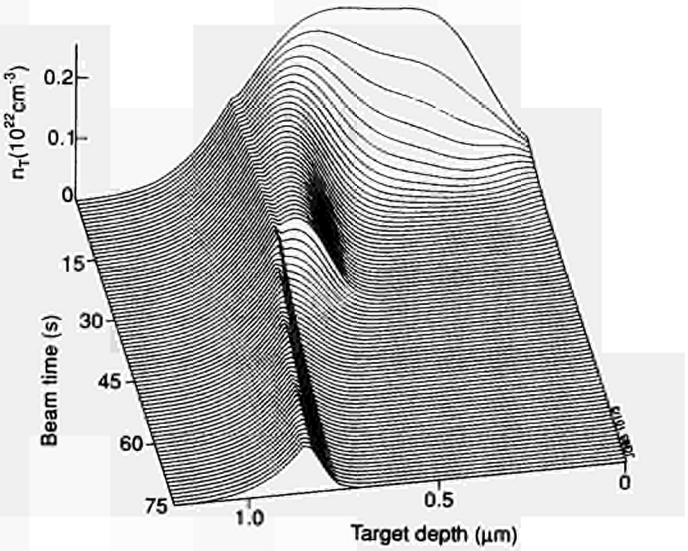

Fig.31: Computed spatial distribution of pre-implanted tritium during subsequent implantation of deuterium.

Figure.30 shows the measured neutron yield as a function of beam fluence. Differing values of beam pulse length were employed for different parts of the experiment to examine the saturated yield as a function of target temperature, which are also shown.

The experimental results indicated that the density of implanted D_2 can be in excess of 10^{28} atoms m^{-3} and the saturation density was be inversely proportional to the surface temperature. This implies that it is the pressure of the implanted deuterium in the surface which determines the limiting value of saturated density. The solid curve in Fig.30 shows the results of a computation using the local mixing model combined with the calculated deposition profile of the implanted species within the copper target. This model also includes the experimentally observed 1/T dependence of the saturated density, where T denotes the temperature of the surface being implanted. The only fitted parameter in the code is the saturated density of hydrogen in copper at room temperature. Based upon published values, this corresponds to 1.7×10^{28} atoms m^{-3}, which is 20% of the atomic density of copper.

Application of this model to the removal of tritium from the injectors shows that although the major part of the implanted tritium is relatively easily removed from the average penetration depth, the tritium implanted close to the end of the penetration depth is more difficult to remove. This is illustrated in Fig.31, which shows the computed depth profile of pre-implanted tritium as a function of the fluence of a deuterium beam used to remove the tritium. The parameters used in this simulation correspond to the values used during the injector clean-up experiment following the PTE. The residual peak of implanted tritium, 0.8mm below the surface, could presumably ultimately broaden by diffusion. Alternatively, it could be removed by the implantation of a more deeply penetrating beam of deuterium (or He).

The apparent lack of importance of diffusion can be attributed to bubble formation as a result of the high implantation flux resulting in deformation/damage to the lattice of the target material. This is consistent with the observation that hydrogen isotopes and helium exhibit similar behaviour in terms of implantation and the exchange of one species by another. If bubble formation is indeed the dominant process for implantation at sufficiently high fluxes, it would be expected that most materials will exhibit similar behaviour in this respect.

Although these experiments were originally foreseen to be specific to injector components, they may well be applicable to energetic plasma-wall interactions in general.

Cryogenics

The Cryogenics Group is responsible for JET cryoplant and the supply of cryogens to the JET site. However, the Group also plays a significant role in supplying cryogenic engineering expertise to all the Project. The very high level of reliability of the cryoplant was maintained to the end of the operational period. Where possible, limited operation has been maintained during the shutdown to supply liquid helium and liquid nitrogen to the various Testbeds.

Table. VI
Performance Data of Upgraded Cryosupply System

HELIUM	
Helium liquefaction capacity or Helium refrigeration capacity	450ℓ/hr at 4.5K 1,400W at 4.5K
He compressor flow	220g/s
He purification	10g/s
Liquid Helium storage	15,000ℓ
Pure Helium storage capacity	1,800m^3
Impure Helium storage low pressure high pressure	 500m^3 6,000m^3
Helium recovery compressors	18g/s
Liquid Helium distribution, outlets for closed loop	10 off
NITROGEN	
Liquid Nitrogen storage	110,000ℓ
Nitrogen evaporation capacity	1,500m^3/h (STP)
Liquid Nitrogen distribution outlets	20 off

Maintenance Activities

The first major maintenance programme of the cryoplant after 10 years of operation has been carried out. This included a complete overhaul of the main helium compressor and the two recovery compressors, re-setting and calibration of safety valves, instrumentation, etc. In addition, the instrumentation of the two NB cryopumps is being upgraded to allow the possibility of baking the pumps (if required) after future operation with tritium.

Upgrade to Cryoplant

The planned major upgrade to the cryoplant to give ~50% increase in refrigeration capacity at 4.2K, to match the increased use of cryogens within the Project, is proceeding satisfactorily. The main characteristics of the upgraded plant are given in Table.VI. Although this indicates the large capacity of the system, what is not evident is the flexibility and wide range of operating conditions required to handle the very differing cryogenic loads. An additional major feature of this plant is the very high degree of computer controlled automatic operation designed into the system from the outset, which minimises the requirements for manpower to operate the plant.

Contracts have been placed for the procurement of the additional liquid helium liquefier/refrigerator (180ℓhr^{-1}), the enhanced liquid nitrogen system and also cryo-transferlines. The necessary enhancement of the existing control systems to accommodate these new systems is underway.

A large liquid nitrogen evaporator with a discharge capacity of 1000m^{3}hr^{-1} has been ordered to provide a fire suppression system for the Torus Hall during the D-T phase of JET operation.

References

(1) E Thompson, D Stork, HPL de Esch and the JET Team. JET Report JET-P(92)68 (to be published in Physics of Fluids B: Plasma Physics).

(2) H Falter, D Ciric, GH Deschamps, HPL de Esch, P Massmann and L Svensson. JET Report JET-P(92)72, (to be published in Proc 17th Symposium on Fusion Technology (Rome 1992)).

ICRF Heating and Lower Hybrid Current Drive Systems

JET is equipped with two distinctly different high power radio frequency systems:

- The Ion Cyclotron Resonant Frequency system is used for high power centralised heating of the JET plasma and also for Fast Wave Current Drive studies. The wide operating frequency range available (23-57MHz) allows variation in the choice of minority ion species used and the localised position of the deposited power or driven current. The position is dependent only on the magnetic field and is insensitive to parameters such as density and temperature. Table.VII summarizes the main characteristics of the RF system. The maximum design power is 24MW in the plasma (3MW per antenna). However, up to 3.5MW on one antenna and 22.7MW total coupled power has been achieved. In preliminary experiments, significant effects on sawtooth behaviour have been achieved by Fast Wave Ion Current Drive near the q=1 surface. New ICRF antenna heating are being installed in JET during the shutdown, designed to take advantage of the new shape of the divertor plasmas and to achieve enhanced coupling. The antenna locations in the torus have also been revised to give four arrays of two

Table VII
Nominal Characteristics of the ICRF Plant

Frequency Range	• 23 to 57MHz (determined by the full field ion cyclotron resonances of D and H), excluding 39-41MHz.
8 Generators	• 4MW output per generator module (20s) (2 tetrodes)
4 Antenna arrays	• Beryllium bars (15° inclination) screen • Four adjacent loops operated with variable phasing.
16 Transmission lines (Generator to antenna)	• Each line 84m long rated at 50kV peak (diam. 230mm, 30Ω)
Feedback loops for	• Plasma position for constant coupling resistance. • RF power level or antennae RF current • Phase between antenna conductors. • Frequency (Δf~200kHz) for matching • Motorised tuning stub for matching • Tetrode screen dissipation and anode efficiency (acting on anode voltage).
8 HVDC Power Supplies : Output (2 tubes) Driver (2 tubes)	• 345A : 16-26kV controlled by tetrode screen and current. • 60A : 9-13kV (remotely preset)

adjacent antenna. Each array has four RF radiating conductors which will provide an enhanced radiated RF spectrum. Variation in the relative phase of the RF currents in the conductors allows this spectrum to be varied for both heating and current drive experiments.

- The Lower Hybrid Current Drive system (at 3.7GHz) can drive a significant fraction of the current flowing in the plasma. This is achieved by launching a lower hybrid wave predominantly in one toroidal direction. This wave accelerates the high energy electrons in the plasma in the same direction as the wave, thus driving a current. Up to 2.3MW of LHCD was coupled to the plasma, and full current drive was demonstrated in a 2MA low density plasma. Towards the end of the campaign, 1.5MW of LHCD power was applied during the ramp-up of a 7MA plasma pulse. This altered the current profile, reducing the internal inductance of the plasma. As a result, the transformer flux swing required to establish the 7MA current was reduced by 2V-s, enabling the plasma pulse flat-top to be extended. To follow the plasma boundary, the LHCD launcher was moved back as the plasma current developed using the launcher's real time position control system. The prototype LHCD launcher (LO) has fulfilled its role in providing engineering, operational and physics experience of LHCD on JET. The L1 launcher is now being prepared for installation. This will be capable of launching three times the power of the prototype (10MW), with the potential of achieving full current drive of 4MA plasmas. Fig.32 shows one ICRF antenna array and the L1 LHCD launcher grill for the pumped divertor configuration in JET.

Technical Achievements with ICRF System

To couple RF power to the smaller, vertically assymetric single-null (bottom X-point) plasmas of the divertor phase, the ICRF "A1" antennae are being replaced with a new "A2" design, which is radially deeper and, to obtain the desired radiated spectrum, are toroidally wider. In addition, to avoid interaction between side protections of these antenna and the edge of the tangential neutral beams, the antennae are being

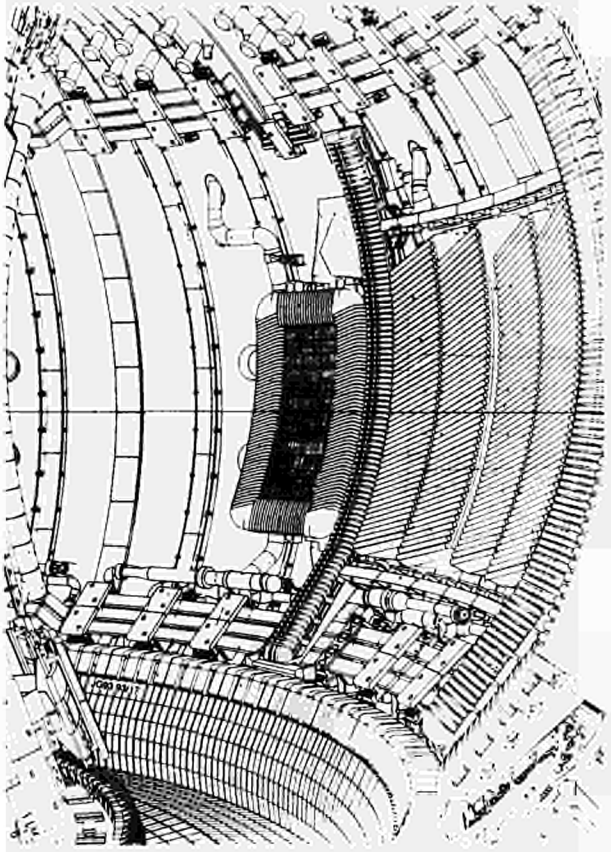

Fig.32: One of the four ICRF heating arrays alongside the LHCD Launcher in the divertor configuration of JET

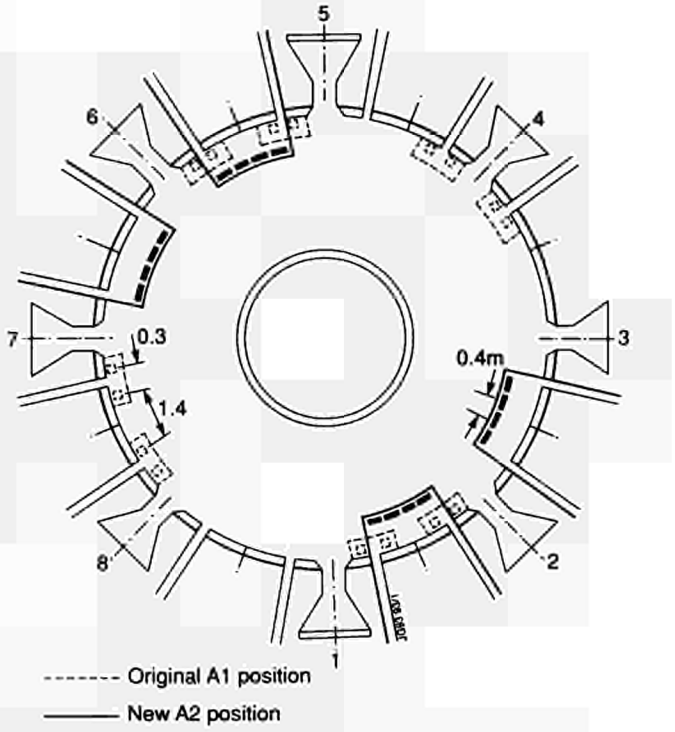

Fig.33: Original ICRF A1 antenna and the new A2 antenna positions in JET.

relocated in the torus and grouped into four pairs (see Fig.33). This also allows improved radiated spectra to be obtained from the four conductors formed by the "array" of two adjacent antennae, to give enhanced FWCD performance. RF coupling between adjacent conductors, which has implications for generator plant control has been reduced by a partially slotted septum. It cannot be eliminated entirely by a full septum as image currents in the septum would impose additional unwanted lobes in the radiated spectrum.

Transmission Line Reconfiguration and Control System Upgrade

The transmission line system design at JET has remained substantially unmodified since its initial installation. About half of the existing ICRF transmission line system is now being re-routed to connect to the new antenna positions. The generator cooling systems and 33kV supplies have been regrouped into new pairs that correspond to the new antenna configuration. In addition, a new tritium containment secondary gas barrier is being included near to the antenna end of the transmission lines (Fig.34).

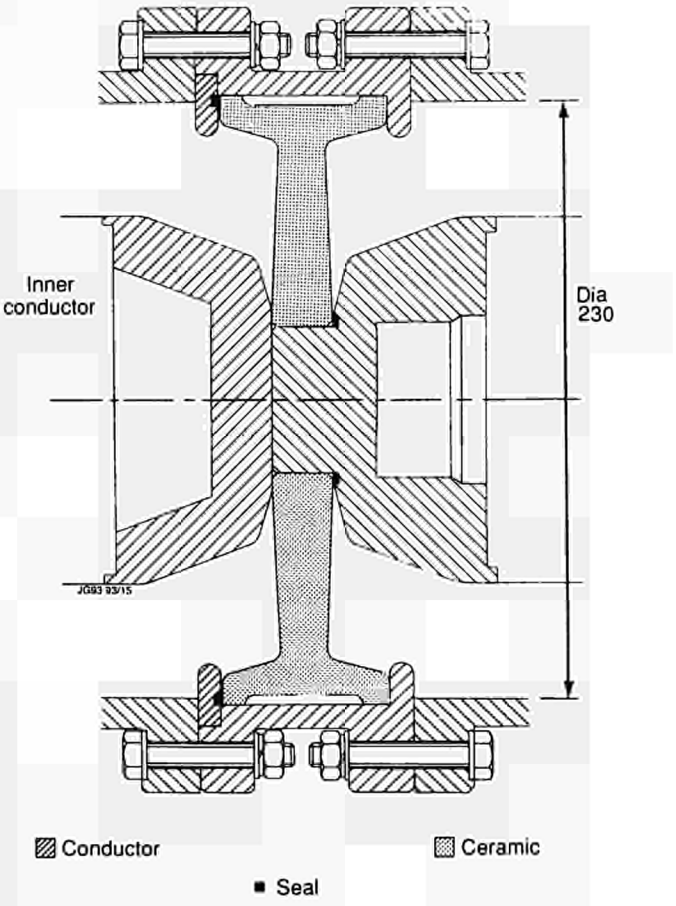

Fig.34: Cross-section of a ICRF transmission line showing the ceramic support of the inner conductor fitted with a gas seal.

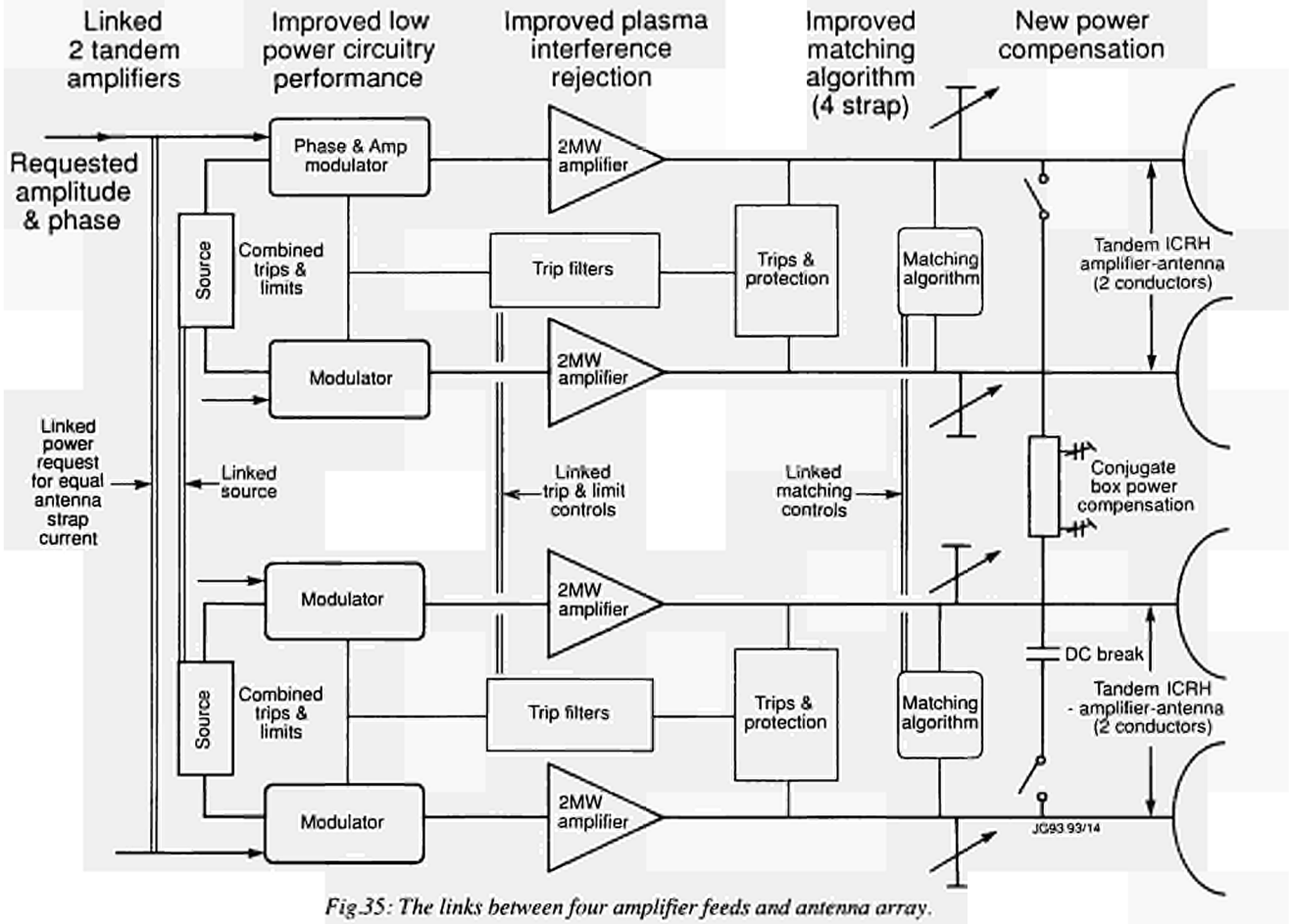

Fig.35: The links between four amplifier feeds and antenna array.

At the start of the shutdown, the A1 ICRF antennae and transmission lines were removed from the torus. In-vessel inspection showed that the antenna were in good condition with no evidence of significant arcing or melting on the screen. The screen was covered on most of the surface with a dark orange/brown layer. Initial analysis suggests this was a mixture of beryllium and beryllium oxide. This covering is indicative of a net deposition on the outer wall.

The new antennae configuration requires an upgrade of the amplitude, phase and matching control of each generator. The revised specification of these controls is shown in Table.VIII. Mutual coupling between each pair of adjacent antennae forming an array means that the amplitude, phase and matching controls of adjacent generators (four outputs) must also be linked (see Fig.35). As was the case with the two amplifiers feeding the two conductors of each A1 antenna, independent power restriction or tripping of one amplifier affects the match of the other, resulting in a trip or power restriction of the latter. This is an unstable situation. Combining or linking the controls of each pair of amplifiers provided a satisfactory solution, and this facility is being extended to groups of four amplifiers.

Individual amplitude and relative phase control of the RF currents in the antenna straps is also extended to groups of four amplifiers for FWCD. New control algorithms are required to maintain matching whilst allowing variable relative phase and therefore effectively a different coupling resistance on each of the four antenna straps. In addition, the upgraded electronics will include the control of the circulating power transfer device called a conjugate box, which optimises the generator power availability. Improved arc protection for the antennae is also being included in this control upgrade.

One of the problems found in previous operation is that of discriminating between

a) damaging arcs or disharges in the antenna and vacuum feedthrough (which can only be extinguished by suppressing the RF power momentarily); and
b) high reflected or reverse power due to eigenmodes, plasma variations, and cross coupling from other antennae, which do not require supression of forward power.

If the RF wave damping in the plasma is low, or when the antenna-plasma distance is large, creating a "duct" around the plasma, cross-talk exists in the form of energy transmitted from one antenna to another, and appears as incoherent

Table. VIII
Upgraded ICRF Plant Control Performance Specification

Frequency	
Operating frequency range (f_O) in 8 bands of 4MHz (39-41MHz are not used)	23-57MHz
Inband frequency deviation (Δf)	200kHz
Frequency regulation better than (Accuracy and Stability for both f_O and Δf)	1kHz
Frequency loop time response to a square pulse (Δf = 500kHz)	1ms
Overshoot	15%
Protection	
Limiter intervention time	<1ms
U/V arc detection time typically	2ms
Trip intervention time	20μs
Trip re-application time	20ms
Ramp-up time to full power on re-application (clock synchhronised)	80ms
Reflection coefficient detector disabled below amplifier output power of	20kW
Generator Performance Parameters	
Amplitude Regulation	
Dynamic range	2.5MW-5kW
Minimum power for regulation	5kW
Regulation accuracy (at any power level)	± 5%
Closed loop response to square pulse (to 5% of reference)	400μs
Amplitude overshoot	< 5%
Maximum Modulation Frequency (square wave excitation)	100Hz
Phase Regulation	
Phase loop dynamic range (any phase offset)	360°
Phase regulation accuracy and stability	± 5°
Phase linearity	± 5°
Phase loop time response to a 180° step (to ± 5°)	100-μs
Overshoot	< 15%
Phase modulation	
Dynamic range (any phase offset):-	360°
Modulation of Operation	
i) Maximum output power	
± 15° variation in set phase for plasma matching.	
± 15° variation in power between amplifiers	
ii) Phase control	
Normal 5% tolerance on set amplitude and phase.	

reflected power back to the generator. Even if the sources are sychronised, this reflected power remains incoherent due to random amplitude and phase modulation by the plasma.

Until 1992, envelope detection was used. The total reflected energy often exceeded the reflected power trip level, when all the generators are run at equal power, and the cross-talk is high. This cross-talk was also sufficient to interfere

Fig.36: New electronics for the ICRF generator for power and control stages

with the "hold" circuits of the frequency and phase feedback loops.

The new protection circuits in the upgrade control system which operate the trips will include pseudo-synchronous detectors and narrow band filtering (see Table. IX). The generator reflected power signal will first be converted to an intermediate frequency of approximately 1.3MHz, which will allow filtering to eliminate energy from generators on adjacent frequencies. Narrow band (20kHz) pseudo-synchronous detection (requiring the presence of the carrier), will provide further filtering of close-to-carrier noise and cross-talk from the plasma. The circuitry takes advantage of ten years advance in technology, to replace outdated electronics (Fig.36), and also of successful experience with a similar system used on the JET Lower Hybrid Current Drive power plant. In addition, the arc detection system will be tested automatically in at low power immediately before each heating pulse as a precaution against electronic failure.

Fast Wave Current Drive Facility

The required antenna directivity for FWCD is achieved by relative phasing of the four conductor currents of each A2 antenna at other than 0 or π between adjacent straps, nominally at π/2, to give the optimum asymmetric radiated spectrum. Mutual coupling between the antenna conductors with this phasing causes assymetry of power inputs to the antenna, due to additional circulating power between the conductors. This would reduce the maximum available coupled power by a factor two in the worst case, if no compensation was used.

Table. IX
ICRF Control and Protection System

	Category	Value	Response Time
(1)	**Terminate the pulse**		
-	Tetrode arc crowbar protection	Overcurrent	10μs
-	Maximum trip count exceeded.	(ρ = 0.5)	255 times
-	Tube dissipation high, limiter not working	1.5MW	5ms
(2)	**Power trip (hold settings and recover)**		recovery 1%/ms
-	Arc in end stage circuitry	UV light	2ms off/20ms on
-	Too high reflectoin coefficient	ρ = 0.5	2μs off/20ms on
(3)	**Limit the output power**		
	[PSU trips shown in brackets]		
-	Anode dissipation	1.3MW	1→5ms
-	Screen grid current	4A [20A]	0.5ms [>20ms]
-	Control grid current	5.5A [6A]	0.5ms [10-20ms]
-	Anode current [both tubes]	160A [345A]	1-5ms
-	Maximum RF voltage on antenna and transmission line (set on operation)	30-40kV	0.5ms
-	RF forward voltage	~ 2MW	1-5ms
-	RF reflected voltage	130kW	1-5ms
(4)	**Requested values**		
	(operating as control loops)		
-	Power, *or antenna currents*	± 0.25dB	
-	Relative Phase	±5°	
-	Nominal Frequency	10kHz ± 1kHz	
-	Coupling resistance via plasma position control	0.1Ω steps	
(5)	**Automatic**		
-	Matching: Uses stubs plus frequency or trombones.	Minimum ρ at stub	f : 0.1ms stub stub: 0.1-1s
-	Anode voltage to minimise anode dissipation (linked to screen current limiter above)	Ig2 = 2.5A	200ms 18-26kV

However, the inter-conductor mutual coupling is essentially a reactive term, and can be cancelled by a high power lossless compensation network containing an equal reactance elsewhere in the antenna feed system. This "conjugate box" network is so-called since its transfer characteristic is the complex conjugate of that of the antenna. Additional power added to one end of the A2 array and subtracted at the other, can be re-circulated via a lossless network connected between the four transmission lines. A compromise which works over most of the frequency and phase range is a single compensator between lines 1 and 4.

The design of this "conjugate box" required a simulation of the A2 antenna and its behaviour for FWCD in combination with such a network. Work has been carried out by JET and Oak Ridge National Laboratory, USA, using plasma, antenna and network modelling codes to predict the launched RF power directivity and wave absorption by the plasma. This includes FWCD efficiency and profile calculations. These combined codes also predict the generator loading and thus the matching control dependence on the phased antenna strap currents.

A practical design of conjugate box is fabricated from a quarter-wave 3dB (symmetrical) power combiner with two ports terminated by variable reactive elements. The compensation is frequency dependent and a compromise in the operating range is achieved by selection of various connecting lengths, shown in Fig.37. For the JET plant, four conjugate box systems are being installed, connecting lines 1 and 4 of each of the four-conductor antenna arrays. The in-line switches allow the conjugate system to be disconnected during normal (high coupling) plasma heating.

The original ICRF matching control system was constrained by the amplitude control system which required a symmetrical match, (only possible at 0 or π phase with the A1 antenna), by imposing equal power outputs from the amplifiers, i.e. no circulating power. To obtain a match and maintain equal but phased antenna currents for FWCD experiments with A2 design, the amplitude regulation control signal is derived from the main transmission line for-

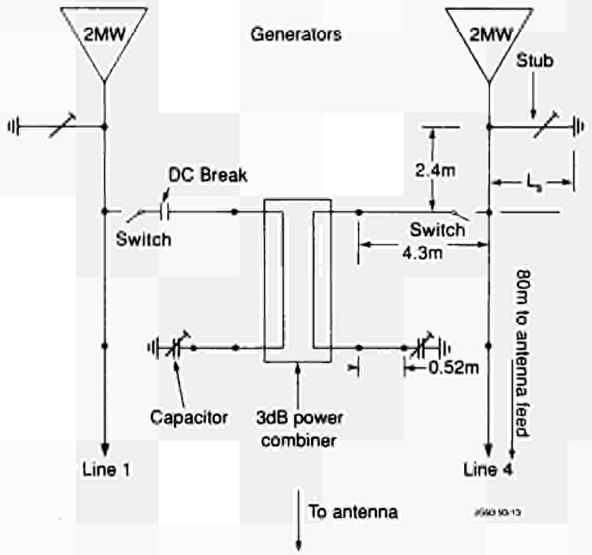

Fig.37: Schematic diagram of the ICRF conjugate box power compensator.

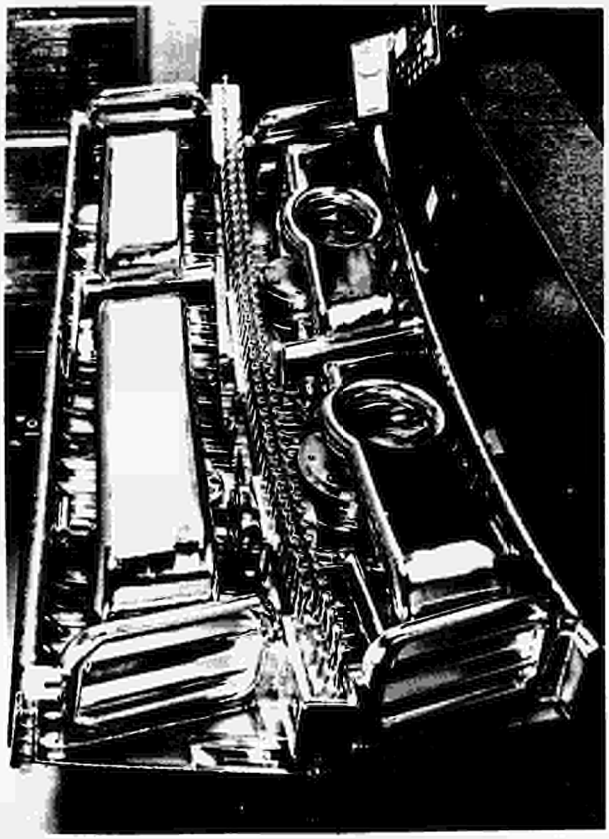

Fig.38: A2 antenna at the manufacturers

ward (V_{fm}) and reflected (V_{rm}) waves, where the vector (V_{fm}-V_{rm}) is proportional to the antenna current, both in amplitude and phase. The individual generators match independently. By regulating to equal currents, the required power imbalance is achieved automatically at the correct match, even though the coupling resistances are unequal.

Design of the A2 Antenna

With the installation of the pumped divertor in JET, the plasma volume is substantially reduced and, in particular the distance from the plasma to the wall is increased by about 300mm or 450mm for the 'fat' and 'thin' plasma configurations, respectively. A new set of eight A2 antennae is being manufactured for use in this configuration. Fig.38 shows the first manufactured antenna assembled without the screen, for inspection at the contractors works. The central conductor, corrugated housing and screen support posts on the septum are clearly visible. These antennae are as large as can be installed through the port, and are a factor 1.5 larger in width and a factor 2 in depth compared to the A1 antennae. The toroidal positions of the antennae in the torus are being re-arranged to give two diagonally opposite groups each of four adjacent antennae to improve the directivity of the launched wave. The opportunity has also been taken to remove the conical ceramic which limits the voltage of the A1 antennae, and the design is such as to enhance the coupling capability, and also the directivity of the spectrum for fast wave current drive experiments.

The duty cycle required of these antennae has been reduced to 1:60, reflecting limits elsewhere in JET, although the 20s pulse duration is retained. The remote handling requirement has also been reduced to a minimum. Only capping of the windows to maintain torus integrity in the event of a window failure is required to be undertaken remotely. The peak RF design voltage for thermal analysis is reduced to 42kV, reflecting previous experience and the improved coupling of the A2 antenna.

The mechanical design of the antenna has been driven by the requirement to limit the forces appearing at the torus wall to less than 50kN. The antennae project far from the wall and are exposed to changing flux during disruptions. Control of the resulting eddy currents has led to a design where it is fabricated from sheet metal 0.5-3mm thick, supported at many points (21 per antenna housing) from the wall. In addition, it has proven necessary to include 0.15Ω ceramic-based resistors in the screen attachments to limit disruption eddy currents through these elements. The resultant forces during a worst case disruption clear predominantly to a torque of typically 50Nm about a vertical axis, with a maximum of 5kN appearing on any one support to the torus.

Table. X
Ceramic Resistors: Disruption Simulation and RF Test Results

Type of Test	Performance Achieved To Date	Required Performance
RF Test Bed		
Subjects a pair of resistors to 20s pulses at 25 - 55MHz. Resistors operate at 300 - 600 C at $1x10^{-6}$ mbar	80A rms for 20s pulses at 48MHz with 10:1 duty cycle. Temp rise during pulse 300C.	60A rms. 20s pulses 60:1 duty
Disruption Simulation Test Bed		
Subjects individual resistors mounted in A2-style jigs to current pulses of up to 1500A peak, 10- 20ms variable duration and shape.	680A peak during quasi-sine wave pulses of 13ms duration (210J deposited energy)	340A 83J

The antenna screen elements are solid beryllium bars and are mounted in pairs, each attached to the housing via one of the ceramic resistors. This resistor comprises a beryllia ceramic block with a thin coating of nickel (~ 5mm) and is shown in Fig.39. The resistance at 300°C is 0.15Ω (± 5%). Sample resistors have been tested extensively both with applied RF power and using a capacitor bank to simulate disruption induced eddy currents. The initial failure mode was arcing which originated at current concentrations at the edge of the metal coating and led to highly local evaporation of the metal. This enhanced the local current concentration and led to propagation of a break in the metallising across the resistor. Careful design to avoid current concentrations has improved the performance so that thermal stress cracking and the thermal diffusivity of the ceramic now limit performance. In particular, the use of beryllia ceramic gave a 20% increase in the current limit over the originally chosen alumina. The performance required and measured during tests is shown in Table. X and Fig.40.

Full power RF tests on a full scale flat model of the antenna indicates that the peak current in the resistors occurs at the cross-over strap, which runs parallel to the screen elements. The margin in resistor current given by these results is about a factor of 4. High power model tests, indicate higher resistor currents and reduced margin. Resolution of this discrepancy is one of the prime objectives of high power tests on the prototype antenna in early 1993.

A full scale model of the upper VTL-side quadrant of the A2 antenna has been extensively tested at high power in the RF testbed. This model incorporates many features of the full antenna, including the cylindrical ceramic, the resistors, nickel plating, and construction typical of the real antenna.

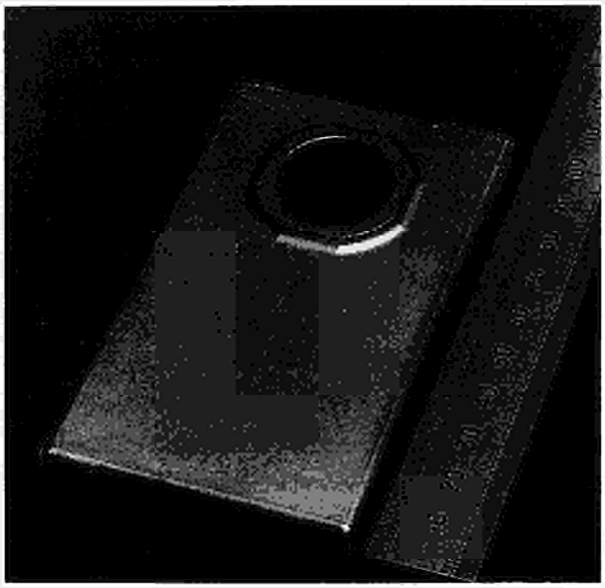

Fig.39: Resistor for two screen bars of an ICRF antenna.

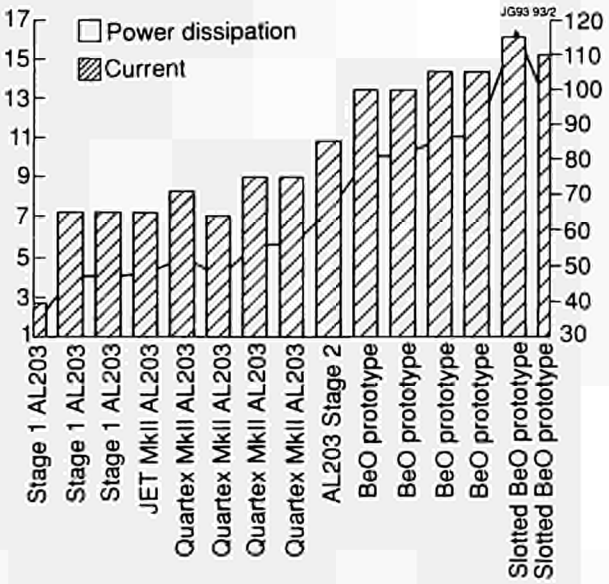

Fig.40: Improvement of Be resistors maximum performance.

Table. XI
Short Assembly RF Test Results

Test Parameter	Measured or Achieved Value
Test Frequencies	55, 42 and 24MHz (approx)
RF Pulse length	20s
RF Peak Line Voltage for reliable operation[1]	50kV at all test frequencies
Maximum Line Voltage Achieved	60kV at 42MHz with 100ms pulses
Peak Line Current for reliable operation[1]	1kA at all test frequencies
Maximum duty cycle[2]	20:1
Peak voltage with Open Circuit Strap[3]	49kV at 28MHz

[1] Typically achievable with no arcing after 4 - 8 hours of multipactor and short pulse conditioning.
[2] Limited by temperature rise in the Pressurised Transmission Line
[3] With gap to screen elements increase to 18mm; 40kV with standard 12mm gap.

The beryllium screen elements of the A2 antenna are replaced by nickel plated aluminium elements. An additional feature of this 'short assembly' is that it can be configured with the strap terminating in either short-or open-circuit (of smooth profile to prevent arcing). The strap in the latter case is only supported by the cylindrical support ceramic and the strap-to-screen gap is increased from 12 to 18mm to eliminate arcing in the absence of a magnetic field. The results achieved are summarised in Table. XI.

The test programme confirmed the viability of important aspects of the A2 design:

- There is no requirement for independent pumping of the vacuum transmission line (except for the interspace of the double ceramic window): the pumping from the torus, estimated to be $100\ell s^{-1}$ at the window, is sufficient to handle the out-gassing during RF pulses. However some form of bakeout and continuous heating along the VTL is desirable. An interlock is necessary to prevent operation too early in the ramp up phase following the initial gas fill of the torus;
- The light weight, fabricated structure of the antenna still offers sufficient thermal heat capacity in the critical areas to limit temperature excursions to acceptable levels during RF pulses;
- With radiative cooling alone, full power operation at up to 20:1 duty cycle is possible whilst operating in an ambient environment of 200°C (with no plasma load). Fig.41 shows a thermal picture of the assembly during such tests. The screen bar pattern is clearly visible as the cooler area. The limit is excessive heating of the VTL inner conductor and of the antenna conductor strap. For comparison, the maximum JET duty cycle is 60:1;
- Vertical displacement of screen elements up to ±5mm in operation due to distortion of the antenna housing or screen mounting posts has no impact on the antenna performance. However, the currents in the ceramic screen resistors is increased and this must be allowed for in their design.

Technical Achievements with the LHCD System

The characteristics of the JET LHCD system are given in Table. XII and a diagram of the main components in the Torus Hall are shown in Fig.42. The frequency of the lower hybrid system has been fixed at 3.7GHz. This choice takes advantage of technical developments made in Tore Supra, France, while being sufficiently high to avoid wave coupling to fast ions and to allow wave penetration to the plasma core

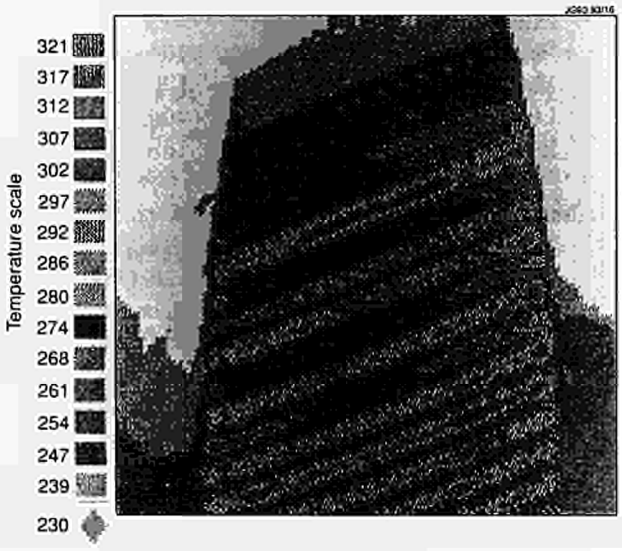

Fig.41: Thermal photograph of high power test on new ICRF A2 antenna

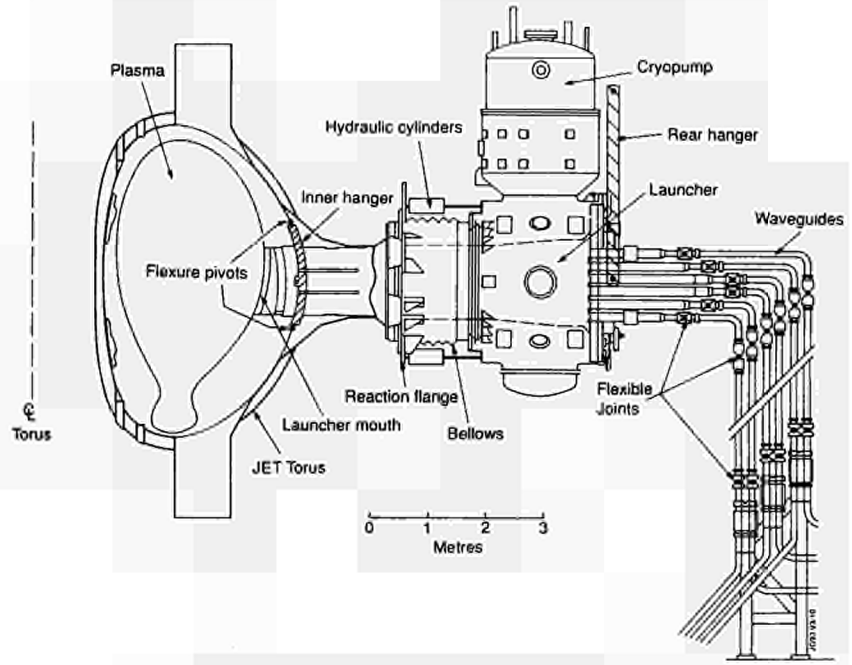

Fig.42: Elevation of the lower hybrid launcher.

Table. XII
Nominal Characteristics of the LHCD Plant

Generator	**Prototype** ***(full system in brackets)***
Frequency	3.7GHz
Number of klystrons	8, (24)
Power (generator)	
10s pulse	4.8MW
20s pulse	4MW, (12MW)
Duty cycle	1/30
Efficiency	42%
Phase control	10° accuracy
Maximum VSWR	1.8
Length of transmission line	40m
Estimated insertion losses	1dB
Launcher	
Number of waveguides	128, (384)
Waveguide material	stainless steel and ZiCu (stainless steel)
Coating	copper + carbon (copper)
Maximum temperature	350°C (450)
Total weight	12 tonnes (15),
Stroke	210mm
Response	5mm/150ms

up to $n_e \sim 3 \times 10^{19}$ m^{-3}. The power generated by each klystron is split via successive hybrid junctions and multijunctions into 16 waveguides at the grill mouth. There are 24 klystrons, each capable of delivering 600kW. The generation of a well-defined wave spectrum with a high directivity is essential for current drive application, and particular emphasis has been placed in controlling the wave phase at the grill mouth in each waveguide. An accuracy of ± 10° has been obtained by tight control of the mechanical dimensions of the multijunction and by feedback control of the phase at the output of each klystron.

The prototype LHCD system, which operated for a total of 12 months (over a 2 year period) up to March 1992, consisted of 8 klystrons operating at 3.7GHz, feeding 16 multi-junction assemblies in a grill launcher, which was mounted on a main port of the torus. The total available generator power was 4.8MW.

Eight of the multi-junctions were designed specifically for JET and are known as LOP (Launcher Zero, Physics). The others were provided by CEN Cadarache, France, using the same design as Tore Supra and are known as LOC (Launcher Zero, Cadarache). LOP was made of copper plated stainless steel, whereas LOC was made of zirconium copper. Both sets of multi-junctions were coated with a carbon anti-multipactor layer. Close to the grill mouth, these were also coated with a beryllium layer from the JET torus evaporators situated next to the launcher.

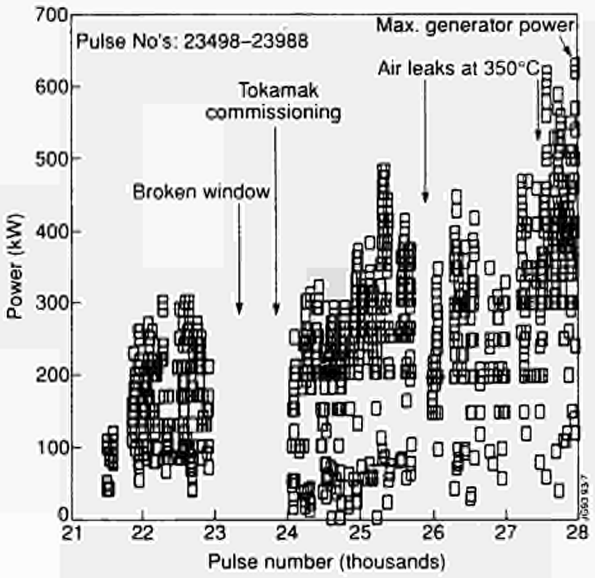

Fig.43: Klystron D4 Pulse History (LOP)

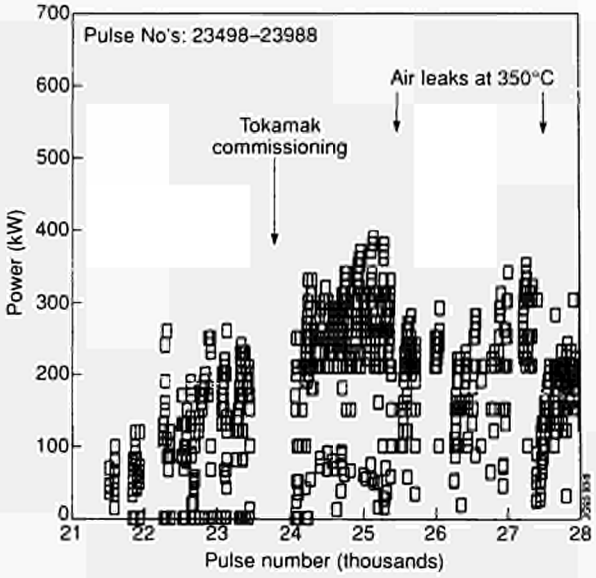

Fig.44: Klystron B4 Pulse History (LOC)

The achieved generator power on LOP was 2 MW compared with an installed capability of 2.4MW, with 1.75MW coupled to the plasma. LOC managed 1.5MW generator power with 1.2MW coupled to the plasma, prior to the major air leaks elsewhere in the torus, but only achieved 600kW generator power after the air leaks. Plasma pulses of one minute duration were obtained with 1MW of LHCD power applied for 50s.

Operation

Operation within the machine started in June 1990 for an initial campaign of five months, followed by a seven-month machine shutdown to change a toroidal field coil. Operation resumed in June 1991 and ended in February 1992 with the shutdown to install the pumped divertor. A total of 1700 pulses were achieved with JET plasmas during the two campaigns. Between campaigns, the multi-junctions were inspected and found to be in generally good condition except for some flaking of the carbon anti-multipactor layer. These flakes were removed from the front of the grill mouth but access to the inner parts of the multi-junction was not possible. Most LHCD pulses were performed in a so-called parasitic mode of operation (i.e. with whatever plasma conditions were being used at the time). Only a total of about six days in the two campaigns was devoted to experiments tailored for LHCD. The LHCD system operated on about 50% of all available plasma pulses.

Figures.43 and 44 show the average power produced by two klystrons during the two campaigns: one klystron fed LOP and the other fed LOC. During the first campaign, power levels were mostly below 200kW per klystron. The multi-junctions did not loose conditioning during the seven-month shutdown between campaigns. Throughout the twelve months of both campaigns, power levels continued to increase slowly as the multi-junctions conditioned. During the second campaign, two uncontrolled air leaks occurred elsewhere on the torus while it was at its operating temperature of 350°C. These had a serious effect on LOC, which was unable to recover its output power level. LOP on the other hand recovered with only minor reconditioning and went on the reach the maximum klystron power on some multi-junctions as the end of the campaign.

Upon inspection of the multi-junctions at the end of the campaign, some minor melting of the stainless steel was noted on LOP at the mid-plane of each multijunction at the grill mouth. This was similar to previous observations on Petula and was associated with breakdown during conditioning but may also arise from occasional arcs seen at the grill mouth during plasma operation.

Coupling to the Plasma

To couple power to the plasma, the electron density in front of the grill must be such that the wave launched by the grill can propagate into the plasma. The parallel refractive index, for which the grill was designed, was $1.4 < n_{//} < 2.3$. Optimum coupling is achieved when the electron density is $1 \times 10^{18} m^{-3}$. Under these conditions, the power reflected back towards the generator is about 1%. With lower densities, the

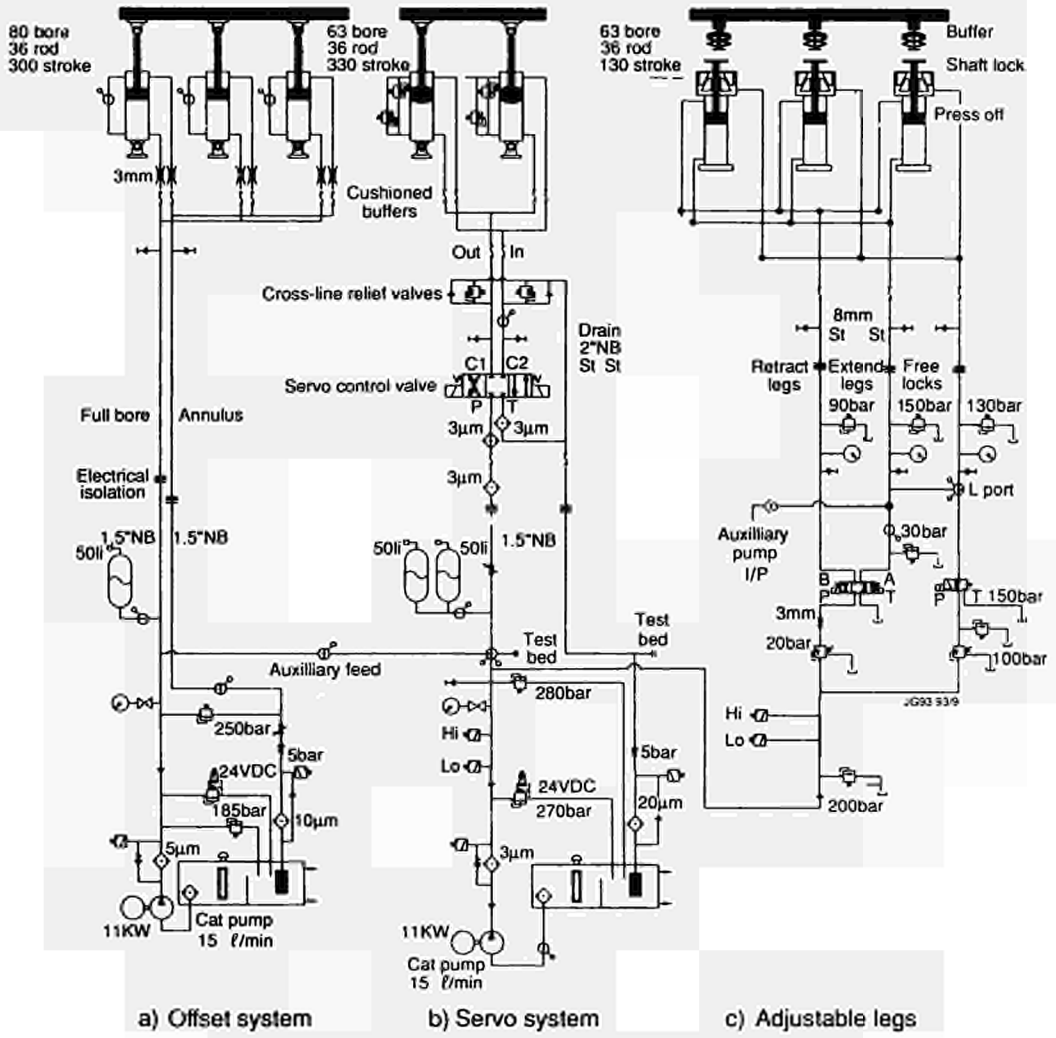

Fig.45: Hydraulic circuits of the LHCD position control system.

reflected power rises and with higher densities arcs tend to occur. In the extreme case of a vacuum in front of the grill, up to 60% of the power is reflected. Thus for satisfactory operation the grill must be in the scrape-off layer of the plasma boundary. Since the plasma boundary can move, for example at an H-Mode transition, the grill mouth also needs to move. To accomplish this the entire launcher can be driven horizontally by a hydraulic system (see Fig.45).

The active position control operates in a closed loop to achieve a static accuracy in position of 0.3mm. This system has a closed-loop resonant frequency of about 4.5Hz, a maximum velocity of 100mms^{-1} and a maximum acceleration of 5ms^{-2} (see Fig.46). The response time to small (5mm) steps is typically 200ms (see Fig.47). The launcher can either be required to follow a predetermined waveform or it can be positioned under feedback control to maintain constant launcher reflection coefficient. An example of the latter is shown in Fig.48. The controlled signal was the total LOP reflected power divided by the total forward power to

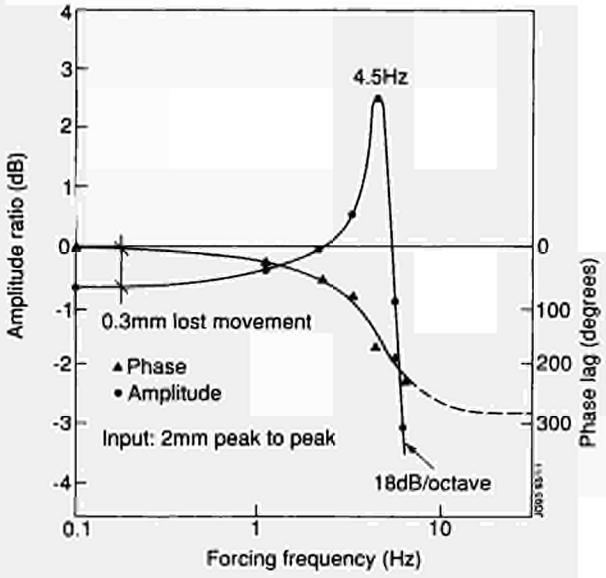

Fig.46: Typical closed loop frequency response near stability limit.

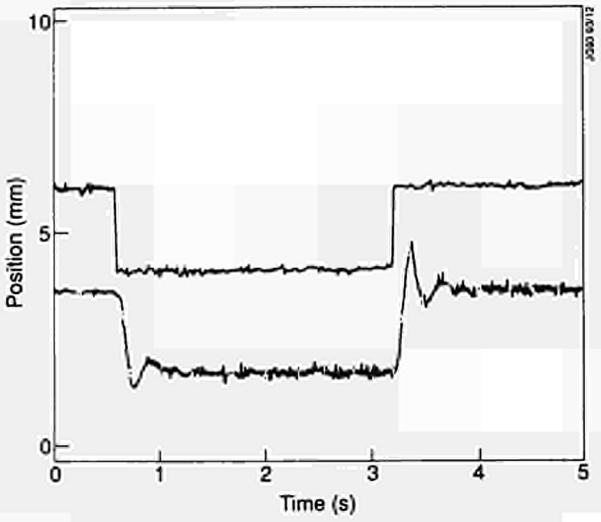

Fig.47: Response to a 2mm step near critical damping

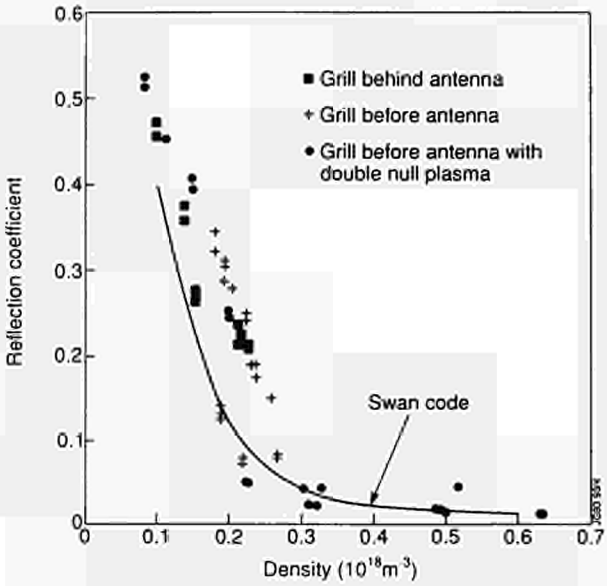

Fig.49: Reflection coefficient as a function of density for various experimental conditions compared with theoretical model of the multi-junctions.

give an average reflection coefficient for the LOP multi-junctions. The requested reflection coefficient was 10%. The launcher was allowed to move within limits of ±10mm about a predetermined waveform to maintain this reflection coefficient. This feedback position system was also used during the current rise of high performance discharge at 7MA in order to compensate for significant changes of the plasma shape during this transient phase.

A further feedback loop on the plasma horizontal position is being implemented to maintain the average reflectivity constant. The new system will have the advantage of a faster time response (30ms) than the hydraulic actuators, but may be incompatible with other requirements on plasma position (for example, to maintain ICRF coupling).

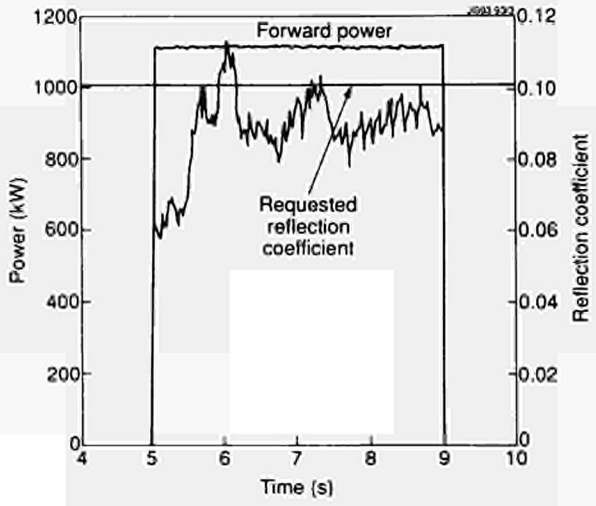

Fig.48: Reflection coefficient with feedback control of the launcher position

A variety of plasma configurations have been used with the launcher:

a) The launcher behind the adjacent ICRF antenna with limiter plasmas touching either just the lower belt limiter or both the upper and lower belt limiters;
b) The launcher in front of the adjacent ICRF antenna with limiter plasmas;
c) The launcher in front of the adjacent ICRF antenna with double-null X-point plasmas.

The density at the grill mouth has been calculated from the distance to the last closed flux surface and the density gradient. The density decay length can be related to the connection length of the magnetic field line in front of the launcher (distance from the grill to the nearest object touching the plasma along the field line). The reflection coefficient is plotted versus this density in Fig.49. These experimental points can be compared with the theoretical model of the grill used in the SWAN code, also plotted in Fig.49. The agreement between theory and experiment is good, thus confirming that the electron density in front of the grill is the important factor for good coupling.

The best coupling was obtained with double-null X-point plasmas where the connection length was long (~30m) and the edge density profile shallow. A low reflection coefficient (<5%) could also be obtained with a limiter plasma of reduced elongation that was not touching the belt limiters but only the ICRF antenna and/or the launcher.

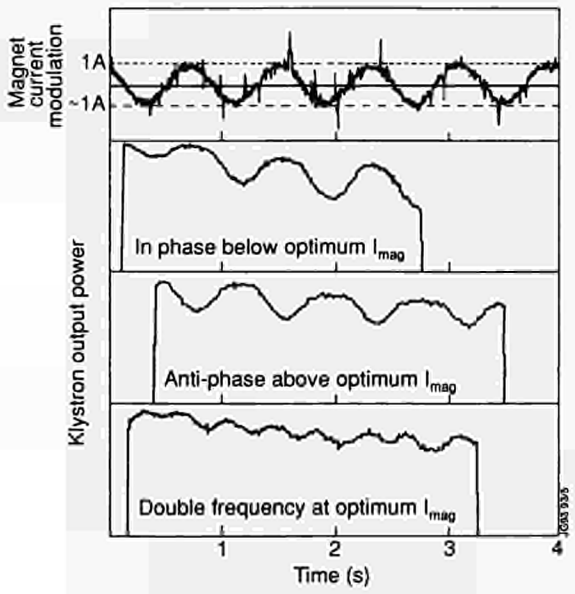

Fig.50: Variation of klystron output power at three different magnet currents and ± 1A modulation of the magnet current.

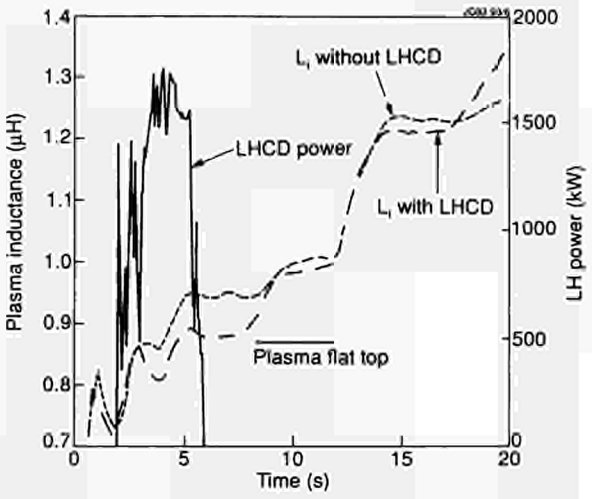

Fig.51: Comparison of 7MA discharges with (Pulse No:27910) and without (Pulse No: 27891) LHCD showing effect on internal inductance and loop voltage.

Shutdown Programme for the Generator

During the shutdown, a programme to enhance and tune the generator has been underway. A major part has been devoted to tuning the klystrons to achieve the maximum power on test loads. A technique for tuning the klystron magnets has been developed. As shown in Fig.50, this involves modulating the magnet current with a sinusoidal current (~1A) about the nominal setting and monitoring the effect of this modulation on the output power with a fixed RF drive input. If the magnet current is below the optimum, the RF power is in phase with the magnet current. Above the maximum, the RF power has the opposite phase to the magnet current and at the maximum the RF power varies at twice the frequency of the magnet current.

Other major parts of the programme are:

a) Calibration of the low power microwave system and investigation of long term drift;
b) Improvements in the noise immunity of the waveguide arc detectors and klystron thermocouples;
c) Implementation of the modifications that were made on the prototype system in the light of operational experience on the other four modules;
d) Installation of an SF6 recovery system to enable the SF6 in the waveguides to be recovered and reused.

Current Drive Experiments

Full current drive of the plasma current has obvious advantages for a reactor as it would allow steady state operation. LHCD has a higher demonstrated current drive efficiency than either ICRF or neutral beam systems. Therefore, its potential for current drive has been assessed in a number of experiments on JET.

Full current drive has also been demonstrated with the prototype system under the following conditions:-

a) 0.4MA constant plasma current with LHCD for 3s;
b) 1.5MA constant plasma current for 6s with ICRF heating and LHCD combined;
c) 2MA for 2s after a ramp down of the plasma current with ICRF heating and LHCD;
d) 1MA constant current for 5s with LHCD and 50% bootstrap current from ICRF heating in a H-Mode plasma at high density (3.6×10^{19} m^{-3}).

In cases (b) and (c), the plasma internal inductance was not constant. Therefore, these are non-equilibrium situations as the change in plasma internal inductance gives an additional component to the reduction in loop voltage.

Flux Saving on 7MA Pulses

During the 7MA campaign, about 1.5MW of LHCD was applied during the ramp-up of the current. This altered the current profile and hence the plasma internal inductance. As shown in Fig.51, the change in internal inductance persisted even after the LHCD pulse had ended, only regaining its normal value during the flat-top. The effect of these changes was a reduction of 2V-s in the transformer flux swing required to establish the 7MA current. This reduced the transformer primary current and hence the losses in the copper primary windings of the transformer: 8MJ of LHCD power resulted in an 80MJ reduction in the transformer losses. The V-s saved were used to extend the flat-top of the plasma pulse by 2s.

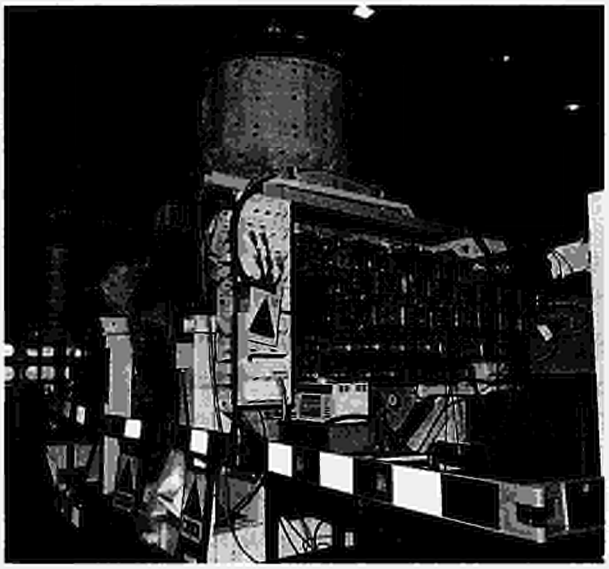

Fig.52: A view of the eight vacuum windows connecting the LHCD waveguides to the rear of the launcher, in its testbed. The cryopump is clearly visible on top

The L1 Launcher

The prototype system has fulfilled its role in providing engineering, operational and physics experience of LHCD on JET. The L1 launcher is now being prepared for installation. This will be capable of launching 10MW into the plasma. Based on the results with the prototype system, this should allow full current drive of a 4MA plasma.

The L1 launcher was originally designed for the plasma profile of the belt limiter configuration. Following a decision in 1990 to install the launcher after installation of the pumped divertor, the shape of the grill mouth was modified to match this plasma. During 1992, the procurement of the modified components was completed and the launcher fully assembled - the completed launcher is shown in the section on Current Drive and Profile Control. This launcher incorporates 48 multijunction units each having eight waveguides at the grill to give a total of 384 waveguides. The power from 24 klystrons is coupled to the grill via 48 vacuum windows, (shown in Fig.52) which shows the launcher assembled on the testbed. The windows may be replaced using remote-handling tools. A cryopump of 85,000ℓs^{-1} is being prepared for installation on top of this launcher. The total mass of the L1 launcher will be ~ 15 tonnes.

The main challenge for the operation of L1 will be the reduction of the excessively long conditioning time. To assist, the carbon layer has not been applied as this tended to outgas and to flake off causing arcs. The baking of the multi-junctions has also been improved with the possibility of operating the multi-junctions at high power in vacuum to provide RF heating of all parts of the waveguide system.

Remote Handling and Waste Management

During 1992, the Remote Handling and Waste Management Group's manpower were heavily committed to shutdown activities and to clean-up associated with the preliminary tritium experiment (PTE). Main progress in these areas is detailed below.

Remote Handling

Maintenance and repair of the tokamak and auxiliary systems in the Torus Hall during the D-T phase of JET will only be possible remotely, (ie controlled from outside the biological shield). Development of the remote handling equipment and procedures for maintenance tasks is carried out by the Remote Handling Groups in Fusion Technology Division. The manpower of these groups is also heavily involved in shutdown activities where remote handling equipment is being deployed, albeit hitherto in hands-on or semi-automatic mode.

Whilst the use of remote handling equipment during JET shutdowns provides an excellent testing ground for the effectiveness and reliability of equipment, it also means that as a consequence of the associated manpower effort, only limited effort has been available for development of full remote handling procedures. Therefore, it is now envisaged that the remote handling for the D-T phase will concentrate on a few essential ex-vessel and in-vessel operations, including gaining remote entry into the vacuum vessel using the telescopic articulated remote mast (TARM) and the articulated boom with special end effectors or the MASCOT IV manipulators. The latter would allow, to a certain extent, to carry out non-planned activities inside and outside the vacuum vessel.

Particular developments are described in the following paragraphs.

Articulated Boom

During March 1992, the Articulated Boom was used to remove 82 large components from within the torus. Many of these components could only be removed after cutting them free and over 132 cuts were made inside the torus. After the campaign of work to remove equipment from the vessel in the first part of the shutdown, the Boom underwent extensive upgrading and modification. It has been totally rewired with insulated cables of low halogen and low smoke mate-

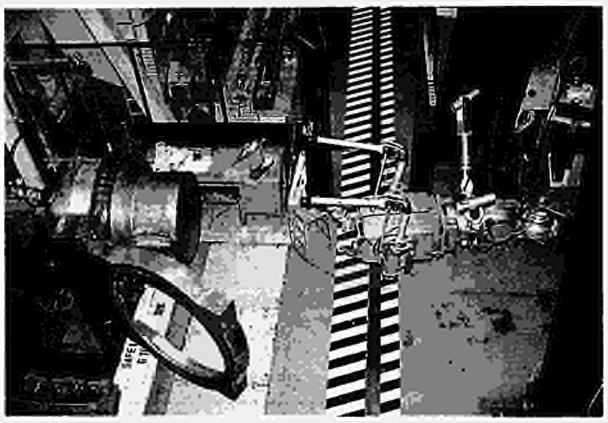

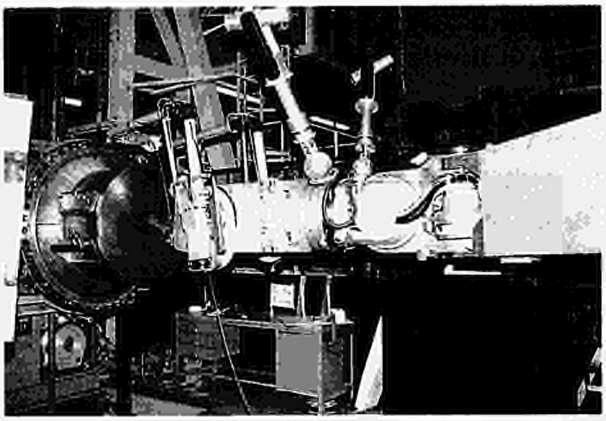

Fig.53: MASCOT IV at (a) start of mock-up; and (b) poised to begin unbolting operation.

rial. Designed for enhanced flexibility, the rewiring accommodates all requirements related to the new boom addition with two joints which bring the total number of joints from five to six.

A new local controller is being prepared for this configuration. The joint control hardware has been specified and complex software is being prepared. Its detailed design is completed, except for the teach/repeat function. Commands and protocol have been defined. To achieve the required speed, the computer hardware (based on Multibus 2) had to be upgraded and the operative system changed from RMX2 to RMX3. A control handbox has been prepared for testing and debugging with the collaboration of JRC ISPRA, Italy, under a Task Agreement, together with an appraisal on testing methodology. The software of the kinematics has been completed and tested using a graphical model.

Following the installation of new actuators and reinforcing plates the boom has been recommissioned for higher speed reducing the insertion time in the vessel to nine minutes from the "pick-up" point, after first adjustment of parameters including velocity feed forward compensation. All joints without a tacho-generator are now controlled with emf feedback. Static and impact load testing where carried out following calculations by JRC ISPRA, Italy, and monitored by a data acquisition system specially designed for this purpose.

Radiation testing of a new miniature camera was undertaken during 1992, at AEA Harwell Laboratory. This camera will now form the basis for a small camera package to replace the existing cameras mounted on the Boom. The new camera package will be physically smaller, provide a colour picture and be less sensitive to noise than the existing units.

Telescopic Articulated Remote Mast (TARM)

The commissioning work has continued with the progressive elimination of residual SW faults. A new Kabelschlepp cable chain was installed along the crane girder and optical fibres were inserted and terminated, optimising the relevant signal levels. In addition to the ongoing commissioning and preparation for A2 antennae installation in 1993, TARM was used as a transporter for MASCOT in remote handling trials.

Figure 53 shows MASCOT applying an impact wrench to port holes during trials on a mock-up of the main vacuum vessel flange.

In-Vessel Inspection System (IVIS)

The four IVIS light guides were dismantled from the machine during the shutdown. The modifications to accommodate the new IVIS viewing tubes are in progress. An international tender action to procure the viewing tubes was completed and the order was placed. Fig.54 shows the tube, with the prism in vacuum, manoeuvred through a "wobbling" bellows. Tests on a prototype in vacuum at elevated temperature have been successfully completed.

A new camera probe was designed, with a special rotary connector. Neutron radiation tests are in progress on the most critical components. These important results are being appraised.

MASCOT

Improvements to the MASCOT manipulator have been achieved especially in the Man Machine Interface (MMI), computer aided teleoperation (CAT) and grippers to increase speed and reliability. The MMI has been made more friendly and manual driven, and the documentation has been clarified. The CAT has been improved to bring sampling time for constraint and weight compensation to below 10ms.

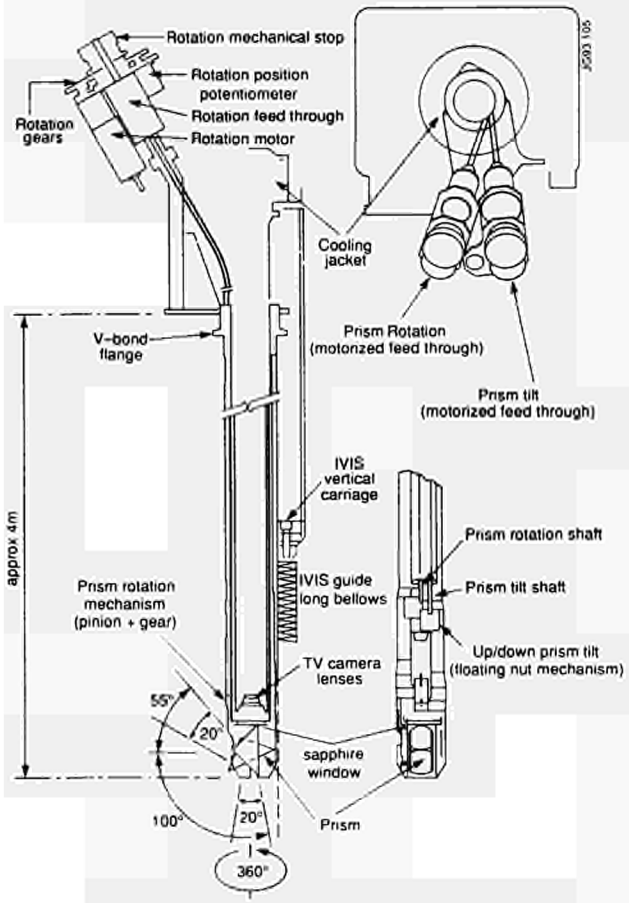

Fig.54: The In-Vessel Inspection System showing a viewing tube with the prism in vacuum manoeuvred through a "wobbling" bellows.

The control of brushless motors has been studied and successfully tested by the Ecole Polytechnique Federale of Lausanne, Switzerland, under an Article 14 contract. This has produced guidelines on improvements to load capacity of MASCOT type manipulators up to 40kg capacity.

After assessment and radiation tests, a new CCD camera is being integrated into the "cyclops" arm. MASCOT has been used on the TARM to perform remote handling trials on the mock-up of the vessel port. This operation has been done in fully remote conditions, and included removal of services, unbolting, replacing the seal, inspecting the seat and smoothing out scratches. Vacuum leak tightness was demonstrated to 10^{-10}mbarℓ s^{-1}.

Navigation and approach to the port was aided by a graphical computer model. Special tools were prepared based on existing tooling and making the necessary modifications to improve gripping for safety and reliability. An integrated team was formed and trained, using personnel seconded to JET by the EC Teleman Project and KFK, Karlsruhe, Germany. CAT algorithms and graphics aids were used when needed in these important trials.

R.H. Mock-ups

To ensure the feasibility of remotely opening and closing the Octant No:5 pumping chamber door, a full size mock-up of the door and its immediate environment was built and the task fully tested during 1992. The remote handling tasks comprise disconnection of door services, removal of the door heater jacket, removal of all 48 door bolts, opening of the door, removal and replacement of the Cefilac door seal and the reversal of the whole process to close the door. Upon completion of these activities the volume immediately behind the door was vacuum pumped and the leak tightness of the seal verified. The success of the trial showed that it is feasible to remotely open the door and leave it in situ whilst the door seal is replaced. Many other data were obtained from the trials including improvements to be made to the JET components and improvements and additions to the remote handling equipment.

Special Tools

Work on special tools was dominated by the operations on the torus and the design and development of new tools for use during the installation on pumped divertor components during Stage III of the shutdown. Many new tools are required for handling, welding and possibly cutting of the divertor module cooling pipes. In addition, new cutting and welding tools are being designed for those small circular ports whose access will be severely limited after installation of the divertor coils.

R.H. Integrated Control System

The new Hand Control Terminal (HCT) has been delivered and acceptance tested at JET. The HCT comprises an Intel 386 microcomputer driving a 16cm Hitachi colour LCD flat screen. The unit is integral with touch screen, LCD display programmable buttons, emergency stop button and a three-axis analogue joystick. Application programs for control of any piece of remote handling equipment (with the exception of MASCOT) can be written and down-loaded into the unit. The first application programme to be implemented is for operation of the TARM and this software is presently being acceptance tested.

The HCT is a hand-held unit of approximately A4 page size and will provide for both hands-on and fully remote operation of remote handling equipment. In this way, the extensive operation of equipment hands-on will yield operators and Man-Machine Interface equipment which is proven and familiar for the fully remote phase.

The TARM Interface cubicle, which connects together all of the service units required by the TARM and thence to the remote handling control room, was ordered during 1992, and delivery is expected in April 1993.

Special End-Effectors

Various new articulated boom end-effectors for handling large components to be installed during the pumped divertor shutdown and those requiring remote handling during the active phase have been designed and are being manufactured. Components requiring new end-effectors comprise, divertor modules, poloidal limiters, inner-wall guard limiters, A2 antennae and the LHCD cadre and cadre extensions.

A handling device for remote replacement of the new LIDAR diagnostic at Octant No:5 has been designed and is now being manufactured. This is a remote handling Class 1 task as the system has to be removed in order to provide access for the Articulated Boom through the pumping chamber and main horizontal port.

Waste Management

Five controlled area facilities which are all equipped to handle components and materials which may be activated and contaminated with tritium and beryllium have been operated in support of the extended shutdown for the installation of the pumped divertor. Wastes generated in these areas are disposed of either as beryllium or low level radioactive waste. These facilities are all ventilated through plant operated in accordance with an Authorisation from the Department of the Environment. Other activities include the provision of all services and equipment for pressurised suit work and respiratory protection, and the operation of a workshop for the fabrication of tents and isolators for contained maintenance work.

In parallel with this work, quality assurance (QA) and waste management procedures (WMP) for waste disposal have been developed further. Low level radioactive waste has been disposed of throughout the year via AEA Harwell Laboratory, to the UK Repository at Drigg, UK. Methods of waste minimisation, waste volume reduction and sampling and analysis techniques have been implemented to reduce waste disposal costs.

The main activities have been as follows.

Torus Access Cabin

The Torus Access Cabin (TAC) was installed on the JET machine at the start of the shutdown in an extended configuration with an enlarged operations box and improved facilities for the transfer of components in ISO-freight containers. The access and change facilities were also improved to allow for quicker entry and exit. Up to six operatives were able to work concurrently in pressurised suits with a modified breathing air supply system. The ventilation plant for the torus and the TAC was extensively modified to take account of the potential tritium levels following the preliminary tritium experiment (PTE). However, tritium levels within the vessel were very low (below the limit of detection on hand-held monitors) and pressurised suits were primarily required to protect against the beryllium hazard.

The TAC provided trouble-free support to the in-vessel programme throughout the shutdown and, in the initial three month period, there were ~1400 suited entries, representing over 5000 man-hours spent in suits inside the vacuum vessel. Following the removal of first wall components and decontamination of the vessel, it was possible to change the classification of the vessel and dispense with the use of suits.

Beryllium Handling Facilities

During the shutdown, the two facilities in the Assembly Hall were integrated into one area with a new materials airlock. A new tritium compatible ventilation system was commissioned, which also serves other areas in the Assembly Hall, including that used for the octant toroidal field coil change.

Fig.55: Grit blasting cubicle in Beryllium Handling Facility

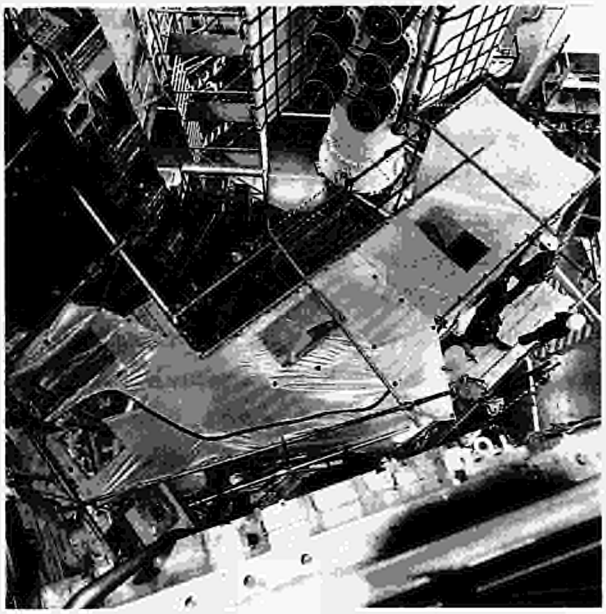

Fig.56: Tent at Octant No:8 for removal of Rotary Valve.

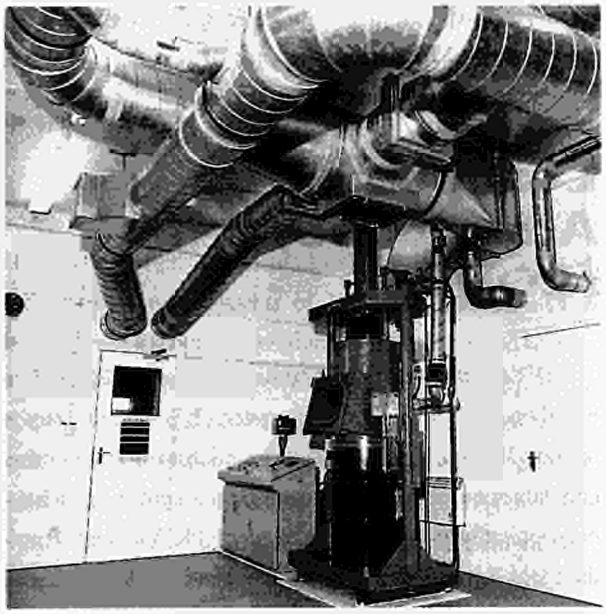

Fig.58: In-drum Compactor.

Main activities in the beryllium handling facility have been the decontamination of tiles and components, for which a new wet grit blasting cubicle was installed (Fig.55). Development of improved techniques for removal of beryllium activity and tritium from components which will be re-used has been ongoing throughout the period.

Suit Maintenance and Isolator Fabrication Area

The suit cleaning and maintenance facility was an area of intense activity during the first three months of the shutdown. Over 1500 suits were cleaned and inspected in the period, requiring over 3500 man-hours inside the controlled area. Suit repairs are also carried out in this area.

The PVC workshop produced around 200 tents and isolators in the period, requiring over 2300m of PVC sheet. These vary in size from small hand isolators and camera bags, up to the large tents used in the octant refurbishment area and those used for the removal of the rotary valves from Octants No:4 and No:8 (Fig.56). The work in these tents was carried out in pressurised suits.

Fig.57: Waste Handling Facility.

Waste Handling Facility

The new Waste Handling Facility (WHF) (Building J30 - Fig.57) was commissioned in January for the start of the shutdown. Principal operations conducted in the area include: sorting and sampling of materials, in-drum compaction of compressible wastes (Fig.58) and preparation for disposal and packaging of component wastes. Initial work concentrated on secondary wastes which consist mainly of disposable clothing and housekeeping waste. By mid-November, around 110 drums of compacted waste had been prepared for disposal and shipped to AEA Harwell Laboratory for disposal at Drigg, UK. Progress was also made on the disposal of wastes accumulated during earlier shutdowns. Towards the end of 1992, work started on the disposal preparation of primary component waste materials. Some of this was packed in 200l drums, which meet the IP2 specification for transport, but other items will be disposed of in half height ISO-freight containers

Waste Disposal

The two main types of specialised waste disposed of during the period were beryllium contaminated solid waste which is disposed of to landfill on a licensed site, and low level solid radioactive waste, disposed of via Harwell to the Drigg repository. Comprehensive waste management procedures and a QA system complying with BNFL requirement (the operators of the Drigg Waste Site) have been developed to

handle this material. The volumes for the radioactive waste are minimised by compaction into 200ℓ drums with the volume reduction factor of 6:1.

Control and Data Acquisition System (CODAS)

The JET Control and Data Acquisition System, CODAS, is based on a network of minicomputers. It is the only way to operate JET and it allows centralised control, monitoring and data acquisition. The various components of JET have been logically grouped into subsystems like Vacuum, Toroidal Field, Lower Hybrid additional heating, etc. Each subsystem is controlled and monitored by one dedicated computer interfaced to the machine and its diagnostics, through CAMAC instrumentation and EUROCARD-based signal conditioning. Embedded front-end intelligence is implemented through CAMAC-based microprocessors for real-time applications. The actions of the various computers are coordinated by supervisory software running in the Machine Console computer. This supervisory function includes the countdown sequence for each plasma discharge. During 1992, the main effort has been devoted to moving CODAS to a UNIX environment. The following sections describe the main activities and report on the current status.

Computer Network Topology and Implementation

The planned computer network described in the 1992 Progress Report has not changed significantly but has been refined. The topology shown in Fig.59 is based on multiple ETHERNET segments connected through bridges. Each segment groups a logical set of subsystem computers and their local server into a cluster. The concept of local servers and of clusters isolated by bridges allows the traffic to be localised on each segment and permits small machines to be used as local servers. To avoid a common performance limiting factor, each computer has a small internal disk (424MB) used exclusively for swapping. This not only improves the swapping performance but decreases the segment traffic significantly. The possibility of grouping the subsystems by affinity gives an additional method of reducing the inter-cluster traffic appearing on CODASnet.

In addition to the CODASnet linking the clusters, Fig.59 shows a JPFnet which has been designed to provide an uncluttered path for the large data collection load. From an operational viewpoint, it is important to be able to monitor conveniently the few (but serious) system error messages, which traditionally go to the "system console". An additional small network, CONSOLEnet, has been devised to cater for this and all error logs can be observed from a single terminal driven by a simple process. It is

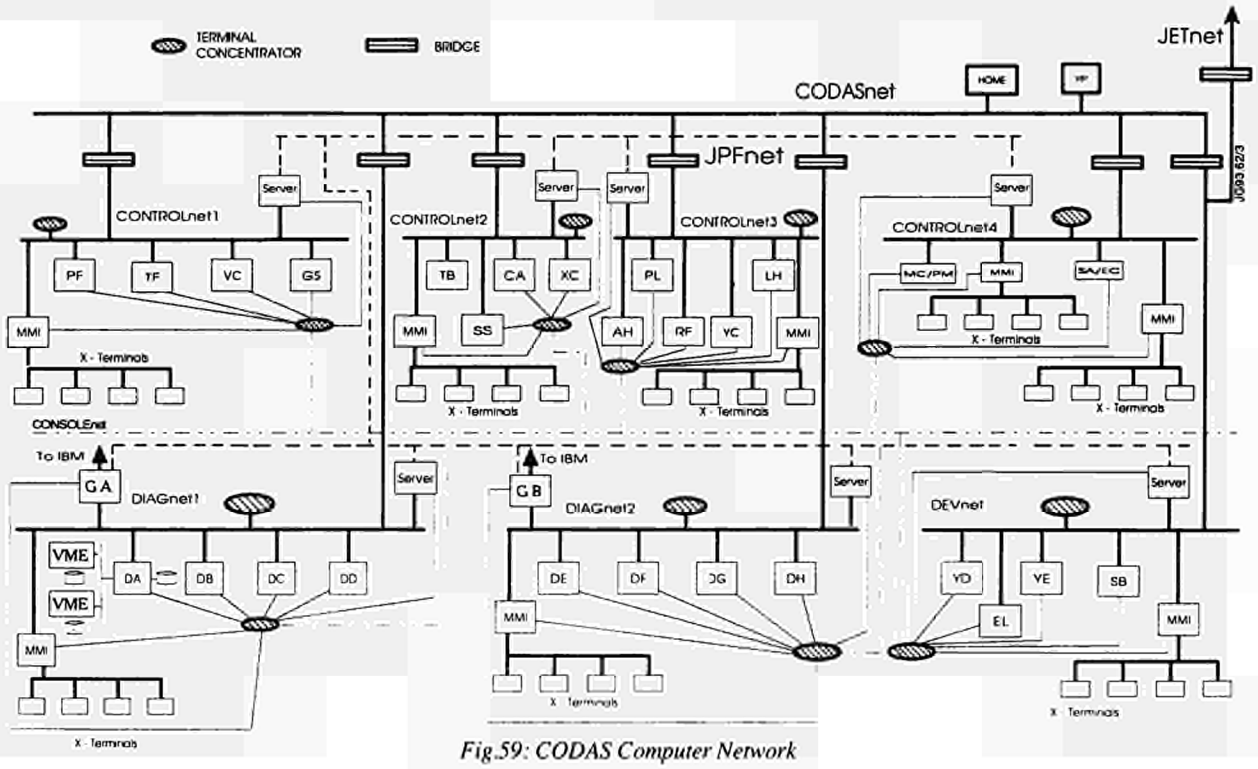

Fig.59: CODAS Computer Network

worth noting the further traffic localisation obtained by the implementation of the connections to the X-terminals used for operation from the control rooms. These are grouped according to the subsystem computers that they most frequently access. Each group is connected to an ETHERNET segment linking them to a service computer included in the relevant cluster.

The cluster concept and the small size of the new components (computers, disk drives, fan-out units, bridges, etc) allowed a modular structure to be implemented. Each cluster is housed in a compact set of three cubicles, in which the local segment consists of one, or more, fan-out units. The inter-cubicle part of CODASnet, JPFnet and CONSOLEnet uses thick ETHERNET. Only Network Information Services and Home reside on CODASnet backbone and are isolated from the on-line part of CODASnet by an additional bridge.

Performance monitoring, problem identification and fault diagnosis tools are required for an efficient operation of the network. A review is presently underway and implementation is expected by the mid-1993.

Computer, Disks, X-terminal and Network Components Procurements

Following full tender action and approval in February, contracts were placed for the procurement of the following equipment:

- Sparc II computers to act as: Subsystem computers; Servers; X-terminal support. Further tests have shown that one Sparc II could support ten X-terminals instead of the six reported in the initial tests in 1991;
- 1.3G Byte disk units ;
- X-terminals - NCD 17Cr;
- SINTROM bridges;
- Fan-out units BICC 1131;
  Transceiver Ringlan 120
  Terminal concentrators, Datability 200 and 300.

All equipment has been subject to strict and formal acceptance tests before installation. The integration of units from multiple vendors did not prove to be too arduous a task and led to significant cost benefits.

Computer and Control Rooms

Taking into account the reduced physical size of the equipment, a detailed study proved the feasibility of re-organising the Computer and Control Room arrangements and of allocating 250m^2 to house the IBM 3090 on the JET site. The CODAS Computer Room has been reduced to 220m^2 leaving some space for further equipment expansion. The new Control Room will use a simple desk arrangement on which X-terminals and other peripherals will be installed.

The open nature of the new system and of the network offers new and welcome operational facilities but, at the same time, brings the potential risks of unwanted interference. The security aspects of JET operation have been assessed and a scheme agreed to control access and actions of CODAS computer users. This control will be applied on a personal basis and will take into account the agreed role of each person and the location from where they execute actions. As an example, an engineer identified by his password, may be allowed to close a circuit breaker only if he is a recognised Power Supply Engineer and if the action is initiated from the JET Control Room. The detailed design of the scheme is underway and the implementation should be completed in 1993.

The previous Control Rooms included a series of 26" overhead displays showing standard computer generated information and pictures from observation cameras. These were not easily visible from distances of more than 5m and their technology was not compatible with the new system. A new scheme has been devised using smaller screens distributed in strategic locations in the control room. A cost effective solution has been identified, which uses Personal Computers emulating X-terminals and driving SVGA (Super Video Graphic Array) screens. The TV signals are captured in frame grabber cards installed in the PCs which can display the pictures in windows. A full prototype will be reviewed with users in the first quarter of 1993.

Installation and Logistic

At the end of operation, CODAS had only a few on-line services to maintain. The most important was the Safety and Access subsystem, which will be in use throughout the shutdown. The others were mainly the test-bed facilities. To provide stand-by and occasional test facilities, eight old computers were reconfigured and relocated. All the other old Norsk Data computers were removed. In a similar way, a few CAMAC based consoles were relocated and the remainder dismantled. Obsolete cabling was removed, new trunking installed, cubicles installed and the new equipment placed in its final location in the Computer Room. The tender action for the control room furniture was issued towards the end of 1992 and the installation should be completed before mid-1993.

CAMAC Interface

As reported in 1991, it was decided to retain the large investment in front end CAMAC instrumentation and to drive CAMAC serial loops from JET-designed VME (Versa Module Eurocard) boards. As part of the computer selection, various methods of interfacing computers to the VME boards were considered and the technical and financial consequences were analysed. The options considered were:

- VME slot(s) available in the computer;
- SCSI interface to VME;
- Parallel computer port connecting to the VME board;
- Computer bus to VME adapter.

The chosen solution is the computer bus to VME adapter. VME crates with partitioned VME bus are installed in each cluster. Each crate has three partitions, each partition is connected to one subsystem computer and provides space for up to four VME serial highway drivers. The installation of this equipment is now complete and all serial highways are operational.

Software Porting

Following the successful integration of the software for the Pellet Testbed subsystem, considerable effort has been concentrated on the move to UNIX. This culminated in the integration of all CODAS subsystems and the successful execution of a software countdown rehearsal in October, in line with the initial planning. This represents a significant milestone in the move of CODAS to a UNIX environment.

At present two subsystems running under UNIX are on-line. One supports the Pellet Testbed and the other the Neutral Beam Testbed. The completion of the transfer of all the software required for the operation of JET is expected before mid-1993. At this time, the Safety and Access Control Subsystem should be moved to UNIX, leading to the decommissioning of the last of the Norsk Data computers. The total effort invested in the move of CODAS has reached 42 man-years and is expected to rise to 46 man-years when the move is completed.

To ease software migration, a set of tools to simplify the porting of FORTRAN code has been developed. The tools automatically perform a number of changes and flag others to be carried out by the programmer. These tools have been used extensively in the porting of the diagnostic software.

Link to the IBM

The relocation of the IBM to the JET site offered new possibilities for higher performance links at lower costs. A tender action was issued for a UNIX/IBM gateway to provide a file transfer rate of about 2MB. The evaluation of this link will be completed early in 1993 and the system will be installed and fully commissioned well before operation resumes.

New Developments

The divertor configuration of JET leads to a substantial increase in instrumentation and diagnostic requirement. The consequences of these requests were a strong demand for powerful front end processing and a significant increase in data volume and channels. After analysis, two lines of action were decided upon as outlined below.

New Electronic Standard

As the CAMAC standard no longer provides the range of required modules at competitive prices, it was decided to extend the CODAS standard to include VME and to deploy VME instrumentation where appropriate. There is no intention of systematically replacing CAMAC by VME. Studies have identified the requirement for a set of VME modules which are now under design or procurement. The use of microprocessors and field-programmable integrated circuits means that fewer hardware designs are needed than in CAMAC, as different functions can be achieved by firmware changes only. Where processing power is required, two types of processors have been selected, both housed in VME modules. One processor will be of the 680x0 family running VxWorks. The other will be DSP (Digital Signal Processor) chips, the TMS320C40, installed in VME carrier boards. The final selection will be made in early 1993. Where VME crates are deployed, these will be connected to their host subsystem computers by independent ETHERNET segments. Software development for the support of this new standard has just started and some low level libraries have been made available under VxWorks.

New Data Collection Scheme

The increase in data volume will require the use of data compression and data reduction where appropriate. This, in itself, is one of the sources of demand for powerful front end processing. The current estimated data volume is about 80MByte per pulse, when all diagnostics are operating. This should be compared with the 30MByte per pulse at the end of the last operation period. In addition, about 150MB per pulse will have to be collected and transferred, as time permits, to the IBM. These data have been named Late Pulse

Table. XIII
Quantitative Information on CODAS Installation

Item	*End 1991*	*End 1992*
CODAS Interface Cubicle	165	156
CAMAC Crates	255	215
CAMAC Modules	3,195	2,675
Eurocard Modules (Signal Conditioning and Power Supplies)	8,180	6,079
CAMAC Serial Loop (Fibre Optic)	25	23
On-line Computers	24	40
Off line and Commissioning Computers	13	7
Size of JPF	33	33
Number of diagnostics on-line with CODAS	42	38
Number of diagnostics under commissioning with CODAS	2	2

Files (LPF). These need not reach the IBM before the next JET pulse, as they will be used for detailed off-line analysis of fast phenomena. The new data collection software has been designed to allow ETHERNET connection to non-CODAS systems, which would have to support a simple message protocol but would have to achieve a minimum performance depending on the data volume to be collected. This new scheme will be developed and tested during the first half of 1993.

Evolution of Existing Systems

Tables XIII and XIV provide quantitative data on CODAS installation, while Figs.60 and 61 provide information on the evolution of JET data acquisition over the years. The reduced quantity of electronic modules deployed arises from the removal of the CAMAC-based consoles. During 1992, six new cubicles were designed, constructed and installed. 264 fully documented improvements were made and 268 maintenance interventions recorded.

Table. XIV
Review of CODAS Electronics Stock Holding
(installed, pre-procurement, loaned and spares)

		End 91	*End 92*
1.	CAMAC system modules	908	911
2.	CAMAC digital I/O modules	910	902
3.	Timing system (CAMAC & Eurocard)	1,430	1,430
4.	CAMAC analogue I/O modules	1,352	1,351
5.	CAMAC display modules	406	375
6.	CAMAC auxiliary controllers	151	151
7.	CAMAC powered crates	280	280
8.	U-port adaptor	215	215
9.	CISS modules	977	1,040
10.	CCTV	690	685
11.	Cubicle frames	354	354
12.	Console devices (not CAMAC)	648	595
13.	Power supply modules	2,097	2,097
14.	Intercom, Public Address, Computer terminal network	731	805
15.	Pool instruments	1,003	1,006
16.	Analogue I/O in Eurocard	2,863	2,922
17.	Digital I/O in Eurocard	4,975	4,977
18.	Eurocard sub-racks	1,024	1,017
19.	JETNet active devices	187	271
20.	VME modules and subracks	5	108
		21,206	**21,492**
		Increase	1.3%

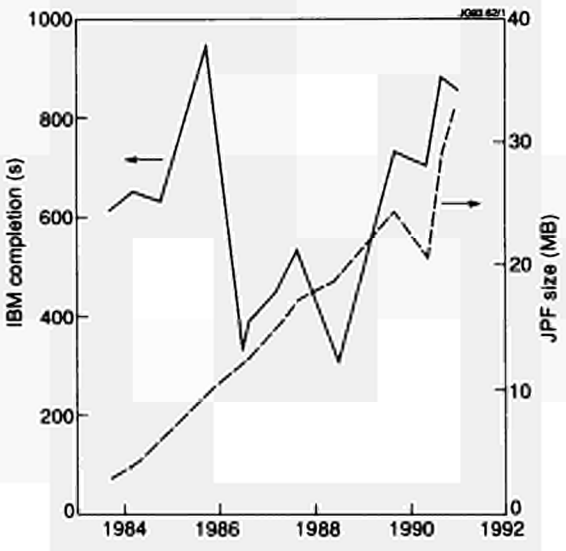

Fig.60: Evolution of JPF size and collection time over the period 1983-1992

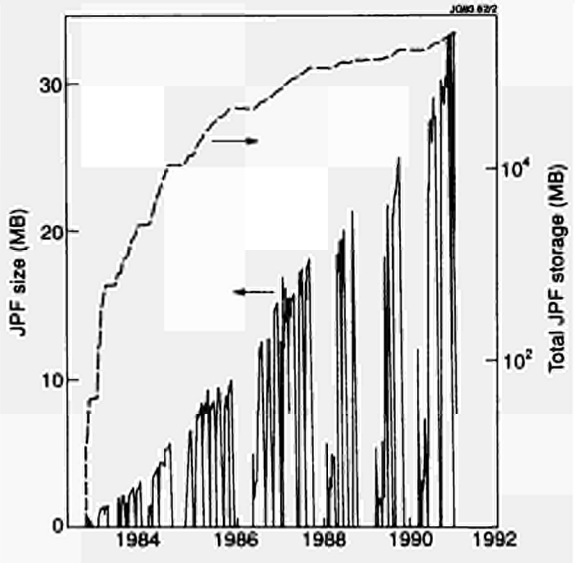

Fig.61: Evolution of JPF size and volume over the period 1983-1992

The interface to the Disruption Feedback Amplifier has been designed, installed and commissioned and will be integrated in the Poloidal Field subsystem. After design and installation, the interface to the Fast Radial Field Amplifier to be used for the vertical stabilisation is being commissioned under UNIX. A significant extension of the Access Control System is underway. This system controls and records personnel access to various areas of JET. The extension led to a redesign of the interface to CODAS. The installation will take place in the first half of 1993.

The Central Interlock and Safety System (CISS) was expanded by an additional controller, PX, installed as a slave of the PF controller. This new controller was required for the inclusion of the divertor, disruption feedback and fast radial field amplifiers into the poloidal field system. This confirmed the suitability of the original design of CISS. The significant extension of the JET cryo-system requires a review and a new design of the Direct Plant Interlock System (DPIS), which uses the CISS technology. Detailed design, implementation and commissioning will be completed in the first half of 1993.

JETNet, the site-wide data network using ETHERNET hardware and Vines software has been extended slightly, especially in the Engineering buildings. There are now 97 segments and 923 outlets. It is now possible to use portable terminals to access CODAS systems and documentation from any point on-site where CODAS has services. Terminals connected in this way provide the fault-finding and commissioning facilities formerly provided by mobile consoles.

The number of JETNet users grew throughout the year as further server computers were connected. At the end of 1992, six servers were available, enough to meet the needs of the whole site. Currently, 356 users are authorised to use JETNet. It provides interconnection between IBM mainframe, UNIX, PCs and Apple Macintosh users for e-mail, as well as shared utilities, programs, data and disk space.

Data Management

The Data Management Group is responsible for the management of JET data and for organisation and control of routine data processing. It is responsible for the provision of a mainframe Computing Service for scientific and engineering computing and for PC, Apple Macintosh and network support, including the provision of appropriate software and hardware systems. The computing service is based on an IBM 3090/300J three-way processor mainframe with two vector facilities. There are 100GBytes of disc storage and a further 1000GBytes of automated cartridge tape storage.

The JET computing Service has been operating since June 1987 and the central computer was upgraded in February 1990 from an IBM 3090/200E to an IBM 3090/300J with three processors, two vector facilities and 256 MBytes of memory (128MB central and 128MB expanded), almost doubling the processing capacity. The upgrade permitted a significant growth of the mainframe computing workload, most critically in the areas of data processing, CAD work from the Drawing Office, interactive (TSO) work and mechanical and electrical design studies. These improvements have significantly enhanced the Project's Design and Data Processing capabilities.

To provide additional storage capacity and ensure compatibility with the latest IBM software and offer higher reliability, the original IBM Mass Storage System (MSS) was replaced in February 1992, by a Memorex-Telex automated cartridge tape library (ATL) with a capacity of about 1000GBytes (four times that of the old IBM MSS). The ATL not only provides storage for backup and dump tapes, that were previously handled using manually operated cartridge tape drives. This, together with the introduction of automated operations via the product AutoMate/MVS, has eliminated the requirement for operator cover, leading to significant staff savings.

The other recent major change has been the relocation of the complete IBM Computer Centre from the UKAEA Harwell Laboratory to the JET site. A new computer room was established in Building J2, with the building work starting at the beginning of the JET shutdown in March 1992. The work involved repositioning of internal walls, extensive refurbishing, and the provision of the required electrical systems, air conditioning and chilled water supplies. The computer room was prepared very efficiently and the move of the equipment took place over the weekend of 17th July 1992, with a minimal interruption, service being restored to users before midday on the Monday (Fig.62).

The relocation of the computer has led to improvements in the following areas:

- improved communications, performance and reliability, with the removal of the need for remote links to access the system;

Fig.62: Installation of the IBM mainframe computer in the Building J2 computer room.

- the potential for greater integration with the CODAS, UNIX systems. Prototype developments for data transfer link between the UNIX (Sun) systems and the IBM show very significant improvement in speed;
- significant cost savings in the areas of communications hardware and of staff.

Overall this should lead to even greater involvement of the mainframe data analysis in connection with control room activities.

The increasing sophistication of JET measurements and analysis techniques have lead to a growth in the JPF size which, during the last operations period reached almost 35MBytes per shot. Various optimizations were made in order to keep the data collection and transmission time within eight minutes from the end of the pulse. The first set of plots from the analysis were returned to the control room within a further two minutes, and the intershot analysis was normally completed in eight minutes from receipt of JPF. In the pumped divertor phase the JPF size may well exceed 80MBytes, and further delayed data will be collected. Developments are in progress to transmit, store and analyse the increased amounts of data.

At present, all the JPFs (in excess of 250GBytes) are stored in compressed form on the Memorex-Telex ATL and a further 90GBytes of analysed data from the intershot and other analysis work is also stored on the IBM system, within the PPF on-line data base.

The Central Physics File (CPF), stored and used under the SAS environment, forms a complete higher level data selection and storage system. A subset of all data is extracted at time points of interest, determined by the Timeslice program and the interactive time slice editor, TED, and stored in the SAS databases. The data are the basis for extended statistical analysis, and the source for other extracts such as the TRANSPORT and EDGE bank. This system is fully automated, and much used in the Project.

The other major area of the group's work is the support of over 450 Personal Computers (PCs), about 80 Apple Macintosh systems, and (together with the CODAS) support for the site wide network. The PCs are used for a wide variety of tasks including word processing, data analysis, data acquisition, program development, terminal emulation, CAD, project planning and circuit design and analysis. The facilities have been significantly extended with the introduction of the sitewide network JETNet. This brings new services such as electronic mail, shared file access with central backup service, access to shared printers and to the UNIX and IBM computer systems.

Diagnostic Systems

The status of JET's existing diagnostic systems at the end of 1992 is summarized in Table XV and their general layout in the machine is shown in Fig.63. The staged introduction of the diagnostic systems onto JET has proceeded from the start of JET operation in June 1983. The present status is that 37 systems are in existence. A further 22 systems are in preparation or in the design stage for operation in the new phase of JET or in the active D-T phase. Table XVI sets out the list of additional diagnostics under construction. Operational experience on the existing diagnostics has been good and most of the systems have operated automatically with minimal manual supervision. The resulting measurements have been of high quality in terms of accuracy and reliability, and have provided essential information on plasma behaviour in JET. Further details on specific diagnostics systems are given below.

Magnetics

The magnetic diagnostic system for the new phase will have two sets of flux and field measurements near the divertor area and a number of extra pick-up coils located near the projected positions of the outboard and inboard plasma surfaces. A back-up set is also provided for these measure-

Table XV
Status of JET Diagnostics Systems, December 1992
Existing Diagnostics

System	Diagnostic	Purpose	Association	Status
KB1	Bolometer array	Time and space resolved total radiated power	IPP Garching	Modified
KC1	Magnetic diagnostics	Plasma current, loop volts, plasma position, shape of flux surface, diamagnetic loop, fast MHD	JET	Upgraded
KE3	Lidar Thomson scattering	T_e and n_e profiles	JET and Stuttgart University	Upgraded
KF1	High energy neutral particle analyser	Ion energy distribution up to 3.5MeV	Purchased from Ioffe St Petersburg	Upgraded
KG1	Multichannel far infrared interferometer	$\int n_e ds$ on six vertical chords and two horizontal chords	CEA Fontenay-aux-Roses	Modified
KG3	Microwave reflectometer	n_e profiles and fluctuations	JET and FOM Rijnhuizen	Modified
KG4	Polarimeter	$\int n_e B_p ds$ on six vertical chords	JET and CEA Fontenay-aux-Roses	Upgraded
KH1	Hard X-ray monitors	Runaway electrons and disruptions	JET	
KH2	X-ray pulse height spectrometer	Monitor of T_e, impurities, LH fast electrons	JET	
KK1	Electron cyclotron emission spatial scan	$T_e(r,t)$ with scan time of a few milliseconds	NPL, UKAEA Culham and JET	Modified
KK2	Electron cyclotron emission fast system	$T_e(r,t)$ on microsecond time scale	FOM Rijnhuizen	
KK3	Electron cyclotron emission heterodyne	$T_e(r,t)$ with high spatial resolution	JET	Upgraded
KL1*	Limiter viewing	Monitor hot spots on limiter, walls, RF antennae, divertor target tiles	JET	Upgraded
KL3	Surface temperature	Surface temperature of target tiles	JET	Upgraded
KM1	2.4MeV neutron spectrometer	Neutron spectra in D-D discharges, ion temperatures and energy distributions	UKAEA Harwell	
KM3	2.4MeV time-of-flight neutron spectrometer		NFR Studsvik	Modified
KM7	Time-resolved neutron yield monitor	Triton burnup studies	JET and UKAEA Harwell	
KN1	Time-resolved neutron yield monitor	Time resolved neutron flux	UKAEA Harwell	
KN2	Neutron activation	Absolute fluxes of neutrons	UKAEA Harwell	Modified
KN3*	Neutron yield profile measuring system	Space and time resolved profile of neutron flux	UKAEA Harwell	Upgraded
KN4	Delayed neutron activation	Absolute fluxes of neutrons	Mol	
KR2	Active phase neutral particle analyser	Ion distribution function, $T_i(r)$	ENEA Frascati	
KS1	Active phase spectroscopy	Impurity behaviour in active conditions	IPP Garching	
KS2*	Spatial scan X-ray crystal spectroscopy	Space and time resolved impurity profiles	IPP Garching	
KS3	H-alpha and visible light monitors	Ionisation rate, Z_{eff}, impurity fluxes from wall and limiter	JET	Upgraded
KS4	Charge exchange recombination spectroscopy (using heating beam)	Fully ionized light impurity concentration, $T_i(r)$, rotation velocities	JET	Modified
KS5	Active Balmer α spectroscopy	T_D, N_D and $Z_{eff}(r)$	JET	Modified
KS6*	Bragg rotor X-ray spectrometer	Monitor of low and medium Z impurity radiation	UKAEA Culham	Upgraded
KS7*	Poloidal rotation	Multichannel spectroscopic measurement of poloidal rotation	UKAEA Culham	Modified
KT2*	VUV broadband spectroscopy	Impurity survey	UKAEA Culham	Upgraded
KT3	Active phase CX spectroscopy	Full ionized light impurity concentration, $T_i(r)$, rotation velocities	JET	Modified
KT4*	Grazing incidence+visible spectroscopy	Impurity survey	UKAEA Culham	Upgraded
KX1	High resolution X-ray crystal spectroscopy	Central ion temperature, rotation and Ni concentration	ENEA Frascati	
KY3*	Plasma boundary probes	Vertical probe drives for reciprocating Langmuir and surface collector probes	JET, UKAEA Culham and IPP Garching	Modified
KY4	Fixed Langmuir probes (X-point belt limiter)	Edge parameters	JET	Modified
KZ3*	Laser injected trace elements	Particle transport, T_i, impurity behaviour	JET	Upgraded
Kγ1	Gamma rays	Fast ion distribution	JET	Modified

* Not compatible with tritium

JG93.131/1

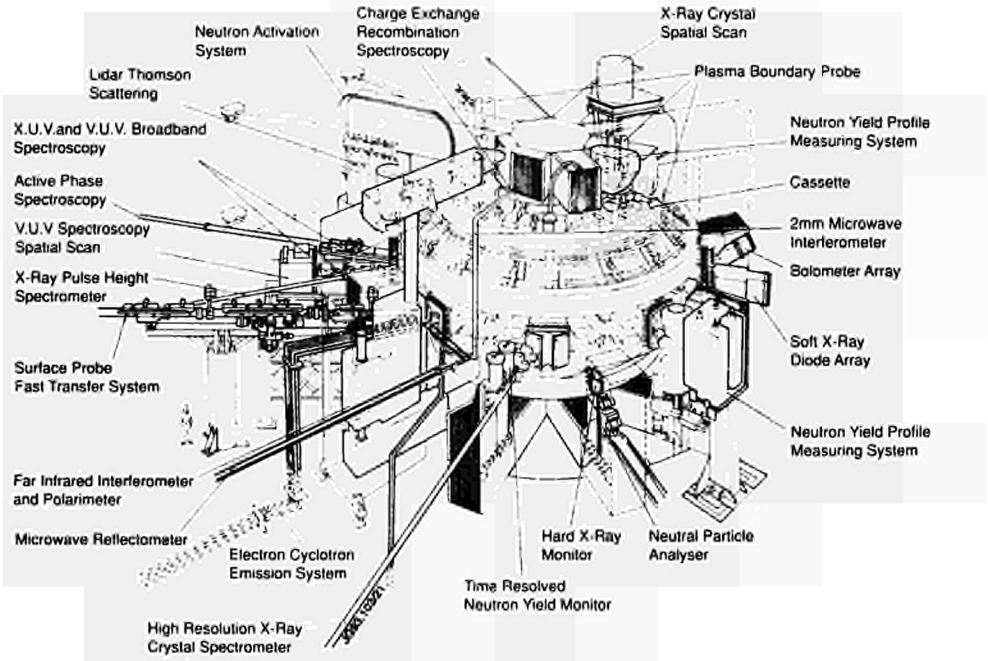

Fig.63: General layout of diagnostics in the JET machine.

ments. The complete set, old and new, will be used for equilibrium reconstruction. Test runs on simulated data indicate that an accuracy of <5mm should be achievable in the identification of the boundary (see Fig.64).

Most new coils are of a single layer ceramic construction as used before. They will operate with bandwidth up to 500kHz. The new ceramic poloidal coils of the set for equilibrium reconstruction will also be used for MHD studies, while the set is further extended at one poloidal position in the toroidal direction. This complete set will allow the study of modes with high m and n numbers.

The data acquisition for the new equilibrium set will be based on VME technology at a rate of up to 10kHz. The MHD signals will be digitised at high rates up to 1MHz, locally stored and selected by means of intelligent triggers. Several new voltage loops will be introduced. Two voltage loops will be attached to the restraint rings at the inboard side of the vessel. These will provide a back-up for external voltage loops and also will provide an absolute reference for flux loops inside vessel. There will also be two voltage loops in the lower divertor coil container with a similar purpose.

Two poloidal voltage loops have now been attached to the inside of the vessel. Estimates indicate that these can be used as diamagnetic loops since the vessel has become sufficiently rigid and this signal will not need to be compensated for the expansion of the toroidal field coil.

Target Langmuir Probes

New Langmuir Probes have been designed for the new divertor geometry. The probe tip will be located in the gaps between the target elements and supported in an isolated holder (Fig.65). The tip is shaped to give the optimum collecting area and the correct orientation to the average field line direction expected. The material will be very fine grain carbon fibre composite. The tip can easily be installed, exchanged and adjusted in height. There will be two coarsely

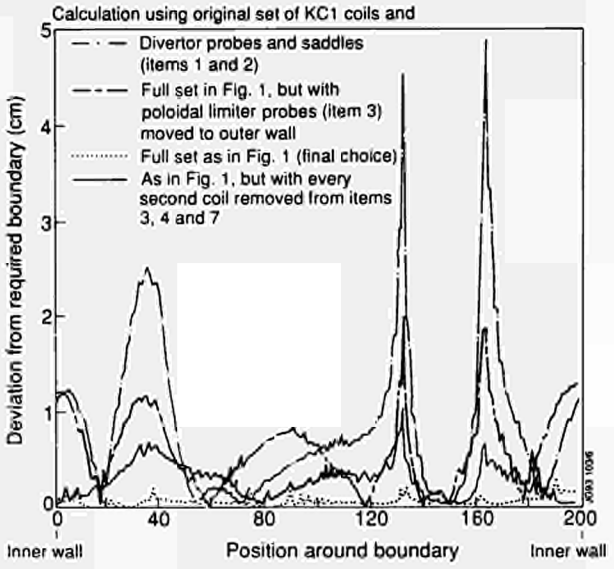

Fig.64: Error in boundary reconstruction (EFIT reconstruction of a PROTEUS equilibrium) with various sets of magnetic detectors. The selected set reduces the errors to below 5mm.

TableXVI
Status of JET Diagnostics Systems, December 1992
Diagnostics under Construction

System	Diagnostic	Purpose	Association	Status
KB3D	Bolometry of divertor region	Power balance of divertor plasma	JET	Mechanical interface manufacture in progress. Final tests of detector element in progress. Procurement of electronics and data acquisition in hand.
KB4	In-vessel bolometer array	Time and space resolved radiated power	JET	Manufacture in progress. Final tests of detector elements in progress. Procurement of electronics and data acquisition in hand.
KC1D	Magnetic pickup coils	Plasma geometry in divertor region	JET	Manufacture in progress.
KD1D	Calorimetry of Mark I divertor targets	Power balance of divertor plasma	JET	Thermocouple installation awaiting delivery of target tiles.
KE4	Fast ion and alpha-particle diagnostic	Space and time resolved velocity distribution	JET	Under construction
KE7	Lidar Thomson scattering	Higher spatial resolution, n_e and T_e in plasma edge	JET	Design
KE9D	Lidar Thomson scattering	T_e and n_e profiles in divertor plasma	JET	In-vessel design complete, procurement in progress.
KG6D	Microwave interferometer	$\int n_e dl$ along many chords in divertor plasma	JET	In-vessel waveguide design complete, procurement in progress.
KG7D	Microwave reflectometer	Peak n_e along many chords in divertor plasma	JET	In-vessel waveguide design complete, ex-vessel microwave design and mockup experiments in progress.
KG8	E-mode reflectometer	Measurement of density profiles in edge and SOL	JET and CFN/ISTLisbon	Design
KJ3	Compact soft X-ray cameras	MHD instabilities, plasma shape	JET	Under construction
KJ4	Compact soft X-ray camera	Toroidal mode number determination	JET	Under construction
KK4D	Electron cyclotron absorption	$n_e T_e$ profile along many chords in divertor plasma	JET	In-vessel waveguide design complete. Ex-vessel microwave design and mockup experiments in progress
KM2	14MeV neutron spectrometer	Neutron spectra in D-T discharges, ion temperatures and energy distributions	UKAEA Harwell	In installation
KM5	14MeV time-of-flight neutron spectrometer		NFR Gothenberg	In installation
KT1D	VUV spatial scan of divertor	Time and space resolved impurity densities	JET	Under construction
KT5D	Toroidal view visible spectroscopy of divertor plasma from Octant No: 7 mid-plane	T_z and V_z, ion temperature and toroidal velocity of impurities	JET	Design in progress. Optics components defined and procurement in progress.
KT6D	Poloidal view visible spectroscopy of divertor plasma using a periscope	Impurity influx, 2-D emissivity profile of lines	JET	Periscope and in-vessel components installed Design of other components and optics in progress
KT7D	VUV and XUV spectroscopy of divertor plasma	Impurity influx, ionization dynamics	JET	Spectrometer in manufacture, mechanical design in hand, procurement of electronics and data acquisition in hand.
KY4D	Langmuir probes in divertor target tiles	ne and Te in the divertor plasma	JET	Thermocouple installation awaiting delivery of target tiles
KY5D	Fast pressure gauges	Neutral flow in divertor region	JET	Manufacture in progress
KY6	50kV lithium atom beam	Parameters of the scrape-off-layer plasma	JET	Source under test. Telescope in manufacture.

JG93.131/2

spaced poloidal sets of eleven probes approximately matching the positions of the magnetic measurements in the divertor module.

In addition, an array of 40 triple probes is planned which will cover the most probable locations of the two strike zones. The triple probes will allow continuous observation of the plasma parameters I_{sat}, T_e and V_{float}. This will be considerable improvement compared to the single probes which must be used in the ramped mode. The triple probes should prove invaluable for fast measurements (10kHz) during ELM activity.

The unit driving the triple probes will deliver up to 10A with the facility of automatic testing of the probe tips and circuit modules. In the event of individual probes failing, remaining probes in the triple probe set will be switched to a single probe mode. The control and data acquisition will be by means of a VME based standard unit.

The long stroke fast scanning probe will be maintained for the new experimental phase. Tests during the last week of previous operation have proven that the CFC probe head is extremely robust. It survived a 2s 10cm deep insertion into a mildly heated divertor plasma (tip temperature ≈ 2500°C). The second stationary probe has been redesigned so that it can also have a long stroke fast scan capability. This probe can carry a variety of heads. In particular, it can expose rotating collector probes and sophisticated retarding field analysers or a plasma ion mass spectrometer.

The Fast Transfer System and the Surface Analysis Station have now been dismantled and removed.

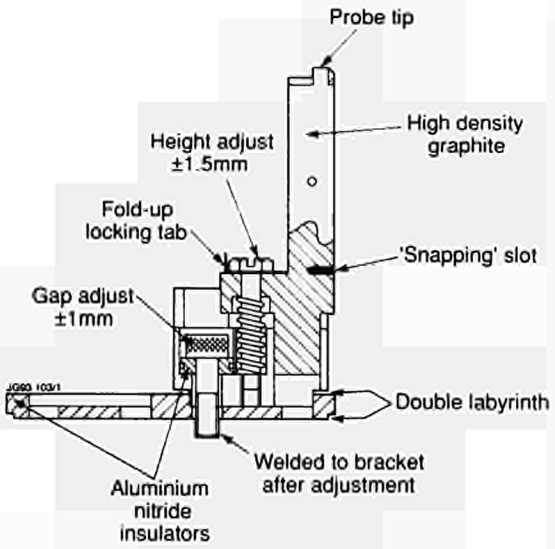

Fig.65: Divertor probe holder

Target Observations

Target observations in visible light and infra-red (IR) are considered vital for the next operational period. These will be used:

- qualitatively, to provide guidance for machine operations and for the optimisation of discharge conditions;
- quantitatively, for evaluating photon fluxes, measuring the temperature distribution on the target and studying fast events (ELM's, X-events, disruptions).

The target will be observed at two toroidal positions (Octant No: 5 and No: 8) from the top and tangentially from the pumping port in Octant No: 1 (wide angle survey camera).

For the observations in the visible and near UV part of the spectrum, two black and white CCD cameras and one colour CCD camera (wide angle view) together with appropriate interference filters will be used. All cameras are being modified to allow either remote or automatic control of their sensitivity by switching the internal integration time. This extends the dynamic range of the cameras significantly. In addition, a 5 channel photon flux detector based on a thermoelectrically cooled CCD will be installed on a vertical port, to measure photon fluxes at five different wavelengths as a function of the major radius and time. This system features high spatial ($\delta R \leq$ 3mm) and medium time resolution ($\delta t \leq 20$ms). Two linear CCD arrays will be used to study fast events. The time resolution of these cameras is about 64μs. These give radially resolved profiles (dR ≤ 3mm) on the target.

It is planned to install a high resolution focal plane cooled IR detector, aligned with the view of the CCD camera. The resolution on the target will be ~3mm, sufficient to observe the poloidal power deposition profile in detail. The selection of a suitable camera is in progress. The CCD video images will be stored on remotely controlled video recorders with an off-line analysis facility, the data of the fast CCD cameras and the IR detector will be stored in a VME data acquisition system. The data of photon flux detector will be stored in the stand-alone PC and transferred to the central storage system.

In-vessel Pressure Gauges

The pressure gauge head has been completely redesigned to make it more robust and easier to manufacture in large quantities (see Fig.66). The new gauge head has been tested successfully and the heads have been delivered. Five modules of the drive electronics are being built. As the total number of gauges in the vessel is 15, a remote switching device is proposed to adapt the mode of operation. Tests have shown that it is an advantage to keep the basic connections to the drive electronics and the filament supply short. The control units are therefore split and connected by optical fibres. Three poloidal sets of five gauges are mounted under the target structure and connected to the surface by means of short pipes, which are 90° toroidally apart.

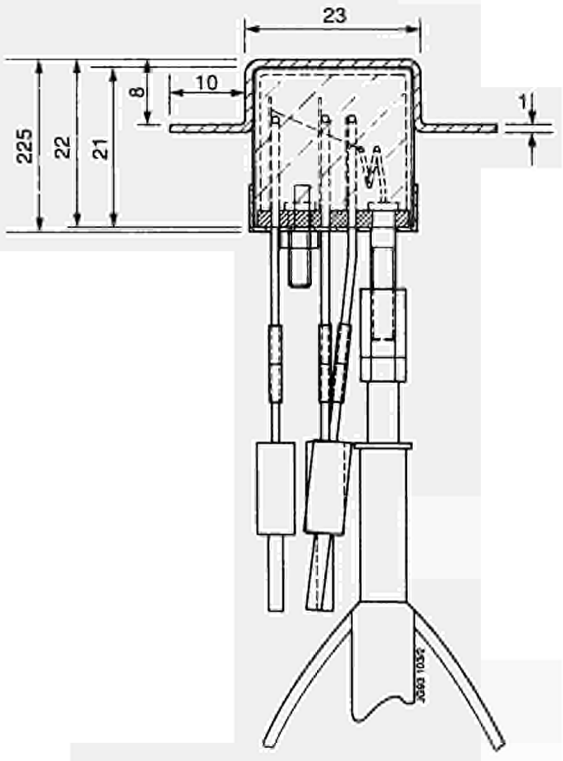

Fig.66: Cross-section of Ionization Gauge.

Lithium Beam Edge Density Diagnostic

Detailed design of the diagnostic and its operating system have been completed successfully. The precise arrangement of some in-vessel protective elements has been changed so that they provide secure protection of the exposed end of the light collection periscope. Most of the major components have either been delivered or are expected shortly.

The lithium source has been assembled and operated using the new control system. Reliable performance has been demonstrated over the required 10s period, with extracted currents >40% higher than design criteria (achieved L_i^+ current > 2mA at ~60keV), with beam divergence close to the anticipated value. The lithium neutralizer is being assembled so that testing of the complete injection system can begin.

The spectrometers and detection equipment are being assembled and tested as items are delivered. All connecting optical fibres and cables are ready for installation. Suitable algorithms have been written, which overcome difficulties in interpretation and allow this diagnostic to be applied to the steep densities expected in JET.

Erosion/Deposition Measurements

For the next generation of tokamaks target erosion is one of the crucial parameters [1]. To relate erosion with plasma parameters, in situ measurements on a shot-by-shot basis are necessary. Several methods have been investigated and assessed for their suitability for JET:

Ellipsometry

Classical ellipsometry has been extended to operate with 2m working distances, this being the shortest distance conceivable in JET [2]. Measurements can readily be made on polished samples of graphite and beryllium, whilst the rough surface of practical samples produces a speckle type pattern from which measurements can still be made. Ellipsometry can be used to measure deposited film thicknesses up to 1mm and has a sensitivity of ~1nm for films on polished surfaces. Erosion can only be measured as the thinning of a pre-deposited layer.

Colour fringe analysis

Thin films when viewed in white light exhibit interference colours which depend on the film thickness. The technique does not depend on specular reflection and is therefore well suited to look at divertor surfaces. In experiments on TEXTOR [3], the technique has been tested by observing a predeposited film on the limiter. A colour television camera has been adapted to observe the colour fringes and software has been developed to calculate the film thickness.

Speckle interferometry

A two wavelength speckle-interferometer produces a fringe pattern reflecting the height contours of the substrate which does not need to be polished or in specular reflection. Tests using the wavelengths 514.5 and 588mm from a CW Ar-ion laser have shown that small steps of ~1mm can be observed. This test was carried out on a laboratory scale of ~0.5m. [4]. Since shot-by-shot erosion in JET is not expected to exceed 1mm, this method cannot be used at JET but has a large potential for next generation machines. These studies have shown that erosion of predeposited film or redeposited film can readily be observed on the JET divertor. However, colour fringe analysis seems to be more suitable than ellipsometry because of the access requirement.

Neutral Helium Beam Target Diagnostics

Two jets of neutral helium are proposed to be injected from between the target elements into the divertor plasma. The flow rate of the two jets can be independently controlled. The spectral emission from the helium can be measured using the periscopes for the D_α emission (Octant No:5). For the electron temperature, the ratio of the 728nm and 706nm lines will be used, whilst for the electron density the ratio of 728nm and 668nm lines.

Neutron Diagnostics for the Next Phase

The neutron diagnostic systems summarized in Table XVII are all expected to be operational at the start of the next campaign. The philosophy underscoring the deployment of these diagnostics is that there will be no clear separation between the operational phase of JET that uses deuterium from that during which deuterium-tritium mixtures will be used. Instead, lengthy periods of deuterium operation interspersed with low level tritium usage may be anticipated, followed (eventually) by the main tritium period during which tritium will be conserved as far as possible, with a possibility of returning to deuterium operation for development of new plasma scenarios. The neutron diagnostics for D-D operation must therefore remain available, in parallel with those specifically for D-T operation, until near the end of the Project. Work is now in progress to implement this philosophy.

Table XVII
Neutron Diagnostic Systems

System	Measured quantities
Time resolved neutron yield monitor. KN1 (Fission chambers) and KM7 (Silicon diodes).	Measures the instantaneous neutron emission strength. Distinction between D-D and D-T neutrons is necessary for triton burnup and low-level tritium diffusion studies.
Activation system. KN2 and KN4. Because of new in-vessel components (divertor), reliable response calculations are possible only for the upper irradiation end inside the vacuum vessel.	Determines absolute neutron yields and hence calibration of time-resolved neutron yield monitors for D-D and D-T neutrons.
2-D neutron camera (D and D-T plasmas). KN3 Upgrade. The upgrade is essential for operation with more than 1 MW of fusion power. It is intended that this diagnostic be in place by the end of 1993.	Measures radial neutron intensity distributions in two directions, the absolute neutron yields, and permits tomographic reconstruction of neutron emission. Study of triton burnup in D-plasmas, to investigate fast particle confinement and to determine n_d/n_e ratios.
Neutron spectrometers (radial and tangential). KM3 - 2.5 MeV neutrons, available. KM2 and KM5 - 14 MeV neutrons, being installed now.	Measurement of neutron energy spectra; separation of thermal and beam-plasma contributions. Identifies neutron production fromICRF-heated particle interactions with impurities. Determines n_d/n_e ratios in D plasmas and n_{fuel}/n_e ratio in D-T plasmas.

Neutron Spectrometers.

The time-of-flight 2.5MeV neutron spectrometer (KM3) is being moved from its position in the Roof Laboratory above Octant No:8 to above Octant No:5. Since the plasma axis for high performance divertor plasmas will be located near 2.90m, instead of 3.25m, it has been necessary to modify the collimation; considerable delay in reassembling the spectrometer has therefore been occasioned. For the same reason, a similar delay has resulted in the installation above Octant No:8 of the 14MeV spectrometer (KM5), constructed by Chalmers University of Technology, Gothenburg, Sweden. The tandem-radiator spectrometer (KM2), constructed by AEA Technology, UK, is to be installed in the Diagnostic Hall, using the beam-line formerly occupied by the Surface Probe Fast Transfer System and thereby avoiding the need for constructing a massive but moveable radiation shield for deployment within the Torus Hall.

Figure.67 shows a 14MeV neutron spectrum, obtained during the Preliminary Tritium Experiment (PTE). It was obtained from an analysis, by Heidelberg University, Germany, of proton recoil tracks in a nuclear emulsion, recorded for Pulse Nos:26147 and 26148. The 14MeV peak was derived from only 30 analyzable tracks. The strength of the

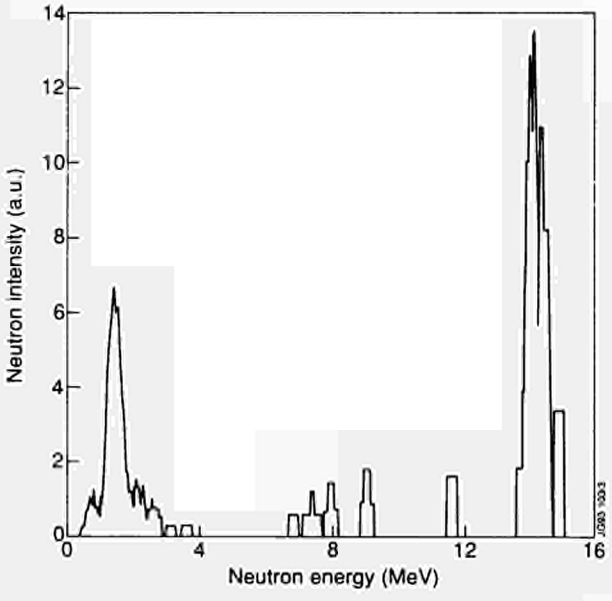

Fig.67: Neutron energy spectrum for D-T discharges Pulses No:26147 and No: 26148, derived from measurements of proton recoil track lengths in a nuclear emulsion. The 14MeV neutrons are distinguished clearly against the weak background of scattered neutrons. The peak just above 1MeV is attributed to (n,p) threshold reactions with ^{13}C in the emulsion.

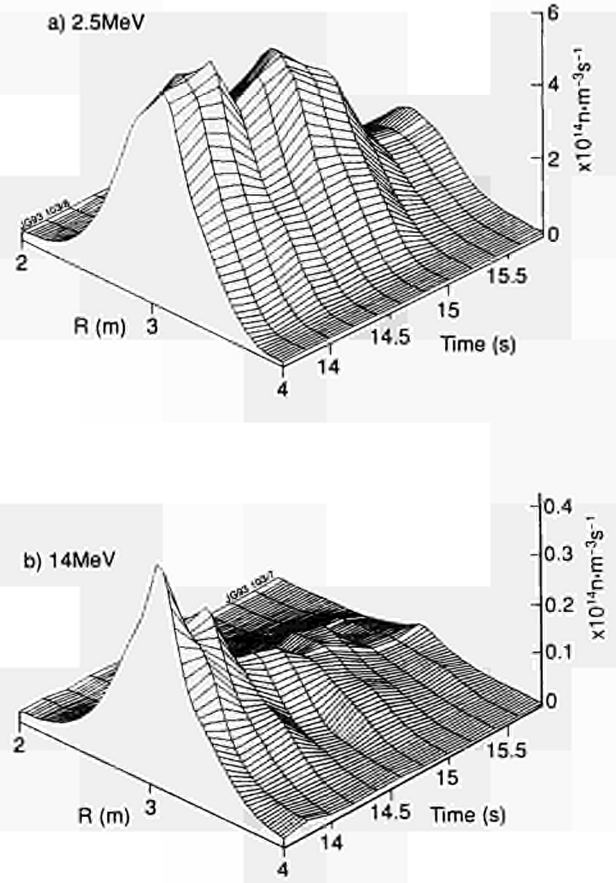

Fig.68:Neutron emissivity profiles along a radial chord at the tokamak midplane plotted versus major radius and time for the (a) 2.5MeV and (b) 14MeV neutrons from (1%) D-T discharge (Pulse No: 26114). Tritium beam injection had terminated by 13.5s and the decay of the thermalized tritium density with a 1.0s decay constant is seen clearly.

neutron emission (~7.2×10^{17} neutrons) is demonstrated by the extreme collimation used: apertures of $1\times1cm^2$ at the vertical of the vacuum vessel and about $4\times1\ cm^2$ in front of the emulsion ~20m distant. The background flux of neutrons is very low in the region 4 to 13MeV. The peak at just above 1MeV is believed to be due to $^{13}C(n,p)^{13}B$ reactions in the emulsion; it has a reaction Q-value of 12.6MeV.

The Neutron Profile Monitor

A major upgrade is being planned for the neutron profile monitor to provide: improved radiation shielding (for D-T operation), remotely adjustable collimation (a choice of two aperture sizes), and provision for three in-line detectors within each collimation channel (a CsI/photodiode for fast-electron bremsstrahlung detection, an NE213 scintillator for D-D neutrons and low intensity D-T neutrons, and a small fast plastic scintillator for high intensity D-T neutrons). The number of channels and their viewing directions will remain unchanged. With these modifications, it will be possible to follow the programme without need for physical access to the profile monitor to exchange detector boxes or collimation in accordance with the programme. It will also be possible, for the first time, to study simultaneously fast electron currents generated through operation of the LHCD system and the effects on the neutron emission profiles.

The capabilities of the present neutron profile monitor were fully exploited during the PTE, when the temporal evolution and 2-D spatial profiles of the 2.5 and 14MeV neutron emissivity from D-D and D-T fusion reactions were measured. These experiments involved D-D fusion production of tritons, tritium beam deposition and diffusion, D-T fusion and the removal of tritium from wall tiles. Four types of plasma conditions were investigated:

(a) High performance deuterium plasmas with deuterium NB injection, which allowed the 14 MeV neutron emissivity due to triton burnup to be observed;

(b) Discharges with 1% tritium NB injection that showed the deposition profiles resulting from T and D beams to be about the same; after injected tritium had thermalized, it was deduced from 2.5 and 14MeV neutron emissivity profiles (Fig.68) that the tritium content decayed with a 1s time constant and that the tritium to deuterium ratio was spatially constant across the plasma, leading to the conclusion that deuterium and tritium have similar particle transport properties;

(c) Two high performance discharges for which two of the sixteen neutral beam injectors operated with 100% tritium, during which the production rate of 14MeV neutrons reached $6\times10^{17}\ n.s^{-1}$. Both the axial 14MeV neutron emissivity and the axial ion temperature saturated before the maximum global emission was reached;

(d) Tritium cleanup discharges, for which the residual tritium entering the plasma produced a spatially constant ratio of tritium to deuterium, providing further evidence for the similarity of their particle transport properties.

The profile monitor has also been exploited in an unexpected way, to obtain tomographic reconstructions of the gamma-radiation emission from reactions between energetic ions produced by ICRF heating and plasma impurity ions. This was only possible since the neutron detectors are sensitive to gamma-radiation and signal processing equipment is provided to distinguish neutron from gamma-ray induced events. Normally, the gamma-radiation background due to neutron scattering and capture in the wall materials is

proportional only to the total neutron emission and is independent of such plasma properties as shape and position. However, with strong ICRF heating, high impurity levels and electronic discrimination levels set to maximize (rather than minimize) the gamma-ray signal, it has been possible to extract signals proportional to the spatial distribution of those ions heated to MeV energies. This has been accomplished for an RF resonance scan (Pulse Nos: 23448 to 23462) in which ~10MW ICRF power, tuned to ^{3}He minority ions using monopole phasing, was applied to 3.5MA deuterium plasmas while the toroidal field was varied from 2.6 to 3.4T in successive pulses; the position of the resonance moved from 2.85 to 3.33m. The tomographic image in Fig.69 was typical. The gamma-ray emission is attributed to ^{3}He ions interacting with ^{9}Be impurity ions; in all cases, a pronounced peak was observed, displaced between 7 and 19cm to the low field side of the resonance layer (the position is uncertain to ±5cm). Almost the entire distribution lies to the low field side, as appropriate to trapped ion orbits.

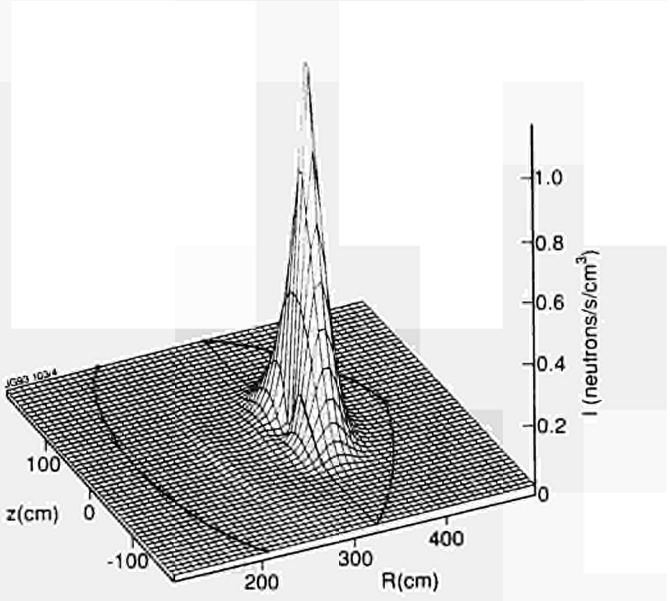

Fig.69: Tomographic reconstruction of gamma-radiation emitted from reactions between MeV ^{3}He ions and ^{9}Be impurity ions during ICRF heating of a D plasma (Pulse No: 23450). The fast ion density distribution is strongly peaked on the machine mid-plane ~0.07m from the low field side of the resonance layer, located at 3.38m. The centre is at 3.01m.

Runaway Electrons

Examination of carbon limiter tiles for their ^{7}Be contents has previously been used as an indication of the intensity of high energy runaway electron currents generated following major plasma disruptions. The present shutdown afforded an opportunity to study a large set of tiles to determine the toroidal symmetry of the activation, which provides an indication of the accuracy with which the tiles are located relative to the magnetic flux surfaces. However, the developing nature of the programme has given rise to some ambiguities. Runaway electrons are generated during major plasma disruptions as a highly transient effect but may also be created continuously during low density operation, as required for LHCD. Such energetic electrons ultimately collide with various plasma facing components, i.e. limiters, X-point tiles and other protecting surfaces. These surfaces are made either of carbon or beryllium. Very energetic electrons (>30MeV) can induce spallation reactions leading to ^{7}Be formation in either material. ^{7}Be cannot be generated through reactions with 14MeV neutrons; it has a 53.3 day half-life and emits a characteristic decay gamma-ray. Unfortunately, another formation mechanism exists; it is generated from ^{9}Be, present either as a limiter material or as impurities in the plasma, by nuclear reactions with (several MeV) ^{3}He ions accelerated by ICRF; redistribution could then bring the ^{7}Be to the dump plate tiles. However, as high power RF heating of minority ^{3}He ions in low density plasmas has not been a strong feature of the campaign, it is estimated that the ^{7}Be found in these tiles is indicative of the presence of very high energy runaway electrons.

A large number of carbon tiles removed from the vacuum vessel at the start of the present shutdown have been examined for their ^{7}Be content. In particular, tiles taken from the inner-most ring of X-point dump plates have been found to have comparable ^{7}Be content (see Fig.70), although an

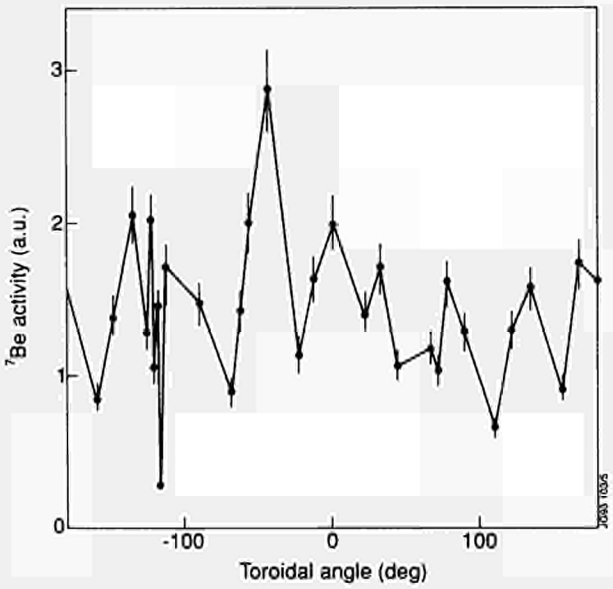

Fig.70: ^{7}Be activity deduced from 478keV decay gamma-rays emitted from a toroidal ring of carbon tiles in the upper dump plates; the radioactive decay has been corrected to refer to the time of the last discharge. A periodic structure is seen, indicating the tiles are nearly equidistant from the last closed flux surface.

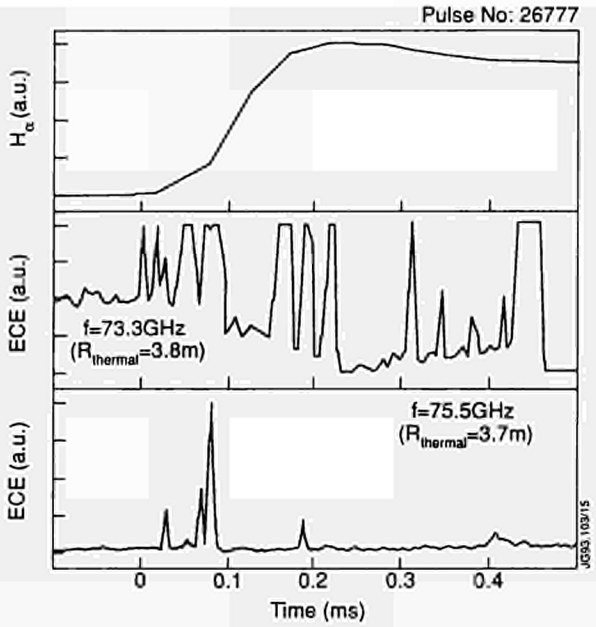

Fig.71:An example of heterodyne radiometer measurements of ECE from near the plasma edge. The signals from two radiometer channels (lower traces) were recorded using the fast data acquisition system, at a sampling rate of 200kHz, around the time of an ELM. They show a compled structure, varying from channel to channel, not seen on the H_α signal (upper trace).

eight-fold periodicity can be discerned, with the highest activity at the joins between structural groups of tiles. Runaway electrons rapidly explore an entire flux surface and will be intercepted and lost at any intruding object. The fact that the observed ^{7}Be production lacks a strong toroidal dependence implies that the X-point tiles are aligned to an accuracy of a few mm. It is estimated that a total of 10^{15} ^{7}Be ions were held in graphite tiles at the end of the 1992 period of operation; production of a ^{7}Be nucleus from ^{12}C is generally accompanied by emission of a neutron. The total number of neutrons associated with disruptions during the last two months of operation is 5×10^{15}, so the ^{7}Be inventory is indeed compatible with production by disruption generated runaway electrons.

Alpha-Particle Diagnostics

The neutron measurements will define the alpha-particle birth profile in space and time. In principle, it should be possible to diagnose the slowing down alpha-particle population through the gamma-ray emission resulting from interactions with beryllium impurity ions in the plasma. This is a difficult measurement and does not have a high probability for success. An extremely high count-rate, gain stable, carefully calibrated gamma-ray detector is required.

Measurements of the loss of energetic alpha-particles to the walls would be most interesting. JET offers a particularly difficult environment for this type of diagnostic due to 350°C wall temperatures. However, it is possible that small diamond solid state detectors may offer appropriate sensitivity and environmental compatibility. These detectors would be wall mounted in a manner reminiscent of Langmuir probes. Sample detectors are being obtained for testing.

Electron Cyclotron Emission (ECE) System

During operation, ECE measurements were made routinely with the standard instrumentation - a rapid scan Michelson interferometer, a grating polychromator and a multichannel heterodyne radiometer. From the measurements, the electron temperature is obtained with good spatial and temporal resolutions. Typical measurements with the heterodyne radiometer using fast data acquisition are shown in Fig.71.

At the beginning of the shutdown, modifications and upgrades of some of the ECE instrumentation were initiated. The in-vessel ECE antennae are being modified to accommodate upward vertical displacement (~0.3 m) of the plasma centre which will result from the new plasma configuration. The fan array of six antennae which view the whole poloidal cross-section has been removed, and will be replaced with three antennae viewing around the new mid-plane location plus a fourth which will have an oblique line-of-sight through the plasma centre. This new arrangement will allow several instruments to make simultaneous measurements on sightlines through the plasma centre. The windows on the vacuum vessel are being changed to double windows so that the system will be fully compatible with the D-T phase.

The heterodyne radiometer is being upgraded in two respects. The antenna spot size is being reduced by installing a Gaussian beam collection system. A pair of relay mirrors inside the vacuum vessel will focus radiation through the vacuum window into a pair of back-to-back scalar feed horns. The small diameter constriction between the two horns will pass only the lowest order mode. The exit feed horn will be connected to oversized waveguide which will transmit the radiation through the biological shield to the radiometer. It is expected that this arrangement will give an antenna pattern of low divergence, with a spot size ~0.1m in diameter. In addition, the frequency coverage of the radiometer is being increased by the addition of two further mixers. Combined with the existing mixers, this will give complete coverage of 73 to 139GHz at ~ 1 GHz intervals. It will then

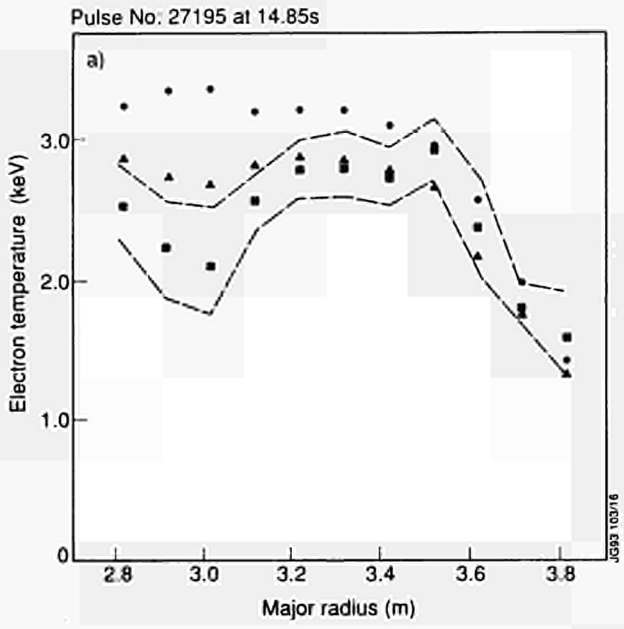

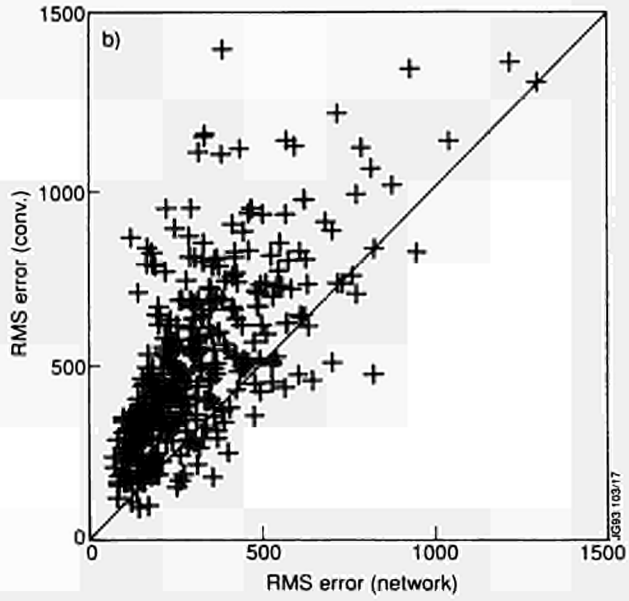

Fig.72: Preliminary results from the neural network analysis of ECE data. (a) shows a typical example of the improved agreement between ECE and LIDAR Thomson scattering T_e profiles. The ECE profile obtained by the conventional analysis (circles) is modified by the network to give a profile (triangles) which is much closer to the LIDAR (squares, with the estimated statistical error as dashed lines). In part (b) the difference between the ECE and LIDAR profiles, characterised as the RMS error across the profile. The error values from the network generated profiles are in general less than those from the conventional analysis.

be possible to measure the electron temperature with a spatial resolution 5 cm in the outer half of the plasma for all toroidal fields between 1.7 and 3.4T. For lower magnetic fields, the measurements will be made using the second harmonic extraordinary mode while for the higher fields the fundamental ordinary mode will be employed.

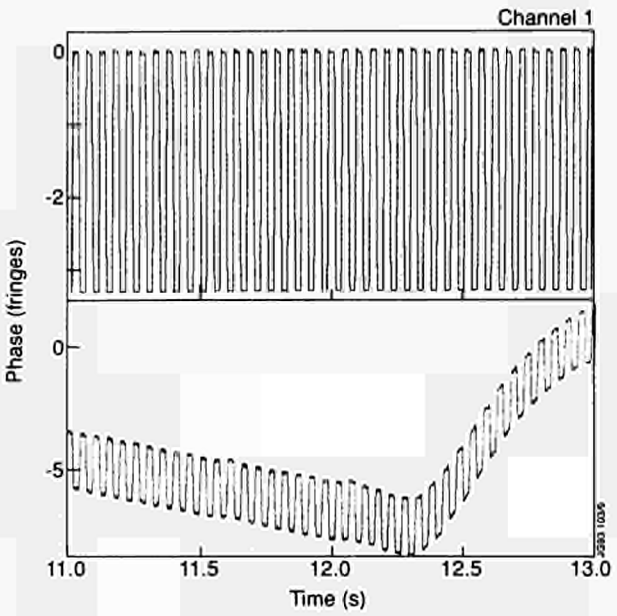

Fig.73: Measured phase changes in one channel of the reflectometer due to the trapeze mode frequency sweep of the source. The channel operates at 18.3GHz and so probes the edge density at 4.3 x 10^{18} m^{-3}. The upper trace is obtained with the back wall of the vacuum vessel and serves as a calibration measurement while the lower trace is obtained with the plasma. At 12.3s, the gas feed is switched on and the density layer moves inwards.

A novel technique using neural networks for the conversion of ECE spectra to electron temperature profiles is being investigated under a contract with AEA Technology, Harwell, UK. The aim is to obtain temperature profiles from ECE measurements with a reduced level of systematic uncertainty, while maintaining the low random uncertainties and good time resolution characteristic of ECE data. This is done by training a neural network to make the conversion from spectrum to profile, using temperature profiles measured by the LIDAR Thomson scattering as examples of the desired result. Various network configurations are being trained on a dataset consisting of about 2000 pairs of simultaneously measured ECE spectra and LIDAR profiles. Preliminary results are shown in Fig.72.

Microwave Reflectometry

The multichannel reflectometer operated routinely and reliably throughout the experimental campaign and provided measurements of the edge electron density profile and measurements of density transients and fluctuations.

A new method has been developed for operating the reflectometer and processing the data. The source frequencies are swept in a trapeze mode in which each frequency sweep up or down is followed by a fixed frequency period (Fig.73). The difference between the upper and lower values

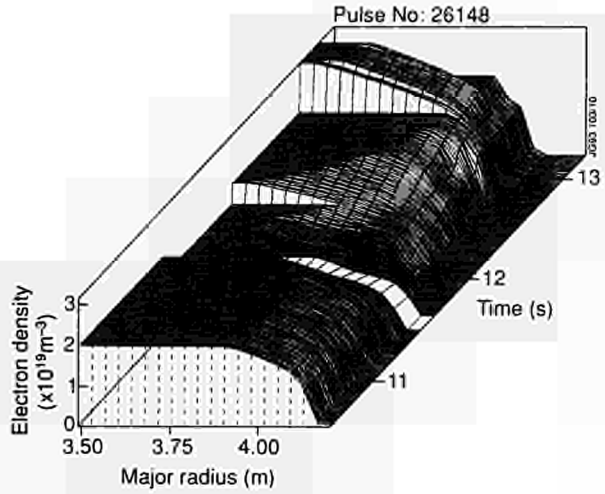

Fig.74: Density profiles measured with the multichannel reflectometer. The changes in the density profile associated with the formation of the X-point at 11.5s and the onset of the H-mode at 12.0s are clearly visible.

of the phase gives the phase difference ($\Delta\varphi$) generated by the frequency sweep (Δf). The group delay, (the difference between the time delay of the microwaves propagating through the plasma path and the reference path, $\tau = (2\pi)^{-1} \Delta\phi/\Delta f$), is readily determined. An accurate continuous measurement of τ for each probing channel is obtained from which the time development of the density profile is obtained by inversion. In the analysis, erroneous fringe jumps are detected and corrected and periods when the return signal from the plasma is lost are identified. This eliminates spurious contributions to the phase measurements. The procedure yields density profiles in which the position of the probed density layers is known absolutely to ± 3cm. Movement of the density layers can be monitored with mm accuracy. The measurement accuracy is so high that it is necessary to correct for the change of the position of the probed density layer due to the finite sweep of the source, and for relativistic modifications of the plasma refractive index. In the latter case, measurements of the electron temperature are included in the analysis. An example of measured density profiles is shown in Fig.74.

Comparisons have been made of density profiles measured with the reflectometer with profiles measured with the LIDAR Thomson scattering system and with the multichannel far infrared interferometer. Usually the profiles agree (Fig.75(a)) but under some conditions there is an apparent systematic difference with the edge of the interferometer profile being at smaller values of the major radius than the reflectometer and LIDAR profiles (Fig.75(b)). The position of the edge of the interferometer profile is determined

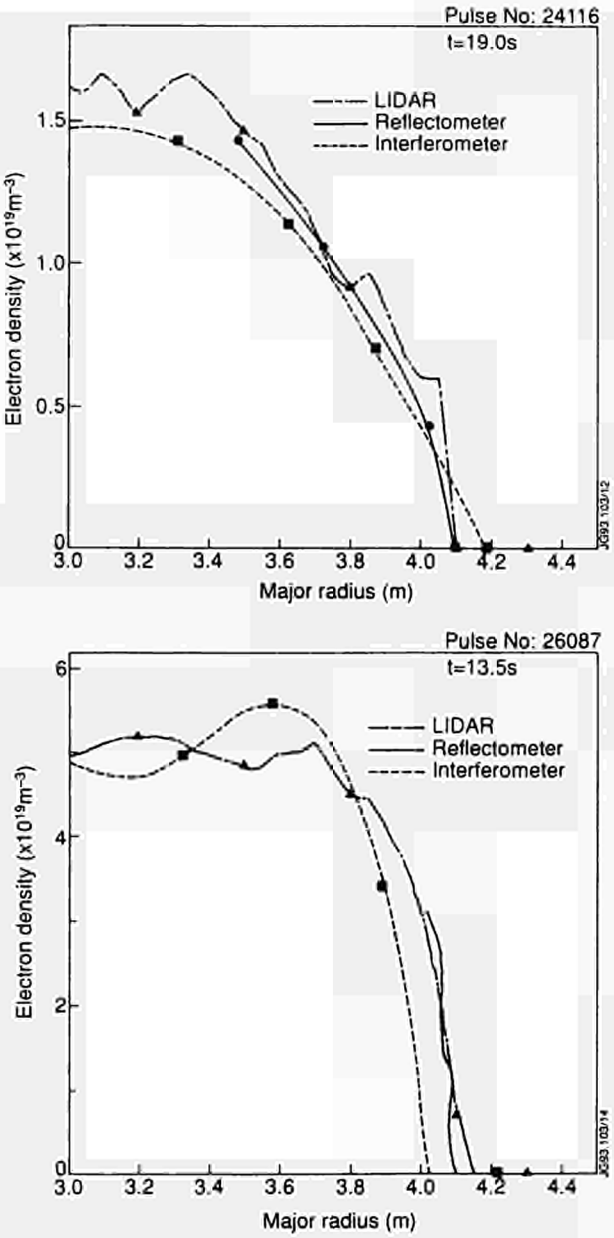

Fig.75: Density profiles measured with the reflectometer compared with those measured by LIDAR Thomson scattering and the far infrared interferometer. The profiles usually agree within the measurement uncertainties as shown in (a), but in some cases significant differences exist as in (b).

by a reconstruction of the magnetic flux contours from independent measurements with the magnetics diagnostic and is believed to be accurate to ±1cm. Investigations are in progress to try to determine the cause of this discrepancy.

JET plasma temperatures are sufficiently high that relativistic modification to the plasma refractive index may have to be taken into account in the reconstruction of the density profiles from the reflectometer measurements. The refractive indices and the cut-off conditions for electromagnetic waves in plasmas were investigated for cold, hot and relativistic plasma models. Significant relativistic modifi-

cations were needed in regimes relevant for reflectometry in large tokamaks. For the extraordinary mode, these effects may shift the location of the reflecting layer by a significant fraction of the minor radius and use of the cold model may lead to considerable underestimations of the density profile (see Fig.76). For the ordinary mode, relativistic effects are smaller but can still be significant. The codes for analysing data from multichannel reflectometer have been modified to take relativistic effects into account.

Thomson Scattering

The LIDAR Thomson scattering system operated reliably until the end of the experimental campaign giving accurate measurements of electron density and temperature profiles on most plasma pulses.

The construction of the new 4Hz ruby laser system was completed and the laser was extensively tested at the manufacturers and again on installation at JET. The key performance parameters are:

Wavelength	694nm
Pulse duration	300ps
Pulse energy	1-2J
Beam divergence	500μrad
Period of pulse train burst	20s
Time between bursts	5-10min
Beam diam	20mm
Repetition rate	4Hz

The roof laboratory was extensively modified so that the new laser and the existing lasers (the 0.5Hz LIDAR laser and the original laser for the single point scattering system) can all be accommodated.

A scheme for combining the beam from the existing 0.5Hz LIDAR ruby laser and the new 4Hz laser beam along the same beam path is being developed (Fig.77). The lasers are set up with orthogonal polarizations. A mirror which reflects vertical and transmits horizontal polarized ruby laser light is used to combine the two beams. A pulsed faraday rotator, triggered synchronously with the 0.5Hz laser, flips this beam polarization into the vertical plane. The divertor LIDAR laser is also combined along the same beam path using another polarization selective mirror. A similar mirror in the vicinity of the floor penetration separates the standard and divertor input beams and directs them down their respective paths to the torus.

The spectrometer is being modified to improve the low temperature limit of the standard LIDAR system. The angle of the first filter in the spectrometer is being changed to extend the lowest measurable temperature from 200eV down to 50eV.

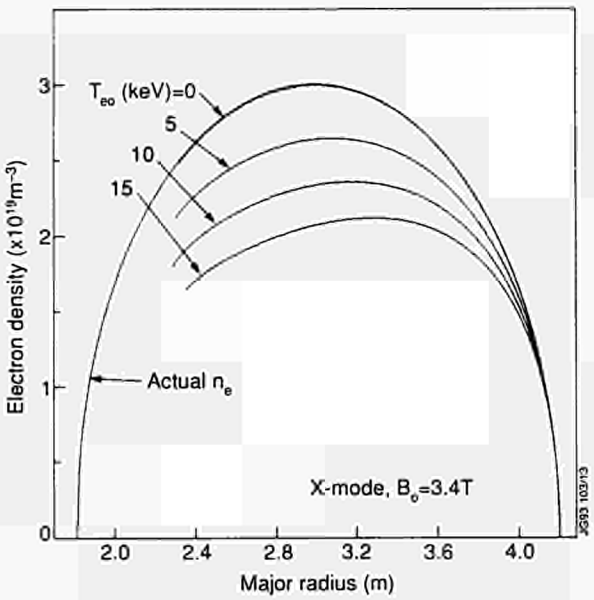

Fig.76: Model density profile and reconstructed density profiles derived using a cold analysis of simulated extraordinary mode reflectometry data. The simulated data were produced numerically from the model density profile, taking relativistic effects into account and assuming a parabolic temperature profile with a central temperature of T_{eo} = 0, 5, 10, 15keV. The central magnetic field was assumed to be 3.4T

Fast Ion and Alpha Particle Diagnostic

The commissioning of the fast-ion and alpha particle system was continued during early-1992, but had to be discontinued before the end of plasma operation due to technical difficulties and equipment failures. The 60kW, 140GHz gyrotron, on loan from the US DoE developed a vacuum leak in the

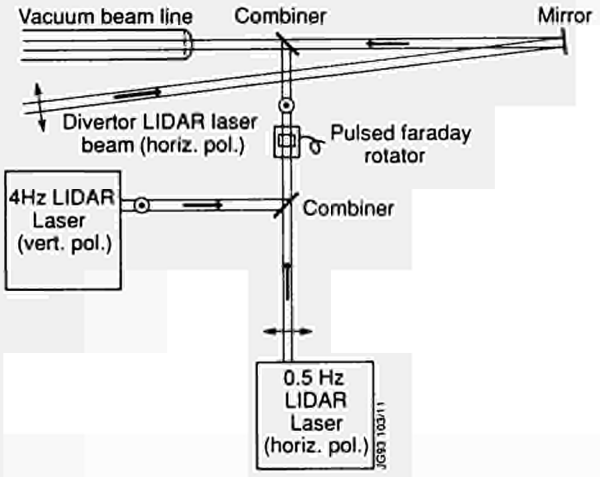

Fig.77: Schematic of the system for combining the beams from the two lasers on the main horizontal LIDAR system with the beam from the laser on the divertor LIDAR system.

window due to long term corrosion and could not be rapidly repaired. Difficulties were also experienced with the power supplies and drives to the steerable mirrors mounted inside the vacuum vessel. Therefore, it was not possible to carry out the planned preliminary scattering experiments. Nevertheless, many technical systems were tested and commissioned and useful experience gained.

The detection system was fully commissioned and used to measure the ECE level in the vertical direction. It is expected that this emission will be the dominant source of noise in the scattering measurements. The emission level at 140GHz and with a central toroidal field of 3.3T was in the range 50 - 500eV depending on plasma conditions - the lower value corresponding to low current ohmically heated plasmas, while the higher value corresponded to plasmas with 30MW of heating. This corresponded closely to the emission (500eV) assumed in initial predictions of signal-to-noise to be achieved in the scattering measurements and so this is encouraging. At lower magnetic fields the plasma radiation increased substantially as expected. Also, with 2MW LHCD, the emission increased substantially, as expected, due to the presence of suprathermal electrons. The equivalent noise temperature of the heterodyne receiver at the receiver antenna was 50 - 80eV, depending on frequency channel. Specialist staff from the Massachasetts Institute of Technology, USA, (under a collaborative agreement with the US DoE) and from ENEA, Frascati, Italy, (under an Article 14 Agreement) spent periods at JET and contributed to these measurements.

At the beginning of the shutdown, a programme of technical improvements to overcome difficulties experienced during commissioning was initiated. Also, substantial modifications are now necessary to make the diagnostic compatible with the new divertor geometry. New in-vessel steerable mirrors for launching and receiving the radiation are being designed and the equipment to drive the mirrors is being improved. The received radiation will be transmitted to the detection waveguide run using small diameter corrugated waveguide specially shaped to go around the divertor coil. The vacuum windows will be replaced by double disk windows and will be mounted vertically to avoid contamination previously observed. With the new divertor geometry, the in-vessel components can no longer be supported externally independent from the vacuum vessel. Instead these will be mounted on the vessel wall. Differential movement between the launch and receive systems is therefore a possibility due to small deformations in the vessel. Also, the launch and receive geometry is no longer symmetric. To maintain alignment between the launch and receive beams, a real-time feedback system which measures and maximises the overlap of the beams is being developed. The system operates by measuring the total scattered power in orthogonal directions with additional receivers. A laboratory facility which utilizes expanded polystyrene beads as a simulated plasma scattering medium is being constructed and will be used to develop and test this system.

Technical difficulties were experienced in the manufacture of the high power (400kW), 140GHz, gyrotron and have delayed the delivery of this tube. However, a short pulse (100ms), high power prototype gyrotron has been loaned to JET as part of the collaborative agreement with the US DoE and will be used for initial system commissioning. The diagnostic will be operated and controlled from the Control Room with a central control system. In operation, the diagnostic will generate a substantial quantity of data and the software to process and analyse the data using the central IBM computer is being developed.

Theoretical work in support of the experimental and technical work has continued. Spatial dispersion was included in the derivation of the equation of transfer and the expression for the scattering cross-section, allowing the dielectric properties of the plasma to be described by models which take thermal motion into account. On the basis of the kinetic description of the plasma, the complete expression was derived, in the cold plasma limit, for the source current which drives the scattered field. Errors in earlier derivations were noted.

Electron Density and Temperature Diagnostics for the Pumped Divertor

Preparation of the divertor LIDAR Thomson Scattering system and the integrated set of microwave diagnostics has continued. These systems will measure the electron density and temperature of the plasma in the pumped divertor region. The design of the LIDAR system is almost complete and several of the most important components have been manufactured and are currently under test. In particular, the in-vessel mirror boom is manufactured and mounted in a test chamber for thermal cycling. A prototype of the double bellows wobble stick drives with an acceptable wind-up under maximum load, has been manufactured and is currently being tested at a temperature of 250°C. Tests have been conducted of some of the in-vessel components and possible optical coatings for use at the elevated vessel

temperatures (~ 400°C). These have shown that it is not possible to use dielectric coatings in the vessel and so it will not be possible to use a mirror to steer the input laser beam. Instead, the beam will be steered by internal reflection in a quartz prism, which has both the input and output faces at the Brewster angle. Tests with a high power laser have shown no damage at the expected energy level. The in-vessel collection mirrors will probably be near surface silver mirrors with a protective coating over the silver. The curved mirror in the collection system will have a cylindrical front face to minimise astigmatism.

Accurate beam steering will be employed so that the laser beam will be directed through the gap in the target plates. However, in case the beam steering fails, tests have been performed to assess possible damage caused by the highly focused laser beam hitting the coil casing. These have shown that in some circumstances damage could occur and so a protective strap is being fitted to the coil casing in this region.

The original intention was to make this measurement with the laser used on the main horizontal LIDAR system by switching the direction of the laser beam when a measurement was required. However, work carried out in collaboration with the Kurchatov Institute, Moscow, Russia has shown that it should be possible to modify the laser used on the original single-point Thomson scattering system to make it suitable for this measurement. The main requirement is to reduce the pulse length to 300ps. This is an attractive possibility since it would make the two systems independent.

Recently new holographic notch filters have been developed. These have a rejection of 10^5 at the ruby wavelength (λ_r) and a transmission of 80% outside the band $\lambda_r \pm 5$nm. Such filters make possible the use of a grating spectrometer to spectrally analyse the scattered signal and the present plan is to use such a device for this system. The detector will be the existing streak-camera fitted with the Peltier cooled CCD camera. The time resolution of the camera is 100ps which when compared with the expected 300ps laser pulse gives an overall spatial resolution of 5cm. The microwave system will consist of a dual frequency interferometer, a multi-frequency "comb" reflectometer and an electron cyclotron absorption diagnostic. Due to limited access in the divertor region, the three systems will share a common set of waveguides and antennae. There will be three sightlines through the divertor plasma, two on the outboard side and one on the inboard side (Fig.78).

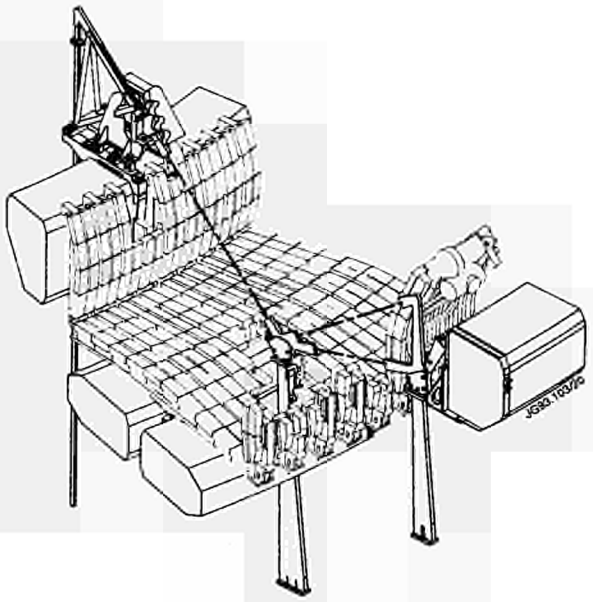

Fig.78: A three-dimensional view of a section of the pumped divertor showing the location of microwave diagnostic antennae and their sightlines across the divertor plasma.The six antennae are arranged in three pairs, giving two lines of transmission through the outboard divertor channel plasma and one on the inboard side.

The dual frequency interferometer is being built by AEA Fusion, Culham Laboratory, UK. To minimise losses, quasi-optical components are used for signal transmission in the vicinity of the sources and detectors. In the original design, which assumed that the source and detection system would be constructed from waveguide components, the upper probing frequency was constrained to be not greater than ~ 170GHz (with the lower probing frequency at 130GHz), but the use of a quasi-optical system allows this constraint to be relaxed and the upper frequency has been increased to 200GHz. For a fixed resolution in the measurement of phase, the increased difference between the probing frequencies to a value of 70GHz improves the accuracy of the measurement of the line integrated density by a factor of 1.48. Delivery is planned for August 1993 and installation and commissioning will be carried out in the Autumn.

The electron cyclotron absorption (ECA) diagnostic will determine the electron density-temperature product (the electron pressure) over a wide range of divertor plasma parameters. It relies on a measurement of the absorption by the plasma of microwave radiation from an external source. Since it is necessary to use conventional microwave sources to obtain sufficient power, and these produce highly coherent radiation, the suppression of standing waves is an important technical issue. This problem has been the focus of much effort. The design adopted uses rapid, linear sweep-

ing of the source frequency, with power from the source being divided between a fixed reference arm and the plasma arm. Mixing of the return radiation from these arms generates a fixed beat frequency in a heterodyne detector. Any radiation which has experienced multipassing due to spurious reflections, and would cause standing waves, can be removed since it causes a different beat frequency. A prototype instrument which operates on this principle has been constructed, to verify the required standing wave suppression and to act as a testbed for microwave hardware. It employs a solid-state source which can be rapidly swept in frequency, has a fixed reference arm, a long oversized waveguide arm and a liquid helium cooled heterodyne detector. Included in the waveguide arm is a variable length cavity to generate the multi-passing of radiation which leads to standing waves. This simulates the imperfections in the long and complex waveguide which transmit radiation to and from the divertor plasma. The reference arm is required to have almost the same length as the waveguide arm, but the power is transmitted as a Gaussian beam in free space, so that multi-passing in this arm is minimised. Measurements with the prototype have highlighted the difficulty of completely suppressing standing waves, but have shown that the optical configuration, and the principle of rapid frequency sweeping, are suitable. The prototype is now being used in the development of the hardware for the linear sweeping of the backward wave oscillator sources to be used in the final system, and for development of signal processing software.

The 'comb' reflectometer, for estimating the peak electron density in the divertor plasma, will be designed and implemented in collaboration with the Centro de Fusão Nuclear, Associação Euratom/IST, Lisbon, Portugal. A prototype 'comb' reflectometer has already been used to estimate the peak density in the X-point region of JET. The maximum probing frequency in reflection was determined by the level of fluctuations on the reflected signals. However, results showed that this method is not always reliable: changes in the plasma, e.g. L- to H-mode transitions, or movements of the reflecting layers can introduce changes in the fluctuation level, which can be confused with changes due to the onset of reflection. To avoid this problem, the instrument being prepared will record simultaneously the transmitted signal as well as the reflected signal. The amplitude of the launched microwave power will be modulated, and the receivers will incorporate narrow band filters at the modulation frequency, so that high signal to noise ratios will be achieved.

Far Infra-Red Interferometer and Polarimeter

Major modifications and refurbishment of the interferometer/polarimeter system were started in 1992, to adjust to the new machine and plasma configurations of the pumped-divertor. The C-frame, housing the optical train for the different interferometer paths, will be rebuilt to accommodate new paths. The finished system will have four vertical chords intersecting the torus mid-plane at major radii R=1.89m, 2.69m, 3.02m and 3.75m. Four lateral chords, injected from the main horizontal port, will intersect the vertical axis (z) through the plasma centre, R=3m, at z=0.2m, -0.15m, -0.38m and -0.61m, giving eight interferometer chords in one poloidal plane. Refurbishment of power supplies, improvements to control of laser output and steering for both the 195μm main interferometer laser and 118μm laser for the compensating interferometer are underway.

New VME based electronics will be employed to count interference fringes, permitting fast tracking of both amplitudes and phase shifts. A prototype of the new fringe counters was tested at the end of the 1992 operating period. The high time resolution achieved during intervals in which rapid plasma changes occur enabled measurement during major disruptions. A large increase of electron density observed during disruptions has provided vital experimental evidence for elucidation of these events in JET [5]. Rates of density increase of up to 6×10^{20} m^{-3} s^{-1} have been measured.

Substantial use of the far-infrared polarimetric measurement of the radial poloidal magnetic field profile employing Faraday rotation continued vigorously during the operation period. Emphasis was placed on direct comparison between Faraday rotation and motional Stark effect measurements of Bq(r). Agreement was found [6], giving further credence to an earlier result that the safety factor on axis in JET remained well below unity throughout a sawtooth cycle. Its magnitude varied with experimental conditions and was typically $0.7 \leq q(0) \leq 0.85$.

Low Energy Neutral Particle Analyser

This instrument was operated routinely during the 1991/92 campaign. It performed measurements for deduction of bulk ion temperature T_i and ratios of the densities of the hydrogenic ions in the plasma. The instrument was disassembled for refurbishment and relocation to a horizontal line-of-sight crossing the plasma centre at Octant No:3. This was necessitated by obstruction of the previous vertical line-of-sight from the bottom of Octant No:1 by the pumped

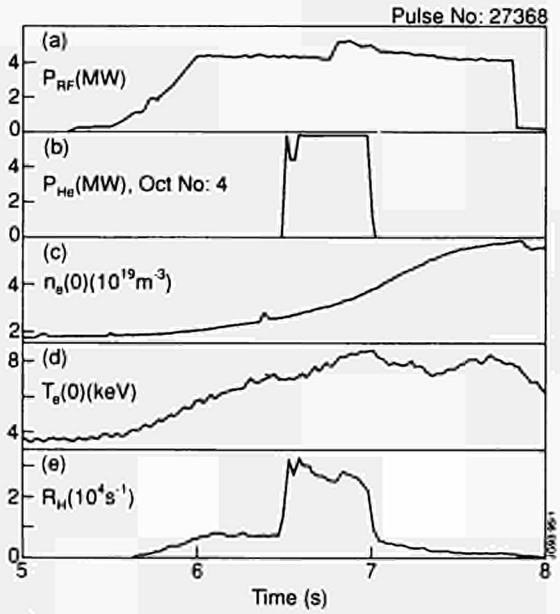

Fig.79: Hydrogen-minority ICRF heating of a deuterium plasma with B_f=2.8T, and I_f=3.5MA, showing traces (a) ICRF heating power at 42.6MHz with deposition peaked near plasma centre, (b) power from 120kV beam of $^4He^0$ atoms from Octant No:4 injectors, (c) central density; (d) central electron temperature; (e) count rate of H^0 flux received in the 0.42MeV channel of the NPA showing good count rate giving low error.

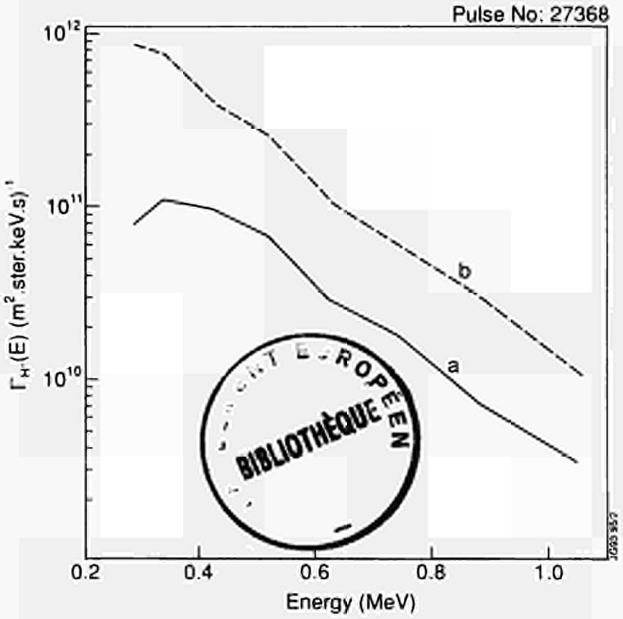

Fig.80: Energy spectra for H^0 at 6.4s and 6.6s, for (a) passive flux and (b) active flux. The former arises due to charge exchange between protons and impurity ions, the latter is a combination of charge exchange with impurity ions and direct charge exchange with $^4He^0$ atoms from Octant No:4 injectors.

divertor. The new location gives an opportunity to improve neutron shielding of the analyser. The old shielding attenuated the neutron flux by a factor < 30 which was just tolerable during the PTE. A new shield, consisting of layers of water extended polyethylene and lead, should give factor ~50 in neutron attenuation. The new assembly will allow more shielding material to be added later if needed.

High Energy Neutral Particle Analyser

A high energy neutral particle analyser (NPA) able to make absolute time resolved measurements of flux and energy spectra of H, D, T, ^{3}He and ^{4}He atoms emitted by the plasma, in the energy range 0.5-3.5MeV, was deployed during the last experimental period. At the end of the campaign, the borrowed prototype device, developed by the A F Ioffe Physical-Technical Institute, St. Petersburg, Russia, was returned to undergo further tests and recalibration using a cyclotron beam source. An instrument suitable for deployment during D-T operations is in manufacture, for installation in 1993.

The NPA was located at the top of torus at Octant No:4 with its vertical line-of-sight intersecting Octant No:4 injected beams at the plasma centre at R=3.07m. The projection of the NPA collimator on the torus mid-plane was 8cmx7cm and the collecting solid-angle was 1.3×10^{-6} sterad; the beam line geometry determined that only atoms with $v_\phi/v_z \leq 7\times10^{-3}$ entered the NPA. The observed flux arises mainly from ions near the plasma centre. Many experiments were carried out to study the creation, transport and loss of high energy ions produced by fusion reactions or by ICRF heating [7,8]. Higher priority is now placed on elucidating the observed efficient neutralisation of MeV energy protons during H-minority ICRF heating of deuterium plasmas [7]. A programme of investigations of atomic collisional processes between impurity ions and MeV protons, and of modelling plasma behaviour in respect of MeV ion neutralisation has started.

Figure 79 shows the evolution of plasma and heating parameters in an ICRF heating experiment. The H^0 flux arose soon after ICRF was applied, independently of He^0 charge-exchange (CX) donor atoms injected from Octant No:4, called the passive flux. The active flux, observed only when the He^0 atom beam was injected, is also shown. Energy spectra of the H^0 flux, $\Gamma_H(E)$, at 6.4s and 6.6s, corresponding to passive and active flux, respectively, are shown in Fig.80. The energy scale for the eight NPA channels has changed from that given previously [7] due to recalibration.

The importance of CX reactions between MeV energy protons and hydrogen- and helium-like ions of carbon and

Table XVIII

	Passive H^0 flux At t = 6.4s	Active H^0 flux At t = 6.6s
1. $n_e(0) \times 10^{19}$ m^{-3}	2.75	2.75
2. T_e (0) keV	6.66	6.97
3. $n(C^{6+}) \times 10^{17}$ m^{-3} [CXRS]	6.73	9.37
4. $n(Be^{4+}) \times 10^{17}$ m^{-3} [CXRS]	7.81	8.3
5. $n(He^{2+}) \times 10^{18}$ m^{-3} [CXRS]	1.43	1.88
6. $n(D^0) \times 10^{13}$ m^{-3} [recycled plus halo]	1	3.1
7. $n(He^0) \times 10^{14}$ m^{-3} [injected for direct CX]	0	7.1
8. $n(C^{5+})/n(C^{6+}) \times 10^{-3}$	1.16	5.71
9. $n(C^{4+})/n(C^{6+}) \times 10^{-5}$	3.83	4.25
10. $n(Be^{3+})/n(Be^{4+}) \times 10^{-4}$	2.89	11.5
11. $n(Be^{2+})/n(Be^{4+}) \times 10^{-5}$	1.06	1.09
12. $n(He^{1+})/n(He^{2+}) \times 10^{-5}$	1.67	16.7
13. $n(He^0)/n(He^{2+}) \times 10^{-6}$	1.09	1.1
14. $n_p \times 10^{18}$ m^{-3}	1.76	1.48
15. T_p keV	280	290
16. $n_p/n_e \times 10^{-2}$	6.4	5.4

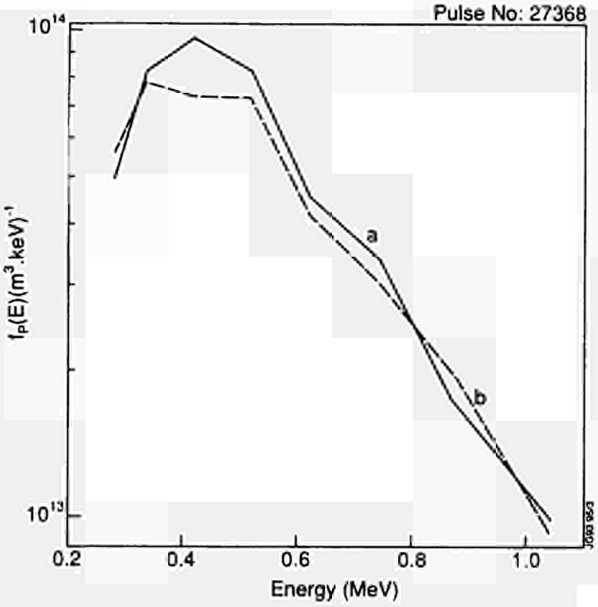

Fig.81: High energy proton energy distribution $f_p(E)$, for (a) passive flux and (b) active flux, deduced from fluxes shown in the previous figure.

beryllium (main impurities in the JET plasma), has now been established. Since the orbital velocity of electrons for these impurity ions is close to that of protons in the energy range 0.3-1.1MeV, cross-sections for electron capture by protons can be large. In spite of the low density of these ions, $\approx 10^{-5}$ of electron density, a large increase in rate of neutralisation of MeV protons can be achieved, a factor of $\approx 10^{-2}$ in relation to radiative recombination and a factor ≈ 10 in relation to CX with injected deuterium or helium atoms.

The densities of hydrogen- and helium-like carbon and beryllium ions present in the plasma during the passive flux, are shown in Table XVIII. Densities of fully ionised impurities, C^{6+}, Be^{4+} and He^{2+}, are measured using charge-exchange resonance spectroscopy (CXRS). Fractional densities of hydrogen-like impurities C^{5+}, Be^{3+}, He^{1+}, and helium-like ones C^{4+}, Be^{2+}, He^0, are deduced from ion balance equations including ion transport and charge-exchange with thermal deuterium. Ion transport is introduced simply by prescribing a model radial impurity ion flux G_z by div $\Gamma_z = n_z/\tau_z$, where n_z is the ion density and τ_z is an empirical impurity ion confinement time, (τ_z = 2.5s was taken). The neutral deuterium density $n(D^0)$ arises from recycling and beam halo. Since the overall proton neutralisation rate giving rise to the passive flux is highly sensitive to the thermal deuterium density, the magnitude of $n(D^0)$ is iterated to obtain a match between the MeV energy proton distribution functions $f_p(E)$ deduced from the passive and active fluxes. This procedure determines $n(D^0)$ in the plasma, which is a new diagnostic application.

Injection of atoms into the plasma is found to increase the density of hydrogen-like impurity ions by a factor 3-5 and less for helium-like ions, giving a corresponding increase in neutralisation rate for MeV protons. This occurs due to CX between the injected atoms and the nuclei of the main impurities (see active H^0 flux in Table XVIII). This corresponds to the experimental observation that the passive flux increased when atoms were injected into the plasma, even far away from the NPA line-of-sight on the opposite side of the torus.

Using the density of different charge donors at the times shown in Table XVIII and corresponding reaction rates for CX with MeV protons, the proton energy distribution fp(E), its effective temperature T_p, and, assuming an isotropic energy distribution like $f_p(E) \sim \exp(-E/T_p)$, a proton density n_p may be deduced, as shown in Fig.81 and in Table XVIII.

Experiments were carried out to demonstrate the ability to measure double charge-exchanged α-particles. Measurements were made on a ^4He plasma at B_ϕ=2.9T, I_ϕ=3.6MA, $n_e(0)=3\times10^{19}$m^{-3}, $T_e(0)$=4.6keV with 2MW of ^3He-minority ICRF heating, producing MeV energy ^3He ions. A 3MW 120 kV $4He^0$ beam was injected into this plasma, providing

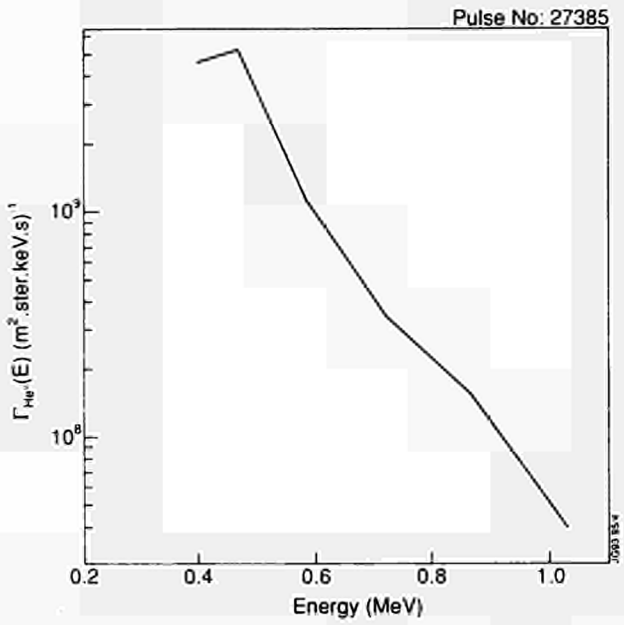

Fig.82: Energy spectrum for $^3He^0$ flux from double-charge exchange of ^3He minority ions with injected ^4He atoms.

donors for the double CX reaction. Measured energy distribution of $^3He^0$ efflux is shown in Fig. 82. Derivation of the energy distribution of ^3He minority ions awaits determination because a contribution to neutralisation of these ions could come from helium-like impurities.

These experiments demonstrate the capability for measurement of MeV helium and hydrogen ions using the NPA-KF1. Efficient neutralisation of MeV protons by intrinsic impurities, without recourse to injected donor atoms, greatly eases exploitation of the new instrument. Success in measurement of double charge-exchanged MeV helium ions creates the possibility of application of this instrument for the measurement of D-T fusion a-particles slowing-down energy spectrum.

In full D-T operation of JET [9], a single PINI source injecting 80kV ^3He or ^4He atom beam should provide sufficient donors for measurement of α-particle slowing-down spectrum in energy range 0.5-3.5MeV. If helium beam injections is not feasible, an alternative scheme for providing charge donors has been prepared requiring injection of a beryllium or lithium pellet [10].

Soft X-ray Measurements

The pulse height analysis system will be reinstalled in the new phase in essentially unchanged form. It will be capable of measuring either the thermal part of the X-ray bremsstrahlung spectrum with a Si(Li) detector or the high energy tail produced in lower hybrid heating experiments with a Ge detector.

The X-ray diode camera arrays were removed from the machine in early 1992 after 7 years of reliable operation. A wealth of information was accumulated about MHD, impurity and pellet effects. The PTE gave an opportunity to observe the effects of high neutron fluxes on the soft X-ray diode arrays. It is important to consider these effects to determine the future role of X-ray systems on JET and ITER and to establish that there is a reasonable understanding of the effects during the discharge (i.e. mainly radiation induced signals and noise) and of longer term effects of radiation damage. The direct effects of neutrons fluxes were studied with detectors in arrays which had been blanked off to remove the flux of soft X-rays from the plasma.

These measurements have shown that, in D discharges, the effects of neutron induced signals are quite small but in the D-T discharges the radiation induced signal can rise to 35% of the X-ray signal. The observed values of the radiation induced signals were in approximate agreement with the results of the radiological calculation which were originally carried out in the early phases of JET to establish safe operating regimes and radiation doses in various parts of the Torus Hall and machine structure. One of the surprising features of the measurements was the very high level of noise associated with the neutron induced part of the signal. This was identified as due to the statistical fluctuation of the high energy particles (typically MeV) from $^{28}Si(n,a)^{25}Mg$ or $^{28}Si(n,p)^{28}Al$ reactions which were responsible for generating the induced signal.

In some cases, these alpha particles or protons were directly observed in the detectors. The fact that effects of neutrons in the X-ray detectors were in reasonable agreement with expectations provides a firm basis for the design of new systems to operate in much higher neutron fluxes. Preliminary studies show that soft X-ray cameras can be designed to operate satisfactorily in the full D-T phase of JET and probably during the initial phases of ITER.

New Compact Soft X-ray Cameras

The mechanical design for the new compact cameras is now completed and contracts have been placed for their manufacture. The new system (Fig.83) consists of a set of compact cameras each of which is based on a pinhole camera with short focal length (≈5 cm) and a single Si chip with 38 individual detectors (size 4x1mm). These compact cameras are mounted either singly in straight pipes which are inserted

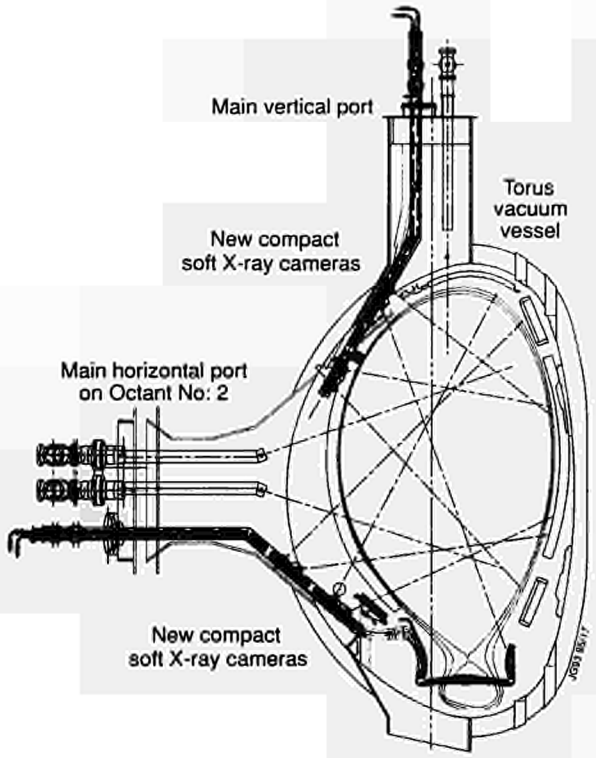

Fig.83: Disposition of proposed new compact soft X-ray cameras in relation to the pumped divertor plasma.

into the vacuum system (KJ4) or in groups mounted in pipes with more complicated geometry (KJ3). The purpose is to obtain many views of one poloidal cross-section of the plasma, to allow accurate determination of the MHD mode structure, plasma shape, etc. In addition, one camera (KJ4) will be installed at a different toroidal position to determine toroidal mode numbers. The construction and installation of these diagnostic systems will take place in 1993.

Most plasma physics diagnostics sample analogue signals throughout the entire plasma pulse at a fixed frequency using an ADC and attached memory, the sampling frequency normally being matched to available memory limits. This technique is adequate for machine operation with a short duration plasma pulse, where the pulse length is typically ~20s, and where sampling frequencies of many 100kHz are required to accurately diagnose the event. The old JET soft X-ray diagnostic, which had limited memory availability, had already implemented real-time event selection to enable events of interest to be selected and sampled at high frequency during a pulse, first using hardware techniques and subsequently using digital signal processors (DSPs). The success of this work and recent developments in microprocessor technology have led to the implementation of a single data acquisition system for all fast diagnostics, the Fast Central Acquisition and Trigger System (Fast CATS).

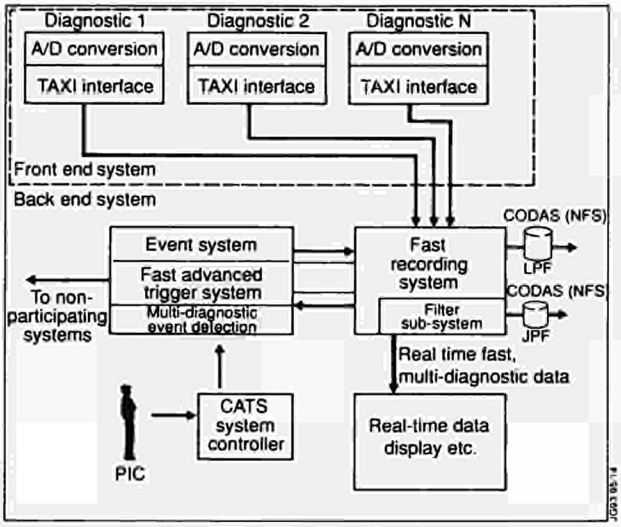

Fig.84: Fast CATS data acquisition system which was developed for the new soft X-ray cameras.

The overall system design is shown in Fig.84. The system consists of two parts, the front-end analogue-to-digital conversion (ADC) and the back-end data collection system. With the back-end system, two levels of trigger algorithms are able to evaluate data from any or all of the participating diagnostics, providing multi-diagnostic triggers. The use of parallel processors makes the system modular in design and extendible.

The front-end ADC cards contain all the signal conditioning electronics and isolation. To reduce noise, each card is powered from a separate linear power supply. The ADC card can accommodate either a trans-impedance or a differential amplifier for current or voltage sources, respectively. To accommodate diverse plasma operating levels, this is then amplified with a gain that is fully adjustable. An eight-pole linear phase analogue filter is included to prevent aliasing of out of band signals or noise that could be present above the Nyquist sampling frequency. The ADC has 12 bits sampling at 1 MHz. The digitised signal can be optionally fed through a digital filter chain to lower the sampling rate and bandwidth as desired. For example, the soft X-ray diagnostic has a 250kHz sampling rate with a 100kHz pass-band and stop band of 125kHz.

Data received from the TAXI interface is placed in memory. Selected channels are passed on to the first level trigger system. The result of this level is sent to the second level trigger, where decisions are made as to the quantity of data to be kept for further analysis. The second level programs implement algorithms that determine the actual class and size of event present. Selection criteria defined by the

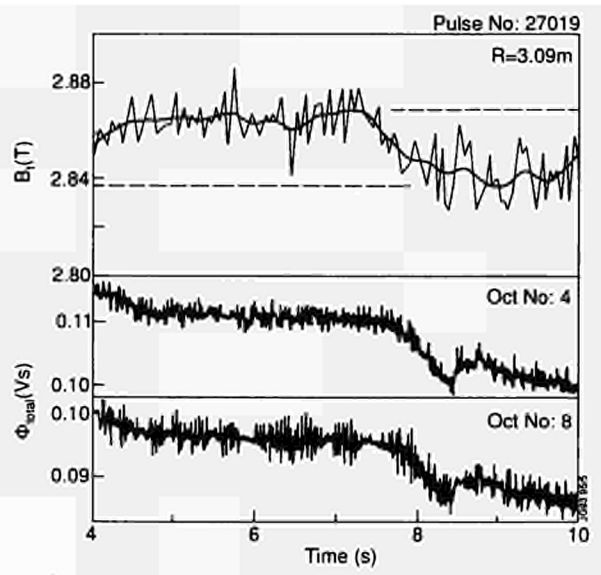

Fig.85: Comparison of the B_t evolution from the Stark measurement with the total toroidal flux from the diamagnetic loop. Clearly F_{total} drops simultaneously with the B_t decrease due to ICRF heating. At JET, two diamagnetic loops have been installed at Octants No:4 and No:8. Despite a small offset they show the same time variation. As JET plasmas are generally paramagnetic, $F_{total}>0$, while the diamagnetism of the plasma shows up in a decreasing F_{total}.

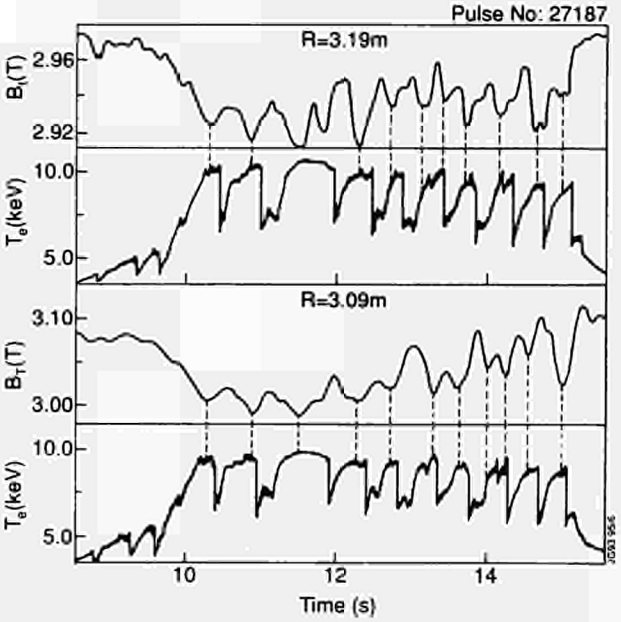

Fig.86: Correlation between sawtooth oscillations of the electron temperature and the measured toroidal magnetic field. In the case that only T_e-oscillations are present, B_t drops when T_e rises and vice versa (data smoothed with a 100ms time constant at 3.19m and 200ms time constant at 3.09m).

operators are then imposed on these results to decide whether that data should be kept.

The Fast CATS system merges data acquisition and event triggering (see Fig.84). This approach allows triggering and data processing of far greater complexity than is possible with separate systems. The use of such a system involving intelligent real-time trigger algorithms and fast data analysis will improve the quantity and quality of diagnostic data, whilst providing valuable input to the design of data acquisition systems for long pulse machines such as ITER.

Charge Exchange Spectroscopy

In parallel with the preparation of new diagnostics for the divertor phase of JET, the main activities in this area were further analysis and interpretation of earlier experimental results and development of future analysis procedures. Some highlights illustrate the progress achieved in three independent areas:

- Substantial progress was made in magnetic field measurements based on the motional Stark effect;
- Fast ion populations were successfully identified in helium beam heating experiments;
- New developments in the analysis procedures for the future Li-beam plasma edge diagnostic have shown a promising extension of the density range and the general applicability of the technique.

Magnetic Field Measurements

The emission spectrum of neutral hydrogen (or deuterium) beams injected into a fusion plasma is characterised by the motional Stark features whose polarisation pattern contains information on magnetic field direction while the Stark wavelength splitting is a direct measure of the toroidal magnetic field. Detecting both quantities simultaneously at several radial positions enables the deduction of local poloidal and toroidal magnetic fields. Present experimental equipment is capable of resolving polarisation angles of ~0.2° and toroidal fields with a statistical error of <0.1%. A further strength of internal magnetic field measurements at JET is the unique combination of Motional-Stark and Far-Rotation techniques. Dedicated experiments with circular magnetic flux surfaces were performed in the experimental campaign. The on-axis value of the safety factor q(0)<1 was confirmed by the two diagnostics. Sweeping of the magnetic axis led to enhanced spatial resolution in both cases, illustrated by sensitive changes of the polarisation angle. The correlation between changes of q(0) at the sawtooth collapse and the preceding sawtooth period was also established.

The most striking potential of the motional Stark technique is its high precision toroidal field measurement. For the first

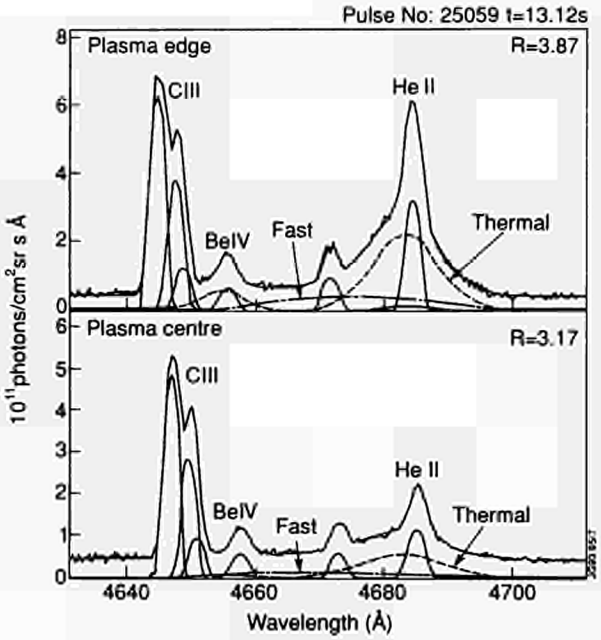

Fig.87: Typical helium charge exchange spectra obtained during helium NB injection. The contributions of the thermal and fast components are slower.

time, diamagnetic effects caused by ICRF heating could be observed. Changes of the diamagnetic toroidal field of ~4% were measured (Fig.85). The evolution of the thermal pressure (measured independently) and comparison with code simulation of the fast ion pressure indicate that the anisotropic pressure build up by fast particles is dominant in the plasma centre. Oscillations of the toroidal magnetic field caused by sawteeth oscillation of the thermal pressure have been resolved (Fig.86).

Fast Ion Densities

The analysis of He+ CX spectra observed in helium beam fuelling and heating experiments has given clear evidence of non-thermal, anisotropic velocity distribution functions. The fuelling process is characterised by a change-over from a distinctly non-Maxwellian distribution function to a dominantly Maxwellian distribution and by a broadening of the deduced fast ion density radial profile (Figs.87 and 88). The fast particle component in the composite charge exchange spectrum is in excellent agreement with predictions based on anisotropic velocity distribution functions obtained from the analytical solution of the NB Fokker Planck equation. Sawtooth oscillations in both thermal and non-thermal alpha-particle densities are found in low-power, low-temperature plasmas with no RF heating and with sawteeth periods comparable to the slowing-down time.

The observation of non-thermal features has opened the access to several potentially promising future activities; alpha-particle slowing-down studies using controlled central sources, although at a much higher power level than that expected in the future D-T phase of JET; further experimental comparison with numerical and analytical modelling of the NB heating process; and an enhanced reliability in the extracted thermal features. The latter point plays an important role in the general diagnostic effort of gaining a consistent overview of the main species (ions and electrons) in a plasma core.

Signal-to-noise levels in the measurement of fast α-particles in the helium fuelling campaign can be extrapolated to thermonuclear fusion α-particle density levels expected for the D-T phase of JET. For next step devices such as ITER, beam penetration and the high level of continuum radiation are major constraints. However, acceptable neutral beam power and energy requirements promise the feasibility of CX α-particle diagnosis in the plasma core.

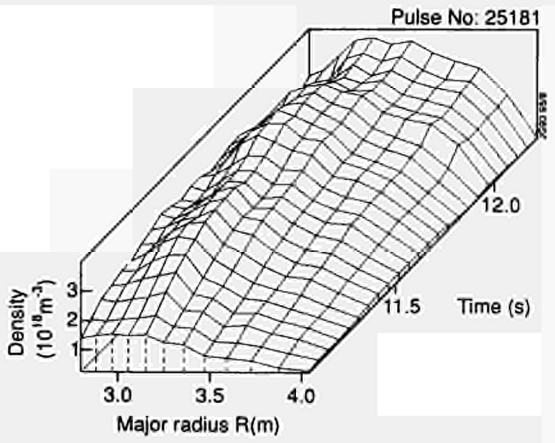

Fig.88: The fast helium ion density obtained from charge exchange spectra similar to those shown in the previous figure.

Li Beam Plasma Edge Diagnostics

Active beam emission spectroscopy with high energy Li beams is a successful technique for determining electron densities of low edge densities (10^{19}m^{-3}) in tokamak plasmas. However, for higher edge densities the extraction algorithm, which is essentially a deconvolution process of the Li beam light emission profile, encounters a singularity point at which numerical instabilities occur. This behaviour is particularly pronounced for noisy input data. An 'integral method' has been developed, which extends the standard approach to much higher densities, and which removes to a large extent the sensitivity on noise levels. The simulations show, for the presently commissioned Li-beam diagnostic system, edge densities up to 4 x 10^{19}m^{-3} may be recovered.

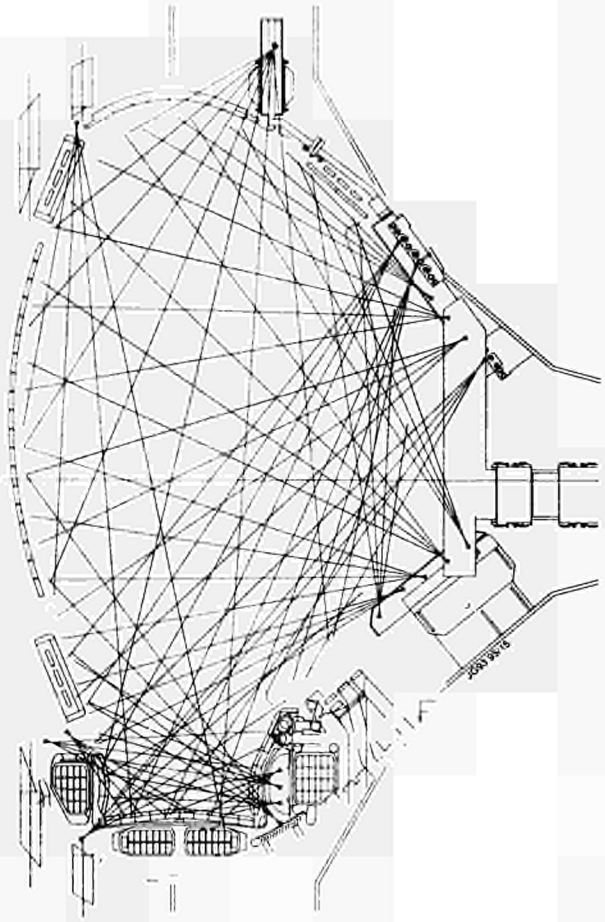

Fig.89: Schematic of the lines-of-sight of the two bolometric systems (KB3 and KB4).

Pumped Divertor Bolometry

To get an accurate tomographic reconstruction of the plasma radiation over the cross-section in the future divertor configuration, a new integrated in-vessel bolometric system has been designed. It consists (see Fig.89) of two main subsystems: the bulk plasma bolometer (KB4) and the divertor bolometer (KB3D). This design involves exposure of the detectors to the high temperatures of the vacuum vessel (300°C during plasma operation and up to 400°C during baking) without the aid of an active cooling system. In these conditions, the only possible detectors are those using metal resistors as sensitive elements. Such bolometers have already been used successfully in JET but with active cooling. They were based on a design, where the resistors in the form of ~35nm thick golden meanders of 1kΩ were deposited on a polymer support. However, this support would melt at the expected temperatures.

Preliminary tests with golden meanders of this thickness on a mica support (see Fig.90) showed that heating at 350°C leads to a progressive random deterioration of the resistors due to irreproducible modification of their resistance. With thicker resistors (> 250 nm), modifications are still observed but they are uniform and become stable after a few thermal treatments. However their lower resistance, would lead to higher power dissipation and to overheating of the bolometers if the applied voltage was not reduced. On the other hand, a lower voltage would reduce the sensitivity of the bolometer.

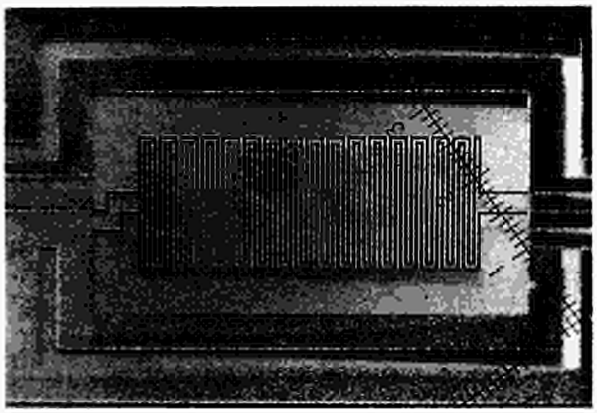

Fig.90: Detail of the gold meanders deposited on mica for preliminary temperature tests.

Platinum resistors of 1kΩ are about four times thicker than gold ones, due to the higher resistivity of that metal. Satisfactory results have been obtained with platinum meanders of initial resistance of 1.5kΩ. Thermal treatment at 500°C have produced an increase in resistance by about a factor 2, but the attained values were proven to remain constant after many thermal cycles at 450°C. On this basis, prototype bolometers are now being produced using ~150nm thick platinum meanders with final resistance of ~1kΩ.

Radial Scan VUV Spectrometer System

The radially scannable VUV spectroscopy diagnostic (KT1) consisted previously of two dual-chrome spectrometers [11, 12], which looked vertically and horizontally into the upper divertor region. The scan was provided by two-faced rotating mirrors running at a maximum speed of 5Hz and provided a minimum time resolution of 100ms. Fig.91 shows the principle of the spectrometer. Each spectrometer has two 10-channel detectors, which allowed the measurement of a spectral line profile over a wavelength range of up to 5 Å. The diagnostic was mainly aimed towards divertor investigations. A major change and upgrade of the diagnostic is now underway to match the demands of the pumped divertor phase of JET and to provide a higher time resolution and better spectral coverage. Three major improvements are being carried out:

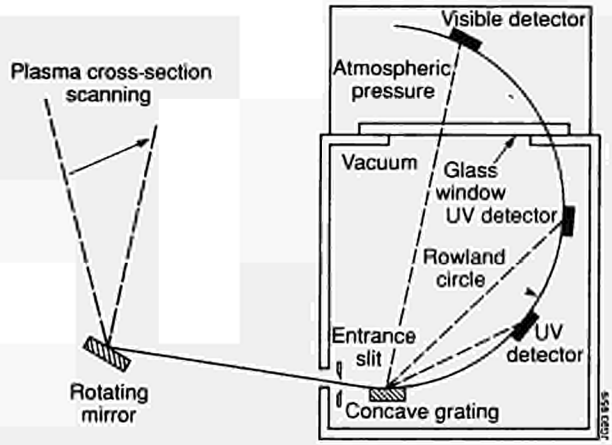

Fig.91: Schematic of the scanning VUV spectrometer KT1.

(a) The two-faced mirror will be replaced by an eight-faced one, reducing the scan repetition time to 25ms at a rotation speed of 5Hz;

(b) The number of channels per detector will be raised from 10 to 32, increasing the wavelength coverage to up to 15Å. Fig.92 shows the set-up of a detector;

(c) Three spectrometers will be installed. Two horizontal looking into the full plasma cross-section and one vertical, mainly covering the divertor region.

The alterations require a complete electrical refurbishment of the instruments and development of new electronic components to provide a high time resolution. Newly developed fast optical pulse transmission modules, with a bandwidth of about 50MHz are being tested under realistic conditions, with one instrument running with a plasma source. At the maximum speed of the rotating mirror of 5Hz, the diagnostic will acquire about 5MBytes and will be connected to VME latching scalers, which can accept 32 channels per module.

X-Ray Spectroscopy of Impurities

A new instrument, a Bragg rotor spectrometer was fully commissioned before the end of 1992 operations. This has

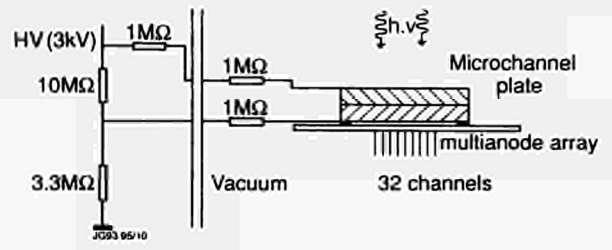

Fig.92: The KT1 UV detector with voltage divider, consisting of two microchannel plates in chevron assembly, which sit on a 32-channel multi-anode array, covering wavelengths of 10-15A°.

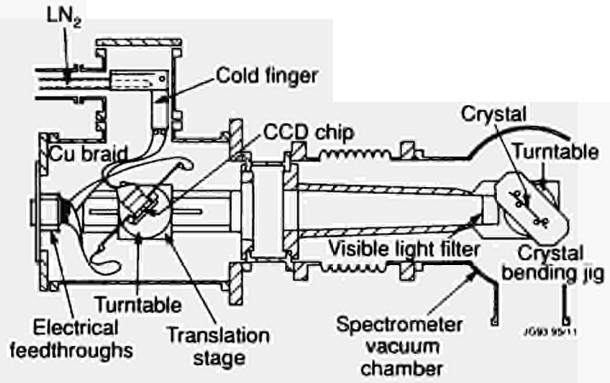

Fig.93: Schematic of the compact curved crystal spectrometer with CCD detector.

two independent sections; a hexagonal rotor gives full spectral coverage between 0.1nm and 10nm to monitor all likely impurities, while a small array of multilayer mirrors and crystals gives good time resolution of representative lines of the main impurities for routine radiated power analysis. Data analysis techniques have been adapted from those used for the VUV-XUV grating instruments.

During the PTE clean-up, the Active Phase Double Crystal Monochromator was tested and found to be clear of tritium contamination. Thus, most of the features necessary for the operation of a soft X-ray spectrometer on a tokamak reactor have been demonstrated. These features include: adequate radiation shielding, tritium isolation of the spectrometer by a thin (1mm) polymer window, and adequate spectral coverage (0.1nm to 10nm) and sensitivity. Studies are now required of neutron damage to diffractors in this situation.

A CCD detector optimised for direct detection of soft X-rays was fitted to a compact high-resolution curved-crystal spectrometer and demonstrated on a tokamak for the first time at JET (see Figs.93 and 94). The CCD detector was developed primarily for astrophysical applications, and consists of an array of 1152x1242 22.5mm square pixels. Cooling by liquid nitrogen allows single photons to be detected with a typical QDE of 50% and an energy resolution of 150eV. CCD arrays are compact, solid state, do not require high vacuum or high voltage and have a standardised readout, and are thus expected to make major contributions to several areas in soft X-ray spectroscopy and imaging.

Impurity Transport Analysis

The time-dependent 1.5-D impurity transport code SANCO has been used extensively during 1992 analysis. It has

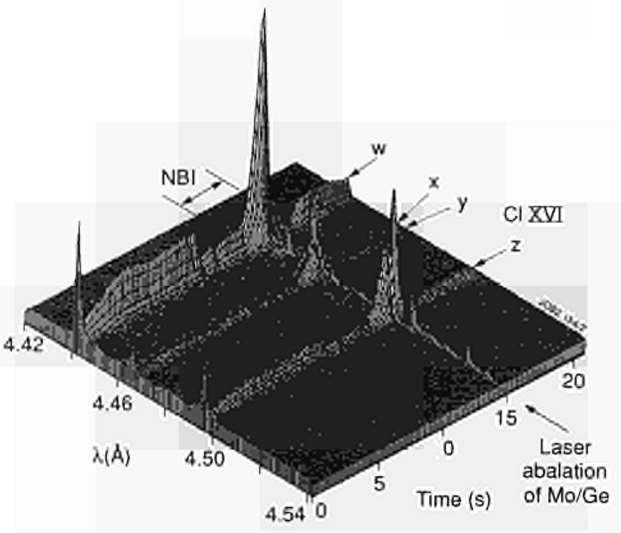

Fig.94: Isometric plot of Cl XVI n=2 resonance lines (w,x,y,zx) during a discharge with a period of NB injection and with transient injection of Mo and Ge. Each time-slice results from compressing the 2-D image onto a single row of the frame store region of the CCD. The time resolution is 40 ms.

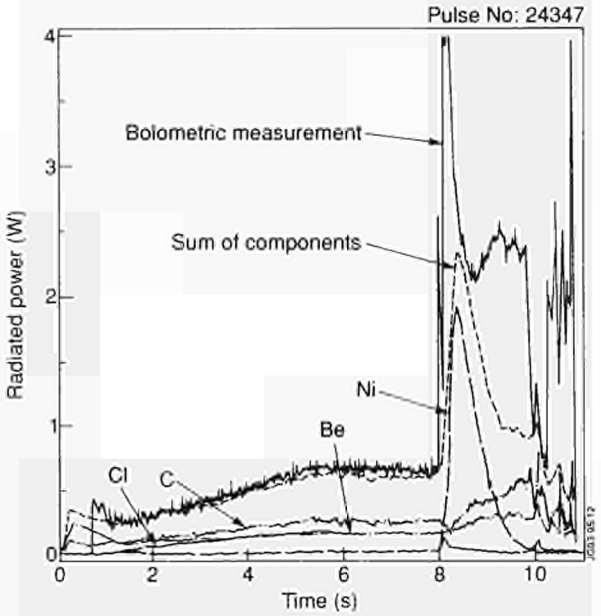

Fig.95: Component and total radiated powers for Pulse No: 24347, illustrating a significant Ni influx.

proven to be highly flexible and has been upgraded in three main areas:

(i) The calculation of the soft X-ray signals has been improved by means of the implementation of the proper filter transmission function in the atomic physics files (ADAS). Previously, the SXR emission profiles were simulated by a "hard" cut-off where only energies above an arbitrary but realistic cut-off were added up into the integral over the energies. The improvement consists of a "filter function", which takes into account the actual beryllium filter thickness, which allows a more realistic description of the SXR emission;

(ii) A central source of impurities has been successfully implemented and has allowed the simulation of the experiments designed to study the transport of helium. The helium beam source rate profiles, modelled by the PENCIL code, are read from the JET PPF's and used as input from the SANCO code;

(iii) A post-processor has been developed to obtain the line integrated signals to be compared with soft X-ray raw data. This facility can make use of either JET or any other geometry.

Impurity transport cases analysed with the SANCO code include also the simulations of injected heavy impurities (Fe, Ni), the study of transport leading to the carbon bloom in high performance discharges and impurity accumulation during PEP-H discharges.

Radiated Power Components and Impurity Concentrations

During 1991/92 operations, the available XUV and VUV spectroscopic data was analysed to give line intensities, elemental radiated power components and impurity concentrations. This allowed an assessment to be made of the global impurity behaviour in JET during this period. It was found that frequent metallic influxes occurred throughout the campaign. This contrasts with the 1990 operations in which Cl was found to be a significant contaminant and where Ni and Cr influxes were observed only towards the end of the campaign, after the displacement of some protective X-point tiles.

In 1991/92, the influxes were most commonly Ni and Cr, the main constituents of inconel. In addition, some Fe influxes were observed and, less frequently, those of Al, Cu and Zn. Fig.95 illustrates elemental radiated power components, together with the bolometric measurement of the total radiated power, for Pulse No: 24347 in which a Ni influx accounts for well over 2MW of radiated power. A locked mode begins 200ms after the impurity influx and the pulse subsequently disrupts. Although, in the main, such influxes are detrimental to plasma performance, they have a positive aspect in that a general reduction in the level of Cl in the plasma was observed. This may well be due to the metals gettering Cl and indeed an anti correlation between, for example, Cl and Ni is observed, as is shown in Fig.96.

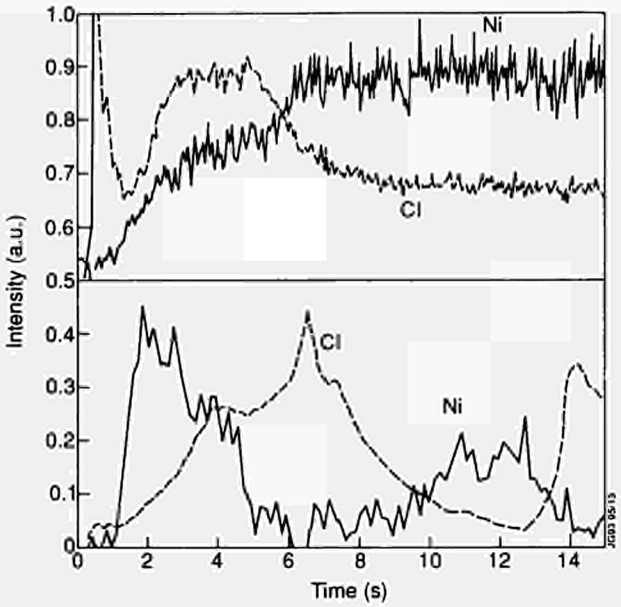

Fig.96: An example of the anticorrelation between the Ni and Cl content of the JET plasma.

During operations, it was not possible to determine the source of the Ni and Cr, the most serious of the metallic contaminants, an investigation suggesting a number of possible sites. It was concluded that many of the releases came from secondary sources, which had resulted from the previous deposition of materials released from a primary source and confirmation was provided by an analysis of a number of inner wall tiles subsequent to operations, which indicated that these were all covered by a film many mm thick and containing ~1% of Ca, Cr, Fe and Ni. The primary source is thought to be exposed pipes on the inner wall of the machine that were eroded during the operations.

Of the low Z elements, Be and C were routinely observed. These impurities originate in the plasma-facing components. During the limiter phase of a pulse, this connection can be seen in that there is a correlation between the low Z impurity dominant in the plasma and the distance of the plasma from the appropriate C or Be limiter. Throughout most of the operations, the use of Be as a getter for O maintained the latter impurity's concentration at ~0.1-0.4% of ne. However, towards the end of the 1991/92 campaign, higher levels of O were observed. At times, these rose to values of ~0.5-1% n_e.

References

[1] J Brooks, Phys. Fluids **8** (1990) 1858

[2] S J Davies and R D Monk, Culham Laboratory Report TAN (92) 2-30

[3] P Wienhold et al, J Nuclear Materials **162-164** (1989) 369

[4] J P Coad et al, JET Report JET-P(92)61 (to be published in J Nuclear Materials)

[5] J A Wesson, et al., 14th IAEA Conf. on Plasma Physics and Controlled Nuclear Fusion Research, Würzburg, 1992, (Paper IAEA-CN-56/A-7-6) to be published in Nuclear Fusion Supplement.

[6] R C Wolf, J O'Rourke, et al., JET Report JET-P(92)99

[7] M P Petrov, et al., Europhysics Conf. Abstracts 16C(1992)II-1031

[8] A V Khudoleev, et al., Europhysics Conf. Abstracts 16C(1992)I-151.

[9] A Gondhalekar, et al., JET Report 1992, JET-R(92)12

[10] J O'Rourke, et al., 1992 to be published.

[11] P Chabert et al., Proc. 16th EPS Conf. on Contr. Fusion and Plasma Physics, Venice 1989

[12] JET Progress Report 1990, Vol.1 (1990)

Summary of Machine Operation

As planned, 1992 operation was for a period of only the first seven weeks of the year. Due to the small amount of time available and due to the severe restrictions on the plasma performance limiting the neutron activation of the vessel (to facilitate subsequent in-vessel work during the shutdown), special attention was given to planning many of the experimental studies. As a consequence, many magnetic field configuration and protection circuit changes (some undertaken overnight and some in the operation session) had to be performed.

The overall operation was successful and resulted in an average of 135 pulses per week, respectively a considerable improvement over the 100 pulses per week during 1991 operation. For example, on one particular day (2-shifts), 52 pulses were achieved. High-current operation was resumed and in a period of two days nearly fifty 7 MA current plasmas were reliably produced. The effects of high current disruptions have been much reduced by improved protection control arrangements (see 1991 Progress Report). Nevertheless, two vacuum leaks and some in-vessel tile damage resulted from plasma disruptions.

Two events significantly hampered operations :

i) a rupture of a diagnostic bellows, due to a control circuit commissioning error, vented the vessel almost to

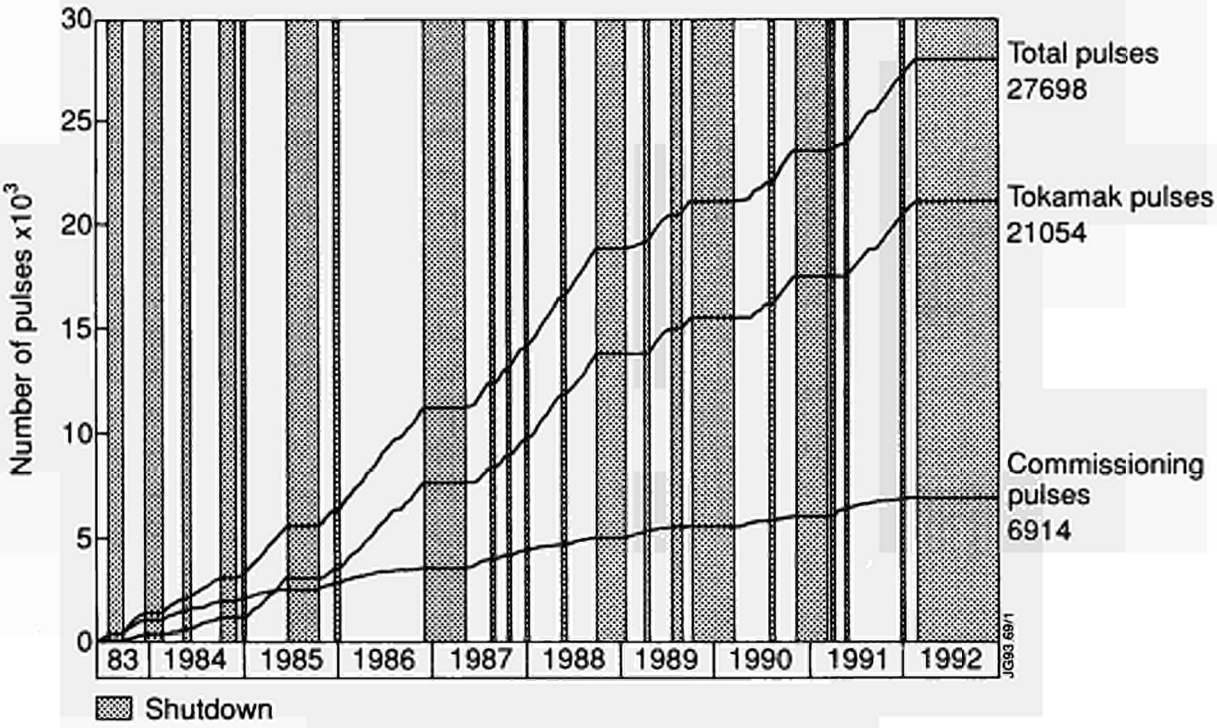

Fig.97: Cumulative totals of JET pulses - 1983 to 1992

atmospheric pressure and the repair and recovery caused a six day loss of operation;

ii) a water leak from the NB Testbed affected the cooling of torus components and control cubicles of the NB injectors. This caused 1.5 days loss of operation, but neutral beam operation was prevented for a subsequent two days.

In spite of these (and lesser) problems, the reliability performance of subsystems was good and allowed effective use to be made of the time available.

During this period, the vacuum exhausts of the torus and neutral beam injector boxes were carefully monitored for tritium, following the PTE in November 1991.

This period included the following activities :

- a study of the effects of ripple in the toroidal field (TF). This was achieved by an arrangement whereby 16 toroidal field (TF) coils were energised and the plasma performance compared with that achieved (at the same magnetic field) with the 32 TF coils;
- extension of the duration of an H mode plasma (to 18s in a 3MA plasma);
- multiple pellet injection (up to 20 per pulse) to study the effect on the radial profiles of plasma quantities;
- divertor studies e.g. radiative gas target, divertor plate temperature feedback control of gas introduction at the divertor region, assessment of the performance of the divertor plates;
- application of RF and LH power to the plasma to study synergistic effects and current-drive studies;
- high plasma current operation (7 MA flat-top extended to 9s by magnetic flux-saving achieved with LH current drive) and additional heating studies (involving up to 28 MW power);
- commissioning of a new power supplies control system, which modifies the primary voltage applied during plasma build-up to ensure that the rate of rise of plasma current is not excessive (which may lead to disruptions);
- studies of the effects of error fields (caused by small deviations from symmetry in the outer poloidal field coil winding) on the growth of locked plasma modes.

The organisational arrangements for operation (Task Forces H, I and P) remained as for 1991 operation. The experimental programme time during 1992 was distributed approximately as follows :

Task Force H :	High Performance	21.6 %
Task Force I :	Impurity Transport and Exhaust	43.1 %
Task Force P :	Physics Issues	35.3 %

The number of pulses in 1992 was 944, bringing the total number of pulses to 27968 (see Fig. 97). The percentage of commissioning pulses in 1992 (less than 10%) was half that in 1990 or 1991. The plasma current distribution (Fig. 98)

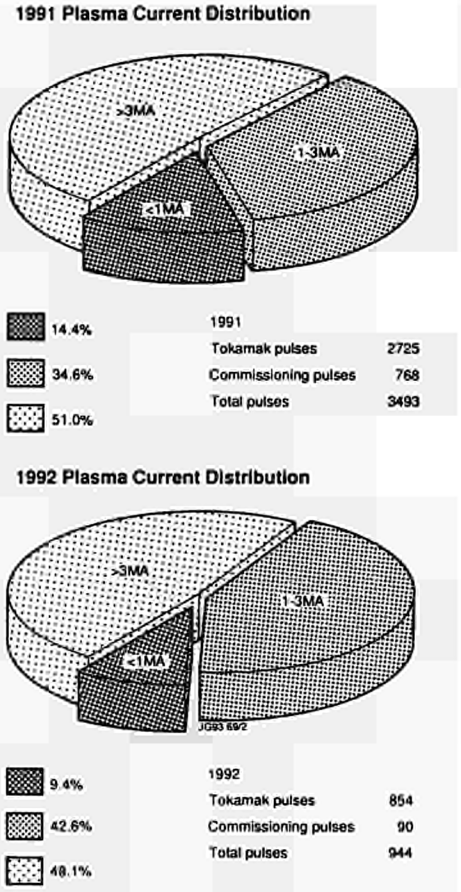

Fig.98: Comparison of numbers of pulses and distributions of plasma currents for 1991 and 1992. The plasma current distributions are for all tokamak pulses.

for 1992 compared with 1991 shows a reduction in the fraction of small plasma currents (<1MA) and high currents (>3MA), and an increase in medium currents (1-3MA).

Summary of Shutdown

Following completion of operations on 21 February 1992, the major shutdown for the installation of the Mark I pumped divertor and associated systems started. It was expected to last until mid-September 1993, but due to additional requirements (notably, the exchange of a second toroidal field coil), it was extended to the end of 1993.

The shutdown activities can be divided into three distinct stages: Stage 1 covers removal of internal and external components from the torus; Stage 2 involves the in situ assembly of the four divertor coils; and Stage 3 comprises the installation of new internal components and the reassembly of external components.

Stage I

Stage 1 (scheduled to mid September, extended to end of October 1992) comprised the following activities:

(i) Removal of internal components; removal of external components; and decontamination of vacuum vessel;

(ii) Exchange of TF Coil No:4.2 with a spare. This required the removal of Octant No:4. Upon reinstatement of Coil No:4.2 in July 92, it was discovered that the neighbouring Coil No:4.3 also had an interturn fault, albeit of much smaller magnitude. The fault in Coil No:4.3 had been masked by the more pronounced fault in Coil No:4.2. It was discovered only after Octant No:4 had been re-instated in the torus. Since it would be impossible to replace TF coils in future due to the presence of internal divertor coils, it was considered prudent to replace Coil No:4.3 with a spare. This added eight weeks to the length of Stage 1 activities;

(iii) Preparations for the building of the divertor coils and for the installation of Stage 3 components. This required the accurate positioning and welding of many supports for in-vessel components, saddle coil crossover bars and vacuum feedthroughs in the bottom of the vacuum vessel, which will be masked by the divertor coils, and therefore could not be fitted after installation of the divertor coils.

At the start of the shutdown, in-vessel activities were influenced by two factors: the tritium-in air and the beryllium-in-air concentrations. Initially, the tritium-in-air concentration was 86Bq/m^3. This fell to ~10Bq/m^3 at the start of the in-vessel cleaning campaign, and subsequently to <1Bq/m^3. Beryllium-in-air concentrations were strongly dependent upon type of work. Concentrations varied from ~30μg/m^3 after initial vessel opening to below detection level after the vessel wash. Therefore, full airline suits were only required for beryllium, and not for tritium.

From March to June 1992, all in-vessel work was carried out in full air-line suits. This involved three entries per day of 4 hours each, with a maximum of 4 operators inside the vessel at any time (maximum 48 in-vessel hours/day) for 7 days per week.

After the vessel cleaning, the vessel was declassified to a Class 1 protection zone, which meant that only simple face masks were needed. Several weeks later, declassification to Class 0 was possible, with no respiratory protection required. However, near inaccessible areas, high levels of Be-contamination were still present inside the vessel. Therefore, operators continued to wear

personal air samplers and when these indicated increased beryllium-in-air concentrations, the class of protection was raised immediately. When airline suits were no longer required, the in-vessel working arrangements were changed to two-shifts, each with two entries of 3 hours with a maximum of eight operators inside the vessel, giving up to 96 in-vessel man hours per day. During the remainder of 1992, 6.5 days per week were worked.

In-vessel radioactivity dose rates fell from 86μSv/hr initially to about 5μSv/hr at the end of 1992. The dose rate was dominated by Co-58 with a half life of 71 days.

Components removed from the vacuum vessel were packed and stored in specially prepared ISO freight containers. Each container was heated and the air from the containers was monitored for tritium as it was exhausted through the stack on Building J25.

Vacuum vessel cleaning also reduced the tritium surface contamination to such an extent that waste could be classified as non-radioactive, unless it contained parts of the activated walls (such as grinding dust or components).

Stage 2

Stage 2 started at the end of October 1992 and was rescheduled for completion by the end of April 1993. The work comprised the fabrication in situ (using prefabricated sections) of divertor Coil Casing Nos:1, 2 and 4 followed by storage of the lower part of the casings below floor level and the lids near the vessel ceiling. Fabrication and storage of Case No:3 at this stage would have limited the handling of prefabricated conductor bar sections to such an extent that sections would have had to be cut shorter and would have involved an increased number of brazed joints. Therefore, it was decided to fabricate Case No: 3 after completion of brazing. After fabrication of the casings, the coils were formed by brazing prefabricated conductor bar sectors inside the vessel. The brazes were checked by radiography. Following brazing, the coils were wrapped with ground insulation and then encased. The interspaces were filled with epoxy, and subsequently thermally cured. After completing Coil Nos:1 and 4, Coil Nos:2 and 3 will be fabricated in parallel and Coil Case No: 3 will be built in the vessel following encasing Coil No:2. During the brazing campaign, two assembly shifts alternated with two radiography shifts so that work continued for 24 hours per day.

In parallel with the in-vessel work, which constitutes the critical path for the divertor shutdown, many ex-vessel activities were carried out. These included a complete survey of all TF coil supports, involving refurbishment of push-pull jacks, and surveying and re-machining of a large number of wedges that provide lateral support.

Furthermore, an extensive programme of trial assemblies of internal vessel components was started using the prototype Octant in the Assembly Hall. These provide important training for personnel, and tests of the installation equipment and assembly procedures.

Stage 3

In parallel with Stage 2 in-vessel activities, intensive effort was devoted to detailed planning of Stage 3, not involving outside companies. Scheduling is in an advanced state and comprises six sub-stages (3A to 3F):

Stage 3A: Installation of coil clamps and heat shields: the divertor coils will be accurately positioned and clamped to supports, followed by installation of coil casings heat shields;

Stage 3B: Installation of upper in-vessel components: including gas introduction pipes, discharge cleaning equipment, dump plates, tile supports, saddle-coil components and diagnostics;

Stage 3C: Installations requiring master survey ring: plasma facing components will be accurately aligned (<1mm). Components include antennae supports, cooling water supports, poloidal limiter and inner wall guard limiter supports, and target plate rails;

Stage 3D: Installation of mid-vessel components: including gas introduction pipes, diagnostics, cryo-baffles, cryo-pump, RF antennae, poloidal limiters, cooling water pipes and manifolds, inner wall guard limiters, saddle coil busbars, LHCD system, and saddle coil components;

Stage 3E: Installation of lower vessel components: including gas introduction pipework, target plate modules, diagnostics, lower saddle-coil elements, poloidal limiter sections and tiles;

Stage 3F: Installation of remaining components: including diagnostics, tiles and RF components.

Installation activities will be accompanied by intensive leak testing and surveying.

Detailed planning suggests 200 in-vessel working days, based on extended double-shift work, are required for the implementation of Stage 3 to complete the shutdown by the end of 1993.

Scientific Achievements during 1992

Introduction

For 1991/92, the system of operation of the scientific programme was the same as that since 1989. The programme operated for a series of campaign periods, the standard being of eight weeks duration (composed of six weeks tokamak operation and two weeks of maintenance/commissioning). Two Programme Leaders were appointed with responsibility for formulating near programme proposals (one campaign ahead) and outline plans (two campaign periods ahead). These proposals were within the broad outline of the JET Development Plan and subject to guide-lines provided by the Experiments Committee. These proposals were presented to the JET Experiments Committee for discussion and approval before implementation.

Programme Leaders for 1991/92 were:

D.J. Campbell and A. Tanga

Three Task Forces implemented the programme, as follows:

H) High Performance

(involving progression to full performance in material limiter and magnetic limiter configurations with currents up to 7MA, with high energy content and including progression to the highest fusion product, long pulse operation, steady state conditions and exploration of operation limits, etc.)

(Task Force Leader: P.J. Lomas)

I) Impurity Transport and Exhaust

(involving optimization of plasma purity and studying exhaust phenomena, and including studies of divertor physics and edge effects; impurity retention; erosion and redeposition; control of boundary instabilities, etc.)

(Task Force Leader: P.R. Thomas)

P) Physics Issues

(involving studies of control and optimization of plasma profile effects (using LHCD, RF, NB and high speed pellet injection, etc.) and optimization of heating effects, especially electron heating. This includes particle and energy transport studies in transient conditions; disruption and sawtooth stabilisation; high beta regimes; α-particle effects and fusion simulation studies; physics issues related to Next Step devices; etc.)

(Task Force Leader: D. Stork)

Task Force Leaders were appointed with responsibility for (i) interacting with and advising Programme Leaders on programme requirements within that task area; (ii) devising and setting out a detailed programme for allocated time within a campaign period; (iii) driving through that task programme (including acting as a Control Room representative); (iv) analysing data (in conjunction with Topic Leaders, if appropriate); (v) disseminating information in the task area through internal meetings and publications (in conjunction with Topic Leaders, if appropriate).

In addition, Topic Groups were formed, as follows:

Topic Group	*Topic Leader*
(a) Transport and Fluctuations;	J.G. Cordey
(b) MHD, Beta Limits and Topology;	J. Wesson
(c) Next-Step Related Issues (including α-particle heating effects)	B. Tubbing

Topic Group subjects are of longer term interest than the immediate tasks undertaken by the Task Force Groups. The Topic Groups are responsible for analysis of results within many areas across the Task Force spectrum, but they also have responsibility for advising Programme Leaders on

programme requirements which are topical and relevant to the Groups areas of activity. In addition, the Groups disseminate information through a number of internal meetings and in external publications.

Programme Execution and Analysis

JET operation during the 1991/92 campaign period was mainly devoted to the exploitation of new facilities; on further improvements in plasma performance; and to further assessment of beryllium and carbon as a first-wall materials. Impurity control in JET, as for other long-pulse high power tokamaks, is of fundamental importance and therefore significant effort has been devoted to this area of study.

The main themes for the 1991/92 Experimental Programme were:

- optimize plasma performance;
- advance understanding in certain key areas of tokamak physics:
  - energy transport and confinement
  - transport of particles and impurities
  - magnetic topology of plasma
  - physics of the H-mode
- establish basis for Pumped Divertor and Next Step physics (including a Preliminary Tritium Experiment);
- complete certain experiments relevant to belt limiter configuration.

During early 1992, the experimental programme was completed with a series of high performance experiments (particularly, limiter experiments up to 7MA). For the remainder of 1992, the Task Forces and Topic Groups retained responsibility for analysis of data taken during their sessions. This applied also to the Tritium Task Force (Task Force Leader: A Gibson), which had been set up to plan and execute the preliminary tritium experiment (PTE). In addition, an Advanced Divertor Study Group (Study Group Leader: G Vlases) had been formed in 1992 to investigate advances in divertor science and technology and to make recommendations for future JET divertor experiments.

The scientific achievements for 1992 are described in the following sections, within the Task Force, Topic Group and Study Group headings.

High Performance

During the short operating period in 1992, a number of experiments started in 1991 were completed. A quantitative

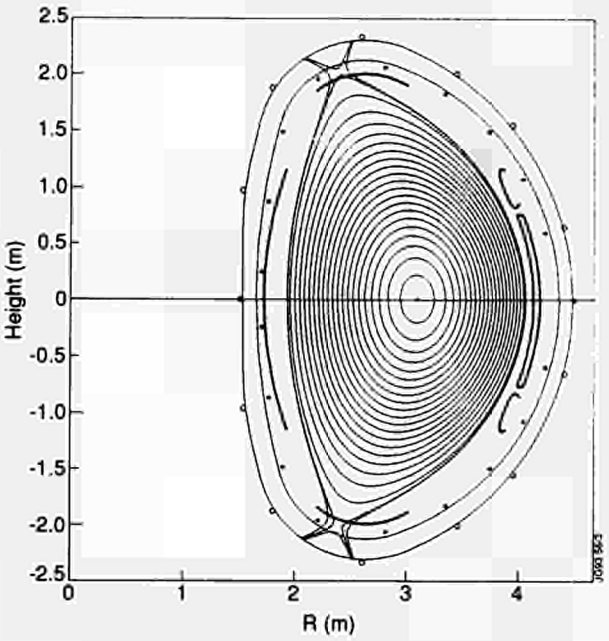

Fig.99: Equilibrium for 5MA DNX discharge (Pulse No: 27278). The magnetic nulls are located about 10cm outboard of the dump plate surfaces.

study of the effect of the magnitude of error fields on operational space was completed and is reported further in the section on MHD, Topology and Beta Limits. H-mode operation in double null was extended to 5MA. A careful experiment to measure transport coefficients with both negative and positive temperature gradients was undertaken on behalf of the Transport Topic Group and is reported in the section of this Report. Finally, the Task Force returned to limiter operation and undertook long pulse and high power operation at 7MA plasma current.

High Current H-mode Experiments

The technical development of high current double-null X-point (DNX) scenarios was described previously [1]. During the 1992 campaign, H-mode plasmas were obtained in the DNX configuration at plasma currents up to 5MA, further extending the H-mode database particularly with respect to confinement current scaling and impurity behaviour. Figure 99 shows the 5MA DNX equilibrium, in which the magnetic null-point is located about 10cm outboard of the surface of the X-point dump-plates. Despite the marginal nature of this X-point configuration, H-modes with ELM-free periods were nevertheless obtained. Figure 100 shows the time evolution of the main parameters of a 5MA DNX H-mode discharge which features both ELM-free and saw-tooth free phases. Figure 101 summarises the global confinement data of DNX H-modes in the range 3-5MA com-

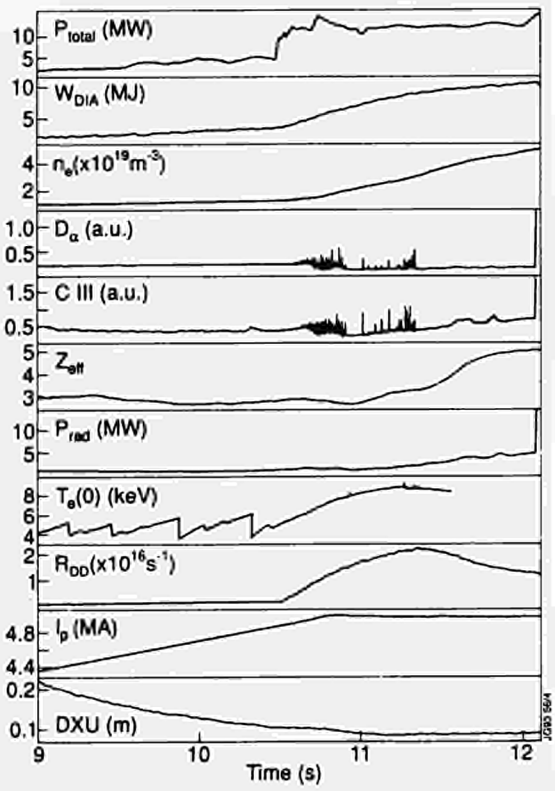

Fig.100: Plasma parameters for 5MA/2.8T DNX H-mode (Pulse No: 27278, 10MW D°, 1.5MW H minority ICRF) with ELM-free and sawtooth free phases. The H-mode reverts to L-mode spontaneously. DXU = upper null distance beyond dump plate surface.

pared with the ITER-90HP power-law scaling [2]. The 5MA data confirms the previously reported trend [1], (i.e. the increase of confinement with current eventually saturates).

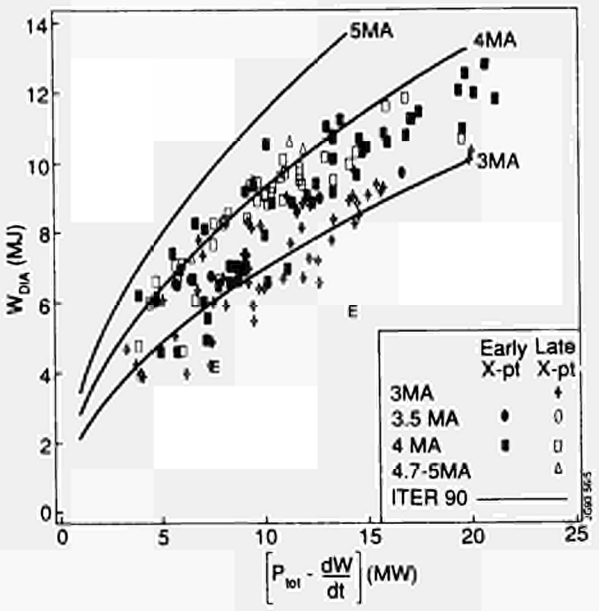

Fig.101: Plot of diamagnetic stored energy versus loss power for 1991-92 DNX 3 - 5MA H-modes, measured during ELM-free periods. Solid curves show the predictions of ITER90-HP scaling.

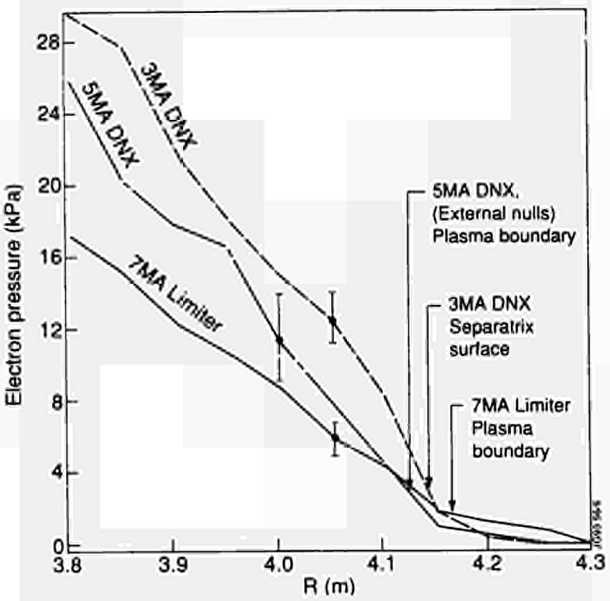

Fig.102: LIDAR measurements of electron pressure on the outboard side at the midplane, comparing 7MA L-mode with 3 and 5MA ELM-free DNX H-modes at similar heating powers, illustrating relative edge confinement properties.

One possible explanation for this effect is the progressive reduction in edge magnetic shear as the X-point location moves beyond the dump-plate surface, on which the plasma directly limits when the X-points are external. Figure 102 compares the edge radial electron pressure profiles measured by LIDAR on the plasma outboard side at the midplane for 3 and 5MA DNX and 7MA belt-limiter configuration plasmas at similar levels of heating power. This indicates that whilst both DNX plasmas exhibit steeper pressure gradients than the 7MA L-mode case, characteristic of H-mode confinement, there is no additional steepening or hence significant further improvement in the edge transport barrier on going from 3 to 5MA. On impurity behaviour, the 5MA DNX discharges are similar to other high power, moderate to high density H-modes (i.e. these tend to terminate in a spontaneous L-mode transition without sudden impurity bloom). It should be noted that these discharges predominantly interacted only with the top graphite dump plates, in order to reduce the risk of damage to the bottom Be plates before completion of other experiments.

Despite the absence of sudden blooms, a further possible and undesirable consequence of the external X-point location is seen in the continuously increasing Z_{eff}, especially during ELM-free phases (Fig. 100), attributable to the lack of divertor impurity screening action. The fuel dilution problem, combined with the observed saturation of confinement, depressed the attainable fusion performance at high current

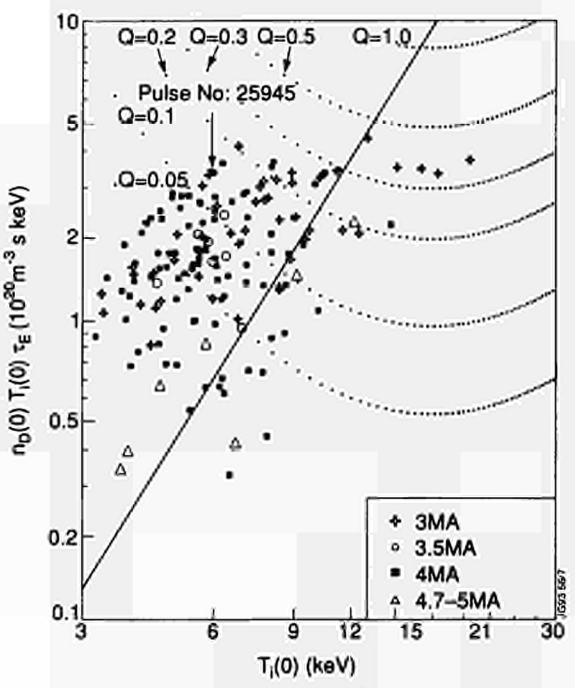

Fig.103: Plot of fusion performance $n_D(0)\ \tau_E T_i(0)$ versus $T_i(0)$ for 1991-92 DNX H-modes. To the left of the solid line, $T_e \sim T_i$. Thermal Q contours assume D:T ratio of 1:1, and stationary stored energy, which is the case for most points with $T_e \sim T_i$.

relative to the best levels achieved at 3MA (Fig.103). The H-mode regimes have potential for further development and exploitation in the divertor phase of operation, resulting in improved plasma purity and confinement in optimised X-point configurations designed for currents up to 6MA.

Programme with 7MA Plasma Current

7MA limiter plasmas were first developed in JET in 1988, at low $q_\psi \sim 2.5$ with essentially no flat-top and with little additional heating. In 1990, these discharges were developed to higher $q_\psi \sim 3.3$, and a flat-top of 3s and additional heating powers raised to ~ 8MW. Unfortunately that programme was terminated by damage to protection plate support rails following disruptions. To avoid such problems, a disruption amelioration programme was undertaken in 1991 to find means of reducing forces on in-vessel components. This work [1], showed a major problem with loss of vertical position stabilisation during the current quench phase of highly elongated configurations. The problem was solved for double-null X-point configurations by ramping down the PFX current (a major part of the elongation control) upon detection of the growth of a stationary mode, and before the current quench.

Thus, one of the major objectives of the 7MA programme in 1992 was to demonstrate the safety and reliability of very

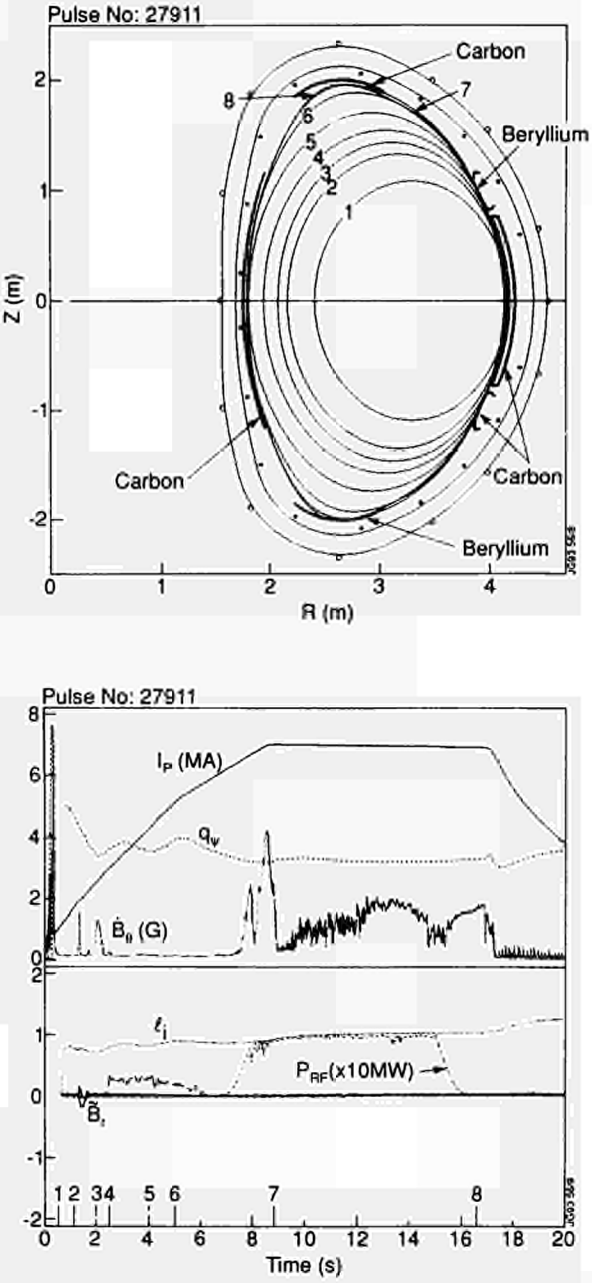

Fig.104: (a) Equilibria at various times marked (b) Corresponding parameters for the 7MA scenario (as marked on lower trace).

high current operation of a tokamak. The original objectives remained of extending the flat-top, demonstrating high power heating and obtaining confinement data.

Operational Aspects at 7MA Current

Figure 104 shows the strong aperture expansion scenario developed for safe early passage through $q_\psi = 4$ and the subsequent ramp to 7MA at $1MAs^{-1}$. The labels on the equilibria correspond to the times marked on the time traces. Passage through $q_\psi = 4$ occurs between equilibria 2 and 3, when the plasma is small and circular. The rotating MHD which appears at this time gave rise to a small amplitude

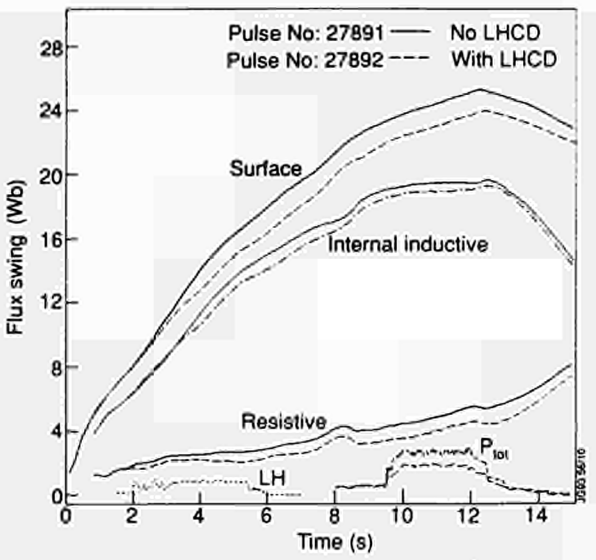

Fig.105: The surface flux swing, internal inductive flux and internal resistive flux for two 7MA pulses with (Pulse No: 27892) and without (Pulse No: 27891) LH in the current rise. The flat top heating powers are similar for the two cases.

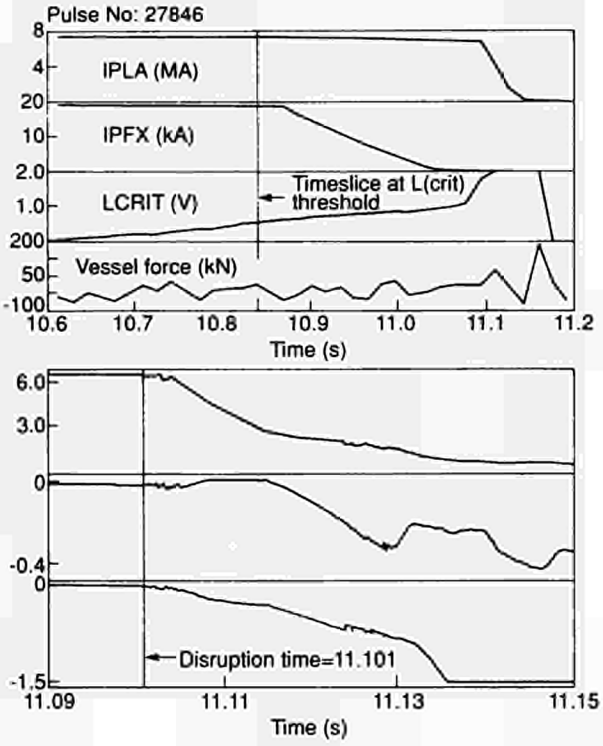

Fig.106: The PFX ramp-down scenario for the 7MA disruption (Pulse No: 27846). The stationary mode was detected by PFPS at the time given by the vertical bar in the upper figure. The lower figure shows the current quench itself on a faster timescale and here the vertical bar marks the start of the current quench.

stationary mode, as shown, but this decayed. In fact, out of 60 successive ramps to 5MA and above, there was only one instance of this mode continuing, but this case was successfully terminated without disruption by the Plasma Fault Protection System (PFPS). From equilibria 3 to 7, both the minor radius and elongation were increased to hold q_ψ at values between 3 and 4, until 7MA was reached. There was some rotating MHD activity as q_ψ undershot towards 3 at about the time of the start of flat-top, but this decayed when a steady $q_\psi = 3.3$ was reached and was replaced by MHD activity associated with sawteeth during additional heating.

Lower Hybrid (LH) power was applied during the current rise. The plasma equilibria receded from the location of the RF antenna as the plasma elongation grew, and therefore, it was necessary to use the real time LH launcher position control to follow this plasma motion to maintain coupling. The LH gave a flux swing saving of 1.4Wb, made up of 0.5Wb inductive and 0.9 Wb resistive, as shown in Fig.105. This inductive saving corresponded to a slower current penetration, but, the plasma remained stable provided that the LH was applied after the $q_\psi = 4$ activity had decayed. The total flux saving corresponds to 2s of flat-top. As shown in Fig.104, this contributed to the flat-top duration of 8.5s. At the end of the flat-top, the primary currents reached limits set, not by actual stresses in the primary coils, but by possible stresses in case of fault conditions.

Of the fifty 7MA pulses in 1992, there was only one disruption, despite heating powers up to ~30MW. This demonstrates significantly higher reliability than is usually the case in other less technically demanding programmes. This reflects the learning process on this scenario over the years, care in preparation, and perhaps significantly, a plasma diagnostic effort organised primarily for "plasma safety" during the course of the experiment.

The sole 7MA disruption in 1992 is illustrated in Fig.106. The stationary mode precursor (labelled LCRIT) was detected by the PFPS system and the PFX shaping current brought to zero before the start of the current quench. As a result, the vertical position shown on an expanded timescale was well controlled down to about 2MA. The resulting force on the vessel was only 200kN (20t). Vessel forces are normally related to the F number, (Fig.107), which is a measure of the elongating fields of the stationary plasma. This 7MA disruption (Pulse No: 27846) and one in 1990 causing vessel damage (Pulse No: 22418) are compared with typical lower current, low F-number disruptions with and without the ameliorating ramp-down. The benefit is clearly obtained reliably, and in the 7MA case reduced the vessel forces from 400 tonnes to only 20 tonnes. No vessel damage resulted and the 7MA programme continued.

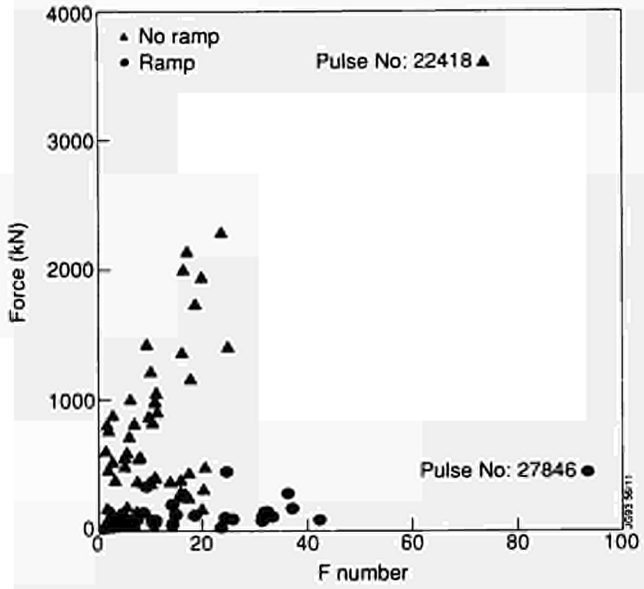

Fig.107: Measured vessel forces during disruptions plotted against F number for cases with and without the PFX ramp-down. The 7MA pulse (No: 27846) from the recent campaign, and the 7MA pulse (No: 22418) from 1990 are marked. The remaining points are 2-4MA DNX configurations from 1991.

High Power Heating at 7MA

Figure 108 shows an example of high power heating at 28MW applied to a 7MA plasma. The heating was made up of 12MW H- minority ICRF together with 16MW of beams. The heating is of sufficient duration to allow the plasma stored energy to reach ~12MJ under steady conditions, which is comparable to the best H-mode results achieved (transiently) on JET at lower current and power. The ICRF heating is slightly off-axis due to a large

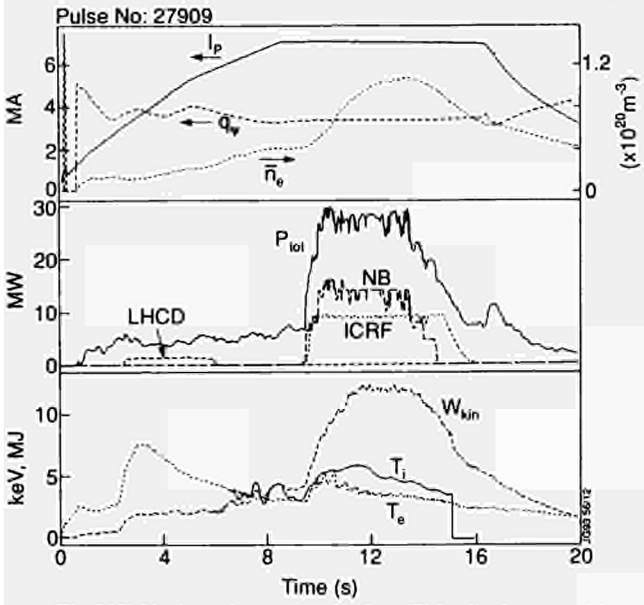

Fig.108: Various time traces for long 7MA discharges with 28MW of additional heating.

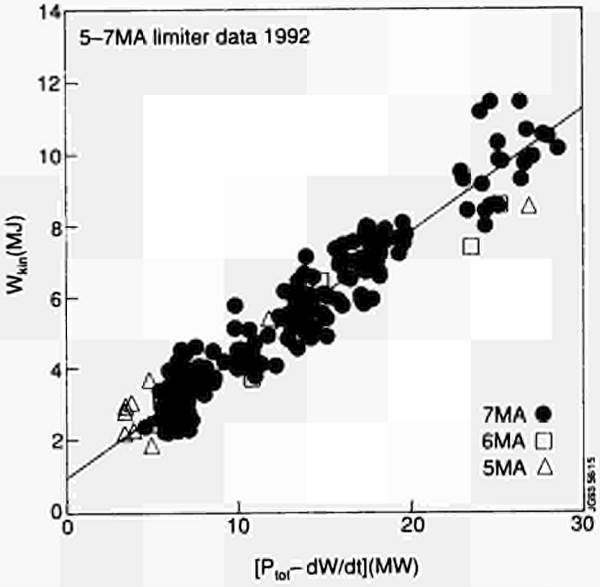

Fig.109: Thermal stored energy plotted against loss power for 5, 6 and 7MA from the 1992 campaign.

paramagnetic effect at 7MA, and the fact that higher frequencies were limited in power. Experiments were carried out with He^3 minority ICRF at lower power (<5MW) with on-axis resonance. This showed that heating results were insensitive to resonance position in this case with large sawtooth inversion radius.

Impurities at 7MA

Plasma equilibrium was balanced magnetically between the upper beryllium belt limiter and the lower carbon belt limiter. However, the dominant heat flux was to the upper limiter. In addition, at these high currents, the scrape-off lengths were very short. These two effects led to very high power densities on the beryllium limiter and consequent melting. Not surprisingly, beryllium was the dominant impurity, with plasma concentrations ~10% at the highest power. Carbon concentrations were a few percent, chlorine ~ 2×10^{-3} and nickel ~ 2×10^{-5}. Estimates of deuterium concentration fell from 0.6 to 0.2 at the highest power. The fusion triple product, $n_D\tau_E T_i$, was therefore only 1.4×10^{20} m^{-3}skeV.

Confinement at 7MA Plasma Current

Long pulse full and half power data were taken at 5, 6 and 7MA and, in addition, there were a further 46 7MA pulses from OH to full power with heating pulse lengths of 1.5 - 2.0s. (i.e. almost but not quite stationary). The thermal stored energy from these pulses is shown in Fig.109 plotted

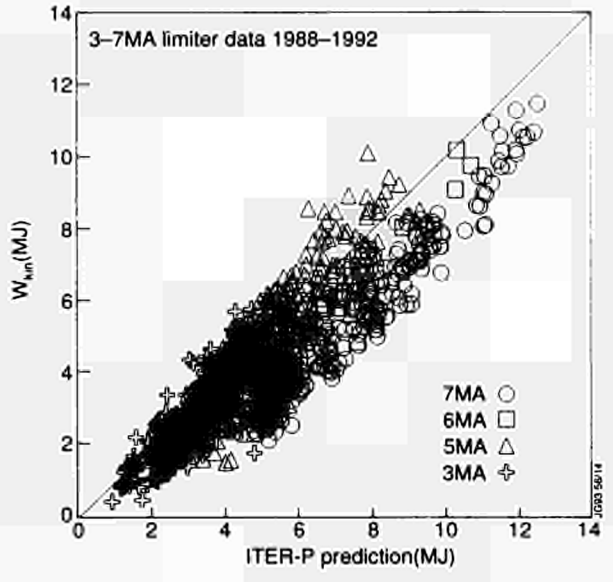

Fig.110: 3, 5, 6 and 7MA limiter datasets from 1988-92 compared with the prediction of the global scaling ITER89P.

against loss power. At the highest power, the global thermal energy confinement there was $\tau_E = 400$ms and the incremental confinement time (given by the slope of the fitted line) was $\tau_{inc} = 340$ms. The 5, 6 and 7MA data were similar at moderate power, but the stored energy at 7MA was significantly higher at full power. This remains true even if the extensive 5-6MA data sets from 1988 are included. These results clearly indicate that the simplest global scalings of $\tau_E \sim I_p/P^{1/2}$ are not adequate in detail. This is confirmed in Fig.110 which shows the complete JET dataset for 3, 5, 6 and 7MA compared with the ITER-P(89) prediction. Although significant deviation might be expected at low heating powers, there remains a 20% deviation at the highest power.

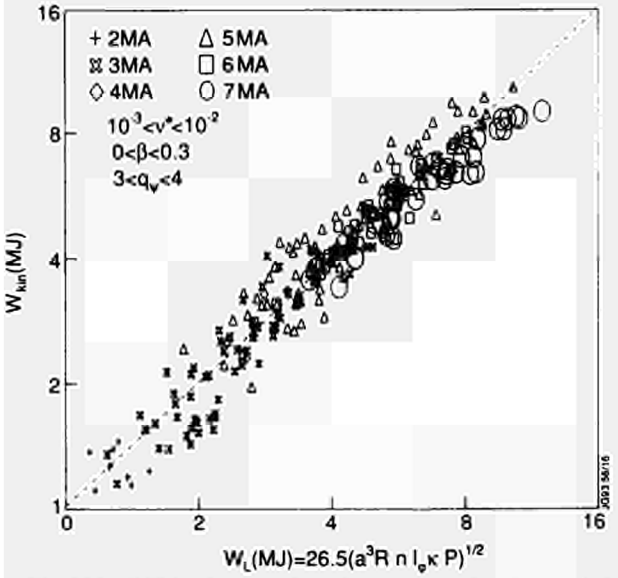

Fig.111: 2-7MA limiter data for restricted values of the dimensionless variables ν^*, β and q_ψ plotted versus the expected long wavelength scaling.

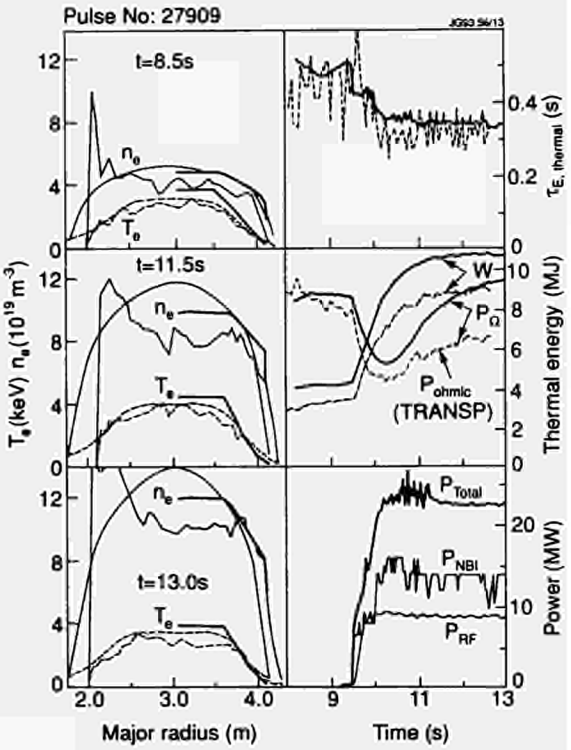

Fig.112: Comparison of the global and local plasma parameters of 7MA pulse (No: 27909) compared with the predictions of the Rebut, Lallia, Watkins model.

These difficulties can be resolved by a dimensionless scaling approach, and Fig.111 shows that, if the range of q_ψ, ν^* and β are restricted, the JET limiter data from 2MA up to 7MA is well represented by a long wavelength global scaling.

As far as local transport is concerned, the Rebut-Lallia-Watkins model can simulate the OH to full power transition at 7MA in terms of both global and local parameters (as shown in Fig.112) with only the edge temperature as a free parameter. The agreement is excellent and within experimental uncertainty.

Conclusions

The 1991/92 experiment did not end with a 'bang' but with a very successful 7MA programme whose technical success leads to improved confidence both for the future of JET and indeed for the viability of high current tokamak fusion reactors. The programme was also scientifically valuable and, in particular, for the completion of the L-mode (limiter) dataset. The 5MA H-mode results look promising for the performance in the divertor phase of JET, where much improved divertor configurations will

be possible at 5MA and above. The error field experiment also has important implications for the future, since it showed that error fields must be controlled to ~1 G, which could be highly demanding.

References

[1] JET Progress Report 1991, No. EUR 14434 EN;
[2] J.P. Christiansen et al, Nucl. Fusion 32 (1992) p 291

Impurity Transport and Exhaust

The objective of the Task Force was to study impurity transport, H-mode and ELM physics and the performance of the divertor. Except for He transport studies the impurity transport results are reported in the section Transport and Fluctuations. All initial observations and results were reported in the 1991 Progress Report. Therefore this report focusses on more detailed analysis of data taken during 1992 and on present understanding of the relevant physics.

Divertor Performance

The investigation of divertor performance concerns the assessment of the Be (lower target) and C (upper target) tiles (Fig.113), erosion and redeposition of the target material, particle transport and density control, impurity retention and model validation. Two additional areas of interest are: (a) the response of the divertor plasma to asymmetric power transported into the two divertor branches (affected by the direction of the ion ∇B drift), and (b) the performance of radiative divertor discharges.

The development of new evaluation methods for the various edge and divertor diagnostics (Langmuir probes, CCD cameras and magnetics) was one of the major tasks. In particular, the determination of the Last Closed Flux Surface (LCFS) with higher accuracy made possible the comparison of measurements in the main plasma scrape-off-layer (SOL) with those at the divertor target. The combination of different diagnostic signals (Langmuir probes, CCD, spectroscopy) from the divertor target and from the SOL yielded a reasonable degree of accuracy.

Accuracy in determining the Last Closed Flux Surface (LCFS)

The position of the LCFS in the SOL and in the divertor must be known to high accuracy to enable measurements on the same flux surface and thus study divertor physics. The XLOC code has produced a substantial improvement with remaining uncertainties <1 cm at the magnetic separatrix strike-points on the divertor target, and in the main plasma SOL.

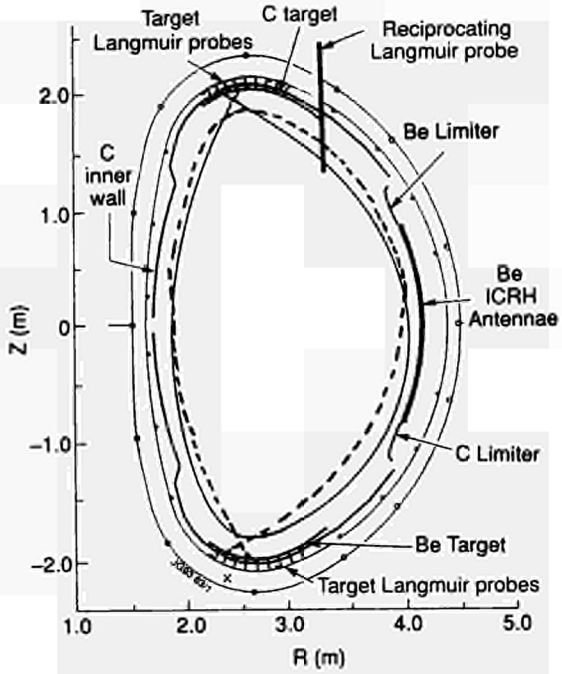

Fig.113: Location of target Langmuir probes and of the fast scanning Reciprocating Langmuir Probe relative to SN upper and SN lower divertor discharges.

On the basis of analytical work on the shape of the flux surfaces [1] at the divertor target, an extensive comparison was possible of Gaussian fits to the Langmuir probe profiles at the target with exponential fits to the SOL profiles measured by the reciprocating probe. The good agreement found between SOL and divertor profiles in SN discharges on the Be target [2,3] suggests that mapping discrepancies are much smaller than 1 cm in outer mid-plane coordinates [2]. However, with the carbon target the same mapping techniques led to inconsistencies of up to an order of magnitude, when comparing the density at the LCFS measured by the reciprocating probe with that obtained from target probes [3]. Although this discrepancy is not understood, it is clear that the reciprocating probe readings were low and those on the target were reasonable (Fig.113).

The accuracy of the location of the LCFS represents a significant improvement over earlier work. However, in order to compare SOL and divertor profiles during H-modes when the profiles are steeper, even greater accuracy is needed, which requires more magnetic flux sensors, as planned for the pumped divertor phase.

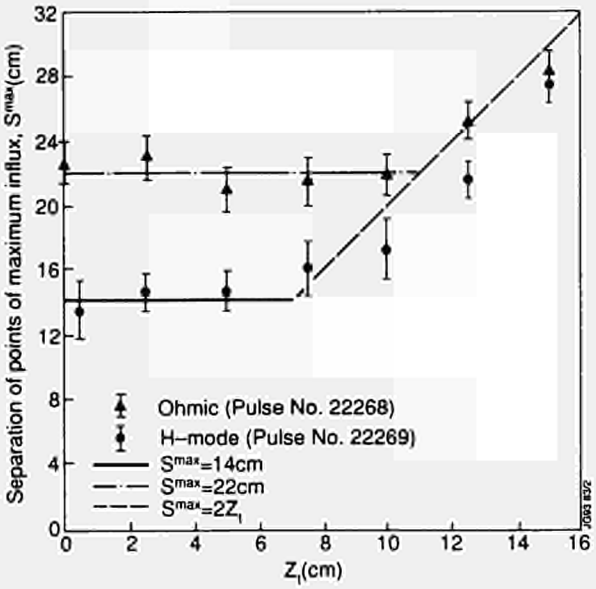

Fig.114: Separation of points of maximum D_α influx from the target versus Δx; compared to model predictions which give S^{max} = const. (Δx=small); S^{max} = 2Δx (Δx=large).

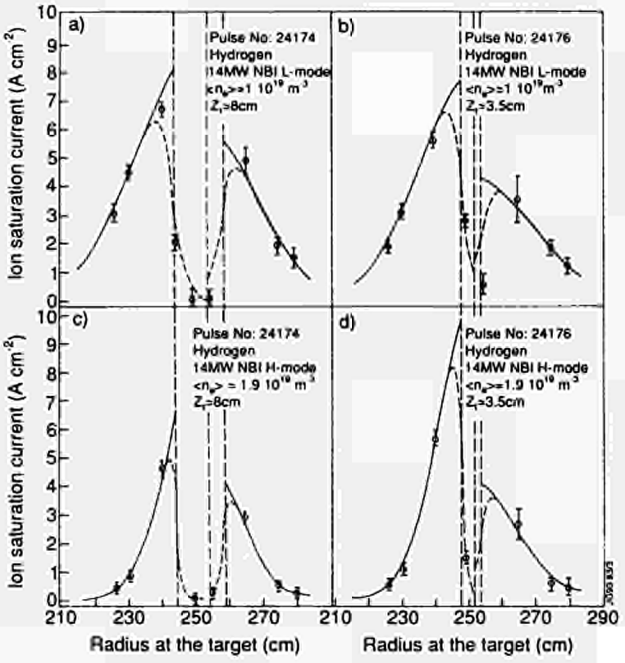

Fig.115: Ion saturation current profiles at the target for two X-point to wall distances in L- and H-mode, respectively. The full lines are fits to the target probe data with no diffusion into the private flux region while the fits represented by the dashed lines include diffusion into the private flux region.

Analytical Modelling of the SOL/Divertor

The Gaussian model profiles[1], taken in conjunction with the variation of field line incidence angle on the target, described the location of the maximum heat and particle flux onto the target in agreement with experimental data (Fig.114). This model has also been used to study the variation of exponential decay lengths in the SOL with main plasma parameters [2]. The sensitivity to $\langle n_e \rangle$, $D_\perp$, and total input power is weak at low densities, and stronger at high densities [3], while the variation with B_Φ is more pronounced:

$$\lambda \sim B_\Phi^{0.4}\ [\Omega]; \quad \lambda \sim B_\Phi^{0.6}\ [L]; \quad \lambda \sim B_\Phi^{1.5}\ [H].$$

Recent results also show a strong dependence on B_Φ in L-mode and in H-mode [4]. One explanation for this scaling is that $D_\perp$ displays an increasing dependence on B_Φ when changing from ohmic (Ω) to L-mode (L) confinement, and an even stronger dependence in H-mode (H). However, the broader, denser SOL obtained at high field contrasts with Bohm diffusion ($D_\perp \sim T_e/B_\Phi$). Another explanation for these dependencies could be based on a strong reduction in parallel transport associated with the increase in connection length. After adding diffusion into the private flux region [5] to the analytical model, a comparison of measured and calculated ion saturation current profiles with and without diffusion into the private flux region has been performed. Fig115 shows that profiles including this diffusion fit the experimental measurements well even over a region within a few cm of the magnetic strike-point on the target.

Another important application of the analytical work was to study the effect of increasing Δ_x on the divertor plasma. Ignoring both the influence of atomic physics and the diffusion into the private flux region, the power peaking factor would increase substantially (up to a factor 10), when Δ_x is increased due to the magnetic flux compression. While the range of Δ_x explored in JET has been relatively restricted (Δ_x <25 cm), it should be up to double this value in the future and should also be large in ITER. Diffusion into the private flux region gives a reduction of the power peaking by a factor ≤2 [6] and this can be further enhanced by atomic processes at the higher density range. These reductions in the predicted power peaking will bring calculations closer to experimental observations [7].

Erosion and Redeposition in the Upper X-point Region

Erosion at the divertor may have serious consequences for ITER unless prompt redeposition greatly ameliorates the effect [8]. Modelling predicts that sputtering of the target will lead to toroidal transport and redeposition back into the erosion zone, with the material eventually drifting to net deposition areas deeper in the SOL. The deposition in the JET divertor region has been analysed to check support for the modelling.

Two continuous toroidal bands of graphite tiles were installed in the upper X-point region for the 1991/92 campaign. Many tiles from each set have been analysed to study impurity movement and the pattern of deposition and deuterium trapping in the X-point region. Studies on the first (flat) set were assisted by including three poloidal tiles across the strike points, coated with ~70μm boron carbide.

Edge effects were observed with the flat divertor tiles, in that a few tiles in each octant experienced high heat loads at one (exposed) edge. All these events occurred at the strike points, and most must have resulted from the short periods of high power operation with ∇B towards the tiles and I_p reversed (counter injection). Patterns of erosion and redeposition can be seen surrounding each of these tile edges, while redeposition is peaked very close to the source. The main distribution of redeposited boron when eroded by sputtering is expected to be at least ~10cm toroidally from the source due to ionisation and transport along field-lines. However, the distribution of redeposited boron was found to be peaked in the private flux region near the source and showed an approximately exponential decrease in concentration away from the eroded edge [9].

The relative amounts of redeposition in the X-point region can be mapped by plotting the amounts of deuterium trapped in the surface due to codeposition. For the flat tiles, the large deuterium concentrations occurred in the private zone, with high concentrations also extending through the inner strike zone and to smaller major radius. In the case of the shaped set of X-point tiles the "ski-slopes" (see Progress Report 1991) facing the ion flux at each strike zone are areas of net erosion. The dominant effects are from plasmas with the ion ∇B drift towards the target and the I_p direction opposite to B_T which is the conventional configuration for upper X-point discharges in JET. Again deuterium levels peak in the private zone and towards smaller major radius.

The conclusions of these surveys is that, under present conditions, erosion at the JET divertor targets is probably dominated by sublimation rather than sputtering. This conclusion is based on the proximity of erosion and redeposition areas, which is incompatible with the expected longer distance transport of sputtered impurity ions.

Effect of the Ion ∇B Drift Direction on the Divertor Plasma

Before describing the findings in detail, a brief definition of the different regimes of the divertor plasma and their major consequences for divertor performance is useful.

There are four different divertor regimes:

- **The low recycling regime:** "constant pressure" along field lines ($P_{Scrape\text{-}off} = 2 \times P_{Div}$); no D^+ flux multiplication in front of target; high target power load, high divertor temperature (T_i and T_e), little impurity retention;
- **The high recycling regime:** "constant pressure" along field lines, reduced divertor temperature, increased particle flux onto the target (flux multiplication > 2); target power load high, better impurity retention due to lower T_i, possibly reduced impurity production depending on target tile material (sputtering yield);
- **The atomic physics regime:** pressure not constant along field lines ($P_{Scrape\text{-}off} >> 2 \times P_{Div}$), power loss perpendicular to field lines due to radiation and CX in the divertor; reduced target power load, less impurity production, divertor temperature (T_e) <10eV, good impurity retention;
- **The gas target regime:** $P_{Scrape\text{-}off} >> 2 \times P_{Div}$; divertor electron temperature very low (<<5eV) due to radiation, neutral deuterons penetrate divertor plasma, slowing down of ion flux towards the target due to ion neutral collisions (τ_p increase in the divertor); Mach number <1 in collisional zone; strongly reduced target power load and target erosion, less impurity production, very good impurity retention if this cold plasma cloud does not extend up to the X-point region (impurities should be ionised in the divertor).

These divertor regimes are considered to be stacked on top of each other starting at the target with the highest density regime achievable and ending with the low recycling regime in the main plasma SOL. The accessibility of the above regimes depends on the main plasma parameters and on the divertor geometry (recycling). The divertor performance improves when moving from a low density high temperature (low recycling) regime towards a high density low temperature regime (high recycling, atomic physics, gas target).

Due to a lower H-mode threshold in single-null X-point plasmas, tokamaks are normally operated with the ion ∇B drift pointing towards the divertor target. In such discharges, a strong asymmetry in conducted power (up to 1:3) between the two divertor branches is observed in JET [10] and elsewhere [11,12]. The consequences of this asymmetry for the plasma parameters in the divertor and for its performance have in general been insufficiently emphasised so far.

In a simple one dimensional analytical model for the SOL such as the two point model [13,14,15], the divertor regime

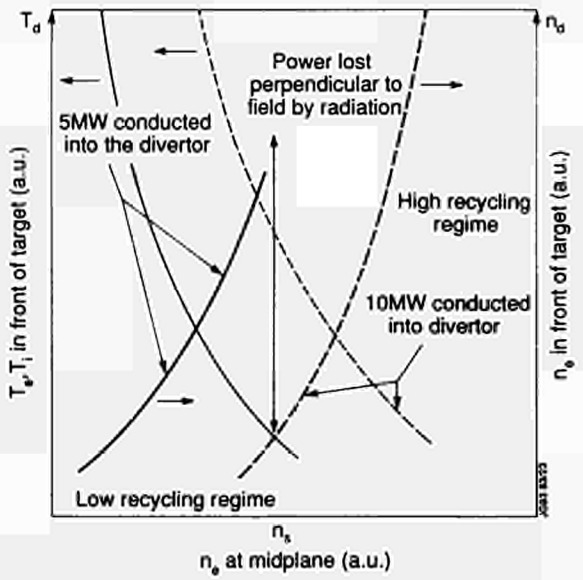

Fig.116: Schematic representation of the dependence of the divertor temperature (T_e, T_i) and density on the scrape-off density in the stagnation point for two different powers conducted into the scrape-off. The curves display the drastic difference in plasma parameters which could occur if a big asymmetry in conducted power between inner and outer strike zone exist.

is mainly defined by the density in the main plasma SOL and by the power flux into the divertor channel. The dependence of the divertor density n_d and temperature T_d on the SOL density n_s and on the power flux parallel to the field lines can be calculated. The power flux conducted into the two divertor branches at a given connection length $L_{//}$, the corresponding divertor densities n_d and temperatures T_d will be different. In addition, different dependencies on the scrape off layer density n_s will be displayed (Fig.116).

In X-point discharges, where the ion ∇B drift was pointing towards the divertor target, the behaviour caused by this strong asymmetry in conducted power is in line with expectations from this model. Figure 117 shows the density at inner and outer strike zones over the line averaged density in the main plasma for both ion ∇B drift directions and many discharges. In the case where the ion ∇B drift was towards the divertor (Fig.117(a)), the inner strike zone density started higher (factor 2) than the outer strike zone density and detached when the main plasma density was increased (high recycling to gas target). The outer strike zone density on the other hand remained relatively low (low recycling regime). When the density increased to where the outer strike zone should enter the high recycling regime, the inner strike zone was starved of power, detached and ultimately caused a density limit disruption. Therefore, it was not possible to achieve a high recycling outer divertor strike zone when the ion ∇B drift was directed towards the divertor target.

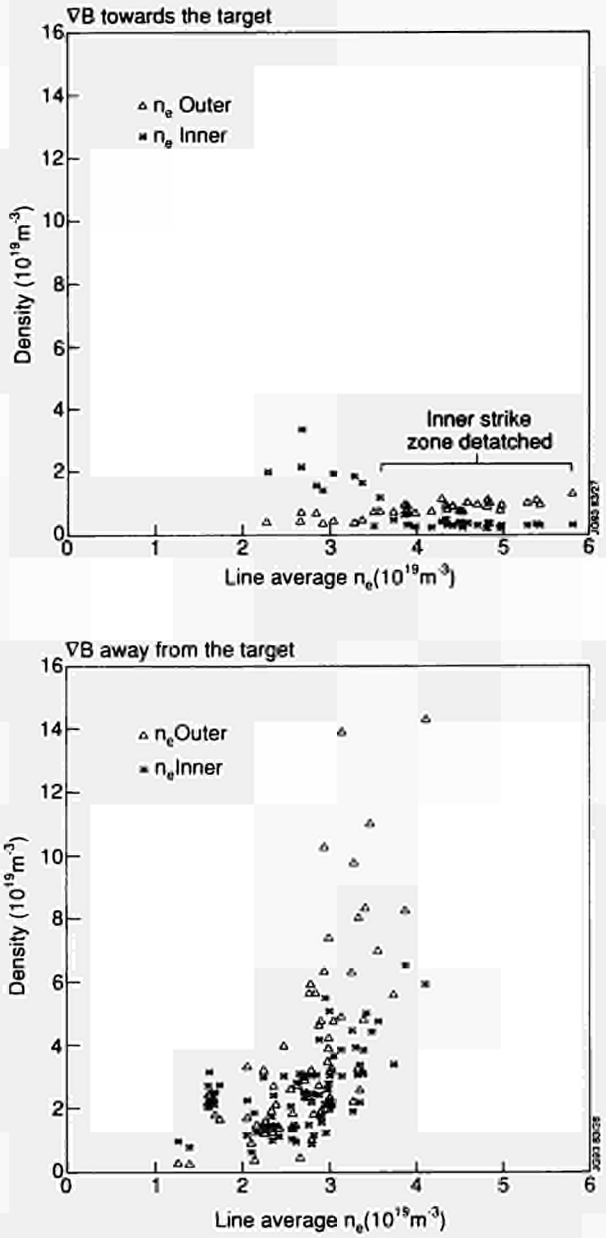

Fig.117: (a) Divertor density at inner (crosses) and the outer (triangles) strike zone versus line averaged density in the main plasma with the ion ∇B drift towards the divertor target; (b) Divertor density at the inner (crosses) and outer (triangles) strike zone versus line averaged density in the main plasma with the ion ∇B drift away from the divertor target.

In discharges with ion ∇B drift pointing away from the divertor target, the conducted power into the two strike zones was more balanced. In these cases, both strike zones were in the same divertor regime for a wide range of densities, allowing achievement of high recycling conditions simultaneously at inner and outer divertor legs (Fig.117(b)).

In addition to the importance of the ion ∇B drift, the X-point to target distance (connection length, divertor volume) also has some influence on the divertor plasma parameters. During an X-point to target distance scan ($\Delta x = 8, 16, 25$ cm) with the ion ∇B drift pointing towards the divertor, a reduced

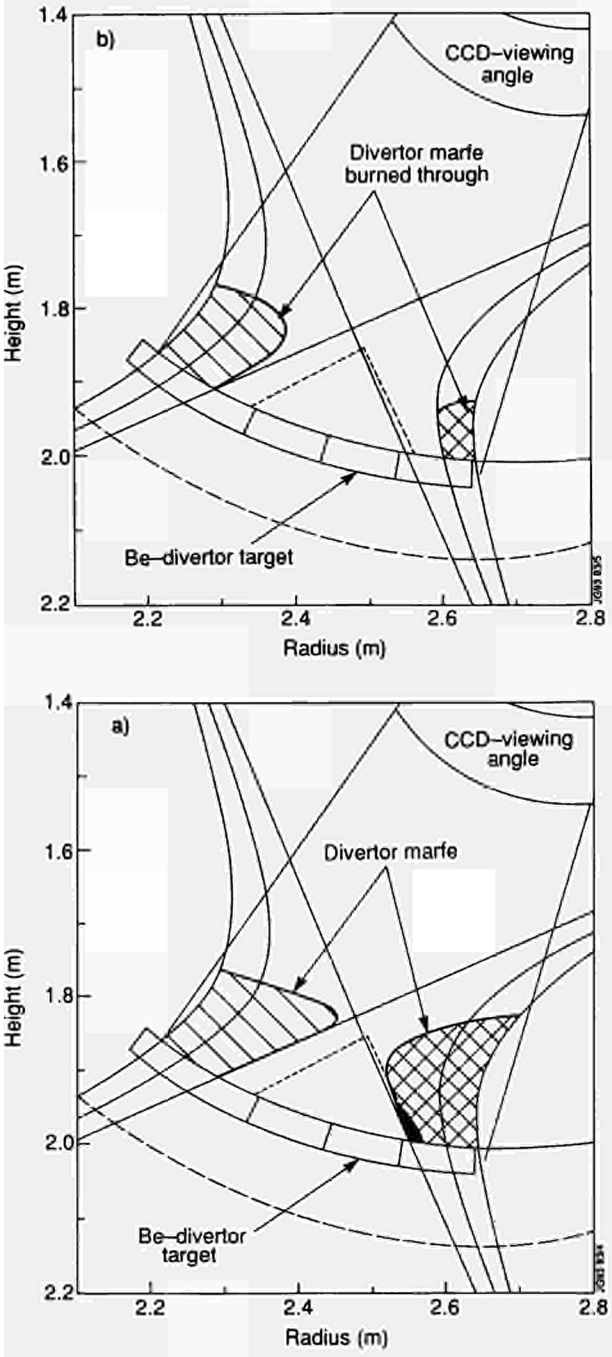

Fig.118: (a) Structure of divertor marfe based on video recordings of D_α radiation. Dark or black regions represent stronger radiation than light shaded areas;(b) Structure of a divertor marfe which is not sustained at the outer strike zone. The radiating cloud is burned through at the inner part of the outer SOL.

asymmetry in the densities and temperatures measured at the two strike zones was observed at the maximum Δx.

However, optimum divertor performance is only possible when the two divertor branches are in the same divertor regime. To achieve this, the conducted power to outer and inner strike zones must be about equal. The only way to obtain about equal power conduction into the two divertor branches is to have the ion ∇B drift pointing away from the divertor target.

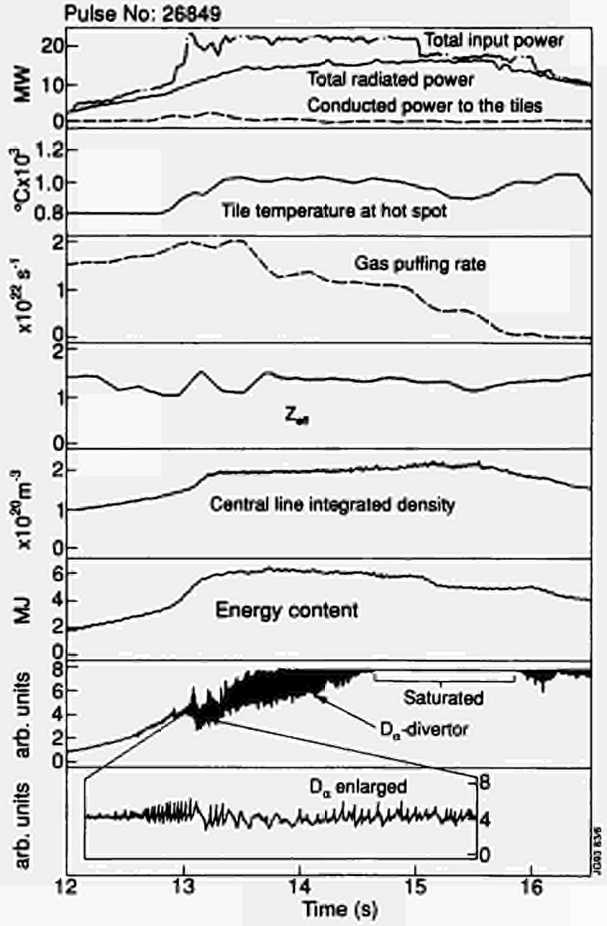

Fig.119: Radiative divertor discharge with 22MW input and 1.0MW conducted power on the target tiles. The quasi-steady state operation of such discharges is demonstrated (Pulse No:26849).

Radiative Divertor Discharges

All radiative divertor experiments were performed in 3MA SN X-point discharges using Be tiles with the ion ∇B drift away from the target. The discharges were heated by a combination of ICRF (10MW) and NB (2 to 12MW) power. One important diagnostic used to assess the quality of a gas target was a CCD camera monitoring the sloped areas of the Be target through a 844.5 nm filter. The signal is a measure of the tile temperature. In some early gas target discharges, the CCD camera used a 1 mm filter, aimed at measuring the tile temperature. However, breakthrough of light from the wings of the Paschen-δ hydrogen line (1004.6 nm) made reliable tile temperature measurements impossible but revealed the geometric structure of the divertor marfe (Fig.118).

In most experiments, a pre-programmed gas puff, required to produce a radiative divertor, was applied at the beginning of the heating pulse and was stepped up with increasing power (1×10^{22} at/s and 2×10^{22} at/s for 12MW and 22MW, respectively). From CCD camera observations, it was concluded that the consequent detachment of the

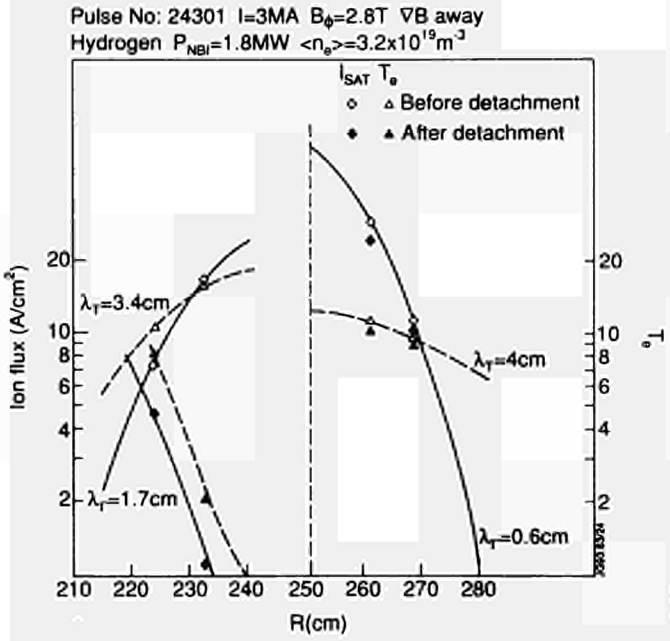

Fig.120: Ion saturation current and T_e at the two divertor strike zones before (open symbols) and after (dark symbols) partial detachment at the inner strike zone. The detachment takes place close to the inner separatrix.

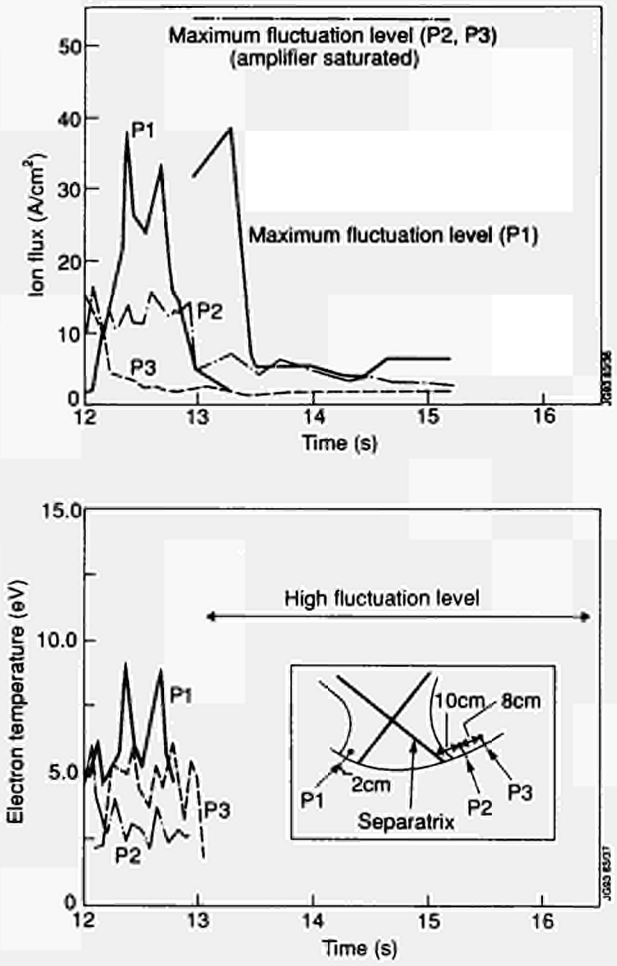

Fig.121: (a) ion saturation current; (b) electron temperature prior to detachment at the inner and the outer strike zone (see inset) for Pulse No:26849. During detachment, the fluctuation level is too high to evaluate probe signals (probably short phases of attachment during power bursts).

plasma from the divertor target always starts at the inner strike zone [16,17] resulting in a marfe-like structure (cold radiating plasma cloud), which fills the inner divertor leg. When increasing the gas puff even further, a second marfe develops at the edge of the outer strike zone (Fig.118(b)) and grows slowly towards the separatrix until it fills the outer divertor (Fig.118(a)). Once this is established, the power conducted to the target (from tile temperature rise) drops below 1MW regardless of heating power applied. At this stage, the divertor marfe can be maintained practically indefinitely by reducing the gas puff rate to a level where it just replaces the particle losses due to wall pumping. Steady state operation (up to 4.0s) with these gas target divertors was demonstrated for various power levels of up to 22MW of ICRF + NB heating (Fig.119).

Fig.119 shows the radiative divertor discharge with 22MW applied. The three curves in the top section represent the power balance by comparing total input power (full line) with the total radiated power (dotted line) and with the power conducted to the target (dashed line), which is only ~1.0MW. The total radiated power is the sum of bulk radiation (6MW) and divertor radiation (10MW). Thus, up to 6MW power is not accounted for in the 2s with 22MW additional heating.

From Fig.119, important plasma parameters such as Z_{eff}, the central line integrated electron density, energy content in the plasma and target tile temperature attain steady state shortly after the start of the high power phase. An important disadvantage of all these discharges is that they do not display H-mode energy confinement regardless of H-mode signature in the D_α signal.

Langmuir probe measurements taken at the divertor target confirm that detachment occurs more easily at the inner strike zone. Some discharges of this type display partial detachment where the divertor plasma close to the separatrix detaches [16] while it remains attached further away from the separatrix (Fig.120). This is in agreement with observations on DIII-D under similar conditions [18], but disagrees with JET CCD observations. Typical electron temperatures at the target prior to detachment were in the range 5 - 10 eV and fall by about a factor 2 when detachment occurs. The reduction in deuteron flux (ion saturation current), however, is typically a factor 5 to 10, which explains the strong decrease in power deposition on the target (Fig.121). During detachment, the probe signals show strong fluctuations with peak values typical of attached plasmas

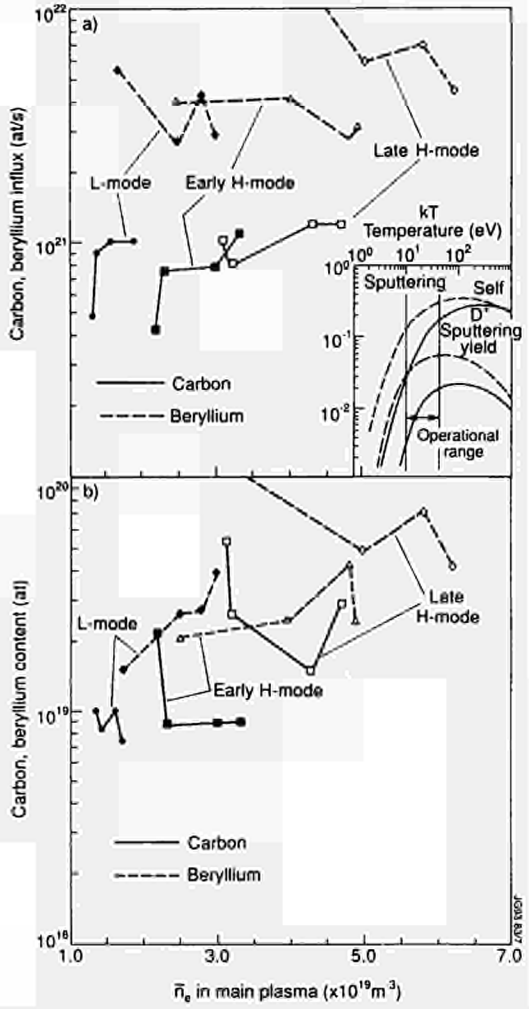

Fig.122: C and Be influxes (a) from the target and the C and Be content; (b) in the main plasma versus volume averaged density in the main plasma. The inset in (a) displays the C and Be sputtering yields (deuteron and self sputtering).

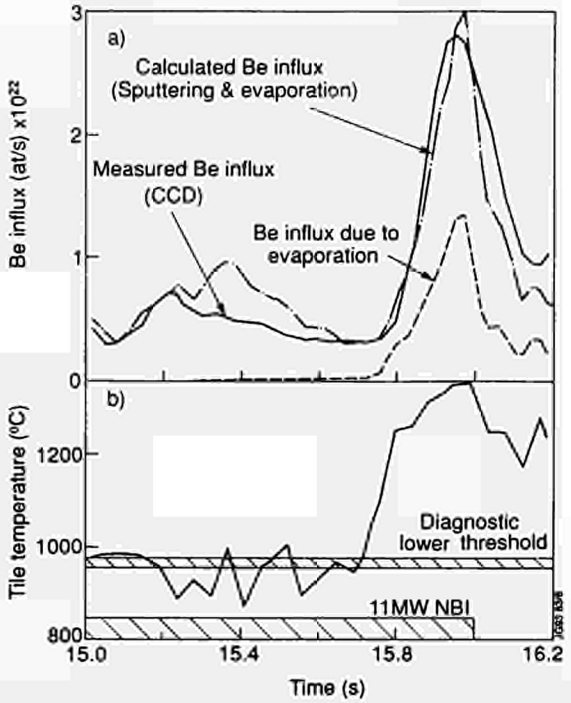

Fig.123: Measured (CCD) and calculated Be influxes (a) taking Be evaporation into account; and (b) tile temperature evolution at the outer strike zone, used to calculate the evaporation rate. The calculated evaporation rate originates from ~10% of the target area but contributes ~50% to the total influx.

superimposed on a low density/low temperature plasma (typical for the private flux region). These fluctuations are also observed with the fast H_α diagnostic (Fig.119) and are associated with short phases of attachment during power pulses due to ELMs or large sawteeth.

To get better operational control of gas puffing rate when producing radiative divertors, a simple tile temperature feedback system was introduced. It consisted of a fibrescope aimed at one of the sloped areas on the outer strike zone of the Be target, which usually sees the highest power deposition. The fibre was coupled through an 815 nm filter to a photo-multiplier. The temperature signal was then transformed by a simple algorithm into a pseudo-electron density signal and fed into the standard density feedback system.

The aim of this second set of radiative divertor experiments was to achieve an H-mode together with a gas target and to test the simple tile temperature feedback system. It turned out that the tile temperature feedback system, when given full control over the gas modules, allowed the H-mode transition to occur before the gas target was established. These discharges displayed an initial ELM-free H-mode phase and made a transition into an ELMy H-mode once the divertor plasma detached. The relatively high ELM frequency deteriorated the energy confinement considerably, resulting in only 1.4 times L-mode confinement.

Comparison of C and Be Target Tiles

The type of discharge used for this comparison was a 3.0MA, 2.8T SN X-point discharge with the ion ∇B drift towards the target and an X-point to target separation of 8.0cm. 2MW NB heating was applied at 12.0s, and this was stepped up to 11MW at 15.0s for 1.0s (Be) or 1.2s (C), respectively. Four discharges of this type with different densities were performed for each target. Three different times were compared. The first time point was during the low power L-mode phase, the second was 0.5s into the high power H-mode phase (early H-mode) and the third was at the end (after 1.0s) of high power H-mode phase (late H-mode).

Since the plasma parameters in front of the two divertor targets were quite similar for similar discharges, the impurity production on the C and Be target can be compared.

From Fig.122(a), it can be seen that throughout the L-mode, and the early H-mode phase, Be influxes are about a factor 3 higher than the C influxes. This is in good agreement with sputtering yields for electron temperatures in the range 10 - 40eV (Fig.122). At the end of the high power phase (late H-mode), Be influxes were considerably higher (up to a factor 30 in the low density discharge) than the C influxes. This behaviour can be explained by the onset of Be evaporation due to target tile temperatures exceeding 1200°C (Fig.123). No significant increase of the C production during the late H-mode can be observed compared to the early H-mode phase, regardless of the fact that the C tile temperature at this time is between 1600°C and 1800°C. When considering Radiation Enhanced Sublimation (RES), which is predicted to be important at these temperatures [19,20,21], it must be kept in mind that only 10% of the target area (sloped tiles) reaches high temperatures, while the rest stays well below 1200 °C. Since Cl^+ ions can travel considerable distances from their birth point, it is unlikely that RES produced C ions hit a hot surface. Therefore, a significant amount of RES self sputtering on hot surfaces can be excluded. When taking this kind of approach, calculated impurity influxes, with and without RES, differ only by a factor of 1.5 to 2. This difference is much too small, when considering the accuracy of our measurements, to make a final decision about the importance of RES, which has not been observed in dedicated experiments on TEXTOR [21], contrary to expectations.

As mentioned, Be evaporation is observed at the end of the 1.0s long 11MW NB heated H-mode phase and unacceptable Be influxes result. Figure 123(a) shows the measured and calculated (sputtering + Be evaporation) impurity influxes, and the contribution of Be evaporation to the total Be influx in the late phase of such a low density H-mode discharge. It can be seen that the influx due to evaporation accounts for almost 50% of the total Be flux, regardless of the fact that it originates only from the sloped tiles (10% of the surface). The second half of the flux can be explained by using a sputtering model including Be self-sputtering and measured plasma parameters in front of the target. From Fig.123, it can be seen that the temperature briefly exceeds 1300°C, above the melting temperature of 1285°C. The discharges with higher densities did not quite reach melting temperature but also suffered from substantial evaporation rates. This underlines the attainment of the power handling limit for the Be target in this type of discharge.

No such limit could be observed for these discharges on C tiles regardless of the high tile temperatures observed.

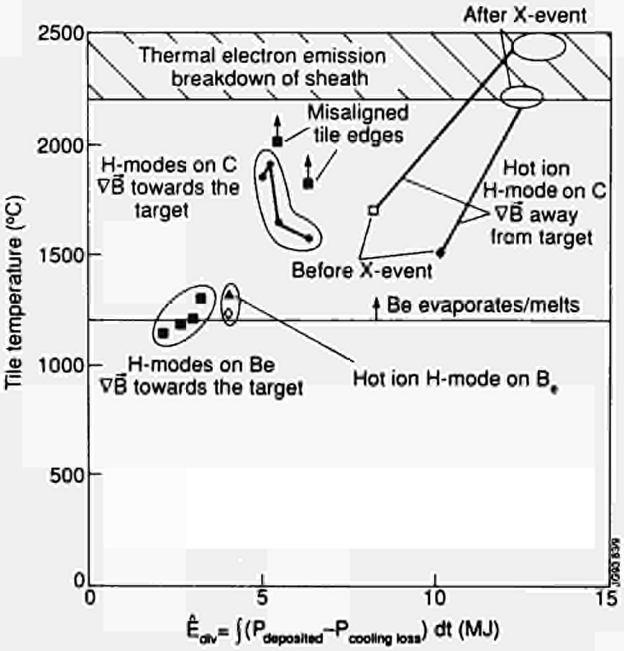

Fig.124: Tile temperature versus accumulated energy on the target for H-modes with ion ∇B drift towards the Be or C target, and for hot ion mode discharges with ion ∇B drift away from the Be or C target.

Only in hot ion H-mode discharges where the C tiles reached temperatures over 2200°C was a strong increase in the C influxes observed (sublimation). In some high performance discharges, such temperatures were reached on exposed tile edges when the plasma was not optimally positioned on the target (normal C-bloom). In most cases, however, a sudden loss of the good confinement phase (X-event), caused a dramatic increase of the power conducted to the target.

Due to this rapid large energy deposition during an X-event, the target tile temperature at the outer strike zone is driven from ~1700°C before the crash to 2500°C. At this temperature, a breakdown (reduction) of sheath potential in front of the target due to thermal electron emission occurred, which could further increase conducted power to the already overheated tiles (limited to factor ~2 by perpendicular transport into flux tube). Visual inspection of recorded C II - CCD images, and tomographic evaluation of spatially resolved VUV spectroscopy, suggested that C atoms (neutrals) can reach the main plasma SOL during this phase. This breakdown of divertor impurity retention (no ionisation in the divertor) together with high impurity production at the target pollutes the plasma severely and causes irreversible loss of high performance. In Fig.124, the observed tile temperatures of these discharges are plotted versus energy accumulated on the target tiles, summarising the power handling capability of the two different target materials.

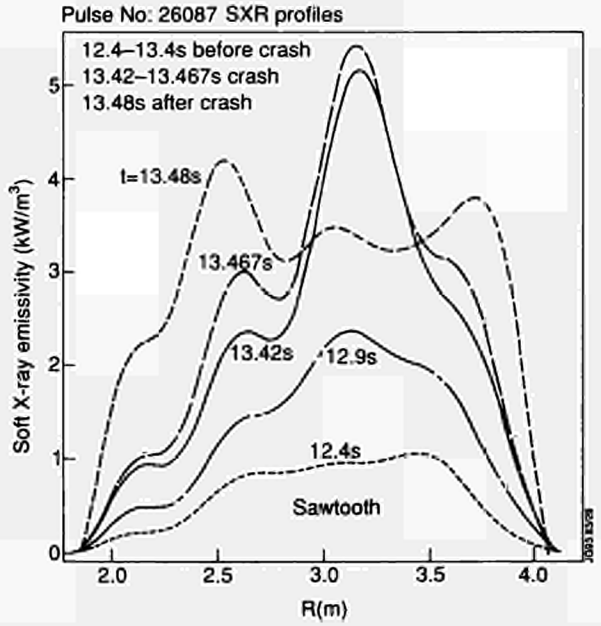

Fig.125: Tomographically reconstructed soft X-ray profiles of Pulse No:26087 before and after the X-event. The crash of the central radiation peak and evolution of pronounced shoulders can be seen.

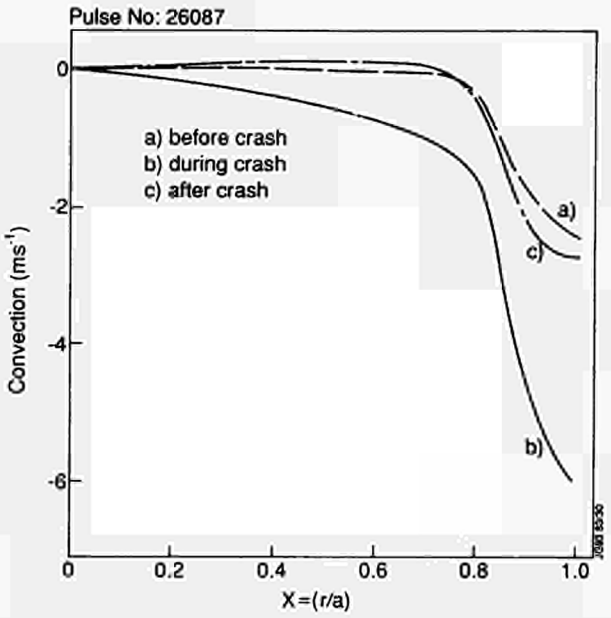

Fig.126: Inward drift velocity from simulations (a) before (b) during and (c) after the X-event. The drastic change of V_{in} in magnitude and radial extent during the X-event is shown.

As shown Fig.124, all Be discharges are close to, or exceed, the power handling capability represented by the melting/evaporation limit at 1200°C. The discharges on the C target have accumulated higher energies resulting in higher tile temperatures. The higher energy loads of C tiles is due to their lower thermal conductivity compared to Be (~2). Fig.124 shows that no discharges on C tiles is limited by the tile temperature except discharges after an X-event.

Impurity Transport in the Main Plasma during an X-event

In the period prior to the neutron rate roll-over (X-event), the soft X-ray (SXR) signals consistently show build-up of a moderate impurity accumulation in the plasma core. Fig.125 shows the time evolution of tomographically reconstructed SXR profiles for Pulse No:26087. The central peaking, occurring in the absence of sawteeth, is a fairly slow phenomenon stretching over ≈1s, compared with the ≤50ms of the fast collapse phase between the neutron yield roll-over and the terminal crash. This peaking is a further indication of the presence of a central region ($\rho \leq 0.3$, ρ = normalised minor radius) of good confinement, where anomalous diffusivity is greatly reduced [22]. However, the amount of carbon in this region according to charge exchange (CX) spectroscopic data can account for only a fraction of the SXR radiation (30-40%). Satisfactory simulations have been obtained with addition of a small concentration (10^{-4}) of Ni or Cl, accumulating in the plasma core. At the plasma periphery, CX carbon profiles show a piling-up at a radial position of $\rho \sim 0.75$, producing 'shoulders' in the SXR profiles. This indicates that, in the outer plasma, inward convection is the dominant transport mechanism for carbon, with a ratio of convection over diffusion up to 10 times L-mode.

During the fast confinement crash, the carbon influx increased rapidly and a fast carbon peripheral pile-up coupled with an increase of the SXR 'shoulders' can be simulated only by stepping up the convective term both in value and in spatial extent, in some cases up to the centre of the discharge. After the crash, the central peak disappears while the 'shoulders' develop further moving outwards. The simulation shows that this behaviour is reproduced by stepping back the convection to previous values (Fig.126).

Due to the massive carbon influx during the confinement crash, plasma profiles undergo rapid changes as far as local dilution and cooling are concerned (e.g. bulk ion profile and its gradient changes substantially). Therefore, the transport time evolution could be compatible with qualitative expectations from a neoclassical transport mechanism, for which $\nabla n_i/n_i$ and $\nabla T_i/T_i$ are the thermodynamical driving forces.

Power Deposition Profiles during Hot Ion H-modes

During high performance hot ion H-mode discharges, a narrow region of high power deposition has been observed

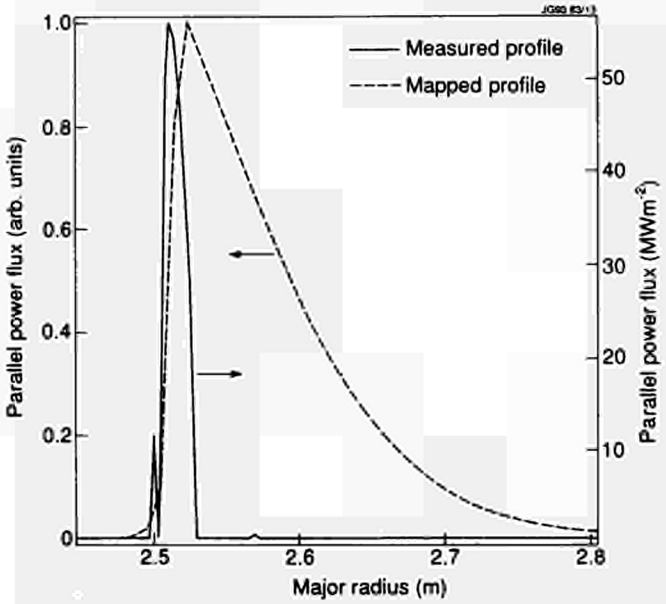

Fig.127: Radial power flux in Pulse No:26087 (outer strike zone) compared with mapped power flux profile (relative units)

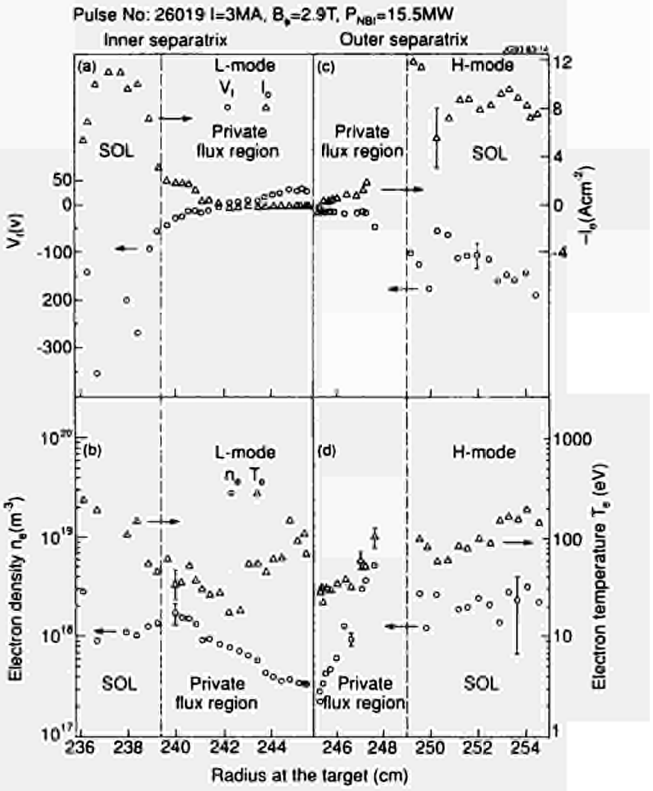

Fig.128: Plasma density and temperature profiles (b, d) and floating voltage and current to the target (a, c) for an NB heated discharge. The results for both strike zones and different confinement regimes are shown (Reversed B_t).

(CCD) on the divertor target at the two strike points of the separatrix. From time and spatially resolved target temperature measurements, radial power flux profiles have been calculated. A general feature of these profiles is a radial decay length at the target of ~1-2cm. This sharp decay contradicts calculated power flux profiles obtained by mapping measured plasma profiles in the main SOL along the magnetic field lines onto the target plate (Fig.127), as well as those obtained by extrapolating measurements of target probes located far away from the separatrix. The narrow profile is superimposed on the wider one and the latter is sometimes below the detection limit of the CCD camera measuring the tile temperature [23].

The existence of a narrow power deposition profile at the strike points is supported by Langmuir probe results [24]. In discharges in which the separatrix is swept over a probe, profiles of plasma parameters in the vicinity of the separatrix have been determined with high spatial resolution (R≤ 1cm). In these cases, the floating voltage shows large negative values, ($V_f \leq$ -100V) for both L and H-mode and both directions of the toroidal field. This observation implies the existence of large currents from the grounded plate to the plasma ($|I_0| \leq 10 Acm^{-2}$). Figs.128(a), (b), (c) and (d) show the profiles of n_e, T_e, V_f, I_0 at both strike zones for a discharge with moving X-point location. The inner and outer probes are crossed by the separatrix at different times, therefore the profiles in Figs128(a) and (b) (inner separatrix) are related to the L-phase of the discharge and the profiles in Figs128(c) and (d) (outer separatrix) to the H-phase. Fig.129 shows clearly a narrow layer (R= 1 - 2cm) of high $|I_f|$ and negative V_f near both separatrices, where the separatrix location is from magnetic data (XLOC) [25].

An estimate of the power flux into this narrow region for the outer separatrix during the H-mode, taking into account the large positive bias of the divertor plate with respect to its floating voltage, gives values of q_p = 125 - 490MW/m² (depending on assumptions about the influence of the secondary electron emission in the sheath) [24]. The total integrated power in this narrow region is then ~ 0.65MW to 2.5MW. This is not only relevant for the global power balance but shows also the intense power deposition that can take place in this narrow region of the target (F=0.31m²). A simple integration of the power flux in the narrow region over the toroidal coordinate for Pulse No:26087 using the CCD measurements gives P ~ 0.16MW which is negligible compared with ~8MW conducted into the SOL. However, the low value obtained contradicts estimates from Langmuir probe data. This discrepancy may be caused by 2D effects of heat conduction in the highly anisotropic graphite.

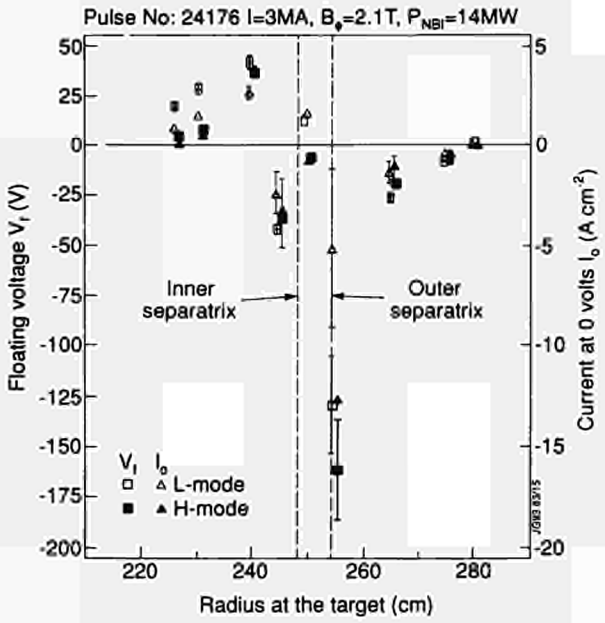

Fig.129: Floating voltage and current to divertor plate for a NB - heated discharge ($I_o > 0$, current towards the plate, $I_o < 0$, current away from the plate)

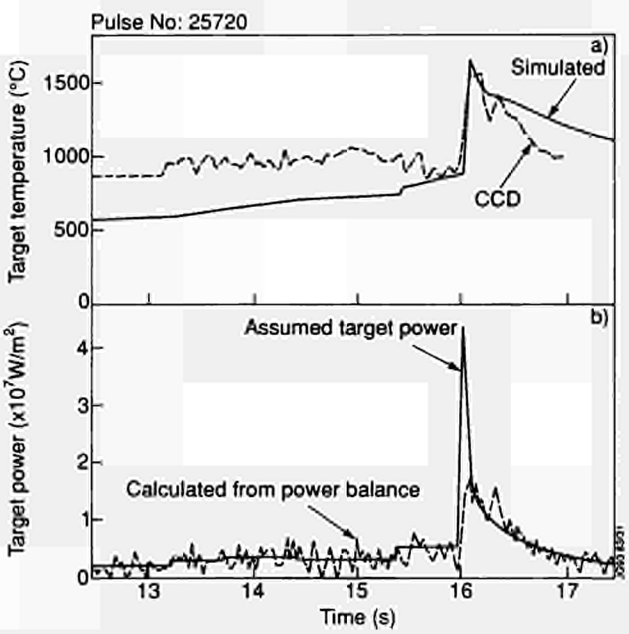

Fig.130: (b) Derived (dashed) and simulated (solid) target power. (a) The simulated target power explains the target tile temperature measured by a CCD camera. The dynamic range of the CCD-camera starts at – 900°C.

A similar behaviour of the floating voltage near the separatrix strike point on the divertor target are also found in low/medium density ohmic discharges in JET. However, the floating voltages are smaller in magnitude than those observed in discharges with additional heating. Results from the reciprocating probe operating in the main SOL are not inconsistent with a strong current flowing away from the target plates in the vicinity of the separatrix [24].

The origin of the narrow region of high floating voltage and power flux at the strike points of the separatrix is not clear. Obviously, a hot electron component in the divertor plasma may explain the observed features. On the other hand, highly non ambipolar plasma transport on the target plates due to steep gradients near the separatrix strike points may be the underlying mechanism. There are severe implications for the local loading of the target plates and a small improvement of the total power balance in H-modes.

Power Balance and Target Tile Temperature

The target load, P_{targ}, in divertor discharges can be evaluated from the global power balance:

$$P_{targ} = P_{div} - a\,P_{div}(rad) - b\,P_{div}(CX)$$

$$\text{where } P_{div} = P_{heat} - P_{rad}(bulk) - dW_p/dt$$

P_{div} is the power conducted into the divertor, P_{heat} is the total heating power, P_{rad}(bulk) is the bulk plasma radiation loss, P_{div}(rad) is the radiation power dissipated in the divertor and P_{div}(CX) is the power loss due to charge exchange processes. "a" and "b" account for a certain proportion of the respective losses dumped onto the target, according to divertor geometry and energy reflection coefficients. In the case of negligible wall losses, the power load on the target, deduced from the target temperature measurements, should be close to the calculated power P_{targ}.

The divertor targets have been monitored with a CCD camera for a series of discharges and target temperatures have been deduced within a dynamic band of ~600°C. The limited range of these measurements can be bolstered in many cases by relative temperatures, deduced from spectroscopic background radiation. The target temperature can be calculated approximately, using a simplified one-dimensional model, which disregards lateral heat diffusion.

The measured tile temperature can thus be simulated by the calculated one, except during fast transient events, such as the H- to L-mode transition or giant ELMs and X-events. In the latter cases, short heat spikes have to be added to the derived target power, in order to explain the observed target temperature rise. Figure 130 shows the measured and the simulated target tile temperature, respectively, for a single-null X-point discharge on the Beryllium target. A comparison between the power calculated from the power balance alone and the simulated target power where a short power spike is taken into account can also be seen. This power spike which marks the end of the H-mode phase, must exceed the one derived from the standard power balance measurements by a factor ≃3 (45MW/m^2) to match the observed tile

temperature rise. The necessity to assume such a short power spike on top of the one obtained from the power balance comes from the low time resolution of some of the signals used for the power balance calculations, which therefore miss these short spikes.

Particle Transport, Density Control and Fuelling

To understand the interrelationship between plasma fuelling, divertor plasma density (i.e. recycling) and main plasma density as well as the role of the material surfaces, fuelling studies were carried out. Comparisons were made between discharges where the location of the external gas fuelling source was changed from the plasma mid-plane to the divertor region. In other experiments, the plasma configuration was changed from limiter to divertor and the resulting density variations were studied. Additional studies comprised discharges with central particle fuelling i.e. by pellet injections or neutral beam injection.

The experimental results were analysed by means of an extended particle balance model [26]. It is based on results from earlier studies [27], where plasma particles which hit the material surfaces were assumed either to diffuse into the material or to leave it by recombination into molecules. Those leaving the surfaces were assumed to fuel the main plasma, however, only with an efficiency of less than unity, while the complimentary remaining ones would return to the surface. Results of the analysis show that for a given external fuelling flux the plasma density and the magnitude of the recycling flux depend, in a non-linear fashion on the pumping capacity of the material surfaces. For quasi-steady state (i.e. plasma density constant but still wall pumping), the plasma particle inventory N can be written in terms of the external fuelling flux as:

$$N = \tau\,[F_r/(1 - R) + F_{ex}]\,\phi$$

where t is the average global particle confinement time in the main plasma, F_r is the fuelling efficiency of recycling particles, F_{ex} is the fuelling efficiency of externally fuelled particles, R is the fraction of the particle flux which recycles, (1 - R) is the pumping efficiency of the wall and ϕ is the external fuelling flux.

For a situation where R is close to unity, the recycling flux dominates the fuelling, unless F is very small. For JET divertor configurations, F can be estimated as 0.1 or less, while R can be close to unity in steady state conditions. In this case, the recycling flux is typically an order of magnitude larger than the external fuelling flux. This explains why the plasma density is almost independent of the fuelling efficiency for the direct fuelling flux, and hence independent of the location of the external gas source. However, during transitional periods, such as a change of plasma configuration or a change of plasma input power as well as plasma fuelling, R can fall to values of 0.5. In these cases, recycling flux and external flux can be of similar order and the attainment of high recycling conditions in a divertor can be temporarily hampered.

Generally, the highest density divertor is achieved for a given main plasma density when one has as little pumping as possible, fuels (externally) directly into the divertor (i.e. $F_{ex} = F$) and restrains the fuelling efficiency for recycling particles. The latter is best obtained by designing a closed divertor, where neutrals are prevented from escaping into the main plasma region. In addition, a low particle confinement time τ is also beneficial. Thus, plasma edge (divertor) fuelling is preferred over central plasma fuelling (i.e. fast pellets), where both the smaller anomalous particle diffusion in the plasma centre and the larger penetration depth for such neutrals contribute to an enhancement of τ. This would in turn reduce the external fuelling flux necessary to sustain plasma density and, thus, the recycling flux in the divertor.

Model Validation and Edge Data Base

A database of experimental JET data relevant to plasma edge physics has been created, using the standard time slicing and data extraction software used to create the Transport Database. The EDGE1D and EDGE2D fluid codes which are both coupled to the NIMBUS Monte-Carlo neutral hydrogen code, have also been used to write data into this standard format. Therefore, the first detailed comparisons have been made between plasma edge diagnostics and code predictions to investigate purely empirical scalings within the data. Work is underway to create a joint JET/DIII-D edge database to extend the parameter range of the data set.

In L-mode discharges, good agreement has been found between code predictions and experimental data. Figure 131 shows the variation of the electron temperature, T_e, measured by the divertor target Langmuir probes at the inner and outer strike zones, with the outer strike point density. Data from the reciprocating probe (RCP) which traverses the SOL near the stagnation point is also shown. The lines overlaid on the figure were generated using the EDGE1D fluid code and shows good agreement with experimental data. The measured differences in T_e between the divertor and SOL are consistent with the EDGE1D predictions based

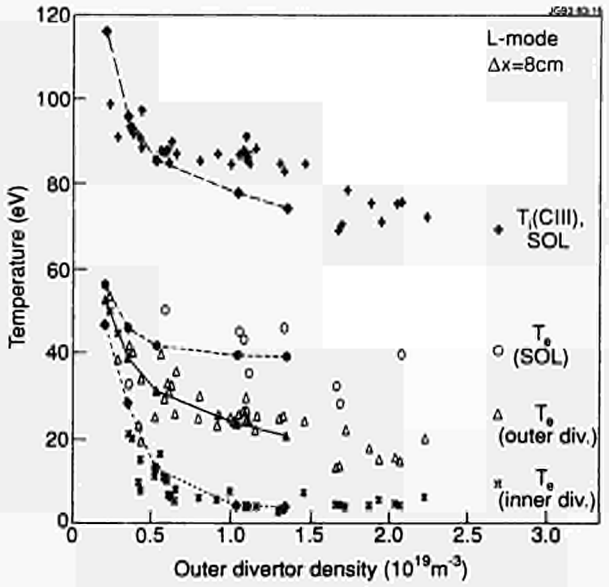

Fig.131: Temperature versus outer divertor density in L-mode discharges on the Be target. Solid symbols represent the code results while the open symbols are measured data.

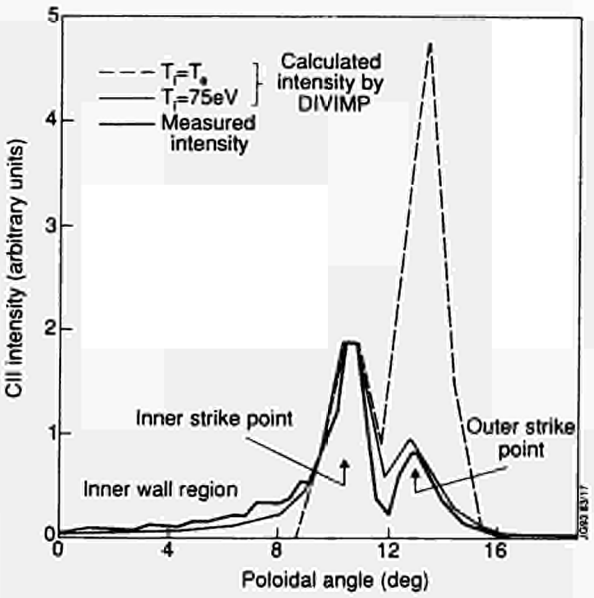

Fig.132: CII intensity versus poloidal angle. The heavy line represents experimental data, the dashed line a DIVIMP simulation, with $T_e = T_i$ and no wall source, and the solid line shows a DIVIMP simulation, with T_i=75eV and a C wall source. Simulations and measurement are normalised at the inner strike zone.

on classical parallel transport. To achieve the observed inner to outer temperature asymmetry the power flow to the outer half of the plasma had to be increased by a factor of three. The experimental results were obtained with ∇B towards the target and show that we can achieve a high recycling low temperature regime at the inner strike zone, whilst the outer divertor remains hot. Much greater symmetry in conducted power was seen with the ∇B drift away from the target. It has yet to be determined whether this effect is due to asymmetries in transport or drift terms not yet included in the models.

Figure 131 also shows the agreement between predicted SOL ion temperatures and the CIII ion temperature measured spectroscopically near the RCP location. Calculations show that in these discharges the ion temperature is sensitive to electron-ion equipartition and ion convection. The correct prediction of upstream ion temperature suggests that the neutral particle code NIMBUS correctly predicts the ionisation sources and that equipartition is consistent with classical theory.

Similar data to that in Fig.131 has been obtained for H-mode discharges with up to 10MW NB heating. Poor agreement with code predictions was obtained unless the power flow into the SOL was assumed to be much smaller than that obtained from the experimental power balance. NIMBUS calculations suggest that a fraction of this unaccounted power may result from charge exchange losses inside the separatrix.

Experimental spectroscopic data from the divertor and SOL cannot usually be directly compared with the output from fluid codes. This problem is being solved by the DIVIMP Monte-Carlo impurity transport code which can be used as a diagnostic simulator. DIVIMP provides a full kinetic description of impurity behaviour in a specified background plasma, which is usually chosen to match the divertor target probe data. The DIVIMP output gives the spatial distribution and temperatures of the different ionisation stages of the impurities. A post processor which is coupled to the JET atomic database ADAS can then integrate the expected spectroscopic emission along the lines-of-sight of any of the spectrometers. Work is in progress to link the output to the PPF system so that simulated signals can be extracted into the Edge Database.

Figure 132 shows the comparison between simulated and measured CII signals from the spatially scanning monochromator. When the temperature near the target is low, the energy dependence of the sputtering yield makes the results sensitive to divertor ion temperature which is not measured. A tail on the experimentally observed distribu-

tion can also be seen in Fig.132 which results from impurities released by the inner wall. DIVIMP simulations have shown that although the sources of impurities originating from the walls of JET are smaller than those originating at the divertor targets they are still a major contributor to the core impurity content. This is due to the relatively poor screening efficiency of the SOL. NIMBUS calculations for the charge exchange sputtering of walls correctly predict the spatial distribution of the wall sources but the experimentally measured impurity sources appear to be larger.

The discovery that wall sources of impurities are a major contributor to the core impurity content provides a strong argument in favour of closed divertor concepts. Such a divertor would reduce the charge exchange flux to the walls in the main chamber and hence the wall source of impurities.

Helium Transport and H-mode Physics

Helium Transport in the Core Plasma

JET measurements have shown that particles are intrinsically much better confined than energy [28,29]. The recognition that the consequent helium ash accumulation threatens long pulse operation of a D-T tokamak has made investigation of helium confinement and removal an important R&D issue for ITER [30]. Exploration of these questions has been undertaken in JET [31] and elsewhere [32,33]. Using 130keV NB helium atoms as a central source in the plasma, the evolution of the resulting fully-ionised helium ion density profiles has been measured in 2.8T, 3.5MA D discharges. L- and H-mode plasmas were compared at similar input power levels by comparing elongated limiter discharges (L-mode) with DN X-point discharges (H-mode). These experiments were performed in sawtooth-free discharges so that differences due to diffusive, local transport could be more easily distinguished.

The main diagnostic for determination of helium ion density profiles is the charge exchange spectroscopy (CXS) system [34]. Reliable determination of helium density profiles and gradients are required, placing great demands on the accuracy and precision of the charge exchange measurements. One known influence on CXS measurements of helium is the so-called plume effect [35]. Since beam attenuation causes the desired prompt signal to vary by up to an order of magnitude, the relative contribution of the plume is found to change over the spatial extent of the measurements, thus directly influencing determination of the gradients. This effect depends critically on the neutral beam and diagnostic geometry.

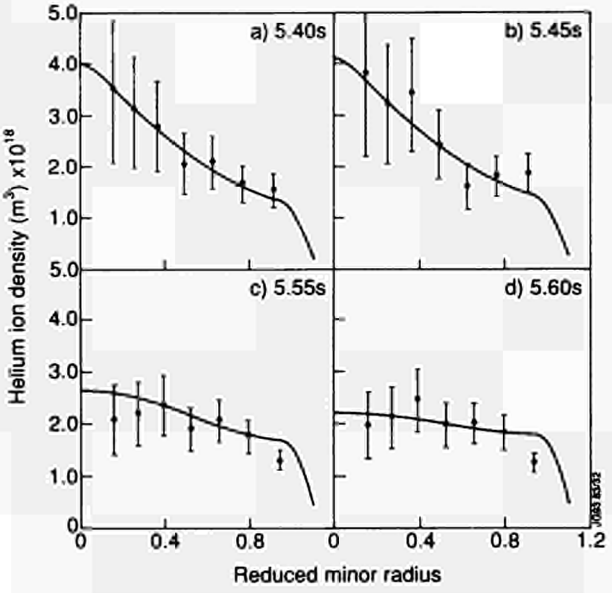

Fig.133: Helium ion density profiles in a typical L-mode discharge. Helium fuelling ends at 5.5s. The points are experimental measurements using CX spectroscopy, and solid curves are simulations of densities using an impurity transport code.

When a neutral beam is injected into a plasma, it is attenuated primarily by a combination of ion impact ionisation and charge transfer with target ions. Since the target ions in the plasma core are fully ionised, the result of the charge transfer collisions is a population of excited hydrogen-like ions. The radiation from these ions as they relax back to their ground state is the basis for CXS (the prompt signal). The hydrogen-like ions are far out of their ionisation balance and thus reionise quickly. However, at the typical ion temperatures in JET, their ionisation length is several metres. Since there is a significant probability of re-excitation and emission before ionisation, these hydrogen-like ions contribute to corruption of both the absolute level and spatial localisation of the impurity density measurement. The expected plume contribution to the measured signal has been calculated for the geometry and plasma conditions specific to the helium experiments [35]. Differences up to 50% were found between deduced helium densities and those if the plume effect was ignored. In fact, in view of the uncertainties, the policy was adopted of disregarding points with predicted plume corrections of more than 30%. In any case, these points are the ones with the largest fitting errors.

The helium ion density profiles are shown in Fig.133 for an L-mode discharge. In this pulse, helium fuelling beams

were on for 1s until 5.5s, after which the helium profile was relaxed to its equilibrium profile. The central peak in the helium density has approximately the same width as the calculated beam particle deposition profile. This peak disappears within 50ms of the termination of central fuelling. Modelling of the evolution of the helium density has been performed using a $1^1/_2$D transport code. During fuelling, the density gradient in the plasma core can be reproduced using a central helium diffusion coefficient of 0.3 ± 0.1 m^2s^{-1}. In contrast, simulating the rapid loss of density peaking requires a core diffusion 4-5 times larger. This large discrepancy is not understood. However, these discharges were specifically designed to be sawtooth-free and had a continually evolving current profile. The requirement, in simulations, of an explicitly time-dependent diffusion coefficient may be related to non-stationary target plasma conditions.

It was not possible to produce any measurable peaking of the helium density profile in H-mode pulses even in discharges with strongly peaked particle fuelling. Thus, it appears that the helium fluxes in the core must be quite large. Exhaust of helium from such an H-mode discharge is then likely to be limited by the size of any reduced particle flux at the plasma edge. As such, conclusions on helium exhaust in H-modes are only possible in experiments which combine a central source and an active helium pumping system. These experiments will be a focus of attention during the divertor phase.

H-mode Physics

H-mode studies during 1992 continued the major themes of the 1991 experiments. Establishing a steady-state H-mode in which plasma parameters were held constant by ELM's was given the highest priority. In addition, further efforts were made to clarify changes in the boundary plasma at the L- to H- transition and to investigating the physics of ELM's.

The improvement in particle confinement associated with the transition to an ELM-free H-mode generally leads to monotonically rising density, impurity content and radiation power. As a result, the H-mode invariably collapses due to radiation on a timescale of 3-5s. In some cases [36], strong gas puffing has been found to maintain a constant impurity content, but the rising density nevertheless caused a radiative collapse. Experiments in the most recent campaign have shown that, under some circumstances, continuous gas-puffing provides a technique for ELM generation which can be maintained for long periods (>18s) and which can allow access to a steady-state H-mode regime [37].

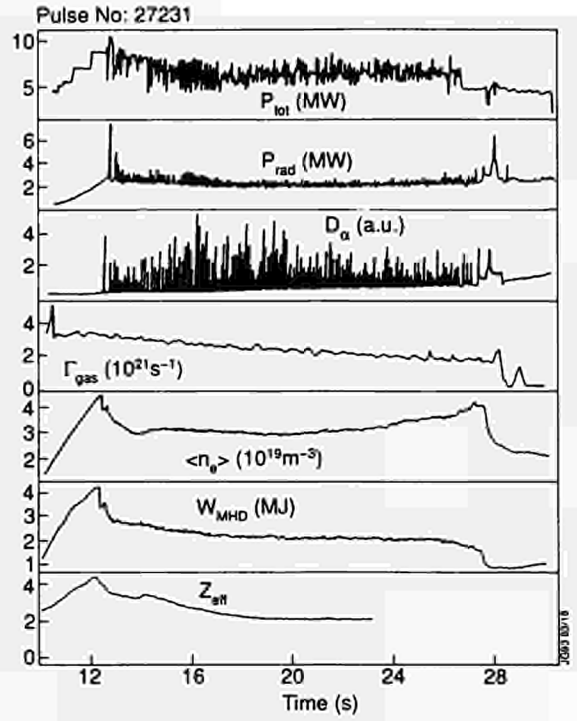

Fig.134: Overview of the discharge with the longest steady-state H-mode. The ELM-free H-mode begins at 10s, and the H-mode is held in steady-state by the onset of ELM's at about 12s.

The main plasma parameters, i.e. density, radiation, temperatures, stored energy and fusion yield, could be held in quasi-steady-state for ~18s, the duration of this period was determined by the length of gas pulse and maximum length of H-mode was set by thermal stresses in the poloidal shaping circuit rather than by plasma physics constraints.

The longest such steady-state H-mode is shown in Fig.134, in which the remarkably constant behaviour of the majority of parameters is clear. It is striking, however, that towards the end of the ELMy period the plasma density began to rise, even though the pre-programmed gas-puffing rate was declining as the pressure in the gas reservoir fell. In addition, the temperature of the target tiles fell, indicating that the ELM's were effective in reducing the peak power deposition on the tiles. As the indications were that Z_{eff} was constant during the ELMy phase, the rise in plasma density appeared to be associated with saturation of the pumping capacity of the first wall. This suggests that further extension of the steady-state regime in JET will require active pumping for density control. Nevertheless, this regime appeared to be robust since it was extended to total powers of 18MW and maintained in steady-state in these conditions for up to 3s, the limit being set by imposed neutron production limits.

As expected, the confinement performance of these discharges was somewhat lower than that of equivalent

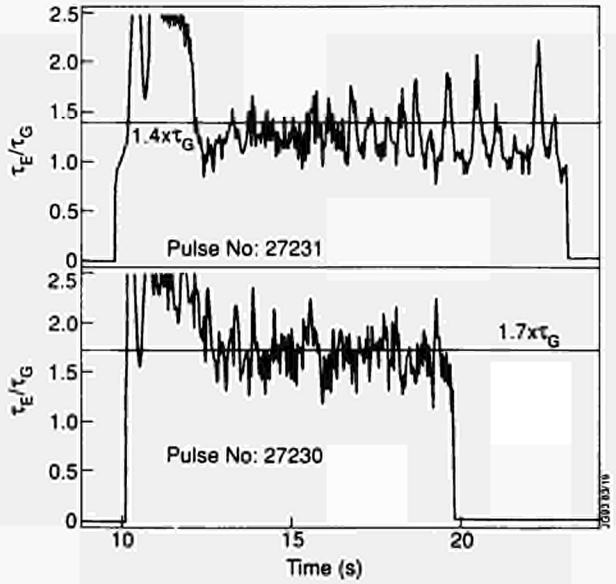

Fig.135: Comparison of confinement enhancement factors of two ELMy steady-state H-modes. In both cases, there is an initial phase of ELM-free H-mode lasting ~2s during which the enhancement factor is well above 2. In Pulse No:27231, a large amplitude n=1 mode persisted throughout the ELMy phase, while in Pulse No:27230, with slightly higher input power, the amplitude of the MHD activity was substantially lower.

ELM-free plasmas. In part, this resulted from the degradation of edge confinement by ELM's and from some reduction in core confinement due to the fact that the ICRF heating was applied ~50cm inboard of the magnetic axis to minimise the influence of sawtooth activity, which was found to have deleterious effects on n=1 MHD activity at the plasma edge. Some of this confinement loss could, no doubt, be regained by optimisation of the ICRF resonance. However, below a power threshold of ~8MW, these plasmas were susceptible to persistent large amplitude n=1 activity (presumably with m=2) which further degraded the energy confinement. Thus, the longest ELMy H-mode had an enhancement factor of 1.4 relative to the Goldston L-mode scaling, while a slightly shorter ELMy H-mode, which also had a slightly higher input power (and, therefore, low-level MHD activity) exhibited an enhancement factor of 1.7.

The confinement enhancement factors of these two pulses, based on the MHD measurement of plasma stored energy (which was in agreement with kinetic measurements), are shown in Fig.135. The degradation of confinement at the onset of ELM's is clear in the two cases. However, in Pulse No:27231, this degradation was substantially more severe and, as shown in Fig.136, can be associated with the growth of an n=1 'locked' mode. Although this mode unlocked at ~15s, a large amplitude rotating n=1 mode persisted throughout the steady-state H-mode in this case and depressed the

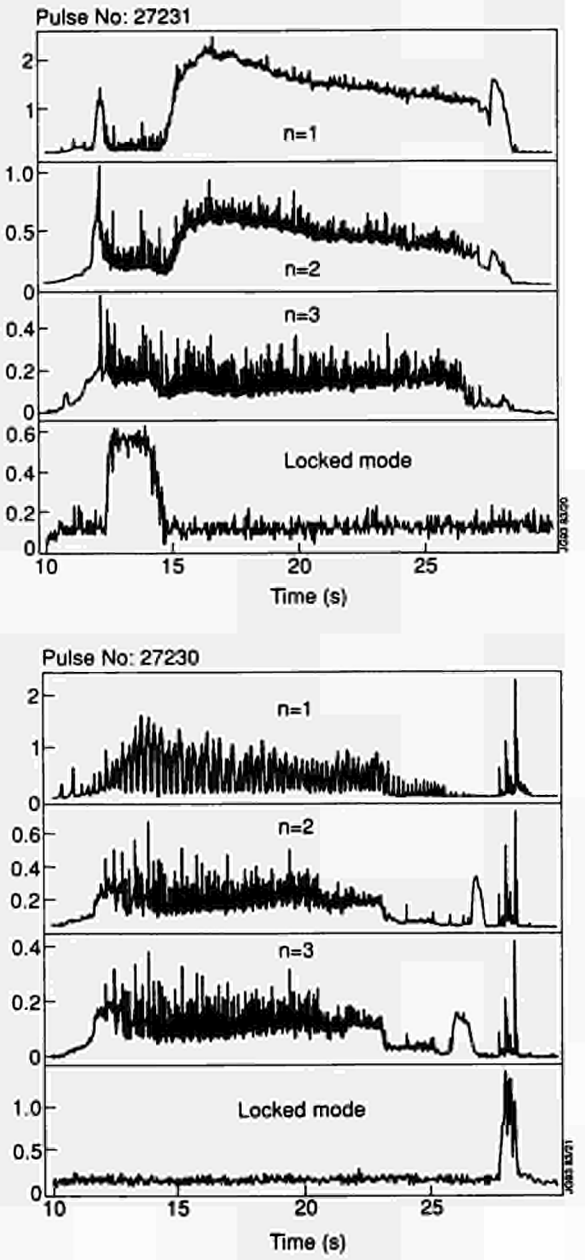

Fig.136: Comparison of MHD activity in n=1,2,3 rotating and n=1 stationary modes for the two pulses of the previous figure. The rotating n=1 mode at ~15s (No:27231) comes from the unlocking of a stationary mode between 12s and 15s. The smaller spikes of n=1 activity (No:27230) coincide with sawtooth collapses.

energy confinement time (Fig.136(a)). In Pulse No:27230, on the other hand, the n=1 activity was significantly lower in amplitude and occurred in bursts coincident with sawtooth collapses (Fig.136(b)). Although this difference in confinement between the two pulses has not been analysed quantitatively, previous analysis of confinement degradation associated with large amplitude MHD activity [38] showed that the degradation could be explained by the flattening of the plasma profiles at the q=2 surfaces and at other integral q surfaces (e.g. q=1) where mode coupling causes other modes to grow.

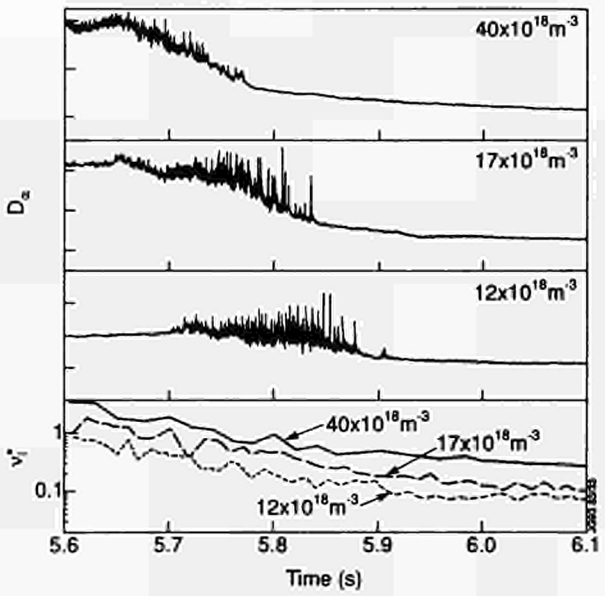

Fig.137: The upper three traces show D_α intesity from a sequence of three sawtooth-free discharges in which the density was reduced on a shot-by-shot basis while the heating power was constant. The 'dithering' nature of the L-to-H transition and the time of the start of the ELM-free H-mode are clear. The lowest trace shows the time development of the normalised ion collisionality, η_i^*, for the three pulses.

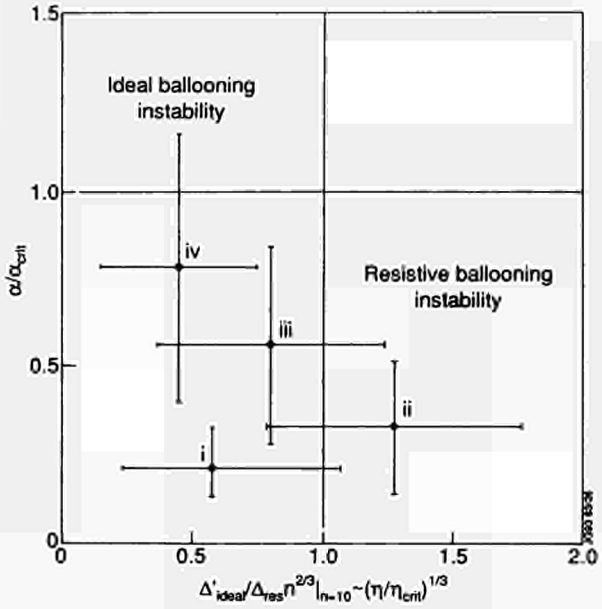

Fig.138: Normalised parameters indicating ideal and resistive ballooning stability: (i) Pulse No:24745, normal low power ELM, (ii) a large singular ELM in hot ion H-mode (Pulse No:27793), (iii) the hot ion H-mode discharges Pulse No:26087, and (iv) Pulse No:26095 at the termination of the high performance phase.

Experiments designed to study the change in edge parameters associated with the L-to-H transition included an investigation of the change in ion collisionality at the H-mode transition as the plasma density was varied at constant power [39]. This experiment, was performed in sawtooth-free plasmas to minimise exterior influences on the transition. Measurements with high spatial resolution were made in the region of 4.01m<R<4.12m while the density was varied on a shot-by-shot basis. In the absence of sawteeth, the L-to-H transition occurred rather slowly with a period of 'dithering'.

Typical results of this experiment are shown in Fig.137, where D_α traces are shown for three of the pulses. The dithering phase and the transition to the ELM-free H-mode are clear. It was found that as the plasma density was lowered (in this case by a factor 3) the time of the L-to-H transition was delayed. However, the temporal development of the edge ion temperature was approximately the same, so that the edge ion temperature at the time of the transition was higher at lower density. Utilising these measurements of T_i, together with measurements of n_e, the normalised collision frequency, η_i^*, was computed and is compared for the three pulses in the lowest panel of the figure. The time evolution of η_i^* is dominated by that of the ion temperature, while the shot-to-shot variation reflects the variation in electron density. The principal conclusion which may be drawn from this series of experiments is that the transition becomes more delayed as the normalised ion collisionality falls, which is contrary to the dependence predicted by certain common orbit-loss theories of the H-mode [40].

The Physics of ELMs

The ELMs occurring during and shortly after the H-mode transition are small and have a high repetition rate (100Hz < f < 1kHz). As the edge electron temperature increases, the ELMs become gradually larger and much less frequent (< 100Hz). All ELMs are primarily observed as a sharp rise in the D_α emission, presumably due to a sudden loss of particles and energy from the outer part of the plasma. ELMs are also detected as short turbulent bursts of magnetic and density fluctuations. When the ELM repetition rate is not too high, these turbulent events occur with irregular intervals and amplitudes, and are often preceded by a period of oscillations with a well-defined frequency, typically 50 to 100kHz.

Present understanding of ELMs in JET assumes the occurrence of resistive ballooning modes. These are radially localised instabilities at the plasma edge with high toroidal mode numbers, driven by large local pressure gradients, and further destabilised by the higher resistivity in the plasma boundary. Non-linear coupling between ballooning modes is thought to cause the turbulent bursts during the ELM itself.

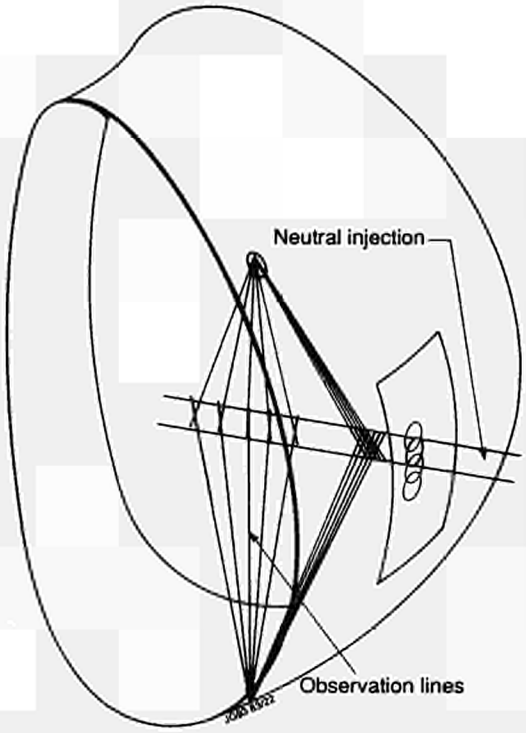

Fig.139: Measured and simulated poloidal rotation and the intensity profile from the CX diagnostic. The simulation assumed a 5cm wide rotation layer just inside the separatrix.

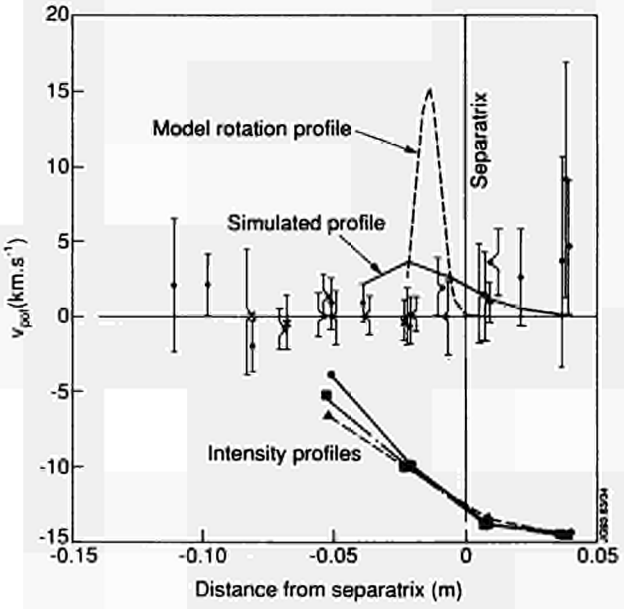

Fig.140: The different contributions to the edge electric field as well as the total E-field versus major radius.

Numerical computations of the stability with respect to high-n resistive ballooning modes have been carried out (Fig.138), determining the largest stable pressure gradient in each point of the plasma. Progress with these ELM stability analyses has been possible due to more detailed knowledge of the density, temperature, and current profiles near the plasma edge. Also important were analytic improvements to ballooning calculations, taking into account resistivity, the finite aspect ratio and shape of flux surfaces close to the separatrix, as well as a pronounced edge current.

The results show that prior to normal ELMs, the edge pressure gradient is significantly lower than the ideal (no resistivity) stability threshold (Fig.138). Nevertheless, instability to modes with toroidal mode numbers n>10 is found by taking the finite resistivity into account. However, in high performance discharges operating at high-beta values very large singular ELMs can be observed in circumstances when the edge pressure gradient is much closer to the ideal stability limit (Fig.138). In these cases, the resistivity is relatively low due to the high edge temperatures. Therefore, the importance of the pressure gradient and of the resistivity in determining the stability of the plasma edge varies from case to case.

Ballooning modes do not cover all aspects of plasma edge stability. Computations of low-n free-boundary resistive modes have shown the destabilising effects of the edge current density built up during the H-mode, in the vicinity of the plasma boundary. These modes have a finite amplitude at the plasma boundary and might be crucial in describing the actual break-up of the outer flux surfaces during an ELM.

Edge Electric Field Measurements on JET

The poloidal rotation diagnostic makes use of visible charge-exchange light arising from a neutral deuterium heating beam. Light is collected from a region near the separatrix by a pair of viewing systems. The two systems are mounted symmetrically in the top and the bottom of the machine. Each viewing system comprises ten 0.6mm optic fibres with imaging lenses. The separation between the individual lines-of-sight in the plasma is 15mm, although the space resolution is limited to about 5cm by the viewing geometry.

The diagnostic measures both the poloidal and toroidal components of plasma velocity from the Doppler shift of the impurity radiation. It also measures the impurity ion temperature from the Doppler broadening and impurity density profiles from the intensity of emitted radiation. Knowledge of these four quantities enables an evaluation of the radial electric field.

Studies have been made of a series of H-modes with the conclusion that the poloidal rotation in these discharges was zero within the accuracy of the measurement (±4kms^{-1}). However, the space resolution of the diagnostic poses a significant limitation on our ability to detect any thin (<5cm) rotating layer.

Figure 139 presents results from several discharges showing measured poloidal rotation at different positions. Also shown is the calculated effect of a thin rotating layer, 1cm FWHM, 15kms^{-1} peak. The calculation shows that despite the limited spatial resolution such a layer would be detectable. Three intensity profiles are plotted at the bottom of the figure from some of these discharges, showing evidence of the steep density gradients that develop in the H-mode.

The ion temperature profiles have small gradients, typically 8kVm^{-1}.The measured intensity profiles indicate a region of 1-2cm width where the impurity density changes by a factor of 10. Figure 140 shows the contributions to the radial electric field arising from the four sources, poloidal and toroidal rotation, ion density and temperature. The solid line shows the sum of the components. The steep ion density gradient is the dominant contribution.

The absence of poloidal rotation in these JET discharges contradicts much of the published data from other experiments [41,42,43]. However, recent results from DIII [44] also show H-modes with low poloidal rotation. The common feature of all the JET and DIII measurements is the edge radial electric field of about -30kVm^{-1} in the H-phase. In JET, the dominant contribution to the electric field comes from the ion density gradients, as ion temperature gradients do not make a significant contribution. In DIII, the reverse is true, and the steep gradients of T_i are the biggest contributor to E_r. These remarks apply only to the developed H-mode, not to the conditions at the moment of transition. At present, the JET measurements do not have as fast a time resolution as those on DIII, so the presence of a fast (< 1ms) localised (<1cm) effect on poloidal rotation at the moment of the H_α drop cannot be confirmed. Improvements to the diagnostic for the forthcoming campaign should allow measurements on these time and space scales.

References

[1] A Loarte and P Harbour, Nuclear Fusion **32** (1992) 681

[2] P Harbour, et al, Journ. Nucl. Mat. **196-198** (1992) 386-391

[3] T. Tagle, et al, Journ. Nucl. Mat. **196-198** (1992) 196-198

[4] J. Watkins, et al, Journ. Nucl. Mat. **196-198** (1992) 829-832

[5 A. Loarte et al, Contributions to Plasma Physics **32** (1992) 486

[6] P Harbour, S Clement, D Ward and A Loarte (Internal Report, 1992)

[7] D. Hill et. al., Bull. Am. Phys. Soc. **37** (1992) 1565

[8] J. Brooks, J. Nuclear Materials **170** (1990) 164

[9] J P Coad, B Farmery, J Linke and and E Wallura, JET-P(92)67, to be published in J. Nuclear Materials.

[10] R. Reichle, et al, EPS Berlin (1991)

[11] R. A. Jong et al, Journal of Nuclear Materials, **196-198** (1992) 800-803

[12] K. Itami et al, Journal of Nuclear Materials **196-198** (1992) 755-758

[13] A. Mahdavi et al, Phys. Rev. Letters, **47** (1981) 1602

[14] M. F. A. Harison et al, 5th INTOR workshop, IAEA Vienna (1981) EUR-FU-BRU/XII

[15] K. Lackner et al, Plasma Phys. and Controlled Fusion **26** (1984) 105

[16] S Clement, SK Erents, N Gottardi, et al, APS 91, Tampa, USA

[17] H Jaeckel, S Clement, N Gottardi, et al, APS 91, Tampa, USA

[18] T. Petrie PSI Conference Monterey 1992

[19] V. Philips private communications

[20] V. Philips et al, Journ. of Nucl. Mat. **179-181** (1991) 25-33

[21] V. Philips et al, PSI Conference, Monterey (1992)

[22] D.Pasini et al, EPS 1992, Innsbruck

[23] D.P. O'Brien, et al, JET Report JET-P(92)57, submitted to Nucl. Fusion

[24] J.Lingertat, et al, Bull. Am. Phys. Soc. **37** no 6 (1992) 1421

[25] A.Loarte, et al, Bull. Am. Phys. Soc. **37** no 6 (1992) 1421

[26] J. Ehrenberg et al, Journ. Nucl. Mat. **196-198** (1992) 992-996

[27] J. Ehrenberg et al, Journ. Nucl. Mat. **176-177** (1990) 226-230

[28] A. Gondhalekar, et al, Plasma Physics and Controlled Fusion **31** 5 (1989) 805.

[29] A. D. Cheetham, et al, Proc.12th International Conference on Plasma Physics and Controlled Nuclear Fusion Research, Nice (1988) 483.

[30] IAEA, ITER Conceptual Design Report, ITER Doc. Series, No. 18, IAEA, Vienna.

[31] T.T.C. Jones, et al, Proc. 18th EPS Conference, Berlin (1991) I-185.

[32] D. L. Hillis, J. Nucl. Mater. (in press).

[33] E. J. Synakowski, et al, Phys. Rev. Lett. **65** 18 (1990) 2255.

[34] A. Boileau, et al, Nucl. Fusion **29** 9 (1989) 1449.

[35] R.J. Fonck et al, Phys. Rev. A **29**, (1984) 3288.
[36] D Stork et al, 31st APS, Anaheim, 1989.
[37] P R Thomas et al, 19th EPS Conference, Innsbruck I 239 (1992).
[38] J A Snipes et al, Nucl Fus **30** 205 (1990).
[39] N Hawkes et al, 20th EPS Conference, Lisbon (1993) (to be published).
[40] K C Shaing, Phys Fluids B **4** 171 (1992)
[41] R. J. Groebner, et al, Phys. Rev. Lett. **64** (1990) 3015
[42] A. R. Field et. al. Nucl. Fus. **32** (1992) 1191
[43] K. Ida et. al. Phys. Rev. Lett. **65** (1990) 1364
[44] R. J. La Haye et. al. GA-A20782 (submitted to Phys. Rev. Lett.)

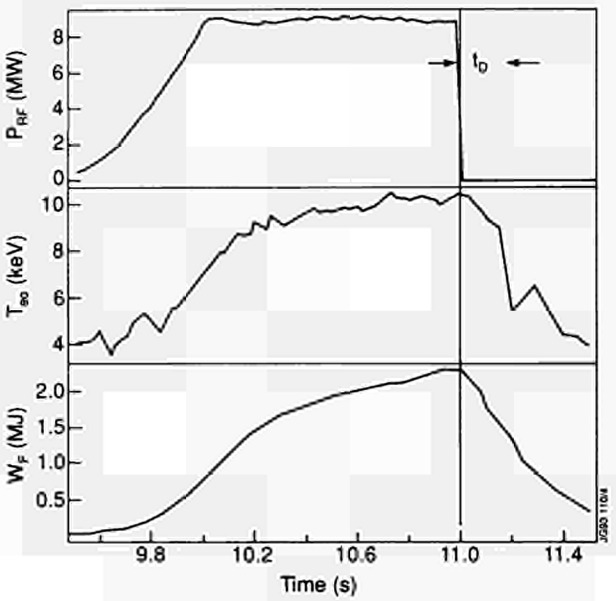

Fig.141: Switch-off of ICRF power showing delay (t_D) to a monster sawtooth crash (second trace).

Physics Issues

In early 1992, a number of experiments on a range of topics were carried out. These included;

- study of the effects of TF ripple on the L-H transition and on fast particle losses;
- confinement scaling in dimensionally-similar discharges;
- monster-sawtooth studies with ICRF switch-off;
- studies of fast electron diffusion;
- 100% current drive using Lower Hybrid waves.

The first of these experiments was performed in conjunction with the 'Physics Issues related to Next Step Devices' Topic Group, and can be found described in that section of the Report. The second topic was studied in conjunction with the 'Transport and Fluctuations' Topic Group, and is reported in detail in that section. The remaining experiments are described below.

1992 Experiments

Monster Sawtooth Studies using delayed ICRF Switch-off

These experiments were aimed at studying the mechanism of sawtooth stabilisation with ICRF power. In the most successful theory [1], stabilisation results from interaction of ICRF-produced fast particles with the m=n=1 mode. Stability is provided by the fast particle content within the q=1 surface, while the force driving the instability increases as the radius of the q=1 surface (r_1) gets larger.

To test these aspects of the theory, a series of 3MA, 3.1T discharges were performed in which the sawtoothing was suppressed by the application of ~9MW of ICRF power on-axis. The ICRF power was switched off at different times during the sawtooth suppression interval, and the time delay for a sawtooth to occur after switch-off was measured (see Fig.141). In these conditions the delay time has a maximum of ~0.3s when the ICRF power is switched off after 0.5-1.0s.

To validate the theory against the observed delays between ICRF switch-off and sawtooth collapse, a heuristic model was constructed. It is postulated that a sawtooth occurs when r_1 reaches a critical value r_{1C}, which depends linearly on the total fast particle energy W_F

$$r_{1C} = r_{1C}(OH) - \delta r_1(OH)(W_F/W_{FO}) \qquad (1)$$

Additionally, the model assumed that r_1 was reduced by an amount $\delta r_1(OH)$ at an ohmic sawtooth crash. Between sawteeth, r_1 grew linearly at a rate (dr_1/dt).

$$r_1 = r_{1C}(OH) - \delta r_1(OH) + (dr_1/dt)t \qquad (2)$$

Finally, the model assumed that W_F grew exponentially with a time constant τ_s when the ICRF power was switched on (at t=0) and decayed with the same time constant when the power was switched off (at $t = t_{so}$).

$$W_F = W_{FO}(1 - \exp(-t_{so}/\tau_S))\exp(-(t - t_{so})) \qquad (3)$$

Experimentally, the linear increase in r_1 (Eq (2) was confirmed by Faraday rotation measurements of the q profile; the exponential evolution of the fast particle energy (Eq (3)) was also confirmed by magnetic measurements). Thus the predictions of this model provide a test of the first assumption, namely that of a critical radius dependent mainly on the fast particle content. Using Eqs.(1)-(3), the delay time between ICRF switch-off and the sawtooth collapse, $t_D = (t - t_{so})$ can be calculated from the condition:

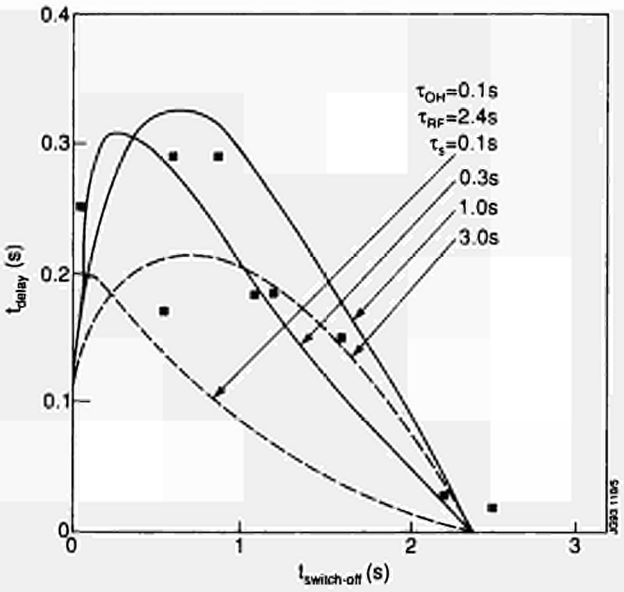

Fig.142: Observed delay time (t_{delay}) between the switch-off of ICRF power and the subsequent collapse of the monster sawtooth as a function of the time of the RF switch-off relative to the start of the monster ($t_{switch-off}$). The various curves show fits to the data using the model described in the text with a range of values for the fast particle slowing-down time (t_s).

$$\exp(-t_D/\tau_S).(1 - \exp(-t_{SO}/\tau_S)) = \alpha(t_{SO} + t_D) - \beta$$

where $\alpha = (dr_1/dt)/\delta r_1(rf)$ and $\beta = \delta r_1(OH)/\delta r_1(rf)$.

α and β were inferred from the ohmic sawtooth period (t_{SO}= 0, $t_D = \tau_{ST}(OH)$), and the intrinsic ICRF sawtooth period, ie. period of sawtooth suppression that resulted when the ICRF power was not switched off ($t_{SO}= \tau_{ST}(rf)$, $t_D = 0$).

Figure 142 shows the observed delay time as a function of the switch-off time. Also shown are the calculations of t_D assuming $\tau_s = 0.1, 0.3, 1.$ and 3s. A reasonable fit to the data is obtained if t_s is in the range 0.3-1s. Since this corresponds to the measured fast-particle rise time in these discharges, it may be concluded that the results of the ICRF switch-off experiments are consistent with the theory of sawtooth stabilisation by fast particles.

Fast Electron Diffusion Studies

The phenomenon of fast electron diffusion has been addressed in a series of dedicated experiments where ejection of energetic electrons from the plasma core has been prompted by a monster sawtooth crash [2]. In these experiments, the fast electron dynamics is determined by transient processes rather than diffusion in near steady-state conditions. Experiments have been performed in 3MA, 3.1T limiter deuterium plasmas, with central density $ne_0 = 2.5 \times 10^{19} m^{-3}$, heated by ICRF up to T_{e0} = 8-10keV and with ~ 1.5MW LH power launched. The fast electron profile, measured by the FEB

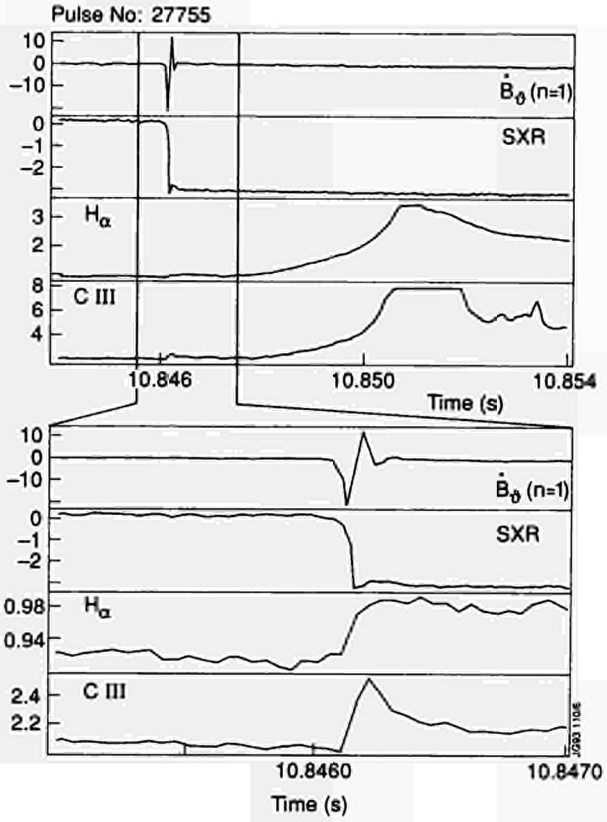

Fig.143: Arrival of an early heat pulse at the plasma edge following the crash of a monster sawtooth. The increase in H_α and CIII light at 10.846s can be attributed to the arrival of fast electrons expelled from the centre by the crash whilst the larger pulses at ~10.85s are associated with the arrival of the usual (thermal plasma) heat pulse.

camera, in these cases was peaked on axis with a half-width at half-maximum of about the radius of the q=1 surface.

There is no obvious influence of the limiter material type (carbon or beryllium) on the fast electron dynamics. The arrival of the heat pulse at the plasma edge after a sawtooth crash is reflected in the time behaviour of the H_α and carbon-light emission for the carbon case shown in Fig143. The traces show that the H_α and CIII emission signals from the proximity of the carbon limiter exhibit a small increase starting less than 0.1ms after the monster crash and lasting about 1ms, followed by a larger increase 2-5ms after the crash. This behaviour is consistent with the arrival on the limiter of a pulse of fast electrons first and the later arrival of the bulk of slower thermal electrons.

The characteristics of the electron transport in this type of sawtooth instability are consistent with the existence of magnetic turbulence which would result from the mixture of magnetic islands and a chaotic region where the magnetic field lines link the inside and outside of the plasma [3]. Since the LH-accelerated electrons at 100-300keV energies are

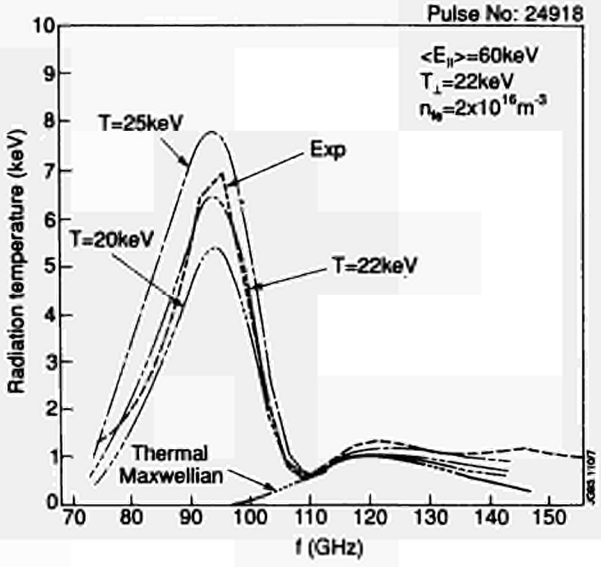

Fig.144: Experimental and simulated non-thermal ECE spectra from an LH assisted discharge. The fast electron density refers to the plasma centre.

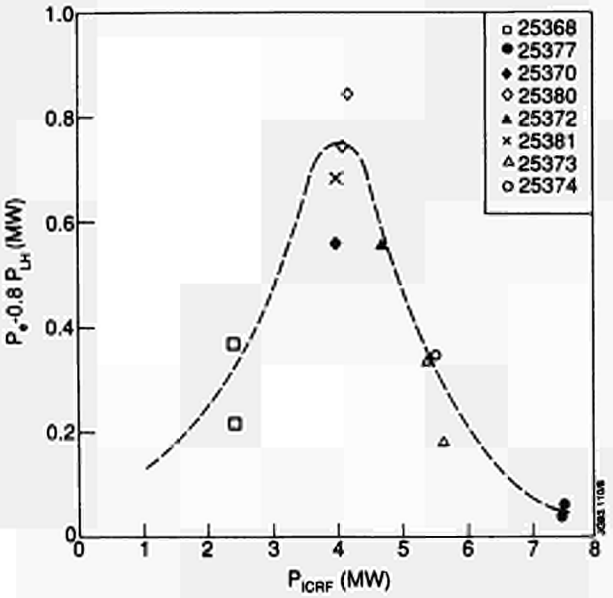

Fig.145: Power coupled from ICRF to the electron population (assuming that 80% of the LH power is coupled to the electrons) as a function of the input ICRF power.

faster than the thermal electrons and are collisionless, these are expected to reach the limiters from around the q=1 region before the bulk electrons. Theoretical predictions of the transit of LH electrons, in the initial phase of ϑ fluctuations, yield values of 0.1-1ms, consistent with the measured values when velocity and space distribution of fast electrons are taken into account. The resulting fast electron diffusion speed at the monster crash is ~$5x10^3 ms^{-1}$.

Lower Hybrid Current Drive

Experiments on Lower Hybrid Current Drive (LHCD) continued in 1992 with the prototype antenna, capable of launching waves at a frequency of 3.7GHz with a narrow wave phase spectrum centred around $N_{//} \approx 1.8$. Full sustainment of the plasma current up to 1.5MA for 6s was achieved, with LH power ~ 2MW, at high toroidal field (B_T > 3T) and relatively low density ($n_e \sim 2 \times 10^{19} m^{-3}$) in ICRF heated discharges [4].

A combined investigation involving the non-thermal Electron Cyclotron Emission (ECE) and Fast Electron Bremsstrahlung (FEB) diagnostics has been carried out to determine the phase space distribution of the fast electrons accelerated by the LH waves [5]. The method assumes the fast electron distribution function to be described by a three temperature maxwellian in velocity space. The radial profile of $T_{//}$ is directly measured by the FEB camera. The parameters and n_{fe} (fast electron density), were then determined by an iteration process until agreement was reached with the ECE spectra, the FEB data and the estimated non-inductive current driven. A typical simulation of ECE non-thermal spectrum is shown in Fig.144. This analysis has also given evidence that the energy of the LH-induced fast electrons increases when ICRF power is applied (LH-ICRF synergy).

Further, on LH-ICRF synergy, the physics mechanism responsible for the acceleration of LH fast electrons in the presence of ICRF heating is still under investigation. A detailed study of the electron power balance via modulation has been carried out. The results show that the amount of ICRF power coupled to the fast electrons as a function of launched ICRF power varies as shown in Fig.145. Up to 20% of the ICRF power can be coupled to the fast electrons at an optimum ICRF power level of 4MW. This behaviour would be consistent with damping after mode conversion of the fast wave at the hydrogen-deuterium resonance rather than direct damping of the fast wave by the Transit-Time Magnetic Pumping (TTMP) and Electron Landau Damping (ELD) mechanisms.

Numerical simulations of the LH wave propagation and absorption were carried out using a ray-tracing code coupled to a two-dimensional (parallel velocity + radial co-ordinate) relativistic Fokker-Planck solver for the fast electron tail [6]. Experimental data on electron temperature, density and magnetic equilibrium were used and the calculation includes fast electron radial diffusion and acceleration due to the residual toroidal electric field. The aim of this exercise is to reproduce not only measured global parameters linked to current drive and profile control (eg. loop

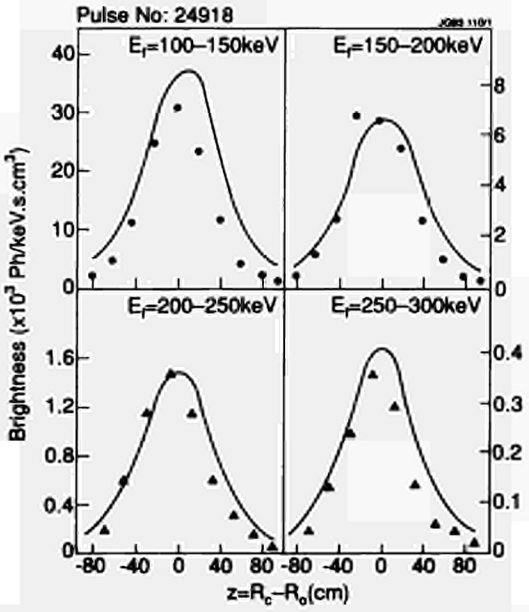

Fig.146: FEB camera radial distribution of fast electrons in several bands for a plasma with 1.9MW LH power at B_T = 3.45T, compared with code simulation.

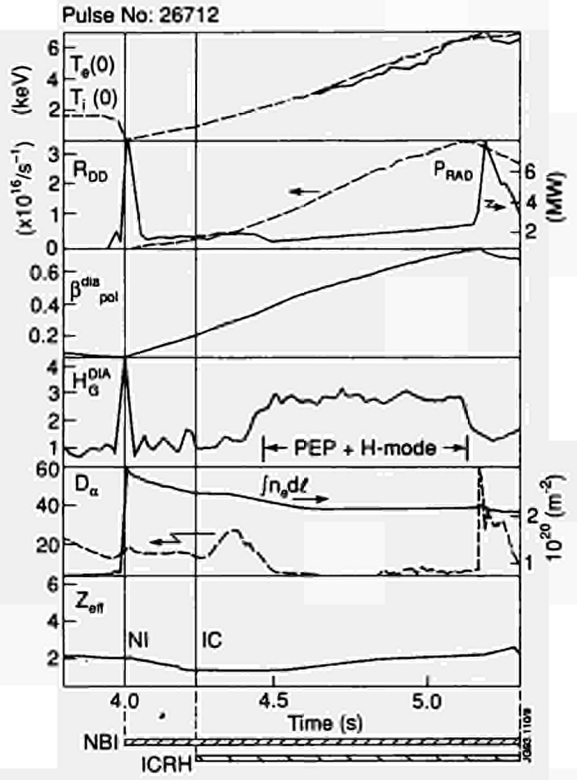

Fig.147: Time development of 3.1MA/2.8T PEP+H-mode after injection of a 4mm pellet at t=4s. This discharge reached a record stored energy of 10MJ (with 11MW NB and 3.3MW ICRF) and showed the longest sustained period (0.6s) with a confinement enhancement relative to Goldston L-mode H_G(DIA)~3.

voltage, internal inductance etc.), but also the hard X-ray (HXR) emission due to fast electron bremsstrahlung measured by the multi-chord FEB diagnostic. The simulation programs taking this data thus include one which calculates the HXR emission spectrum detected by the FEB, with the detector geometry folded in. Results on the radial distribution of fast electrons in several energy bands are presented in Fig.146 for a case with full current drive by LH only, where the problem of modelling the LH-ICRF synergy does not exist. Reasonable agreement can be seen between the code predictions and the measurements.

Further Analysis Work

After completion of the experimental campaign, the Task Force maintained responsibility for analysis of topics it had undertaken during 1991. Broadly, these covered the areas of high-β physics and current drive. Specifically, the analysis covered;

- PEP H-modes;
- high β_ϕ plasmas;
- bootstrap-current dominated discharges at high β_{pol};
- LH current drive.

PEP H-modes

The 1991-2 experimental campaign extended the types of operation in which the Pellet Enhanced Plasma (PEP) regime could be combined with the H-mode (the 'so-called' PEP H-mode). The 1991 Progress Report detailed the improvements in obtaining the PEP-H mode, with different heating schemes (NBI , ICRF and combined). This was the first attainment of the mode with 6mm diameter pellets.

The longest duration of a PEP+H mode enhanced confinement phase significantly above normal H-mode scaling was extended to 0.6s. The discharge development (Pulse No:26712 at 3.1MA, 2.8T) is shown in Fig.147. An enhancement in energy confinement over Goldston L-mode scaling (H_G(DIA)) of ~3 is reached for 0.6s. This compares to a range $2.0 < H_G(DIA) < 2.4$ for typical JET H-modes. The stored energy reached 10MJ, a record for PEP+H modes using 4mm pellets. The stored energy in this discharge (with 11MW NB and 3.3MW ICRF) is competitive with the best of the PEP+H modes formed with 6mm pellets at 4MA with ~25-27MW combined heating power (see Fig.148), but it has about double the neutron yield. In general, the PEP's derived from 6mm pellets had a larger region of density enhancement, but central densities were too high for the heating powers available. Their development still requires further optimisation.

Other general features of the PEP+H mode dataset were that the longest duration H-mode phases were associated

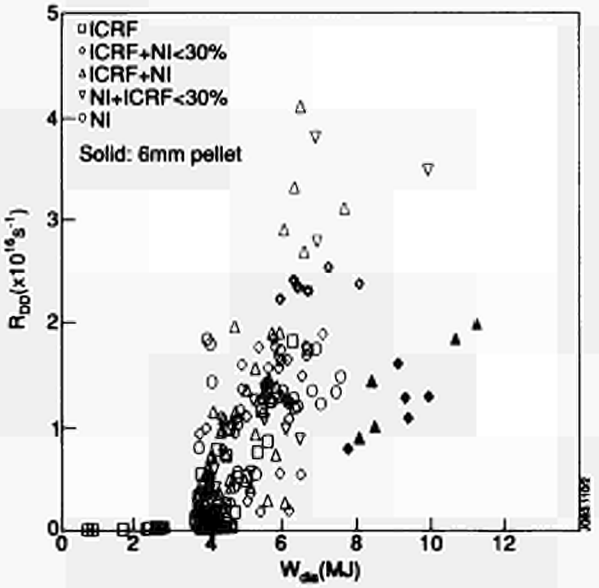

Fig.148: PEP dataset showing peak D-D reaction rate (R_{DD}) and stored energy (W_{DIA}) for the JET discharges with 4 and 6mm pellets. The data is marked by heating scheme.

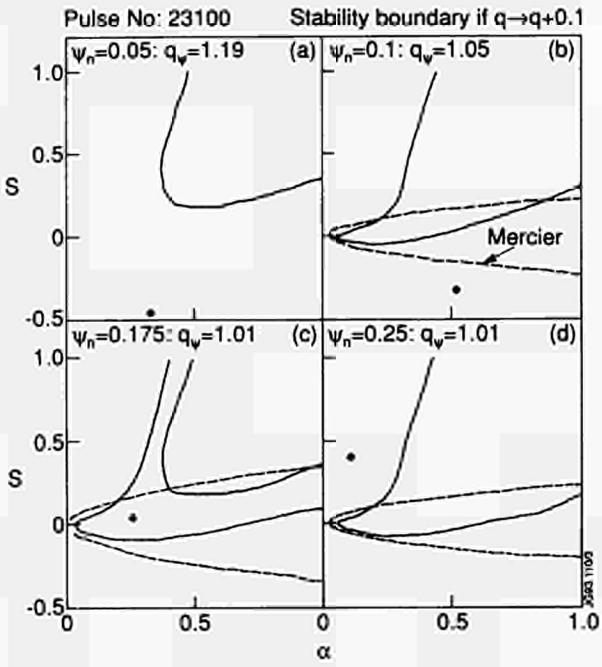

Fig.149: Comparison of experimental values of shear ($s = rq'/q$) and normalised pressure α ($\alpha = -2\mu_0 Rp'q^2/B_T$) with the stability boundaries for ideal ballooning and Mercier modes. Data is for Pulse No:23100 just before the time identified as the PEP collapse. Graph (c) shows the change in boundary of the unstable region if the fitted q value at $\psi_n = 0.175$ is increased by 0.1 (approximately the error in the fitting procedure).

with NB heated discharges whilst the best overall neutron performance came predominantly from combined heating discharges. The enhancement in neutron yield obtained by adding a modest amount (3MW) of ICRF power to a NB-heated PEP could be as large as a factor 2 and came from thermal-thermal reactions arising from the increased central temperature from the centrally-deposited power.

MHD Stability in PEP+H-Modes

The collapse of the PEP enhanced phase usually occurred before the termination of the H-mode phase. The discharge in Fig.147 was unusual in this respect. The collapse was associated with a wide variety of MHD activity. Sometimes fast (1,1) MHD events occurred which were preceded by n=3 modes and followed by n=2 modes. Such behaviour [7], consistent with a non-monotonic q-profile with an off-axis minimum, was discussed in the 1991 Progress Report in the section on MHD, Beta Limits and Topology.

It has previously been postulated [8], in analyses of the PEP phenomenon in the L-mode, that the central part of the PEP is in the second stability regime against high-n ballooning modes and Mercier modes. This is shown in Fig.149 for a PEP+H mode equilibrium for Pulse No: 23100 at 6.6s just prior to the termination of the PEP phase in this pulse. The termination of the PEP phase is identified by the decline in the D-D neutron rate.

The analysis uses measured pressure and shear profiles and the code IDBALL [9] based on the method of Greene and Chance [10]. It can be seen that access to the second stability region is much improved by the presence of negative shear and that the profiles have developed such that the experimental profile is unstable against ballooning and Mercier modes for $0.15 < \psi_{norm} < 0.2$. Whether or not this unstable region leads to the collapse is open to question, as the high frequency, high-n MHD activity which might be expected from ballooning modes is difficult to identify with present diagnostics and, indeed, no unambiguous identification exists. Moreover, Fig.149(c) shows the effect of a change of +0.1 to the local q which is within the errors of the measurement. This places the data back into the stable region, so it is possible that the ballooning limit is unable to act before some other phenomenon causes the collapse. Investigations are still in progress.

Impurity Behaviour in PEP+H-modes

The behaviour of impurities in the PEP+H phase is extremely complex. Impurity accumulation is often seen in the centre of the PEP+H plasma, and is often associated with MHD activity[7]. An example of impurity accumulation is shown in a PEP L-mode plasma generated by using a 4mm pellet injected at t=6.0s followed by 10MW ICRF and 5MW NB heating (Fig.150). The PEP phase collapses at ~6.7s and this is associated with a growing (1,1) mode, which is

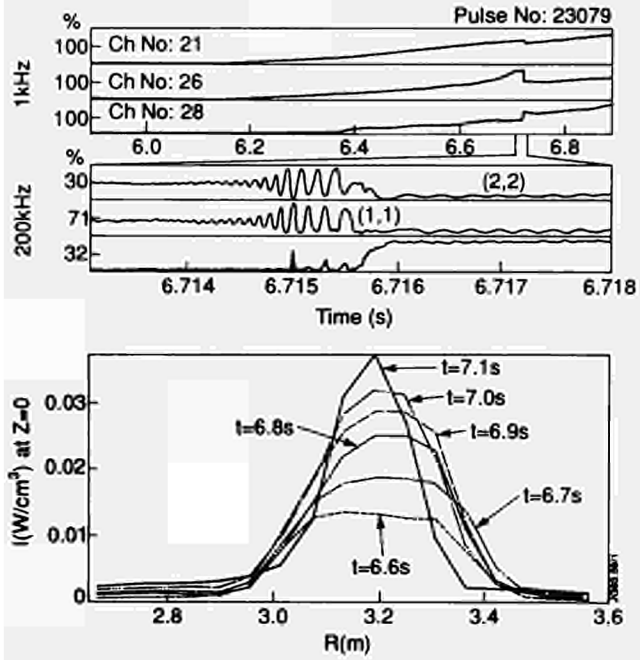

Fig.150: Soft-X-ray traces showing MHD modes associated with a PEP crash at 6.7s and (lower trace) Soft-X-ray profile showing strong impurity accumulation associated with the crash.

succeeded by a (2,2) mode after the crash. This collapse causes flattening of the q-profile and a strong peaking of the soft X-ray (SXR) emission profile, indicating a jump in the central concentration of impurities (also shown in Fig.150).

Examples both of impurity accumulation and of cases where outflow of impurities from the centre occurs can be seen in PEP L- modes, PEP+H and their successor phases. Comparison of these two cases is shown in Figs.151(a) and (b), which shows the same discharge as Fig.150. The first post-pellet phase of both discharges, lasting ~0.8s, shows a moderate central impurity accumulation. After this, there was a sudden collapse in the neutron yield for the PEP L-mode Pulse No: 23079, (Fig.151(a)). As already noted, this is accompanied by an increase in the level of SXR central radiation which implies an almost complete depletion of the central deuterium. However, the temperature does not decline but bulk Z_{eff} and radiated power show strong increases at the time of the neutron collapse. On the other hand, the PEP+H mode Pulse No: 24470 (Fig.151(b)),

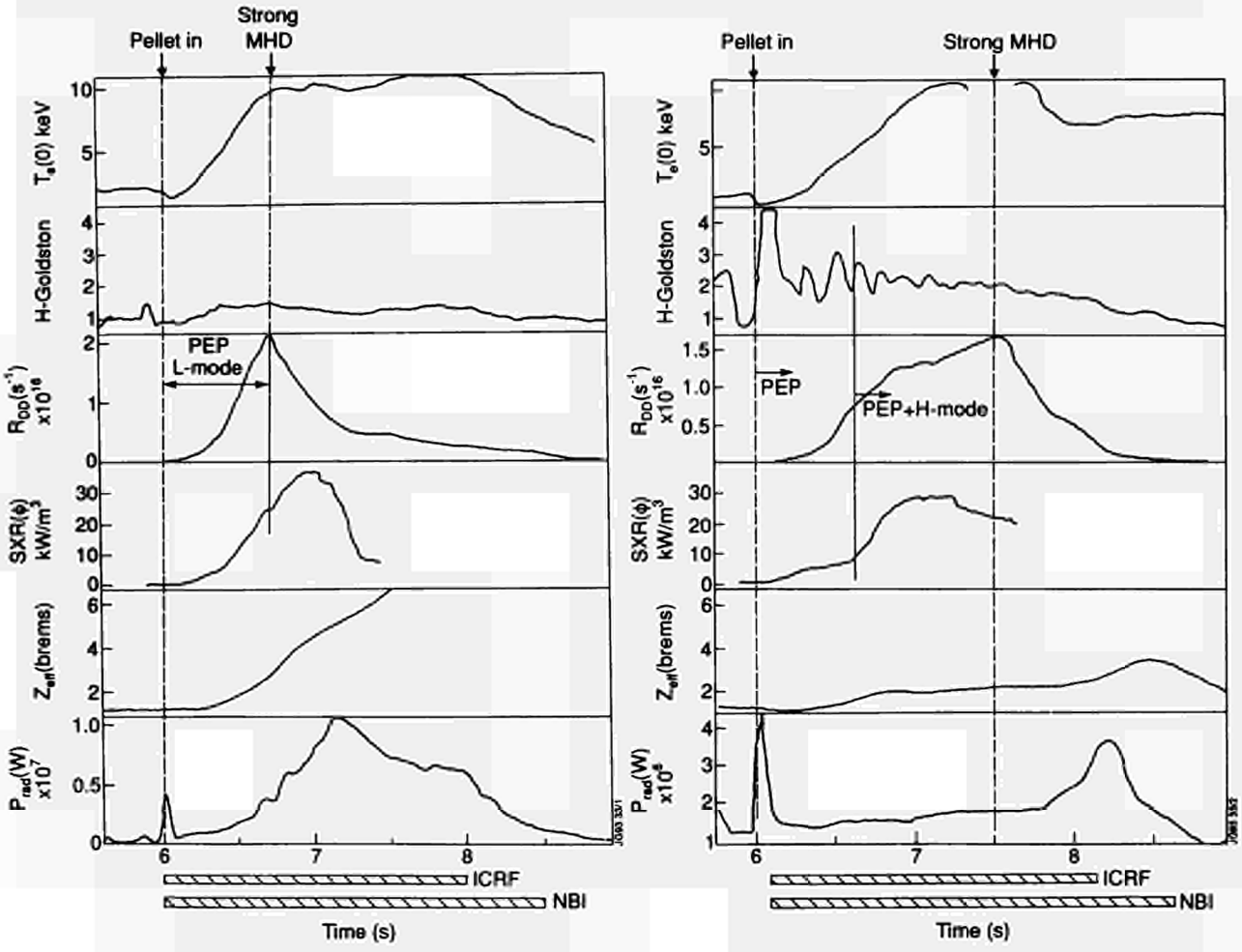

Fig.151: (a) Overview of PEP L-mode pulse shown in previous figure. Note accumulation of impurities developing from 6.7s; (b) PEP H-mode pulse showing similar initial phase as (a) (up to ~5.6s), but then transition to the H-mode and impurity development which shows control of Z_{eff} and P_{rad} with (from ~6.2s) some evidence of impurity outflow.

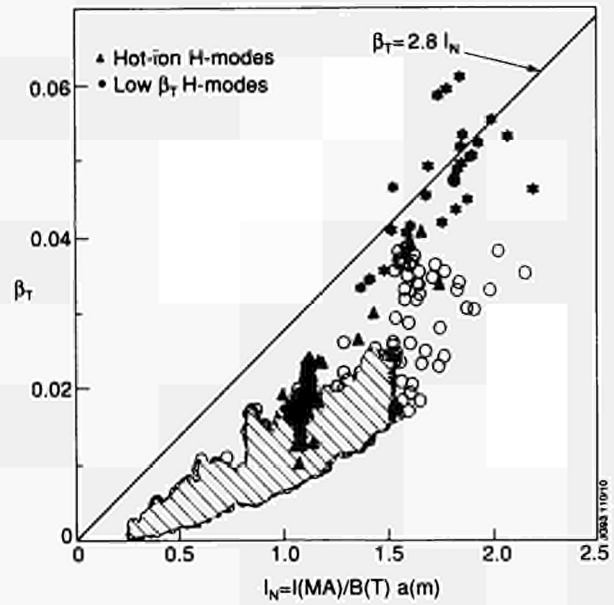

Fig.152: JET dataset for toroidal beta (β_ϕ) against normalised current (I_N = I/Ba). The hot ion (HI) H-modes and the low B_T H-modes with NB heating are highlighted. The cross-hatched area indicates the bulk of the dataset.

shows behaviour which is the inverse in many respects. A slow transition to the H-mode occurred, which resulted in increased neutron and SXR signals in a phase lasting a further ~500ms. The bulk Z_{eff} reached approximately steady-state conditions, whilst the decline of central SXR signal and slight increase of neutron rate indicated increasing purity in the central plasma. This third phase lasts for ~500ms, and in this time, β_{POL} was saturating and confinement enhancement H^G(DIA) had dropped to 'normal' H-mode values (~2). Thus, a transition was made to normal H-mode confinement (Fig.151(b)) despite the existence of a peaked density profile (which persisted until after t=6s).

The differences which lead one discharge to irreversible collapse, whilst another makes a successful transition to an H-mode, are still under investigation. In particular, it is still unclear whether or not these differences can also explain the observed difference in impurity transport.

High β_ϕ Plasmas

Analysis has continued on the high toroidal β (β_ϕ) discharges obtained in 1991 (1991 Progress Report). The dataset for β_ϕ against the normalised plasma current I_N (= I/aB in units of MA, m and T), is shown in Fig.152. This emphasises the subsets of data pertaining to the high β_ϕ discharges at low-B_T and the high β_ϕ hot-ion (HI) H-modes. These subsets were extended in the 1991 campaign. As shown in Fig.152, the best of the low-B_T discharges reached β_ϕ ~ 3.2-3.3 I_N. This is ~20% higher than the Troyon limit [11].

The low B_T H-modes have been extensively analysed for MHD activity and ballooning instability [12] and this work is covered in detail in the section on MHD, Beta Limits and Topology.

Confinement Systematics of Hot-Ion H-modes at High β_ϕ

The hot-ion H-modes (defined by $T_i > 1.5\ T_e$) reach a limit in JET discharges at 80-90% of the Troyon limit (β_ϕ ~ 2.2-2.4 I_N). The reasons for this limitation, which quite often begins as a 'soft' limitation for up to ~200ms before a β_ϕ collapse occurs, are still unclear. These are discussed further in the sections on MHD, Beta Limits and Topology and on Further Analysis of the Preliminary Tritium Experiment.

The existence of the soft limitation in some cases motivates the question of whether the ideal ballooning limit affects the plasma pressure profile in some regions of these discharges. A ballooning analysis of low-q (q_{95}~2.8) hot-ion H-modes at 3MA/1.8T shows that the pressure gradient limits at around 60-70% of the ideal ballooning gradient in the region $0.4 < r/a < 0.8$. This saturation can be seen on the electron and ion temperatures in these regions, which become approximately constant for around 200ms before the β collapse. (The centre of the discharge is approximately at the ideal ballooning limit, but this represents a relatively small plasma volume with little effect on the global confinement). One possible limitation mechanism is that the local *resistive ballooning limit has been reached*. At the temperatures involved (T_e ~ 4keV in these low q cases), mode numbers of n > 30-40 would be needed for instability and such modes are thought to be weak in their effect.

The systematics of the global confinement of hot-ion H-modes at high normalised β (β_ϕ/β_ϕ^T) has been investigated. One of the strongest systematics shows that energy confinement (τ_E) varies inversely with effective ion charge (Z_{eff}) at fixed I_p and B_T. It is important to note that this may imply some density dependence since $Z_{eff} \propto 1/\langle n_e \rangle$ in these discharges.

The global confinement is also dependent on B_T in a stronger manner than for the bulk of ordinary JET H-modes, all of which have $0.75\ \beta_\phi^T < \beta_\phi < 0.88\ \beta_\phi^T$, as a function of B_T. The energy confinement was calculated *near to the time of maximum neutron yield* before confinement saturation had set in. Two enhancement factors were calculated; H_G(DIA), ratio of diamagnetic energy confinement time to Goldston L mode scaling value; and H^{th}(J/DIII), the ratio of

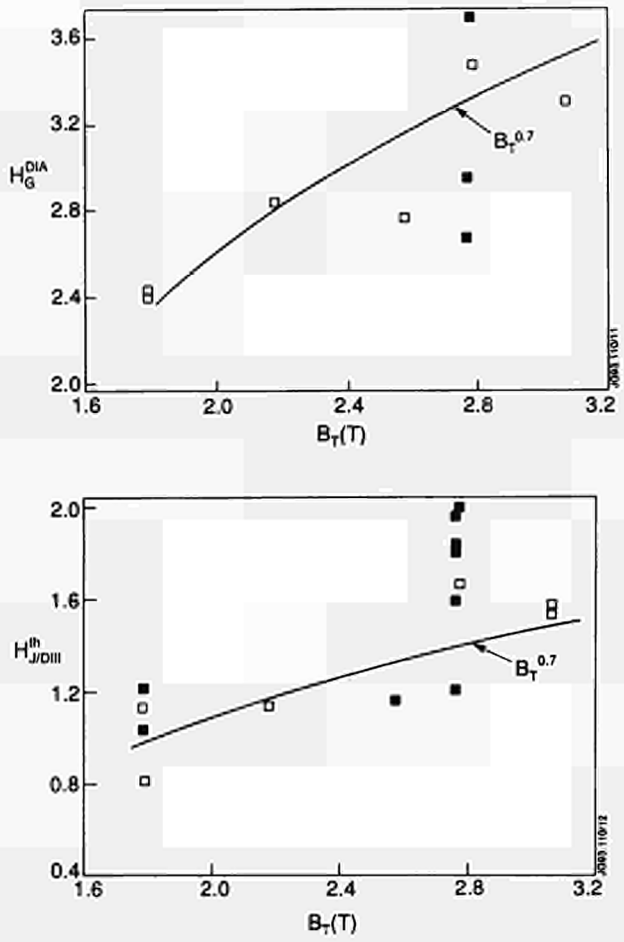

Fig.153: Confinement enhancement factors for: (a) Goldston L-mode scaling (H_G^{DIA}); and (b) JET-DIIID H-mode scaling ($H^{th}_{J/DIII}$) for 3MA Hot Ion (HI) H-modes. Data plotted versus toroidal field. Open symbols indicate plasmas with $2.0<Z_{eff}<2.2$.

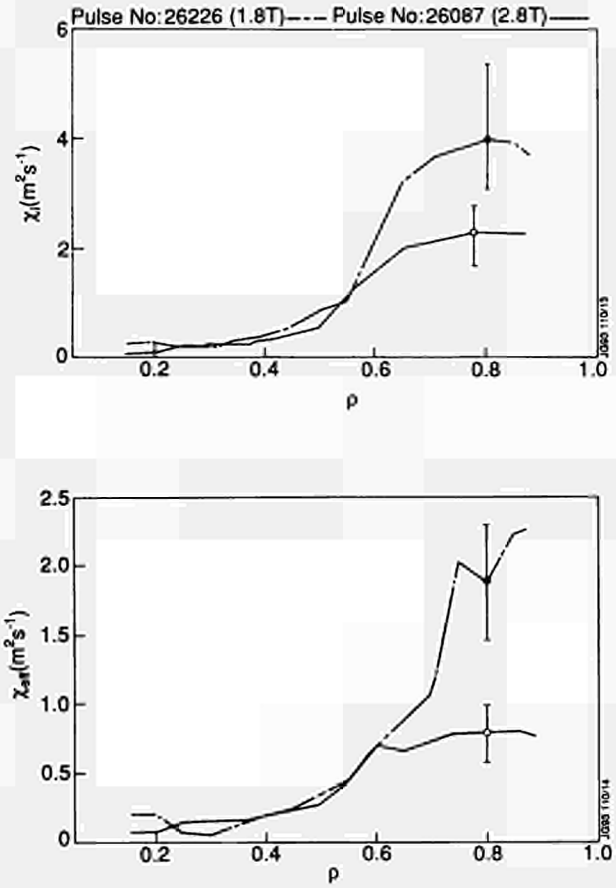

Fig.154: (a) Ion thermal diffusivity (χ_i) from local transport analysis using TRANSP for two 3MA HI H-modes at 1.8T and 2.8T; (b) Effective thermal diffusivity (χ_{eff}) from the same TRANSP analysis.

thermal (kinetic) energy confinement time to JET/DIII-D H-mode scaling law ($\tau_{E,J\ DIII} = 0.106\ P_{Loss}^{-0.46} I_p^{1.03} R^{1.48}$) [13]. The 'normal' values for the bulk of JET H-modes are $2.0 < H_G(DIA) < 2.2$ and $1.0 < H^{th}(J/DIII) < 1.2$, so Figs.153(a) and (b) show that these hot-ion H-modes exhibit enhanced global confinement at the higher toroidal field values. A scaling of $H \sim B_T^{0.7}$ is consistent with the data, compared to the $\tau_E \sim B_T^{0.2}$ scaling which emerges from 'standard' H-mode databases (eg. ITER-92H [14]).

Local transport analysis with the TRANSP code revealed that the origin of this toroidal field scaling (TF) is in the reduced transport in the outer region ($r/a > 0.5$). Figs.154(a) and (b) show that the ion thermal conductivity (χ_i) and the effective thermal conductivity (χ_{eff}) are both very low in the central region of the plasma, with values of $< 0.4\ m^2s^{-1}$ (< 3 x neoclassical), being achieved in common with other hot-ion H modes [15]. There was no discernable TF scaling in this regime. However, in the outer part of the plasma, the transport seemed to increase strongly as the TF was lowered. The relationship of this phenomenon to resistive ballooning effects, or transport models such as the Rebut-Lallia-Watkins model [16] (which predicts amongst other things a $\chi_{i,e} \propto 1/B_T$ dependence), needs further work and probably further experiments.

Bootstrap-dominated Discharges at High β_{POL}

The prospects for steady-state operation of a fusion reactor are significantly improved if a substantial fraction ($\geq^2/_3$) of the plasma current can be driven by the bootstrap mechanism. The production of plasmas, approaching this condition, has been reported from TFTR [17] and JT-60 [18] and was achieved, for the first time with pure RF heating, by JET during 1991 (see 1991 Progress Report).

In the JET high bootstrap current experiments, plasmas at 1-1.5MA/2.8-3.1T were heated with up to 10MW of D(H) dipole ICRF heating, in a double-null X-point configuration. A large bootstrap current was obtained in ELM-free H mode plasmas. In the best cases, the poloidal β (β_{POL}) rose to a value of about 2 and the interpreted bootstrap current reached 70% of the plasma current [19].

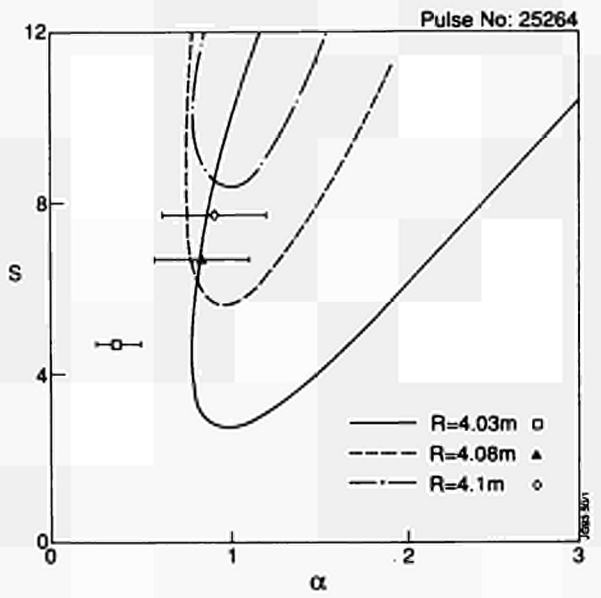

Fig.155: Marginal stability boundaries in the $S(= r/q\,(dq/dR))$ and $\alpha(= -(2\mu_o r^2/RB_q^2)(dP/dR))$ plane for the high bootstrap fraction discharge Pulse No: 25264 (I_{bood}/I_p~0.7). Data are evaluated just before the β_{POL} decline. The unstable regions are in the upper right region enclosed by the stability boundaries.

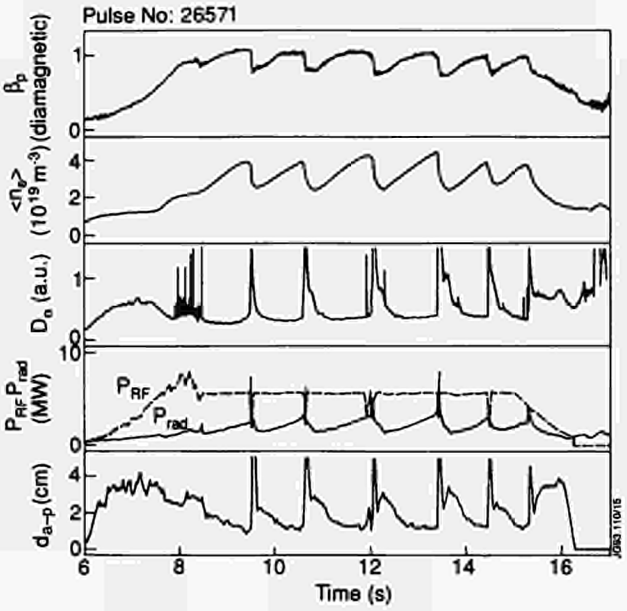

Fig.156: Repetitive β_{POL} collapses in a 1.5MA/2.8T ICRF heated H-mode.

Stability of Bootstrap-dominated Discharges

The H-mode phase of the bootstrap-dominated discharges was typically terminated by a large ELM resulting in a substantial loss of plasma density and energy. There are two candidate mechanisms for this phenomenon. The separation of the plasma and the RF antennae decreases significantly during the H-mode phase, resulting in a strong plasma-antennae interaction, which could be seen on the infra-red camera. Therefore, it is plausible that the RF antennae are disturbing the plasma boundary conditions in a manner which eventually leads to a collapse.

Another possible hypothesis rests on the basis of an ideal ballooning stability analysis of some of the high β_{POL} discharges. As the ELM-free period develops, the edge density gradients (and hence pressure gradients) become very large (dn_e/dr ~2 x 10^{20}m^{-4}) and significantly higher than 'normal' JET H modes. An ideal ballooning analysis, using the method described above, performed on a 1MA bootstrap-dominated discharge shortly before the β_{POL} decline, is shown in Fig.155. The analysis uses LIDAR profiles for density and temperature and equilibrium derived from the EFITJ code. Figure 155 shows that access to the second-stability region occurs very near the plasma edge, but at the time of the collapse, the edge profiles are (within error bars) very close to marginal stability. Apart from the error bars in Fig.155, there are significant experimental uncertainties in the evaluation of the current density near the edge. An upper bound for the edge current density can be found from a collisionless bootstrap model, which increases the current density in this analysis by a factor ~3. This would significantly improve access to the second stability region.

It is hoped to improve on the edge measurements in this regime using the new high resolution LIDAR developed for the pumped divertor phase of JET [20] and reflectometer measurements for the density. In addition, the modifications to the NB system should enable the long pulse heating of low current H-modes in 1994 and should provide H-modes without the accompanying proximity of the ICRF antennae. This should help resolve the ambiguity between the two competing mechanisms. If the above ballooning analysis holds up under further investigation, then it is clear that these high β_{POL} discharges suffer from a collapse mechanism similar to the 'X event', which terminates the high performance hot-ion H-modes.

Often, the H-mode phases in these bootstrap experiments were re-established quickly after a β_{POL} collapse giving rise to a series of H-modes, as shown in Fig.156. In this case, the average β_{POL} per cycle is almost 90% of the peak value.

Confinement in Bootstrap-dominated Discharges

The energy confinement in these bootstrap-dominated discharges is significantly enhanced over the standard scalings. The enhancement relative to Goldston L-mode (H_G(DIA)) is ~3-3.5 and is in line with other high β_{POL} results on JT-60U (obtained in the L-mode). The enhancement relative to the JET-DIIID H-mode scaling (H^{th}(J/DIII) is ~1.6-1.7. The

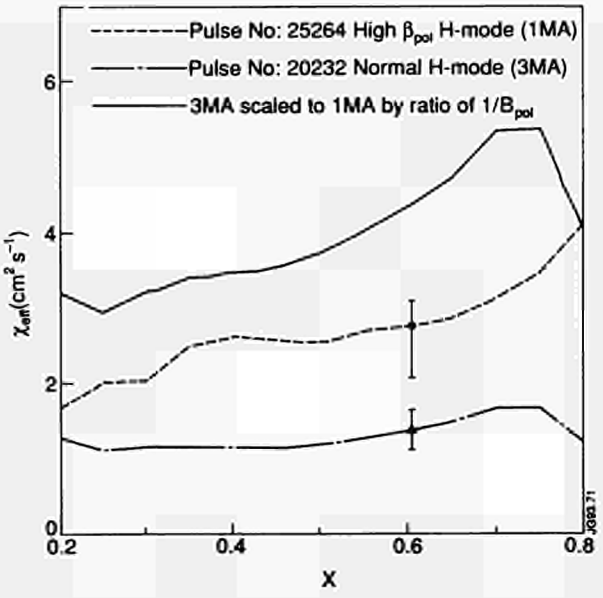

Fig.157: Radial profiles of effective thermal diffusivity (χ_{eff}) obtained from TRANSP analyses of the 1MA/2.8T high β_{POL} H-mode Pulse No:25264 (small dashes) and the 3MA/2.8T ICRF heated H-mode discharge Pulse No:20232 (dot-dash). The 3MA data scaled to 1MA using χ_{eff}(scaled) = χ_{eff}(3MA)(B_{POL}(3MA)/ B_{POL}(1MA)) is also shown (dashed lines). Error bars show the typical range of χ_{eff} established at various times during the H-mode periods.*

bootstrap-dominated H-modes are obtained at much lower current and higher q_{edge} than the 3MA H-modes used in the derivation of the JET-DIIID H-mode scaling.

There are no 'ordinary' (medium-q, low β_{POL}) 1-1.5MA H-modes in the JET dataset with which to make direct comparison, so it is unclear whether the favourable confinement enhancement originates in a positive scaling with q_{edge}, which is not covered in the scaling expression or even in a less favourable exponent for the confinement dependence on plasma current than the $\sim I_p^{1.0}$ result used. The existence of a high enhancement relative to the Goldston scaling, the dataset for which does contain data in the same I_p and q_{edge} ranges would argue against these two explanations. It is important to pursue the origin of this confinement enhancment. Although either of the preceding explanations would not be favourable for a steady-state reactor concept based on the bootstrap current, the alternative possibility that the confinement enhancement could be identified as a *consequence* of a high value of β_{POL}, would have attractive features for such a reactor concept. Such a consequence might arise, for example, as a result of a second stability regime opened up to the plasma by the presence of the bootstrap current.

Figure 157 shows a first attempt to find the regions of the plasma where a simple plasma current scaling of energy confinement gives an inadequate picture of the local transport. The value of effective thermal diffusivity (χ_{eff}) profile obtained in a TRANSP analysis of the 3MA ICRF heated H-mode (Pulse No: 20232, [15]) is scaled by the relevant value of $1/B_{POL}(x)$ and compared with TRANSP analyses of bootstrap dominated H-modes at 1MA. A simple scaling of $\chi_{eff} \propto 1/B_{POL}$ gives significantly worse transport than the χ_{eff} obtained at the lower current over most of the minor radius ($\rho \leq 0.8$). Thus, the confinement enhancement would appear to be distributed fairly uniformly in the inner volume of the plasma, in contrast to the H-mode enhancement itself usually appears primarily in the outer plasma.

The high β_{POL} discharges have a somewhat higher (10-20%) shear than the ICRF heated H-modes, but preliminary investigations show that a very strong inverse dependence of χ_{eff} on shear ($\chi_{eff} \propto S^{-\alpha}$ with $|\alpha| >> 1$) would be necessary to bring the 3MA data into line with the 1MA data. This is contrary to the experience from the JET confinement studies during current ramps [21] which gave results of $\chi_{eff} \sim S^{-\alpha}$ with $0 < |\alpha| < 1$.

References

[1] F Porcelli et al, *Sawtooth stabilisation by fast ions: a comparison between theory and experiments*, Proc 17th EPS Conf on Controlled Fusion and Plasma Physics, Amsterdam (1990). Europhys Conf Abstracts 14B, Vol II, 327.

[2] M Hugon et al, *Diffusion of fast electrons after a monster sawtooth crash*, Proc of 19th EPS Conf on Controlled Fusion and Plasma Physics, Innsbruck 1992.

[3] P H Rebut et al, Proc 11th Int Conf on Plasma Physics and Controlled Nuclear Fusion Research, Kyoto 1986.

[4] F Rimini et al, *Full Current Drive with Lower Hybrid waves at JET*, Proc Europhys Topical Conf on RF Heating and Current Drive of Fusion Devices, Brussels 1992.

[5] M Brusati et al, *Phase space distribution of fast electrons induced by Lower Hybrid waves in JET*, Proc Europhys Topical Conf on RF Heating and Current Drive of Fusion Devices, Brussels 1992.

[6] J Jacquinot et al, Proc Europhys Topical Conf on RF Heating and Current Drive of Fusion Devices, Brussels 1992, (to be published in Plasma Physics and Controlled Fusion).

[7] M Hugon et al, Nucl Fusion **32**(1992), 33.

[8] R Galvao et al, *Ideal Ballooning Stability at JET Discharges*, Proc 16th EPS Conf on Controlled Fusion

and Plasma Physics, Venice (1989). Europhysics Conf Abstracts 13B(II), 501.

[9] L C Appel, T C Hender and S Zhu, TAN(92)4-2, AEA Culham Laboratory Report (1992).

[10] J M Greene and M S Chance, Nucl Fusion **21**(1981), 453.

[11] F Troyon et al, Plasma Phys Contr Fusion **26**(1984), 209.

[12] D Stork et al, *High βStudies in the H-mode and Hot Ion H Mode in JET*, Proc19th EPS Conf on Controlled Fusion and Plasma Physics, Innsbruck 1992, Vol I, 339.

[13] D P Schissel et al, Nucl Fusion **31**(1991), 73.

[14] O J W F Kardaun et al, *ITER: Analysis of the H-mode confinement and threshold databases*, Proc 14th Int Conf on Plasma Phys and Contr Nucl Fusion, Wurzburg (1992) (IAEA-Vienna, in press).

[15] B Balet et al, Plasma Phys and Contr Fusion **34**(1) (1992), 3.

[16] P H Rebut, P P Lallia and M L Watkins, Proc 12th Int Conf on Plasma Phys and Contr Nucl Fusion, Nice (1988) (IAEA-Vienna, 1988), Vol 2, 191. With modification in JET Report R(89)16, 184.

[17] M C Zarnstorff et al, Phys Rev Lett **60**(1988), 1306.

[18] M Kikuchi et al, Nucl Fusion **30**(1990), 265.

[19] The JET Team, presented by D Stork, *Long Pulse Operation of JET and its Implications for a Reactor*. Proc 14th Int Conf on Plasma Phys and Contr Nucl Fusion, Wurzburg (1992) (IAEA-CN-56/A-7-7) (IAEA Vienna, in press).

[20] C Gowers et al, *Electron Pressure Gradient Measurement on JET H-mode and Pellet fuelled discharges from the new High Resolution LIDAR Scattering System*, contrib paper 34th APS-DPP meeting (Seattle, 1992) JET-IR(92)09.

[21] C D Challis, J P Christiansen, J G Cordey et al, Nucl Fusion **32**(1992), 2217.

Transport and Fluctuations

The main effort during 1992 was devoted to an analysis of the data obtained during the 1991/92 campaign. Further experiments with strong on-axis ion cyclotron resonance heating applied to a standard JET discharge with-and without-pellet injection, were completed to confirm the local diffusive nature of the heat transport. These experiments and progress with the analysis in other fields are described below.

Global Confinement Analysis: ITER/JET

The collaboration between the six tokamak teams (ASDEX, DII-D, JET, JFT-2M, PBX-M and PDX) that lead to a joint global H-mode confinement database (ITERH.DB1) [1] has continued. The Working Group has assembled and analysed an improved second version of this database (ITERH.DB2). New H-mode data from ASDEX, DIII-D, JET and JFT-2M have been added [2] so that in comparison with ITERH.DB1 the type of H-mode (ELMy/ELM-free) and the isotope composition are more evenly distributed over the six tokamaks in ITERH.DB2. The database now also includes ECH, ICRH and combined ICRH + NBI heated H-mode data. Furthermore, better estimates of several of the relevant plasma parameters have also been provided. In particular, more precise estimates of the thermal confinement time are now available because of improved estimates of such quantities as the fast particle content and anisotropy, and the power losses due to charge exchange and unconfined orbits.

Power-law scalings for both the total and thermal confinement time have been determined by regression analysis on the data in ITERH.DB2 [3]. The analysis has shown that the total confinement time is independent of density. In contrast, the data indicate a density dependence of the thermal confinement time in the form $\tau_{th} \propto n^{0.3}$. At the same time, the dependency on major radius is strong and of the form $\tau_{th} \propto R^{1.95}$ (ELM-free). If the density is not included in the regression, the dependency on major radius is $\tau_{th} \propto R^{1.4}$ which is similar to the dependency in existing L-mode scalings like ITER89P[4]. However, the extrapolations to ITER-like parameters by the scaling with density included are almost a factor of 1.4 higher than the other scaling (Fig.158). The data also show signs that a simple power-law scaling may not be the best representation. For example, the strength of the isotope and toroidal field dependencies do vary with the power input [3]. This indicates that a two term scaling such as an offset-linear type scaling may be a better solution. Both these problems will be studied in more detail by the Working Group.

The Working Group has also assembled a joint H-mode power threshold database (ITERTH.DB1) [2,3] and it includes data from ASDEX, DIII-D, JET, JFT-2M, and PBX-M. The following objectives are being pursued: a) predict the plasma parameter region where H-mode can be expected

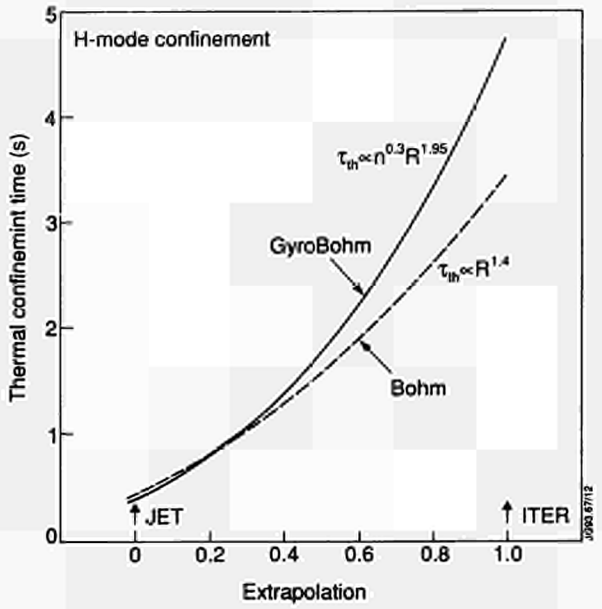

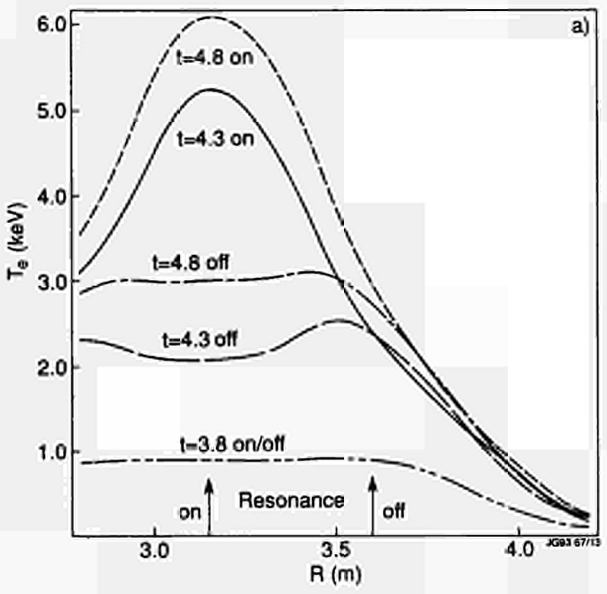

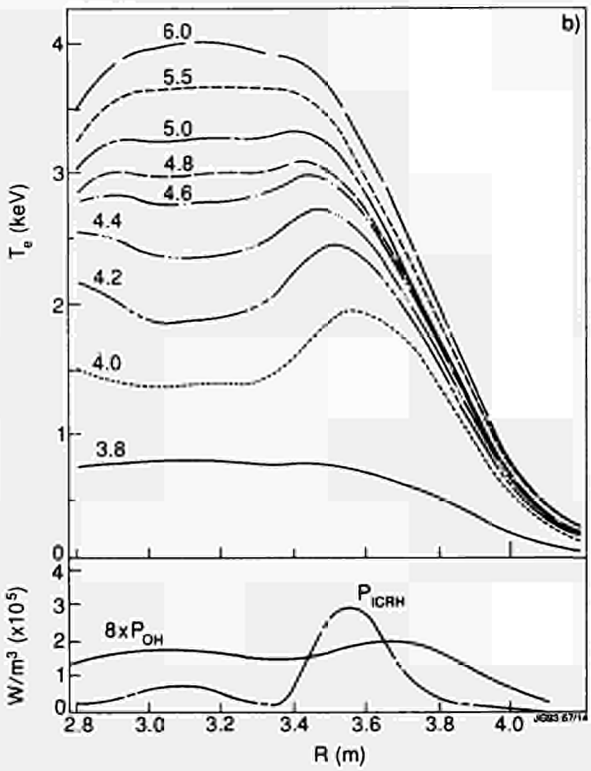

Fig.159: (a) The electron temperature profile at three different times for the purely on and off-axis heated discharges; (b) The electron temperature profile for the off-axis heated case.

Fig.158: The thermal confinement time predicted by the two ELM-free H-mode scalings given in Ref[3]. The extrapolation parameter used as x-axis is EXTP = $\sum \log_{10}(x/x_j^{ITER})$ where x_j = {I,B,P,M,k,a/R,R,n} and x_j^{ITER} = {22MA, 4.85T, 200MW, 2.5amu, 2.2, 0.36, 6m, 12.5 x $10^{19}m^{-3}$}. For JET, x_j^{JET} = {3MA, 3T, 20MW, 2amu, 1.8, 0.4, 3m, 3x$10^{19}m^{-3}$}. The parameter EXTP is varied from -3.15(JET) to 0(ITER) along a straight line in the 8-dimensional space given by $\log_{10}(x_j/x_j^{ITER})$, j = 1 to 8. The two scaling expressions shown are:

$$\text{gyroBohm: } \tau = 4.8\, I^{0.95} B^{0.2} p^{-0.65} M^{0.45} k^{0.65} (a/R)^{0.05} R^{1.95} n^{0.3}$$

$$\text{Bohm: } \tau = 3.46\, I^{1.08} B^{0.09} p^{-0.56} M^{0.49} k^{0.54} (a/R)^{-0.07} R^{1.4}$$

with the parameters being normalized to the ITER values x_j^{ITER}.

in future devices; b) contribute to the L-H transition physics; and c) investigate pedestal effects.

On- and Off-Axis Heating Experiments

The original off-axis heating experiments following pellet injection were completed in 1988 [5]. During 1992, these experiments were repeated and supplemented with on-axis and mixed on- and off-axis ICRH discharges. The difference in the response of the axial electron temperature to the on- and off-axis heating is shown in Fig.159(a) where the off and on-axis temperature profiles are compared at three different times. In the outer region beyond the off-axis heating location, the profiles are similar, as would be expected but in the inner region the profiles are markedly different.

The evolution of the electron temperature for the off-axis heated pulse, is given in Fig.159(b). Note that the profile remains hollow for approximately one second and only becomes slightly peaked about 2s after the start of heating. The reason for this behaviour can be understood from the power balance. Initially the off-axis heating produces a hollow temperature profile with a shape close to the shape of the heating profile. Heat is then conducted away from the peak of the temperature profile towards the centre and edge. Due to the large thermal inertia of the plasma centre it takes a long time for the centre to reach the temperature of the region of heating. Eventually the ohmic heating dominates over the thermal inertia term and the electron temperature profile becomes marginally peaked in the centre with an outward heat flux.

Analysis of the data [5] shows that the total heat flux Q can be described by a local diffusive model $Q = -\chi_\eta \nabla T$ for

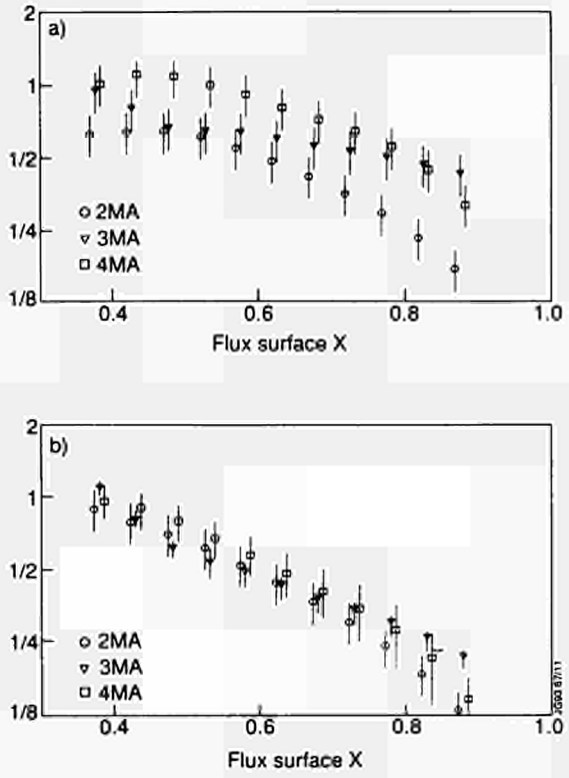

Fig.160: (a) Heat flux normalised to the gyro-Bohm scaling expression versus the normalised radius x; (b) Heat flux normalised to the Bohm scaling expression versus radius x, for the three discharges at I = 2, 3, 4 MA.

a large range of ∇T (including $\nabla T > 0$) and that any heat pinch term would have to be very small indeed.

The data has also been compared with three models of local transport: (a) $\chi \propto |\nabla T|$; (b) $\chi \propto T^{2.5}$; and (c) the RLW critical temperature gradient model. All are found to give a reasonable fit to both the off- and on-axis heated pulses.

Larmor Radius Scaling Experiments

Tests of specific transport models often produce ambiguous answers, which arise from collinearities in the experimental data. In experiments on dimensionally similar discharges which only differ in the values of one single dimensionless parameter, transport scaling with respect to that parameter can be studied. Experiments on JET have been carried out to keep all parameters fixed except for the normalised Larmor radius ρ_*. In these experiments the plasma current, toroidal field, density, ion cyclotron frequency and power level are varied in a predetermined pattern which yields fixed values of collisionality, beta and safety factor. From a range of 16 almost similar pulses, the three most similar pulses with currents of 2, 3 and 4MA have been selected for a full transport analysis. The dependence of heat flux q upon ρ_* is tested by normalising q as $q/(q_{Bohm}\, \rho_*^{x_\rho})$ where x_ρ = 1, 0, 1 correspond to MHD, Bohm and gyroBohm scaling forms. Figure 160 shows this ratio between the 4MA and 2MA pulses of the normalised flux. The experimental data shows convincingly that local L-mode confinement scales with ρ_* according to the Bohm scaling, as does the global confinement. A similar conclusion has been reached from experiments on TFTR and DIII-D. These three major Tokamaks have provided the key element requirement for extrapolations towards a reactor.

Enhanced Confinement Regimes

During the series of hot-ion H-mode experiments completed during the 1991/92 campaign, a new enhanced confinement regime was found. The new regime is similar to the V-H mode seen in DIII-D, with values of the confinement time about twice the usual H-mode scaling (ITERH92-P) and a factor three above the Goldston L-mode scaling expression. This improved confinement follows a second transition during the H-mode. The transition is clearly visible on a confinement time plot of τ_E and is usually coincident with the disappearance of ELMs during the H-mode as seen in the D_α signal. The high confinement is associated with reduced energy transport near the edge. A fraction of the plasma volume is believed to access the second stable regime to ideal high-n ballooning modes. This fraction increases from the edge inwards as the plasma goes further into VH-mode. The VH-mode is often terminated by an X-event which is thought to be associated with an MHD instability. The improvement in confinement from L-mode to H-mode coincides with the development of steep gradients in the temperature and density profiles near the edge. The improvement in confinement from H-mode to VH-mode is a consequence of the broadening of the steep gradients.

The local transport evolution calculated using TRANSP shows a reduction in ion diffusivity at the onset of the ELMS with the bootstrap current increasing continuously from the H-phase through the ELMing H-phase into the VH-phase. The second regime access in the edge region of VH-mode discharges is afforded by this large bootstrap current which broadens and moves inward to small minor radius. In Fig.161, the marginally stable boundaries for a flux surface close to the edge are plotted together with $\alpha \propto p'$ calculated from experimental data showing that for the VH-phase the pressure gradients are in the second stable region. During the ELMing period, the more accurate reflectometer data, is not available so that the estimate of α during this period is questionable. At the onset of confinement degradation, the experimental pressure gradients are seen to decrease coinci-

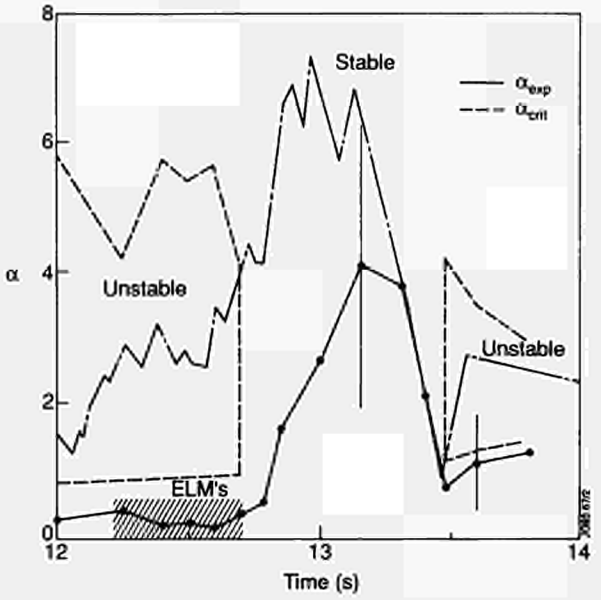

Fig.161: The ideal ballooning boundaries given by α_{crit} plotted together with α_{exp} and the confinement time τ as calculated from TRANSP. As the confinement time increases during the VH-mode the plasma edge enters into the 2nd stable region.

dent with the rise of MHD activity. However, access to the ideal second stability region is maintained.

Isotope Scaling

The dependence of energy and particle confinement in JET on the plasma ion species was studied by means of a full global and local transport analysis of a series of discharges with fixed geometric configuration, plasma current (3MA) and toroidal field, but with different ion species H, D and He^3. The main results of the analysis are summarized in Figs.162 (a), (b) and (c).

Figure 162(a) shows the total and thermal energy confinement time as a function of density. The thermal energy confinement time in D is ~15% larger than in H at all densities. This difference is somewhat larger in total energy confinement times (Fig.162 (b)) due to larger fast ion component with deuterium injection, but it does not exceed 25%. Interestingly, the particle confinement time in D is 50% larger than in H as shown in Fig.162(c). In fact, the difference in particle confinement times, and hence increased convective losses with H is partly responsible for poorer energy confinement in H. No significant difference was observed in thermal energy confinement time or in particle confinement time of D and He^3 discharges.

In summary, JET results point to very weak dependence of the thermal energy confinement time on ion species ($\tau_E \propto A_i^{0.2 \pm 0.1}$) and do not support the hypothesis used in most

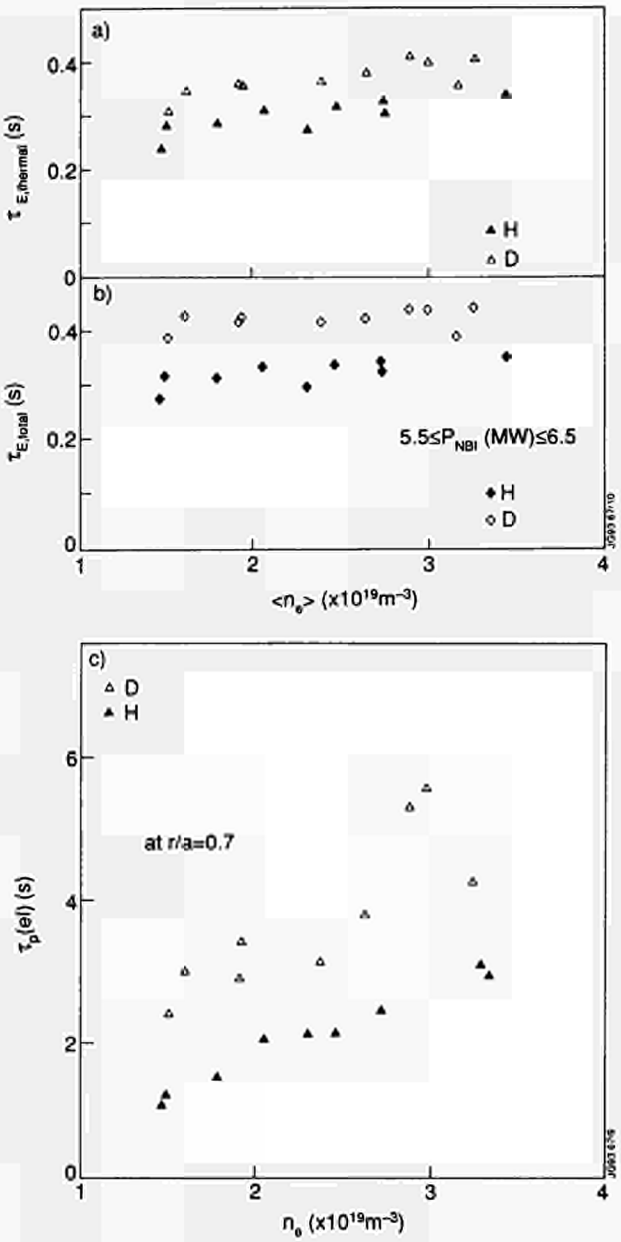

Fig.162: (a) Thermal energy confinement time versus volume average density; (b) Total energy confinement time (thermal + fast) versus volume average density; (c) Particle confinement time versus density.

scaling laws of a square root dependence on the isotope mass, A_i. Further information is available elsewhere [5,6].

New Analysis of Sawteeth Induced Heat Pulse Propagation

A new analysis technique has been developed for the study of the decay rate of sawteeth perturbed T_e profiles to investigate further, electron transport in the spatial zone between the inversion radius and mixing radii. For many JET pulses, four or five ECE grating polycrometer channels with high time resolution are located between these radii. This allows

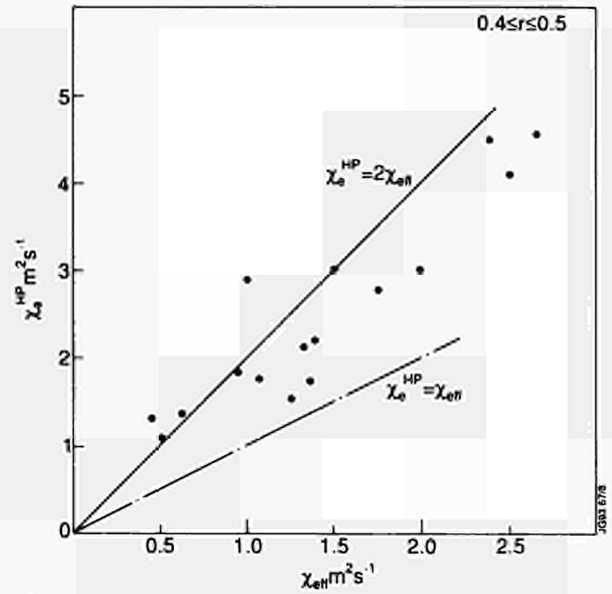

Fig.163: The correlation between the electron heat diffusivity obtained from heat pulse propagation analysis and effective heat diffusivity obtained from power balance.

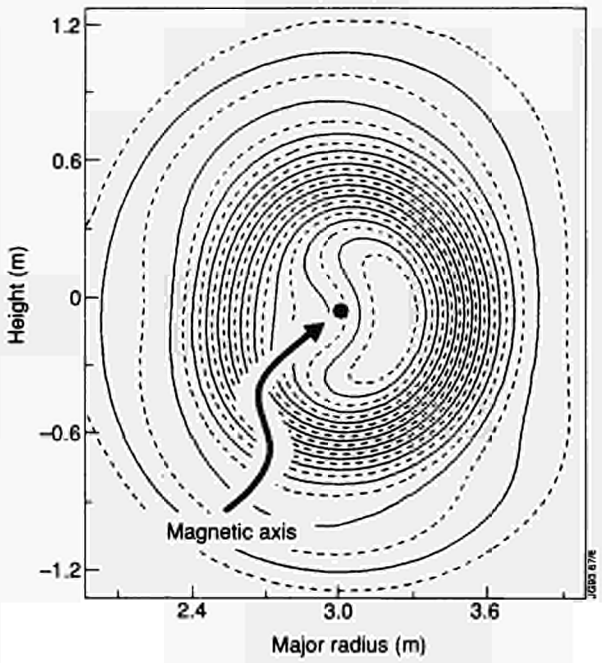

Fig.164: Contour plot of the soft X-ray emissivity during counter-injection beam heating after injection of Ni into the discharge (JET Pulse No: 24375)

the measurement of the electron temperature perturbation profile and to a separation in time of the crash event from the transport processes under study, by beginning the analysis a few milliseconds after the crash.

A comparison between the observed dynamic electron heat diffusivity, χ_e^{HP}, and the effective heat diffusivity, χ_{eff}, from power balance calculations, are shown in Fig.163. The data presented are from JET L- and H-mode plasmas with currents ranging from 1.5MA to 5 MA, toroidal field about 3T, with ICRH, NBI and ICRH + NBI heating, and with ^{4}He, D and H, gas filling. Typically, the time decay between the beginning of the crash and the start of the analysis was about 2ms. For most pulses examined, the heat wave, a few milliseconds after the crash, behaved in a diffusive manner.

Preliminary analysis of the variations in χ_e^{HP} due to change in plasma parameters have demonstrated that these variations are generally consistent with those observed in χ_{eff}. A correlation between slow heat pulse propagation and regimes with very good confinement, e.g. in the hot-ion H-mode was clearly seen.

Poloidal Asymmetries in NB Counter-Injection Experiments

A poloidal assymetry is expected in the impurity density profile in plasmas which are strongly rotating in the toroidal direction, due to the differential centrifugal force on the different impurity species. Balanced by the pressure and the parallel ambipolar electric field forces, this force should result, when the poloidal flows are small, in a marked selective accumulation of the heaviest ions on the outside of the torus. The relative in/out poloidal modulation of the impurity density due to this effect can be roughly approximated, in the limit of small inverse aspect ratio and trace concentration of the heavy impurity I, by

$$\frac{\tilde{n}_I}{\overline{n}_I} = \frac{1}{1+Z_{eff}} X \qquad (1)$$

where $X = \varepsilon m_I v_\phi^2 / T$ and v_ϕ, T are the ion toroidal velocity and temperature. In JET counter-injection experiments [7] this effect could be clearly detected by soft X-ray tomography (see Fig.164). The parametric dependence of these poloidal modulations and their absolute values appear to agree with the above equation up to values of $\tilde{n}_I / \overline{n}_I$ in excess of 0.5, while no appreciable modulation (in/out or up/down), has been observed in several comparable co-injection experiments (see Fig.165). This circumstance could be explained for example, by the presence of an impurity poloidal velocity of about (e/q)V_j in the latter case, that is absent in the former.

Investigation of dependence of Impurity Transport on n_e, P_{add}, I_p, and B_T in L-mode

Dedicated experiments to study the dependence of impurity transport with operational parameters of the discharge were performed at the end of the experimental campaign using the laser blow-off technique. The discharges were in helium

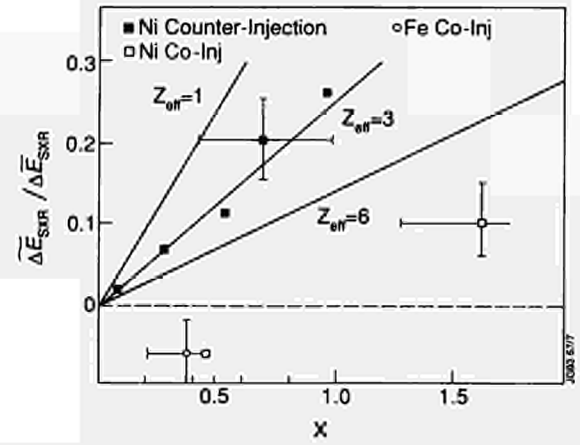

Fig.165: Relative in/out modulation of the soft X-ray emissivity perturbation after metal injection in beam heated plasmas. The straight lines represent the prediction of Eq.(1) for different values of Z_{eff} in a D plasma.

plasma and the following ranges of parameters were explored: $<n_e>$: 1 to 5x10^{19}m^{-3}; P_{add}: 0 to 20MW; I_p: 2 to 5MA; B_T: 1.45 to 3.2T; T_e : 2.5 to 6keV; q(a) : 3 to 6.5.

Clear phenomenological scalings of the impurity containment time with the density (see Fig.166), the additional power (Fig.167), the current and the magnetic field have been identified. From the combined analysis of the density and power scalings it appeared that the level of anomalous diffusion in the confinement region increases with the plasma temperature (or with its gradient), while keeping the temperature profile constant, very large variations of the density profile do not appreciable affect the propagation of the injected impurity.

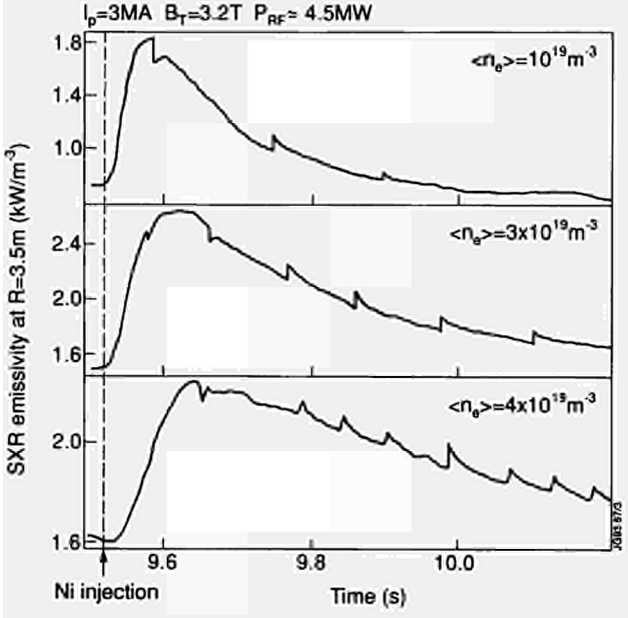

Fig.166: Time behaviour of local soft X-ray emissivity at R = 3.5m for different values of average electron density $<n_e>$. At constant heating power, the transport is slower for higher densities.

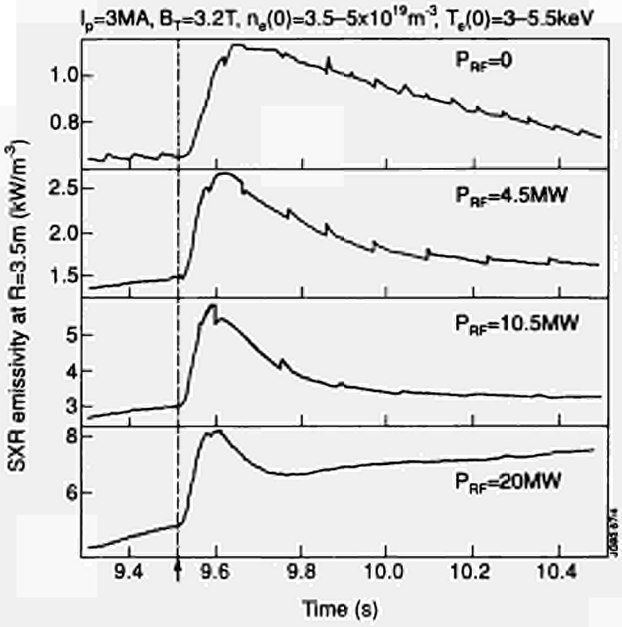

Fig.167: Time behaviour of the local soft X-ray emissivity at R = 3.5m for different values of the additional RF heating power P_{RF}. For larger heating power, the transport is faster.

The presence of a zone of reduced transport in the centre of the discharge was confirmed and the dependence of its size on the current and the magnetic field has been determined (Fig.168). The data clearly show that the diameter of the zone of reduced diffusion increases when the value of q(a) is decreased with little or no dependence on B_T, or n_e, if the q profile is kept constant. The detailed spatial analysis tend to suggest a strict correlation between a high level of anomalous diffusivity and strong magnetic shear.

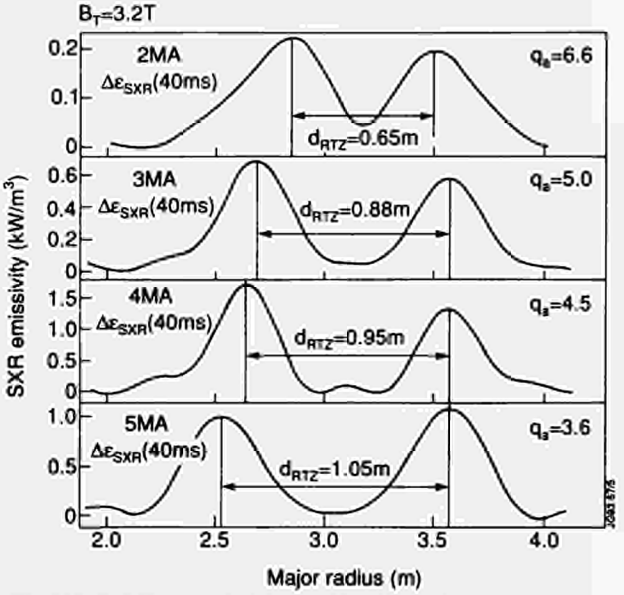

Fig.168: Soft X-ray emissivity profiles 40ms after Ni injection at different values of the total plasma current (I_p = 2-5MA). The size of the reduced transport zone (measured by distance d_{RTZ} between peaks) increases when the safety factor at the edge q_a is decreased.

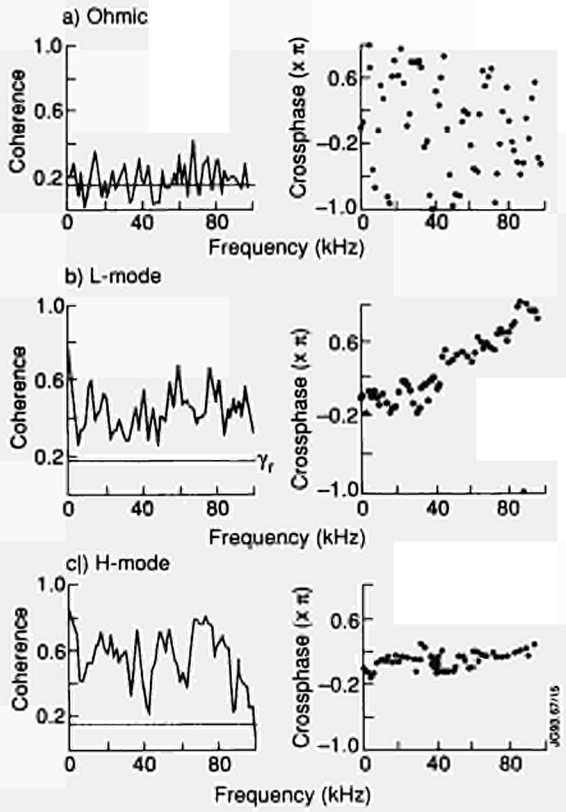

Fig.169:Coherence and cross phase measurements under (a) ohmic, (b) L-mode and (c) H-mode conditions

Density Fluctuation Measurements using Correlation Reflectometry

Development of correlation reflectometry as a technique for investigating density fluctuations has continued. In 1992, attention was concentrated on making measurements with the toroidal correlation reflectometer. This device consists of two independent reflectometers which probe the plasma in the mid-plane through two antennae toroidally separated by 155mm. One of the reflectometers is the standard multichannel instrument, while the other has been specially constructed for this measurement. The probing radiation is polarized in the ordinary mode and so reflection is from the plasma frequency layer. Both reflectometers operate at the same radiation frequency (29 or 34GHz) so that the two reflecting layers are always at the same radius. For most of the measurements, the reflecting layer is located in the boundary of the plasma (3.75<R<4.0m). The detection systems in both cases are of the homodyne type and the data is usually recorded with a bandwidth of 100kHz.

The measurements are analysed using standard spectral analysis techniques. From the analysis, the crosspower spectrum, $G(\omega)$, the crossphase spectrum, $q(\omega)$, and the coherence spectrum, $\gamma(\omega)$, are determined. The value of the coherence is between unity (identical signals) and zero.

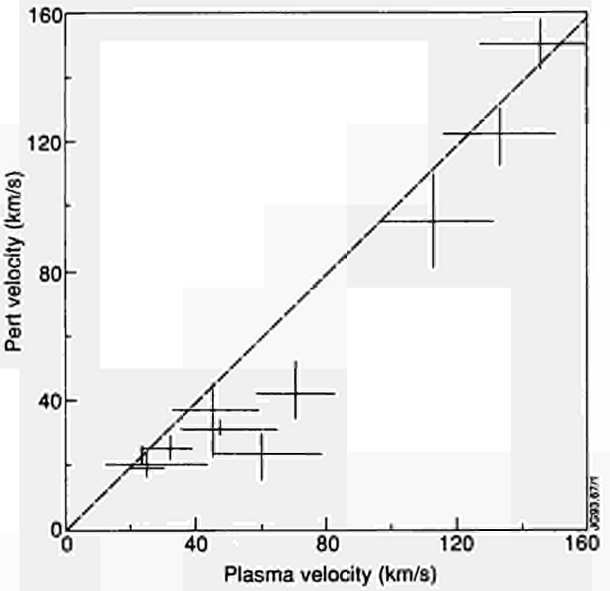

Fig.170: Comparison between measured toroidal velocity of the perturbations and toroidal velocity of the plasma measured with the CX diagnostic for a range of neutral beam powers (2-15MW).

However, for a finite length data set, there is a lower level of statistical significance, γ_r, which represents the coherence between two independent random signals. For these measurements, γ_r is typically 0.18.

Measurements were made for a range of plasma conditions: ohmic, L-mode and H-mode. Under ohmic conditions, the level of coherence was generally at the random level (γ_r) and the crossphase spectrum showed wide scatter. Typical measurements are shown in Fig.169(a). Under L-mode conditions, the level of coherence was significant across the entire frequency band and the cross phase increased linearly with frequency (Fig.169(b)). As the NB power was increased, the slope of the cross phase decreased. In H-mode, the level of coherence was significant, but the cross phase was independent of frequency (Fig.169(c)).

As in the case of earlier radial measurements, the results were interpreted in terms of perturbations in the density profile, ie fine-scale density structures. The measurements did not show any eveidence for such structures under ohmic conditions. However, under L-mode conditions, the high level of the coherence, combined with the frequency dependence of the cross-phase, suggested that the structures rotated toroidally. The phase difference was due to the rotation, and it can be shown that the slope of the cross phase spectrum was simply related to the rotation velocity. It is instructive to compare the rotation velocity of the fine-scale density structures obtained with the toroidal correlation reflectometer with the local plasma rotation obtained independently with the charge exchange (CX) diagnostic. This

is shown in Fig.170 for a wide range of neutral beam powers (2-15 MW). It can be seen that, within measurement uncertainties, the two velocities agree. The uncertainty in the CX measurement includes a contribution due to the uncertainty on the radial location of the reflecting layer.

Under H-mode conditions, the frequency independence of the cross phase suggests that the structures were either moving toroidally at very high velocity or, more plausibly, poloidally. The CX diagnostic indicated that, under these conditions, there was usually a poloidal component to the plasma motion of similar magnitude to the toroidal component. Therefore, it is most likely, that, under these conditions, the reflectometer measurements were dominated by the poloidal motion. To investigate this, a poloidal correlation reflectometer is required.

References

[1] Christiansen, J.P., Cordey, J.G. Thomsen, K., et al., Nucl. Fusion **32** (1992) 291.

[2] Thomsen, K., et al., H-mode Confinement and Threshold Database Work, Rep. JET-R(92)07, JET Joint Undertaking, (1992).

[3] Kardaun, O.J.W.F., Ryter, F., Stroth, U., et al., IAEA-CN-56/F-1-3, 14th International Conference on Plasma Physics and Controlled Nuclear Fusion Research, IAEA, Würzburg (1992) to be published in Nuclear Fusion Supplement.

[4] Yushmanov, P.N., Takisuka, T., Riedel, K.S., et al., Nucl. Fusion **30** (1990) 1999.

[5] The JET Team, The Transport of energy and particles in JET plasmas, IAEA-CN-56/D-3-4, 14th International Conference on Plasma Physics and Controlled Nuclear Fusion Research, IAEA, Würzburg (1992) to be published in Nuclear Fusion Supplement.

[6] F. Tibone et al., Dependence of Confinement on Plasma Ion Species in JET, JET Report JET-P(92)79, submitted to Nuclear Fusion.

[7] R. Giannella et al. Proc. 19th EPS Conference on Controlled Fusion and Plasma Physics, Innsbruck 1992, Vol. 1, p 279.

MHD, Topology and Beta Limits

During 1992, studies of magnetic hydrodynamics (MHD) phenomena were undertaken in three principal areas:

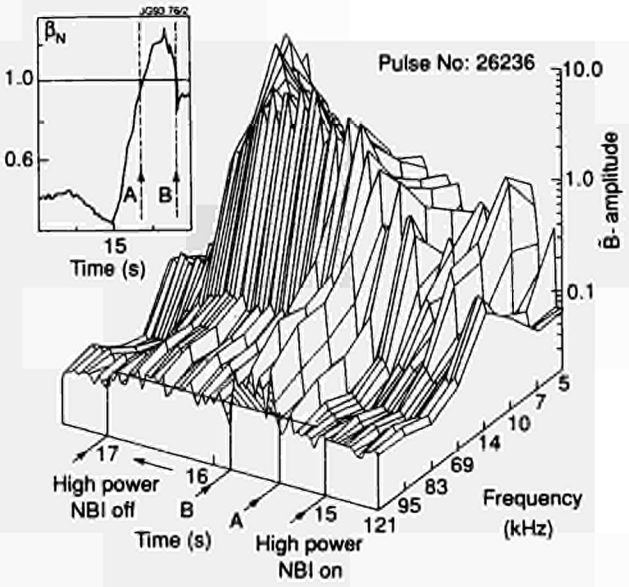

Fig.171: High frequency MHD activity as a function of time during the high power heating phase of β_N>1 (Pulse No: 26236). The peak at <10kHz represents n = 1 activity at the plasma rotation frequency.

- high performance plasmas and β-limitation;
- the causes and consequences of disruptions;
- experimental and theoretical studies relating to sawtooth oscillations.

The main advances are described in the following paragraphs.

High Performance Plasmas and β-Limitation

The performance of high-β plasmas is subject to deterioration at high-β either in a progressive limitation of β or as a sudden event. This has led to studies of the associated MHD phenomena of fishbone instabilities, edge localised modes and ballooning modes. Two particular areas of investigation were high-β plasmas at low toroidal magnetic field and hot-ion H-modes.

Characteristics of the Low B_T H-modes

In Pulse No: 26236 with a low toroidal field, 1.1 T and a current of 2MA, a β of 6% was obtained, corresponding to 1.2 times the Troyon limit [1]. The plasma was close to the hot-ion regime with $T_i(0)$ = 12keV and T_e (0) = 5.5keV at a pulse time of 15.4s. All the highest β discharges show a similar occurrence of high frequency MHD activity in the range 70 - 120kHz. This is broadband in nature and grows as the normalised β_N (=β/β' where β' = 2.8I(MA)/aB) exceeds unity (see Fig.171). This may be the manifestation of high mode number ballooning modes. It is not possible with the

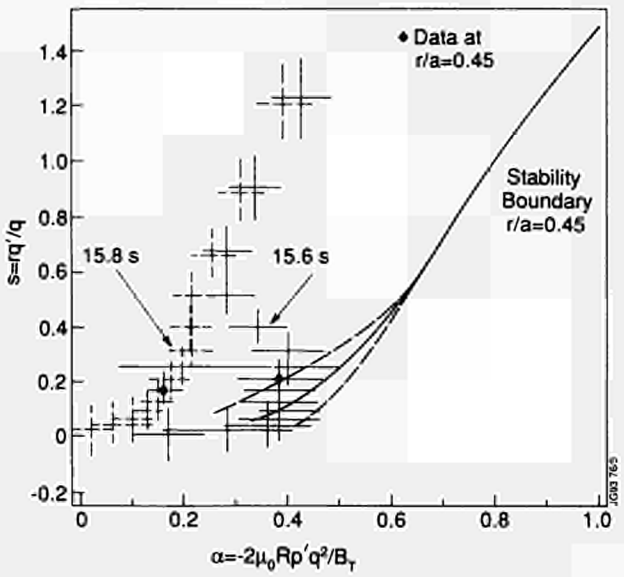

Fig.172: Ballooning stability curve for Pulse No: 26236, at r/a = 0.45, compared with (s, α) profiles at 15.6s and 15.8s (after collapse). The dashed lines around the stability boundary indicated uncertainly due to q profile errors. ◊ indicates the data point to be compared to the curve at each time.

diagnostics available to determine the radial location of the activity.

A preliminary stability analysis using a high-n ballooning code [2], supplemented by the HBT code [3] at low shear, has been performed on data from Pulse No:26236. Thermal pressure profiles were established from LIDAR and ECE measurements of $T_e(r)$, and Charge Exchange Recombination Spectroscopy (CXRS) measurements of $T_i(r)$ and $Z_{eff}(r)$. Polarimetry measurements of Faraday rotation profile were used, together with measured pressures and magnetic measurements as constraints to two equilibrium fitting codes (IDENTD and EFIT). The two codes, which were in good agreement, can essentially be interchanged. Some results are shown in Fig.172. The plasma profile at 15.6s (near the peak β value) has a trajectory in the s-α plane ($s = rq'/q$, $\alpha = 2\mu_o Rp'q^2/B^2_\phi$), which approaches close to 100% of the ideal MHD ballooning limit around the surface r/a = 0.45. The data at 15.8s, taken during the collapse of β, shows that the central pressure is lost principally due to collapse of the ion temperature.

Hot Ion H-modes

These discharges had a plasma current of 3MA and toroidal fields of 1.8 to 3.1T, and included the highest performance discharges. In extending the analysis, many forms of MHD activity, including fishbones, were seen in the H-modes with well-peaked current profiles. There is no regularity in the β threshold for low n and fishbone activity, however, and it is not clear whether the existence of such activity limits the plasma performance. There are strong bursts of high frequency MHD activity above 70kHz (as in the β_N>1 discharges) and these occur generally at high β. The threshold for such high frequency activity decreases with increasing Z_{eff}, and is generally around 0.75 - 0.95 of the peak normalized β. This high frequency activity may be linked to high n modes, and the Z_{eff} dependence may indicate resistive ballooning activity.

Further analysis was performed on the global and local confinement properties of these discharges, especially on the effect of the toroidal field variation, and this is described in the section related to Physics Issues.

Causes and Consequence of Disruptions

Although there have been extensive and detailed studies of disruptions in JET, there remain important unresolved issues. The role of plasma cooling in fast disruptions has been studied together with the behaviour of the energetic electrons produced in these disruptions. Recently the surprising sensitivity of the plasma to error fields has been explored experimentally, providing clear evidence that small errors can lead to disruption.

Fast Disruptions

The complicated pattern of behaviour of fast disruptions in JET is now reasonably well understood. The early phase is associated with MHD instability, current re-distribution, a negative voltage within the plasma and energy loss. In fast disruptions, this is followed by a sudden plasma cooling, now thought to be due to a massive localised influx of impurity. The increase in resistivity leads to the release of the trapped negative voltage followed by a large positive voltage. It is the associated electric field in the plasma which can produce a large current of runaway electrons.

Runaway Electrons

With carbon limiters, large runaway currents are produced. With X-point configurations, the currents are less and with beryllium limiters there are generally few runaway electrons. In some discharges, the runaways carry a large fraction of the original current for a considerable time. These runaway electrons have energies of tens of MeV and the current is located at a small major radius. They are generally stably confined but are subject to sudden unexplained loss. While they are confined they lose energy by synchrotron

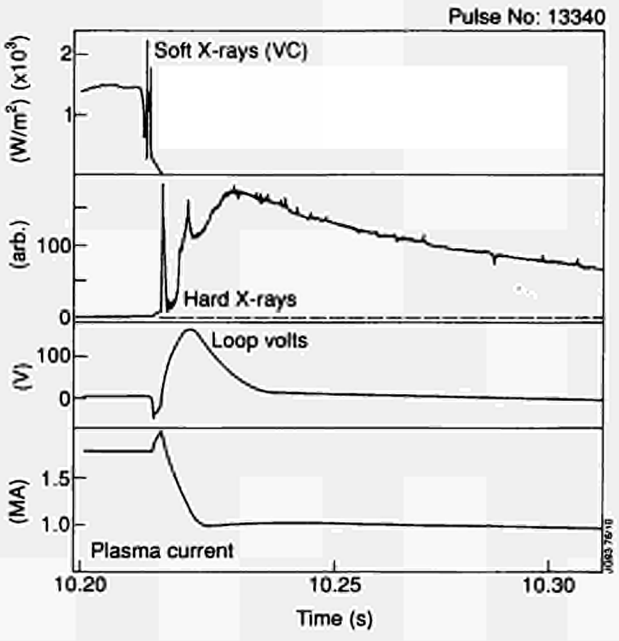

Fig.173: The time development of the soft and hard X-rays, the loop voltage and plasma current, following a disruption.

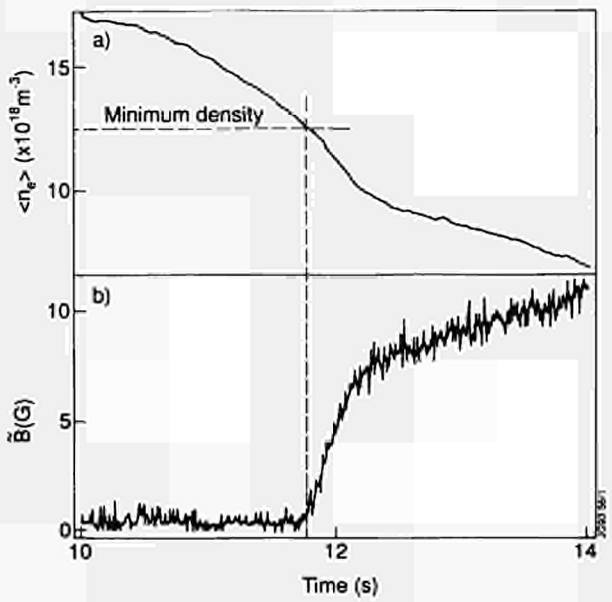

Fig.174: Growth of a magnetic field perturbation as the density decreases below the minimum value for stable operation.

radiation, but since the electrons are relativistic the current persists. The behaviour is illustrated in Fig.173.

Once the runaway regime has been reached the energy of the runaways increases rapidly. Calculations show that energies up to 36MeV are reached in 12ms, in approximate agreement with the characteristic rise time seen in the hard X-ray signal. After a substantial runaway current is produced, the loop voltage drops to around zero and the hard X-ray signal observed by the X-ray diode arrays then shows a smooth decay. This signal is believed to originate in bremsstrahlung radiation from the runaways.

The hard X-ray signal originates in bremsstrahlung radiation from runaway-background plasma interactions. This radiation is highly peaked in the direction of the runaways and is observed in the hard X-ray detectors only after scattering from material in the region of the main horizontal ports. The efficiency of detection above threshold depends only weakly on energy and the observed decay represents a gradual loss of energy from the runaway beam principally by synchrotron radiation. Typical timescales are about 75ms which correspond to synchrotron loss times of relativistic electrons in orbits with Larmor radii of 12cm. This is very much less than the major radius of the orbit and probably corresponds to the effective radius of the electrons as they move in the combined toroidal and poloidal field. An alternative explanation would be that the electrons were scattered from their original trajectories parallel to the magnetic field. A scattering angle of ~5° would be sufficient to account for the observed decay time.

The Effect of Error Fields

The poloidal and toroidal field coils generate small error fields, that is components of magnetic field which are not axisymmetric. A large quantity of evidence points to the conclusion that error fields cause disruptions if the plasma density drops to below a minimum value [4]. This conclusion has now been tested with dedicated experiments.

The number of turns used in each of the vertical field coils (P4) is either 39 or 61. The difference between the two configurations, with respect to the plasma equilibrium, is that of a very small change in the curvature of the poloidal field. However, each configuration generates different error fields. For the plasmas used in this particular experiment, the resonant m = 2, n = 1 component of the magnetic field at the q = 2 surface was larger when using only 39 turns by a factor of ~2.5 (i.e. 0.4 G (61 turns), and 1.0 G (39 turns)).

A limiter plasma was used in the experiment, with no additional shaping currents, to minimise the number of sources of error field. There were small additional sources from the primary coil (P1) and toroidal field system, but the total error field was dominated by that from vertical field coils. The plasma density was ramped down slowly between 10 and 15s after the start of plasma current. The minimum density for each plasma was taken as the density immediately before growth of a helical perturbation of the magnetic field (Fig.174). Plasmas with various values of safety factor on the last closed flux surface, q(a), were produced by varying the toroidal field. The results from both configurations of the vertical field coils are shown in Fig.175.

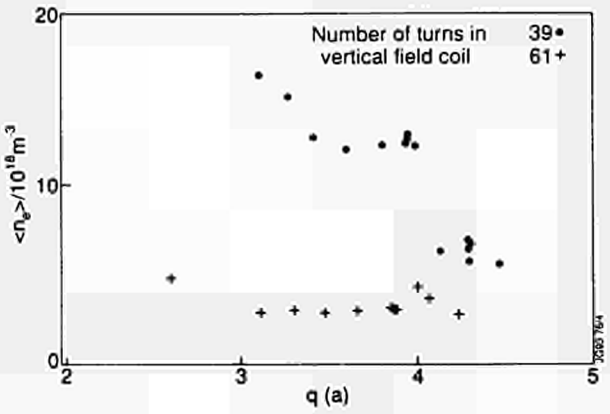

Fig.175: Measurement of the minimum density for the two configurations of the vertical field coils, as a function of q(a).

The results demonstrate that the minimum density was much larger when only 39 turns were used in each of the vertical field coils (larger error field), for a given plasma equilibrium. The helical phase of the measured perturbation was close to that predicted from the error field source in the vertical filed coils (differing by 2 (± 5)° over a sample of 35 plasmas). Hence it is deduced that error fields are responsible for the minimum density limit.

The increase in the minimum density at lower values of q(a) is explained by the movement of the q = 2 surface towards the plasma edge. This brought the surface closer to the error field source and also reduced the stability of the plasma with respect to the natural m = 2, n = 1 tearing mode. The increase in minimum density prevented the production of stable plasmas with q(a) ≤3 using 39 turns in the coils, since the high density limit in these plasmas was at $<n_e>$ = 22 (±1) x 10^{18} m^{-3} (for 3 < q(a) < 5). The abrupt increase at q(a) = 4, for the plasmas using 39 turns, is not understood.

The value of the minimum density was highly reproducible during the experiment, for a given plasma equilibrium. However, the internal inductance, ℓ_i, was not an important parameter for determining the stability of the plasma with respect to the effect of error fields, in contrast with previous suggestions [5].

Sawtooth Oscillations

Further studies have been undertaken to clarify both the pattern of behaviour of sawtooth oscillations and underlying physics. For the first, soft X-ray tomography has been a most powerful tool. Experiments were carried out to investigate the mechanism of sawtooth stabilisation by application of ICRF heating. Since the value of safety factor, q, is crucial to understanding sawteeth and since measurements have often been in conflict, measurements were carried out using two different techniques: Faraday rotation and motional Stark effect. Further theoretical investigations have been carried out, concentrating on the reconnection process.

Tomographic Analysis of Sawtooth Behaviour

The variety of sawteeth in JET can be divided into two main groups: precursorless sawteeth and those with m = n = 1 precursors. The latter are predominantly found in NB heated discharges, with a corresponding fast toroidal rotation. It is found that their collapse is a sequence of two energy loss processes. Either of these may be stabilised during the collapse, giving rise to the apparently different types of sawtooth behaviour observed.

These NB heated discharges, where rotation frequencies of up to 20kHz are measured, have been analysed with high spatial resolution by means of a rotational soft X-ray tomography code. For such high rotation frequencies, soft X-ray data from only a quarter rotation cycle can be used, during which time the emissivity changes little.

Three classes of sawtooth collapse are observed: partial; intermediate; and complete. Partial sawteeth flatten the temperature profile only near the q = 1 surface. Intermediate sawteeth represent a stage between the partial and complete collapse, exhibiting postcursor oscillations of considerable amplitude. For complete sawteeth, the collapse is followed by very small or no postcursor oscillations.

The early dynamics of all three classes of sawteeth are the same, that is there is a radial displacement of the hot core together with growth of an m = n = 1 island. The partial sawtooth is rapidly stabilised before the centre is reconnected. The core moves back to the plasma centre on a much slower timescale, leaving the hot core unaffected and the temperature profile flattened in the region of q = 1 surface. For complete sawteeth, the island size and displacement of the hot core continue to increase to where the peak emissivity starts to decrease until finally profiles across the whole plasma core have been flattened. Since the emissivity in the non-reconnected core drops, it can be concluded that reconnection is not the only process of plasma redistribution.

This is shown most clearly in the analysis of the intermediate sawtooth collapse. Just as in the complete collapse, energy is transported across closed flux surfaces. This process is stabilised, however, before the whole pressure is released from the core. The presence of two loss processes is confirmed by an analysis of the growth rate for the

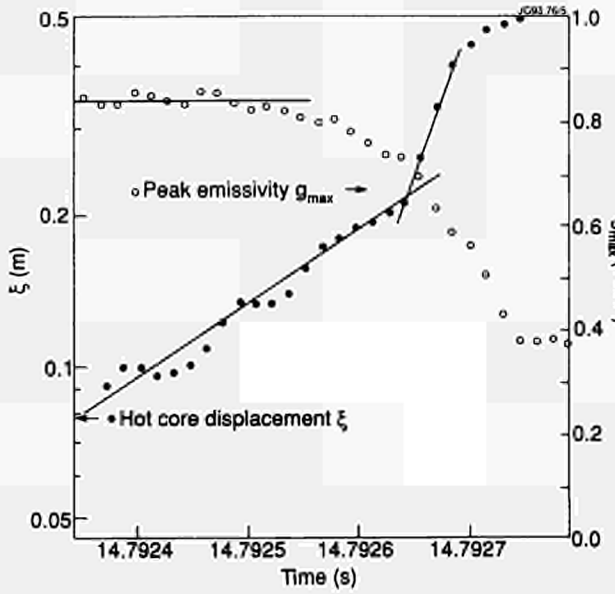

Fig.176: The peak emissivity together with the displacement of the hot core as a function of time for a complete sawtooth collapse. In the first place, there is a "slow" reconnection, and in the second, a fast central energy loss.

complete collapse. Two growth rates are found for the core displacement. The change in growth rate from slow ($\gamma \sim (300\mu s)^{-1}$) to fast ($\gamma \sim (100\mu s)^{-1}$), coincides with the onset of the central pressure release (Fig.176). A two stage process for the sawtooth instability provides a probable explanation for the seemingly inconsistent observations made in different tokamaks. Depending upon machine parameters and plasma profiles, stabilisation of the collapse will occur at different stages during both loss processes and thus give rise to the complex spectrum of observations.

Tomographic Reconstruction and the Snake

The tomographic method used in the sawtooth studies described above is an extension of an algorithm originally developed for circular plasmas in ASDEX 2. Its static version performs the tomography in flux co-ordinates rather than the polar co-ordinates of the original Cormack method. The rotational version makes use of the rotation of MHD modes to increase the poloidal resolution. It has been tested in numerical simulations and by reconstructing pellet induced snakes. Snakes are far too localised to be resolved by static tomography. The snake size deduced from rotational tomography (Fig.177) is in good agreement with that deduced from the raw data traces, clearly demonstrating the reliability of the method.

RF Switch-off Experiments

These experiments were aimed at studying the mechanism by which sawteeth are stabilised with ICRF heating power.

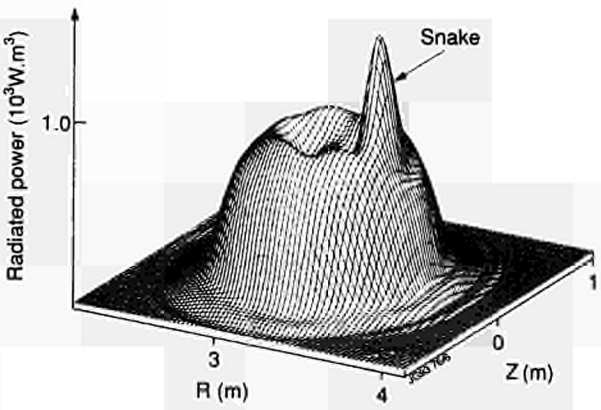

Fig.177: Reconstruction of soft X-ray emission showing a "snake".

In a series of 3MA, 3.1T discharges, sawtoothing was suppressed by application of about 9MW of ICRF heating power on-axis. The ICRF power was switched off at different times during the sawtooth suppression interval, and the time delay for a sawtooth to occur after switch-off was measured. In the experimental conditions, it was found that this delay time had a maximum of about 0.3s when the ICRF power was switched off after 0.5 - 1s.

This has been described further in the section on Physics Isssues.

Comparison of Poloidal Field Measurements

The central safety factor, q_o, in sawtoothing JET discharges has been measured to reach values of ~0.75, using far-infrared polarimetry (Faraday rotation), but until recently this result has not been corroborated by an independent diagnostic. A second measurement of the poloidal field, which has been successfully developed at JET in recent years, makes use of the motional Stark effect (MSE). A direct comparison between these two techniques has been made. The measurements are made by an 8-channel DCN (195μm) polarimeter and by a 4-channel visible beam-emission spectrometer, which measures both the magnitude of the Stark splitting and the polarisation of the multiple components.

The most important sources of error in the determination of the q-profile in JET are: (i) uncertainties in the geometry, particularly the radial variation of the flux surface elongation κ; (ii) the line integrated nature of the Faraday rotation diagnostic coupled with the small number of probing chords; and (iii) systematic offsets in the pitch angles measured using motional Stark effect polarimetry. The geometrical errors were minimised by making the measurements in strictly circular discharges. This has been verified by the

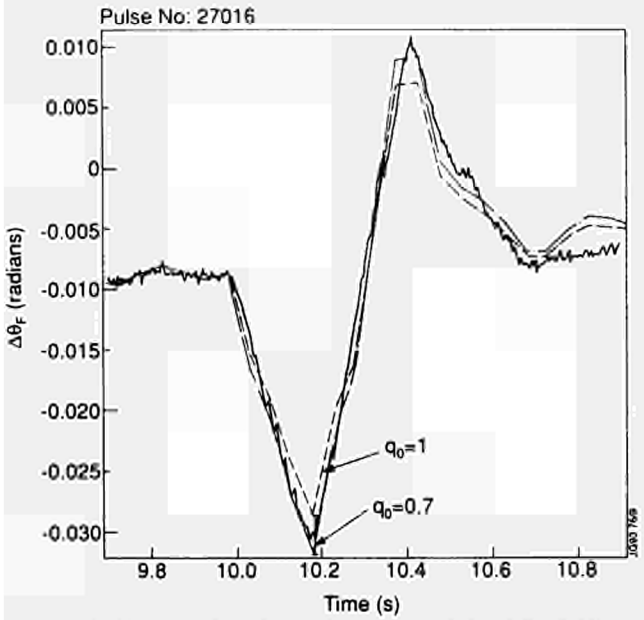

Fig.178: Change in Faraday angle on a central chord (R = 3.02m) during a radial plasma sweep. The figure also shows the calculations undertaken assuming q_o = 1 (dashed line) and q_o = 0.7 (solid line).

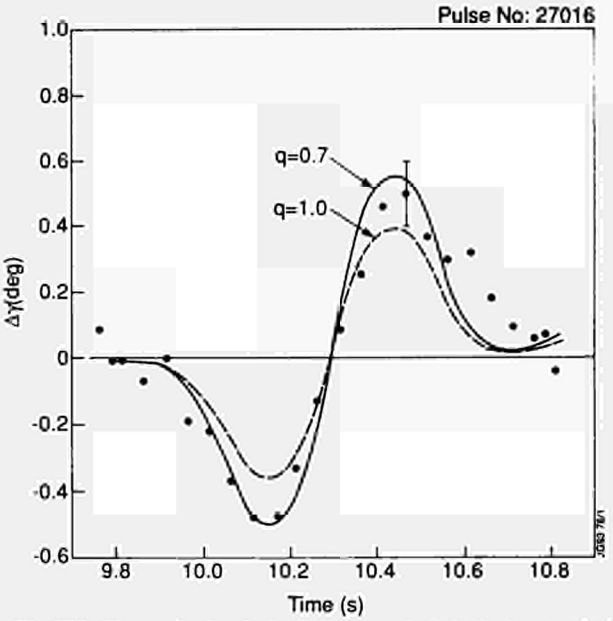

Fig.179: Change in the pitch of the magnetic field during a radial plasma sweep, inferred from MSE measurements. Also shown are calculations assuming vanishing shear and q = 0.7 (solid line) and 1.0 (dashed line).

equilibrium identification code IDENTD (which incorporates both magnetic and polarimetric measurements) and by tomographic inversion of the soft X-ray emmissivity. Both determinations give $\kappa = 1$ within 3%. The other errors were reduced by introducing major radius sweeps of the plasma column. This increased the effective spatial resolution of the diagnostics, since successive time points probe different relative positions in the plasma. It also eliminated systematic offsets because only the differential changes in the measurements were examined.

Figure 178 shows the time evolution of the central chord of the polarimeter as the plasma is displaced in and out across the line-of-sight in a 3MA, 2.8T discharge. Note that the periodic modulation arising from sawtoothing have been subtracted to highlight the effect of the radial sweep. Also shown are the calculated values of the Faraday angle under the assumption that: (i) the q-profile is flat within the SXR inversion radius; or that (ii) the q-profile is hollow within this radius, reaching a value of 0.7 at the axis. The latter assumption fits the data within its error bars, while the former does not. Figure 179 compares the effect of the same radial sweep on the MSE measurement with simulations. Since this is a local measurement, it only depends on the local value of the safety factor and its radial derivative. The simulations are made assuming (dq/dr) = 0, at the measurement position, so that the inferred value of q represents an upper bound. As with the variation of the Faraday angle, the change in the observed pitch angle is consistent with a value of q well below unity inside the q = 1 surface.

Thus, under these optimized conditions, both diagnostics lead to similar inferences regarding the safety factor profile. The consistent result which emerges is that the safety factor is well below unity throughout the sawtooth cycle. The actual value depends on experimental conditions, but values in the range 0.7 - 0.85 are typical.

Sawtooth Theory

A model for the stability of resistive internal kinks, which encompasses both effects of fast particle pressure and the local (q = 1) magnetic shear, has been developed. Sawtooth stabilisation by the fast particle pressure is most effective with on-axis ICRF heating. With off-axis current drive from ICRF waves in low β_p discharges, the modification of the local shear near q = 1 may play the most important role.

Theoretical attention has turned to the processes by which magnetic reconnection takes place in high temperature plasmas. In JET plasmas, it is probable that sawtooth reconnection is collisionless. Magnetic reconnection can remain a virulent process at high temperature, contrary to predictions based on collisional models. In fact, for JET parameters, the initial growth rate of collisional m = 1 tearing modes compares favourably with the observed sawtooth relaxation time. The nonlinear m = 1 mode evolution is not yet clear. The indications are that the ion Larmor radius plays an essential role in the nonlinear stage, where it limits the width of the ion flow channel around the reconnecting q = 1 surface.

References

[1] Troyon F., et al., Plasma Phys. Contr. Fusion **26** (1984), 209.

[2] Green J.M. and Chance M.S., Nucl. Fus. **21** (1981), 453.

[3] Huysmans G.T.A., et al., FOM Instituut voor Plasmafysica, Rijnhuizen Report, 90-194.

[4] JET Progress Report 1991, No. EUR 14434 En, 135.

[5] JET Progress Report 1989, No. EUR 12808 EN, 118.

Physics Issues Relating to Next Step Devices

The objective of the Topic Group was to carry out experiments on issues of particular relevance to Next Step devices, that were not already part of the JET programme. This work was carried out in close cooperation with the various Task Forces. The responsibility for analysis and documentation has been divided between the Topic Group and the Task Forces. In particular, a report on experiments on high bootstrap current is detailed in the section on Physics Issues, while a report on the experiments on the simulation of helium slowing down and ash behaviour can be found in the section on Impurity Transport and Exhaust. This section reports on experiments on toroidal field ripple, and on the progress made on the analysis of the experiments with ion cyclotron heating at high minority concentration.

Toroidal Field Ripple

The primary objectives of these experiments [1,2] were to address the issues of stochastic diffusion losses [3,4] of fast particles, as well as to investigate any additional effects caused by toroidal field high ripple. JET was operated with 16 toroidal field (TF) coils in a variety of operation conditions (enhanced field ripple). Reference experiments were carried out with the full set of 32 coils (small TF ripple). Halving the number of coils results in an increase of the ripple on the magnetic axis from a negligible value ($<10^{-6}$) to about 10^{-3}, and an increase of the ripple at the plasma edge from about 10^{-2} to 10^{-1}. Data was obtained on: the reduction of the confinement and heating of L-mode plasmas; on suppression of high quality H-mode behaviour; on suppression of plasma rotation; on loss of ion-cyclotron fast minority tail particles; and on the reduction of the triton burn-up.

For analysis of this experiment, and for the prediction of fast particle losses due to ripple in general, a novel approach

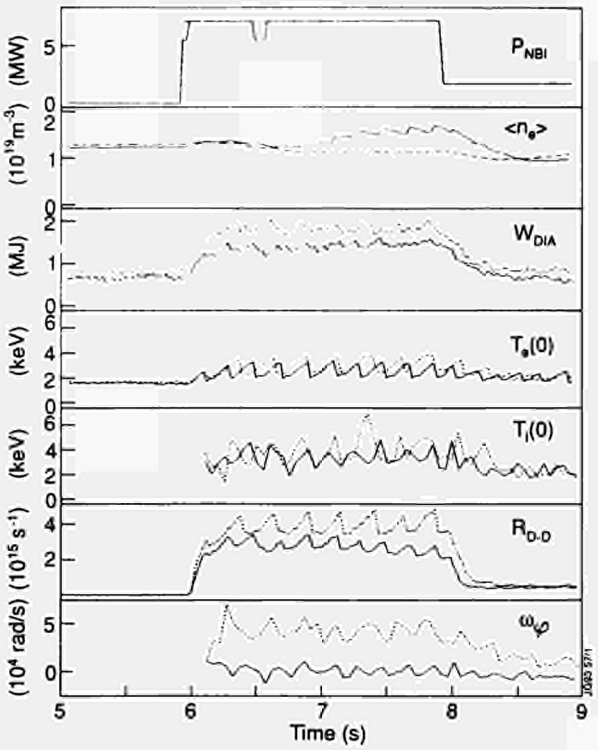

Fig.180: Comparison between NB L-mode discharges with 16 (solid traces) and 32 (dashed traces) coils. Shown are NB power, diagmagnetic stored energy, volume-average density, central electron and ion temperatures, D-D fusion reaction rate and central rotation velocity.

to the calculation of the stochastic diffusion losses was developed. The method is based on the theoretical observation that the stochastic diffusion losses for small ripple can be described by a diffusive scattering of banana-orbit averaged particle parameters. Once the relevant diffusion coefficient is known, the bounce average procedure leads to orders of magnitude savings in computational time compared to full Guiding Centre Following Monte Carlo Codes. A Bounce Average Monte Carlo code on the basis of this method, was developed.

The experiment with 16 toroidal field coils was subject to operational limitations. First, due to concerns about stresses in the toroidal field coils, the toroidal field was restricted to 1.4T. Secondly, on the basis of worst-case calculations of possible heat-loads due to escaping fast particles on inconel in-vessel components, the input powers were limited to 8MW NB power for 2s, or 5MW ICRF heating for 0.5s, respectively.

In Fig.180, a comparison between 16 and 32 coil operation is shown for an L-mode discharge with NB injection. The toroidal field was 1.4T, the plasma current was 2.5MA, and the plasma was limited on the inner-wall. The densities of the two discharges were equal, until at 7s, a carbon influx occurred for the 16 coil case. This was thought to be due to

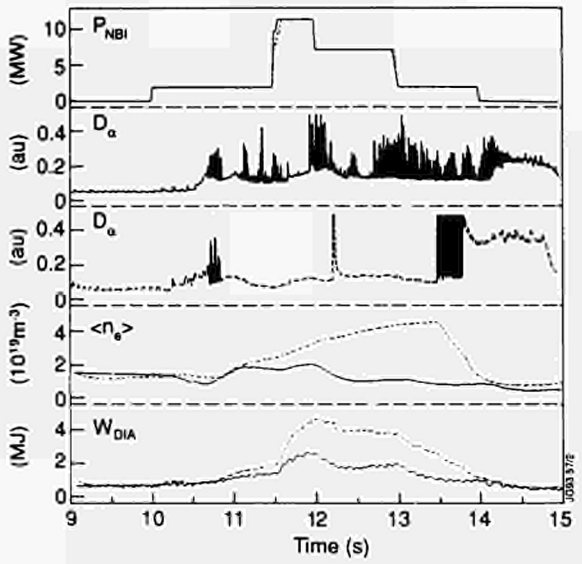

Fig.181: Comparison of NB H-mode discharges with 16 (solid traces) and 32 (dashed traces) coils. Shown are NBI power, vertical D_α signals for 16 and 32 coils respectively, volume average density and diamagnetic stored energy.

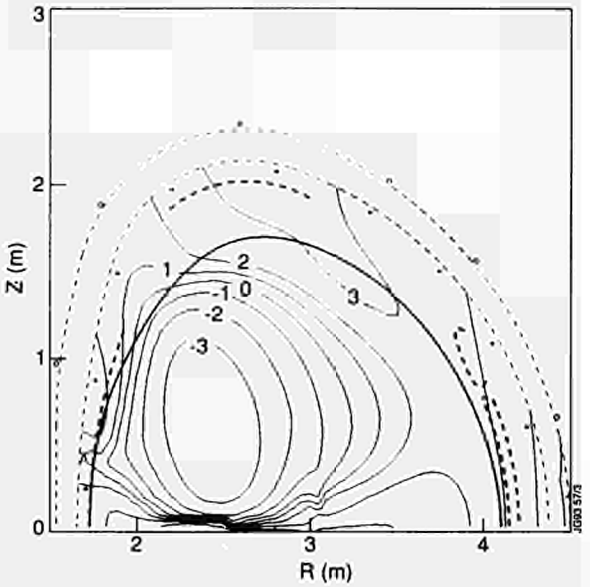

Fig.182: Contours of log (D_R), the effective stochastic diffusion coefficient for 1MeV protons. The R, z coordinate represented the position of the banana tip.

a localisation of the heat load on the inner-wall in the rippled field. The diamagnetic energy was reduced by about 30% in the 16 coil case. This represents a reduction of about 10% in central electron temperature, about 20% in ion temperature, and about 25% in the D-D reaction rate. In the 16 coil case, the plasma rotation was suppressed over the entire plasma cross-section.

The reduction of the stored energy results, in principle, from two effects. First, there is a loss of NB fast ions, due to the ripple loss cone. It was calculated, with a full representation of the NB source (as obtained from the PENCIL code), that about 7% of the beam power is lost as a result of direct trapping of injected ions into the ripple wells and of pitch angle scattering of NB ions into the wells. Since this loss only affects the NB deposition near the plasma edge, the expected effect on the plasma stored energy is significantly smaller than the 7% loss of NB power. Second, there is an increase of thermal energy transport due to ripple effects. The expected effect was deduced on the basis of theoretical calculations [4]. The ripple-induced heat conductivity was added to the heat anomalous conductivity derived for the 32 coil reference case by the TRANSP code. A TRANSP predictive run was then performed to predict the plasma stored energy and temperature for a 16 coil case. The result was that the simulated reductions of the central ion temperature was less than 5%, while the experimental value of the reduction was 20%. It thus appears, that the losses are larger than theoretically predicted.

A comparison between H-mode discharges with NB power for 16 and 32 coil cases is shown in Fig.181. H-mode discharges were made in a double-null X-point configuration at 2.0 and 2.5MA. With 32 coils, ELM-free H-mode operation could readily be obtained. At the lower toroidal field, the H-mode threshold was low, at about 1.5MW. With 16 coils, the threshold for the H-mode appears not to be significantly higher. However, ELM-free H-modes could not be sustained for longer than a few tens of milliseconds, with power levels up to 10MW. It is not clear what is the cause of the loss of the H-mode, although a probable cause is the transport across the separatrix induced by the high ripple at the plasma edge (10% at outer midplane).

The loss of ICRF fast minority particles was explored by second harmonic heating of an H-minority species. A high energy neutral particle analyser [5] was used to measure the flux of neutral hydrogen H^0, in a vertical line of sight, in the energy range between 0.3 and 1.0MeV. The toroidal field was 1.4T, the plasma current was 2.5MA, and the ICRF resonance location was varied by changing the ICRF frequency. High energy minority particles were subject to stochastic diffusion losses. These losses result from non-exact cancellation of the vertical drift, averaged over the bounce motion of banana particles. Particle loss is in the vertical direction, as both the particle energy and the magnetic moment are conserved. An expression for an effective diffusion coefficient is due to Yushmanov [4]. In Fig.182, the diffusion coefficient is shown for 1MeV H particles.

Using the newly developed Bounce Average Monte Carlo code with this diffusion coefficient, the losses of minority particles during their slowing down history were calculated. For the case of an ICRF resonance location of 3.3m major radius, the typical loss time was 30ms. The predictions of this method are in reasonable agreement with those derived from the measured reduction of the H^0 flux. If stochastic diffusion is switched off in the calculation, no such agreement with the experiment could be found. Work is underway at present to extend the Monte Carlo code with a ICRF velocity space diffusion operator.

Fast particle losses were also studied by measuring the burn-up of 1MeV tritons generated by D-D reactions. The NB input power in the 16 and 32 coil cases were adjusted so that the emission of 2.5MeV neutrons (i.e. the D-D reaction rate) were the same. Theoretical predictions gave a reduction of the triton burn-up (defined basically as the fraction of the tritons that undergo a D-T fusion reaction) by less than 25%. An analysis of the experiment using the TRAP-T code, which takes into account slight differences in the background plasma parameters, leads to an observed reduction of between 30 and 60%. Work is underway to investigate why the measured losses do exceed the predicted ones. This is focussing on the effect of sawteeth, which have not been taken into account in the TRAP-T modelling.

In parallel with these developments, a study was carried out [6] into the effect of finite orbit width on the stochastic diffusion threshold, noting that the Bounce Average Monte Carlo code uses a zero banana width approximation. Trapped ions moving along trajectories with banana turning points on the high field side of the torus have been found to be strongly affected. In particular, orbits close to the so-called pinch orbit are very sensitive to the magnetic field ripple. Orbits with turning points close to the horizontal midplane are less easily perturbed than suggested by the small banana width theory. However, when the results are applied to the ripple experiments on JET, the number of ions lost due to stochastic diffusion is only moderately affected.

High Minority ICRF Heating

The usual minority heating at low concentrations would be a limitation in a reactor where the heating of about a 50-50 D-T mixture is required. Adding another minority such as H or He^3 would not be desirable from the fuel dilution viewpoint. Moreover, the resulting high tail energies at low concentrations not only contribute to the total plasma pressure, which is limited by MHD instabilities, but also transfer its power mainly to electrons. It is shown that in a reactor, a balanced mixture can be heated efficiently by ICRF power at $f = f_{CD}$ with a low-field-side antenna exciting predominantly a spectrum at $k_{//} \cong 4m^{-1}$. Further, ICRF heating at high minority concentration has been tested experimentally in JET with H-minority in He^3 plasmas [7,8] accompanying low-tail energies and improved background ion heating.

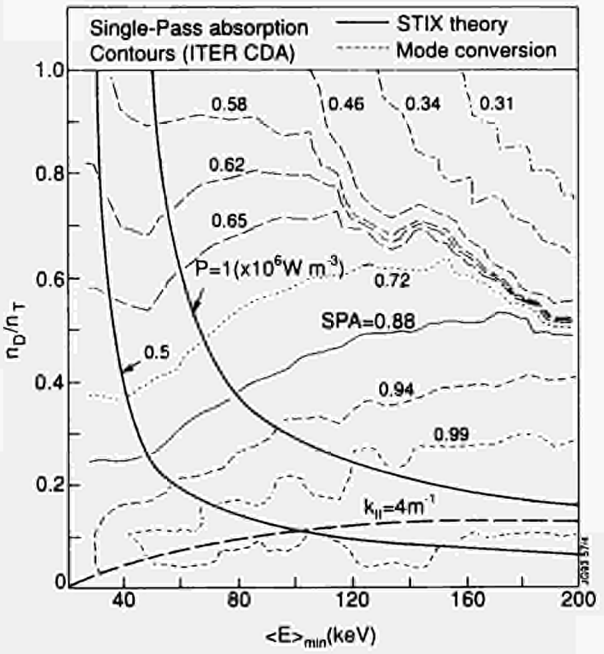

Fig.183: Single pass absorption contours in a n_d/n_T versus minority <E> diagram in a ITER CDA D-T plasma. Other plasma parameters are: T_e=15keV, n_{e0}=9x10^{19}m^{-3}, T_i=15keV, R_0=6m, a_p=2.2m, f=36MHz, B_f=4.85T and $k_{//}$=4m^{-1}.

The ICRH operation domain of a reactor or an ITER-like machine) can be conveniently described by the diagram shown in Fig.183, where the single-pass absorption (SPA) contours of the fast wave launched from a low-field-side antenna are drawn in a n_D/n_T versus $<E>_{min}$ plot. The generator frequency is $f=f_{CD}$ and the parameters are as shown. The average energy of the minority-ion tail $<E>_{min}$ is calculated using the full isotropic Stix [9] model for given RF power densities. The SPA values are then calculated using ray tracing techniques with rays launched in the equatorial plane. The waves are damped by ion cyclotron damping, electron transit-time magnetic pumping (TTMP) and e-Landau damping. The α-particle damping is not included here. The threshold for mode conversion is also shown which appears for $n_D/n_T > 0.1 - 0.15$. For a low-field-side launch, mode conversion and the ion-ion hybrid cutoff layers are encountered only after the wave has had a chance to be significantly absorbed at the D-cyclotron layer. Indeed, the large size and hot ITER plasmas permit strong damping (see Fig.183) even at large deuterium concentrations before

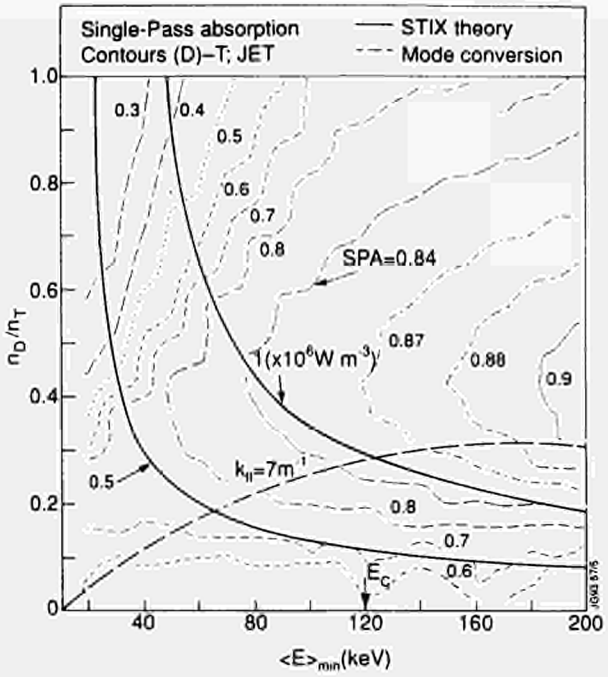

Fig.184: Single pass absorption contours in a n_D/n_T versus minority <E> diagram in a D-T plasma similar to previous figure. Other plasma parameters are: T_e=8keV, n_{e0}=6x10^{19}m^{-3} and T_T=8keV, R_0=3m, a_p=1.1m, f=25MHz, B_f=3.5T and $k_{//}$=7m^{-1}.

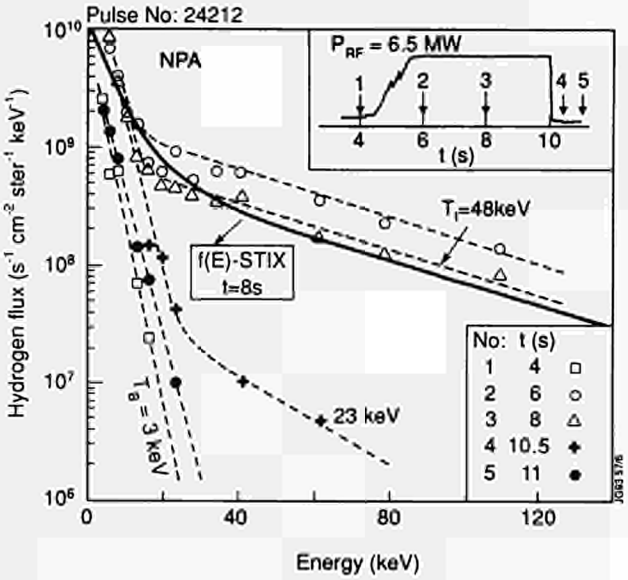

Fig.185: Hydrogen flux as a function of the particle energy during the high minority heating experiments ($n_H/n_{He3} \cong 0.53$). The inset shows the ICRF power trace and the arrows indicate the time slices during the RF pulse at which the data is plotted. The solid line shows the isotropic Stix distribution for the 3rd time slice.

the mode conversion is encountered and therefore it becomes irrelevant in such devices. From experience in JET, a SPA > 0.3 would not produce large eigenmodes which are deleterious for antenna matching. Thus, $n_D/n_T < 1.2$ can be used in ITER. A possible scenario would be to apply a square wave ICRF pulse with D-concentration rising to its maximum value in about 5s. According to this diagram, the operation would follow the P_d curves from low to high background ions. A similar diagram drawn for the D-T phase of JET is shown in Fig.184 which shows a somewhat reduced operating range ($n_D/n_T > 0.4 - 0.6$).

The high minority concentration scenario in JET has been tested experimentally using hydrogen as the resonating species in He^3 plasmas [7], which allows high single-pass damping for JET parameters similar to that obtained for ITER except that $k_{//} \cong 7m^{-1}$ for JET, and $\cong 4m^{-1}$ for ITER, imposed by the respective antennae designs. In the experimental results [7], significant (>0.3) damping per pass at high concentration is inferred by the absence of eigenmodes despite being above the mode conversion threshold. In Fig.185, the H-minority perpendicular ion energy distribution function is shown as measured by a mass resolved neutral particle analyser for $n_H/n_{He^3} = 0.53$. The theoretically calculated distribution function from the Stix model is also shown for the time-slice 3 and a good agreement is found. Low tail energies permit significant ion heating [7]. Tail temperatures obtained from such measurements are plotted in Fig.186 as a function of minority concentration. Fitted to a central point, the broken line drawn represents the expected $[n_H/n_e]^{-1}$ dependence of the tail temperature from the Stix model [9].

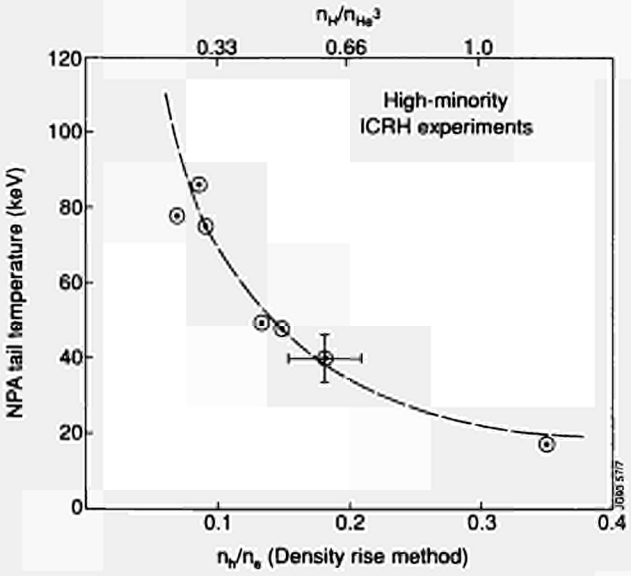

Fig.186: A plot of the H-minority tail temperature as a function of n_H/n_e for the high-minority heating experiments. The broken line was drawn by fitting to a central point and shows the expected $[n_H/n_e]^{-1}$ dependence.

The successful operation of ICRF at minority ion concentrations approaching majority and evidence of improved ion heating gives confidence in deuterium cyclotron heating of a 50/50 D-T plasma of a reactor. In fact, there will be flexibility to work in a range of concentrations ($0.05 \leq n_D/n_T \leq 1.2$). Sawtooth stabilization processes will be maximum at low concentration, but will lead to some penalty such as in maximum thermal β available. Maximum direct ion heating will be achieved when $n_D/n_T \cong 0.3$. Finally, deuterium rich scenarios ($n_D/n_T \cong 1.1\text{-}1.2$), which are advantageous for tritium inventory purposes, can be heated by ICRF but at the expense of a reduction of direct ion heating. Single-pass absorption will further improve when damping on α-particles in a reacting plasma is included, which will increase the range of D-minority concentration that can be used, but in this condition the amount of direct ion heating would drop further.

References

[1] Sadler, G., Barabaschi, P., Bertolini, E., et al., in Controlled Fusion and Plasma Physics (Proc. 19th Eur. Conf., Innsbruck, Austria, 1992).

[2] Tubbing, B.J.D., and JET Team, in Plasma Physics and Controlled Nuclear Fusion Research (Proc. 14th IAEA Conf., Wurzburg, Germany, 1992).

[3] Goldston, R.J., White, R.B., Becoulet, A., Phys. Rev. Lett., **47** (1981) 647.

[4] Yushmanov, P.N., in Reviews of Plasma Physics Vol. 16, Plenum Publ. Corp., New York, 1990.

[5] Petrov, M.P., Afanasyev, V.I., Corti, S., et al., in Controlled Fusion and Plasma Physics (Proc. 19th Eur. Conf. Innsbruck, Austria, 1992).

[6] Eriksson, L-G., Helander, P., '*Finite orbit width effects on stochastic ripple diffusion*', submitted to Nucl. Fus. See also JET-P(92)98.

[7] Jacquinot J. et al, Plasma Physics and Controlled Fusion, 1993 (to be published)

[8] Bhatnagar, V.P. et al, Nuclear Fusion, 1993 (to be published)

[9] Stix, T.H., Nuclear Fusion, **15** (1975) 737.

Analysis of Preliminary Tritium Experiments

Following the Preliminary Tritium Experiments (PTE) carried out in November 1991, further analysis of data has continued throughout 1992. It has led to a coordinated series of papers, which will be published in the Nuclear Fusion journal during 1993.

The following subjects have been covered:

- Neutron Emission Profile Measurements during the Tritium Experiments;
- Release of Tritium from the First Wall;
- Particle and Energy Transport during the PTE;
- Ion Cyclotron Emission Measurements during the Deuterium-Tritium Experiments.
- Discharge Termination of High-Performance Discharges.

Further details on these subjects are described in the following paragraphs.

Neutron Emission Profile Measurements during the Tritium Experiments

The JET Neutron Emission Profile Monitor was used to simultaneously obtain the local 2.5MeV and 14MeV neutron emissivity profiles during a series of discharges in which one or two of the 80keV beam sources had a mixture of 1% T and 99% D, to study tritium beam deposition and diffusion of thermalized tritium. During these discharges, the rate of production of 14MeV neutrons was less than half the rate of 2.5MeV neutrons, so that it was possible to obtain simultaneous 2.5 and 14MeV neutron emissivity profiles without significant interference of the 14MeV neutrons.

At 12s into Pulse No:26114, the deuterium beam power was increased to 8MW, and at 12.5s, an additional 1MW, 80keV beam with 1% tritium was switched on, giving an injected tritium power of ~13kW, compared to a total injected power of 9MW. The 1% tritium beam was turned off at 13.5s, and replaced with a 1MW beam of pure deuterium. The diffusion of tritium was examined by following the evolution of the neutron emissivity profiles after the 1s injection pulse of tritium.

The ratio of n_T/n_D was obtained as a function of space and time using the neutron emissivity and beam-plasma reactivity ratios based on a weighted average of the beam energies. The neutron emissivities were sufficiently intense to obtain the density ratio over the inner ±50% of the plasma radius. The first time-interval analyzed was 13.6-13.7s, thereby excluding the beam-plasma contribution from the tritium beam, since the tritium injection ended at 13.5s. In Fig. 187(a), the ratio n_T/n_D and its radially-averaged value are plotted versus major radius for two time points during the tritium density decay phase of Pulse No:26114. The data are shown

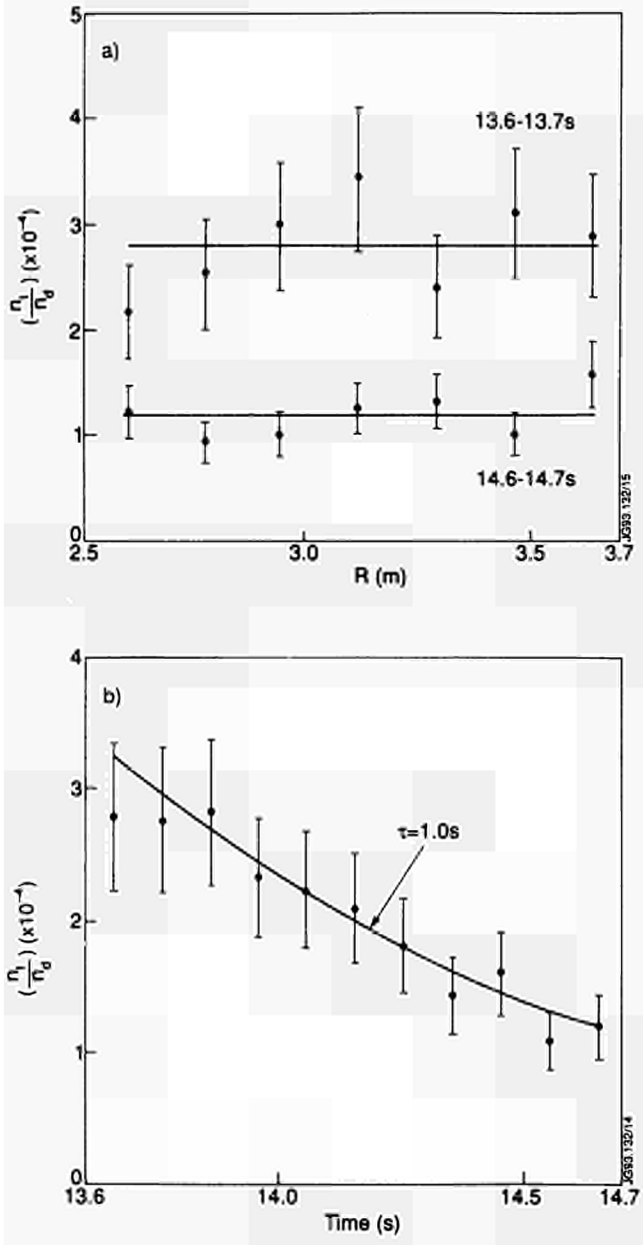

Fig.187: (a) The ratio n_T/n_D and its radially-averaged value plotted versus major radius for two different time points during the tritium density decay phase of Pulse No: 26114; (b) The radially-averaged density ratio n_T/n_D plotted as a function of time. The fitted exponential curve has a 1.0s decay.

with experimental error bars of ±20%, attributable to error propagation from the line-integral measurements, tomographic inversion and the ratios of the 2.5 and 14MeV neutron emissivities. Within experimental errors, the density ratio was constant as a function of major radius during all time intervals between 13.6 and 14.7s. The electron density profile was flat over the radial region investigated. At 13.7s, the deuterium density profile implied from CXRS measurements was also relatively flat, with a value at half the plasma radius equalling 85% of the axial value.

In Fig.187(b), the radially-average density ratio n_T/n_D is plotted as a function of time. The fitted exponential curve has a 1.0s delay time. The initial value of n_T/n_D is $3x10^{-4}$, a reasonable value since about 10^{-3} of the injected beam particles were tritium, and additional pure deuterium was added by gas puffing. The trend of the exponential decay was not affected by the sawtooth crash at 14.085s, which temporarily flattened the emissivity profiles.

Based on the experimental observations that the deuterium and tritium beams had similar spatial deposition profiles, and that the density n_T/n_D was spatially constant, a reasonable hypothesis is that thermalized deuterium and tritium have approximately the same diffusive behaviour.

During the initial tritium clean-up discharges after the high fusion power experiments, additional information was obtained on tritium diffusion properties in the plasma. Two or three half-second bursts of 2MW of deuterium neutral beams at 140keV were added to probe the tritium density in the plasma by giving an enhanced, beam-plasma dominated neutron yield for obtaining n_T/n_D. The 2.5 and 14MeV neutron emissivity profiles were found by tomographic inversion to have the same shape. Examples are shown in Fig.188 for Pulse No:26150 and No:26165, where the local 2.5MeV and 14MeV neutron integrated yields per unit volume derived from tomograpy are plotted. The 2.5 and 14MeV profiles maintained similar shapes, while varying between the two discharges, as the quantity of tritium released from the walls diminished. The ratio of emissivities is constant across the profile, and therefore the ratio n_T/n_D is constant throughout the plasma.

Since almost all the deuterium and tritium enter the plasma at its boundary (either from gas puffing or wall release) with only a very low level increase (≈5%) of density from beam injection, the spatially constant density ratio n_T/n_D provides further evidence that deuterium and tritium have similar particle diffusion properties. It had been observed that the particle flux G for electrons and impurities can be described by the equation $G_x = -D_x \nabla n_x + n_x v_x$ with diffusion coefficients D_x and pinch velocity v_x, and that the ratio D_x/v_x is the same for all species x = D or T. In the relatively stationary condition of these cleanup discharges with surface fuelling, G_x became a small and D_x/v_x approximately equalled $\nabla n_x/n_x$ for each species. The electron density profile was more rounded in these cleanup discharges than the profiles observed in Pulse No:26114 and No:26148, and ∇n_x was non-zero. Since both density profiles had the same shape and hence the same $\nabla n_x/n_x$ profile, $D_t/v_t = D_d/v_d$.

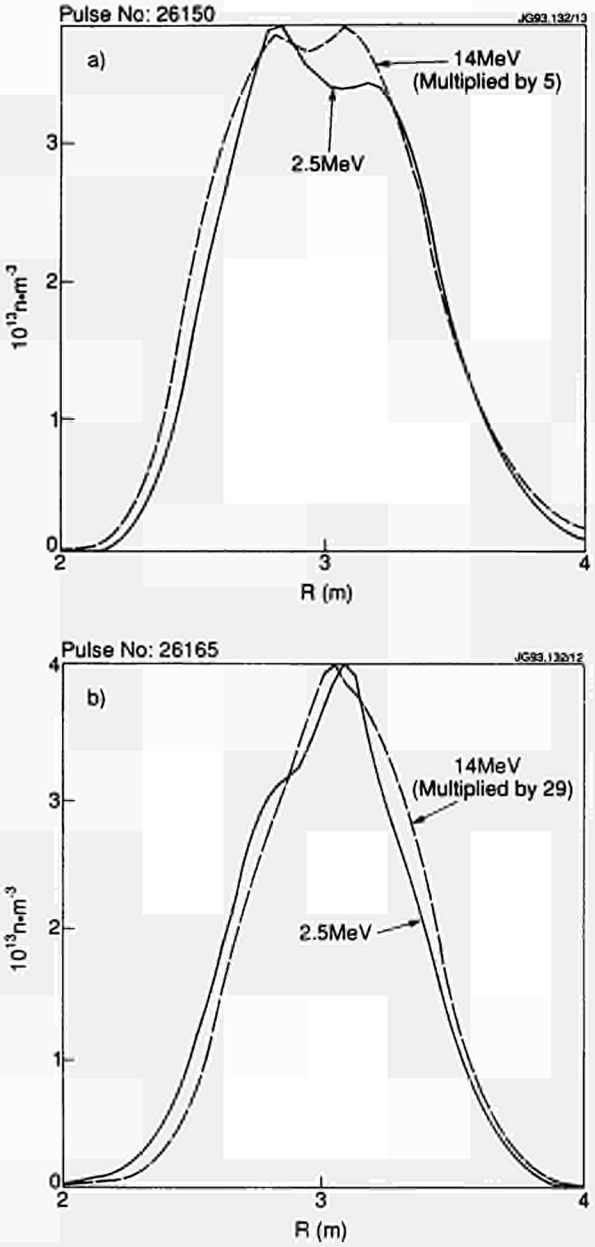

Fig.188: The 2.5 MeV and (scaled up) 14 MeV neutron emissivities plotted along the major radius chord through the magnetic axis for (a) Pulse No: 26150 and (b) Pulse No: 26165 during the cleanup experiments.

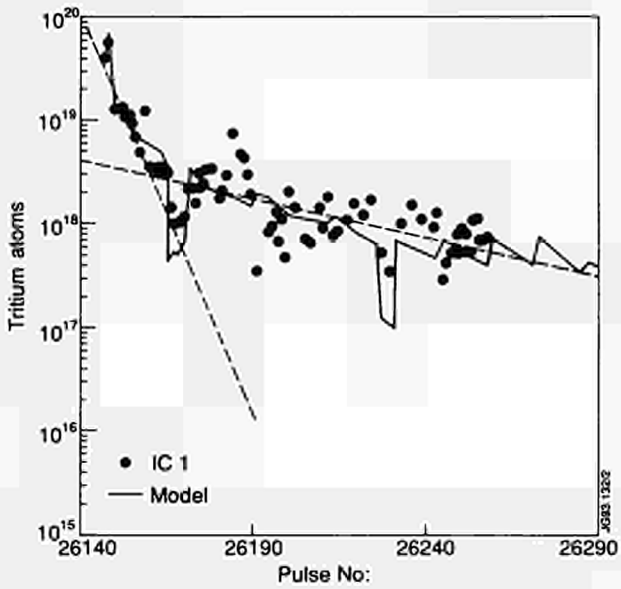

Fig.189: The number of tritium atoms released from the JET vacuum vessel as a function of Pulse. The two PTE shots were Pulse Nos:26147 and 26148. The data are integrated over the first 560s of outgassing after the shot and are ion chamber measurements for the first week after the PTE shots. The solid curve is the prediction of the model described in the text. The dashed lines are the results of a simple two reservoir model for the wall.

Using the expression for G and the continuity equation, it can be shown that in Pulse No:26114, since the relative rates of deuterium fuelling by beams and the tritium time-dependent density loss are the same in the central region of the plasma, then $D_t=D_d$ and $v_t=v_d$ individually.

Release of Tritium from the First Wall

During the PTE, an estimated 2×10^{12} Bq (1.1×10^{21} atoms) of tritium was injected into the vacuum vessel. A series of experiments was performed whose purpose was to deplete the torus of tritium, to compare the effectiveness of different methods of tritium removal, and to obtain a quantitative understanding of the processes involved. The effectiveness of the cleaning procedures was such that the normal tokamak programme was resumed one week after the PTE and routing of exhaust gases to atmosphere after two weeks. The release of tritium from the vessel was found to scale with the deuterium release from the vessel, suggesting that dilution and mixing of the hydrogen isotopes in the vessel walls is important.

High density, disruptive tokamak discharges were found to be the most successful plasma pulses for tritium removal. Purges with deuterium gas were also effective and have the advantage of operational simplicity. Helium discharges, on the other hand, resulted in low tritium release from the vessel walls. It was demonstrated that the tritium release rate could be predicted using data from hydrogen to deuterium changeover experiments. Using the superior quality of data available from the tritium clean-up experiment, the physical mechanisms necessary to describe the hydrogenic uptake and release from the torus were identified. The release of tritium was reproduced using a model which incorporated implantation into a thin surface layer as well as diffusion of tritium into and out of the bulk material.

The PTE experiment offered a unique opportunity to study the isotopic exchange processes in a large tokamak

and to follow the release rate over nearly four orders of magnitude in concentration. The primary objective of removing most of the tritium was successfully accomplished. The tritium inventory was reduced to 3.4×10^{19} atoms at the end of the operations (i.e. 3% of the injected tritium).

A number of different methods of removing tritium were compared. Standard ohmic discharges were reasonably effective and additional heating produced only a marginal improvement. The most effective method was disruptive discharges in deuterium which were two times better than standard discharges. After about a factor two operation the tritium level was sufficiently low that evacuation into the sealed-off backing line could be discontinued and use of the conventional backing pumps resumed (see Fig.189).

An initially surprising result was that even though tritium was injected only during X-point conditions, the tritium was found to be rapidly distributed uniformly over all the tokamak surface. This occurred as a result of charge exchange neutral fluxes to the wall which were large enough to maintain an equilibrium isotopic balance over large areas of the vessel. Using the results of a Monte Carlo neutral transport code, even in the limiter phase of the second PTE shot significant contamination of the plasma should be expected. As such, at least with geometries and neutral fluxes typical of JET, careful control of the plasma position during termination was ineffective in maintaining localised tritium contamination of the vessel wall.

The release of tritium between discharges was modelled using existing theories, which have previously been used to model ion beam experiments with graphite. However, it was necessary, to include an additional mechanism, diffusion, to model the long term release of tritium from the torus. The calculated depth distribution of tritium in the vessel wall is shown in Fig.190 for several times after the PTE. This model gives good agreement with the time dependence of the outgassing between discharges, the shot-to-shot release, and the tritium inventory long after the tritium experiment. Using the model, it was calculated that the final tritium inventory in the torus could have been reduced by a factor of 1.6, if the clean-up campaign had been started immediately after the PTE rather than waiting for 40 hours.

Soaking of the torus at pressures of ~2Pa of deuterium was found to be an effective, operationally simple way of removing tritium from the machine. Although the equilibration time between the gas load and the vessel walls was not measured, it is estimated from other experiments to be about 5 minutes. If this molecular exchange process can be shown

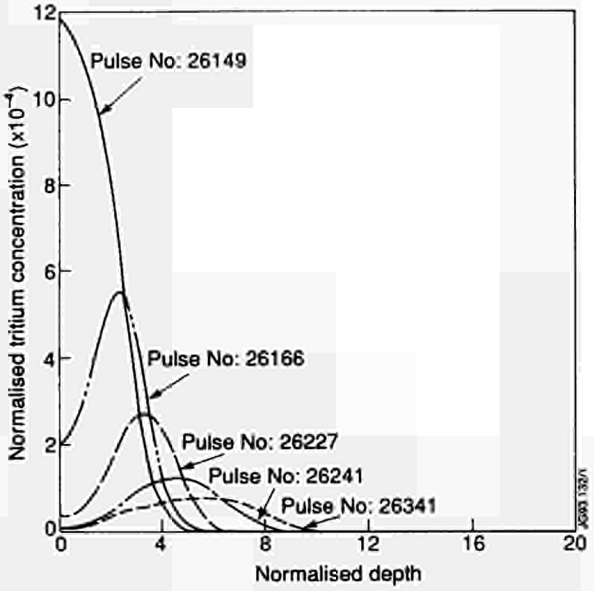

Fig.190: Calculated depth profiles of tritium at various stages after the tritium injection (Pulse Nos: 26147 and 26148 were the two PTE discharges). The tritium levels are normalised to the saturation concentration of hydrogen in carbon. The depth is normalised to one implantation layer (8nm).

to access the entire implantation layer of the vessel wall, it may be possible to remove tritium more quickly, and thus with lower diffusion losses to the bulk wall material, using gas purges rather than plasma discharges.

The data obtained has enabled a much better understanding of the principal processes occurring. This should enable the behaviour of tritium in the next tritium phase to be predicted with some confidence. However, because the rates of physical processes are dependent on material properties, the absolute values of the model parameters will change if the vessel materials are changed. Therefore, an isotope exchange experiment with hydrogen and deuterium is necessary to validate the model parameters for different machine conditions.

Discharge Termination of High Performance Discharges

The main issues in the termination of high performance discharges were the role of the carbon bloom and the high confinement. The discharges considered are hot ion H-mode discharges similar to the discharges used for the preliminary tritium experiment (PTE). The time of the sharp rollover of the neutron yield is defined as the time of the termination. With the improved carbon divertor tiles installed in Summer 1991, only a very small increase in the ratio of C to D radiation was seen by visible edge spectroscopy, before the termination, and the temperature of the hot-spots on the

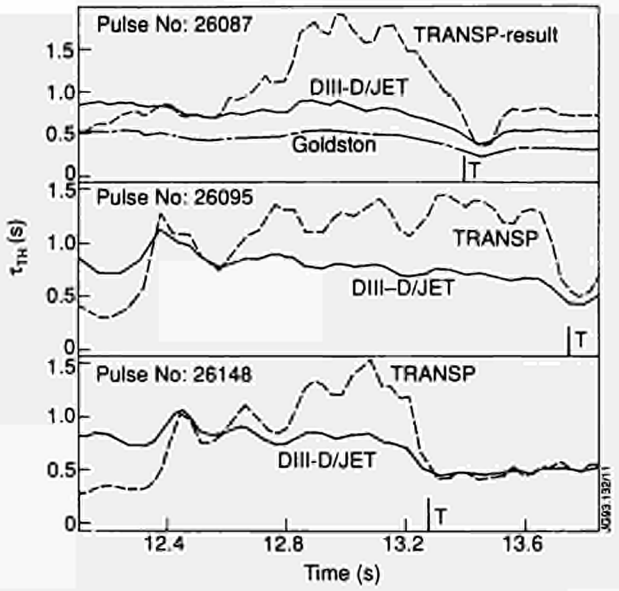

Fig.191: Temporal evolution of the thermal confinement time.

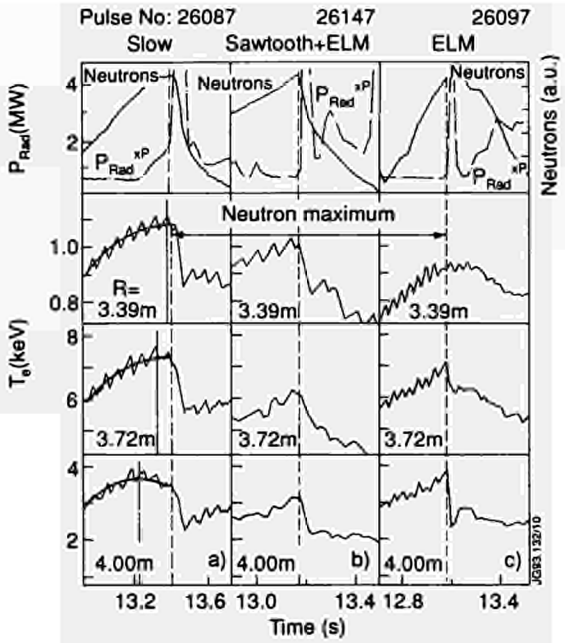

Fig.192: Three typical cases of termination: "slow"; Sawtooth + ELM; and ELM.

target tiles stayed below 1600°C. This excluded a thermal bloom as a cause of the termination e.g. by triggering resistive modes. During and immediately after the termination i.e. on a time-scale of less than 40ms, the temperature of the hot-spots on the target tiles increased well above 2000°C, a radiation spike of several MW was observed and the C to D ratio increased, indicating the occurrence of a bloom. After a bloom, the discharges did not recover to the high performance state.

A statistical analysis of many discharges, in which the evolution of the temperature of the target tiles was calculated from power balance considerations, showed that the block had a well defined thermal threshold beyond which large impurity influxes set in. This threshold was regularly and quickly surpassed at the termination of high performance discharges, when these lost their particularly good confinement. Figure 191 shows that the thermal confinement time τ_{TH} reached values up to 2 times higher than DIII-D/JET scaling would predict. The time T marks the rollover of the neutron yield. The thermal confinement time decreased sharply for Pulse No:26095 and No:26148 simultaneously with T - within the time resolution of the analysis. For Pulse No:26087, the decay of the confinement seemed to start already well before T. When the high confinement was lost, the additional heat flow to the target heated it to bloom temperature. Three different types of termination could be distinguished as indicated in Fig.192.

In the first case labelled "slow" (i.e. in Pulse No: 26087), the electron temperature evolved as if a cold wave propagated from the plasma edge towards the centre. At the time when this cold wave started at the edge, the influx of light impurities increased near the separatrix, both the C and the D signal rose, the confinement degraded and the target temperature started to rise slightly, which was all in line with an edge transport enhancement under conditions of hollow impurity profiles. For this discharge, the temporal evolution of the total plasma pressure profile at the edge had been estimated using the reflectometer measurements of the electron density and extrapolations of the electron temperature together with the assumptions that the ion pressure was the same as the electron pressure. Under these assumptions, the total pressure profile at the edge was found to be so steep that the implicated bootstrap currents were large enough to give access to the second stability regime at the plasma edge. Figure 193 shows the temporal evolution of α_{ideal}, which is proportional to the experimental pressure gradient and the evolution of α_{ideal}, which is the boundary within which ideal ballooning modes are unstable. Also shown is the evolution of the diamagnetic energy confinement time τ_E^{DIA}. The similarity in the evolution of α_{exp} and τ_E^{DIA} during the high confinement phase suggest that the confinement was edge dominated and that the loss of the second stability at the edge may cause the loss of the good overall confinement. The reasons for loss of edge confinement are still unclear. Possible alternative reasons considered are resistive modes, kinks from the high bootstrap current, and a local β-limit at

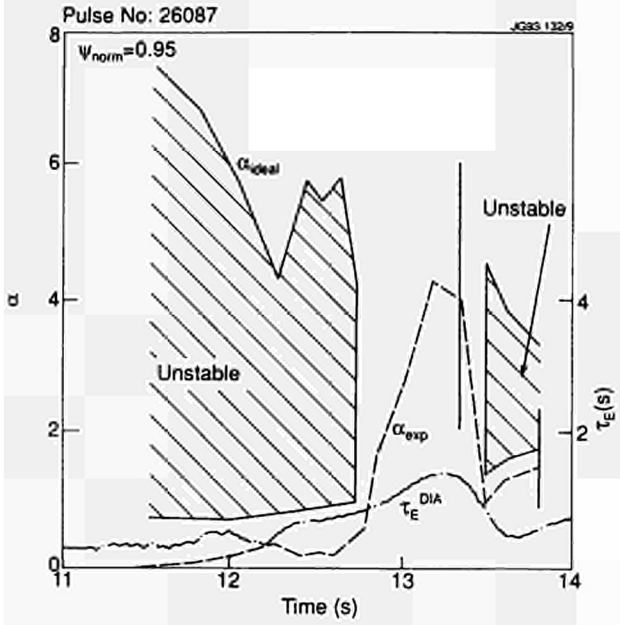

Fig.193: Access to the second stability regime at the plasma edge during the time of high confinement.

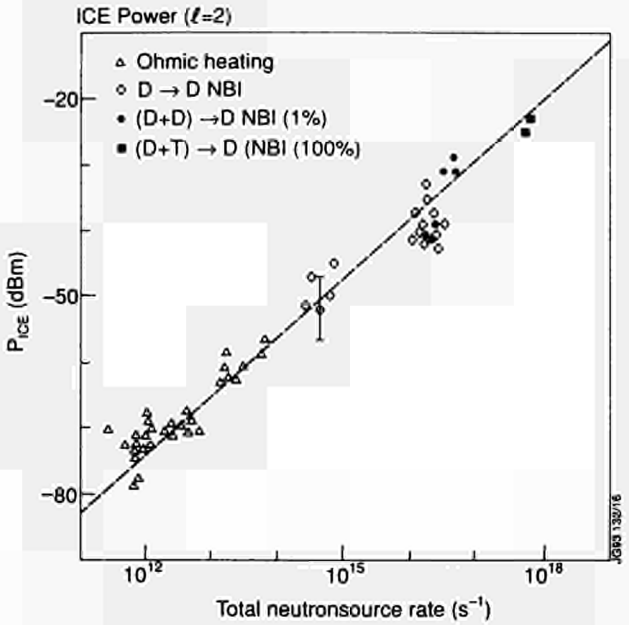

Fig.194: Correlation between ICE intensity P_{ICE} and total neutron emission rate R_{NT} for a variety of ohmic and NB heated discharges, over six decades of signal intensity. The measurement frequency corresponds to the second harmonic of the deuterium or alpha-particle ion cyclotron frequency evaluated at the outer mid-plane plasma edge of the plasma.

the edge. To harden up on any of these possibilities a better spatial resolution of experimental edge data is needed.

The second case of termination shown in Fig.192 (i.e. Pulse No:26147), is a combination of sawtooth and giant ELM, which reduces the electron temperature over the whole plasma cross-section. Both discharges of the PTE and Pulse No:26788 had this termination scenario. One possibility of explaining such a coincidence is the MHD coupling of an internal kink with the plasma edge at higher β values.

The third case of termination (Fig.192 is a giant ELM - the most common type of high performance discharges. The electron temperature steps down at the edge, up to the q=1 surface, but remains stable in the centre. In this type of termination, resistive ballooning modes may be implicated. During the giant ELM, the convective inward drift velocity is stepped up in spatial extent and value. Together with the hollow profiles of light impurities before the termination, this sweeps the impurities rapidly far into the plasma.

The last two cases do not only ask for better spatial resolution of experimental data at the edge but also for much higher temporal resolution. Any progress in understanding the mechanisms of improved confinement may help in understanding the loss of confinement, which has been identified as the step preceding the bloom.

Ion Cyclotron Emission Measurements during Deuterium-Tritium Experiments

In the course of the PTE, where combined deuterium and tritium neutral beam injection generated D-T fusion power, ion cyclotron emission (ICE) was detected. This was measured using an ICRF antenna in reception mode in the frequency range n ≤ 180MHz. The ICE spectra contained superthermal, narrow, equally spaced emission lines which corresponded to successive cyclotron harmonics of deuterons or α-particles at the outer mid-plane, close to the last closed flux surface at major radius R ~ 4.0m. The ICE signal fluctuated rapidly in time, and was extinguished whenever a large-amplitude edge-localized MHD mode (ELM) occurred. The detected RF power spectra in D-D and D-T discharges were similar in form. However, on changing the gas feed to the NB injectors from pure deuterium to mixed deuterium and tritium at constant power, the intensity of the ICE increased in proportion to the neutron flux. This indicated that fusion α-particles - and not beam ions - provided the free energy for generating ICE. This result constituted the first detection of RF emission from confined α-particles in a fusion experiment. In pure deuterium discharges, ICE was generated by the primary D-D fusion products: the most likely single candidate driving the ICE in this case was the 3MeV fusion proton.

The JET ICE database, which now extends over a range of six decades in signal intensity, shows that the time-averaged ICE power increased almost linearly with total neutron flux (Fig.194). The rise and fall of the neutron flux during a time-evolving D-T discharge was closely followed

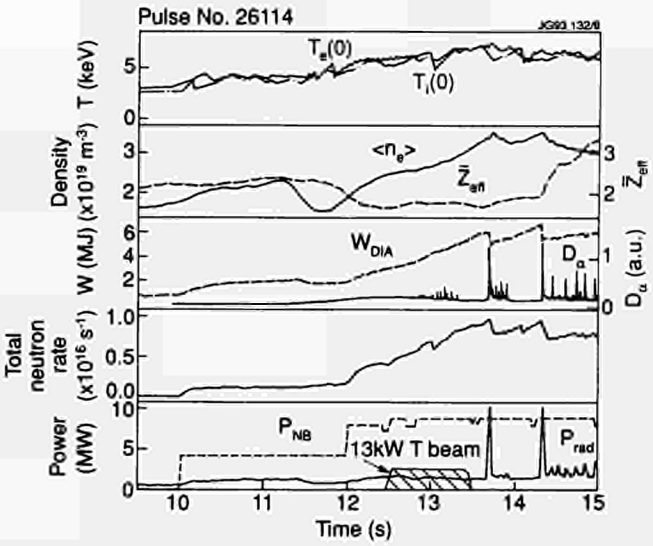

Fig.195: Time evolution of the central electron and ion temperatures, the volume-averaged electron density, the line average Z_{eff} the plasma diamagnetic energy, the edge D_α emission, the total neutron (2.5 MeV + 14 MeV) rate and the neutral beam power (total and tritium) and radiated powers for Pulse No:26114.

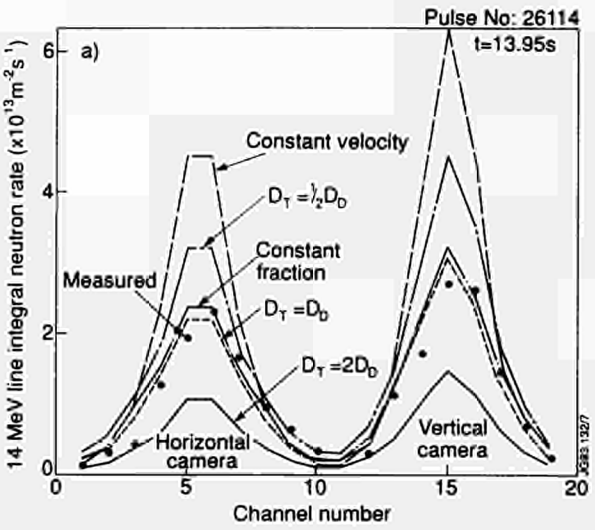

Fig.196: The measured and simulated line integral rates of 14 MeV neutrons for Pulse No:26114 at t = 13.95s (i.e. 0.45s after the tritium beam was switched off) using different mixing models. All the simulations with the "proportional diffusivities" model assume the same values for D_T/D_D and v_T/v_D.

by that of the ICE intensity, which was delayed by a time of about the α-particle slowing-down time (~0.5s). This feature is well-modelled by TRANSP code simulation of the density of deeply trapped α-particles reaching the plasma edge. Drift orbit calculations revealed a class of fusion products, born into trapped orbits in the core plasma, which made orbital excursions of sufficient size to reach the outer mid-plane edge. There, the energetic α-particle or fusion proton velocity distribution was both anisotropic and not monotonically decreasing, and was potentially unstable to relaxation at multiple ion cyclotron harmonics. A linear ion cyclotron instability model is being developed to explain the superthermal ICE in terms of the collective excitation of cyclotron harmonic radiation by a diffuse, high energy ion population. These measurements show how ion cyclotron emission provides a unique diagnostic for confined fusion alpha-particles.

Particle and Energy Transport during PTE

The transport properties of several high fusion performance JET pulses obtained during this series were analysed using the TRANSP code [2]. Good simulations of various measured quantities, particularly of neutron emission profiles, have given considerable confidence in the internal consistency of the data which is used as input data to the code.

Particle Transport

One objective of these experiments was to determine the characteristics of the particle transport of the thermalised tritium and deuterium and to derive particle diffusivities of each species. TRANSP simulations were performed assuming three different mixing models which determine the thermal tritium and deuterium density profiles[3]. The "constant fraction" model assumes that both species have the same radial profile shape ($\nabla n_D/n_D = \nabla n_T/n_T$). In the "constant velocity" model, the radial velocities of the two species are assumed to be identical ($v_T = v_D$). Finally, the "proportional diffusivities" model imposes $D_D/D_T = v_D/v_T$ = constant, where D_D and D_T are the deuterium and tritium particle diffusivities. Once the density profiles are known, the D-D and D-T neutron emission profiles and total emission rates are computed and the validity of each mixing model assessed by comparing simulations and measurements.

By definition, the three models predict similar density profiles, if the deuterium and tritium source terms are similar. This is the case in all the hot ion H-mode D-T pulses, where there is simultaneous NB fuelling of D and T. Therefore, the models cannot be distinguished in such discharges. This was one of the reasons that neutral beam injection was chosen for the tritium experiment (i.e. the result would be independent of mixing model). This would not have been the case with tritium gas puffing. In Pulse No: 26114 (a medium density H-mode D-T discharge with 1% tritium injected) the tritium beam was terminated abruptly, thereby making the source rates dissimilar and particle transport could then be studied throughout the tritium decay. The main characteristics of the pulse are shown in Fig.195. Figure 196 shows a comparison between measured 14MeV

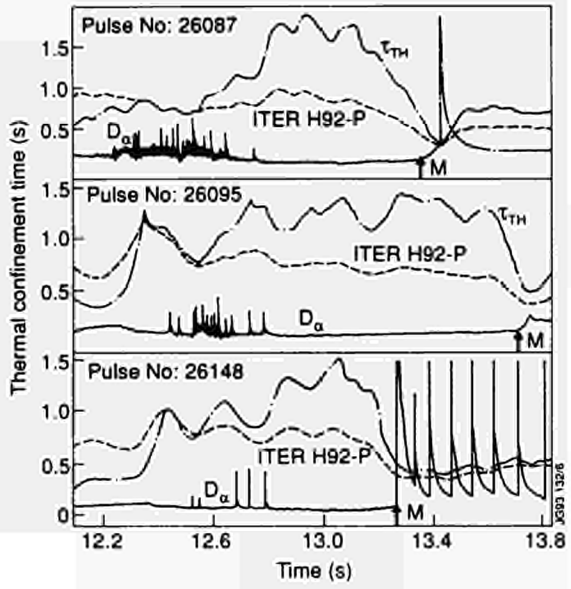

Fig.197: The time evolution of thermal confinement time τ_{th} compared to values predicted by ITERH92-P H-mode scaling, and D_α emission from the edge for a) Pulse No:26087 b) Pulse No:26095 c) Pulse No:26148. M indicates times of the maximum measured total neutron rate in each pulse.

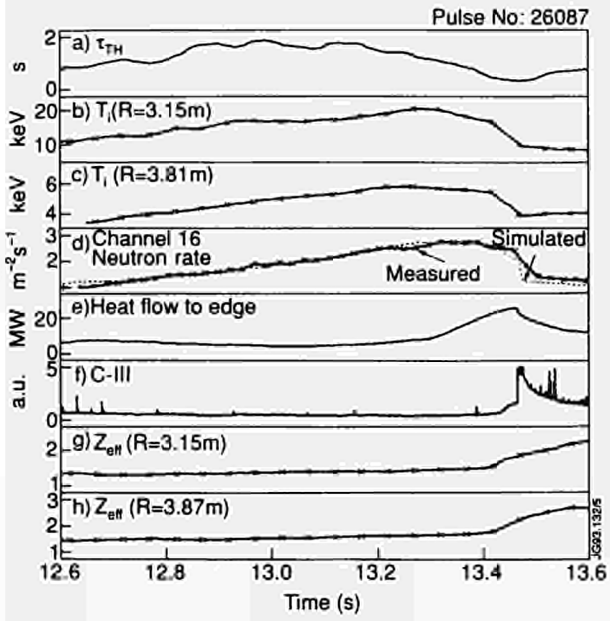

Fig.198: Time evolution of a) thermal confinement time τ_{th}, b) central and c) edge values for ion temperature, d) measured and simulated 2.5 MeV line-integral neutron rates for a central (No:16) neutron camera channel, e) calculated heat flow to X-point target, f) measured C-III light emission from edge, g) central and h) edge values for effective charge Z_{eff} for Pulse No:26087. Symbols (x) mark measured data points.

time integral neutral emission rates and simulated values using three different mixing models. The "constant velocity" model predicts a peaked tritium density profile which leads to neutron emission rates much greater than measured ones. The "proportional diffusivities" model, with $D_T/D_D = v_T/v_D = 1$ predicts a flatter tritium density profile leading to a good fit between the measured and simulated emission rates. As the tritium and deuterium flows are proportional in this discharge, the "constant fraction" model gives an equally good fit to the data. However, given the uncertainties in the measurements and the simulation, a weak mass dependence on the diffusion coefficients cannot be ruled out.

For Pulse No: 26148, where two of the neutral beam sources were fuelled with pure tritium, the measured D-T neutron data were only accurately reproduced if it was assumed that each recycled ion is returned to the plasma as a neutral of the same species, implying that the isotope ratio in the plasma and the wall quickly reach equilibrium. The effective tritium diffusivity D_T^{eff}, defined by the ratio of the particle flux and the density gradient, is similar to the deuterium D_D^{eff} observed in similar pure deuterium discharges being low in the centre (~ $0.25 m^2 s^{-1}$) and increasing sharply towards the edge (~ $2 m^2 s^{-1}$).

Energy Transport

This series of pulses generally had very good confinement. However, the enhanced performance phase was only maintained for a short time (~ 1s), before the ion temperature decreased causing a dramatic drop in the thermal-thermal component of the neutron yield. Figure 197 shows the different evolution of the thermal confinement time, τ_{TH}, for three high performance Pulses No: 26087 (the best D-D discharge), No: 26095 (a D-T discharge with a small amount of injected tritium) and No: 26148 (the best D-T discharge). During the enhanced phase, values of τ_{TH} about twice the value predicted by ITERH92-P scaling was reached[4].

Generally, it was impossible to state that the confinement had definitely been lost before the peak neutron rate was reached due to the poor time resolution of the data used in the calculation of t_{TH}. However, for Pulse No: 26087 the good confinement was clearly lost prior to the peaking of the neutron emission rate and this pulse was chosen for detailed analysis with TRANSP. Figure 198 shows the time evolution of several key parameters for this pulse during the period of high confinement and its subsequent deterioration. The degradation in performance from 13.2s onwards, as shown by τ_{TH}, is reflected in the time evolution of the measured temperature profiles, which flatten from the edge causing the thermal-thermal component of the neutron yield to fall. As the power being deposited on the X-point target plates builds up, the impurity level increases, finally leading to the massive impurity influx (the carbon bloom)[5].

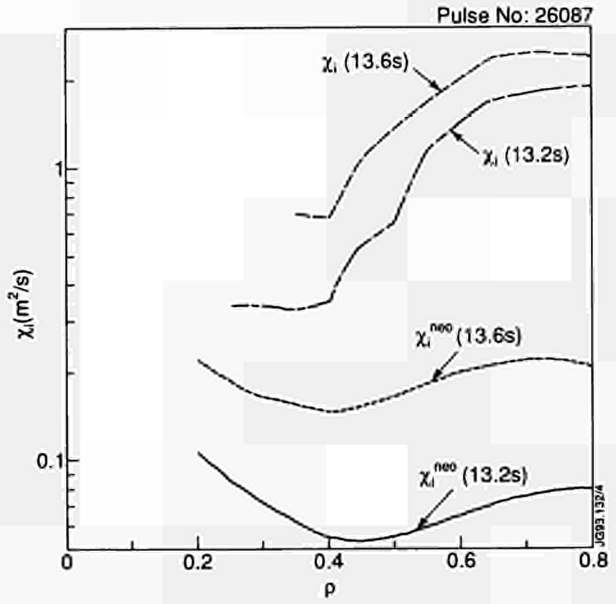

Fig.199: Ion thermal conductivity c_i and neoclassical prediction χ_i^{neo} versus normalised radius during (t = 13.2s) and after (t = 13.6s) the period of enhanced confinement for Pulse No:26087.

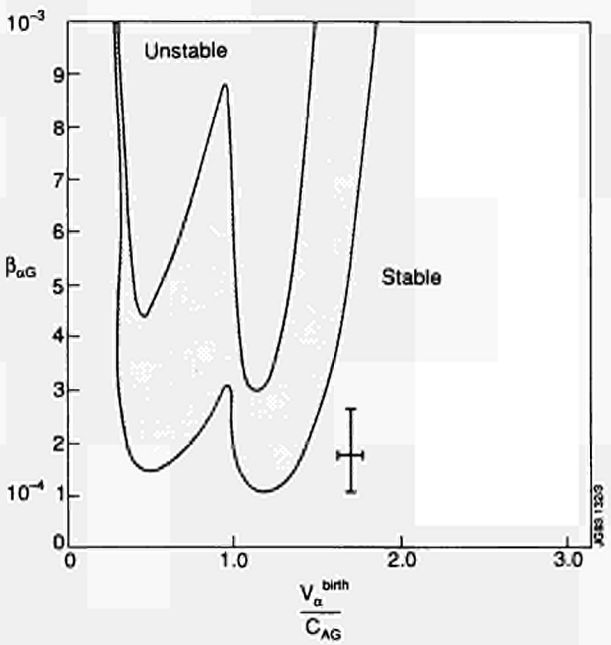

Fig.200: Stability boundary for TAE mode with n = 4, m = 3,4 at time of maximum $\beta_{\alpha G}$ (Pulse No:26148). Parameters at the q_G = 7/6 surface are as follows: $r_G/a = 0.47 \pm 0.04$; $n_e = (3 \pm 0.3) \times 10^{19} m^{-3}$; $n_D = (1.8 \pm 0.2) \times 10^{19} m^{-3}$; $n_T = (2.0 \pm 0.2) \times 10^{19} m^{-3}$; $n_{imp} = (2.0 \pm 0.2) \times 10^{18} m^{-3}$; $T_i = (11 \pm 1)$ keV; $T_e = (7.5 \pm 0.5)$ keV; $L_\alpha/a = 0.15 \pm 0.5$; $\beta_{\alpha G} = (1.7 \pm 0.7) \times 10^{-4}$; $B_T = 2.8T$. It is assumed $T_i = T_D = T_T$. The hatched region reflects the sensitivity of marginal stability curve to variations of relevant parameters within corresponding error bars. Also shown are the values of $\beta_{\alpha G}$ and v_α^{birth}/C_{AG} at the selected time.

Transport analysis shows that >85% of the input power goes through the ion channel and the main loss is ion heat conduction, convection only becomes important near the edge. Figure 199 shows that the pulse has good central confinement ($\chi_i \approx 0.3 m^2 s^{-1}$) during the enhanced confinement phase and the edge value ($\chi_i \sim 2 m^2 s^{-1}$) is lower than that of a conventional H-mode. The edge conductivity starts to rise soon after 13.1s, closely followed by the central value. Initial loss of confinement at the edge is confirmed by the behaviour of the calculated thermal confinement time profiles. The coefficient of particle diffusivity has a similar shape but does not show initial loss of confinement at the edge. After the "carbon bloom", good confinement is lost and the plasma reverts to normal H-mode behaviour.

Possible Explanations for Confinement Behaviour

MHD activity (n = 1 mode) was present in Pulse Nos: 26087, 26095, and 26148. The most prominent activity was fishbone bursts [6], but there was no correlation between increase in MHD activity and loss of confinement. All pulses showed ELMs before the enhanced phase, as shown by the D_α signal in Fig.197, but these cease as the performance improves.

TRANSP calculations showed that at about the time the confinement started to fall in Pulse Nos: 26087 and 26095, β was being limited at about 0.75 of the Troyon beta limit [7]. This was not the case in Pulse No:26148, which was terminated by a sawtooth and giant ELMs.

One obvious reason for the saturation of the ion temperature could be that the neutral beams were prevented from heating the centre of the plasma due to increasing density. However, TRANSP calculations showed that although the fast particle source rate was falling at the centre, the heating power continued to rise because the energy transferred from the fast ions was becoming greater with increasing density.

The stabilisation of the η_i mode due to the peaking of the density gradient has been investigated but seems to be unlikely, since although η_i was increasing during the collapse phase, it was also quite high during the early part of the discharge.

All these pulses exhibited some of the characteristics found in the DIII-D VH-mode[8]; particularly steep edge gradients and a large edge bootstrap current (0.8 MA in a total plasma current of 3 MA). These edge features led to a consideration of marginal ballooning stability and a time-dependent calculation has been performed for some of these discharges. The results indicate that entry of the edge of the plasma into the second ideal ballooning stability region showed a clear correlation with the improvement of confinement in the edge region and hence the generally enhanced

performance of the plasma. It was not clear however whether the high edge current density initiated or was a consequence of this enhanced confinement, nor whether shear stabilised modes other than the above were playing a role.

For the discharge with a high concentration of tritium, it has been suggested that α-particle driven instabilities could affect the energy confinement and toroidicity induced Alfvén eigenmode (TAE)[9] have been investigated for Pulse No: 26148. The mode which is considered most likely to be unstable for this pulse has been analysed [10] and Fig.200 shows the marginal stability boundary for this mode, at the time when the α-particle production reaches its maximum, where C_{AG} is the Alfvén speed and v_{α}^{birth} denotes the α-particle birth velocity. The experimental point at this time is also plotted with error bars and lies outside of the unstable domain on its right, corresponding to $v_{\alpha}/C_{AG} > 1$. In conclusion, the α-particle driven global Alfvén modes were stable in Pulse No: 26148.

Summary

The TRANSP code has been used to study particle transport of D and T and possible reasons for enhanced performance behaviour in the series of pulses, which included the first tritium experiments. The particle transport of both species is similar being driven by their local density gradients. All the plasmas had the enhanced confinement phase showing reduced ion thermal conductivity and particle diffusivity across the whole plasma. No clear explanation has been found for the existence of such good performance or for its degradation, which in the pulse most extensively analysed clearly happens some time before the final impurity influx.

References

[1] The JET Team, Nuclear Fusion **32** (1992) 187.
[2] Goldston, R.J., et al., J. Comput. Phys. **43** (1981) 61.
[3] Balet, B, et al., to be published in Nuclear Fusion.
[4] Kardaun, O.J.W.F., et al., in Plasma Physics and Controlled Fusion Research 1992 Proc. 14th Int. Conf. Würzburg, Germany, IAEA-CN-56/F-1-3.
[5] Pasini, D., et al., J. Nucl. Mater. **176 & 177** (1990) 186.
[6] Nave, M.F., et al., Europhys. Conf. Abstracts (Proc. 19th European Conference on Controlled Fusion and Plasma Physics), EPS, Innsbruck, Vol. 16C, Part I, (1992) 439.
[7] Troyon, F., et al., Plasma Phys. and Control. Fusion **26** (1984) 209.
[8] Jackson, G.L., et al., Phys. Fluids **B, 4(1),** July 1992.
[9] Cheng, C.Z., Phys. Fluids **B3** (1991) 2463 and references therein.
[10] Kerner, W., et al, European Conference on Controlled Fusion and Plasma Phys, Lisbon, 1993.

Advanced Divertor Studies

Introduction and Overview

The present pumped divertor programme consists of two phases. In the first (Mark I), inertially-cooled target blocks of CFC or beryllium are mounted on a water-cooled support structure to speed cooling between discharges. The second version, for installation in 1995, was based upon actively-cooled copper elements to which thin Be plates were brazed ("Hypervapotrons") to permit thermally steady state operation at high powers.

During 1992, an ad hoc Advanced Divertor Study Group was set up to study the question of possible improvements to the pumped divertor, for the purpose of optimising its performance and reliability. At that time, the design of Mark I was nearly finished, but the Mark II design was only partly completed.

The study was motivated by two factors:

(a) it had been generally accepted recently that "conventional" divertors, wherein the SOL power flows directly to the target plates, will lead to unacceptably high heat loads in Next Step devices. The exhaust power must be distributed over a much larger divertor surface area than can be obtained by simply tilting the plates, and radiation and charge exchange processes are the leading candidates for accomplishing this. The Mark I divertor geometry, which was to have been taken over directly into the hypervapotron-based Mark II phase, is not well suited to achieving such divertor conditions, principally because it is too "open";

(b) Second, there was continuing concern about the reliability of brazing Be plates to Cu hypervapotrons, and the severe risk to the programme, especially in the D-T phase, which a failed braze would imply.

The ad-hoc group was detailed to study both the physics and engineering of various divertor designs, within the constraints imposed by the JET schedule. The group came to the following conclusions:

- To the extent possible, the divertor should be "closed", (i.e. it should allow as few as possible of the neutrals

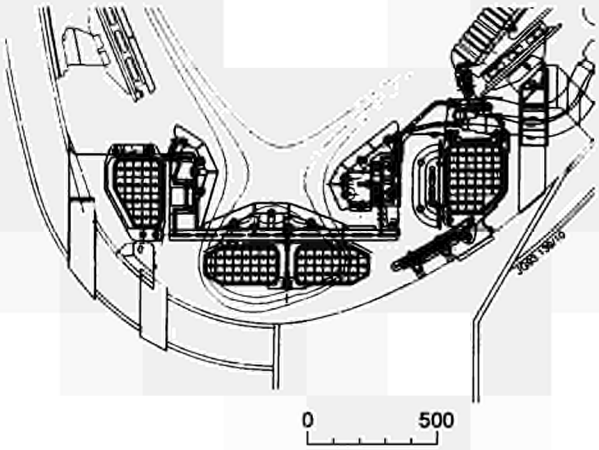

Fig.201: Cross-section of the inertial Mark IIA divertor

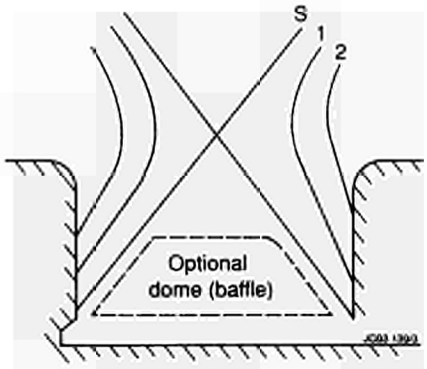

Fig.202: Vertical target divertor with optional baffle

recycling from the target plate to escape from the "divertor region" below the X-point). Closing the divertor leads to higher density and lower temperature in the divertor. This reduces impurity production, enhances impurity retention, and facilitates access to the "atomic physics" regime where radiation and charge exchange are increased, decreasing the conducted power load to the plates. In addition, the wetted area should be made as large as possible by reducing the angle of incidence of the field line on the target to the limit allowed by target alignment tolerances;

- Only minor changes, specifically with respect to final machining of the target blocks to maximimize their effective wetted area, could be made to the Mark I design due to time constraints;
- An inertially cooled version of Mark II, offering high performance (relative to Mark I), flexibility, and minimum risk could be built in about the same time schedule as the hypervapotron-based Mark II. It would allow testing of recent divertor concepts, and could be designed to form the basis for an extended programme.

The inertial Mark II divertor proposed to replace the original hypervapotron design has several innovative features. It is based on a water-cooled, rigid, toroidally continuous floor-and-sidewall structure upon which large tiles can be mounted with a high degree of alignment, permitting small magnetic field line incidence angles with corresponding large wetted area. The design is such that the divertor geometry, which plays a crucial role in divertor performance, can be readily changed by an exchange of tiles and tile holders, requiring only a relatively short machine intervention. Inertial Mark II divertor has a heat handling capacity which meets or exceeds that of the hypervapotron design for pulse lengths of 5 - 10s at high power, depending on plasma conditions. It can accommodate either Be or CFC tiles, allowing investigation of the two leading candidate target materials for Next Step devices.

The remainder of this report deals first with the physics considerations surrounding the design of Mark II, with emphasis on the role played by divertor geometry. The technical design of the proposed Inertial Mark II is then described briefly.

Divertor Physics and the Effect of Geometry

The three main functions which a divertor should perform can be summarized as:

- handle the heat load (power exhaust) at acceptable erosion rates;
- control impurity content in the main plasma by reducing sources and retaining impurities in the divertor;
- remove He ash.

The divertor plasma parameters (n_e, n_i, T_e, T_i, . .) depend most sensitively on two quantities, the power crossing the separatrix (P_{sol}) and the mid-plane separatrix density (n_b). For fixed power, divertor performance improves dramatically as the midplane density is raised. However, when both variables are fixed, the divertor geometry itself can play a major role. Generally speaking, the more "closed" the divertor, the higher its plasma density and the lower its temperature, contributing to improved performance.

The effects of divertor geometry can be divided into two categories. First, there is the purely geometric effect of increasing the wetted area, upon which the conducted power

falls, by tilting the plates relative to the poloidal flux surfaces. The second effect arises from the fact that by tilting the plates, the recycling neutrals can be directed either towards the private flux region, in "vertical target" designs, or towards the divertor sidewalls, in "domed horizontal target" designs. Examples of these generic target geometries are shown in Figs.201 and 202. In either case, fewer neutrals head directly back towards the main plasma than is the case for divertors with targets oriented orthogonally to the poloidal flux surfaces. More importantly, the distribution of ionization sources in the divertor is dramatically altered by tilting the plates. This can lead to a major redistribution of plasma profiles in the divertor [1], which in turn can lead to enhanced volumetric losses from radiation and charge exchanges. Pumping performance can also be enhanced, particularly when "pumping baffles" are introduced.

Heat Handling Capability

The term *"basic"* heat handling capability refers to the ability of the divertor design to accept the scrape-off layer power transmitted directly to the plates by conduction and convection in the absence of any significant volume energy sinks, such as radiation and CX in the divertor region; this is often called the "conducted power." This situation constitutes a "worst case" for a divertor, and can arise for high power, low density operation. When significant volumetric radiative or CX energy sinks are present, in which case the divertor is said to operate in the "atomic physics" regime, the conducted power can be greatly diminished. This is referred to as "enhanced" heat handling capability.

The *"basic"* conducted power to the plates, for a given input power to the SOL, is most robust against changes in midplane density or recycling changes induced by geometry, while the losses leading to *enhanced* heat handling capabilities of a particular design are dependent not only on midplane density, but on geometry as well. The only way to reduce the *basic* conducted power per unit area is to increase the "wetted area" upon which the power falls. The more orthogonal the target is to the poloidal flux surfaces, and the further it is from the X-point, the higher is the power per unit area. Therefore, the effective wetted area can be increased by either tilting the plates, or moving them closer to the X-point, which increases the flux expansion. The amount of tilting allowable depends on the smallest permissible angle between the magnetic field (total) and the plate, which depends on tile size, gap size, and alignment tolerances. An alternative to increasing wetted area is to sweep. However, this should be avoided if possible. Sweeping reduces the degree to which the divertor can be closed, and it may affect main plasma performance adversely by introducing unwanted effects into the main plasma edge. In addition, it is not a technically preferred solution for ITER and beyond.

The second major factor affecting the heat loading is the toroidal utilization factor, which is the fraction of the ideal wetted area which is actually usable. Low toroidal utilization factors result from combinations of low field angle, small tiles with large gaps, and poor alignment tolerances. The toroidal utilization factor in Mark I is quite low, but in the proposed inertial Mark II, it is close to the optimum, as a result of the use of large tiles, small gaps, and improved alignment tolerances.

Enhanced divertor radiation can be produced by operating at as high a divertor density (volume averaged) as possible. Generally speaking, "closing" the geometry is beneficial. The degree to which a divertor radiates is influenced, by the type and amount of radiating material. It is possible that radiation from hydrogen, along with that from the intrinsic impurities (carbon or beryllium), may suffice to substantially reduce the conducted power. However, simulations and scaling arguments suggest that extra radiation produced by impurity puffing in the divertor may be necessary, and such experiments will be conducted in the next JET campaign. Introducing the impurity atom into the divertor plasma some distance away from the targets, which can be controlled to a certain extent by geometry, increases the radiation per atom, but may adversely affect the retention of impurities.

Charge exchange can in some cases be beneficial in removing energy from the ion channel. However, charge exchange very near the target plates does not help much, and can actually lead to heating of the plasma if the fast reflected atoms arising from ions accelerated through the sheath make a CX collision with lower energy ions near the target. Therefore, cold neutrals must be introduced away from the target for this mechanism to be effective, and the degree to which this can be accomplished depends strongly on target and baffle design.

Impurity Control.

Numerical and analytical studies both indicate that, to retain impurities produced at the target it is necessary to reduce the divertor ion temperature to ≤ 20eV [2]. This also strongly reduces (in the case of Be), or nearly eliminates (in the case of C), the production of impurities, since the sputtering

yields falls off rapidly at low plasma temperature. For a given SOL power, this is most effectively accomplished by raising mid-plane density. However, here again the geometry can play an important role. If the divertor design is very open, the divertor density achieved for a given P_{SOL} and n_b will be significantly reduced, so that closure again is important. Closure has another very strong influence on the impurity content of the main plasma in that it reduces the sputtering of impurities at the main chamber walls arising from cold neutrals charge exchanging with relatively energetic ions inside the separatrix. It is difficult to shield against such wall-produced impurities. Optimization of divertor design with respect to impurity control is relatively complicated, as it is affected by the distribution of sources and of flow, both of which depend sensitively on the geometry

It should be stressed that the ion temperature must be reduced below ~20eV on both sides of the divertor for effective impurity control (as well as for enhancing radiation, etc.). If the power flow into the divertor is greatly unbalanced, when the ion —B drift is towards the target, it is not possible to create the desired high recycling/atomic physics regime on both sides of the divertor simultaneously. This argues strongly for operation with "reversed" ion ∇B drift, as was used in the PTE, even though the H-mode threshold is raised.

Pumping

In any design, some of the neutrals recycled at the target plate escape immediate reionization and enter either the private flux region or the regions external to the divertor plasma. If a baffle or pump duct is placed there, these can be "scooped off" and led to the pumping chamber. Without such a baffle, these will re-enter the plasma somewhere and be re-ionized. Gaps in the target plates themselves (Mark I and the original Mark II) are not very effective for pumping, as has been shown by modelling with the Monte Carlo neutral code EIRENE. Vertical plate designs lend themselves quite readily to enchanced pumping, although other designs can probably also be made to work. For He transport studies, the ability to pump with the cryopump should lead to significant advances in our ability to interpret He transport experiments.

JET Divertor Geometries

Mark I (and original Mark II)

The geometry of Mark I (and the original Mark II hypervapotron design) is a relatively wide, U-shaped trough with nearly vertical sides. It was designed to accommodate a large family of equilibria and to permit high amplitude sweeping. Due to the 1cm gaps between narrow (3cm) tiles, and relatively poor alignment tolerances achievable, it has a small toroidal utilization factor, and sweeping will be required for all but modest power inputs. The geometry is very "open" for most equilibria of interest, which may limit access to the high recycling/atomic physics regime. However, elevated X-point equilibria having their strike zones on the vertical side walls can probably be produced, permitting investigation of "vertical target" divertor geometries at modest powers and currents.

Inertial Mark II

The basic concept of the Mark II proposal, described in more detail later, is to use a rigid, toroidally continuous, water cooled base structure upon which target/baffle structures of various designs can be mounted. The rigid base allows for good tile alignment and thus permits the use of large tiles, with small incidence angles, resulting in large wetted areas. The wetted area depends on the particular magnetic equilibrium chosen, but is typically a factor of four or more larger than in Mark I, virtually eliminating the need for sweeping.

The degree to which the divertor geometry can be optimized in JET is restricted by the geometry of the lower part of the vessel, including the divertor coils, which cannot be changed due to time constraints. Specifically, the divertor floor cannot extend below the top of the case around the lower divertor coil pair, so that the divertor "depth", distance from the X-point to the bottom of the divertor plasma channels, is limited by X-point heights.

Past experience indicates that on-axis NB heating is necessary to guarantee the high performance achieved in PTE-like (hot ion mode) discharges. This limits the position of the magnetic axis to ~20cm above the vessel midplane for effective heating, which, in turn, limits the height of the X-point, for the "fat" equilibria, which have large volume and good vertical stability, to about 30cm above the case of the central divertor coils. For this limited X-point to divertor floor distance, a true "deep-slot" design is not possible. The divertor geometry selected for these equilibria, referred to as Mark IIA, is of the "domed horizontal target" type, shown in Fig.201. The poloidal flux surfaces shown correspond to the separatrix and the surfaces 1 and 2cm beyond the separatrix at the outer midplane, for a 5MA "fat" equilibrium. Relative to Mark I, the target is tilted upwards in the centre. This serves the dual purpose of increasing the wetted area and redistributing the re-cycled neutrals, which tend to come off

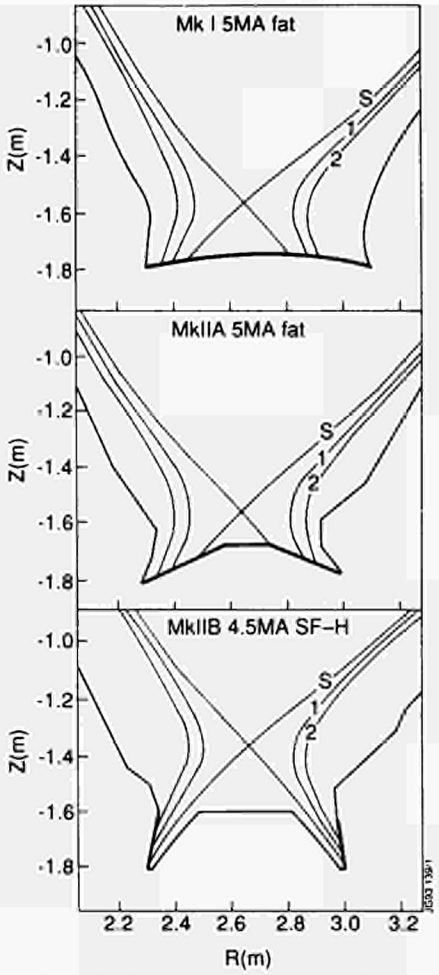

Fig.203: Geometries used for simulations

the targets perpendicularly. In addition, the side walls are brought in, in this version, to about the 2cm line. This Mark IIA design accommodates all the standard "fat" and "superfat" equilibria developed for pumped divertor phase operation, and can also accommodate a certain amount of sweeping of the strike points across the target, if found to be necessary.

A deeper, "slot-like" divertor can also be envisaged if the magnetic axes of the equilibria are allowed to rise to about 50cm above the midplane, so that NB heating is then somewhat off-axis. This version of the divertor is referred to as Mark IIB. An example is shown in Fig.203(c) for 4.5MA equilibrium. In this version, the targets are nearly vertical side walls, and the high "centre dome" is inserted to reflect neutrals back into the lower part of the divertor plasma. It can easily incoporate openings for pumping or gas puffing, either near its base, or higher up, to test various ITER-relevant ideas on enhancing CX and radiation losses. Using vertical targets, rather than an orthogonal one at the bottom of the slot, increases the wetted area and thus keeps heat loads to manageable values even for high power, low density

Table XIX: Input for Comparison Cases

Config	P_{SOL}(MW)	Equilibrium	$n_{ib}(10^{19}m^{-3})$
Mark I	20	5 MA, F	2.5
Mark IIA	20	5 MA, F	2.4
Mark IIB	20	4.5 MA, SF	2.4

shots, for which it is difficult to radiate large fractions of the SOL power. An alternative is to remove the centre dome entirely, creating a true "vertical target" divertor in which recycling neutrals which pass through the divertor fan enter the private flux region and tend to impinge on the full length of the opposite divertor leg, which helps to increase the volume over which radiation and CX effects are important. Alternatively, the geometry can be arranged so that the strike zone is on the outward-facing sides of the dome, creating a "deep slot" version of Mark IIA, which results in a different distribution of density, temperature, and radiation in the divertor volume than for the vertical target designs.

Code Predictions of Divertor Performance

The performance of Mark I and versions of Mark II has been modelled using EDGE2D, which is a full 2-D version of EDGE1D [3]. It is a multi-species fluid code which treats hydrogen and all the ionization stages of a single impurity, either carbon or beryllium. Impurities are introduced self-consistently by a sputtering model. Hydrogenic and impurity neutrals are followed by the Monte Carlo code NIMBUS to compute particle sources, with NIMBUS called automatically according to prescribed criteria. Symmetry between inner and outer divertors is not assumed. EDGE2D incorporates a distorted (non-orthogonal) mesh approximation near the target to handle inclined plates.

The geometries are shown in Fig.203. Mark IIA is a domed horizontal plate design, and Mark IIB is a vertical slot, which fits raised X-point "superfat" equilibria. It is not optimized, but is included to illustrate generic behaviour of such a configuration.

Comparison of Local Plasma Parameters

Three cases have been selected (see Table XIX), one for each geometry, to illustrate the differences in local parameters that geometry produces. Each uses an input power to the SOL of 20MW, evenly split between ions and electrons. The midplane separatrix densities are nearly the same (see Table XIX). All cases were run with Be as an impurity, but only in one was the radiation computed correctly with the

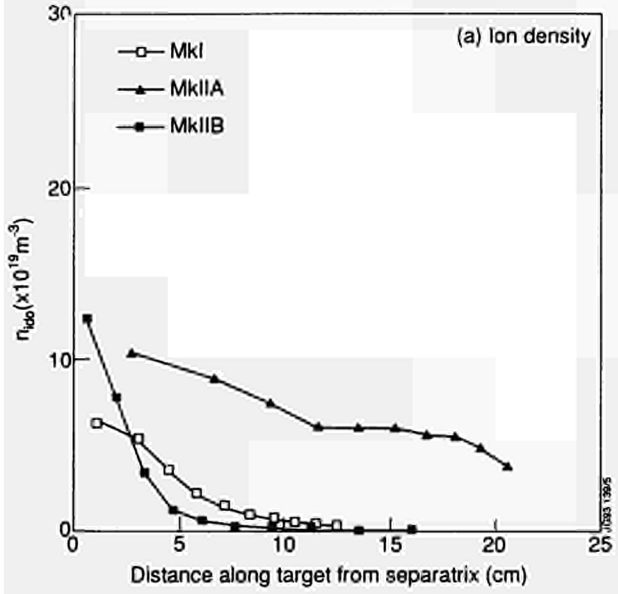

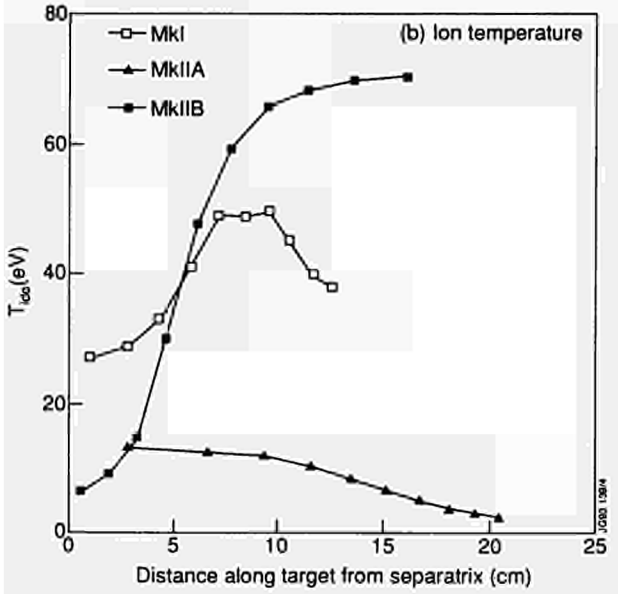

Fig.204: Target profiles of (a) ion density and (b) ion temperature

full multi-species code version. Since the impurity radiation is always a small fraction of the input power, it probably does not significantly affect the results shown here.

Figure 204 shows the distribution of ion density and temperature across the target plate for the three cases. Both Mark II designs have larger wetted areas than Mark I. Case IIA produces the most uniform distribution of temperature and density, with the ion temperature remaining low across the entire target face, which is desirable for retention of impurities. Mark I produces a relatively high ion temperature and correspondingly low density, (i.e. it does not enter the desired high recycling regime for the given input parameters). The vertical slot geometry (Mark IIB) gives a narrow region of high density and low temperature, outside which the divertor plasma becomes hot but very rarified. The behaviour of the density and temperature profiles varies dramatically with geometry. Comparing Mark IIA and Mark IIB geometries, the former, for which neutrals are reflected towards the outer separatrix layers, tends to form a thicker, more uniform SOL, which is reflected also in the midplane profiles (Fig 205). The vertical slot, which reflects neutrals in the opposite direction, (i.e. towards the separatrix), produces a narrow SOL of higher density and lower temperature. In this case, the flux tubes close to the separatrix are in a high recycling mode, while the outer ones are high temperature, low recycling, with low particle content.

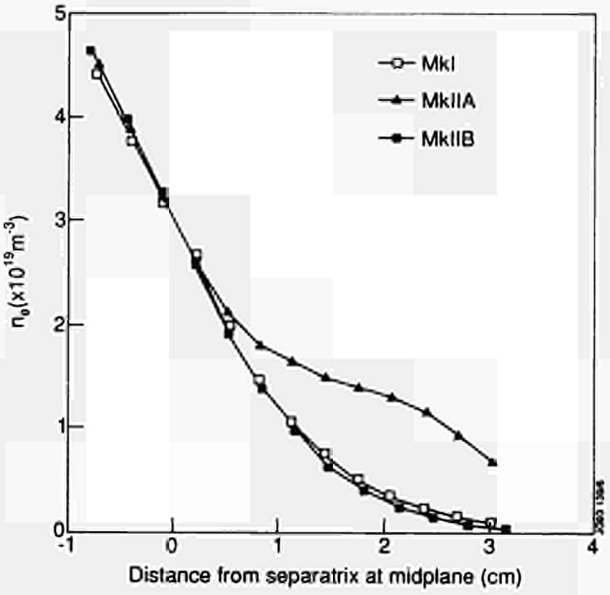

Fig.205: Midplane electron density profiles in the SOL

The power distribution across the outer divertor target is shown in Fig.206. Mark IIA has a much broader profile than Mark I, with a lower peak by a factor of ~2, and that the area under the curves, the conducted power to the plate, is lower for both versions of Mark II than for Mark I. The power densities shown assume that 100% of the toroidal wetted length is available, but in Mark I the toroidal utilization factor is only about 40%, compared with better than 80% in Mark II. Therefore, the real power loading on Mark I would be about 2.5 times higher than that shown, increasing the differences between Mark I and Mark II.

Global Parameters: Effect of n_{lb} and Geometry

A total of eleven runs were carried out for the three geometries in Fig.202, all with input powers of 20MW, but

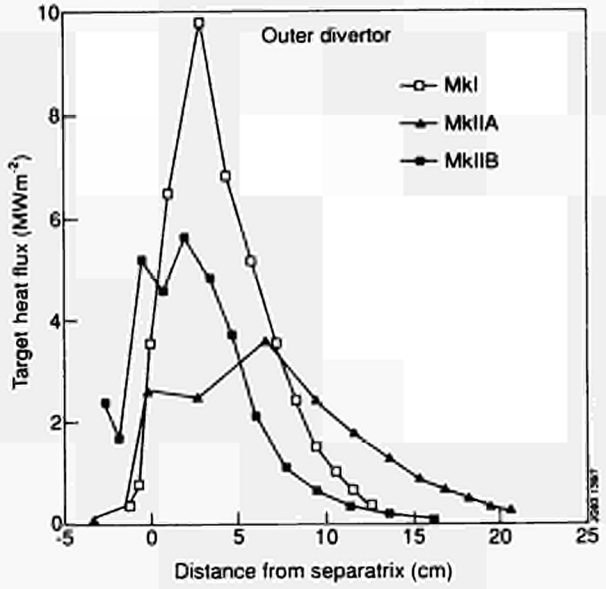

Fig.206: Heat deposition profile on the outer divertor target

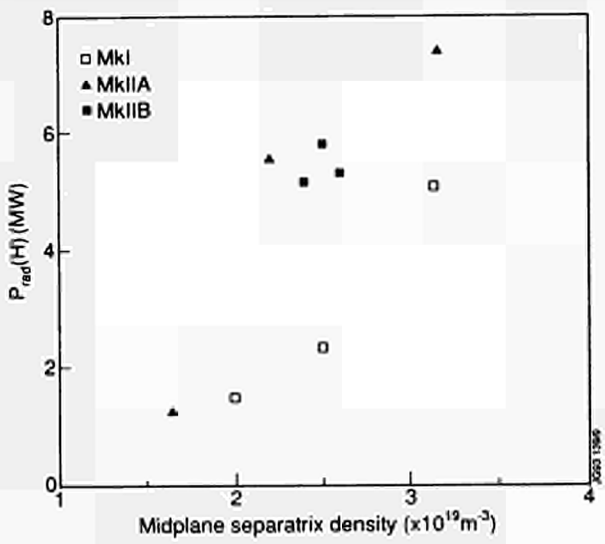

Fig.208: Estimated power lost by hydrogen radiation

with variations in the midplane separatrix density, n_{ib}. Some of the runs were with Be, and the others with C. Two were full multi-species calculations, while the rest used the average charge state version of the code.

One measure of the degree to which a divertor enters into the high recyling atomic physics regime is the total number of hydrogen ions, N_{div}, contained in the divertor, the higher the value of N_{div}, the more likely that significant amounts of radiation can be produced. Fig.207 shows N_{div} versus n_{ib}, for fixed power into the SOL. It can be seen that for each geometry, N_{div} increases rapidly with n_{ib}, which is expected from simple models of divertors. However, Mark I, the most open of the three geometries, developed a significantly lower particle content than the two Mark II geometries, which entered more easily into a high inventory mode as the midplane density is increased.

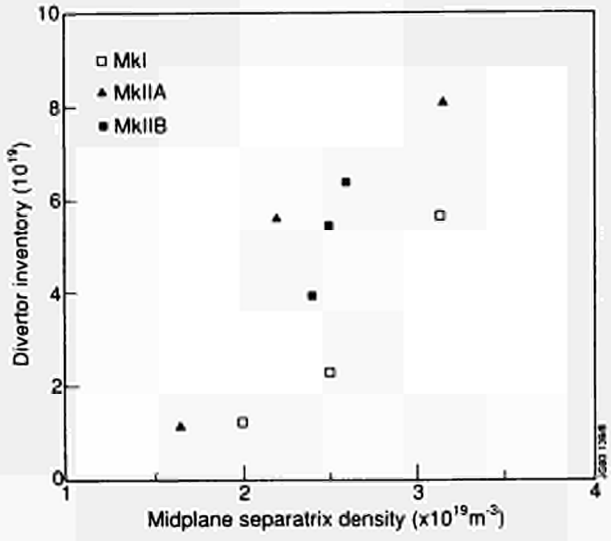

Fig.207: Total number of ions in the divertor versus midplane ion density

Radiation in the divertor will arise during ionization of the recycling hydrogen neutrals and from impurities sputtered from the targets and sidewalls. Fig.208 shows the hydrogen radiation for each case, which is estimated as twice the direct ionization energy (i.e. an effective ionization energy of about 40eV per ion.) This is directly proportional to the hydrogen flux to the target. Again, the Mark II versions both have significantly higher recycling fluxes, and therefore higher hydrogenic radiation. The total hydrogen radiation approaches 8MW in these cases, which is a signifcant fraction of the input to the electron channel. These calculations suggest that for the "gas target" experiments at JET and DIII-D, which had relatively clean plasmas and very high midplane and divertor densities, the high measured radiative losses may be attributable primarily to hydrogenic, rather than impurity radiation.

The radiation arising from the intrinsic impurity production at the target has been examined for two cases, using the full multi-species version of the code. Relevant data is shown in Table XX. In each case, the total radiated power was low, reaching only 1.14 MW in the best case (Mark IIB with a carbon plate). A more interesting figure is the radiation per sputtered impurity ion. For the case with a nearly orthogonal target, Mark I, the number is relatively low. However, for Mark IIB, each carbon atom radiates, on average, about 2keV. This is believed to be because, in this geometry, the sputtered ions tend to enter the plasma further

Table XX: Total Impurity Radiation and Radiation per Sputtered Impurity Atom: Full Multi-Species Calculation

Config.	Impurity	n_{ib} ($10^{19}m^{-3}$)	Γ_{d,H^+} ($10^{23}s^{-1}$)	Y_{eff} (%)	$\Gamma_{d,zo}$ ($10^{21}s^{-1}$)	$P_{RAD,Z}$ (MW)	$P_{RAD,Z}/\Gamma_{d,zo}$ (eV/particle)
Mark I	Be	2.5	5.6	2.85	15.6	0.50	201
Mark IIB	C	2.5	14.3	0.25	3.5	1.14	2037

upstream, and thus have a longer lifetime in the plasma. A pure vertical target design, without the domed centre baffle, may be even better. It is also worth noting that Be may perform better than C. At a given divertor ion temperature, which must be kept low for impurity retention, Be sputtering coefficient is considerably larger than that for C. In addition, Be vapour pressure is large at high target temperatures, adding to the Be content of the divertor plasma.

It has been proposed that charge exchange may constitute a significant loss to the ion channel [4], and if it occurs sufficiently far away from the target plates, it can help to distribute the heat load over a larger area. EDGE2D calculates this effect fully self-consistently. In these simulations, CX losses of up to 2.5MW were found for Mark IIB, with lower values for Mark I and Mark IIA.

Technical Design

A toroidally continuous structure was chosen to enable accurate tile alignment. This structure, as shown in cross-section in Fig.201, (with the Mark IIA tile geometry) could be assembled inside the machine from 48 sections, each compatible with vessel entry. A continuous structure also significantly simplifies the attainment of mechanical stability. Although the forces due to halo currents may be large, the inherent rigidity of a continous ring enables the support structure to withstand these forces internally. Each module is made up from a 4cm thick baseplate and two 10cm thick fabricated sidewalls. The modules are pre-assembled during manufacture with dowel locations to form a complete ring, the machining of which then enables very accurate tile locations. The inherent stiffness of the sidewall structure allows hinged corner joints to be used, thereby leaving a reasonable large pumping gap open to the cryo-pump. The volume between the main plasma and the divertor/pumping chamber is closed by thin sheet baffles. Since the structure is internally stable it is mounted at only one poloidal position, thereby easing the problems associated with thermal expansion.

A substructure is used to support the tiles accoding to the chosen divertor geometry. Each tile should be attached by a single spring-loaded central bolt and supported on corner pads. Each module is fitted with its own tile carrier, but adjacent tiles share corner support pads, so that tile-to-tile step accuracy is dependent only on the tolerance of tile thickness. Replacement of a damaged tile is carried out by exchanging a complete carrier, an operation which can be performed by remote handling.

Cooling of the support structure is required to prevent overheating of the divertor coil epoxy. The present design of the coil and heat shields can withstand radiation from a 350°C surrounding structure, as required for bake-out. The required cooling is modest, with an estimated maximum load of $15kW/m^2$. A water flow of $7kgs^{-1}$ would be adequate with a 1.0°C film drop and a 2°C bulk temperature rise.

The power handling capability of this design has been significantly improved, relative to Mark I, by maximising the total wetted area. The poloidal wetted length is increased by inclining the target plates to the poloidal flux surfaces, while the toroidal length is increased (by a factor of >2 for most magnetic equilibria), by using carefully aligned large tiles with small inter-tile gaps. The optimum tile length is determined by thermal bowing and lies between 15 and 30cm, depending on the material properties.

With the tolerances achievable in the present design, the sum of the step and angular tolerances amounts to an effective maximum step size of 0.7mm between the 15 - 30cm long tiles, permitting the use of very small angles of incidence between the magnetic field and the target. Figure 209 shows the power per leg which can be accommodated for a 1000°C temperature rise (above the pre-pulse temperature of about 350°C) for 5 and 10s pulses for two types of carbon fibre material, and for a 700°C rise for beryllium tiles. The 2-D CFC has been oriented with the matting in the plane defined by the vertical and toroidal directions, which maximizes thermal conduction away from the surface while minimizing bowing. From Fig.209, the inertially-cooled

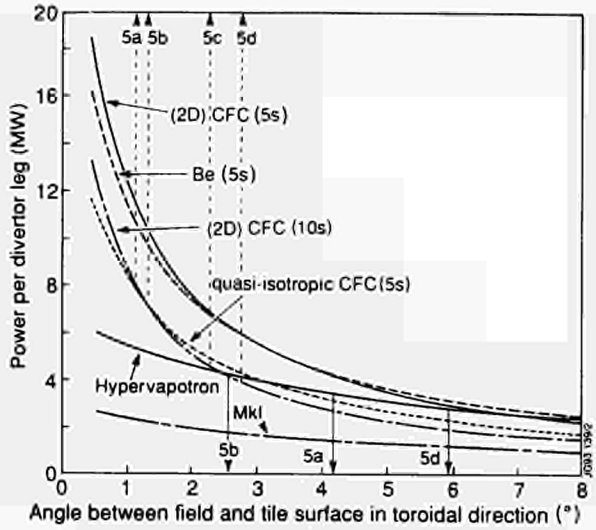

Fig.209: Power handling capability of various JET divertor designs

Mark II with C-tiles out-performs the hypervapotron version for periods up to 10s for equilibria with field angles below 2°, and for a several seconds for higher field angles. The Mark I, hypervapotron Mark II, and inertially cooled Mark II can all be swept, with a resultant gain in power handling which is approximately proportional to the field angle of incidence. For a 4° angle, a factor of ~3 could be achieved. The Mark I and hypervapotron Mark II were designed to rely upon sweeping, while for most equilibria and plasma powers of interest, inertial Mark II can operate without sweeping, as shown in the figure. In addition, the inertial Mark II is expected to produce larger volumetric power losses, further increasing its advantage over the older designs.

Conclusions

The simulations, while preliminary, all tend to confirm that a closed divertor will function more effectively than an open one, which can be deduced from analytical divertor models. Although closing the divertor means reducing the SOL flow outside the divertor, the gains in power exhaust performance, through entrance into the high recycling/atomic physics regime, and the improved impurity behaviour seem to more than offset the effect of the reduced flow.

The Mk II configurations, while differing from each other in performance, outperformed the more open Mark I in nearly every respect, at fixed input power and SOL midplane density.

Mark IIA produced a relatively uniform plasma across a broad target, and is clearly a great improvement over Mark I. It is a relatively conservative design, which will be further optimized by moving the sidewalls closer, and perhaps increasing the height of the centre dome.

Mark IIB is an example of a family of deeper slot geometries which is considered to be more "ITER relevant". Such geometries can be investigated in JET by raising the X-point. Mark IIB performs well in terms of divertor particle inventory, peak density, radiation per impurity atom, hydrogen radiation, and CX losses. However, the rather hot, rarefied outer layers of the divertor plasma allow the escape of more impurities than the "outward facing" designs such as Mark IIA.

From the limited number of simulations performed so far with the full multi-species version of the code, it seems that radiation from sputtered impurities will always be small for a high recycling, low temperature divertor. This suggests that injected impurities will be needed, a topic which should be investigated both computationally and experimentally as soon as possible.

Divertor optimization is a difficult problem involving many factors. Further work will be undertaken on optimization of the "deep" version of Mark II. This will include investigation of high dome- and unbaffled-vertical target designs, as well as of the effect of puffing and pumping opening in the divertor walls. Simulation of He transport in the SOL and divertor for the various candidates will also be addressed.

A technical conceptual design has been developed which has large wetted area to eliminate the need for sweeping. It allows various target plate geometries can be tested, with only a short machine intervention required to change the configuration. This permits the the investigation of the effect of geometry on divertor performance, leading to optimization of a Next Step divertor.

References:

[1] G. Vlases et. al. Proceedings of 14th IAEA Conference on Plasma Physics and Controlled Nuclear Fusion Research (IAEA CN 56/A-5-1) (Würzburg, Germany, 1992)

[2] G. Vlases and R. Simonini, Proc. 18th EPS Conference on Controlled Fusion and Plasma Heating, vol. III, p 221 (Berlin, 1991)

[3] M. Keilhacker et. al., Nuclear Fusion **31** 535 (1991).

[4] M. L. Watkins and P.-H. Rebut, Proc. 19th EPS Conference on Controlled Fusion and Plasma Heating, vol. II, p. 731 (Innsbruck, 1992)

Theory

The purpose of theoretical work at JET is twofold; it aims to increase physical understanding of plasma behaviour in JET and hence predict theoretically the performance of future experiments; and it assists experimentalists and engineers with present problems. The main activities are described below in the areas of analytic and predictive theory.

Analytic Theory

Analytic theory has supported the experimental programme by detailed interpretation of JET discharges. Progress has been achieved in the areas of equilibrium calculations, of discharge identification with emphasis on fishbone events and on an ELM database, of stability analysis and MHD spectroscopy, of energetic particle effects, of transport and of plasma heating. In addition, assessment of plasma theory, in particular models for L- to H-mode transitions, has been undertaken.

Equilibrium Reconstruction

The results of equilibrium reconstruction form the backbone of theoretical analysis and an essential part of many diagnostic systems in use at JET. The accurate determination of the magnetic field configuration close to the plasma boundary has become increasingly important in recent years, with the recognition of the pivotal role played by edge physics in determining the overall performance of tokamak fusion devices. Plasma boundary analysis will receive even more emphasis for the pumped divertor phase at JET.

Methods (XLOC[1], FBC[2]) have recently been developed at JET which give an accuracy of ~1cm in the plasma boundary position when compared with independent diagnostics such as the Langmuir probe and CCD camera at various positions around the boundary, and, in particular, with the X-point position. This has given confidence in the execution and interpretation of experiments where the position of the plasma boundary has been a significant parameter under investigation. One result is the dependence of H-mode performance on X-point position relative to the vessel [3].

The magnetic reconstruction codes presently in use at JET are XLOC and FBC for the calculation of the plasma boundary, IDENTC/D and EFITJ being used for full equilibrium reconstruction. XLOC is a 'local' expansion technique which is used routinely at JET. FBC, which was developed to provide accurate boundary data for IDENTD,

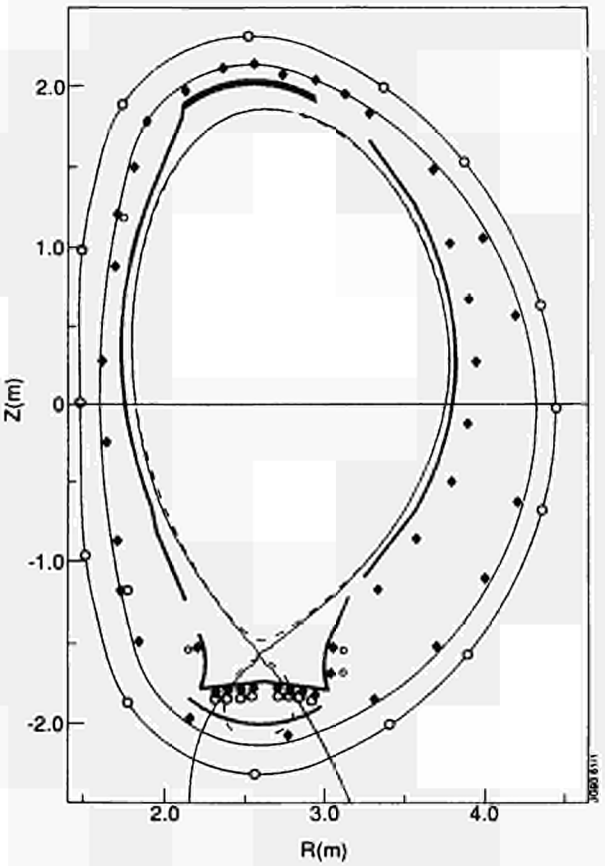

Fig.210: XLOC boundary (solid curve) superimposed on a boundary line computed by EFITJ for a 5MA (fat) pumped divertor configuration. Also shown are proposed magnetic diagnostics.

uses global toroidal eigenfunctions. A version of XLOC has been implemented, which is used for real-time display of the plasma boundary during operation. The codes IDENTD and EFITJ make use of magnetic, pressure profile, Faraday rotation, motional Stark and q-profile data. These codes complement each other: IDENTD is a finite domain code for the vessel area only; whereas EFITJ is an infinite domain code, which uses the poloidal field coil measurements as well. These codes have the ability to reconstruct accurate q-profile information, such as negative shear [4], which is an important prerequisite for stability analysis. EFITJ can additionally include finite edge current effects.

The equilibrium analysis is presently being upgraded for use with the pumped divertor. EFITJ, XLOC and FBC already have versions which work for the pumped divertor, and IDENTD is being upgraded. The design of the magnetic field measurement system was performed using EFITJ resulting in a substantial upgrading of the system giving better coverage around the plasma boundary, as shown in Fig.210. The use of XLOC (FBC) for real time shape control of the plasma boundary is also planned for the pumped divertor phase.

MHD Spectrum and Stability

MHD spectroscopy (i.e. identification of ideal and dissipative MHD modes for the purpose of diagnosing tokamaks and optimising their stability properties), requires a numerical tool which accurately calculates the dissipative MHD spectra for measured equilibria. The spectral code CASTOR (Complex Alfvén Spectrum for TORoidal Plasmas), together with the equilibrium solver HELENA [5], provides such a tool. A specific code, CSCAS [6], was developed for studies of the continuous part of the ideal spectrum.

The interpretation of the MHD signals measured in coils outside the plasma requires the inclusion of a vacuum region. In collaboration with FOM Nieuwegein, The Netherlands under an Article-14 contract [7] and two study contracts [8] and in collaboration with IPP Garching, Germany, the resistive spectral code CASTOR was extended to a plasma-vacuum-wall system. It is found that the stabilising influence on the tearing mode, which can be very effective for modes in the plasma centre, is not effective for modes localised near the plasma boundary. In particular, it has been shown that resistive free-boundary instabilities can exist without an underlying ideal instability.

The calculation of the vacuum solution was extended to take into account antenna currents in the vacuum region. This version of CASTOR computing the plasma response allows modelling of the excitation of global Alfvén waves, TAE, by utilising the saddle coils. The plasma response yields maxima at the frequency of global Alfvén modes, where the corresponding plasma damping is given by the width of these maxima. In this joint effort, CASTOR has been extensively applied to identify possible resistive MHD instabilities for the explanation of the ELM precursor and to analyse global Alfvén modes. The structure of the code allows for extension to other dissipative terms, such as thermal conductivity, a generalised Ohm's law and energetic particle effects.

Global Alfvén Waves

Energetic particles preferentially destabilise global MHD modes, which experience no damping, i.e. are easily excited. Apart from the marginally stable internal kink modes, another branch, defined by the toroidicity induced Alfvén eigenmodes, is important. It has been argued that fusion born alpha-particles can destabilise global Alfvén modes and, hence, are lost by the particle-wave resonance.

Usually, the stable Alfvén branches exhibit continua corresponding to eigenmodes where every field line oscil-

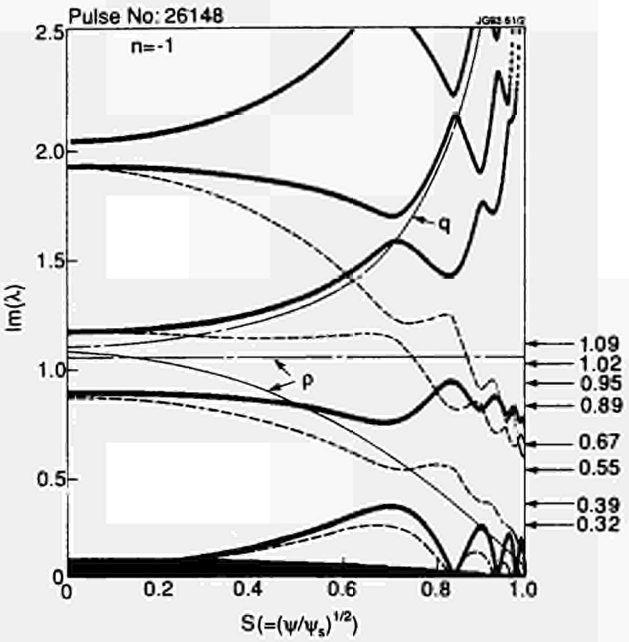

Fig.211: The radial dependence, $s = (\psi/\psi_s)^{1/2}$, of the Alfvén continua for the PTE (Pulse No: 26148) for n = 1, for parabolic density profile r(s) given by the solid lines and for constant density given by broken lines. The global Alfvén eigenmodes as computed by CASTOR are indicated by arrows showing TAE in the first gap and EAE in the second gap. The frequency Im(λ) is normalised to the Alfvén frequency defined on the magnetic axis.

lates with its own local frequency $\omega_A(r)=k_{//}v_A(r)$. If a coherent oscillation is enforced within such a continuum, e.g. by antenna excitation, this 'friction' yields resonant absorption. This effect accounts for the **continuum damping**.

The toroidal curvature induces a poloidal mode coupling which is the strongest on rational surfaces, where the cylindrical continuum frequencies are at least four-fold degenerate. The effect of the mode coupling is to remove these degeneracies which gives rise to "avoided crossings" and, by consequence, to "gaps" in the continuous spectrum of finite aspect ratio tokamaks. The size of these gaps is proportional to the strength of the poloidal mode coupling. In addition global Alfvén waves exist with a frequency inside these gaps. The interaction of these gap modes with ideal continuum modes causes phase-mixing so that these modes are damped by resonant absorption.

The Alfvén sub-spectrum of the PTE (Pulse No: 26148) are displayed in Fig.211. Two gaps are important, the toroidicity induced at $\omega / \tilde{\omega}_A \sim 0.5$ and the elongation induced gap at $\omega / \tilde{\omega}_A \sim 1.0$. Here $\tilde{\omega}_A$ denotes the characteristic Alfvén frequency defined at the magnetic axis. Further gaps which are due to triangularity, etc, need not be considered. The width of the lowest gap decreases with increasing toroidal wave number as the radial position of maximum

coupling gets nearer to the magnetic axis. The second gap does not experience such an aspect ratio dependence, (i.e, the gap remains wide). For this configuration, four discrete modes have been found, respectively, inside the toroidicity and elongation induced gap. Their frequencies are indicated in Fig.211.

The influence of the continuum damping has been studied quantitatively. The damping is computed in resistive MHD, where for asymptotically small resistivity, the damping is finite and independent of h. For a parabolic density profile (Fig.211), the gaps corresponding to the coupling of different m and $\tilde{m} = m + 1$ have the same width. Therefore the discrete Alfvén modes do not experience continuum damping except those at the bottom at $\omega_A = 0.32$ and 0.89 (normalised to $\tilde{\omega}_A$). For a high density pedestal near the plasma boundary, simulated by the extreme case of constant density (broken lines in Fig.211), the gaps are now shifted relative to each other.This yields finite damping. The magnitude of this continuum damping strongly depends on the magnitude of the singular contribution. Numerical calculations imply that a weekly damped TAE mode has a damping of $-\gamma/\omega_A = 10^{-3}$ (as obtained for $\omega_A = 0.3\tilde{\omega}_A$, for constant density). In contrast, a strongly damped TAE exhibits damping of (obtained for $\omega_A = 1.0\tilde{\omega}_A$, for constant density).

Collisionless Magnetic Reconnection

Collisionless reconnection - considered to be a fundamental process in Astrophysics - can be observed in JET plasmas close to thermonuclear breakeven conditions. In particular, due to the high temperatures which have been attained in recent experiments, this process is thought to occur during the relaxation phase of sawtooth oscillations. Magnetic reconnection can remain a virulent process at high temperature, contrary to predictions based on collisional models. In fact, for JET parameters, the initial growth rate of a collisional m = 1 tearing modes compares favourable with the observed sawtooth relaxation time. The nonlinear m = 1 mode evolution has not yet been clarified. Indications are that the ion Larmor radius plays an essential role in the nonlinear stage, where it limits the width of the ion flow channel around the reconnecting q = 1 surface.

Nonlinear Model for Fishbones

A simple heuristic non-linear model has been developed to study the fishbone repetition cycle. Including ion-diamagnetic effects in resistive MHD two-fluid theory, an expression for the growth rate for the fishbone mode can be obtained [9]. The growth rate is proportional to the density of resonant super-thermal ions, and the mode decay is due to plasma resistivity. An equation for the density of the resonant ions is obtained assuming that a constant source of ions is provided by auxiliary heating, and loss of fast particles is due to ergodization of fast particle orbits. In this model, the loss rate is proportional to the square of the mode amplitude.

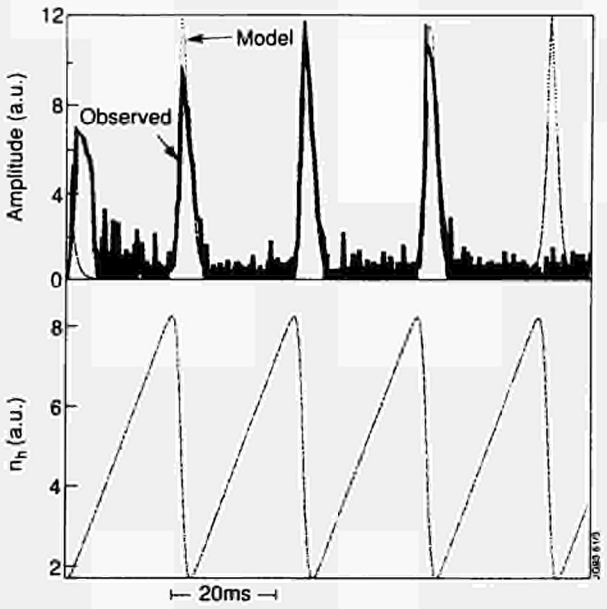

Fig.212: Fishbone amplitude measured by a magnetic pick-up coil, mode amplitude and density of fast ions calculated for n = 2.

The following non-linear system of equations describes the evolution of the mode amplitude, A, and the density of fast ions, n_h:

$$\partial A / \partial t = -\gamma_\eta A + \gamma_{MHD}(n_h / n_0)A$$

$$\partial A n_h / \partial t = S_h - \gamma_L n_{crit} A^\nu$$

γ_{MHD} is the ideal MHD stability parameter; γ_η is the resistive damping; S_h is the source of fast ions; and $\gamma_L n_{crit}$ is a measure of the fast particle loss rate. It is expected that $1 \le \nu \le 2$; $\nu = 1$ assumes a secular loss of the resonant ions, while $\nu = 2$ corresponds to losses following orbit stochasticity.

The comparison with the experimental data shows good agreement with the model. Qualitatively the model predicts both bursts and continuous oscillations, and the observed relation between amplitude and the period of repetition of the bursts. A fit of the cycle solution with the experimental bursts is obtained for n = 2 (see Fig.212), suggesting that orbit stochasticity is the main loss mechanism.

Ion Cyclotron Resonance Heating

The time dependent PION-T code, which calculates ICRF-power deposition and velocity distributions of resonating

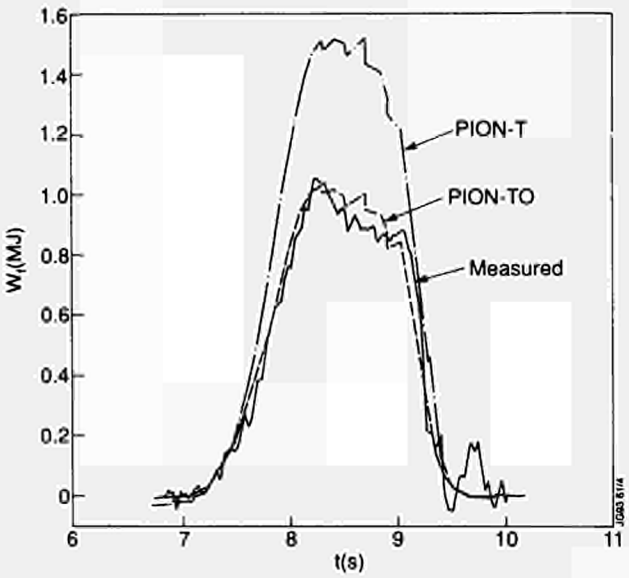

Fig.213: Comparison between the calculated and measured anisotropic energy content for a JET discharge.

ions, has been upgraded to take finite orbit width effects into account. The upgraded version, which is called PION-TO, is now run as part of the so-called secondary processing chain where the necessary input data are taken directly from the experimental data banks at JET. A comparison between code simulations and experimental results has been carried out. Figure 213 shows a comparison between the calculated and measured anisotropic energy content of the resonating ions for a JET discharge. Results from both a version without orbit effects (PION-T) and the version with orbit effects are shown. When orbit effects are neglected the calculated energy content becomes too large. With orbit effects included it is possible to simulate the time evolution of the anisotropic energy content fairly well. The reason for the lower energy content when orbit effects are included is the enhanced slowing down the fast ions experience when they reach out to colder parts of the plasma. The good agreement for the anisotropic energy content gives further support to the claim that the fast ions slow down classically. Furthermore, the non-thermal neutron yield from (D-D) reactions, caused by second harmonic heating of deuterium, during hydrogen minority heating in deuterium has also been simulated. Fairly good agreement between the calculated and measured yield can be obtained provided the hydrogen concentration, the only input quantity for which there are no reliable measurements, is suitably chosen.

Particle Turbulent Transport

Particle transport is conveniently analysed in the test particle approximation. In this limit, the effect of the particle motion on the bulk plasma is neglected. The condition for the applicability of this approximation is that the total charge of the particles belonging to a given class is much smaller than the total electron charge. A typical example of test particles occurring in JET experiments are diluted impurities, like those produced by laser blow-off.

The theoretical analysis of the ion motion takes advantage of the fact that, for almost any situation (including MHD), one needs to know only the electric component of the electromagnetic field (the only significant exception being the motion in a magnetostatic field like the ripple). In this framework, the numerical study of the motion of test particles in a given two-dimensional **E x B** field has been carried out, with the specific task of assessing the validity of various analytic approximations to the particle diffusivity [10]. The results are expressed in terms of the only dimensionless parameter of the problem, the quantity $K = v_E \tau_c / \lambda_c$ (Kubo number) where v_E is the r.m.s. drift velocity and τ_c and λ_c are the correlation time and the correlation length of the turbulent field, respectively. As expected, the quasilinear theory is recovered in the regime $K \ll 1$, where the diffusivity D scales like $D \sim K$. In the opposite limit $K \gg 1$, the asymptotic scaling $D \sim K^{-0.20 \pm 0.04}$ is obtained.

The actual comparison with the measured impurity diffusivity requires good experimental knowledge of the spectrum of the electric field fluctuations. Alternatively, the spectrum can be derived theoretically. This has been carried out recently for a simplified model of plasma turbulence [11]. In that case, the associated test particle diffusivity must be calculated in the regime of large Kubo numbers. However, more realistic models of plasma turbulence require extensive numerical analysis. To this extent, an assessment of the state of the art of the numerical simulations of reduced fluid models of plasma turbulence has been carried out [12].

Predictive Theory

Activity in predictive theory was directed towards two main areas:

- development, validation and predictive use of codes and models for the simulation of the edge plasma;
- development and validation of transport models for the simulation of the plasma inside the last close flux surface.

A considerable amount of work was dedicated to the analysis and interpretation of experimental data in the Transport and Fluctuations area and is described in that section of the Report.

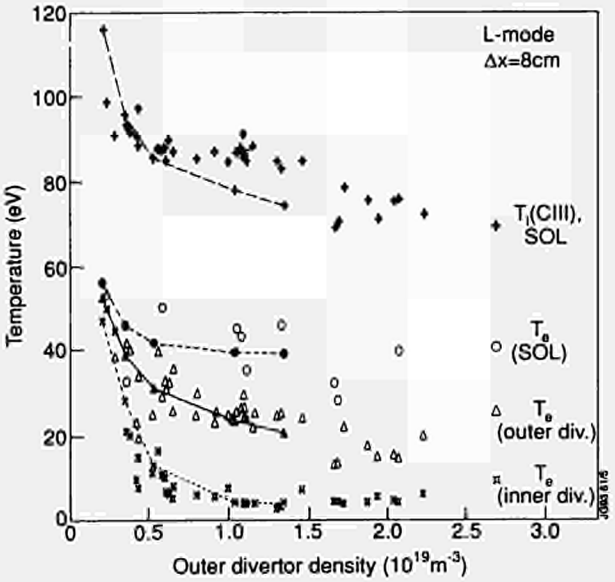

Fig.214: Temperature versus outer divertor density - L-mode, SNX, Be target. Solid symbols - Code results; Open symbols - Experiment.

Modelling Edge Plasma Physics

Code and Model Development

The code EDGE2D was extended to include the treatment of impurities. All the ionization stages of an impurity can now be followed by the code taking into account self-consistently sputtering at the walls, via the Monte Carlo code NIMBUS dealing with all kinds of neutral species and radiation. A simplified approach based on an average charge impurity ion is also available in the code. Beryllium and carbon have been considered so far but the extension to other species is straightforward.

To treat correctly divertor targets with an arbitrary inclination with respect to magnetic field lines, an updated version of the code (EDGE2D/U) was written with an implicit nine-point finite difference discretization scheme.

In addition, a new 2D code, EDGE2D/N, was set up to investigate basic physics phenomena in a divertor, such as relative roles of transport and atomic physics. EDGE2D/U can treat a straight divertor channel with plates orthogonal to the poloidal magnetic field lines, avoiding complications related to the real geometrical configuration. A very accurate Newtonian method is used to solve the difference equations, and a diffusion approximation, much faster than the Monte Carlo approach, is used for the neutral species.

The standard five moment set of Braginskii transport equations in one version, the EDGE1D code, was extended to a 13-moment description with the parallel viscosity tensor and parallel heat flux treated as independent variables. The 21-moment classical transport coefficients, previously implemented in EDGE1D and EDGE2D only for cases with low impurity density, were extended to allow for arbitrary impurity densities. Such code and model development is described in Refs [13-15].

Model Validation

During the last experimental campaign, a series of experiments was performed, using either Be or C target tiles. The experiments were designed to scan parameters, such as the level of power, the density in the scrape-off-layer (SOL) and the position of the magnetic X-point that had been shown by results of edge plasma modelling to be important in determining the production and retention of impurities in a divertor. Comparisons of experimental results and simulations have been carried out for a series of discharges, using both EDGE1D and EDGE2D. Results obtained so far have shown a satisfactory agreement between the predicted trends of temperature and density at the target plates and experimental observations [16-18]. An example is given in Fig.214 [18].

In addition, results from the simulation have proven to be very useful to resolve inconsistencies between experimental results from different diagnostics, e.g. temperature measurements from fixed probes at the 'divertor' targets and reciprocating probes in the SOL away from the targets. While much more experimental, theoretical and computational work is required to develop validated edge plasma models, the work carried out so far at JET is a good starting point in this field and shows that the existing models are at least not in contradiction with experiments and be used, with caution, to support design work related to the JET and ITER divertors.

Divertor Simulations

The EDGE codes were extensively used to simulate the performance of the JET pumped divertor. In particular, various "advanced" geometries for the divertor were studied for the second phase (Mark II) and compared with predictions for the first phase (Mark I). For Mark II configurations, a "slot" design and a baffled vertical plate design were considered, showing the advantages of configurations more closed to recycling neutrals with respect to Mark I, in minimizing the impurity content in the SOL outside the divertor, since:

a) lower temperature and higher densities can be obtained in the divertor reducing the impurity production and favouring the friction force keeping impurities in the

divertor region with respect to thermal forces pushing them out;

b) the sputtering of impurities by neutrals outside the divertor is reduced.

In addition, the Mark II configurations have more favourable power density deposition profiles at the targets, thus reducing or eliminating the need for sweeping. The possibility of obtaining a highly radiating divertor plasma was explored, showing that a key parameter in this respect, as well as for the entrenchment of impurities on the divertor, is the power per particle entering the SOL. Results so far show that beryllium alone is unable to produce the required level of radiation in the Mark I configuration. The Mark II configurations and other impurity species are presently being studied.

An interesting result of these predictive calculations, still to be tested experimentally, is that the density decay length at the targets (and also as far away from the targets as in the midplane zone) depend strongly on the inclination of the plates [13]. However, this geometry effect is counteracted by enhancing the anomalous perpendicular particle transport. Only further experimental work and simulations will possibly determine the edge transport coefficients with sufficient accuracy to allow satisfactory predictions. So far, only sensitivity studies of divertor performance to various model assumptions have been possible. Results on divertor modelling have already been published [18].

Energy Transport Models

As a result of simulations and local transport analysis carried out with the predictive $1^1/_2$ D transport code JETTO, new energy transport model of the Bohm type were developed. They are very simple and depend on two (or at most three) non-dimensional local quantities, but still possess the global and local energy confinement properties observed experimentally in L-mode discharges.

Recent results of local transport analysis in various devices, such as JET, TFTR and DIIID, indicate that a local energy transport model of the Bohm type should allow the best description of transport phenomena of experiments devised to determine the dependence of these coefficients on plasma quantities, by keeping non-dimensional local plasma parameters constant or by changing them in a controlled way. Thus the thermal conductivity c is conveniently written as: $\chi = (cT/eB_0)F$, where the Bohm transport coefficient is written in terms of the toroidal magnetic field B_0 and F is a function of non-dimensional local quantities, such as the plasma β, the safety factor q or the shear parameter s, but does not depend on the normalised gyroradius ρ^*. The number of possible non-dimensional variables in F can be represented by a simple combination in the function F of only two (or at most three) parameters, by choosing:

$$F = \alpha\, r\, q^2/L_p \text{ or } F = \alpha\, q^2/(L_p s)$$

where α is a number, L_p is the scale-length of variation of the pressure and s is the shear parameter.

The global energy confinement properties of the coefficients proposed can be derived analytically, showing that these are close to those of the so called ITER89 scaling law. Taking into account the linear dependence of χ on the temperature gradient, it is found, that, in steady-state and in the absence of sawtooth activity, the thermal energy confinement time is approximately given, by:

$$\tau \propto R^{3/2}\, I\, P^{-1/2}\, n^{1/2}\, B_0^{-1/2}$$

It can also be shown that a dependence of the global energy confinement on the internal inductance ℓ_i close to the one observed experimentally is implied by the coefficients. The code JETTO was used to test the local transport properties of the coefficients by simulating JET discharges. The discharges to be simulated were chosen as being representative of the main transport features of L-modes.

The simulations include:

- ρ^* scaling experiments testing the Bohm type nature of the model;
- current ramp experiments, testing the dependence of χ on the current density distribution;
- off-axis heating experiments, testing the resilience of electron temperature profiles predicted by the model.

Computed and experimental results are in good agreement in all cases showing that these simple energy transport coefficients are a valid starting point for the derivation of a more complete local transport model of the Bohm type to be used for predictions and comparisons with results obtained with existing models of the gyro-Bohm type.

An assessment of various published versions of theoretical electron and ion energy transport models was completed in collaboration with AEA Technology, Culham Laboratory, UK. The models were tested against JET experimental results using the interpretive transport code FALCON. The aim of the study was to establish a basis for the development of a satisfactory, theory-based transport model. However, the results obtained indicate that none of the models considered, gyro-Bohm or resistive MHD type, describe the experimental observations with sufficient accuracy.

References

[1] D. O'Brien et al., Nuclear Fusion, in print (1993)

[2] W. Zwingmann et al., to be prublished at 20th EPS Conference, Lisbon (1993)

[3] D. O'Brien et al., Nuclear Fusion **32**, 1351 (1992)

[4] M. Hugon at al., Nuclear Fusion **32**, 33 (1992)

[5] G.T.A. Huysmans, J.P. Goedbloed and W. Kerner, *Isoparametric Bicubic Hermite Elements for Solution of the Grad-Shafravov Equation*, Proc. CP90 Conf. on Computational Physics, Proc., World Scientific Publication Co., (1991)a., p.371.

[6] S. Poedts and E. Schwarz, *Computation of the Ideal MHD continuous Spectrum in Axisymmetric Plasmas*, to appear in J. Comp. Physics, (1993).

[7] G.T.A. Huysmans, J.P. Goedbloed and S. Poedts, *External Resistive Modes and Toroidicity Induced Alfvén Eigenmodes in Tokamaks*, Rijnhuizen Report 91-209, 1991.

[8] J.P. Goedbloed, et al., *"MHD Analysis of JET Single-null Discharges by Extending and Applying CASTOR"*. J.P. Goedbloed, et al., *"Analysis of Global Alfvén Modes by The Extension of CASTOR with an External Antenna"*, FOM Institute voor Plasmafysica.

[9] B. Coppi, S. Migliuolo, F. Porcelli, Phys. Pluids **31**, 1630 (1988)

[10] M. Ottaviani, "Scaling laws of test particle transport in two-dimensional turbulent velocity fields", Europhysics Letters, 20, 11 (1992).

[11] M. Ottaviani and J.A. Krommes, *"Weak and strong turbulence regimes of the forced Hasegawa-Mima equation"*, Phys. Rev. Letters, 69, 2923 (1992).

[12] M. Ottaviani, *"Direct simulations of turbulent transport in fusion devices"*, Proceedings of the IAEA Technical Committee Meeting on Advances in Simulations and Modelling of Thermonuclear Plasmas, (Montreal, June 1992) and JET Report JET-P (92)58.

[13] A. Taroni et al, Plasma Phys. **32** (1992), 438

[14] S Weber et al, *Plasma Edge Modelling Using the Neutral Diffusion Approximation*, JET Report, JET IR(92)03

[15] G Radford, Plasma Phys. **32** (1992), 297

[16] G Vlases et al, J.Nucl. Mat. **196-198** (1992), 392

[17] R. Simonini et al, J. Nucl. Mat. **196-198** (1992), 369

[18] G. Vlases et al, XIV IAEA Conference on Plasma Physics and Controlled Nuclear Fusion Research, (Paper IAEA-CN-56/A-5-1) (Würzburg, Germany, 1992) to be published in Nuclear Fusion Supplement.

Summary of Scientific Progress

The 1992 experimental campaign essentially sought to extend and complete the experimental investigations addressed during the 1991 campaign. As outlined in the 1991 Progress Report, the major themes of the programme during the period 1991-1992 were:

(i) to exploit new facilities (such as the continuous X-point targets, improvements in the poloidal field circuit, enhancements to heating systems and new diagnostics);

(ii) to advance understanding in several key areas of tokamak physics (such as energy and particle transport, impurity production and transport, magnetic topology and H-mode physics);

(iii) to improve fusion performance;

(iv) to address issues central to the Pumped Divertor and to Next Step devices;

(v) to complete certain experiments relevant to the belt limiter configuration.

Since many of the experiments relevant to themes (i), (iv) and, in particular, (iii) were completed in the 1991 campaign, these had a lower priority in the 1992 experiments. This permitted more time to be allocated to experiments designed to improve physics understanding in several areas and to experiments aimed at completing the programme of studies utilizing the belt limiter. Nevertheless, significant advances in pumped divertor and Next Step issues were also made.

The major constraint on the programme during this period was the requirement to limit neutron production, in order to minimize vessel activation at the start of the current major shutdown. Since much of the vessel activation had been contributed by the first tritium experiment, inevitably neutron production had to be strictly controlled. While this limited the duration of experiments at the highest power levels, it did not prevent significant advances being achieved in several areas. This review concentrates on those areas where significant new results were obtained during the 1992 experiments.

Tokamak Physics Studies

Energy and Particle Transport

A range of experiments has been performed to study the detailed behaviour of local energy transport and to investigate the underlying processes responsible for this behaviour.

Two of the most recent experiments involved the study of plasmas with negative temperature gradients in the plasma core and the analysis of dimensionally similar plasmas. In the first, off-axis ICRF heating was applied to a discharge following pellet injection. This established a plasma with negative values of $n\nabla T$ in the plasma core. By analyzing the subsequent evolution of profiles in such plasmas, it was possible to determine whether a simple diffusive model in which the thermal diffusivity is a function of the local values of electron temperature and its gradient provided an adequate description of thermal transport in JET. It was found that this was indeed the case and that the contribution of a heat pinch term must be very small.

Non-dimensional scaling experiments aimed to explore the processes responsible for anomalous thermal transport, by comparing local thermal transport coefficients in plasmas, in which selections of fundamental parameters, such as β, ν^* or ρ^*, were held constant while another was varied. Studies in JET focussed on the identification of the variation of local transport with normalized local Larmor radius, ρ^* ($=\rho_i/a$), since this should permit the scale-length of the turbulent processes involved in anomalous transport to be calculated. In these experiments, which utilized on-axis ICRF heating (to maintain a constant heating profile) at several magnetic fields, the variation of local radial heat flux in the various discharges was best described by a model in which the local thermal diffusivity did not depend on the normalized Larmor radius - the so-called Bohm scaling.

The experimental difficulties inherent in determining particle transport coefficients have restricted the depth of understanding of particle confinement. However, it is known that particles are confined more effectively in JET plasmas than is energy. Moreover, it is emerging that the control of particle fluxes may be a more severe problem in Next Step devices than the achievement of high energy confinement. Not only must the fuel concentrations be controlled, but impurities must be screened and helium must be efficiently exhausted to prevent fuel dilution. In spite of its importance for maintaining ignition, little quantitative data exists on this last problem, but recent studies have yielded some insight.

Experiments have been performed in sawtooth-free plasmas, in both L- and H-modes, utilizing helium neutral beam injection. Local measurements of the helium density profile can be derived from active charge exchange recombination spectroscopy (CXRS), although the complexities of analyzing the emission spectrum are considerable and the resultant uncertainties great. Nevertheless, it was observed that, in L-mode discharges with helium NBI, the helium density profile could be simulated using a diffusion coefficient of 0.3 ± 0.1 m^2s^{-1}. However, the decay of the helium density profile following the termination of central helium fuelling, required a diffusion coefficient, which was a factor of 4-5 larger. The source of this discrepancy is not understood, but the non-stationary plasma conditions may be relevant. In H-modes, it was not possible to establish a helium density profile with measurable peaking, indicating that particle fluxes in the bulk plasma must be large. Therefore, in such a situation, helium exhaust is expected, to be dominated by edge transport, which cannot be addressed adequately in the present JET configuration. However, the active pumping expected to be available in the divertor phase should permit a more thorough investigation of this question.

H-Mode Studies

H-modes in JET are usually ELM-free and this leads to monotonically rising density and radiation, which causes the H-mode to collapse on a timescale of 3-5s. It is recognized that for Next Step devices it will be necessary to establish a long-pulse steady-state H-mode and that this will most probably be achieved by utilizing regular ELM activity to degrade the edge confinement barrier. In JET, it has been possible to establish such a regime for periods of up to 18s by combining moderate to high power heating (ICRH and NBI) with gas-puffing at rates of ~50-100mbℓs^{-1}. In this regime, the majority of plasma parameters, e.g. density, temperatures, energy, fusion yield, impurity content and radiation could be maintained in quasi-steady state.

It was found that energy confinement was generally in the range of 1.4-1.7 times that predicted by the Goldston L-mode scaling, so that, as anticipated, some degradation of energy confinement accompanies the degradation of particle confinement, which permits the maintenance of the steady state. It was also observed that large amplitude MHD activity could grow and that this was related to the total input power, the problem being more severe at lower power. This MHD activity was responsible for the degradation from 1.7 to 1.4 times Goldston L-mode scaling observed in the longest H-modes. Furthermore, ICRF heating was applied significantly off-axis in these experiments to reduce the influence of sawtooth activity on edge MHD and this is also expected to contribute part of the degradation of energy

confinement relative to ELM-free H-modes. An additional important observation was that during the last few seconds of the H-mode, the plasma density started to rise, indicating that wall-pumping had saturated and that further extension of this regime in time would require active pumping.

Experiments have been performed to investigate the change in edge conditions associated with the L-to-H transition. In particular, the change in ion collisionality at the plasma edge associated with the transition has been investigated using local measurements of ion temperature obtained from a new, high resolution edge CXRS diagnostic. In a sequence of sawtooth-free plasmas (to eliminate the tendency of sawtooth heat pulses to trigger the H-mode transition), the H-mode transition was increasingly delayed relative to the start of additional heating as the target density fell. More significantly, increasing delay until the H-mode transition correlated with decreasing normalized ion collisionality, in contrast to predictions derived from certain theories of the L-to-H transition, which are based on the model of a change in edge poloidal velocity shear resulting from an increasing radial electric field gradient in the plasma edge.

MHD Stability

The discovery of the phenomenon of 'monster' sawteeth, in which sawteeth are stabilized by central heating with ICRF or NB power, has stimulated extensive experiments to clarify the underlying stabilization mechanism. This has led to the development of the idea that sawteeth can be stabilized by a population of energetic particles which are accelerated by ICRF waves or by NB injection. This theory predicts that stabilization is associated with a peaked profile of fast particles within the q=1 surface, but that the m=1 mode becomes more unstable as the q=1 radius expands, as can occur due to resistive diffusion of the current profile. Recent experiments have investigated this prediction by switching off the ICRF heating at varying times during sawtooth-free periods, to observe the delay until a sawtooth collapse occurs. To relate the experimental observations to theory, polarimetric measurements of the evolution of the q=1 radius and magnetic measurements of the fast particle content have been used to construct a model of the behaviour of these critical quantities during the ICRF pulse. On this basis, these experiments have shown that the behaviour of the delay from RF switch-off until the sawtooth collapse is consistent with that expected from the fast particle stabilization theory.

Pumped Divertor and Next Step Physics Studies

Pumped Divertor Studies

Considerable efforts have been made during the campaign to establish an experimental database for the validation of the modelling of the Pumped Divertor. Detailed experiments have studied, for example, divertor impurity retention, the effects of the ion ∇B-drift and the relative merits of carbon and beryllium as divertor target materials. A key experiment has been the attempt to establish a 'gas target', or radiative divertor plasma. The requirement for such an approach arises from the excessive power densities, in excess of $10MWm^{-2}$, to which divertor targets in Next Step devices will be exposed unless a substantial fraction of the power efflux is radiated. The constraints on bulk plasma impurity concentration, plasma density and MHD stability imply that most of this radiation will have to occur outside the separatrix (i.e. in the divertor).

The most successful attempts to establish a radiative divertor utilized the beryllium target in a single-null X-point configuration. In the majority of experiments, a preprogrammed gas-puff was applied from the commencement of additional heating and was increased with increasing heating power. For example, over the range 12 to 22MW, the gas-puff rate was increased from 180 to $360mb\ell s^{-1}$. The regime could be maintained in a stable state with less than 1MW of power conducted to the divertor if the gas-puff rate was subsequently reduced to that required to replace particles lost by wall pumping. Quasi-steady state operation was demonstrated at powers of up to 22MW and for pulse lengths of up to 4s. In a more advanced scenario, a control loop was established using thermal radiation from the divertor target to maintain the gas-puff rate. This permitted the gas target regime to be brought under feedback control. The demonstration of this regime is of major significance for the development of reactor-relevant scenarios. However, to date, it has not been possible to combine the radiative divertor with high confinement H-modes, since the bulk plasmas in these discharges either remained in the L-mode or exhibited ELMy H-mode behaviour with a confinement enhancement factor of 1.4.

Toroidal Field Ripple Experiments

Establishing the acceptable amplitude of toroidal field ripple for a tokamak reactor is fundamental to the design of a Next Step tokamak. By operating JET with 16 (rather than 32) toroidal field coils, it was possible to compare plasma

performance with theoretical predictions, particularly in relation to fast particle confinement. Experiments were performed in L- and H-mode, using ICRF and NB heating in plasma configurations with 16 and 32 coils. In the former case, the edge toroidal field ripple was 15%, while in the latter less than 1%.

In L-mode plasmas with 16 coils, central ion heating with NB injection was reduced relative to plasmas with 32 coils and the efficiency of ICRF heating fell significantly as the minority ion resonance was moved to larger major radius. Both effects led to a significant degradation of energy confinement with 16 coils compared to the 32 coil case. Moreover, it was observed that, in the former case, the plasma rotation was suppressed across the entire plasma. The reduction of fast particle confinement due to the enhanced ripple, as measured either by triton burn-up measurements or neutral particle analysis, was in line with expectations and fast ion spectra were in agreement with the predictions of stochastic ripple diffusion theory. However, in NB-heated L-mode discharges, a loss of 30% of stored energy was observed for the 16 coil case. This is larger than that expected on the basis of beam fast ion losses and is not understood.

A striking difference in H-mode behaviour between the 16 and 32 coil cases was also observed. Whereas, with 32 coils, ELM-free H-modes with high energy confinement could be achieved readily at NB powers of 1.5MW, only ELMy H-modes could be obtained with 16 coils, even at NB powers as high as 12MW. The energy and particle confinement of these H-modes was significantly poorer than in the 32 coil plasmas. It is believed that enhanced fast ion transport due to the loss of ripple well trapped ions may be responsible, since this would not permit a high edge temperature gradient to develop.

7MA Limiter Plasmas

Although 7MA plasmas were first produced several years ago, recent improvements in the design of the vessel protection tiles and the advances made in disruption control during the present programme have increased the margin of safety for high current operation and have allowed more extensive experimentation at 7MA than had previously been possible. Significant progress has been made as a result. The flat-top duration of 7MA plasmas has been extended to nearly 9s, by employing LHCD and additional heating to reduce flux consumption, and additional heating experiments have been carried out at total powers of up to 28MW. Energy confinement of these discharges is good, with total stored energies of up to 12MJ being achieved (close to the highest H-mode value of 12.7MJ).

In addition to their significance as a technical achievement, these experiments provided an opportunity to explore how energy confinement varied with plasma current at currents beyond those previously explored in tokamaks. As q_ψ is close to 3 (~3.3) they also permit the influence of the large sawtooth inversion radius to be investigated. By comparing the thermal energy confinement with that obtained in similar 5 and 6MA limiter plasmas, it was shown that, at the highest powers the stored energy increases with plasma current. Moreover, the stored energy increases linearly with power and the offset term (P_{loss}=0) is small. At the highest powers the energy confinement of these discharges is in line with that expected on the basis of common scaling laws (e.g. Goldston, ITER-P). Analysis of local transport finds that the thermal diffusivity outside the sawtooth region is independent of power. In addition, comparison with the results of modelling based on Rebut-Lallia scaling shows that this model gives good agreement with profile and global plasma parameters for the high power experiments.

The major problem observed during these experiments lay in the domain of power handling, Since the plasma position could not be optimized to share power between the beryllium and carbon limiters (since the plasma-wall clearance at the top and bottom of the vessel was insufficient), substantial melting of the beryllium limiter occurred in high power experiments. As a result, relatively poor values of n_D/n_e were obtained, the plasma density was high and the ion temperature was low. Therefore, the best value of the fusion triple product produced at 7MA current was $n_i(0)T_i(0)\tau_E$ ~$1\times10^{20}m^{-3}keVs$, substantially below the best values achieved in 3MA H-mode plasmas.

Conclusions

The experiments described are the highlights of the last few weeks of the 1991/1992 experimental programme. During the 1991/1992 campaign, experiments have ranged over wide areas of tokamak physics. The programme for this period, the final experimental period before the major upgrade to the pumped divertor phase, encompassed several objectives, all of which were successfully accomplished. Amongst the major achievements of this campaign were: the first demonstration of the use of tritium in a tokamak and the production of 1MW of fusion power; the performance of extensive high power heating experi-

ments at 7MA; the demonstration of high current (2MA) AC operation of the tokamak; the detailed comparison of carbon and beryllium as divertor target materials and an extensive exploration of divertor physics; the investigation of the effect of large field ripple on thermal and fast particle confinement; the attainment of long pulse operation in both L- (60s) and H-modes (18s); and the demonstration of minority ion current drive using an ICRF phased array.

In addition, a wide range of tokamak physics issues has been addressed, covering fundamental processes influencing energy and particle transport. MHD stability and the H-mode transition; exploring the limits of β_p and β_t in tokamaks and the processes which limit the values attainable; optimizing the efficiency of RF (LHCD and ICRF) current drive; exploiting current profile modifications to influence MHD stability; and investigating the parameters which influence the performance of the divertor in terms of power handling and impurity screening.

These studies have significantly advanced knowledge of tokamak physics and have improved technological capabilities, laying the foundation for a successful transition to the new phase of JET, which will exploit the pumped divertor to address key questions relating to the control of heat and particle exhaust and of impurity influxes.

Progress towards a Reactor

During the 1991/92 campaign, significant progress was made in determining the conditions required in a reactor. By using tritium, it had been possible to check predictions made in previous years concerning the power output and to assess whether the thermonuclear Q in JET with a D-T

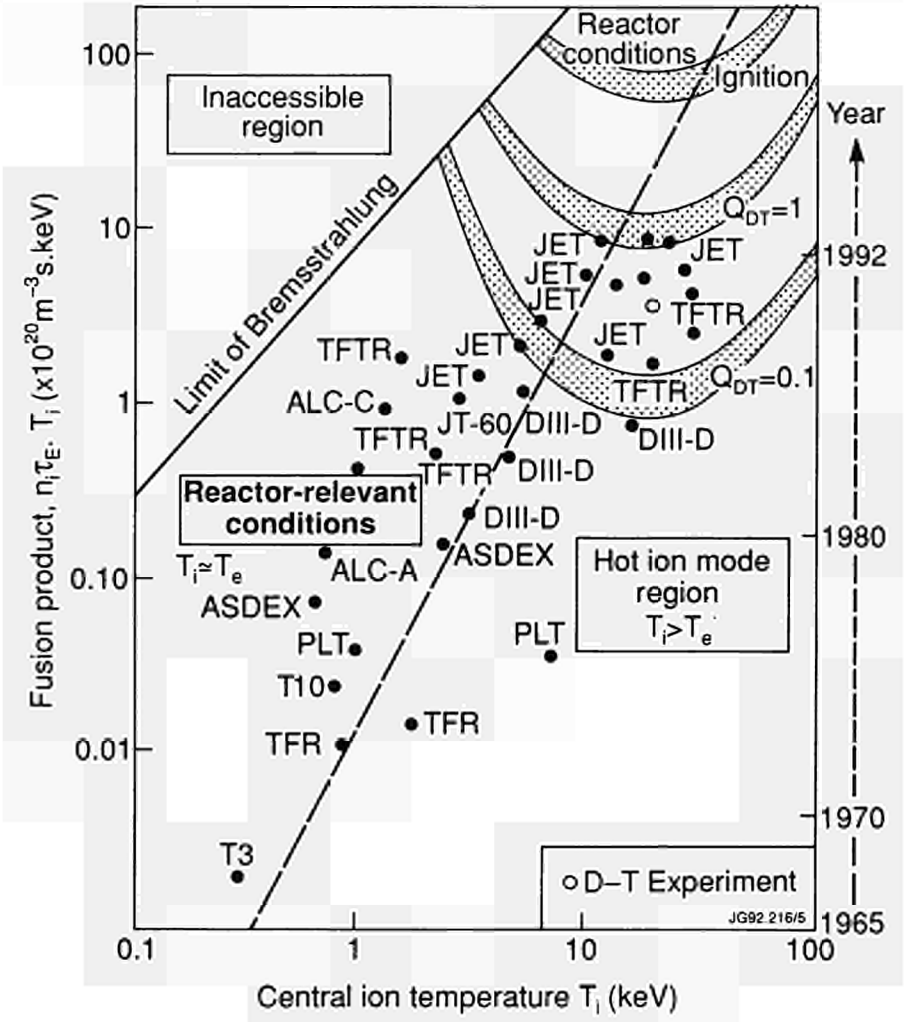

Fig.215: Triple fusion product ($n_D T_i \tau_E$) as a function of ion temperature, T_i for a number of tokamaks worldwide.

mixture were actually valid. In particular, the tritium experiments enabled detailed checks of computer codes used in predictions of D-T performance. The outcome was that indeed the previous code predictions of Q_{DT} close to breakeven have been fully justified. During 1992, further analysis of the high performance discharges obtained during the first tritium series of experiments was completed. The overall picture was unchanged with the hot-ion H-mode plasmas having the highest Q_{DD} ($5x10^{-5}$) and the extrapolated Q_{DT} was 1.14.

In early 1992, a series of 7MA limiter L-mode plasmas with high power combined ICRF and NB heating was developed. Although these pulses achieved a high stored energy (~12MJ) the $n_D T_i \tau_E$ was $<1.4x10^{20} m^{-3} keVs$ at a temperature of 4.5keV. The main problem encountered was the high impurity levels giving rise to a low deuterium concentration $n_D/n_e<0.5$.

The actual preliminary tritium pulses had a somewhat lower Q_{DT} than the highest values obtained. The actual equivalent value Q_{DT} was 0.46. This was due to the reduced value of the fusion product $n_D T_i \tau_E$ in these particular pulses caused by the early onset of the "carbon bloom". The $n_D T_i \tau_E$ values of the high performance pulses in both impure deuterium and in the D-T pulses are compared in Fig.215 with data from other machines to illustrate the progress that has been made over the last 30 years.

Developments and Future Plans

In 1978, the original objectives of JET were set out in the JET Design Proposal, EUR-JET-R5, as follows:

'The essential objective of JET is to obtain and study a plasma in conditions and dimensions approaching those needed in a thermo-nuclear reactor. These studies will be aimed at defining the parameters, the size and the working conditions of a Tokamak reactor. The realisation of this objective involves four main areas of work:

i) the scaling of plasma behaviour as parameters approach the reactor range;

ii) the plasma-wall interaction in these conditions;

iii) the study of plasma heating; and

iv) the study of α-particle production, confinement and consequent plasma heating.

The problems of plasma-wall interaction and of heating the plasma must, in any case, be solved in order to approach the conditions of interest.

An important part of the experimental programme will be to use JET to extend to a reactor-like plasma, results obtained and innovations made in smaller apparatus as a part of the general tokamak programme. These would include: various additional heating methods, first wall materials, the control of the plasma profiles and plasma formation.'

At the start of 1992, the Project had almost completed its planned Phase III - Full Power Optimization Studies. The general objectives of the experimental programme were to optimize performance and to explore the domain of high performance plasmas, studying aspects of plasma physics and engineering including: profile and heating effects; exhaust phenomena; and divertor edge physics. Priority was given to study of the power and energy handling capability of newly installed plasma facing components in regimes relevant to the Next Step and to the New Phase of JET.

Extensive studies had been made in the first and third areas of work of JET's objectives: reactor relevant temperatures (up to 30 keV), densities (up to $4 \times 10^{20} m^{-3}$) and energy confinement times (up to 1.7s) had been achieved in separate discharges. The second area of work had been well covered in the limiter configuration for which JET was originally designed. However, the highest performance JET discharges had been obtained with a 'magnetic limiter', (or X-point configuration). The duration of the high performance phase of these discharges exceeded 1.5s; this was achieved by careful design of the targets and specific operation techniques, but is limited, ultimately, by an unacceptably high influx of impurities, characterized by a rapid increase in electron density, effective ionic discharge and radiated power (referred to as the 'bloom').

The fourth area of work had been started by earlier studies of energetic particles produced as fusion products or by ion cyclotron resonance heating (ICRH). It was addressed further during 1991 by the first tokamak plasma experiments in deuterium-tritium mixtures. The high performance achieved in deuterium discharges, together with the experience gained in making substantial modifications to JET in a beryllium environment and with significant vessel activation, gave confidence that an experiment with about 10% tritium in the plasma could be performed and would provide data that could be used to plan an effective campaign of deuterium-tritium experiments in 1996.

During 1991, the JET Council had approved the policy of a step-wise approach to the introduction of tritium in advance of the full D-T phase of JET operations. As a first such step, after having obtained all necessary regulatory approvals, JET successfully carried out a preliminary tritium experiment (PTE-1) in November 1991 (as already described). A release of fusion energy in the megawatt range in a controlled fusion device had been achieved for the first time in the world.

The most recent experiments on JET achieved plasma parameters approaching breakeven values for about a second, resulting in large bursts of neutrons. However, in spite of the plasma pulse continuing for many seconds after reaching peak plasma values, the neutron count fell away rapidly as impurities entered the plasma and lowered its performance. This limitation on the time for which the near-breakeven conditions could be maintained is due to the poisoning of the plasma by impurities (the 'bloom'). This has further emphasised the need to provide a scheme of impurity control suitable for a Next Step device.

At its meeting on 19th December 1991, the Council of Ministers adopted Decisions concerning the Euratom Fusion Programme in the period to the end of 1994 and a modification to the Statutes of JET, which prolonged its statutory lifetime by four years until 31st December 1996. The extension will allow JET to implement the new Pumped Divertor Phase of operation, the objective of which is to establish the effective control of plasma impurities in operating conditions close to those of the Next Step. This programme of studies will be pursued before the final phase of full D-T operations in JET.

During 1992, a large proportion of JETs effort was devoted to shutdown work for the new pumped divertor phase of operations. The first stage of the shutdown in 1992 involved removal of components and replacement of faulty toroidal magnetic field (TF) coils. The second stage involves assembly of the four divertor coils and casings inside the vacuum vessel and this was in progress at the end of the year. It is believed to be the first time that a full manufacture and assembly of coils has been undertaken in such a confined space, and the work is being done to demanding standards to ensure the highest reliability during subsequent operations. Intensive design and procurement activities for the pumped divertor components to be installed in the third stage of the shutdown have continued.

Present achievements show that the main objectives of JET are being actively addressed and substantial progress is being made. The overall aim for JET can be summarised as a strategy "to optimise the fusion product ($n_i T_i \tau_E$). For the energy confinement time, τ_E, this involves maintaining, with full additional heating, the values that have already been reached. For the density and ion temperature, it means increasing their central values $n_i(0)$ and $T_i(0)$ to such an extent that D-T operation would produce alpha-particles in sufficient quantities to be able to analyse their effects on the plasma.

The enhancements to JET aim to build up a high density and high temperature plasma in the centre of the discharge (with minimum impurity levels) where alpha-particles could be observed, while maintaining an acceptably high global energy confinement time τ_E. The mechanisms involved are to decouple the temperature profile from the current density profile through the use of lower hybrid current drive and neutral beam injection to ensure that, at higher central temperatures, the current density in the centre does not reach the critical value that causes sawteeth oscillations.

This involves the following:

a) Increasing the Central Deuterium Density $n_D(0)$ by:
   - injecting deuterium pellets and high energy deuterium beams to fuel the plasma centre and dilute impurities;
   - injecting pellets to control the influx of edge material;
   - stabilising the m=2, n=1 magnetic oscillations present at the onset of a disruption with magnetic perturbations produced from a set of internal saddle coils which will be feedback controlled;

b) Increasing the Central Ion Temperature, $T_i(0)$ by:
   - trying to lengthen the sawtooth period;
   - controlling the current profile (by lower hybrid current drive in the outer region, and by counter neutral beam injection near the centre) to flatten the profile;
   - on-axis heating using the full NB and ICRF additional heating power (24MW, ICRH, and 20MW, NB)

c) Increasing the Energy Confinement time τ_E by:
   - increasing to 6MA the plasma current in full power, H-mode operation in the X-point configuration;

d) Reducing the impurity content, by:
   - using beryllium as a first-wall material to decrease the impurity content;
   - controlling new edge material by using the pumped divertor configuration.

In parallel, preparations for the full D-T phase of operations have continued. In particular, JET has completed installation of all the main components of the active gas handling system and commissioning is underway. At the end of the shutdown, JET will be in a position to begin its programme of operations to demonstrate effective methods of power exhaust and impurity control in operational conditions close to those envisaged for ITER before the final phase of full D-T operations. ITER relevant studies will provide stimulation to JET and JET's results will make an important contribution to the development of the ITER design. The following sections describe various developments underway on JET to implement these systems.

Current Drive and Profile Control

The main objectives of current drive and profile control remain:

- to suppress sawtooth activity and to benefit from higher core reactivity by sustaining peaked profiles of both density and temperature;
- to modify local values of the current gradient and improve energy confinement in the plasma centre;
- to assess the efficiency required for non-inductive operation of large tokamaks.

At the 1992 IAEA Conference on Plasma Physics and Controlled Nuclear Fusion Research (Würzburg, Germany), all major experiments, including JET, presented data showing that proper shaping of the plasma current leads to improved plasma confinement, at least on a transient timescale. Maintaining these improved confinement scenarios (high poloidal beta plasmas, central shear reversal (PEP's mode) in quasi-steady-state) is challenging and might lead to a significant enhancement of reactor operation.

Non-inductive current drive efficiencies are of paramount importance in order to assess the feasibility of a steady-state tokamak reactor at ignition. Such estimates [1,2] indicate that steady-state operation is only possible if:

- improved current drive efficiencies at high density in low aspect ratio tokamaks are demonstrated;
- improved confinement properties together with stable high bootstrap operation are demonstrated;
- advanced divertor technology allows low density operation to be feasible.

The main tool which is being prepared to control the plasma current profile in JET is the generation of non-inductive plasma current by means of Lower Hybrid (LH) waves. First results with a prototype system (LO) have already been obtained. The full system (L1) will be installed during the 1993 shutdown. A high directivity ICRF antenna is also being prepared to drive a substantial amount of non-inductive current by means of either minority current drive or direct electron magnetic pumping. These antennae (A2) will also be installed during the 1993 shutdown. Non-inductive current drive can also be produced by neutral beams (NB) and by the bootstrap current.

A large quantity of data on current drive has been obtained during the 1991/2 experimental campaign, including the achievement of:

- 2MA full current drive discharge with LHCD in combination with ICRF heating;
- discharges where the bootstrap current was up to 70% of the total current in ICRF heated plasma. The corresponding energy confinement time was up to 1.7 times H-mode scaling;
- good control of sawteeth by producing localised minority ion current drive near the q=1 surface [3].

These data are encouraging for profile control and current drive application to future large experiments. Synergistic effects between LH and ICRF waves might lead to improved current drive efficiencies. As well, the proposed scenario to drive the full current in a reactor can be assessed during the pumped divertor phase of the JET campaign. This will involve:

- a seed current generated at the plasma centre by ICRF fast wave current drive (independent of density) or NBI current drive;
- large bootstrap current, in excess of 50% of the total required current, generated near mid-radius;
- LH current drive generated in the outer plasma region.

ICRF Current Drive

During the 1991/92 experimental campaign, the ICRF control system was upgraded to allow the antenna straps to carry currents of equal amplitude but arbitrary phase in a limited range of plasma conditions [3]. With this facility, travelling waves were launched into JET to perform current drive experiments. Fast magnetosonic waves can drive plasma current either by direct damping on the electrons or by asymmetrical heating of the minority ions. In the first method, the waves are absorbed at the Landau resonance and drive current by a combination of parallel momentum transfer and asymmetric heating in a completely analogous way to Lower Hybrid Current Drive (LHCD). The principle difference between fast wave current drive and LHCD is in the interaction mechanism, which for fast waves is a coherent admixture of Transit Time Magnetic Pumping (TTMP) and Electron Landau Damping (ELD). Fast wave damping by electrons is weak in JET but has been observed in experiments using phase velocities close to the electron thermal velocity. Substantially increased damping will occur in reactor grade plasmas, especially at the higher phase velocities appropriate for current drive, where the power deposition will be peaked on-axis regardless of the plasma density; the fast wave has no accessibility problems at high density [4]. Consequently this method is especially attrac-

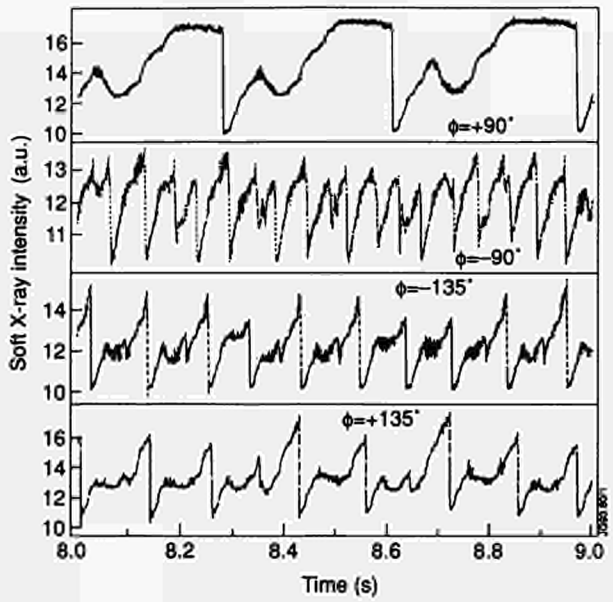

Fig.216: Sawtooth control using second harmonic fast wave ion current drive.

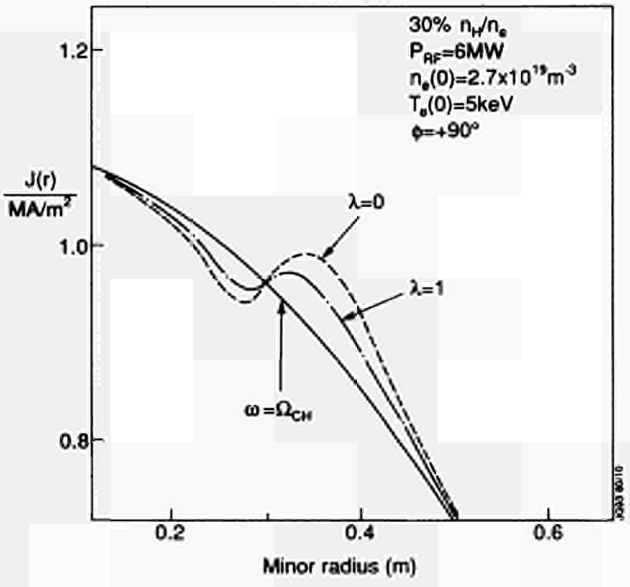

Fig.217: Fast wave non-inductive current profile superimposed on the ohmic current density profile.

tive for seeding the bootstrap current, which is presently seen as providing the bulk of the plasma current in a steady-state tokamak.

Experiments on ion current drive by asymmetric cyclotron heating have been carried out on JET and have successfully demonstrated, for the first time, many of the features of this method [5]. The non-inductive current profile is bipolar and strongly localised at the resonance layer. In the experiments, the current was driven close to the q=1 surface in order to affect the stability of the sawteeth. With waves directed in a clockwise direction (viewed from above the tokamak), the sawteeth were destabilised becoming higher in frequency and smaller in amplitude. With waves travelling anticlockwise, stability was increased and monster sawteeth were produced. Similar behaviour was found with both fundamental minority and second harmonic ICRF heating. An example of the latter is shown in Fig.216. With a phase of 90° between current straps, the sawtooth period was changed by a factor of five as the direction of the waves was reversed by changing the sign of the phasing. With 135° phasing, the sawteeth were unaffected and provided a reference case since the directivity of the antenna was much weaker than for $\varphi = 90°$. This correlation between the sawtooth stability and the wave direction has been modelled theoretically [6] on the basis of magnetic shear stabilisation of the resistive kink instability, which is thought to be responsible for the sawtooth crash.

A characteristic feature of fast wave ion current drive, expected theoretically, is an optimum fast ion energy at which the current per unit power is a maximum. Experimental evidence for this was obtained by scanning the RF power. Travelling waves in the anticlockwise (stabilising) direction created monster sawteeth for power levels between 2.5MW and 5MW. Above 5MW, the sawtooth period decreased with increasing power. A scan of minority concentration at fixed power (5MW) also showed a decrease in the stabilising effect as the minority density was raised, again as expected theoretically.

Theoretical calculations of the non-inductive current have been made using ray tracing and 2-D bounce averaged Fokker-Planck codes. A typical current density profile is shown in Fig.217 superimposed on a JET ohmic current profile. Clearly the RF driven current will substantially modify the current density profile and even produce a

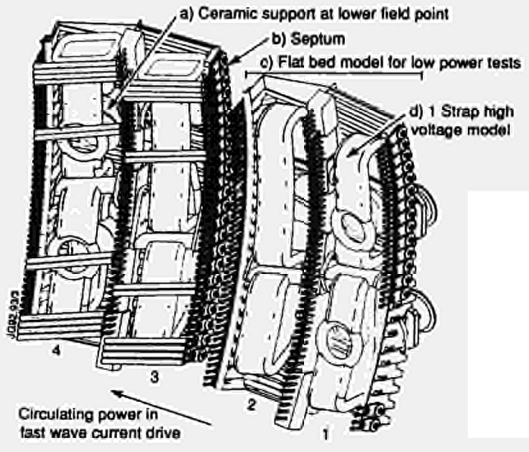

Fig.218: A2 antenna module showing current strap geometry, Faraday shields and disruption protection resistors.

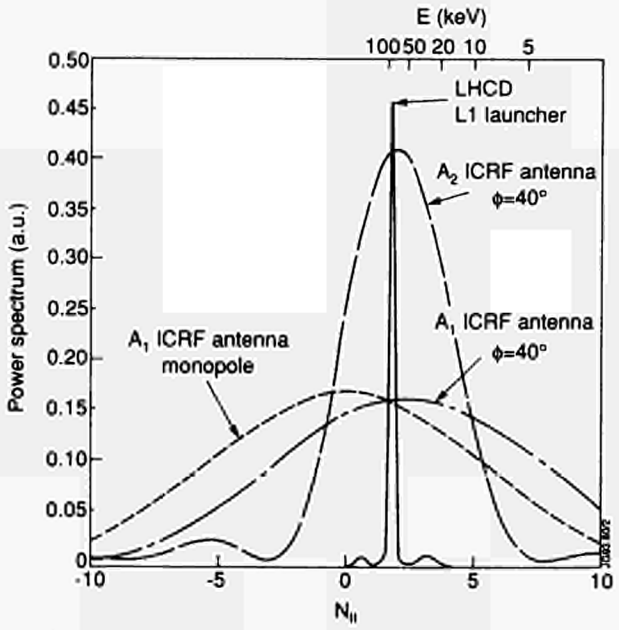

Fig.219: Comparison of $N_{//}$ spectra from the A1 and A2 antennas and the Lower Hybrid launcher.

positive gradient at the q=1 surface. Perturbations of about 100kA/m^2 can either cancel or double the local shear produced by the ohmic current, depending on the wave direction. Such changes can account for the observed changes in sawtooth stability on the basis of resistive kink mode theory.

The new A2 antenna [7] will bring several improvements to both the electron and ion fast wave current drive schemes as well as to the synergism with LHCD [8]. These antennae will be mounted in adjacent pairs to give four phased current straps instead of two, with the toroidal spacing between straps similar to that in the A1 design as shown in Fig.218. As a result the $k_{//}$ wavevector spectrum will be a factor 2-3 narrower than for the A1 as shown in Fig.219. For 90° phasing, the peak power occurs close to $k_{//} = 4m^{-1}$, as in the A1 design but, for equal total radiated powers, the maximum spectral power density is increased twofold. For the electron current drive scheme, this means that twice as much power is available to accelerate the electrons of interest. This will be particularly effective in synergism experiments, where success depends on damping the fast wave on electrons driven by lower hybrid waves, a condition which requires the best possible overlap of the $N_{//}$ spectra of the ICRF and LHCD launchers. The maxima of the A1 and A2 spectra coincide with the LHCD spectrum for a phasing of ≈40° and in this situation, the A2 antenna should be twice as efficient as the A1 in accelerating the LHCD superthermal electrons.

The A2 system will also be fitted with a power compensator between the outer lines of each set of four, as shown in

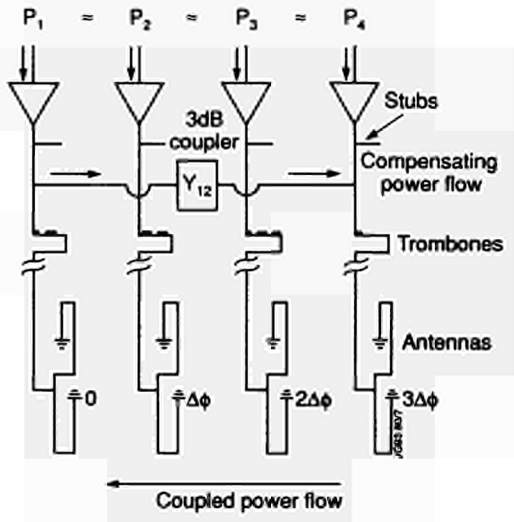

Fig.220: Schematic of a four-strap A2 antenna, generators, transmission lines, power compensator and tuning elements.

Fig.220. Due to the coupling between the antenna straps, phasings used to launch travelling waves necessarily produce a power flow from one side of the antenna to the other, as indicated. Without a compensator, the generators need to be run at unequal power levels to produce equal currents in the straps as required for good directivity. This is particularly true at low plasma coupling resistance. Thus, the maximum power available is limited in just the situation where the antenna directivity is maximum, since at low coupling the plasma tends to filter out unwanted high k_z components due to image currents.

The power compensator counters the power coupled across the array by transferring power between the end feedlines at a location close to the tuning stubs. There is no need to compensate the inner lines since the inner straps are essentially transparent to the power flow. The compensator consists of a 3dB coupler with adjustable capacitors on two of the four ports to control the magnitude and direction of the power flow.

The system has been designed in collaboration with Oak Ridge National Laboratory (ORNL), USA, under a JET-USDoE agreement. In this collaboration, JET has the use of extensive ORNL modelling tools and ORNL will participate in RF physics and technical experiments at JET. These tools include two models of the A2 antennae [9]. One model treats the array as cascaded coupled transmission lines with each segment of a strap coupled to the corresponding segment of the other straps. A more sophisticated model takes the complex geometry into account by including the effect of coupling between straps, between different sections of the same strap and between the straps and the

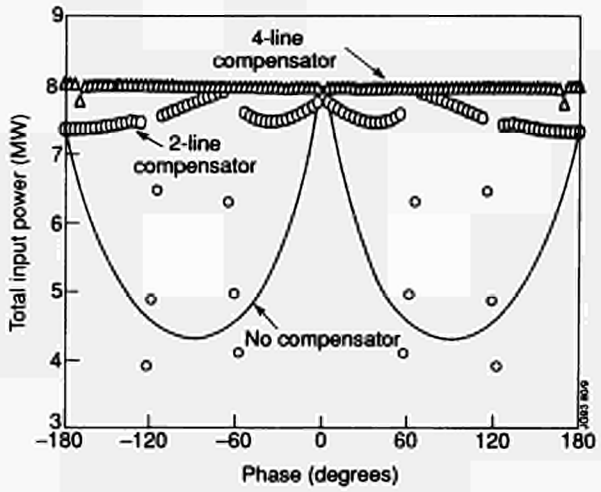

Fig.221: Effect of the power compensator to increase the total power capability in current drive phasing mode.

connecting links. A 2-D magnetostatic code is used to calculate the mutual and self-coupling coefficients. The more complex model has been particularly successful in reproducing the measured coupling coefficient (S_{12}) of a two-strap array representing half of the A2 antenna. In JET, a third model is under development which solves the full electromagnetic problem in a simplified geometry but includes the coupling to the plasma. The presence of plasma both reduces the coupling and filters out the unwanted high $k_{//}$ components due to image currents.

The impedance matrix at the input to the antenna, given by these models, is used as the load in a simulation of the power delivery system comprising the generators transmission lines, power compensator, variable capacitors and tuning elements (trombones and stubs). This simulation calculates the values of the capacitors for equal powers from the generators and equal antenna currents at the lower strap ground connections, and also derives the trombone and stub lengths for matching to the generators. One of the first results of this code was that the present trombones were too short (0.5m) to obtain matches over the whole frequency and phasing ranges. Consequently, trombones with a range of 1.5m are being ordered. The effectiveness of the power compensator is shown in Fig.221, where the maximum power with and without the compensator is plotted against the phase difference between straps. A factor two increase in power can be gained by using compensation at $\pi/2$ phasing. There is little advantage in adding compensators to the inner straps and the compensator is unable to operate at 60° and 120°. In these cases, the phase difference between the outer line voltages is 180° and 0°, respectively, so that there is no power flow through the compensator.

The new system is designed to operate with an upgraded version of the A1 automatic phase, amplitude and matching control circuits. An additional servo is required to maintain equal generator powers by tuning the variable capacitors, but this will operate on a relatively slow time-scale since the priority will be to achieve a match, albeit with a transient unbalance of the generator powers.

Design of the A2 antenna has been completed. A model of one quadrant has been extensively tested at high RF power and has been shown to sustain 20s pulses at 50keV. Manufacture of the antennae is well advanced with the prototype due for delivery in February 1993. The first production unit will be delivered in February 1993 and completed in May. The high power model tests show that the most critical components in the antennae are the resistors, which restrict disruption currents flowing in the screens. Tests of individual resistors for RF losses and eddy current losses showed that beryllium oxide resistors could withstand 20% more current than the alumina resistors chosen initially. Such beryllium resistors are being fitted to the A2 antennae. Measurements using Rogowski coils on a full scale low power model show much lower resistor currents.

Four new transmission lines and modifications to 16 existing lines are being made to accommodate the new A2 antennae. The conical ceramics in the A1 vacuum transmission lines have been replaced by ceramics inside the antenna and these have been positioned so that the RF electric field on the surface of the ceramics is always perpendicular to the ambient tokamak magnetic field in order to reduce high voltage breakdown. The removal of the conical ceramics makes the transmission lines more open to the torus which, in general, will produce a better vacuum in the transmission lines but at a cost of increased sensitivity to changes in the vessel pressure, for example during gas fuelling.

Lower Hybrid Current Drive

The prototype Lower Hybrid Current Drive (LHCD) system operated during the 1991/1992 experimental campaign. The campaign has enlarged the existing database providing a firmer basis to earlier results. Flux saving experiments during the current ramp-up in the 7MA experiments were also performed at the end of the experimental period. The main characteristics of the LHCD system are listed in Table XXI [10]. The prototype system has most of the main technical features of the complete system, which is being tested in the first half of 1993 and will be installed on JET at the end of the 1993 shutdown.

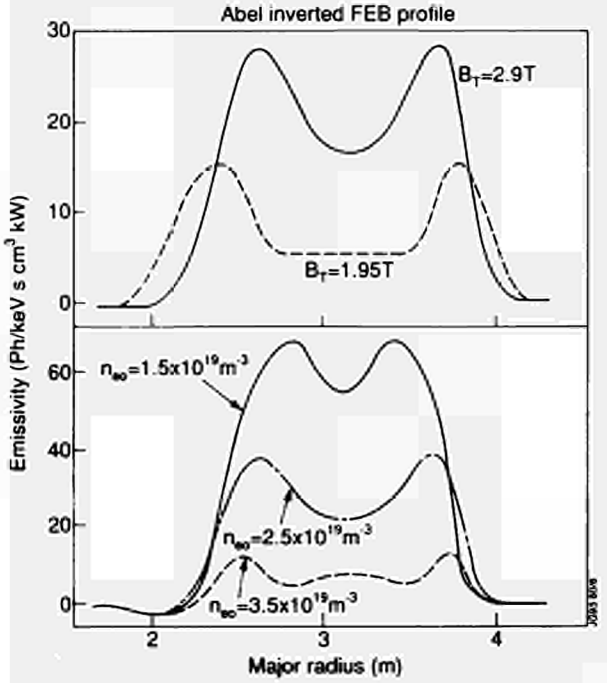

Fig.222: Influence of the magnetic field and of the plasma density on the radial profiles of fast electrons.

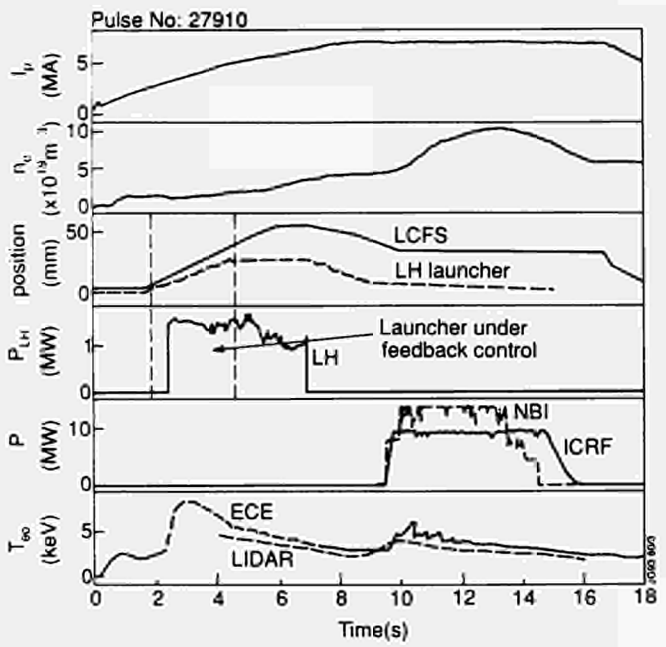

Fig.223: LH power during ramp-up of a 7MA discharge. Launcher position has followed closely the last closed flux surface.

The Lower Hybrid campaign during the last operational period was characterised by two main lines of activities [2]. The first activity was assessing the LHCD system performance level in terms of current drive, flux saving and current profile control capability, to provide a database for realistic extrapolations for current drive and active current profile control experiments during the pumped divertor phase and, on a longer time-scale, to reactor applications. The second line of activity has concentrated on the characterisation of the fast electron population to investigate current drive physics issues, such as the dependence of lower hybrid wave penetration upon global plasma parameters and wave spectrum, and the comparison with theoretical and computational models. The main diagnostic tools during the campaign were the magnetic diagnostics, providing information on the loop voltage and plasma internal inductance, the electron cyclotron emission (ECE) diagnostic and the fast electron Bremsstrahlung (FEB) cameras, the latter developed specifically for Lower Hybrid operation.

Most of the Lower Hybrid campaign was carried out in conjunction with Ion Cyclotron Resonance Frequency (ICRF) [11] operation, to provide a high electron temperature plasma

Table XXI - Parameters of the JET LHCD system

	Prototype	Final
Frequency	3.7 GHz	3.7 GHz
N. of Klystrons	8	24
(launched) Power (max)	3.5 MW	10 MW
Launcher waveguides	128	384
Multijunction phasing	90°	90°
Central $N_{//}$	1.8	1.8
Range in $N_{//}$	1.4 - 2.3	1.4 - 2.3
Width of $N_{//}$ spectrum	0.4	0.2
Phase accuracy	10°	10°
Directivity	70%	80%
Density limit	8 x 10^{20} m^{-3}	8 x 10^{20} m^{-3}
Power Handling	4 - 5 kW cm^{-2}	4 - 5 kW cm^{-2}
(Estimated) driven current (in ICRF heated plasmas)		
at n_e = 2 x 10^{19} m^{-3}	2 MA	(5 MA)
at n_e = 4 x 10^{19} m^{-3}	(1 MA)	(2.5 MA)

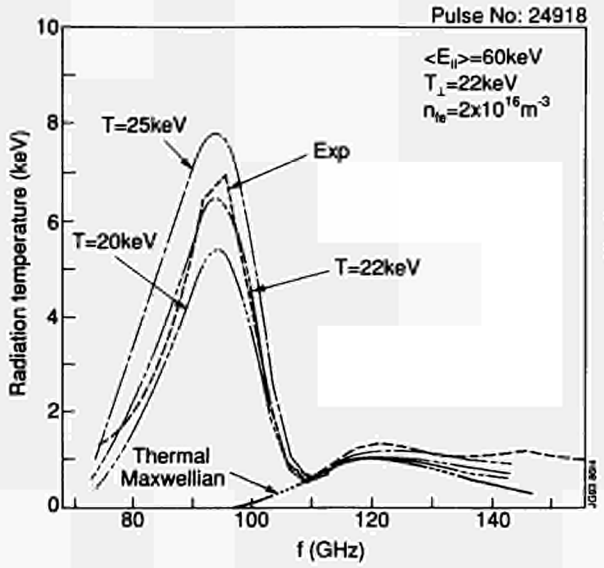

Fig.224: Experimental and simulated non-thermal ECE spectra for a full current drive pulse.

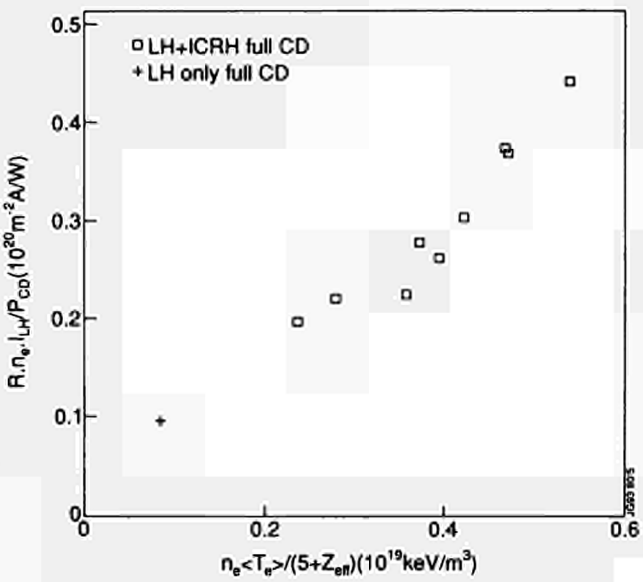

Fig.225: Current drive efficiency versus plasma pressure.

target to increase the current drive efficiency. This scenario has allowed identification of a synergistic effect between ICRF and LHCD systems, which led to record current drive efficiencies of up to 0.45 x $10^{20}m^{-2}A/W$.

The main results achieved with the prototype LHCD system and implications for future operation are as follows:

- Fast electron profiles, observed experimentally, are qualitatively in agreement with theory [12]. Fast electron penetration increases with magnetic field and decreases with electron density and broadening of the launched wave spectrum. The measured effect is systematically enhanced with respect to theoretical predictions. These results are summarised in Fig.222;
- Full current drive in almost steady-state conditions has been achieved in limiter and double-null (DN) plasmas [13]. At low electron temperature of T_e ~ 1keV, 0.4MA was driven by LH alone with 1.5MW of coupled power. At higher temperatures of T_e ~ 5keV, during the application of ICRF, 2MA was maintained in a limiter, low beta plasma, at plasma densities of n_e ~ 2.5 x 10^{19} m^{-3} and 2.8T toroidal magnetic field. Close to 2MW of LH power have been coupled to a 1MA DN H-mode discharge, in conjunction with 3MW of ICRF, maintaining the full plasma current for 4s with 40% bootstrap contribution;
- Flux savings of ~ 2V-s resulted from application of ~1.5MW of LH power during the low density current ramp-up phase of 7MA limiter plasmas [14], allowing an extension of the current flat-top by 2s to a total of 9s. In these discharges, the active launcher position control was used with a preprogrammed waveform, allowing the launcher to track the plasma surface for optimum coupling, as shown in Fig.223. Flux savings of up to 5V-s have been achieved with 1MW LH pulses of 50s duration during the 2MA one-minute long pulses at a toroidal field of 1.9T [15]. Upgradings to the LHCD position control system are being implemented, which will allow direct feedback to the launcher position from the measured reflection coefficient;
- Synergistic effects between ICRF and LHCD have been observed, where LH induced fast electrons are further accelerated in the presence of the ICRF wave up to energies ~400 to 500keV, well in excess of the parallel Landau damping resonance energy of ~100keV for a launched $N_{//}$ ~ 1.8 [16]. This result is substantiated by FEB measurements of the photon temperature obtained in the range 100 to 300keV, which show a photon temperature increase from 60 to 140keV when 3MW ICRF was added to 2.3MW LH in a limiter 1.5MA plasma at 3.3T toroidal field and 2.4x$10^{19}m^{-3}$ central electron density. The synergy was further confirmed by tangential soft X-ray viewing line measurements. Combined analysis of FEB and ECE data have shown [17] that the plasma current is driven by a fast electron population with an average density of 3.5 x $10^{15}m^{-3}$ and energies in excess of 300keV, characterised by temperatures of 800 and 80keV, respectively, in the direction parallel and perpendicular to the total magnetic field. These results are summarised in Fig.224;

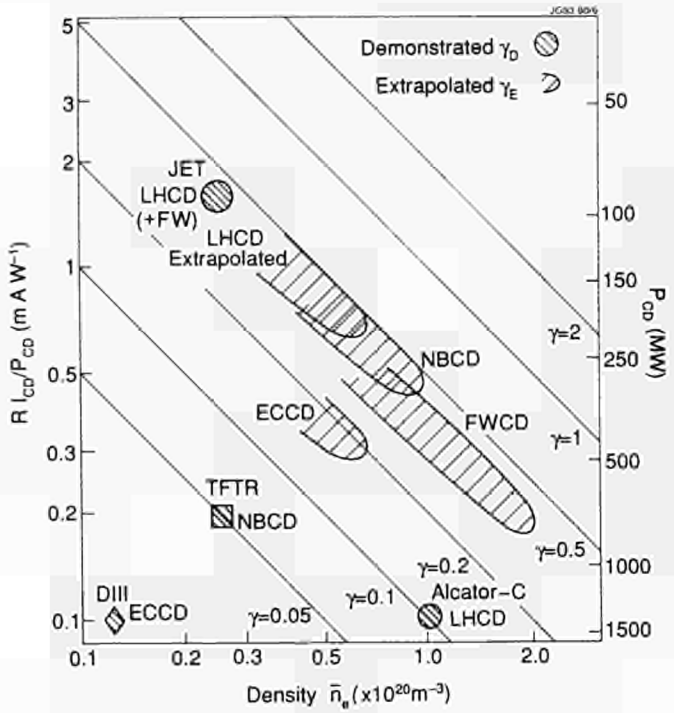

Fig.226: Comparison between demonstrated and extrapolated current drive efficiencies. P_{CD} refers to the required power for a reactor (as defined in Ref [1]).

- The Lower Hybrid wave-plasma coupling has been studied in limiter and DN plasmas, with the edge plasma parameters associated with L- and H-mode and with different positions of the launcher with respect to the toroidal limiters and neighbouring ICRF antenna [18]. The power reflection coefficient increases quadratically with parameter $d/L_{//}^{1/2}$, where d is the radial plasma-launcher distance and $L_{//}$ is the connection length of the magnetic field line. Reflection coefficients below 5% have been achieved, in agreement with theoretical expectations. A reflection coefficient of ~ 1% has been achieved in DN plasmas where the connection length exceeds of 30 m and the shallow density gradient facilitates the launcher positioning at the optimum electron density of ~10^{18} m^{-3};
- The current drive efficiency γ = nRI/P has been deduced taking into account the ICRF contribution to fast electrons, estimated at up to 18% of the total ICRF power, and the amount of bootstrap current generated. The efficiency increases with electron temperature, and values up to $\gamma \geq 0.4 \times 10^{20}$m^{-2}A/W have been obtained during synergistic conditions. Within the range of plasma parameters, the LHCD system has operated so far in JET ($n_{e0} < 3 \times 10^{19}$ m^{-3}, B > 2.8 T), γ does not depend upon plasma pressure, as shown in Fig. 225. This result is important for reactor extrapolation studies, where efficiency values ranging between 0.6 and 1.5 x 10^{20} m^{-2}A/W are required at plasma densities of ~10^{20} m^{-3}, depending upon the value of the poloidal β and consequently the amount of bootstrap current which can be generated by other heating mechanisms. As shown in Fig226, LHCD has the highest efficiency to date among the various CD methods, comparable to the extrapolated value for a 20keV average electron temperature ITER tokamak [1]. If a 20% recirculating power fraction to the CD system is assumed, as a realistic figure in terms of reactor economics, it is seen that an efficiency of $\gamma \sim 2 \times 10^{20}$ m^{-2}A/W would be required at an operating density of 2 x 10^{20} m^{-3}. High field, high aspect ratio regimes would be favourable in this respect, but the present database is not sufficient to identify an operation regime for ITER [2]. Further experiments, in particular, taking advantage of synergistic effects, should explore this possibility.

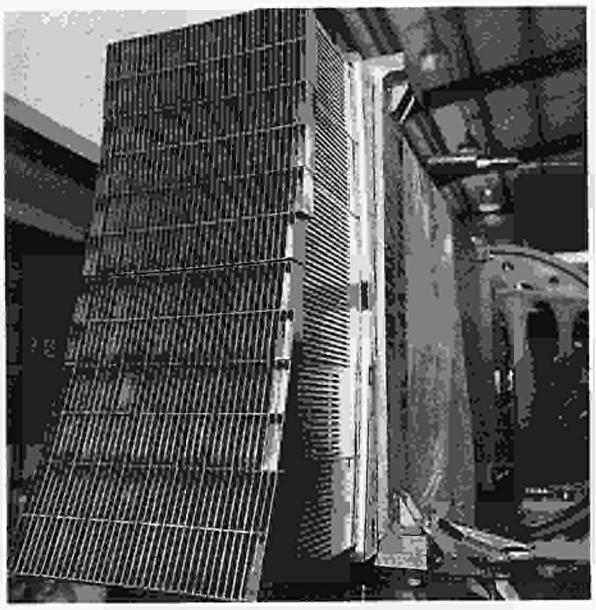

Fig.227: View of the L1 launcher mouth.

The L1 launcher for the final LHCD system has been modified to take into account the new pumped divertor geometry. Manufacture and assembly of the launcher was completed during 1992. The full assembled launcher is shown in Fig.227. The grill comprises 384 waveguides each 9 x 72 mm, as shown in Fig.228. The phase distribution at the grill has been measured for each multijunction module and found to be within ± 10° of the nominal values. The launcher is now installed in the vacuum vessel and undergoing high

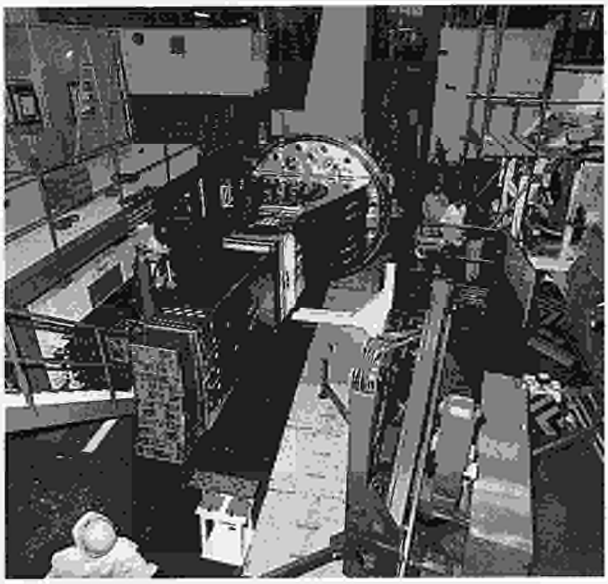

Fig.228: View of the L1 launcher prior to its installation in the Testbed.

power RF testing under vacuum. This test assembly which shows the 48 waveguide vacuum windows is shown in the section on ICRF Heating and Lower Hybrid Current Drive Systems. This launcher will be able to match the lower elongation "fat" plasma divertor configuration on JET, but it is unlikely that good coupling could be achieved in the highly elongated "thin" plasma.

The conventional launcher design presents a number of technical limitations which are associated with difficulties found in the conditioning and in its power handling properties. Alongside the coupling difficulties in a high power loading reactor environment, these aspects call for alternative launcher concepts to be considered. A conceptual solution has been under study at JET based on the new "hyperguide" concept [19]. The particular design is a TE_{012} overmoded waveguide ~ 5 m long with high power transmission capability. These results are confirmed by numerical calculations. The hyperguide can be operated with good vacuum conditions allowing avoidance of electron resonance zones, where breakdowns are more likely to occur. Such a system in JET is compatible with the present LH vacuum vessel and L1 end plate. This alternative does not address the problem of the coupler to the plasma, and could accommodate either a short conventional waveguide mouth or a quasi-optical coupler.

Experience with the prototype LHCD system has indicated that the handling capability of the multijunction type launcher is difficult and the conditioning to full power operation a time consuming activity, with an average generator power increase of ~75 kW per 100 JET pulses. New loads are now being tested and will be installed in the Torus Hall on the fourth port of the 3dB hybrid junctions feeding two multijunctions from each klystron line, to implement HF baking facilities in vacuum at high reflection coefficient. Upgrading in the launcher position control, in particular, the implementation of a feedback system on the reflection coefficient, will also contribute to the plant power handling capability during operation.

References

[1] P-H Rebut, D Boucher, C Gormezano, BE Keen, ML Watkins, Europhysics Conference on RF Heating and Current Drive of Fusion Devices, Brussels, July 1992. (To be published in Plasma Physics and Controlled Fusion).

[2] J Jacquinot, V Bhatnagar, C Gormezano and JET Team, Europhysics Conference on RF Heating and Current Drive of Fusion Devices, Brussels, July 1992. (To be published in Plasma Physics and Controlled Fusion).

[3] G Bosia and J Jacquinot, IAEA Technical Committee Meeting on Fast Wave Current Drive in Reactor Scale Tokamaks, Arles, France, 1991, p 471.

[4] J Jacquinot, M Bures and the JET Team JET Report JET-P(91)58, to be published in Physics of Fluids.

[5] D F H Start et al., Proc. of the 19th EPS Conference on Controlled Fusion and Plasma Physics, Innsbruck, Austria 1992, Vol 2 p 897.

[6] F Porcelli et al., Proc. of the 13th EPS Conference on Controlled Fusion and plasma Physics, Innsbruck, Austria, 1992, Vol 2 p 901.

[7] A Kaye et al., JET Report JET-P(92)46, submitted to Fusion Engineering and Design.

[8] C Gormezano et al., 14th IAEA International Conf. on Plasma Physics and Controlled Nuclear Fusion Research, Wurzburg, Germany, 1992.

[9] R H Goulding et al., Proc. of the 17th Symposium on Fusion Technology, Rome, 1992, paper Z:15, to be published.

[10] M Pain et al., Proc. 13th Symp. on Fusion Engineering, Knoxville, USA, 1989.

[11] D Start et al., Proc. IAEA Tech. Comm. Meeting on Fast Wave Current Drive in Reactor Scale Tokamaks, Arles, France, (1991).

[12] M Lennholm et al., Proc. Europhysics Conference on RF Heating and Current Drive on Fusion Devices, Brussels, Belgium, July 1992.

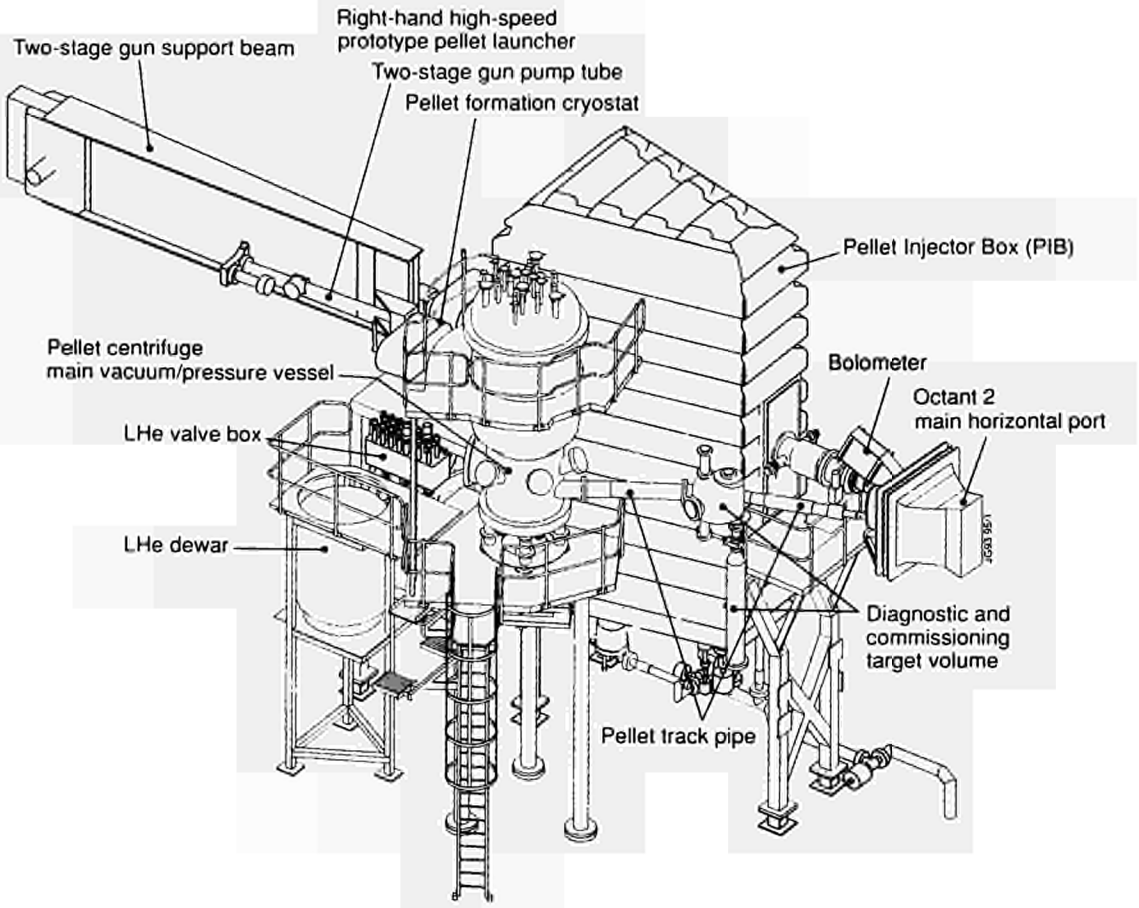

Fig.229: 3-D diagram of pneumatic and centrifuge pellet injectors.

[13]F Rimini et al., Proc. Europhysics Conference on RF Heating and Current Drive on Fusion Devices, Brussels, Belgium, July 1992.

[14]P Lomas et al., Proc. 14th IAEA Conf. on Plasma Physics and Controlled Nuclear Fusion Research, Wurzburg, Germany, 1992.

[15]M Brusati et al., Proc. 19th European Conference on Controlled Fusion and Plasma Physics, EPS, Innsbruck, Austria, Vol. 16C (Part 1), (1992) 307.

[16]C Gormezano et al., Proc. IAEA Tech. Comm. Meeting on Fast Wave Current Drive in Reactor Scale Tokamaks, Arles, France (1991).

[17]M Brusati et al., Proc. Europhysics Conference on RF Heating and Current Drive on Fusion Devices, Brussels, Belgium, July 1992.

[18]A Ekedahl et al., Proc. Europhysics Conference on RF Heating and Current Drive on Fusion Devices, Brussels, Belgium, July 1992.

[19]M Pain et al., JET Report JET-P(92)94, submitted for publication in Fusion Engineering and Design.

Pellet Injection

After the return of the ORNL launcher (see Torus Systems section) and the cancellation of a repetitive high-speed Advanced Pellet Launcher (APL) for budgetary reasons, JET plans to employ two high-speed single-shot pneumatic (formerly called "prototype") pellet launchers and a mechanical pellet centrifuge for the next experimental campaign. Detailed descriptions of the performance and design features of these devices were given in previous Progress Reports. Therefore, only a brief account will be given, combined with a more detailed description of the progress of work. Fig.229 shows a diagram of the planned centrifuge installation in the Torus Hall alongside the pellet injector box (PIB). In the rear, the two high-speed launchers can be seen with their respective two-stage guns supported by a large beam. Preparation work for their implementation on the torus is detailed in the Torus Systems section of the Report.

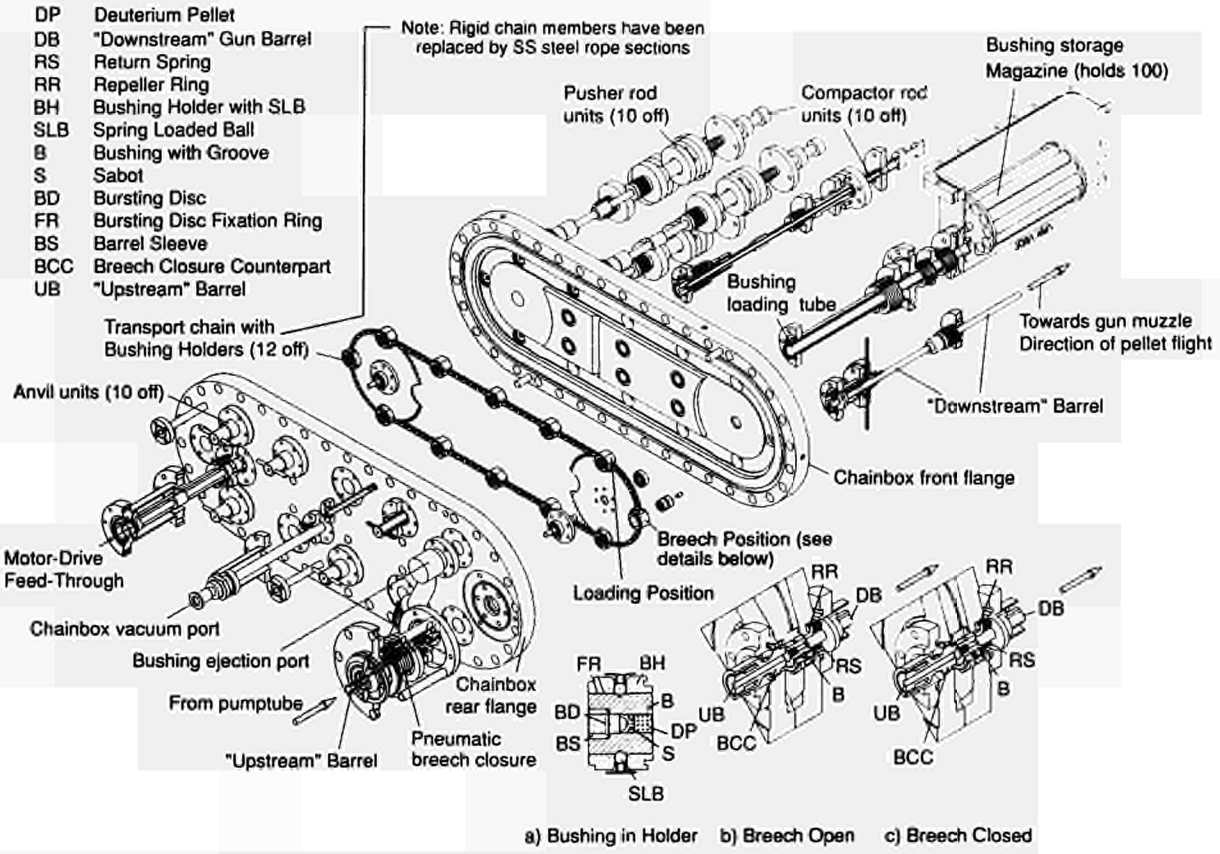

Fig.230: Exploded view of the cryostat cold box of the JET high-speed pellet launcher.

The High-Speed Pneumatic Prototype Launcher

This launcher is to accelerate sabot supported 6mm deuterium pellets to speeds up to 4kms^{-1} by using two-stage light gas gun driver technology (3m long, 60mm ID pump tube and a 0.6kg titanium piston) for deep to central plasma fuelling purposes. Sabots are small plastic pistons, set behind the deuterium pellets to protect them from the hot driving gas. These sabots, needed for pellet velocities in excess of about 3 kms^{-1} and being accelerated with the pellet, are made from two halves of equal mass, which will split after leaving the barrel due to aerodynamic forces and can be eliminated from the pellet path by a shear cone. Pellets are formed by cryo-condensation into bushings - ca 20mm long barrel sections - which are pre-loaded with bursting discs and sabots. The cryo-condensation is performed outside the gun breech in a cryostat with the capability of forming in one thermal cycle and then storing ten pellets in their bushings, which can be moved one per tokamak pulse into the breech immediately before the shot. This is carried out by means of a transport chain as shown schematically in Fig.230.

The high-speed launcher did not achieve its performance goals to be implemented on the torus in time for the previous experimental campaign, due to technical difficulties with the cryostat part of the launcher. Commissioning work, carried out at the pellet injection testbed, has proven the gun performance to be satisfactory apart from an occasional problem. If the piston, being pushed back after a shot by gas fed to the second stage via the barrel, does not end up at rest at its exact foreseen position at the first-stage entrance valve due to the dynamics of this process the timing in the two-stage gun process is influenced and the amount of foreland gas may be too small to warrant the safe reflection of the piston in the front of the pump tube. Such an event deforms the piston and jams it in the pump tube (the pump tube can be recovered by honing only after the piston is machined out). The piston is now equipped with a CoSm magnet and its exact position can now be monitored outside the pump tube, and interlocking with this magnet signal measurement will now prevent the seizure of the piston.

The major stumbling block was the lack of performance of the cryostat failing to permit accelerated pellets and finally even sabots. The commissioning process has turned out to be very tedious. This is due to the fact that, in the complex sequence of forming and transporting pellets and firing them, a verification of a successful launch is only

possible by the final in-flight photography and (destructive) target impact documentation. In addition, modifications to the cryostat which need to be made in the commissioning usually require a very time consuming dis-assembly and re-assembly of the LHe cryostat, with the added complexity of also being a mechanical gear box. One of the major pieces of repair work was the replacement of the rigid chain members (between the bushing holders) and their chain wheels by stainless steel rope sections and newly designed transport wheels and bearings. Careful and painstaking analysis had revealed that the accuracy requirements for the chain to place the bushings within 50μm into the breech axis, so that the self-alignment of conical breech parts could then assure the perfect (within 20μm) alignment during the shot, could not be guaranteed by the old system due to mechanical over-determination and subsequent progressive deterioration of the systems accuracy. Failure of the chain transport to meet this requirement resulted in a breech alignment mismatch, which destroyed pellets and sabots when they left the bushing during the shot. In addition, this in turn led to wear of the barrel breech parts, which were to assure the alignment, under the very high forces (15kN actuator force enhanced during the two-stage gun pulse, in which the second-stage driver gas acts on the free upstream barrel end, to 35kN on areas less than $1cm^2$) necessary to seal the two breech gaps. The modifications have now been carried out and commissioning operation is being continued.

In testbed operation, the control and data acquisition system, was changed over to the new UNIX based control system; although being one of the first subsystems to be converted only a few occurences interfered with launcher operation and the controls are now reliably in place.

Two of the prototype launchers, the second being a mirror image of the first, are under preparation for the next experimental period to be installed side by side at the rear of the Pellet Injector Box (PIB) in the Torus Hall. The two-stage gun of the second launcher is commissioned and the cryostat is in a late state of assembly (with the modifications resulting from the commissioning of the first one being carried over to it immediately).

The Pellet Centrifuge

The pellet centrifuge will deliver long strings, approaching 1 minute in duration, of 2 and 3mm pellets at repetition frequencies of up to $40s^{-1}$ with velocities between 50 and $600ms^{-1}$. This will provide shallow fuelling with minimum recycling beyond the separatrix for the divertor plasma in the next experimental programme phase. Each size of deuterium ice pellet will be launched from an individual extruder unit into the central part of the centrifuge rotor, the stop cylinder ensuring the proper starting conditions for the pellet on the rotor arm. The design of centrifuge rotor and stop cylinder follow very closely the centrifuge developed for ASDEX Upgrade (IPP Garching, Germany), who also advise under contract. The extruder is of a new design by JET to provide the much larger number of pellets per pulse. It is also novel, in the sense that in the final version, it will attempt to cool the deuterium ice dynamically from the 14°K (at which ice is extrudable), to 7°K, at which it should be accelerated, during the extrusion process..

The major procurement contracts concern the vacuum vessel (simultaneously at 23bar pressure vessel to contain possible hydrogen deflagration), the pellet centrifuge rotor mounted on top of a turbopump rotor, and parts of the cryopump. These contracts have been placed and delivery (somewhat delayed) is now scheduled for early 1993. The cryopump let to smaller contracts for the LHe and LN_2 reservoirs, LHe quilted panels (already delivered), LN_2 baffles and thermal shields will be assembled at JET. The extruder units, providing the pellets to the stop cylinder/rotor section of the centrifuge, have been conceptually designed and the various qualifications of manufacturing methods for the cryogenic extruder sections (friction welding of SS - Cu transitions, e-beam welding and spark erosion cutting) are being carried out. Trials with the bread-board version (inclusive of the respective electronics) of the chopper magnet - which cuts the extruded ice column in portions of pellet size at a rate of up to $40s^{-1}$ are well advanced. Contracts for: the track - guiding pellets in a slightly curved arc to the torus; target volume section of the vacuum vessel; auxiliary Roots blower sets for deuterium pumping from the target volume during routine pellet commissioning and helium compression at the extruder helium outlet; are in preparation.

Tritium Handling

Following the extension of the Project to the end of 1996, the Active Gas Handling System (AGHS) will be required to be fully operational before the start of the full D-T phase of JET scheduled for 1996.

The installation of the systems in the Active Gas Handling (AGH) building has been completed (Fig.231). The function of these systems is to collect exhaust gases from the

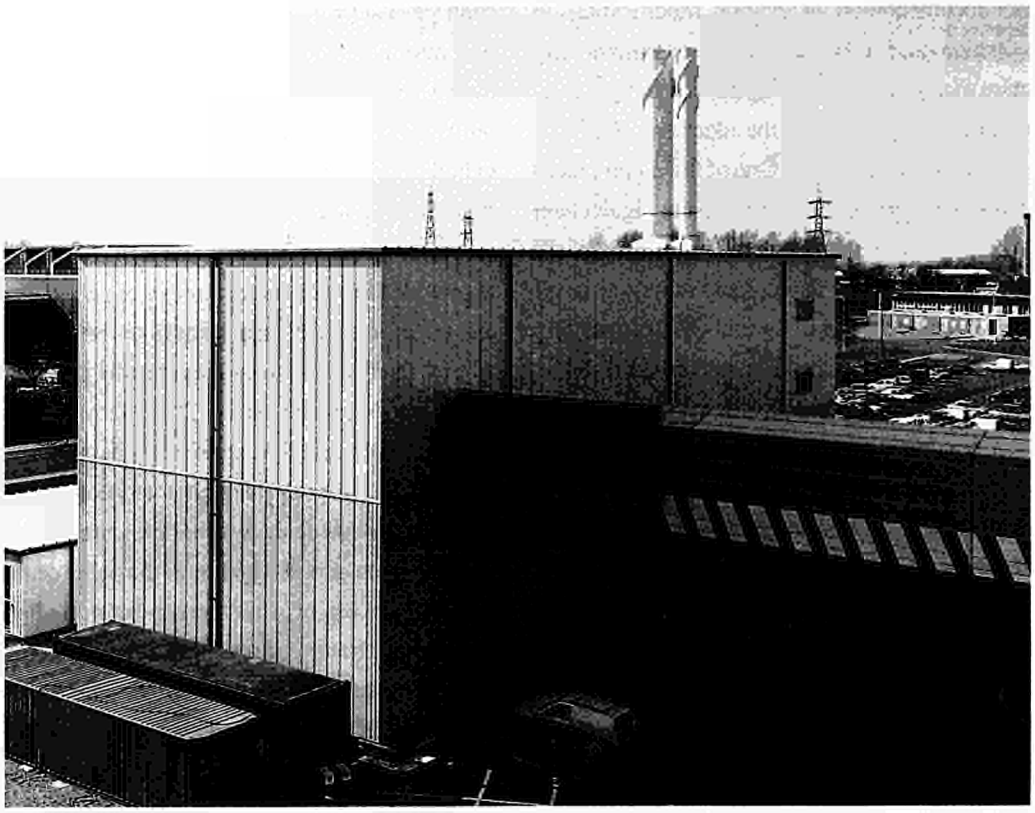

Fig.231: The Active Gas Handling System Building and enclosed lines from the torus.

torus, to remove impurities and to separate pure deuterium and tritium so that it can be stored for re-injection through neutral beam, pellet or torus gas introduction as required (Fig.232). Significant progress in commissioning during 1992 was made in: Exhaust Detritiation, Gas Chromatography and the Analytical Laboratory. In addition, a series of tests and modifications to improve the performance of the Cryodistillation System (CD) was carried out.

Exhaust Detritiation

Initially tested in 1991 after installation, the Exhaust Detritiation system (Fig.233) met its specification regarding water retention in adsorbers. Minor excursions after adsorber regeneration were eliminated by modification of the regeneration sequence. The performance of the catalytic recombiner for methane (CH_4) gas was tested: at various temperatures, 1% CH_4 was injected into the full exhaust detritiation design air flow of 500m^3h^{-1} for the duration of 1 minute. At the end of each CH_4 pulse samples were taken at the ED outlet and analysed by gas chromatography (GC-AN). CH_4 combustion started at approximately 250°C catalyst temperature in agreement with the manufacturers data for a gas mixture of 0.3% CH_4, 3%0_2, 1%CO_2 95.7% N_2, combustion was nearly complete at a catalyst temperature of 350°C, achieving > 99.7% combustion of CH_4. The recombiner was designed for and operated at a temperature of 500°C and thereby has been shown to have a sufficient safety margin for combustion of (tritiated) methane. Furthermore, improvements for the exhuast detritiation system have been identified for implementation in 1993: an additional water condenser should reduce drier loading and a new regeneration method should achieve 100% humidity removal from adsorbers.

Gas Chromatographic System

The Gas chromatographic system is designed for separation of D-T mixtures with a throughput of 20 moles per day (Fig.234). The separation of the hydrogen isotope mixtures consisting of the six hydrogen molecules H_2, HD, HT, D_2, DT and T_2 into pure product streams T_2, D_2 and H_2 can be carried out in a displacement gas chromatographic system. The column packing employed is 18 % (weight) palladium deposited on porous Al_20_3. The isotopic dependence of the solubility of hydrogen in palladium is the physical origin for the isotope separation. Due to the fact that the heavier hydrogen isotopes prefer to stay in the gas phase in comparison to the lighter ones when in contact with palladium, the heavier isotope will pass faster through the column packing

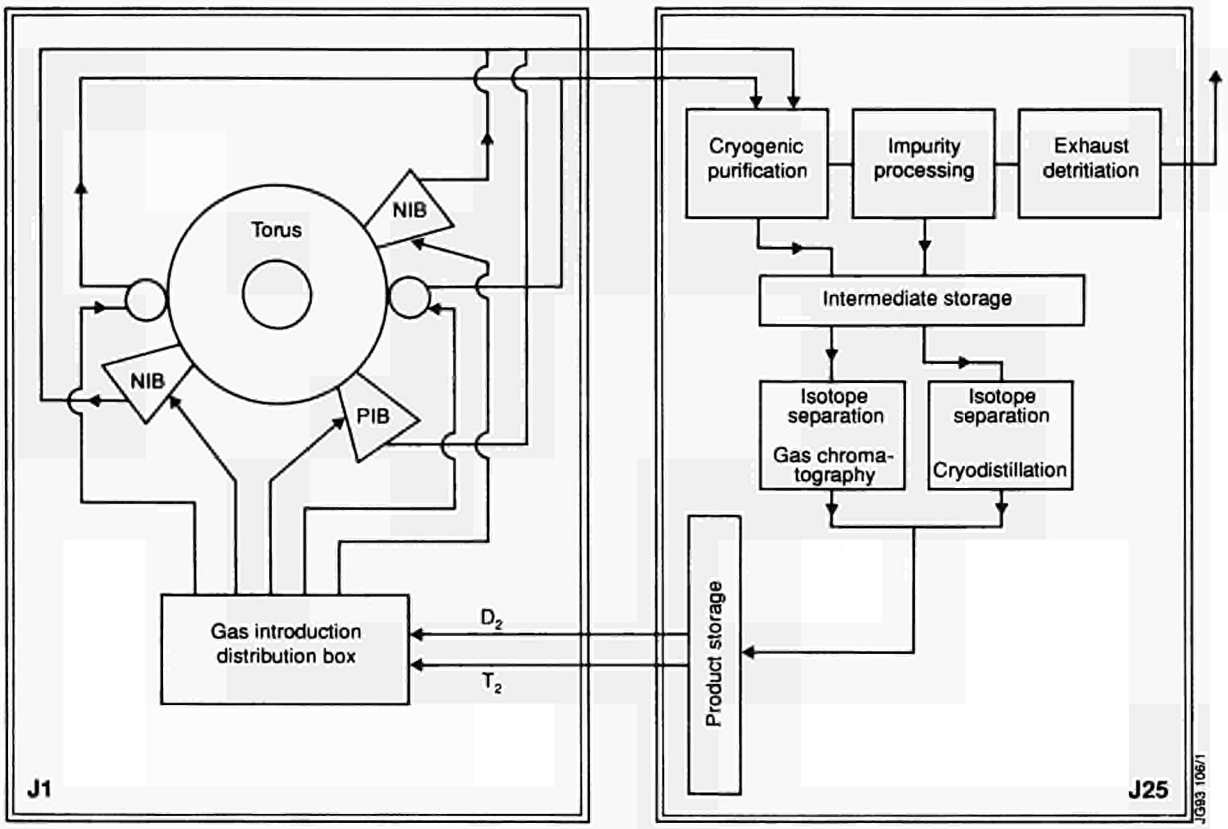

Fig.232: Block diagram of functions of Active Gas Handling System

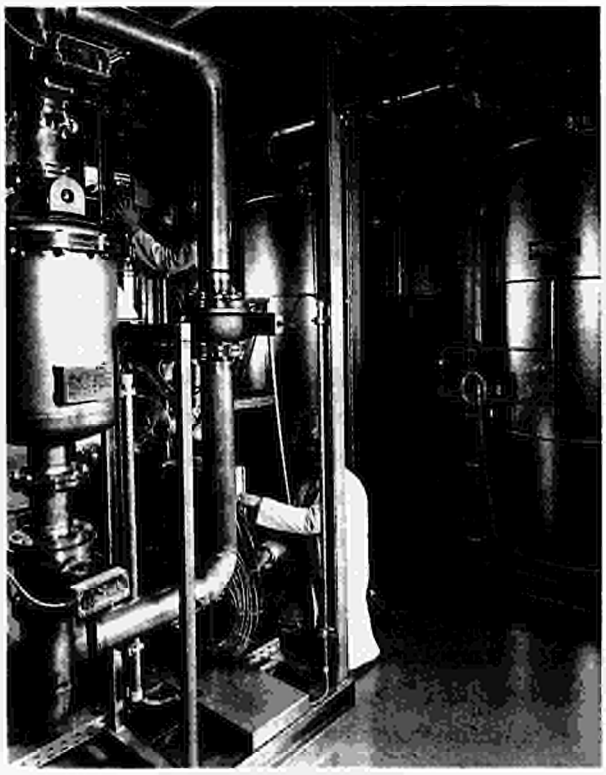

Fig.233: Exhaust detritiation system

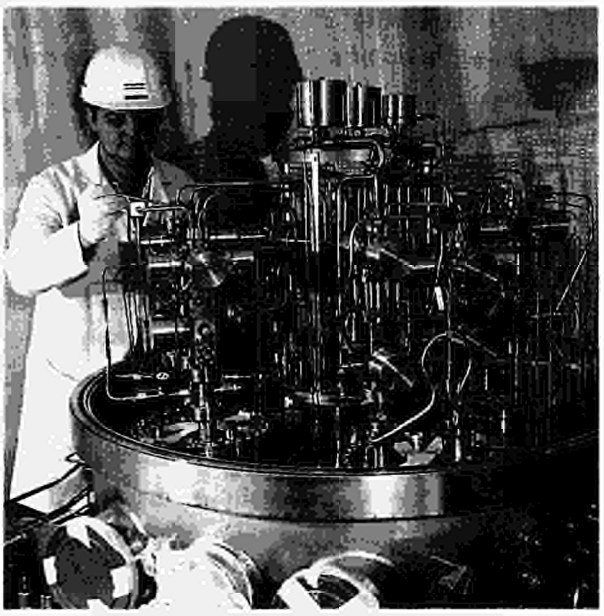

Fig.234: Gas chromotography equipment

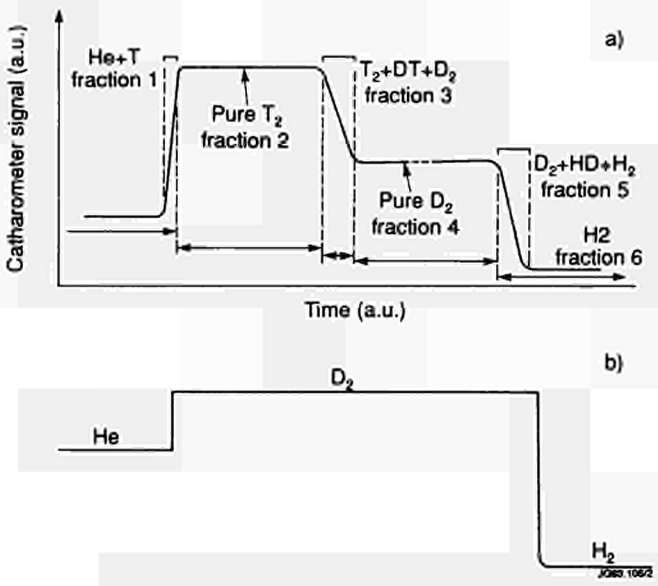

Fig.235: (a) Expected katharometer signal; and (b) experimental katharometer signal;

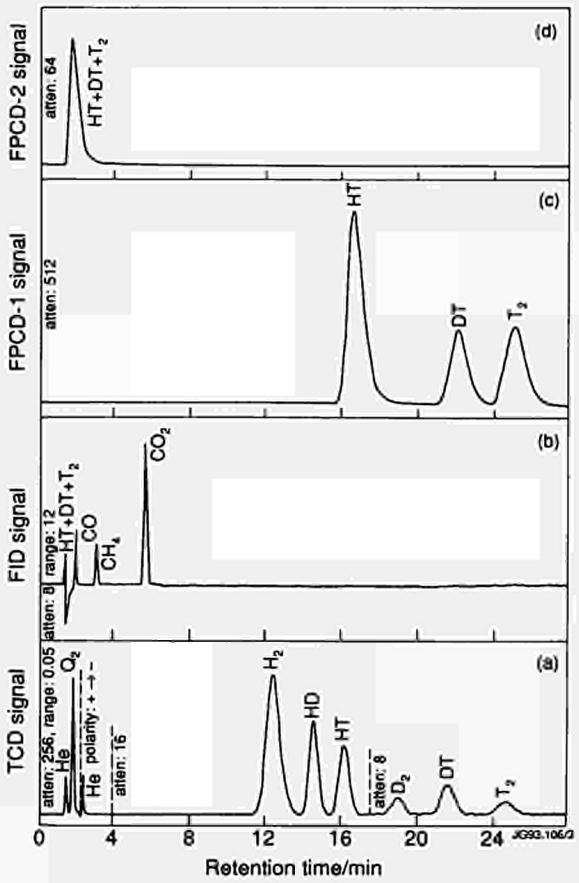

Fig.236: Gas chromatography output signals

than the lighter ones, which are more often absorbed into the palladium packing and therefore delayed.

Separation runs with the system have been performed in the following way: a certain amount of hydrogen gas mixtures (up to about 5 moles) can be introduced into the hydrogen free, helium filled columns. Pure H_2 gas is used to displace the hydrogen mixture through the Pd-packing. The gases which leave the columns can be measured by katharometers. Fig.235(a) shows the expected katharometer signals [4], and Fig.235(b) shows the experimental values. With the exception of the missing T_2 signal (because no tritium was used in these tests) the two curves are similar. The conclusion is that the system works well and the interfractions of mixed gases He and D_2 or D_2 and H_2 are very small, an indication for sharp separation.

The first runs were performed semi-automatically and with a gas mixture of 50% protium and 50% deuterium. Further commissioning will be undertaken with other gas mixtures, including tritium. Finally, the system will be tested for its full design performance, ie the fully automatic separation of pure T_2 and D_2 from H/D/T mixtures.

Analytical Laboratory

An Analytical Laboratory was designed as a central facility for the Active Gas Handling (AGH) System with the purpose of analysing all gas species exhausted by JET and treated in the different subsystems of the AGH plant.

A special gas chromatograph was built by CFFTP, Canada, for the detection of the six hydrogen molecules, helium, carbon monoxide, carbon dioxide, methane and higher carbon hydrides, nitrogen oxygen and water. The separation of the gas species is carried out via commercially available packed columns. Two flow proportional counter detectors (FPCDs), one thermal conductivity detector (TCD) and one flame ionisation detector (FID) are used.

A series of tests were carried out to confirm that the required performance was achieved. This included the use of a small quantity of tritium. Figure 236 shows the response of the gas chromatograph system after the injection of the following gas mixture: 0.96% He, 1.41% H_2, 0.81% HD, 0.82% HT, 0.13% D_2, 0.28% DT, 0.16% T_2, rest Ne and very low level of impurities: CO, CH_4 and CO_2. All gas species are detected and separated clearly with the exception of Ne, which is used as the carrier gas. CO, CH_4 and CO_2 were not introduced during the production of the gas mixture but are known to be created during longer storage periods of tritium in stainless steel containers due to reaction of the atomic tritium with oxygen and carbon in the steel. The FPCDs are very sensitive instruments and can analyse tritium concentrations down to the ppb range. They can also be used to determine the amount of tritiated methane and tritiated higher hydrocarbons.

Table XXII
JET Programme Schedule: 1989 - 1996

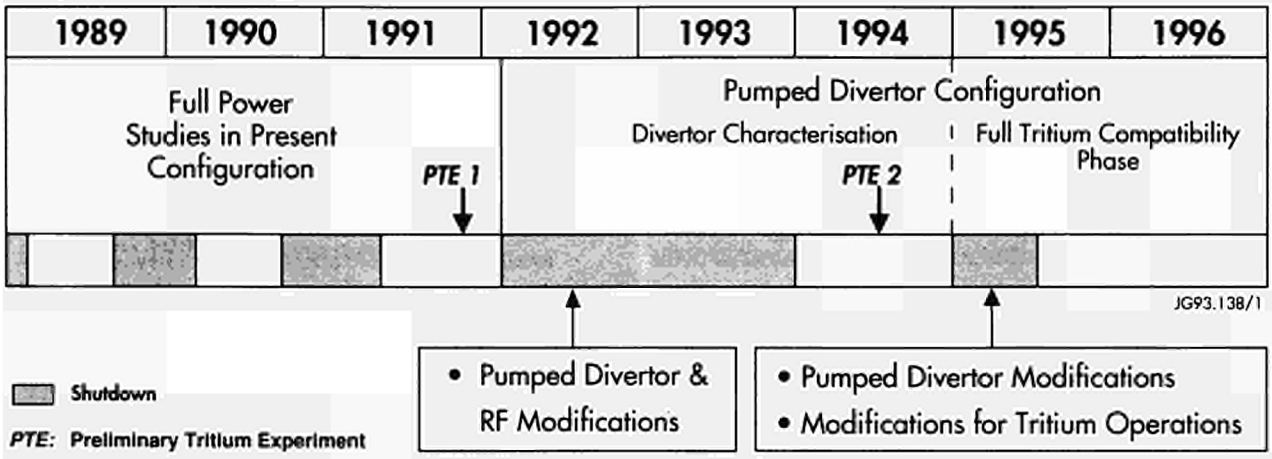

The FID can analyse methane and higher hydrocarbons, as well as CO and CO_2, when a catalyst for conversion to methane is used in front of the FID. The TCD is used for the determination of the gas species with higher concentrations (up to 100%).

A detailed description of the design and the performance of the GC-system has been published [2].

Safety Approval for Tritium Operation

All the Design Safety submissions for the Active Gas Handling System have been issued to the Safety and Reliability Directorate (SRD) of the UKAEA. Apart from minor issues which can readily be resolved, the design of the system has been accepted as meeting the UKAEA standards. Effort is now concentrated in producing the justification documents which will permit active commissioning to begin. As well as providing an overall assessment of the accidental risk from the plant, these will deal with issues of operational safety management.

For the torus systems, SRD have specified that a rigorous hazard analysis methodology should be used to identify any hazards arising from the design and operation of the machine in the D-T phase. Work has started with a series of Hazard and Operability studies (HAZOPs) which will be used to identify those systems which require a detailed safety justification involving Failure Mode and Effect Analysis (FMEA) and Fault Tree analysis.

In accordance with the Authorisations issued by the Department of the Environment, careful monitoring of the effect of the Preliminary Tritium Experiment in November 1991 has continued. This confirms that the experiment has had negligible environmental impact.

References

[1] F Botter, J Gowman, J L Hemmerich, B Hircq, R Lässer, D Leger, S Tistchenko, M Tschudin: Fusion Technology 14, 562 (1988)

[2] R Lässer, B Grieveson, J L Hemmerich, R Stagg, T Dowhyluk, K Torr, R Massey, P Chambers: JET Report JET-P(92)78

Future Plans

The JET Programme is divided into phases governed by the availability of new equipment and fitting within the accepted life time of the Project. Phase I (Ohmic Heating Studies) was completed in September 1984, and Phase II (Additional Heating Studies) in October 1988. Phase III (Full Power Optimization Studies) ended in February 1992. The scientific aims of Phase III were to obtain maximum performance in limiter configuration (currents up to 7MA) and to optimize X-Point Operation (currents up to 6MA) including a comparison of H-modes in X-point configuration using beryllium (lower X-point) with carbon (upper X-point) dump plates. The programme to 1996 is shown in Table XXII.

JET future plans are dominated by the insertion of a new phase of the Project (Phase IV: Pumped Divertor Configuration and Next-Step Oriented Studies). This phase is subdivided into a Divertor Characterization Plasma and a Full Tritium Compatibility Phase. The final Full Tritium Compatibility Phase, is now scheduled to start in 1995. This new phase has now been formally approved and has extended the lifetime of the Project by four years up to the end of 1996.

The aim of the new phase is to demonstrate, prior to the introduction of tritium, effective methods of impurity control in operating conditions close to those of a Next-Step Tokamak with a stationary plasma (10s-1m) of 'thermonuclear grade' in a single-null axisymmetric pumped divertor configuration. This configuration can only be achieved in JET by using divertor coils internal to the vessel.

Following the approval by the JET Council of the stepwise approach to the introduction of tritium in advance of the full Tritium Phase, a first preliminary tritium experiment (PTE1) was carried out and successfully completed in November 1991. A second tritium experiment (PTE2) is scheduled for the first half of 1994 at a point, yet to be determined, when divertor operation has been well established, but in time to allow the necessary period of radioactive decay before the following shutdown. The information derived from these preliminary tritium experiments will provide a safer approach to the full tritium phase and will help to optimize the active handling and waste management arrangements.

More information on the future phases of the Project are indicated below.

New Phase (first part): Pumped Divertor Configuration Phase IVA (Divertor Characterization Phase) (February 1992 - December 1994)

In February 1992, the Project entered an extended shutdown to install the components relevant to the new pumped divertor. This will be concluded by the end of 1993. This is involving intensive in-vessel work to install the following equipment:

- lower divertor structure with Mark 1 carbon target plates (inertially cooled);
- pumping chamber and cryopump;
- internal divertor coils and necessary power supplies;
- poloidal limiters;
- new ICRF heating antennae (A2);
- full lower hybrid current drive (LHCD) system with its modified launcher;
- divertor diagnostics;
- high-speed pellet launcher (for plasma core injection);
- centrifuge pellet launcher (for plasma edge injection);
- disruption control system using internal saddle coils.

The single-null X-point pumped divertor configuration should enable JET to progress towards extended high power operation with 40MW additional heating using neutral beam and ICRF power (e.g. plasma currents of 6MA for up to 3s, 3MA for up to 5s). The control of disruptions using saddle coils system and the control of sawteeth using the full power LHCD systems should also be studied.

Experiments during the subsequent operating period in 1994 will concentrate on establishing and characterising plasma behaviour in the pumped divertor configuration. The programme will focus on:

- establishing reliable operation in the new configuration;
- studying the control of impurities, plasma density and exhaust, and power loading on the target plates; and
- assessing power handling using the full range of ancillary equipment.

The centrifugal pellet injector will be used for repetitive fuelling. In addition, the prototype fast pellet injector will deliver one pellet per tokamak discharge.

At the end of the shutdown, the RF capabilities of JET will have been enhanced significantly with the installation of the A2 RF antennae and of the full L1 LHCD launcher. The exploitation of these systems in a range of heating and current drive scenarios will also be an integral part of the programme during this phase.

CFC carbon divertor target plate tiles will be installed for the first period of operation with the Mark I divertor (inertially-cooled plates). This will allow initially a more rapid characterisation of plasma behaviour and build-up of high performance in the divertor configuration particularly at low density. When pumped divertor operations are well established, a decision will be taken on whether to replace the CFC tiles with beryllium tiles during a short intervention.

A second Preliminary Tritium Experiment (PTE2) is provisionally scheduled to take place (subject to the necessary formal approvals) about halfway through the operating period. A decision whether or not to proceed with this experiment, together with its timing and objectives, will be taken at a later date in the light of the early experience of operation in the new pumped divertor configuration. Account will also be taken of the evolving R & D needs of the overall European Fusion Programme.

At this stage, it appears likely that PTE2 could also involve a full scale application of the tritium handling system at JET. Such a demonstration well in advance would help to optimise the active handling and waste management arrangements for full D-T operations at JET and would be of importance in establishing technological aspects of the Next Step.

Preparations for D-T operations will continue during this period, including finalisation of remote handling tests and commissioning of the Active Gas Handling System with tritium (subject to consent by the approving bodies).

New Phase (second part): Pumped Divertor Configuration - Phase IVB (Full Tritium Compatibility Phase) (January 1995 - December 1996)

This phase will start with a major shutdown scheduled for early-1995. The main in-vessel task will be to install the Mark II (actively cooled) divertor. As presently conceived, this would involve replacing the inertially-cooled divertor target plates with actively-cooled hypervapotron elements, which should allow the divertor to accept the incident power level from operation with full plasma heating in steady state. In addition, it should be possible to install other enhancements aimed at improving performance in the new configuration or for the D-T experiments (e.g. enhanced pellet injection or fuelling system, modification to LHCD or additional heating systems). In parallel, ex-vessel activities would focus on bringing all the systems and subsystems to full tritium compatible status.

Operations would resume in mid-1995 and the use of tritium would start near the end of 1995, subject to the approval of the JET Council and to the necessary official consents. Decisions on the precise programme of experiments during this phase will be taken at a later date, in the light of experience during the characterisation phase (including the possible PTE2) and of the Fusion Programme needs at that time. The general plans envisage the re-establishment of pumped divertor operation and experimental progress towards reliable steady-state operation at high heating power. The experimental programmes will be directed at the physics of alpha-particle production, confinement and heating. Key additional information will be generated from the experience of tritium operations on a reactor relevant scale - tritium retention, remote maintenance and plasma diagnostics with large neutron and gamma backgrounds. This experience of D-T operation in a reactor relevant scale tokamak should provide information essential for ITER design and construction.

Appendix I

JET Task Agreements 1992

Title	*Associations (JET Responsible Officer)*	*Duration of Agreement*
RF HEATING DIVISION		
LOWER HYBRID CURRENT DRIVE ON JET • Exchange of knowledge • Design and construction of special items • High power tests	EUR-CEA CADARACHE (CEA/TA4) (J. Jacquinot)	Now Completed. The prototype launcher built by CEA has been installed and operated successfully
LH AND ICRF EFFECTS ON JET • CD efficiency including transport • Synergistic effects between FWCD and LHCD • Modulated heating modelling • Minority CD experiments • Effect on RF CD on MHD stability	EUR-UKAEA CULHAM, UK (J.Jacquinot)	In Progress: detailed comparison with JET experiments on LH and FW synergy, fast electron transport and minority CD
EXPERIMENTAL DIVISION I		
EDGE PLASMAS & PLASMA SURFACE INTERACTIONS	CULHAM, UK (CUL/TA2) (P.E.Stott)	Started July 1992
PLASMA WALL INTERACTIONS	GARCHING, GERMANY (IPP/TA2) (P.E.Stott)	Started Jan. 1984
NEUTRON PRODUCTION RELATED PHYSICS AND ASSOCIATED DIAGNOSTICS	SWEDEN (NFR/TA1) (P.E.Stott)	Started Jan 1984.
PLASMA SURFACE INTERACTIONS	SWEDEN (NFR/TA1) (P.E.Stott)	Started July 1987

Title	*Associations (JET Responsible Officer)*	*Duration of Agreement*
NEUTRON PRODUCTION RELATED PHYSICS	HARWELL, UK (HAR/TA1) (P.E.Stott)	Started Jan. 1984,
NEUTRON PRODUCTION RELATED PHYSICS AND ASSOCIATED DIAGNOSTICS	FRASCATI, ITALY (ENEA/TA3) (P.E. Stott)	Started Jan. 1986,
MICROWAVE REFLECTOMETRY & EDGE FLUCTUATIONS	CIEMAT, SPAIN (CIEMAT/TA1) (P.E. Stott)	Started Dec. 1991
EXPERIMENTAL DIVISION II		
BULK IMPURITY PHYSICS AND IMPURITY RELATED DIAGNOSTICS	EUR-IPP GERMANY (P.R. Thomas)	Started Feb. 1983
SPECTROSCOPIC MEASUREMENTS INTERPRETATION AND IMPURITY ANALYSIS	EUR-CEA CADARACHE, FRANCE (P.R. Thomas)	Started July 1984
IMPURITIES AND OTHER TOPICS	EUR-AEA CULHAM, UK (P.R. Thomas)	Started June 1987
THEORY		
ANALYSIS OF LOCAL TRANSPORT IN JET AND COMPARISON WITH THEORETICAL MODELS	EUR-UKAEA CULHAM, UK (F. Tibone)	Started Jan. 1991

Appendix II

List of Articles, Reports and Conference Papers Published in 1992

1. The JET neutron emission profile monitor.
Adams J M Jarvis O N Sadler G J Syme D B Watkins N
Joint European Torus (JET). May 1992. Preprint JET-P(92)27. (submitted to Nuclear Instruments and Methods).

2. ELM precursors in JET.
Ali-Arshad S Campbell D Colton A Cripwell P de Kock L Kramer G J Nave M F F Neill G F
Papers submitted to the 19th European Conf. on Controlled Fusion and Plasma Physics, Innsbruck, 1992. Preprint JET-P(92)37, pp.157-162.

3. Generation of signals for disruption precursor control.
Ali-Arshad S Morris A W Nicholson P Trotman D L Vickers A J
JET papers presented to Course and Workshop on Diagnostics for Contemporary Fusion Experiments, Varenna, Italy, 27 August - 6 September 1991.

4. DIOSCUR-divertor optimization and steady current study of a tokamak aimed at steady state operation with reactor relevant plasma parameters.
Alladio F Tanga A et al
Fusion Engineering. 14th IEEE/NPSS Symp., San Diego, 1991. 2 vols. Piscataway, IEEE. 1992. p.426.

5. MHD limiting phenomena in high performance JET plasmas.
Alper B Edwards A W Gill R D Pasini D Smeulders P
Papers submitted to the 19th European Conf. on Controlled Fusion and Plasma Physics, Innsbruck, 29 June - 3 July 1992. Joint European Torus (JET). May 1992. Preprint JET-P(92)37, pp.223-228.

6. The tritium clean-up experiment in JET.
Andrew P L Aldwell-Nichols C J Coad J P Dietz K J Ehrenberg J Goodall D H J Hemmerich J Horton L How J Lasser R Lomas P Loughlin M McCracken G M Peacock A Saibene G Sartori R Thomas P Winkel T
JET papers submitted to 10th Int. Conf. on Plasma Surface Interactions, Monterey, USA, 30 March - 3 April 1992. Joint European Torus (JET). May 1992. Preprint JET-P(92)32, pp.127-149.

7. Interpretation of deuterium pumping by plasma- facing beryllium surfaces.
Andrew P L Peacock A T Pick M A
JET papers submitted to 10th Int. Conf. on Plasma Surface Interactions, Monterey, USA, 30 March - 3 April 1992. Joint European Torus (JET). May 1992. Preprint JET-P(92)32, pp.169-185.

8. Derivation of nuclear parameters for delayed neutron measurements of neutron yields for D-T plasma operation at JET.
Angelone M
Joint European Torus (JET). 1992. Preprint JET-P(92)28. (submitted for publication in Fusion Technology).

9. Axisymmetric toroidal equilibrium with incompressible flows.
Avinash K Bhattacharyya S N Green B J
Plasma Physics and Controlled Fusion vol.34 no.4 April 1992 pp.465-473.

10. Confinement of high performance JET plasmas.
Balet B Cordey J G Stubberfield P M Thomsen K
Controlled Fusion and Plasma Physics. 18th European Conf, Berlin, 3-7 June 1991. Contributed papers. Geneva, European Physical Society. 1991. pp.I-9 - I.12.

11. Determination of local transport coefficients by heat flux analysis and comparisons with theoretical models.
Balet B Cordey J G Stubberfield P M
Plasma Physics and Controlled Fusion vol.34 no.1 January 1992 pp.3-31.

12. Heat transport with strong on/off-axis heating.
Balet B Boucher D Cordey J G Muir D G Neudatchin S V Schmidt G
Papers submitted to the 19th European Conf. on Controlled Fusion and Plasma Physics, Innsbruck, 29 June - 3 July 1992. Joint European Torus (JET). May 1992. Preprint JET-P(92)37, pp.139-144.

13. Heat transport with strong off-axis heating.
Balet B Cordey J G Muir D G Schmidt G L
Nuclear Fusion vol.32 no.7 July 1992 pp.1261-1264. (Preprint JET-P(92)04).

14. Particle transport during the tritium experiments in JET.
Balet B Cordey J G Jones T T C Konig R Marcus F Sadler G Stubberfield P M von Hellermann M

Papers submitted to the 19th European Conf. on Controlled Fusion and Plasma Physics, Innsbruck, 1992. Joint European Torus (JET). Preprint JET-P(92)37, pp.49-54.

15. The design features of secondary containments for the JET active gas handling system and their role in mitigating both chronic and accident tritium releases.
Ballantyne P R Bell A C Hemmerich J L
Fusion Technology vol.21 no.2 pt.2 March 1992 (Procs. 4th National Topical Meeting on Tritium Technology in Fission, Fusion and Isotopic Applications, Albuquerque, New Mexico, 29 September-4 October 1991) pp.49-54.

16. Methodology and results of risk assessment of interconnections within the JET active gas handling system.
Ballantyne P R Bell A C Konstantellos A Hemmerich J L
Fusion Technology vol.21 no.2 pt.2 March 1992 (Procs. 4th National Topical Meeting on Tritium Technology in Fission, Fusion, and Isotopic Applications, Albuquerque, New Mexico, 1991) pp.477-482.

17. Bragg rotor spectrometer for the JET tokamak.
Barnsley R Patel A Peacock N J Smith R T C
Review of Scientific Instruments vol.63 no.10 pt.II 1992 (Procs. 9th Topical Conf. on High Temperature Plasma Diagnostics, Santa Fe, New Mexico, 1992) p.5022.

18. Bragg spectroscopy of impurities during the JET preliminary tritium experiment.
Barnsley R Brzozowski J Coffey I H Lawson K D Patel A Patel T K Peacock N J Schumacher U
Review of Scientific Instruments vol.63 no.10 pt.II 1992 (Procs. 9th Topical Conf. on High Temperature Plasma Diagnostics, Santa Fe, New Mexico, 1992) p.5023.

19. Components of P_{rad} and Z_{eff} derived from X-ray spectroscopy of the main impurities in JET.
Barnsley R Brzozowski J Coffey I H Lawson K D Melnick I M Patel A Patel T K Peacock N J
Papers submitted to the 19th European Conf. on Controlled Fusion and Plasma Physics, Innsbruck, 29 June - 3 July 1992. Joint European Torus (JET). May 1992. Preprint JET-P(92)37, pp.217-222.

20. Observations of suprathermal electrons in the edge region of JET H-mode plasmas.
Bartlett D V Porte L Costley A E Jones S E Smith R Zolfaghari A
Papers submitted to the 19th European Conf. on Controlled Fusion and Plasma Physics, Innsbruck, 29 June - 3 July 1992. Joint European Torus (JET). May 1992. Preprint JET-P(92)37, pp.79-84.

21. A model for analytical performance prediction of hypervapotron.
Baxi C Falter H D
Joint European Torus (JET). August 1992. Preprint JET-P(92)56.

22. Optimization of thermal design for nitrogen shield on JET cryopump.
Baxi C B Obert W
Fusion Engineering. 14th IEEE/NPSS Symp., San Diego, 1991. 2 vols. Piscataway, IEEE. 1992. pp.1218-1221.

23. Pellet fuelling deposition measurements on JET and TFTR.
Baylor L R Schmidt G L Houlberg W A Milora S L Gowers C Bailey W Gadeberg M Kupschus P Tagle J A Owens D K Mansfield D K Park H
Nuclear Fusion vol.32 no.12 December 1992 pp.2177-2188. (Preprint JET-P(92)73).

24. Routine tritium releases from JET.
Bell A C Ballantyne P Caldwell-Nichols C Wykes M
Fusion Technology vol.21 no.2 pt.2 March 1992 (Procs. 4th National Topical Meeting on Tritium Technology in Fission, Fusion, and Isotopic Applications, Albuquerque, New Mexico, 1991) pp.506-511.

25. Safety aspects and approvals of the first JET tritium experiment.
Bell A C Wykes M Breen B J
Fusion Engineering and Design vol.19 no.2 September 1992 (Topical Issue on the first JET tritium experiment) pp.169-178. (Preprint JET-P(92)14).

26. The JET divertor coils.
Bertolini E Celentano G Last J R Tait J Tesini A Dal Mut G D'Urzo C Ghirlanda L Laurenti A Maragliano A Veardo A
IEEE Transactions on Magnetics vol.28 no.1 January 1992 (12th Int. Conf. on Magnet Technology, Leningrad, USSR, 23-28 June 1991) pp.275-278.

27. The JET Project.
Bertolini E and JET Team
Energia Nucleare vol.8 no.3 September/December 1991 pp.5-26.

28. The JET project: key experimental results and technical development towards breakeven plasmas.
Bertolini E
Status and Perspectives of Nuclear Energy: Fission and Fusion. Procs. Int. School of Physics, 'Enrico Fermi'. Course 116, Varenna, Villa Monastero, 10-20 July 1990. Amsterdam, North-Holland. 1992. pp.331-370.

29. The JET divertor coils - manufacture and assembly.
Bertolini E Dal Mut G Dolgetta N D'Urzo C Last J R Laurenti A Presle P Maragliano A Tesini A Veardo A
JET Papers presented at 17th Symp. on Fusion Technology (SOFT-17), Rome, Italy, 14-18 September 1992 Joint European Torus (JET). September 1992. Preprint JET-P(92)72, pp.127-133.

30. Fast wave current drive efficiency calculations for JET A2-antennas.
Bhatnagar V P Jacquinot J Start D F H

Fast Wave Current Drive in Reactor Scale Tokamaks (Synergy and Complementarity with LHCD and ECRH). IAEA Technical Committee Meeting, Arles, 23-25 September 1991. Association EURATOM-CEA sur la Fusion, Centre d'Etudes de Cadarache, 1992. pp.110-120.

31. Bulk-ion heating by high-concentration minority ICRH in the JET tokamak.
Bhatnagar V P Challis C D de Esch H P L Gowers C Jacquinot J O'Rourke J Start D F H Stork D Tubbing B J D
Papers presented to Europhysics Topical Conf. on RF Heating and Current Drive of Fusion Devices, Brussels, 7-10 July 1992. Joint European Torus (JET). May 1992. Preprint JET-P(92)31, pp.7-12.

32. High-concentration minority ion-cyclotron resonance heating in the JET tokamak.
Bhatnagar V P Jacquinot J Start D F H Tubbing B J D
Joint European Torus (JET). July 1992. Preprint JET-P(92)49. (submitted to Nuclear Fusion).

33. ICRF heating and synergistic LH and fast-wave current drive in JET.
Bhatnagar V P Jacquinot J Gormezano C Start D F H and JET Team
Radio Frequency Power in Plasmas. 9th Topical Conf., Charleston, 19-21 August 1991. New York, American Institute of Physics, 1992. pp.115-124.

34. ICRH H-modes produced with Be-screen antennas and coupling-resistance position feedback control.
Bhatnagar V P Bosia G Bures M Campbell D Fessey J Gottardi N Jacquinot J de Kock L Lowry C Morgan P Smeulders P Start D F H Stork D Summers D Thomas P Thomsen K Tubbing B J D Vlases G Ward D
Controlled Fusion and Plasma Physics. 18th European Conf., Berlin, 3-7 June 1991. Contributed papers. Geneva, European Physical Society, 1991. pp.I-369 - I-372.

35. Dynamics of a steady-state D-T burning tokamak plasma.
Bickerton R J
Joint European Torus (JET) 1992. Report JET-R(92)03.

36. Comments on 'Relativistic effects in microwave reflectometry'.
Bindslev H
Joint European Torus (JET). December 1992. Preprint JET-P(92)101. (submitted to Physics of Fluids B).

37. Relativistic dielectric effects in millimeter wave diagnostics for large tokamaks.
Bindslev H
JET papers presented to Course and Workshop on Diagnostics for Contemporary Fusion Experiments, Varenna, Italy, 27 August - 6 September 1991. Joint European Torus (JET). December 1991.

38. Relativistic effects in reflectometry.
Bindslev H
Papers presented to the IAEA Technical Committee Meeting on Reflectometry, JET Joint Undertaking 1992. Joint European Torus (JET) Preprint JET-P(92)55, pp.13-24.

39. Relativistic effects in plasma reflectometry.
Bindslev H
Plasma Physics and Controlled Fusion vol.34 no.11 November 1992 pp.1601-1618. (Preprint JET-P(92)35).

40. Automatic analysis of JET charge exchange spectra using neural networks.
Bishop C M Roach C M von Hellermann M G
Joint European Torus (JET). November 1992. Preprint JET-P(92)90. (submitted to Nuclear Fusion).

41. Neural networks and expert systems to solve the problems of large amounts of experimental data at JET.
Blackler K
Joint European Torus (JET) Preprint JET-P(92)13. (submitted to Procs. 2nd Int. Workshop on AI and Expert Systems for High Energy and Nuclear Physics).

42. The soft X-ray real time fast trigger system.
Blackler K Edwards A Holm J
Joint European Torus (JET) Report JET-R(92)06.

43. Model for MHD activity during density limit disruptions in tokamaks.
Bondeson A Parker R D Hugon M Smeulders P
IAEA Technical Committee Meeting on Avoidance and Control of Tokamak Disruptions, Culham Laboratory, 10-12 September 1991.

44. Simulation of MHD activity during density limit disruptions in tokamaks.
Bondeson A Parker R Hugon M
Controlled Fusion and Plasma Physics. 18th European Conf., Berlin, 3-7 June 1991. Contributed papers. Geneva, European Physical Society. 1991. p.II-41.

45. Radioactive waste management at JET.
Booth S J Collins D Newbert G
JET Papers presented at 17th Symp. on Fusion Technology (SOFT-17), Rome, Italy, 1992 Joint European Torus (JET). September 1992. Preprint JET-P(92)72, pp.47-53.

46. Waste management at JET during tritium operations.
Booth S J Newbert G
Fusion Technology vol.21 no.2 pt.2 March 1992 (Procs. 4th National Topical Meeting on Tritium Technology in Fission, Fusion, and Isotopic Applications, Albuquerque, New Mexico) pp.719-723.

47. The nonlinear behaviour of fishbones.
Borba D Nave M F F Porcelli F
Joint European Torus (JET). November 1992. Preprint JET-P(92)82.

48. Scrape-off layer based modelling of the density limit in beryllated JET limiter discharges.
Borrass K Campbell D Clement S Vlases G
Joint European Torus (JET). July 1992. Preprint JET-P(92)44. (submitted for publication in Nuclear Fusion).

49. Phased antenna arrays for fast wave power generation.
Bosia G Jacquinot J
Fast Wave Current Drive in Reactor Scale Tokamaks (Synergy and Complementarity with LHCD and ECRH). IAEA Technical Committee Meeting, Arles, 23-25 September 1991. Association EURATOM-CEA sur la Fusion, Centre d'Etudes de Cadarache, 1992. pp.471-495.

50. Predictive modelling and simulation of energy and particle transport in JET.
Boucher D Rebut P-H
Papers presented to IAEA Technical Committee Meeting on Advances in Simulation and Modelling of Thermonuclear Plasmas, Montreal, 15-17 June 1992. Joint European Torus. September 1992. Preprint JET-P(92)51, pp.1-27.

51. The simulation of energy and particle transport, heat and density pulse propagation and H-mode confinement in JET and a reactor.
Boucher D Rebut P-H Watkins M L
Controlled Fusion and Plasma Physics. 18th European Conf., Berlin, 3-7 June 1991. Contributed papers. Geneva, European Physical Society, 1991. pp.I-177 - I-180.

52. Study of particle transport in the JET tokamak.
Boucher D Rebut P-H Watkins M
C. R. Academy of Science Paris vol.315 no.II 1992 pp.273-278. (Preprint JET-P(92)23).

53. The thermal instrumentation and power accountability of the JET neutral injection system.
Browne A Bickley A J Challis C D de Esch H P L Ewers D T Hogben C H Jensen J Z Jones T T C Stork D Svensson L Tivey R Todd J M Young D Young I D
JET Papers presented at 17th Symp. on Fusion Technology (SOFT-17), Rome, Italy, 14-18 September 1992 Joint European Torus (JET). September 1992. Preprint JET-P(92)72, pp.103-109.

54. Long pulse operation in JET.
Brusati M Bures M Clement S Ehrenberg J Horton L Jones T T C Lawson K Lomas P Morgan P Nielsen P Sartori R Schmidt G Stamp M F Summers D
Papers submitted to the 19th European Conf. on Controlled Fusion and Plasma Physics, Innsbruck, 29 June - 3 July 1992. Joint European Torus (JET). May 1992. Preprint JET-P(92)37, pp.145-150.

55. Phase space distribution of fast electrons induced by lower hybrid waves in JET.
Brusati M Airoldi A Bartlett D Froissard P Gormezano C Jacquinot J Ramponi G Rimini F da Silva R P Tanzi C P
Papers presented to Europhysics Topical Conf. on RF Heating and Current Drive of Fusion Devices, Brussels, 7-10 July 1992. Joint European Torus (JET). May 1992. Preprint JET-P(92)31, pp.31-36.

56. Recent results from the lower hybrid current drive experiment on JET.
Brusati M Ekedahl A Froissard P Gormezano C Jacquinot J Lennholm M Lomas P J Pain M de Andrade M C R Rimini F Schild P Start D F H
Radio Frequency Power in Plasmas. 9th Topical Conf., Charleston, 19-21 August 1991. New York, American Institute of Physics, 1992. pp.233-242.

57. The sawtooth collapse in rotating JET plasmas.
Buchse R Campbell D J Edwards A W Gill R D
Papers submitted to the 19th European Conf. on Controlled Fusion and Plasma Physics, Innsbruck, 29 June - 3 July 1992. Joint European Torus (JET). May 1992. Preprint JET-P(92)37, pp.43-48.

58. Assessment of beryllium Faraday screens of the JET ICRF antennas.
Bures M Jacquinot J J Stamp M F Summers D D R Start D F H Wade T D'Ippolito D A Myra J R
Nuclear Fusion vol.32 no.7 July 1992 pp.1139-1145.

59. Enhanced performance of neutral beam heated hot-ion H-modes on JET by central ICRF heating.
Bures M Balet B Campbell D Cottrell G A Elevant T Eriksson L-G Jacquinot J Jarvis N Jones T Konig R Lomas P Marcus F Righi E Sadler G Start D F H Tanga A van Belle P von Hellermann M
Papers submitted to the 19th European Conference on Controlled Fusion and Plasma Physics, Innsbruck, Austria, 29 June - 3 July 1992. Joint European Torus (JET). May 1992. Preprint JET-P(92)37, pp.55-60.

60. Low particle confinement H-mode observed during ICRF heating on JET.
Bures M Campbell D J Gottardi N A C Jacquinot J J Mattioli M Morgan P D Pasini D Start D F H
Nuclear Fusion vol.32 no.4 April 1992 pp.539-548.

61. The design and performance of the JET ionisation chambers for use with tritium.
Caldwell-Nichols C J Hemmerich J L Lasser R Milverton P
JET Papers presented at 17th Symp. on Fusion Technology (SOFT-17), Rome, Italy, 14-18 September 1992 Joint European Torus (JET). September 1992. Preprint JET-P(92)72, pp.159-165.

62. Radiation monitoring, environmental and health physics aspects during the first JET tritium experiment.
Caldwell-Nichols C J Russ R M Bell A C Davies N Haigh A D Jones H D Serio L
Fusion Engineering and Design vol.19 no.2 September 1992 (Topical Issue on the first JET tritium experiment) pp.149-160.(Preprint JET-P(92)06).

63. Highlights of recent JET operation.
Campbell D J Tanga A JET Team
Joint European Torus (JET). 1992. Preprint JET-P(92)26. (submitted to Plasma Physics and Controlled Fusion).

64. Recent results on confinement in JET.
Campbell D J and JET Team
Transport and Confinement in Toroidal Devices. 2nd Workshop on Magnetic Confinement Fusion, Santander, 2-6 July 1990. Bristol, Adam Hilger. 1992. pp.11-14.

65. New DIII-D tokamak plasma control system.
Campbell G L Lazarus E A et al
General Atomics, San Diego. September 1992. Report GA-A21036. (Paper presented at 17th Symp. on Fusion Technology, Rome, 14-18 September 1992).

66. ρ scaling of confinement in dimensionally similar discharges in JET and DIII-D.
Carlstrom T N DeBoo J C Waltz R E Christiansen J P
American Physical Society Bulletin vol.37 no.6 November 1992 (Program of 1992 Annual Meeting of the APS Division of Plasma Physics, Seattle, 16-20 November 1992) Paper 3E5, p.1410.

67. A nanometer notch filter with high rejection and throughput.
Carolan P G Selden A C Bunting C A Nielson P
Review of Scientific Instruments vol.63 no.10 1992 (Procs. 9th Topical Conf. on High Temperature Plasma Diagnostics, Santa Fe, New Mexico) pp.5161-5163.

68. The installation of the JET pumped divertor systems inside the vacuum vessel.
Celentano G Macklin B Scott S Tait J
Fusion Engineering. 14th IEEE/NPSS Symp., San Diego, 1991. 2 vols. Piscataway, IEEE. 1992. pp.396-399.

69. Density fluctuations and spectral broadening during the lower hybrid current drive experiment on ASDEX.
Cesario R Paoletti et al
Associazione EURATOM-ENEA sulla Fusione, Frascati. November 1991. Report RT/NUCL/91/25.

70. Magnetic field measurements at JET based on the Faraday and motional Stark effects.
Challis C von Hellermann M Keegan B Konig R Mandl W O'Rourke J Wolf F Zwingmann W
Controlled Fusion and Plasma Physics. 18th European Conf., Berlin, 3-7 June 1991. Contributed papers. Geneva, European Physical Society. 1991. pp.IV-229 - IV-232.

71. Bootstrap current dominated ICRH plasmas in JET.
Challis C D Gimblett C G Hender T C Jacquinot J O'Brien D P O'Rourke J Smeulders P Stamp M Stork D Stubberfield P Tibone F Tubbing B J Zwingmann W
Papers presented to Europhysics Topical Conf. on RF Heating and Current Drive of Fusion Devices, Brussels, 7-1992. Preprint JET-P(92)31, pp.1-6.

72. Current ramp experiments on the scaling of energy confinement.
Challis C D Christiansen J P Cordey J G Gormezano C Gowers C W Kramer G J O'Rourke J Stubberfield P M Taroni A Tibone F Tubbing B
Nuclear Fusion vol.32 no.12 December 1992 pp.2217-2228. (Preprint JET-P(92)15).

73. High bootstrap current ICRH plasmas in JET.
Challis C D Hender T C O'Rourke J Ali-Arshad S Alper B de Blank H J Gimblett C G Han J Jacquinot J Kramer G J Kerner W O'Brien D P Smeulders P Stamp M Stork D Stubberfield P M Summers D Tibone F Tubbing B Zwingmann W
Joint European Torus (JET). September 1992. Preprint JET-P(92)76.

74. Reliability study of the JET neutral injection system.
Challis C D Bickley A J Browne A de Esch H P L Fogg M Jones T T C Stork D Svensson L
Fusion Engineering. 14th IEEE/NPSS Symp., San Diego, 1991. 2 vols. Piscataway, IEEE. 1992. pp.62-65.

75. The effect of radial electric field on fast ion losses in divertor tokamaks.
Chankin A V Summers D D R McCracken G M
Papers submitted to the 19th European Conf. on Controlled Fusion and Plasma Physics, Innsbruck, 29 June - 3 July 1992. Joint European Torus (JET). May 1992. Preprint JET-P(92)37, pp.151-156.

76. Parallel currents in the scrape-off layer of JET diverted discharges.
Chankin A V Clement S de Kock L Erents S K Harbour P J Tagle J A
JET papers submitted to 10th Int. Conf. on Plasma Surface Interactions, Monterey, USA, 30 March - 3 April 1992. Joint European Torus (JET). May 1992. Preprint JET-P(92)32, pp.95-108.

77. Power supplies for the stabilisation of plasma vertical position: Recent upgrades and future development.
Chiron D Bonicelli T Huart M Garribba M Mondino P L Noll P
Fusion Engineering. 14th IEEE/NPSS Symp., San Diego, 1991. 2 vols. Piscataway, IEEE. 1992. pp.513-516.

78. Current scaling of plasma confinement.
Christiansen J P Challis C Cordey J G Gormezano C Gowers C Kramer G O'Rourke J Taroni A Tibone F Tubbing B Stubberfield P M

Papers submitted to the 19th European Conf. on Controlled Fusion and Plasma Physics, Innsbruck, 29 June - 3 July 1992. Joint European Torus (JET). May 1992. Preprint JET-P(92)37, pp.37-42.

79. Evidence for a local diffusive model of transport in a tokamak.
Christiansen J P Balet B Boucher D Challis C D Cordey J G Gormezano C Gowers C Kramer G Muir D G Neudatchin S V O'Rourke J Schmidt G Stubberfield P M Taroni A Tibone F Tubbing B
Plasma Physics and Controlled Fusion vol.34 no.13 December 1992 (19th EPS Conference on Controlled Fusion and Plasma Physics, Innsbruck, 29 June - 3 July 1992) pp.1881-1888. (Preprint JET-P(92)54, pp.9-18).

80. Global energy confinement H-mode database for ITER.
Christiansen J P Cordey J G Thomsen K Tanga A; JET Team; DIII-D Research Team; ASDEXTeam; PDX & PBX-M Teams; JFT-2M Group
Nuclear Fusion vol.32 no.2 February 1992 p.291.

81. Experience in the installation programme of the JET active gas handling system.
Chuilon P Bell A C Hemmerich J L
Fusion Technology vol.21 no.2 pt.2 March 1992 (Procs. 4th National Topical Meeting on Tritium Technology in Fission, Fusion, and Isotopic Applications, Albuquerque, New Mexico, 1991) pp.359-364.

82. Deuterium ice production by extrusion technique for a repetitive high speed 6mm diameter pellet injector.
Claudet G Disdier F Kupschus P
JET Papers presented at 17th Symp. on Fusion Technology (SOFT-17), Rome, Italy, 14-18 September 1992 Joint European Torus (JET). September 1992. Preprint JET-P(92)72, pp.175-181.

83. Edge measurements in the divertor region in high density discharges at JET.
Clement S Erents S K Gottardi N Harbour P J Jaeckel H Janeschitz G de Kock L Loarte A Lowry C Saibene G Summers D Tagle J A Vlases G
Papers submitted to the 19th European Conf. on Controlled Fusion and Plasma Physics, Innsbruck, 29 June - 3 July 1992. Joint European Torus (JET). May 1992. Preprint JET-P(92)37, pp.61-66.

84. Assessment techniques for measurement of target erosion/redeposition in large tokamaks.
Coad J P de Kock L Koch A Weschenfelder F Wienhold P Wilhelm R
Joint European Torus (JET). August 1992. Preprint JET-P(92)61. (submitted to J. Nuclear Materials).

85. Deuterium and tritium release on venting the JET torus to air after the beryllium phase.
Coad J P Gibson A Haigh A D Kaveney G Orchard J
Controlled Fusion and Plasma Physics. 18th European Conf., Berlin, 3-7 June 1991. Contributed papers. Geneva, European Physical Society, 1991. pp.III-81 - III-84.

86. Experience with boron-carbide coated target tiles in JET.
Coad J P Farmery B Linke J Wallura E
Joint European Torus, 1992. Preprint JET-P(92)67. (submitted for publication in Journal of Nuclear Materials).

87. Experimental investigation of ELMs and associated fluctuations in JET.
Colton A L Ali-Arshad S Cripwell P Porte L
JET papers submitted to 10th Int. Conf. on Plasma Surface Interactions, Monterey, USA, 1992. Joint European Torus (JET) 1992. Preprint JET-P(92)32, pp.239-254.

88. Measurement techniques for plasma edge parameters related to the H-mode in JET.
Colton A L Porte L Sips A C C
JET papers presented to Course and Workshop on Diagnostics for Contemporary Fusion Experiments, Varenna, Italy, 27 August - 6 September 1991.

89. Measurements of ELMs and associated fluctuations with the multichannel reflectometer system.
Colton A L Cripwell P J
Papers presented to the IAEA Technical Committee Meeting on Reflectometry, JET Joint Undertaking, 4-6 March 1992. Joint European Torus (JET). July 1992. Preprint JET-P(92)55 , pp.55-67. (Also issued as JET-P(92)36).

90. Ray tracing in JET plasmas for the 140 GHz collective scattering diagnostic.
Comiskey M
JET papers presented to Course and Workshop on Diagnostics for Contemporary Fusion Experiments, Varenna, Italy, 27 August - 6 September 1991.

91. An assessment of theoretical models based on observations in the JET tokamak. Part I: Ion heat transport due to ∇T_i instabilities.
Connor J W Maddison G P Wilson H R Corrigan G Stringer T E Tibone F
Joint European Torus (JET) 1992. Preprint JET-P(92)63. (submitted to Plasma Physics and Controlled Fusion).

92. Alpha-particle diagnostics for the D-T phase.
Conroy S W Bergsaker H Coad J P Jarvis O N Marcus F B McCracken G M Pitts R A Sadler G van Belle P Zhu J
Controlled Fusion and Plasma Physics. 18th European Conf., Berlin, 3-7 June 1991. Contributed papers. Geneva, European Physical Society. 1991. pp.IV-265 - IV-268.

93. Electron heating in JET by ICRH.
Cordey J G Christiansen J P Core W Cottrell G Eriksson L-G Kovanen M A Lomas P Start D F H Taroni A Tibone F

Controlled Fusion and Plasma Physics. 18th European Conf., Berlin, 3-7 June 1991. Contributed papers. Geneva, European Physical Society, 1991. pp.III-385 - III-388.

94. ITER: preliminary analysis of energy confinement H-mode database.
Cordey J G DeBoo J C Kardaun O Kaye S M Miura y Schissel D P Suzuki N Thomsen K Christiansen J P Itoh S I Itoh K Matsuda T Mori M Post D E Ryter F Takizuka T Tamai H Tanga A Taylor R Wagner F
Procs. 13th Int. Conf. on Plasma Physics & Controlled Nuclear Fusion Research, Washington, DC., 1-6 October 1990. Vol.3. Vienna, International Atomic Energy Agency. 1991. pp.443-452.

95. Progress toward a tokamak fusion reactor.
Cordey J G Goldston R J Parker R R
Physics Today vol.45 no.1 January 1992 p.22.

96. The transport of energy and particles in JET plasmas.
Cordey J G and JET Team
JET papers presented at 14th IAEA Conf. on Plasma Physics and Controlled Nuclear Fusion Research, Wurzburg, Germany, 30 September - 7 October 1992. Joint European Torus (JET). December 1992. Preprint JET-P(92)84, pp.35-51.

97. A note on the calculation of NBI fast ion distribution functions.
Core W G F
Joint European Torus (JET). November 1992. Report JET-R(92)11.

98. Fast ion current density profile in a tokamak with symmetric launch ion cyclotron resonance heating.
Core W G F Cottrell G A
Nuclear Fusion vol.32 no.9 September 1992 pp.1637-1641. (Preprint JET-P(92)25).

99. First results from the JET time of flight neutral particle analyser.
Corti S Bracco G Moleti A Zanza V
Controlled Fusion and Plasma Physics. 18th European Conf., Berlin, 3-7 June 1991. Contributed papers. Geneva, European Physical Society. 1991. pp.IV-253 - IV-256.

100. Neutral particles analysis in JET.
Corti S Bracco G Moleti A Zanza V Khudoleev A V Kislyakov A I Petrov M P Petrov S Ya
JET papers presented to Course and Workshop on Diagnostics for Contemporary Fusion Experiments, Varenna, Italy, 27 August - 6 September 1991.

101. A collective scattering diagnostic to measure fast-ion and alpha-particle distributions in JET.
Costley A E Bindlev H Comisky M Fessey J Hammond N Hoekzema J A Hughes T P Machuzak J Roberts P Stevens A Stott P E Taylor E Woskov P
JET papers presented to Course and Workshop on Diagnostics for Contemporary Fusion Experiments, Varenna, Italy, 27 August - 6 September 1991.

102. Measurement of the toroidal motion of fine- scale density structures in JET plasmas.
Costley A E Cripwell P Fukuda T
Papers submitted to the 19th European Conf. on Controlled Fusion and Plasma Physics, Innsbruck, 29 June - 3 July 1992. Joint European Torus (JET). May 1992. Preprint JET-P(92)37, pp.67-72.

103. Measurements of electron cyclotron emission and absorption.
Costley A E
JET papers presented to Course and Workshop on Diagnostics for Contemporary Fusion Experiments, Varenna, Italy, 27 August - 6 September 1991.

104. Microwave reflectometry.
Costley A E
JET papers presented to Course and Workshop on Diagnostics for Contemporary Fusion Experiments, Varenna, Italy, 27 August - 6 September 1991.

105. Millimetric measurement systems at the JET project.
Costley A E
Joint European Torus (JET). September 1992. Preprint JET-P(92)74. (submitted to Procs. 'MM92' Conf. and Exhibition, Brighton, October 1992).

106. A "comb" reflectometer: A simple device for determining the peak density in difficult experimental situation.
Costley A E Fessey J
Papers presented to the IAEA Technical Committee Meeting on Reflectometry, JET Joint Undertaking, 4-6 March 1992. Joint European Torus (JET). July 1992. Preprint JET-P(92)55, pp.81-87.

107. Identification of ion cyclotron emission from fusion alpha particles during JET deuterium- tritium experiments.
Cottrell G A Bhatnagar V P da Costa O Dendy R O Edwards A Jacquinot J Nave M F F Schmid M Sibley A Smeulders P Start D F H
Plasma Physics and Controlled Fusion vol.34 no.13 December 1992 (19th EPS Conference on Controlled Fusion and Plasma Physics, Innsbruck, 29 June - 3 July 1992) pp.1969. (Preprint JET-P(92)54, pp.1-8. Also issued as JET-P(92)37).

108. Ion cyclotron emission measurements during JET deuterium-tritium experiments.
Cottrell G A Bhatnagar V P da Costa O Dendy R O Jacquinot J McCune D C Nave M F F Smeudlers P Start D F H
Joint European Torus (JET). December 1992. Preprint JET-P(92)96. (submitted to Nuclear Fusion).

109. Measurements of the distribution of impurity line radiation in JET with scanning VUV spectrometers.
Coulon J-P Jackel H Janeschitz Giannella R
Diagnostics for Contemporary Fusion Experiments, Varenna, 27 August - 6 September 1991. Report EN 36321 ORA.

110. Correlation reflectometry measurements at JET.
Cripwell P Costley A E Fukuda T
Papers presented to the IAEA Technical Committee Meeting on Reflectometry, JET Joint Undertaking, 4-6 March 1992.Joint European Torus (JET). July 1992. Preprint JET-P(92)55, pp.69-79.

111. Evidence of fine scale density structures on JET under additional heated conditions.
Cripwell P Costley A E
Controlled Fusion and Plasma Physics. 18th European Conf, Berlin, 3-7 June 1991. Contributed papers. Geneva, European Physical Society. 1991. pp.I-17 - I-20.

112. Numerical simulation of fluctuation measurements by reflectometry.
Cripwell P
Papers presented to the IAEA Technical Committee Meeting on Reflectometry, JET Joint Undertaking, 4-6 March 1992. Joint European Torus (JET). July 1992. Preprint JET-P(92)55, pp.25-37.

113. Observation of velocity dependence and line-of-sight effects in ion temperature and toroidal rotation velocity measurements in JET.
Danielsson M Kallne E Zastrow K-D von Hellermann M Mandl W Morsi H Summers H P
Controlled Fusion and Plasma Physics. 18th European Conf., Berlin, 3-7 June 1991. Contributed papers. Geneva, European Physical Society. 1991. pp.IV-273 - IV-276.

114. On comparison of spectroscopically deduced central ion temperatures and plasma rotation at JET.
Danielsson M von Hellermann M G Kallne E Mandl W Morsi H W Summers H P Zastrow K-D
Review of Scientific Instruments vol.63 no.4 pt.I April 1992 pp.2241-2247.

115. Experience with helium neutral beam systems.
de Esch H P L Massmann P Bickley A J Challis C D Deschamps G H Falter H D Hemsworth R S Jones T T C Stork D Svensson L Young D
Fusion Engineering. 14th IEEE/NPSS Symp., San Diego, 30 September - 3 October 1991. 2 vols. Piscataway, IEEE. 1992. pp.86-89.

116. Local confinement in neutral beam heated JET discharges.
de Esch H P L Tibone F Balet B Bickley A J Challis C D Cordey J G Jones T T C Stork D von Hellermann M
Controlled Fusion and Plasma Physics. 18th European Conf., Berlin, 3-7 June 1991. Contributed papers. Geneva, European Physical Society, 1991. pp.I-189 - I-192.

117. Excitation of neutral helium by electron impact.
de Heer F J Hoekstra R Kingston A E Summers H P
Joint European Torus (JET). February 1992. Preprint JET-P(92)09. (submitted to Nuclear Fusion supple. series "Atomic and Plasma- material Interaction Data for Fusion").

118. A new assessment of cross section data for helium excitation by protons.
de Heer F J Hoekstra R Summers H P
Joint European Torus (JET). February 1992. Preprint JET-P(92)10. (submitted to Nuclear Fusion supple. series "Atomic and Plasma- material Interaction Data for Fusion").

119. Fourier analysis of sawtooth heat pulse propagation and comparison with other methods using JET data.
de Luca F Gorini G Hogeweij G M D Jacchia A Kramer G Lopes Cardozo N J Mantica P Sips A C C
Joint European Torus (JET). March 1992. Preprint JET-P(92)18. (submitted to Nuclear Fusion).

120. Fatigue of inertial beryllium elements for the JET Mark I pumped divertor.
Deksnis E B Falter H D Massmann P Miele P Pick M A
JET Papers presented at 17th Symp. on Fusion Technology (SOFT-17), Rome, Italy, 1992 Joint European Torus (JET) 1992. Preprint JET-P(92)72, pp.33-39.

121. Spectral emission characteristics of beryllium near tokamak plasma-wall boundaries.
Dickson W J Breger P Loarte A Morsi H Stamp M F Summers H P
JET papers presented to Course and Workshop on Diagnostics for Contemporary Fusion Experiments, Varenna, Italy, 27 August - 6 September 1991.

122. Vacuum problems and solutions related to the tritium experiment at JET.
Dietz K J and JET Team
Joint European Torus (JET). September 1992. Preprint JET-P(92)70.

123. Experience with high heat flux components in large tokamaks.
Dietz K J et al
Fusion Engineering and Design vol.16 1991 (Procs. 2nd Int. Symp. on Fusion Nuclear Technology, Karlsruhe, Germany, 2-7 June 1991). p.229.

124. Full-wave simulations of current profiles for fast magnetosonic wave current drive.
Dmitrieva M V Eriksson L-G Gambier D J
Joint European Torus (JET) 1992. Report JET-R(92)09.

125. Operation of the lower hybrid current drive system.
Dobbing J A Bosia G F Brinkschulte H W Brusati M Ekedahl A C Gormezano C Jacquinot J G Kaye A S Lennholm M Pain M S Rey G Rimini F Schild P A J

JET Papers presented at 17th Symp. on Fusion Technology (SOFT-17), Rome, Italy, 14-18 September 1992 Joint European Torus (JET). September 1992. Preprint JET-P(92)72, pp.183-189.

126. Status and prospects of controlled thermonuclear fusion.
Duchs D F Hellsten T
Joint European Torus (JET). October 1992. Preprint JET-P(92)88. (submitted to Muon Catalysed Fusion).

127. Destruction of drift surfaces in tokamaks through small magnetic field perturbations.
Duchs D F Montvai A
JET Contributions to 4th European Fusion Theory Conf., Aspenas, Sweden, 17-19 June 1991.

128. Influence of external tokamak coil imperfections on the structure of the boundary layer magnetic field.
Duchs D F Montvai A
Contributions to Plasma Physics vol.32 no.3-4 1992 (3rd Int. Workshop on Plasma Edge Theory in Fusion Devices, Bad Honnef, Germany, 22-24 June 1992) pp.198-203. (Preprint JET-P(92)52).

129. Recent steps towards a controlled thermonuclear fusion reactor with results from the JET tokamak device.
Duchs D F
Joint European Torus (JET). November 1992. (Invited lecture presented at the Int. Symp. on Physics and High Technology, Seoul, Korea, 22-23 October 1992).

130. Subdiffusive behaviour of Hamiltonian motion in overlapping island domains.
Duchs D F Montvai A Riedel K S
American Physical Society Bulletin vol.37 no.6 November 1992 (Program of 1992 Annual Meeting of the APS Division of Plasma Physics, Seattle, 16-20 November 1992) Paper 7R9, p.1542.

131. Global sawtooth instability measured by magnetic coils in the JET tokamak.
Duperrex P A Pochelon A Edwards A W Snipes J A
Nuclear Fusion vol.32 no.7 July 1992 pp.1161-1180.

132. A comparison of JET sawtooth behaviour in plasmas with co- and counter neutral beam injection.
Edwards A W Bickley A Buchse R Challis C D Konig R Marcus F B O'Rourke J Stork D
Papers submitted to the 19th European Conf. on Controlled Fusion and Plasma Physics, Innsbruck, 1992. Joint European Torus Preprint JET-P(92)37, pp.85-90.

133. Material related aspects of density control in JET plasma discharges.
Ehrenberg J Andrew P Horton L Janeschitz G de Kock L Philipps V
JET papers submitted to 10th Int. Conf. on Plasma Surface Interactions, Monterey, USA, 30 March - 3 April 1992. Joint European Torus (JET). May 1992. Preprint JET-P(92)32, pp.151-167.

134. Influence of plasma configuration and poloidal shaping on the coupling of the lower hybrid waves in JET.
Ekedahl A Brinkschulte H Brusati M Dobbing J A Gormezano C Jacquinot J Kaye A Lennholm M Pepe da Silva R Rimini F Schild P Tagle J A
Papers presented to Europhysics Topical Conf. on RF Heating and Current Drive of Fusion Devices, Brussels, 7-10 July 1992. Joint European Torus (JET). May 1992. Preprint JET-P(92)31, pp.19-24.

135. The new JET 2.5-MeV neutron time-of-flight spectrometer.
Elevant T van Belle P Grosshog G Hoek M Jarvis O N Olsson M Sadler G
Review of Scientific Instruments vol.63 no.10 pt.II October 1992 (Procs. 9th Topical Conf. on High Temperature Plasma Diagnostics, Santa Fe, New Mexico, 15-19 March 1992) pp.4586-4588.

136. Calculation of fast wave current drive efficiencies and profiles with a global wave code.
Eriksson L G Hellsten T
Fast Wave Current Drive in Reactor Scale Tokamaks (Synergy and Complementarity with LHCD and ECRH). IAEA Technical Committee Meeting, Arles, 23-25 September 1991. Association EURATOM-CEA sur la Fusion, Centre d'Etudes de Cadarache, 1992. pp.98-106.

137. Broadening of ICRH produced fast ion profiles due to orbit effects.
Eriksson L-G Porcelli F
JET Contributions to 4th European Fusion Theory Conf., Aspenas, Sweden, 17-19 June 1991.

138. Finite orbit-width effects on stochastic ripple diffusion.
Eriksson L-G Helander P
Joint European Torus (JET). December 1992. Preprint JET-P(92)98. (submitted to Nuclear Fusion).

139. Modelling of ICRH on JET.
Eriksson L-G
JET Contributions to 4th European Fusion Theory Conf., Aspenas, Sweden, 17-19 June 1991.

140. Non-standard high energy ion orbits.
Eriksson L-G Berk H Porcelli F Stankiewicz R
Papers submitted to the 19th European Conf. on Controlled Fusion and Plasma Physics, Innsbruck, 1992. Joint European Torus Preprint JET-P(92)37, pp.229-234.

141. Observations of toroidal plasma rotation induced by ICRH in JET.
Eriksson L-G Giannella R Hellsten T Kallne E Sundstrom G
Plasma Physics and Controlled Fusion vol.34 no.5 May 1992 pp.863-871.

142. Ohmic ion temperature and thermal diffusivity profiles from the JET neutron emission profile monitor
Eposito B Marcus F B Adams J M Conroy S Jarvis O N Loughlin M J Sadler G van Belle P Watkins N
Joint European Torus (JET). December 1992. Preprint JET-P(92)102. (submitted to Plasma Physics and Controlled Fusion).

143. $T_i(r)$ profiles from the JET neutron profile monitor for ohmic discharges.
Esposito B Marcus F B Adams J M Conroy S Jarvis O N Loughlin M J Sadler G van Belle P Watkins N
Controlled Fusion and Plasma Physics. 18th European Conf., Berlin, 3-7 June 1991. Contributed papers. Geneva, European Physical Society. 1991. pp.IV-277 - IV-280.

144. High resolution LIDAR Thomson scattering at JET.
Fajemirokun H Gowers C Hirsch K Kajiwara T Nielsen P Salzmann H
JET papers presented to Course and Workshop on Diagnostics for Contemporary Fusion Experiments, Varenna, Italy, 27 August - 6 September 1991.

145. Hydrogen isotope exchange in the JET neutral beam injection system.
Falter H D Ciric D Deschamps G H de Esch H P L Massmann P Svensson L
JET Papers presented at 17th Symp. on Fusion Technology (SOFT-17), Rome, Italy, 14-18 September 1992 Joint European Torus (JET). September 1992. Preprint JET-P(92)72, pp.87-93.

146. Implantation and desorption of tritium and tritium recovery from the JET neutral beam injectors.
Falter H D Thompson E Ciric D de Esch H P L
JET papers submitted to 10th Int. Conf. on Plasma Surface Interactions, Monterey, USA, 1992. Joint European Torus (JET). May 1992. Preprint JET-P(92)32, pp.289-300.

147. Thermal test results of the JET divertor plates.
Falter H D Altmann H Baxi Ch Deschamps G H Hemsworth R S Martin D Massmann P
Joint European Torus (JET). July 1992. Preprint JET-P(92)48.

148. SINBAD–Afast neutral beam particle deposition code.
Feng Y Wolle B
Joint European Torus (JET) 1992. Report JET-R(92)13.

149. A locked mode associated with low density in JET.
Fishpool G M Campbell D J Fitzpatrick R Haynes P S
IAEA Technical Committee Meeting on Avoidance and Control of Tokamak Disruptions, Culham Laboratory, 10-12 September 1991.

150. Measurements of the poloidal structure of locked modes in JET.
Fishpool G M
JET papers presented to Course and Workshop on Diagnostics for Contemporary Fusion Experiments, Varenna, Italy, 27 August - 6 September 1991.

151. He^{2+}-H collisions: experimental charge exchange cross sections and their relevance for alpha particle diagnostics at JET.
Frieling G J Hoekstra R Morgenstern R de Heer F J
Atomic Physics of Highly Charged Ions. 5th Int. Conf. on the Physics of Highly Charged Ions, Giessen, 10-14 September 1990. Invited lectures and contributed papers. Berlin, Springer-Verlag. 1991. pp.163-164.

152. Fast electron dynamics during LHCD in JET.
Froissard P Brusati M Adams J M Ekedahl A Gormezano C Jarvis O N Pasini D Peysson Y Ramos de Andrade M C Rimini F Sadler G
Controlled Fusion and Plasma Physics. 18th European Conf., Berlin, 3-7 June 1991. Contributed papers. Geneva, European Physical Society, 1991. pp.III-389 - III-392.

153. Heat transmission at the divertor sheath of DIII-D.
Futch A H Cuthbertson J W Buchenauer D A Hill D N Matthews G F Lowry C Porter G D Jong R A
American Physical Society Bulletin vol.37 no.6 November 1992 (Program of 1992 Annual Meeting of the APS Division of Plasma Physics, Seattle, 16-20 November 1992) Paper 8Q11, p.1567.

154. Control and operational aspects of the MASCOT 4 force feedback servomanipulator for JET.
Galbiati L Raimondi T Garetti P Costi G
Fusion Engineering. 14th IEEE/NPSS Symp., San Diego, 1991. 2 vols. Piscataway, IEEE. 1992. pp.563-566.

155. Comparison of impurity and electron particle transport in JET discharges.
Giannella R Hawkes N C Lauro-Taroni L Mattioli M O'Rourke J Pasini D
Plasma Physics and Controlled Fusion vol.34 no.5 May 1992 pp.687-697.

156. Comparison of the impurity and electron particle transport in JET discharges.
Giannella R Hawkes N C Lauro-Taroni L Mattioli M O'Rourke J Pasini D
Controlled Fusion and Plasma Physics. 18th European Conf., Berlin, 3-7 June 1991. Contributed papers. Geneva, European Physical Society, 1991. pp.I-197 - I-200.

157. Poloidal asymmetry of impurity in co- and counter-injection experiment at JET.
Giannella R Christensen M de Angelis R Gottardi N Lauro-Taroni L Mattioli M Pasini D
Papers submitted to the 19th European Conf. on Controlled Fusion and Plasma Physics, Innsbruck, 29 June - 3 July 1992. Joint European Torus (JET). May 1992. Preprint JET-P(92)37, pp.115-120.

158. Experiments using D-T plasmas in the JET tokamak.
Gibson A and JET Team
JET papers presented at 14th IAEA Conf. on Plasma Physics and Controlled Nuclear Fusion Research, Wurzburg, Germany, 30 September - 7 October 1992. Joint European Torus (JET). December 1992. Preprint JET-P(92)84, pp.25-34.

159. Fusion found–the deuterium-tritium reaction in the JET tokamak.
Gibson A
Plasma Physics and Controlled Fusion vol.34 no.4 April 1992 pp.407-409.

160. Effects of neutrons on the JET soft X-ray detectors.
Gill R D Alper B Edwards A W
Papers submitted to the 19th European Conf. on Controlled Fusion and Plasma Physics, Innsbruck, 29 June - 3 July 1992. Joint European Torus (JET). May 1992. Preprint JET-P(92)37, pp.19-24.

161. Generation and loss mechanisms of runaway electrons following disruptions in JET.
Gill R D Edwards A W
Papers submitted to the 19th European Conf. on Controlled Fusion and Plasma Physics, Innsbruck, 1992. Joint European Torus, 1992. Preprint JET-P(92)37, pp.13-18.

162. Snake-like density perturbations in JET.
Gill R D Edwards A W Pasini D Weller A
Nuclear Fusion vol.32 no.5 May 1992 pp.723-735.

163. Spontaneous appearance of snakes in JET.
Gill R D Edwards A W Pasini D Wolfe S W
Controlled Fusion and Plasma Physics. 18th European Conf., Berlin, 3-7 June 1991. Contributed papers. Geneva, European Physical Society. 1991. pp.II-49 - II-52.

164. Investigations of impurity control in JET using fueling and interpretation of experiments using the LIM impurity code.
Gondhalekar A Stangeby P C Elder J D
Joint European Torus (JET). October 1992. Preprint JET-P(92)89. (submitted to Nuclear Fusion).

165. Long pulse high power heating of JET plasmas.
Gondhalekar A Bamsley R Jones T T C Morgan P D Lomas P Pasini D Stamp M F Stangeby P C Summers D Tagle J A Tanga A
Controlled Fusion and Plasma Physics. 18th European Conf, Berlin, 3-7 1991. Contributed papers. pp.I-25 - I-28.

166. Perturbative measurement of suprathermal electron diffusion in JET.
Gondhalekar A Bartlett D Lomas P Martin-Solis R O'Brien M
Papers submitted to the 19th European Conf. on Controlled Fusion and Plasma Physics, Innsbruck, 29 June - 3 July 1992. Joint European Torus (JET). May 1992. Preprint JET-P(92)37, pp.169-174.

167. Specification of a helium atom beam required for neutral particle analysis and for charge exchange resonance spectroscopy applications in JET.
Gondhalekar A
Joint European Torus (JET). November 1992. Report JET-R(92)12.

168. Release of tritium from the JET vacuum vessel after high power discharges.
Goodall D H J Andrew P Ehrenberg J McCracken G M Peacock A T Saibene G Sartori R van Belle P
JET papers submitted to 10th Int. Conf. on Plasma Surface Interactions, Monterey, USA, 30 March - 3 April 1992. Joint European Torus (JET). May 1992. Preprint JET-P(92)32, pp.205-222.

169. Lower hybrid current drive experiments on JET.
Gormezano C Bosia G Brusati M Dobbing J Ekedahl A Froissard P Jacquinot J Kaye A Lennholm M Naito O Pain M Paoletti F Pasini D Ramos de Andrade C Rey G Rimini F Schild P
Controlled Fusion and Plasma Physics. 18th European Conf., Berlin, 3-7 June 1991. Contributed papers. Geneva, European Physical Society, 1991. pp.III-393 - III-396.

170. Non-inductive current drive in JET.
Gormezano C and JET Team
JET papers presented at 14th IAEA Conf. on Plasma Physics and Controlled Nuclear Fusion Research, Wurzburg, Germany, 30 September -7 October 1992. Joint European Torus (JET). December 1992. Preprint JET-P(92)84, pp.1-23.

171. Synergistic effects between lower hybrid and fast magnetosonic waves in JET.
Gormezano C Brusati M Ekedahl A Froissard P Jacquinot J Rimini F
Fast Wave Current Drive in Reactor Scale Tokamaks (Synergy and Complementarity with LHCD and ECRH). IAEA Technical Committee Meeting, Arles, 23-25 September 1991. Association EURATOM-CEA sur la Fusion, Centre d'Etudes de Cadarache, 1992. pp.244-259.

172. Phased operation of the JET A_2 antenna arrays.
Goulding R H Batchelor D B Hoffman D J Jaeger E F Ryan P M Stallings D C Bhatnagar V Bosia G Kaye A S Wade T J
American Physical Society Bulletin vol.37 no.6 November 1992 (Program of 1992 Annual Meeting of the APS Division of Plasma Physics, Seattle, 16-20 November 1992) Paper 5S23, p.1494.

173. Electron pressure gradient measurements on JET H-mode and pellet fuelled discharges from the new high resolution LIDAR scattering system.

Gowers C Fajemirokun H Kajiwara T Nielsen P Schunke B
American Physical Society Bulletin vol.37 no.6 November 1992 (Program of 1992 Annual Meeting of the APS Division of Plasma Physics, Seattle, 16-20 November 1992) Paper 3Q4, p.1421.

174. Thomson scattering diagnostics for contemporary fusion experiments: I - Conventional Thomson scattering.
Gowers C
JET papers presented to Course and Workshop on Diagnostics for Contemporary Fusion Experiments, Varenna, Italy, 27 August - 6 September 1991.

175. Thomson scattering diagnostics for contemporary fusion experiments: II - LIDAR Thomson scattering.
Gowers C
JET papers presented to Course and Workshop on Diagnostics for Contemporary Fusion Experiments, Varenna, Italy, 27 August - 6 September 1991.

176. Status and prospects of JET tritium operation.
Haange R Ballantyne P Bell A C Booth S J Caldwell-Nichols C Chuilon P Hemmerich J L Jaeger J-F Konstantellos A Lasser R Newbert G Wong D Wykes M E P
Fusion Technology vol.21 no.2 pt.2 March 1992 (Procs. 4th National Topical Meeting on Tritium Technology in Fission, Fusion, and Isotopic Applications, Albuquerque, New Mexico, 1991) pp.253-255.

177. The behaviour of neutral particles in the private region of X-point discharges in JET.
Haas G Duchs D Ehrenberg J Lesourd M Montvai A Reichle R Summers D
Controlled Fusion and Plasma Physics. 18th Euro. Conf., Berlin, 3-7 June 1991. Contributed papers. Geneva, European Physical Society. 1991. pp.III-101 - III-104.

178. A new approach to scaling of the scrape-off layer and divertor plasma in JET.
Harbour P J Clement S de Kock L Jackel H J Lesourd M Loarte A O'Brien D P Summers D D R Tagle J A
JET papers submitted to 10th Int. Conf. on Plasma Surface Interactions, Monterey, USA, 1992. Joint European Torus (JET) 1992. Preprint JET-P(92)32, pp.321-333.

179. An analysis of trapped particle effects on fast wave current profiles.
Hellsten T Eriksson L G
Fast Wave Current Drive in Reactor Scale Tokamaks (Synergy and Complementarity with LHCD and ECRH). IAEA Technical Committee Meeting, Arles, 23-25 September 1991. Association EURATOM-CEA sur la Fusion, Centre d'Etudes de Cadarache, 1992. pp.48-58.

180. The cryogenic diffusion pump - an advanced design for fusion reactor primary pumping and fuel processing.
Hemmerich J L
Fusion Technology vol.21 no.2 pt.2 March 1992 (Procs. 4th National Topical Meeting on Tritium Technology in Fission, Fusion, and Isotopic Applications, Albuquerque, New Mexico, 1991) pp.276-281.

181. Gas recovery system for the first JET tritium experiment.
Hemmerich J L Lasser R Winkel T
Fusion Engineering and Design vol.19 no.2 September 1992 (Topical Issue on the first JET tritium experiment) pp.161-168. (Preprint JET-P(92)05).

182. A systematic approach to the design of a large scale detritiation system for controlled thermonuclear fusion experiments.
Hemmerich J L
Joint European Torus (JET). July 1992. Preprint JET-P(92)50. (submitted to Fusion Technology).

183. Marfe stability.
Hender T C Wesson J A
Controlled Fusion and Plasma Physics. 18th European Conf., Berlin, 3-7 June 1991. Contributed papers Geneva, European Physical Society. 1991. pp.IV-81 - IV-84.

184. High-β_p MHD activity in JET.
Hender T C Alper B Ali-Arshad S de Blank H J Challis C D Gimblett C Han J Jacquinot J Kramer G J Kerner W Nave M F O'Brien D P O'Rourke J Smeulders P Stamp M Summers D Tibone F Tubbing B Zolfaghari A Zwingmann W
Papers submitted to the 19th European Conf. on Controlled Fusion and Plasma Physics, Innsbruck, 1992. Joint European Torus Preprint JET-P(92)37, pp.259-264.

185. Monte Carlo calculations of efficiency, resolution, and response functions for the new neutron time-of-flight spectrometer at JET.
Hoek M
Nuclear Instruments and Methods in Physics Research A, vol.A323 no.3 1992 pp.656-670. (Preprint JET-P(92)39).

186. Charge transfer in collisions of protons on helium.
Hoekstra R Summers H P de Heer F J
Joint European Torus (JET). February 1992. Preprint JET-P(92)08. (Preprint of paper to be submitted for publication in Nuclear Fusion supplement series "Atomic and Plasma-material Interaction Data for Fusion").

187. Hydrogen, deuterium, and tritium isotope exchange experiments in JET.
Horton L D Andrew P Bracco G Conroy S Corti S Ehrenberg J Goodall D H J Jarvis O N Lomas P Loughlin M Peacock A T Saibene G Sadler G Sartori R Stamp M P Thomas P R van Belle P
JET papers submitted to 10th Int. Conf. on Plasma Surface Interactions, Monterey, USA, 1992. Joint European Torus (JET). 1992. Preprint JET-P(92)32, pp.51-64.

188. Measurement of helium transport in JET.
Horton L D Denne-Hinnov B Gondhalekar A Lauro-Taroni L Jones T T C von Hellermann M
JET papers presented at 14th IAEA Conf. on Plasma Physics and Controlled Nuclear Fusion Research, Wurzburg, Germany, 30 September - 7 October 1992. Joint European Torus (JET). December 1992. Preprint JET-P(92)84, pp.67-73.

189. Pellet penetration experiments on JET.
Houlberg W A Attenberger S E Baylor L R Gadeberg M Jernigan T C Kupschus P Milora S L Schmidt G L Swain D W Watkins M L
Nuclear Fusion vol.32 no.11 November 1992 pp.1951-1966. (Preprint JET-P(92)19).

190. AC operation of JET tokamak: Modification of the JET poloidal field system.
Huart M Chiron D Dolgetrta N Garribba M Noll P Tubbing B Benfatto I
Fusion Engineering. 14th IEEE/NPSS Symp., San Diego, 30 September - 3 October 1991. 2 vols. Piscataway, IEEE. 1992. pp.181-186.

191. Spectral simulation and analysis at JET.
Hughes I G Briden P Barnsley R Giannella R Summers H P Coffey I H McWhirter R W P
JET papers presented to Course and Workshop on Diagnostics for Contemporary Fusion Experiments, Varenna, Italy, 27 August - 6 September 1991.

192. Joint European Torus (JET) - Regulatory aspects of radioactive waste management.
Hughes P
Fusion Technology vol.21 no.2 pt.2 March 1992 (Procs. 4th National Topical Meeting on Tritium Technology in Fission, Fusion, and Isotopic Applications, Albuquerque, New Mexico. 1991) pp.389-394.

193. Current rise studies.
Hugon M Balet B Christiansen J P Edwards A Fishpool G Gimblett C G Gottardi N Hastie R J Lomas P van Milligen B Neill G O'Rourke J Sips G Smeulders P Stubberfield P M Tagle T Wolfe S
Controlled Fusion and Plasma Physics. 18th European Conf, Berlin, 3-7 June 1991. Contributed papers. Geneva, European Physical Society. 1991. pp.I-41 - I-44.

194. Diffusion of fast electrons after a monster sawtooth crash.
Hugon M Bartlett D Brusati M Froissard P Gormezano C Morgan P Porte L Rimini F Stamp M
Papers submitted to the 19th European Conf. on Controlled Fusion and Plasma Physics, Innsbruck, 29 June - 3 July 1992. Joint European Torus (JET). May 1992. Preprint JET-P(92)37, pp.163-168.

195. Shear reversal and MHD activity during pellet enhanced performance pulses in JET.
Hugon M van Milligen B Ph Smeulders P Appel L C Bartlett D V Boucher D Edwards A W Eriksson L-G Gowers C W Hender T C Huysmans G Jacquinot J J Kupschus P Porte L Rebut P H Start D F H Tibone F Tubbing B J D Watkins M L Zwingmann W
Nuclear Fusion vol.32 no.1 January 1992 pp.33-44.

196. Design of the JET pumped divertor.
Huguet M Altmann H Barabaschi P Bertolini E Dietz K Deksnis E Falter H Froger C Garribba M Kaye A Last J R Lobel R Martin E Massmann P Noll P Obert W Papastergiou S Peacock A Pick M Rebut P H Rossi L Sborchia C Sannazzaro G Tesini A Tivey R
Fusion Engineering. 14th IEEE/NPSS Symp., San Diego, 1991. 2 vols. Piscataway, IEEE. 1992. pp.440-443.

197. Technical aspects of the first JET tritium experiment.
Huguet M Haange R Bell A C Booth S J Caldwell-Nichols C Carmichael A Chuilon P Davies N Dietz K J Delvart F Erhorn F Falter H Green B J Grieveson B Haigh A Hemmerich J L Holland D How J Jones T T C Laesser R Laveyry M Lupo J Miller A Milverton P Newbert G Orchard J Peacock A Russ R Saibene G Sartori R Serio L Stagg R Svensson S L Thompson E Trevalion P Usselmann E Winkel T Wykes M E P
Fusion Technology vol.21 no.3 Pt.2A May 1992 (Procs. 10th Topical Meeting on The Technology of Fusion Energy, Boston, Mass., 7-12 June 1992) pp.1317-1323.

198. Technical aspects of the first JET tritium experiment.
Huguet M Bell A C Booth S J Caldwell-Nichols C Carmichael A Chuilon P Davies N Dietz K J Delvart F Erhorn F Falter H Green B J Grieveson B Haange R Haigh A Hemmerich J L Holland D How J Jones T T C Laesser R Laveyry M Lupo J Miller A Milverton P Newbert G Orchard J Peacock A Russ R Saibene G Sartori R Serio L Stagg R Svensson S L Thomson E Trevalion P Usselmann E Winkel T Wykes M E P
Fusion Engineering and Design vol.19 no.2 September 1992 (Topical Issue on the first JET tritium experiment) pp.121-132.(Preprint JET-P(92)07).

199. MHD stability analysis of high-β JET discharges.
Huysmans G T A Hender T C Kwon O J Goedbloed J P Lazzzaro E Smeulders P
Plasma Physics and Controlled Fusion vol.34 no.4 April 1992 pp.487-499.

200. MHD stability models of edge localized modes in JET discharges.
Huysmans G T A de Blank H J Kerner W Goedbloed J P Nave M F F
Papers submitted to the 19th European Conf. on Controlled Fusion and Plasma Physics, Innsbruck, 1992. Joint European Torus Preprint JET-P(92)37, pp.265-270.

201. Impurity edge transport in the vicinity of the beryllium belt limiters in JET.

Hwang A Elder J D Goodall D H J McCracken G M Stangeby P C Summers D D R
JET papers submitted to 10th Int. Conf. on Plasma Surface Interactions, Monterey, USA, 30 March - 3 April 1992. Joint European Torus (JET). May 1992. Preprint JET-P(92)32, pp.187-203.

202. JET recent results on wave heating and current drive; consequences for future devices.
Jacquinot J Bhatnagar V P Gormezano C and JET Team
Joint European Torus (JET). October 1992. Preprint JET-P(92)77. (submitted to Plasma Physics and Controlled Fusion).

203. Joint European Torus results with both fast and lower-hybrid wave consequences for future devices.
Jacquinot J Bures M JET Team
Physics of Fluids B vol.4 no.7 pt.2 July 1992 (Invited and review papers from the 33rd Annual Meeting of the APS Division of Plasma Physics, 4-8 November 1991) pp.2111-2121.

204. D-^{3}He fusion in the Joint European Torus tokamak - recent experimental results.
Jacquinot J Sadler G J and JET Team
Fusion Technology vol.21 no.4 July 1992 (Special Issue on D-^{3}He Fusion) pp.2254-2264.

205. Radial carbon flux profiles in the upper divertor in JET at high target load.
Jaeckel H J Lingertat J Summers D D R Clement S Lesourd M Matthews G F Maggi C F Summers H P
Papers submitted to the 19th European Conf. on Controlled Fusion and Plasma Physics, Innsbruck, 29 June - 3 July 1992. Joint European Torus (JET). May 1992. Prepint JET-P(92)37, pp.205-210.

206. Comparison of plasma performance with beryllium and carbon divertor targets in JET.
Janeschitz G and JET Team
JET papers presented at 14th IAEA Conf. on Plasma Physics and Controlled Nuclear Fusion Research, Wurzburg, Germany, 1992. Joint European Torus (JET). December 1992. Preprint JET-P(92)84, pp.75-86.

207. Dependence of He retention on X-point plasma parameters in JET.
Janeschitz G Gottardi N Jaeckel H Coulon J P Denne B Giannella R Haas G Lawson K Tagle T
Controlled Fusion and Plasma Physics. 18th Euro. Conf., Berlin, 3-7 June 1991. Contributed papers. Geneva, European Physical Society. 1991. pp.III-97 - III-100.

208. Divertor performance on carbon and beryllium targets in JET.
Janeschitz G Konig R Lauro-Taroni L Lingertat J Matthews G Stamp M Vlases G Campbell D Clement S de Kock L Eckstein W Ehrenberg J Gottardi N Harbour P Horton L Jackel H Lesourd M Loarte A Lowry C Roth J Saibene G Summers D Tagle J A Thomas P R von Hellermann M
JET papers submitted to 10th Int. Conf. on Plasma Surface Interactions, Monterey, USA, 1992. Joint European Torus (JET). May 1992. Preprint JET-P(92)32, pp.33-49.

209. High power operation with a radiative divertor in JET.
Janeschitz G Clement S Gottardi N Lesourd M Lingertat J Lowry C Radford G Saibene G Stamp M Summers D Taroni A Thomas P R Vlases G
Papers submitted to the 19th European Conf. on Controlled Fusion and Plasma Physics, Innsbruck, 1992. Joint European Torus Preprint JET-P(92)37, pp.127-132.

210. Neutron and γ-ray diagnostics: I - Characterization of the neutron emission.
Jarvis O N
JET papers presented to Course and Workshop on Diagnostics for Contemporary Fusion Experiments, Varenna, Italy, 27 August - 6 September 1991.

211. Neutron and γ-ray diagnostics: II - Derivation of plasma parameters.
Jarvis O N
JET papers presented to Course and Workshop on Diagnostics for Contemporary Fusion Experiments, Varenna, Italy, 27 August - 6 September 1991.

212. Neutron measurements from the preliminary tritium experiments at JET.
Jarvis O N
Review of Scientific Instruments vol.63 no.10 pt.II October 1992 (Procs. 9th Topical Conf. on High Temperature Plasma Diagnostics, Santa Fe, New Mexico, 15-19 March 1992) pp.4511-4516.

213. Triton burnup in JET - profile effects.
Jarvis O N Adams J M Conroy S W Marcus F B Sadler G J Watkins N van Belle P
Controlled Fusion and Plasma Physics. 18th European Conf, Berlin, 3-7 June 1991. Contributed papers. Geneva, European Physical Society. 1991. pp.I-21 - I-24.

214. Fusion energy production from a deuterium- tritium plasma in the JET tokamak.
JET Team
Nuclear Fusion vol.32 no.2 February 1992 p.187.

215. JET status and prospects.
JET Team
Fusion Engineering. 14th IEEE/NPSS Symp., San Diego, 1991. 2 vols. Piscataway, IEEE. 1992. pp.162-167.

216. The JET preliminary tritium experiment.
Rebut P-H and JET Team
Joint European Torus (JET). July 1992. Preprint JET-P(92)53. (invited talk given at 1992 Int. Conf. on Plasma

Physics, Innsbruck,Austria, 29 June - 3 July 1992. To be published in Plasma Physics and Controlled Fusion).

217. JET contributions to ITER R&D programme.
Gambier D J Tubbing B J D
Joint European Torus (JET), 1992. Report JET-R(92)08.

218. Latest results from JET.
Stott P E and JET Team
JET papers submitted to 10th Int. Conf. on Plasma Surface Interactions, Monterey, USA, 30 March - 3 April 1992. Joint European Torus (JET). May 1992. Preprint JET-P(92)32, pp.301-319.

219. High current, high power H-modes in JET.
Jones T T C Balet B Brusati M Bures M Hugon M Lawson K D Lomas P J Morgan P D Morsi H W Nielsen P Sadler G Sartori R Start D F H Summers D D R Tanga A Taroni A Thomsen K Ward D J
Papers submitted to the 19th European Conf. on Controlled Fusion and Plasma Physics, Innsbruck, 29 June - 3 July 1992. Joint European Torus (JET). May 1992. Preprint JET-P(92)37, pp.187-192.

220. Simulated ash transport experiments in JET using helium neutral beams and charge exchange spectroscopy.
Jones T T C von Hellermann M G Bickley A J Boucher D Breger P Challis C D Christiansen J P Cottrell G A Davies J F de Esch H P L Fogg M Frieling J Giannella R Gondhalekar A Koenig R W T Lomas P J Magyar G Mandl W Marcus F B Morgan P D Morsi H Prentice R Sadler G Stamp M F Stork D Summers H P Svensson L Tanga A Taroni A Thomas P R Thompson E Wolf R
Controlled Fusion and Plasma Physics. 18th European Conf., Berlin, 3-7 June 1991. Contributed papers. Geneva, European Physical Society, 1991. pp.I-185 - I-188.

221. Hydraulic position control of the JET microwave antenna.
Kaye A Walker C Paling P
Joint European Torus (JET). October 1992. Preprint JET-P(92)87. (submitted to Procs. Institute of Mechanical Engineers Seminar on Machine Actuators and Controls).

222. Present and future JET ICRF antennae.
Kaye A Brown T Bhatnagar V Crawley P Jacquinot J Lobel R Panissie H Plancoulaine J Rebut P-H Wade T Walker C
Joint European Torus (JET). July 1992. Preprint JET-P(92)46. (submitted to Fusion Engineering and Design).

223. Progress in ICRH and lower hybrid launcher development.
Kaye A S
Joint European Torus (JET). October 1992. Preprint JET-P(92)80. (invited paper presented to Europhysical Topical Conf. on Radio Frequency Heating & Current Drive of Fusion Devices, Brussels, July 1992, and to be submitted to Plasma Physics and Controlled Fusion).

224. The new phase of JET: the pumped divertor.
Keen B E Watkins M L JET Team
Joint European Torus (JET). March 1992. Preprint JET-P(92)17. (submitted to Europhysics News.)

225. Recent JET results and consequences for future devices.
Keilhacker M and JET Team
JET papers presented at 14th IAEA Conf. on Plasma Physics and Controlled Nuclear Fusion Research, Wurzburg, Germany, 30 September - 7 October 1992. Joint European Torus (JET). December 1992. Preprint JET-P(92)84, pp.1-23.

226. MHD modelling of plasma equilibrium and stability.
Kerner W
Papers presented to IAEA Technical Committee Meeting on Advances in Simulation and Modeling of Thermonuclear Plasmas, Montreal, 15-17 June 1992. Joint European Torus. September 1992. Preprint JET-P(92)51, pp.57-123.

227. Measurement of MeV hydrogen minority ions in JET using neutral particle analysis.
Khudoleev A V Afanasyev V I Corti S Gondhalekar A Maas A C Petrov M P
Papers presented to Europhysics Topical Conf. on RF Heating and Current Drive of Fusion Devices, Brussels, 7-10 July 1992. Joint European Torus (JET). May 1992. Preprint JET-P(92)31, pp.43-48.

228. Current state of the neutral beam based diagnostics at JET.
Konig R Summers H P von Hellermann M Mandl W Frieling J Horton L D Breger P Morsi H Wolf R
JET papers presented to Course and Workshop on Diagnostics for Contemporary Fusion Experiments, Varenna, Italy, 27 August - 6 September 1991.

229. The JET active gas handling plant process control system.
Konstantellos A Hemmerich J L Bell A C Mart J Yorkshades J Walker K Skinner N Jones G Delvart F
Papers presented to 4th Topical Meeting on Tritium Technology in Fission, Fusion and Isotopic Applications, Albuquerque, New Mexico, 29 September - 4 October 1991.

230. The JET active gas handling plant process control system.
Konstantellos A Hemmerich J L Bell A C Mart J Yorkshades J Walker K Skinner N Jones G Delvart F
Fusion Technology vol.21 no.2 pt.2 March 1992 (Procs. 4th National Topical Meeting on Tritium Technology in Fission, Fusion, and Isotopic Applications, Albuquerque, New Mexico, 1991) pp.365-370.

231. Modelling and simulation of thermal and closed loop control behaviour of uranium-bed assemblies.
Konstantellos A Karditsas P J
Joint European Torus 1992. Preprint JET-P(92)83. (submitted to Journal of Systems and Control Engineering).

232. Finite orbit effects in ICRF heated tokamak plasmas.
Kovanen M A Core W G F Hellsten T
Nuclear Fusion vol.32 no.5 May 1992 pp.787-799.

233. Modelling of the observed particle and heat fluxes in the X-point region in JET.
Kovanen M A Reichle R Lazzaro E Summers D D R Taylor T S
Nuclear Fusion vol.32 no.5 May 1992 pp.863-872.

234. Monte Carlo study of high power (D)T ICRF heating in JET.
Kovanen M A
JET Contributions to 4th European Fusion Theory Conf., Aspenas, Sweden, 17-19 June 1991.

235. Monte Carlo study of high power (D)T ICRF heating in JET.
Kovanen M A
Nuclear Fusion vol.32 no.6 June 1992 pp.945-950.

236. Electron density fluctuation in JET measured with multichannel reflectometry.
Kramer G J Sips A C C Lopes Cardozo N J
Joint European Torus (JET). December 1992. Preprint JET-P(92)97. (submitted to Plasma Physics and Controlled Fusion).

237. Measurement of density transients using the multichannel reflectometer at JET.
Kramer G J Sips A C C Costley A E
Papers presented to the IAEA Technical Committee Meeting on Reflectometry, JET Joint Undertaking, 1992. Joint European Torus (JET) Preprint JET-P(92)55, pp.39-54.

238. High thermonuclear yield on JET by combining enhanced plasma performance of ICRH-heated, pellet-peaked density profiles with H-mode confinement.
Kupschus P Balet B Bartlett D Boucher D Challis C Corrigan G Corti S Edwards A Eriksson L G Gill R Gormezano C Gowers C Holm H Hugon M Jacquinot J Lawson K Morsi H Neill G Oosterbeek H O'Rourke J Pasini D Porte L Rimini F Sadler G Schmidt G Sips G Smeulders P Start D Stubberfield P Taroni A Tibone F Tubbing B von Hellermann M van Milligen B Zwingmann W
Controlled Fusion and Plasma Physics. 18th European Conf, Berlin, 3-7 June 1991. Contributed papers. Geneva, European Physical Society. 1991. pp.I-1 - I-4.

239. A review of electron impact collisional excitation data for the oxygen-like isoelectronic sequence.
Lag J Summers H P
Jont European Torus (JET). 1992. Preprint JET-P(92)24. (submitted to Atomic Data & Nuclear Data Tables).

240. Analytical equipment for the JET Active Gas Handling Plant.
Lasser R Caldwell-Nichols C J Dallimore J Grieveson B Hemmerich J L Konstantellos A Laveyry M Milverton P Stagg R Yorkshades J
Fusion Technology vol.21 no.2 pt.2 March 1992 (Procs. 4th National Topical Meeting on Tritium Technology in Fission, Fusion, and Isotopic Applications, Albuquerque, New Mexico, 1991) pp.406-411.

241. Gas chromatographic analysis of the gas compositions in the active gas handling plant of JET.
Lasser R Grieveson B Hemmerich J L Stagg R Dowhyluk T Torr K Massey R Chambers P
Joint European Torus (JET). October 1992. Preprint JET-P(92)78. (submitted to Review of Scientific Instruments).

242. Numerical study of the calibration factors for the neutron counters in use at the Joint European Torus.
Laundy B J Jarvis O N
Joint European Torus (JET) 1992. Preprint JET-P(92)60. (submitted for publication in Fusion Technology).

243. Particle and impurity transport in JET versus neoclassical theory.
Lauro-Taroni L Giannella R
Papers submitted to the 19th European Conf. on Controlled Fusion and Plasma Physics, Innsbruck, 1992. Joint European Torus 1992. Preprint JET-P(92)37, pp.109-114.

244. Results from edge spectroscopy in JET.
Lawson K D Barnsley R Denne-Hinnov B Giannella R Gottardi N Hawkes N C Morgan P D Patel T K Peacock N J Stamp M F
Controlled Fusion and Plasma Physics. 18th Euro. Conf., Berlin, 3-7 June 1991. Contributed papers. Geneva, European Physical Society. 1991. pp.III-109 - III-112.

245. Neoclassical poloidal flow bifurcation in the H mode transition.
Lazzaro E Lucca F Nardone C Tanga A
Plasma Physics and Controlled Fusion vol.34 no.6 June 1992 pp.893-905.

246. Neoclassical poloidal flow bifurcation in the H mode transition.
Lazzaro E Lucca F Nardone C Tanga A
Controlled Fusion and Plasma Physics. 18th European Conf., Berlin, 3-7 June 1991. Contributed papers Geneva, European Physical Society. 1991. p.IV-201.

247. Parametric studies of fast electron profiles and comparison with numerical modelling for lower hybrid current drive in JET.
Lennholm M Brusati M Ekedahl A Froissard P Gormezano C Jacquinot J Ramos de Andrade C Rimini F Schild P
Papers presented to Europhysics Topical Conf. on RF Heating and Current Drive of Fusion Devices, Brussels, 7-10 July 1992. Joint European Torus (JET). May 1992. Preprint JET-P(92)31, pp.37-42.

248. The behaviour of the divertor target plates during high performance hot-ion mode discharges at JET.
Lingertat J Lesourd M Summers D D R
American Physical Society Bulletin vol.37 no.6 November 1992 (Program of 1992 Annual Meeting of the APS Division of Plasma Physics, Seattle, 16-20 November 1992) Paper 3Q5, p.1421.

249. Effect of the magnetic flux geometry of a poloidal divertor on the profiles and parameters at the target.
Loarte A Harbour P J
Nuclear Fusion vol.32 no.4 April 1992 pp.681-686.

250. Plasma parameters in the vicinity of the Separatrix strike points on the divertor target plates in JET.
Loarte A Clement S Lingertat J Tagle J A
American Physical Society Bulletin vol.37 no.6 November 1992 (Program of 1992 Annual Meeting of the APS Division of Plasma Physics, Seattle, 16-20 November 1992) Paper 3Q3, p.1421.

251. Radial density profiles in a poloidal divertor modelled by diffusion across a region with variable connection length.
Loarte A
Contributions to Plasma Physics vol.32 no.3-4 1992 (3rd Int. Workshop on Plasma Edge Theory in Fusion Devices, Bad Honnef, Germany, 22-24 June 1992) pp.468-473. (Preprint JET-P(92)52, pp.35-48; JET-P(92)43).

252. High power heating of 7MA limiter plasmas in JET.
Lomas P and JET Team
JET papers presented at 14th IAEA Conf. on Plasma Physics and Controlled Nuclear Fusion Research, Wurzburg, Germany, 1992. Joint European Torus (JET) 1992. Preprint JET-P(92)84, pp.87-94.

253. The performance of high current belt limiter plasmas in JET.
Lomas P J Bartlett D Brusati M Cottrell G Christiansen J P de Esch H Fishpool G Giannella R Gondhalekar A Hugon M Jones T T C Magyar G Marcus F Prentice R Sadler G Sartori R Stamp M Tanga A Taroni A Tibone F
Controlled Fusion and Plasma Physics. 18th European Conf, Berlin, 3-7 June 1991. Contributed papers. Geneva, European Physical Society. 1991. pp.I-13 - I-16.

254. Reassessment of the interpretation of sawtooth-induced pulse propagation.
Lopes Cardozo N J Sips A C C
Controlled Fusion and Plasma Physics. 18th European Conf., Berlin, 3-7 June 1991. Contributed papers. Geneva, European Physical Society, 1991. pp.I-225 - I-228.

255. Ion temperature and fuel dilution measurements using neutron spectroscopy.
Loughlin M J Adams J M Conroy S Elevant T Hawkes N Jarvis O N Marcus F B Morsi H Olsson M Sadler G van Belle P von Hellermann M
Controlled Fusion and Plasma Physics. 18th European Conf., Berlin, 3-7 June 1991. Contributed papers. Geneva, European Physical Society. 1991. pp.IV-281 - IV-284.

256. Neutron yields from the preliminary tritium experiment in JET.
Loughlin M J Balet B Clipsham E Rapisarda M
American Physical Society Bulletin vol.37 no.6 November 1992 (Program of 1992 Annual Meeting of the APS Division of Plasma Physics, Seattle, 16-20 November 1992) Paper 3Q1, p.1420.

257. Profile effects on ion temperature measurements derived from neutron spectrometry.
Loughlin M J
JET papers presented to Course and Workshop on Diagnostics for Contemporary Fusion Experiments, Varenna, Italy, 27 August - 6 September 1991.

258. Results of JET operation with continuous carbon and beryllium X-point target plates.
Lowry C G Ady W N Campbell D J Carman P Clement S Deksnis E B Gondhalekar A Harbour P J Horton L Janeschitz G Lesourd M Lingertat J Pick M A Saibene G Summers D D R Thomas P R
JET papers submitted to 10th Int. Conf. on Plasma Surface Interactions, Monterey, USA, 30 March - 3 April 1992. Joint European Torus (JET). May 1992. Preprint JET-P(92)32, pp.83-94.

259. Receiver calibration on the JET fast ion and alpha particle diagnostic.
Machuzak J S Woskov P P Bindslev H Comiskey M Fessey J Hoekzema J A Hughes T P Orsitto F
Review of Scientific Instruments vol.63 no.10 pt.II October 1992 (Procs. 9th Topical Conf. on High Temperature Plasma Diagnostics, Santa Fe, New Mexico, 15-19 March 1992) pp.4648-4650.

260. Edge conditions with high peripheral ion temperatures in JET.
Maddison G P Yushmanov P N Weisen H Gimblett C G
Contributions to Plasma Physics vol.32 no.3-4 1992 (3rd Int. Workshop on Plasma Edge Theory in Fusion Devices, Bad Honnef, Germany, 22-24 June 1992) pp.462-467.

261. Beam emission spectroscopy as a comprehensive plasma diagnostic tool.
Mandl W Wolf R C von Hellermann M G Summers H P
Joint European Torus (JET). November 1992. Preprint JET-P(92)93. (submitted to Plasma Physics and Controlled Fusion).

262. Fourier analysis of sawtooth heat pulse propagation and comparison with other methods using JET data.
Mantica P De Luca F Gorini G Jacchia A Hogewij G M D Lopes Cardozo N J Kramer G J Sips A C C
Nuclear Fusion vol.32 no.12 1992 pp.2203-2216.

263. JET progresses towards fusion power.
Maple J H C
Nuclear Engineering vol.37 no.461 December 1992 pp.44-46.

264. JET experiments with 120 keV ^{3}He and ^{4}He neutral beam injection.
Marcus F B Adams J M Bartlett D V Bhatnagar V Bickley A J Bures M Campbell D J Challis C D Christiansen J Conroy S Cordey J G Core W Corti S Cottrell G de Esch H de Kock L Elevant T Eriksson L G Falter H Giannella R Gill R D Gondhalekar A Gottardi N A Hemsworth R Jacquinot J Jarvis O N Jones T T C Konig R Lomas P Loughlin M Lowry C Magyar G Mandl W Massmann P Morgan P Morsi H Nielsen P Obert W O'Rourke J Prentice R Sadler G Smeulders P Stamp M Start D F Stork D Summers D Summers H Svensson L Tanga A Taroni A Thomas P R Thompson E Tubbing B Tibone F van Belle P von Hellermann M Watkins N
Controlled Fusion and Plasma Physics. 18th European Conf, Berlin, 3-7 June 1991. Contributed papers. Geneva, European Physical Society. 1991. pp.I-45 - I-48.

265. JET experiments with 120keV ^{3}He and ^{4}He neutral beam injection and neutron diagnostic applications.
Marcus F B Adams J M Bartlett D V Bhatnagar V Bickley A J Bures M Campell D J Challis C D Christiansen J Conroy S Cordey J G Core W Corti S Cottrell G de Esch H de Kock L Elevant T Eriksson L G Falter H Giannella R Gill R D Gondhalekar A Gottardi N A Hemsworth R Jacquinot J Jarvis O N Jones T T C Konig R Lomas P Loughlin M Lowry C Magyar G Mandl W Massmann P Morgan P Morsi H Nielsen P Obert W O'Rourke J Prentice R Sadler G Smeulders P Stamp M Start D F Stork D Summers D Summers H Svensson L Tanga A Taroni A Thomas P R Thompson E Tubbing B Tibone F van Belle P von Hellermann M Watkins N
Plasma Physics and Controlled Fusion vol.34 no.8 August 1992 pp.1371-1378. (Preprint JET-P(92)11).

266. Neutron profile measurements during the tritium experiments in JET.
Marcus F B Adams J M Bond D S Conroy S Howarth P J A Jarvis O N Loughlin M J Sadler G Smeulders P van Belle P Watkins N
Papers submitted to the 19th European Conf. on Controlled Fusion and Plasma Physics, Innsbruck, 29 June - 3 July 1992. Joint European Torus (JET). May 1992. Preprint JET-P(92)37, pp.7-12.

267. Design of in-vessel water circuits and ceramic electrical break for the JET pumped divertor.
Martin E Hodapp T Dietz K J Celentano G Middleton R Mills S Pick M Rebut P-H
JET Papers presented at 17th Symp. on Fusion Technology (SOFT-17), Rome, Italy, 14-18 September 1992 Joint European Torus (JET). September 1992. Preprint JET-P(92)72, pp.25-31.

268. Deuterium depth profiles and impurities on the Be coated carbon belt limiter in JET.
Martinelli A P Hughes I Behrisch R Peacock A T
Controlled Fusion and Plasma Physics. 18th Euro. Conf., Berlin, 3-7 June 1991. Contributed papers. Geneva, European Physical Society. 1991. pp.III-153 - III-156.

269. Deuterium trapping and impurity collection on a 1990 JET Be belt limiter.
Martinelli A P Peacock A T Behrisch R
JET papers submitted to 10th Int. Conf. on Plasma Surface Interactions, Monterey, USA, 30 March - 3 April 1992. Joint European Torus (JET). May 1992. Preprint JET-P(92)32, pp.255-270.

270. Lifetimes and oscillator strengths for Be I - Be III.
Martinson I Summers H P Westerlind M Gaupp A
Joint European Torus (JET). August 1992. Preprint JET-P(92)62. (submitted for publication in Physica Scripta).

271. Modifications and characteristics of the JET positive ion neutral injectors for the first tritium experiment.
Massmann P Falter H D Bickley A J Deschamps G H Hurford D Thompson E
JET Papers presented at 17th Symp. on Fusion Technology (SOFT-17), Rome, Italy, 14-18 September 1992 Joint European Torus (JET). September 1992. Preprint JET-P(92)72, pp.71-77.

272. Impurity profiles at the JET divertor targets compared with the DIVIMP code.
Matthews G F Elder J D Gottardi N A C Harbour P J Horton L DJackel H J de Kock L Loarte A Maggi C F O'Brien D P J Simonini R Spence J Stamp M F Stangeby P C Stott P E Summers H P Tagle J von Hellermann M
JET papers submitted to 10th Int. Conf. on Plasma Surface Interactions, Monterey, USA, 30 March - 3 April 1992. Joint European Torus (JET). May 1992. Preprint JET-P(92)32, pp.17-31.

273. Plasma ion mass-spectrometry in the TEXTOR boundary.
Matthews G F Elder D McCracken G M Monk R D Pitts R A Samm U Schweer B Stangeby P C
JET papers submitted to 10th Int. Conf. on Plasma Surface Interactions, Monterey, USA, 30 March - 3 April 1992. Joint European Torus (JET). May 1992. Preprint JET-P(92)32, pp.223-238.

274. Fast and slow waves launched from a fast-wave waveguide array.
McWilliams R Edrich D Wolf N S Brusati M
Nuclear Fusion vol.32 no.4 April 1992 pp.687-689.

275. The assessment of non-metallic inclusions in steels and nickel alloys for ultra high vacuum applications.
Meriguet P J-L
Joint European Torus (JET). February 1992. Report JET-R(92)01.

276. The design, development and use of pipe cutting tools for remote handling in JET.
Mills S F Loving A Irving M
Fusion Engineering. 14th IEEE/NPSS Symp., San Diego, 30 September - 3 October 1991. 2 vols. Piscataway, IEEE. 1992. pp.559-562.

277. The new fast radial field amplifier for the control of the plasma vertical position in JET.
Mondino P L Bonicelli T Hrabal D Klein R Marchese V Ostrom R Timmert H P
JET Papers presented at 17th Symp. on Fusion Technology (SOFT-17), Rome, Italy, 14-18 September 1992 Joint European Torus (JET). September 1992. Preprint JET-P(92)72, pp.119-125.

278. Reactive power compensation for the JET pulsed loads supply.
Mondino P L Bonicelli T Hrabal D Klein R Kruger K H Marchese V Murphy G Schultz W
JET Papers presented at 17th Symp. on Fusion Technology (SOFT-17), Rome, Italy, 1992 Joint European Torus (JET) 1992. Preprint JET-P(92)72, pp.111-117.

279. Mapping techniques for solving non-integrable Hamiltonian systems.
Montvai A Graf Finck von Finckenstein K Duchs D F
Joint European Torus (JET) 1992. Report JET-R(92)05.

280. The evolution of Z_{eff} during H-mode operation in JET.
Morgan P D Ellis J J Morsi H W Oord E Oster J Stamp M F Thomsen K von Hellermann M G Zastrow K-D
Controlled Fusion and Plasma Physics. 18th European Conf., Berlin, 3-7 June 1991. Contributed papers. Geneva, European Physical Society, 1991. pp.I-361 - I-364.

281. Irradiation of optical fibres at JET through 14MeV neutron production.
Morgan P D
JET Papers presented at 17th Symp. on Fusion Technology (SOFT-17), Rome, Italy, 1992 Joint European Torus (JET) 1992. Preprint JET-P(92)72, pp.167-173.

282. Fluid description of nickel as a diagnostic impurity.
Morsi H W Sack C
Papers submitted to the 19th European Conf. on Controlled Fusion and Plasma Physics, Innsbruck, 29 June - 3 July 1992. Joint European Torus (JET). May 1992. Preprint JET-P(92)37, pp.247-252.

283. A new diagnostic for the tritium phase of JET covering the visible and UV wavelength range.
Morsi H W Hatzky R von Hellermann M Mandl W McKillen R R Mijnarends M Millward P Nielsen P Reid J Roberts P Ryan J Thomas P Viaccoz B
Controlled Fusion and Plasma Physics. 18th European Conf., Berlin, 3-7 June 1991. Contributed papers. Geneva, European Physical Society. 1991. pp.IV-261 - IV-264.

284. Multichannel fluctuation data analysis by the singular value decomposition method. Applications to MHD modes in JET.
Nardone C
Plasma Physics and Controlled Fusion vol.34 no.9 September 1992 pp.1447-1465. (Preprint JET-P(92)01).

285. Power threshold for L-H mode transition in JET.
Nardone C Bhatnagar V P Campbell D Gottardi N Lazzaro E O'Brien D Tanga A Weisen H
Controlled Fusion and Plasma Physics. 18th European Conf., Berlin, 3-7 June 1991. Contributed papers. Geneva, European Physical Society, 1991. pp.I-377 - I-380.

286. Material transport by erosion and redeposition on surface probes in the scrape-off layer of JET.
Naujoks D Behrisch R Coad J P de Kock L
Joint European Torus (JET). December 1992. Preprint JET-P(92)64. (submitted to Nuclear Fusion).

287. Energetic particle driven instabilities at JET.
Nave M F F Borba D Cripwell P von Hellermann M Kerner W Porcelli F Sadler G Smeulders P
Papers submitted to the 19th European Conf. on Controlled Fusion and Plasma Physics, Innsbruck, 29 June - 3 July 1992. Joint European Torus (JET). May 1992. Preprint JET-P(92)37, pp.271-276.

288. Observation of MHD structures in JET temperature profiles.
Nave M F F Edwards A W Hirsch K Hugon M Jacchia A Lazzaro E Salzmann H Smeulders P
Nuclear Fusion vol.32 no.5 May 1992 pp.825-835.

289. Pumping speed and thermal load analysis of the JET appendage cryopump by Monte Carlo calculation.
Obert W Perinic G
Vacuum vol.43 nos.1/2 January/February 1992 Vacuum '91: Conf. of Vacuum Group of the Institute of Physics, University of Salford, UK, 30 July - 2 August 1991) pp.163-166.

290. Regeneration and tritium recovery from the large JET neutral injection cryopump system after FTE.
Obert W Anderson J Bell A Davies J Jenkins E Mayaux C Perinic G Saibene G Sartori R Thompson E Walthers C
JET Papers presented at 17th Symp. on Fusion Technology (SOFT-17), Rome, Italy, 14-18 September 1992 Joint European Torus (JET). September 1992. Preprint JET-P(92)72, pp.79-85.

291. Analysis of neutron energy spectra from neutral beam heated plasmas in the JET tokamak.
Olsson M van Belle P Conroy S Elevant T Sadler G
Joint European Torus (JET). March 1992. Preprint JET-P(92)22. (submitted to Plasma Physics and Controlled Fusion).

292. JET experience in recovery from large air leak incidents.
Orchard J C Peacock A T Saibene G
Joint European Torus (JET). September 1992. Preprint JET-P(92)66. (submitted to Journal of Nuclear Materials).

293. Predicted precision of ion temperature and impurity fractional density measurements using the JET collective scattering diagnostic.
Orsitto F
Joint European Torus (JET). November 1992. Report JET-R(92)10.

294. Direct simulations of turbulent transport in fusion devices.
Ottaviani M
Papers presented to IAEA Technical Committee Meeting on Advances in Simulation and Modeling of Thermonuclear Plasmas, Montreal, 1992. Joint European Torus. 1992. Preprint JET-P(92)51, pp.29-55. (Also issued as JET-P(92)58).

295. Scaling laws of test particle transport in two-dimensional turbulence.
Ottaviani M
Europhysics Letters vol.20 no.2 15 September 1992 pp.111-116. (Preprint JET-P(92)38).

296. Edge current density in H-mode discharges at JET.
O'Brien D P Challis C Cordey J G Ellis J J Jackson G Lao L L Stubberfield P M Taylor T S
Controlled Fusion and Plasma Physics. 18th European Conf., Berlin, 3-7 June 1991. Contributed papers. Geneva, European Physical Society, 1991. pp.I-373 - I-376.

297. Equilibrium analysis of iron core tokamaks using a full domain method.
O'Brien D P Lao L L Solano E R Garribba M Taylor T S Cordey J G Ellis J J
Nuclear Fusion vol.32 no.8 August 1992 pp.1351-1360.

298. Local expansion method for fast plasma boundary identification at JET.
O'Brien D P Ellis J J Lingertat J
Joint European Torus (JET). August 1992. Preprint JET-P(92)57. (submitted to Nuclear Fusion).

299. 3D Fokker-Planck calculations of electron and ion distributions in tokamak plasmas.
O'Brien M R Cox M Warrick C D Zaitsev F S
Joint European Torus (JET). July 1992. Preprint JET-P(92)42. (paper presented to IAEA Technical Committee Meeting on Advances in Simulation and Modelling Thermonuclear Plasmas, Montreal, 15-18 June 1992).

300. An analytic solution of the inhomogeneous coupled diffusion problem.
O'Rourke J
Joint European Torus (JET). 1992. Preprint JET-P(92)40. (submitted to Plasma Physics and Controlled Fusion).

301. Comparison of poloidal field measurements on JET.
Wolf R C O'Rourke J Edwards A W von Hellermann M
Joint European Torus (JET). December 1992. Preprint JET-P(92)99. (submitted to Nuclear Fusion (letters)).

302. Evolution of the current profile in JET high bootstrap current plasmas.
O'Rourke J Challis C D Jacquinot J O'Brien D Stamp M F Stork D Stubberfield P Tibone F Tubbing B J Zwingmann W
Papers submitted to the 19th European Conf. on Controlled Fusion and Plasma Physics, Innsbruck, 29 June - 3 July 1992. Joint European Torus (JET). May 1992. Preprint JET-P(92)37, pp.97-102.

303. Measurements of the electron source distribution and implications for particle transport.
O'Rourke J Kramer G J Simonini R Sips A C C
Papers submitted to the 19th European Conf. on Controlled Fusion and Plasma Physics, Innsbruck, 29 June - 3 July 1992. Joint European Torus (JET). May 1992. Preprint JET-P(92)37, pp.91-96.

304. Measurements of the electron source distribution and particle transport coefficients in JET.
O'Rourke J Gowers C Kramer G J Morgan P D Simonini R Sips A C C
Joint European Torus (JET). 1992. Preprint JET-P(92)86. (submitted to Plasma Physics and Controlled Fusion).

305. Perturbative measurements of the electron transport matrix using ICRF power modulation.
O'Rourke J Rimini F G Start D F H
Nuclear Fusion vol.32 no.10 1992 pp.1861-1866.

306. Poloidal field measurements on JET: A comparison.
O'Rourke J Edwards A W von Hellermann M Wolf R
American Physical Society Bulletin vol.37 no.6 November 1992 (Program of 1992 Annual Meeting of the APS Division of Plasma Physics, Seattle, 16-20 November 1992) Paper 3Q2, p.1420.

307. The role of the plasma current distribution in L-mode confinement.
O'Rourke J Balet B Challis C Cordey J G Gowers C Jacquinot J Kramer G Tibone F Stubberfield P
Controlled Fusion and Plasma Physics. 18th European Conf, Berlin, 3-7 June 1991. Contributed papers. Geneva, European Physical Society. 1991. pp.I-37 - I-40.

308. The Hyperguide: a new concept of lower hybrid launcher.
Pain M Brusati M Gormezano C Jacquinot J Schild P
Joint European Torus (JET) 1992. Preprint JET-P(92)94. (submitted to Fusion Engineering and Design).

309. Impurity transport in JET.
Pasini D Denne-Hinnov B Giannella R Hawkes N Lauro Taroni L Magyar G Mattioli M Weisen H

Controlled Fusion and Plasma Physics. 18th European Conf, Berlin, 3-7 June 1991. Contributed papers. Geneva, European Physical Society. 1991. pp.I-33 - I-36.

310. Measurements of impurity transport in JET.
Pasini D Giannella R Lauro Taroni L Mattioli M Denne-Hinnov B Hawkes N Magyar G Weisen H
Plasma Physics and Controlled Fusion vol.34 no.5 May 1992 pp.677-685.

311. Scaling of impurity transport in JET.
Pasini D Giannella R Lauro-Taroni L Magyar G Mattioli M
Papers submitted to the 19th European Conf. on Controlled Fusion and Plasma Physics, Innsbruck, 29 June - 3 July 1992. Joint European Torus (JET). May 1992. Preprint JET-P(92)37, pp.121-126.

312. Tritium retention in first wall material at JET after the First Tritium Experiment (FTE).
Peacock A T Coad J P Kietz K J Knight A P
JET Papers presented at 17th Symp. on Fusion Technology (SOFT-17), Rome, Italy, 14-18 September 1992 Joint European Torus 1992. Preprint JET-P(92)72, pp.9-15.

313. Operational experience with a remote radiation hard quadrupole residual gas analyser.
Pearce R Winkel T
Joint European Torus (JET). September 1992. Preprint JET-P(92)69. (submitted to Procs of IVC-12/ICSS-8).

314. Latest JET experimental results on the sawtooth.
Pearson D Campbell D J Edwards A W O'Rourke J
Controlled Fusion and Plasma Physics. 18th European Conf., Berlin, 3-7 June 1991. Contributed papers. Geneva, European Physical Society. 1991. pp.II-25 - II-28.

315. Neutral particle analysis in the MeV range in JET.
Petrov M P Afanasyev V I Corti S Gondhalekar A Khudoleev A V Korotkov A A Maas A C
Papers submitted to the 19th European Conf. on Controlled Fusion and Plasma Physics, Innsbruck 1992. Joint European Torus 1992. Preprint JET-P(92)37, pp.133-138

316. Analysis of outgassing after JET-discharges under beryllium first wall conditions.
Philipps V Ehrenberg J
Joint European Torus (JET). July 1992. Preprint JET-P(92)41. (submitted for publication in J Vac Sci Techn.).

317. Evidence of halo currents in JET.
Pick M A Noll P Barabaschi P Marcus F B Rossi L
Fusion Engineering. 14th IEEE/NPSS Symp., San Diego, 1991. 2 vols. Piscataway, IEEE. 1992. pp.187-190.

318. Optimising X-point target plates.
Pick M A Deksnis E Dietz K J Lowry C Parsons W Tivey R
JET papers submitted to 10th Int. Conf. on Plasma Surface Interactions, Monterey, USA, 30 March - 3 April 1992. Joint European Torus (JET). May 1992. Preprint JET-P(92)32, pp.109-126.

319. Damping of global Alfven waves in tokamaks due to resonant absorption.
Poedts S Kerner W Goedbloed J P Keegan B Huysmans G T A Schwarz E
Joint European Torus (JET). January 1992. Preprint JET-P(92)03. (submitted for publication in Plasma Physics and Controlled Fusion).

320. Effects of radiation on insulation materials.
Pohlchen R
Advances in Cryogenic Engineering Materials vol.38 Pt.A 1992 (Procs. 9th Int. Cryogenic Materials Conf. (ICMC), Huntsville, Alabama, 1991) pp.261-269.

321. Review of NB_3SN magnets completed or under manufacture and relevant for future fusion magnets.
Pohlchen R
Joint European Torus (JET). May 1992. Report JET-R(92)04.

322. Collisionless magnetic reconnection in laboratory plasmas.
Porcelli F
Joint European Torus (JET) 1992. Preprint JET-P(92)85. (submitted to Procs. Varenna Theory Workshop, 1992).

323. Resistive internal kinks and ICRF phasing current drive.
Porcelli F Bhatnagar V P Bosia P Cherubini A Jacquinot J Start D Taroni A
Papers submitted to the 19th European Conf. on Controlled Fusion and Plasma Physics, Innsbruck, 29 June - 3 July 1992. Joint European Torus (JET). May 1992. Preprint JET-P(92)37, pp.211-216.

324. First results with the upgraded ECE heterodyne radiometer on JET.
Porte L Bartlett D V Campbell D J Costley A E
Controlled Fusion and Plasma Physics. 18th European Conf., Berlin, 3-7 June 1991. Contributed papers. Geneva, European Physical Society. 1991. pp.IV-357 - IV-360.

325. Physics aspects of the ITER design.
Post D Cordey J G et al
Fusion Engineering. 14th IEEE/NPSS Symp., San Diego, 1991. 2 vols. Piscataway, IEEE. 1992. p.4.

326. JET 250mm stroke moving Langmuir probe system - design and operational experience.
Prior P C S Hancock C J de Kock L Millward P Nicholson C J Tagle J A
JET Papers presented at 17th Symp. on Fusion Technology (SOFT-17), Rome, Italy, 14-18 September 1992 Joint European Torus (JET). September 1992. Preprint JET-P(92)72, pp.143-149.

327. Geometry of drift surfaces near magnetic separatrix in a tokamak with poloidal divertor.
Putvinskii S
Joint European Torus Preprint JET-P(92)02. (submitted for publication in Plasma Physics and Controlled Fusion).

328. On the plasma confinement in the m=1, n=1 kink distorted central core.
Putvinskii S
Joint European Torus (JET). July 1992. Preprint JET-P(92)47. (submitted to Nuclear Fusion).

329. The application of moment equations to scrape off layer plasmas.
Radford G J
Contributions to Plasma Physics vol.32 no.3-4 1992 (3rd Int. Workshop on Plasma Edge Theory in Fusion Devices, Bad Honnef, Germany, 1992) pp.297-302. (Preprint JET-P(92)52).

330. Trends in remote handling device development.
Raimondi T
Fusion Engineering & Design vol.18 1991 (Procs. 2nd Int. Symp. on Fusion Nuclear Technology, Karlsruhe, Germany, 2-7 June 1991 (ISFNT 2)), pp.445-452.

331. JET results and the approach to a fusion reactor.
Rebut P H
JET Team Status and Perspectives of Nuclear Energy: Fission and Fusion. Procs. Int. School of Physics, 'Enrico Fermi'. Course 116, Varenna, Villa Monastero, 10-20 July 1990. Amsterdam, North-Holland. 1992. pp.307-329.

332. Controlled nuclear fusion.
Rebut P-H Gambier D J
La Recherche no.242 April 1992 pp.436-444.

333. A fusion reactor: continuous or semi-continuous?
Rebut P-H Boucher D Gormezano C Keen B E Watkins M L
Joint European Torus (JET). August 1992. Preprint JET-P(92)65. (Invited talk to Europhysics Conf. on RF Heating and Current Drive of Fusion Devices, Brussels, Belgium, 7-10 July 1992. To be published in Journal of Plasma Physics and Controlled Fusion).

334. Impact of JET results on the concept of a fusion reactor.
Rebut P-H
Sakharov Memorial Lectures in Physics. Procs. 1st Int. Sakharov Conf. on Physics, Moscow, 21-31 May 1991. 2 vols. New York, Nova Science, 1992. pp.633-652.

335. Magnetic confinement fusion: Recent results at JET and plasma for the future.
Rebut P-H
Joint European Torus (JET). March 1992. Preprint JET-P(92)21. (invited talk to 3rd Euro. Particle Accelerator Conf., Berlin, 24-28 March 1992).

336. Perspective on nuclear fusion.
Rebut P-H
Joint European Torus (JET). March 1992. Preprint JET-P(92)20. (invited talk at 3rd Conf. on Clean Energy for Europe in Transition, Paris, 30 March - 3 April 1992).

337. The ITER challenge.
Rebut P-H Boucher D Gambier D J Keen B E Watkins M L
Joint European Torus (JET). December 1992. Preprint JET-P(92)92. (invited talk to 17th Symp. on Fusion Technology, Rome, Italy, 14-18 September 1992). (submitted to Fusion Engineering and Design).

338. The JET preliminary tritium experiment.
Rebut P-H and JET Team
Plasma Physics and Controlled Fusion vol.34 no.13 December 1992 (Joint Conf. of 9th Kiev Int. Conf. on Plasma Theory, 9th Int. Congress on Waves and Instabilities in Plasmas, & 19th Euro. Phys. Soc. Conf. on Controlled Fusion and Plasma Physics, 1992) pp.1749-1758.

339. Power loading and radiation distribution at the X-point target in JET for normal and reversed toroidal field.
Reichle R Clement S Gottardi N Jaeckel H J Lesourd M Summers D D R
Controlled Fusion and Plasma Physics. 18th Euro. Conf., Berlin, 3-7 June 1991. Contributed papers. Geneva, European Physical Society. 1991. pp.III-105 - III-108.

340. Termination of high performance plasmas in JET.
Reichle R and JET Team
American Physical Society Bulletin vol.37 no.6 November 1992 (Program of 1992 Annual Meeting of the APS Division of Plasma Physics, Seattle, 16-20 November 1992) Paper 3Q6, p.1421.

341. Modelling of fast ion orbit effects on electron heating profiles in minority ICRF scenarios.
Righi E Cottrell G A Eriksson L-G Start D F H Tibone F
Papers presented to Europhysics Topical Conf. on RF Heating and Current Drive of Fusion Devices, Brussels, 1992. Joint European Torus (JET). 1992. Preprint JET-P(92)31, pp.13-18.

342. Full current drive with lower hybrid waves in JET.
Rimini F G Brusati M Challis C D Froissard P Gormezano C Jacquinot J
Papers presented to Europhysics Topical Conf. on RF Heating and Current Drive of Fusion Devices, Brussels, 7-10 July 1992. Joint European Torus (JET). May 1992. Preprint JET-P(92)31, pp.25-30.

343. Remote handling mock-up trials of replacement of a JET neutral beam ion source.
Rolfe A C Burgess T Removille J

Fusion Engineering. 14th IEEE/NPSS Symp., San Diego, 30 September - 3 October 1991. 2 vols. Piscataway, IEEE. 1992. pp.567-571.

344. The new first wall protection at JET.
Rossi L Deksnis E Lomas P Martin E Mohanti R Pick M A Saibene G
JET Papers presented at 17th Symp. on Fusion Technology (SOFT-17), Rome, Italy, 14-18 September 1992 Joint European Torus (JET). September 1992. Preprint JET-P(92)72, pp.17-23.

345. Beryllium safety at JET.
Russ R M Haigh A D Booth S J
Fusion Engineering. 14th IEEE/NPSS Symp., San Diego, 30 September - 3 October 1991. 2 vols. Piscataway, IEEE. 1992. pp.596-599.

346. Health physics and environmental implications of JET's first tritium experiment.
Russ R M Bell A C Caldwell-Nichols C J Haigh A D Patel B Serio L
JET Papers presented at 17th Symp. on Fusion Technology (SOFT-17), Rome, Italy, 1992 Joint European Torus (JET) 1992. Preprint JET-P(92)72, pp.55-61.

347. Effects of enhanced toroidal field ripple on JET plasmas.
Sadler G Barabaschi P Bertolini E Conroy S Corti S Deksnis E Dietz K J de Esch H P L Gondhalekar A Green B Huart M Huguet M Jacquinot J Jarvis O N Khudoleev A Loughlin M J Konig R Last J Maas A Petrov M Putvinskii S Sborchia C Stork D Tubbing B van Belle P
Plasma Physics and Controlled Fusion vol.34 no.13 December 1992 (19th EPS Conference on Controlled Fusion and Plasma Physics, Innsbruck, 29 June - 3 July 1992) pp.1971-1976. (Preprint JET-P(92)37, pp.1-6. Also issued as JET-P(92)54).

348. ^{3}He-D fusion yield studies in JET.
Sadler G Christiansen J P Cottrell G A de Esch H P L Eriksson L Giannella R Gondhalekar A Jacquinot J Jarvis O N Jones T T C Lomas P J Loughlin M J Magyar G Marcus F B Prentice R Stamp M Start D F Tanga A Taroni A van Belle P Willen U
Controlled Fusion and Plasma Physics. 18th European Conf, Berlin, 3-7 June 1991. Contributed papers. Geneva, European Physical Society. 1991. pp.I-29 - I-32.

349. The plasma fault protection system: Disruption control in JET.
Saibene G Budd T Card P Green B Noll P Reed K van der Beken H Tanga A
IAEA Technical Committee Meeting on Avoidance and Control of Tokamak Disruptions, Culham Laboratory, 10-12 September 1991.

350. Tritium accounting during the first tritium experiment at JET.
Saibene G Sartori R Andrew P How J King Q Peacock A T
Fusion Engineering and Design vol.19 no.2 September 1992 (Topical Issue on the first JET tritium experiment) pp.133-148. (Preprint JET-P(92)34).

351. Low cycle fatigue testing of Inconel 600 and life assessment of JET vacuum vessel.
Sannazzaro G Sborchia C Huguet M Sonnerup L
Fusion Engineering. 14th IEEE/NPSS Symp., San Diego, 1991. 2 vols. Piscataway, IEEE. 1992. pp.385-387.

352. Determination of the ion thermal diffusivity from neutral emission profiles in decay.
Sasao M Adams J M Conroy S Jarvis O N Marcus F B Sadler G van Belle P
Papers submitted to the 19th European Conf. on Controlled Fusion and Plasma Physics, Innsbruck, 29 June - 3 July 1992. Joint European Torus (JET). May 1992. Preprint JET-P(92)37, pp.241-246. (Also issued as JET-P(92)75).

353. Fuelling of JET limiter and X-point plasma by deuterium pellet injection.
Schmidt G L Bartlett D Baylor L Bures M Edwards A Gadeberg M Gottardi N Jones T Kupschus P Lomas P Morgan P Morsi H Nielsen P O'Rourke J Sadler G Start D F H Stubberfield P Tanga A Ward D
Papers submitted to the 19th European Conf. on Controlled Fusion and Plasma Physics, Innsbruck, 1992. Joint European Torus 1992. Preprint JET-P(92)37, pp.253-258.

354. X-ray measurements from the JET and ASDEX tokamaks.
Schumacher U Barnsley R Fussmann G Asmussen K Chu C C Janeschitz G
Atomic Processes in Plasmas. 8th American Physical Society Topical Conf., Portland, 25-29 August 1991. New York, American Institute of Physics. 1992. pp.131-143.

355. Discussion of the possible combination of the LIDAR technique with Rayleigh scattering.
Schunke B Nielsen P Gowers C
JET papers presented to Course and Workshop on Diagnostics for Contemporary Fusion Experiments, Varenna, Italy, 27 August - 6 September 1991.

356. A LIDAR based Thomson scattering diagnostic for the JET divertor region.
Schunke B Nielsen P Gowers C Wilson D
JET papers presented to Course and Workshop on Diagnostics for Contemporary Fusion Experiments, Varenna, Italy, 27 August - 6 September 1991.

357. Working in the heart of JET.
Scott S
Professional Engineering January 1991 pp.13-15.

358. Decontamination of the JET vacuum vessel from beryllium and tritium.

Scott S M Buttgereit H F Celentano G Malone K
JET Papers presented at 17th Symp. on Fusion Technology (SOFT-17), Rome, Italy, 1992 Joint European Torus (JET). September 1992. Preprint JET-P(92)72, pp.41-46.

359. Modelling impurity control at JET.
Simonini R Taroni A Keilhacker M Radford G Spence J Vlases G Watkins M L Weber S
JET papers submitted to 10th Int. Conf. on Plasma Surface Interactions, Monterey, USA, 1992. Joint European Torus (JET). May 1992. Preprint JET-P(92)32, pp.1-16.

360. Electron density profile measurements in JET with the O-mode reflectometer.
Sips A C C Colton A L Costley A E Kramer G J Prentice R
JET papers presented to Course and Workshop on Diagnostics for Contemporary Fusion Experiments, Varenna, Italy, 27 August - 6 September 1991.

361. Interpretation of heat and density pulse propagation in tokamaks.
Sips A C C Lopes Cardoso N J Costley A E Hogeweij G M D O'Rourke J
Controlled Fusion and Plasma Physics. 18th European Conf., Berlin, 3-7 June 1991. Contributed papers. Geneva, European Physical Society, 1991. pp.I-193 - I-196.

362. Measurement of density profiles using the multichannel reflectometer at JET.
Sips A C C Kramer G J Beurskens M Costley A E Prentice R
Papers presented to the IAEA Technical Committee Meeting on Reflectometry, JET Joint Undertaking, 4-6 March 1992. Joint European Torus (JET). July 1992. Preprint JET-P(92)55, pp.1-12.

363. MHD studies in JET.
Smeulders P Edwards A Fishpool G Hender T C Hugon M van Milligen B Nardone C Neill G Porte L Wolfe S Zwingman W
Controlled Fusion and Plasma Physics. 18th European Conf., Berlin, 3-7 June 1991. Contributed papers. Geneva, European Physical Society. 1991. pp.II-53 - II-56.

364. Measurement of sputtering yields at the JET beryllium and carbon X-point tiles.
Stamp M F Thomas P R
Papers submitted to the 19th European Conf. on Controlled Fusion and Plasma Physics, Innsbruck, 1992. Joint European Torus Preprint JET-P(92)37, pp.199-204.

365. Fast wave heating and current drive on JET: Present results and future plans.
Start D F H Bhatnagar V P Bosia G Brusati M Bures M Campbell D Challis C Cottrell G A Cox M Edwards A Eriksson L G Froissard P Gormezano C Gowers C Hugonard S Jacquinot J Kupschus P Gottardi N O'Brien M R Pasini D Porcelli F Righi E Rimini F Sadler G Stork D Tanga A Thomsen K Tibone F Tubbing B Von Hellermann M
Fast Wave Current Drive in Reactor Scale Tokamaks (Synergy and Complementarity with LHCD and ECRH). IAEA Technical Committee Meeting, Arles, 23-25 September 1991. Association EURATOM-CEA sur la Fusion, Centre d'Etudes de Cadarache, 1992. pp.226-242.

366. Observation of fast wave ion current drive effects on sawteeth in JET.
Start D F H Bhatnagar V P Bosia G Brusati M Bures M Campbell D Cottrell G A Cox M de Esch H P L Edwards A Eriksson L-G Gormezano C Jacquinot J Lomas P Marcus F B O'Brien M R Porcelli F Rimini F Stork D Tanga A Tubbing B Warrick C D Wesson J
Papers submitted to the 19th European Conf. on Controlled Fusion and Plasma Physics, Innsbruck, 1992. Joint European Torus. 1992. Preprint JET-P(92)37, pp.73-78.

367. Control of carbon blooms and the subsequent effects on the H to L mode transition in JET X-point plasmas.
Stork D Campbell D J Clement S Gottardi N de Kock L Lowry C G Morgan P D Reichle R Saibene G Smeulders P Summers D D R Thomas P R
Controlled Fusion and Plasma Physics. 18th European Conf., Berlin, 3-7 June 1991. Contributed papers. Geneva, European Physical Society, 1991. pp.I-357 - I-360.

368. High β studies in the H-mode and hot ion H-mode in JET.
Stork D Alper B Ali-Arshad S de Blank H J de Esch H P L Edwards A Hender T C Konig R Kramer G J Marcus F B Nave M F O'Brien D P O'Rourke J Smeulders P Stamp M Tibone F Tubbing B J D Zolfaghari A Zwingmann W
Papers submitted to the 19th European Conf. on Controlled Fusion and Plasma Physics, Innsbruck, 1992. Joint European Torus 1992. Preprint JET-P(92)37, pp.193-198

369. Long pulse operation of JET and its implications to a reactor.
Stork D and JET Team
JET papers presented at 14th IAEA Conf. on Plasma Physics and Controlled Nuclear Fusion Research, Wurzburg, Germany, 1992. Joint European Torus (JET). December 1992. Preprint JET-P(92)84, pp.95-108.

370. Book Review: Plasma physics and controlled nuclear fusion research 1990 - Supplement to Nuclear Fusion.
Stott P E
Plasma Physics and Controlled Fusion vol.34 no.8 August 1992 p.1443.

371. The development of plasma measurement techniques and their impact on fusion research.
Stott P E
Reports on Progress in Physics vol.55 no.10 October 1992 p.1715-1768. (Preprint JET-P(92)16).

372. Diagnostics for contemporary fusion experiments (Report on the Course and Workshop, Int. School of Plasma Physics "Piero Caldirola", Villa Monastero, Varenna, Italy, 27 August to 6 September 1991.
Stott P E
Nuclear Fusion vol.32 no.1 January 1992 pp.167-176.

373. Measurements at the plasma edge.
Stott P E
JET papers presented to Course and Workshop on Diagnostics for Contemporary Fusion Experiments, Varenna, Italy, 27 August - 6 September 1991.

374. Present status of tokamak research and diagnostics.
Stott P E
JET papers presented to Course and Workshop on Diagnostics for Contemporary Fusion Experiments, Varenna, Italy, 27 August - 6 September 1991.

375. Present status and future developments of JET diagnostics.
Stott P E
Soviet Journal of Plasma Physics (English translation of Fizika Plazmy) vol.18 no.4 April 1992 pp.9-24.

376. Recent developments of diagnostics at JET.
Stott P E
Review of Scientific Instruments vol.63 no.10 pt.II 1992 (Procs. 9th Topical Conf. on High Temperature Plasma Diagnostics, Santa Fe, New Mexico, 1992) pp.4696-4701. (Preprint JET-P(92)33).

377. Summary of the meeting.
Stott P E
JET papers presented to Course and Workshop on Diagnostics for Contemporary Fusion Experiments, Varenna, Italy, 27 August - 6 September 1991.

378. Different forms of the energy conservation equation, or is energy convection 5/2kTΓ or 3/2kTΓ
Stringer T E
JET Contributions to 4th European Fusion Theory Conf., Aspenas, Sweden, 17-19 June 1991.

379. Neoclassical impurity flux in the presence of anomalous transport.
Stringer T E
JET Contributions to 4th European Fusion Theory Conf., Aspenas, Sweden, 17-19 June 1991.

380. Neoclassical transport in the presence of fluctuations.
Stringer T E
Nuclear Fusion vol.32 no.8 August 1992 pp.1421-1432.

381. Neoclassical impurity flux in the presence of anomalous transport.
Stringer T E
Joint European Torus (JET). August 1992. Preprint JET-P(92)59. (submitted to "Theory of Fusion Plasmas". Procs. Joint Varenna-Lausanne Int. Workshop on Fusion Theory, Varenna, 24-28 August 1992).

382. Energy confinement in high performance JET D-T plasmas.
Stubberfield P M Balet B Cordey J G O'Brien D P Thomsen K von Hellermann M
Papers submitted to the 19th European Conf. on Controlled Fusion and Plasma Physics, Innsbruck, 1992. Joint European Torus 1992. Preprint JET-P(92)37, pp.25-30.

383. The effects of particle drift orbits on flux deposition profiles at the JET X-point target.
Summers D D R Lesourd M Reichle R Schulz J-P Zhu Y
Controlled Fusion and Plasma Physics. 18th European Conf, Berlin, 3-7 June 1991. Contributed papers. Geneva, European Physical Society. 1991. pp.I-5 - I-8.

384. Atomic spectroscopy in highly ionised plasmas.
Summers H P Thomas P Giannella R von Hellermann M Dickson W Lawson K Mandl W Briden P
Atomic Physics of Highly Charged Ions. 5th Int. Conf. on the Physics of Highly Charged Ions, Giessen, 10-14 September 1990. Invited lectures and contributed papers. Berlin, Springer-Verlag. 1991. pp.17-21.

385. Atomic processes relevant to neutral beam based tokamak diagnostics.
Summers H P von Hellermann M Breger P Frieling J Horton L D Konig R Mandl W Morsi H Wolf R de Heer F J Hoekstra R Fritsch W
Atomic Processes in Plasmas. 8th American Physical Society Topical Conf., Portland, 25-29 August 1991. New York, American Institute of Physics. 1992. pp.111-120.

386. The requirements for collision data on the species helium, beryllium and boron in magnetic confinement fusion.
Summers H P von Hellermann M de Heer F Hoekstra R
Joint European Torus (JET). July 1992. Preprint JET-P(92)45. (submitted to Nuclear Fusion (Supple. Series)).

387. Spectral emission from beryllium in plasmas.
Summers H P Dickson W J Boileau A Burke P G Denne-Hinnov B Fritsch W Giannella R Hawkes N C von Hellermann M Mandl W Peacock N J Reid R H G Stamp M F Thomas P R
Plasma Physics and Controlled Fusion vol.34 no.3 March 1992 pp.325-352.

388. The gas introduction system used for tritium neutral beam injection into JET.
Svensson L Martin D Browne A Cooper D Davies J F Falter H D Jones T T C Thompson E
JET Papers presented at 17th Symp. on Fusion Technology (SOFT-17), Rome, Italy, 14-18 September 1992 Joint

European Torus (JET). September 1992. Preprint JET-P(92)72, pp.95-101.

389. Edge radial profiles and transport in JET X-point plasmas.
Tagle J A Bures M Campbell D Clement S de Kock L Erents S K Harbour P J Loarte A Lowry C
Controlled Fusion and Plasma Physics. 18th Euro. Conf., Berlin, 3-7 June 1991. Contributed papers. Geneva, European Physical Society. 1991. pp.III-93 - III-96.

390. Power flow thickness and edge density scaling in the scrape-off layer of JET.
Tagle J A Clement S Erents S K Harbour P J de Kock L Loarte A Richards S D
Controlled Fusion and Plasma Physics. 18th Euro. Conf., Berlin, 3-7 June 1991. Contributed papers. Geneva, European Physical Society. 1991. pp.III-149 - III-152.

391. Probe edge measurements in JET X-point plasmas for various heating and plasma conditions.
Tagle J A Clement S Loarte A de Kock L Harbour P J O'Brien D Erents S K Janeschitz G Nicholson C Vince J
JET papers submitted to 10th Int. Conf. on Plasma Surface Interactions, Monterey, USA, 30 March - 3 April 1992. Joint European Torus (JET). May 1992. Preprint JET-P(92)32, pp.271-288.

392. Dynamics of plasma disruptions and vertical instability in JET.
Tanga A
IAEA Technical Committee Meeting on Avoidance and Control of Tokamak Disruptions, Culham Laboratory, 10-12 September 1991.

393. A high performance and long pulse tokamak.
Tanga A Roccella M Tubbing B J D Sack C H
EURATOM-ENEA sulla Fusione. May 1991. Report RT/NUCL/90/48.

394. Hot-ion and H-mode plasmas in limiter configuration in JET.
Tanga A Jones T T C Lomas P Nardone C Sartori R Tibone F von Hellermann M Watkins M L
Controlled Fusion and Plasma Physics. 18th European Conf., Berlin, 3-7 June 1991. Contributed papers. Geneva, European Physical Society, 1991. pp.I-365 - I-368.

395. Study of plasma disruptions in JET and its implications on engineering requirements.
Tanga A Garribba M Hugon M Johnson M F Lowry C Nardone C Noll P Pick M Saibene S Sannazzaro G
Fusion Engineering. 14th IEEE/NPSS Symp., San Diego, 991. 2 vols. Piscataway, IEEE. 1992. pp.201-204.

396. DIOSCUR-divertor optimization and steady current study of a tokamak aimed at steady state operation with reactor relevant plasma parameters.
Tanga A Alladio F et al
Associazione EURATOM-ENEA sulla Fusione, Frascati. February 1992. Report RT/NUCL/91/28.

397. Local transport analysis in L and H regimes.
Taroni A Sack Ch Springmann E Tibone F
Controlled Fusion and Plasma Physics. 18th European Conf., Berlin, 3-7 June 1991. Contributed papers. Geneva, European Physical Society, 1991. pp.I-181 - I-184.

398. The multi-fluid codes EDGE1D and EDGE2D: models and results.
Taroni A Corrigan G Radford G Simonini R Spence J Weber S
Contributions to Plasma Physics vol.32 no.3-4 1992 (3rd Int. Workshop on Plasma Edge Theory in Fusion Devices, Bad Honnef, Germany, 22-24 June 1992) pp.438-443. (Preprint JET-P(92)52, pp.13-24).

399. Non-linear regimes in resistive MHD equations.
Tebaldi C
JET Contributions to 4th European Fusion Theory Conf., Aspenas, Sweden, 17-19 June 1991.

400. Steady state H-modes in JET.
Thomas P R Campbell D J Gondhalekar A Lowry C J
Papers submitted to the 19th European Conf. on Controlled Fusion and Plasma Physics, Innsbruck, 29 June - 3 July 1992. Joint European Torus (JET). May 1992. Preprint JET-P(92)37, pp.175-180.

401. Tritium experiments in JET.
Thomas P R and JET Team
Joint European Torus (JET) 1992. Preprint JET-P(92)71.

402. The use of neutral beam heating to produce high performance fusion plasmas, including the injection of tritium beams into JET.
Thompson E Stork D de Esch H P L and JET Team
Joint European Torus (JET) 1992. Preprint JET-P(92)68. (submitted to Physics of Fluids B, Plasma Physics).

403. The use of neutral beam heating to produce high performance fusion plasmas, including the injection of tritium beams into JET.
Thompson E and JET Team
American Physical Society Bulletin vol.37 no.6 1992 (Program of 1992 Annual Meeting of the APS Division of Plasma Physics, Seattle, 1992) Paper 1I3, p.1353.

404. H-mode confinement and threshold database work.
Thomsen K Campbell D J Cordey J G and JET Team
Joint European Torus (JET) 1992. Report JET-R(92)07.

405. Dependence of confinement on plasma ion species in JET.
Tibone F Balet B Bures M Cordey J G Jones T T C Lomas P J Lawson K Morsi H W Nielsen P Start D F Tanga A Taroni A Thomsen K Ward D J

Papers submitted to the 19th European Conf. on Controlled Fusion and Plasma Physics, Innsbruck, 29 June - 3 July 1992. Joint European Torus (JET). May 1992. Preprint JET-P(92)37, pp.181-186.

406. Dependence of confinement on plasma ion species in JET.
Tibone F Balet B Bures M Cordey J G Jones T T C Lomas P J Lawson K Morsi H W Nielsen P Start D F Tanga A Taroni A Thomsen K Ward D J
Joint European Torus (JET). October 1992. Preprint JET-P(92)79. (submitted to Nuclear Fusion Letters).

407. AC plasma current operation in the JET tokamak.
Tubbing B J D Gottardi N A C Green B J How J A Huart M Konig R Lowry C G Lomas P J Noll P O'Rourke J J Rebut P-H Stork D Tanga A Taroni A Ward D J
Nuclear Fusion vol.32 no.6 June 1992 pp.967-972.

408. The impact of increased toroidal field ripple in JET.
Tubbing B and JET Team
JET papers presented at 14th IAEA Conf. on Plasma Physics and Controlled Nuclear Fusion Research, Wurzburg, Germany, 1992. Joint European Torus (JET) 1992. Preprint JET-P(92)84, pp.109-116.

409. Real time plasma boundary determination for display and control using transputers.
van der Goot E Ellis J J O'Brien D P
JET Papers presented at 17th Symp. on Fusion Technology (SOFT-17), Rome, Italy, 14-18 September 1992 Joint European Torus (JET). September 1992. Preprint JET-P(92)72, pp.135-141.

410. Comparison of measured JET divertor performance with edge models.
Vlases G Janeschitz G Matthews G Radford G Simonini R Taroni A Campbell D Clement S Harbour P Horton L Keilhacker M de Kock L O'Brien D Spence J Stamp M Summers D Tagle J Thomas P von Hellermann M Watkins M
JET papers submitted to 10th Int. Conf. on Plasma Surface Interactions, Monterey, USA, 30 March - 3 April 1992. Joint European Torus (JET). May 1992. Preprint JET-P(92)32, pp.65-81.

411. Divertor physics at JET: experimental results and modelling.
Vlases G and JET Team
JET papers presented at 14th IAEA Conf. on Plasma Physics and Controlled Nuclear Fusion Research, Wurzburg, Germany, 30 September - 7 October 1992. Joint European Torus (JET). December 1992. Preprint JET-P(92)84, pp.117-129.

412. Atomic modeling and spectroscopic diagnostics.
von Hellermann M G Summers H P
Review of Scientific Instruments vol.63 no.10 pt.II 1992 (Procs. 9th Topical Conf. on High Temperature Plasma Diagnostics, Santa Fe, New Mexico, 15-19 March 1992) pp.5132-5139. (Preprint JET-P(92)29).

413. Investigation of alpha particle slowing-down features in helium neutral beam fuelling experiments at JET.
von Hellermann M G Core W G F Frieling J Horton L D Konig R T Mandl W Summers H P Wolle B
Papers submitted to the 19th European Conf. on Controlled Fusion and Plasma Physics, Innsbruck, 29 June - 3 July 1992. Joint European Torus (JET). May 1992. Preprint JET-P(92)37, pp.103-108.

414. Observation of alpha particle slowing-down spectra in JET helium beam fuelling and heating experiments.
von Hellermann M G Core W G F Frieling J Horton L D Konig R W T Mandl W Summers H P
Joint European Torus (JET). 1992. Preprint JET-P(92)95. (submitted to Plasma Physics and Controlled Fusion).

415. Development of the JET ICRH plant.
Wade T J Jacquinot J Bosia G Sibley A Schmid M
Joint European Torus (JET). October 1992. Preprint JET-P(92)81. (submitted to Fusion Engineering).

416. High power (22 MW) ICRH at JET and developments for Next Step devices.
Wade T J Jacquinot J Bosia G Sibley A Schmid M
Fusion Engineering. 14th IEEE/NPSS Symp., San Diego, 30 September - 3 October 1991. 2 vols. Piscataway, IEEE. 1992. pp.902-907.

417. Real time position control of the JET LHCD launcher.
Walker C I Gormezano C Kaye A Helholm M Paling P Price R Schild P
JET Papers presented at 17th Symp. on Fusion Technology (SOFT-17), Rome, Italy, 14-18 September 1992 Joint European Torus 1992. Preprint JET-P(92)72, pp.1-7.

418. Tritium retention in JET cryopanel samples.
Walthers C R Jenkins E M Mauaux C Obert W Naruse Y
Fusion Technology vol.21 no.2 pt.2 March 1992 (Procs. 4th National Topical Meeting on Tritium Technology in Fission, Fusion, and Isotopic Applications, Albuquerque, New Mexico, 1991) pp.883-885.

419. Influence of ∇B drift direction on H-modes in JET.
Ward D Bhatnagar V Bures M Campbell D Clement S Fessey J Gottardi N Harbour P de Kock L Lowry C Morgan P Nardone C Reichle R Saibene G Smeulders P Stock D Summers D Thoms P Thomsen K Vlases G
Controlled Fusion and Plasma Physics. 18th European Conf., Berlin, 1991. Contributed papers. Geneva, European Physical Society, 1991. pp.I-353 - I-356.

420. Impurity influx model of fast tokamak disruptions.
Ward D J Wesson J A
Nuclear Fusion vol.32 no.7 July 1992 pp.1117-1123.

421. Energy exhaust through neutrals in a tokamak divertor.
Watkins M L Rebut P-H
Papers submitted to the 19th European Conf. on Controlled Fusion and Plasma Physics, Innsbruck, 1992. Joint European Torus 1992. Preprint JET-P(92)37, pp.235-240.

422. Boundary ion temperatures and ion orbit losses in JET.
Weisen H Bergsaker H Campbell D J Erents S K de Kock L C J M McCracken G M Stamp M F Summers D D R Thomas P R von Hellermann M Zhu J
Nuclear Fusion vol.31 no.12 1991 pp.2247-2269.

423. Measurement of impurity densities and Z_{eff} in JET using X-ray tomography.
Weisen H Pasini D Weller D Edwards A W
JET papers presented to Course and Workshop on Diagnostics for Contemporary Fusion Experiments, Varenna, Italy, 27 August - 6 September 1991.

424. Sawtooth oscillations and disruptions in JET.
Wesson J and JET Team
JET papers presented at 14th IAEA Conf. on Plasma Physics and Controlled Nuclear Fusion Research, Wurzburg, Germany, 1992. Joint European Torus (JET). December 1992. Preprint JET-P(92)84, pp.131-141.

425. Theory of Marfe stability.
Wesson J A Hender T C
Joint European Torus (JET). February 1992. Preprint JET-P(92)12. (submitted to Nuclear Fusion).

426. Engineering design of the JET divertor Lidar Thomson scattering system.
Wilson D Nielsen P Schunke B Gowers C
JET Papers presented at 17th Symp. on Fusion Technology (SOFT-17), Rome, Italy, 1992 Joint European Torus (JET) 1992. Preprint JET-P(92)72, pp.151-157.

427. Migration of tritium in the JET vacuum system following the first tritium experiment.
Winkel T Haigh A D Holland D
JET Papers presented at 17th Symp. on Fusion Technology (SOFT-17), Rome, Italy, 1992 Joint European Torus (JET). 1992. Preprint JET-P(92)72, pp.63-69.

428. A time-dependent Fokker-Planck code for neutron rate interpretations.
Wolle B Eriksson L-G Tsintsadze L N
Joint European Torus (JET). February 1992. Report JET-R(92)02.

429. Time-dependent neutron rate interpretation for neutral beam heated tokamaks.
Wolle B Eriksson L-G
Joint European Torus (JET). May 1992. Preprint JET-P(92)30. (submitted for publication in Plasma Physics and Controlled Fusion).

430. The exhaust detritiation system for the JET Active Gas Handling Plant - engineering, construction, installation and first commissioning results.
Wong D P Hemmerich J L Monahan J J
Fusion Technology vol.21 no.2 pt.2 March 1992 (Procs. 4th National Topical Meeting on Tritium Technology in Fission, Fusion, and Isotopic Applications, Albuquerque, New Mexico, 1991) pp.572-576.

431. Deduction of central plasma parameters from line-of-sight averaged spectroscopic observations.
Zastrow K-D Morsi H W Danielsson M von Hellermann M G Kallne E Konig R Mandl W Summers H P
Journal of Applied Physics vol.70 no.11 1 December 1991 pp.6732-6742.

432. ECE correlation radiometry as a diagnostic for MHD ballooning modes on JET.
Zolfaghari A Barlett D V Costley A E Cripwell P Kesner J Luckhardt S C Porte L Ramos J J Woskov P P
JET papers presented to Course and Workshop on Diagnostics for Contemporary Fusion Experiments, Varenna, Italy, 27 August - 6 September 1991.

433. Fast ECE correlation radiometry for MHD fluctuation measurements in JET and PBX-M.
Zolfaghari A Luckhardt S Woskov P Jones S Kesner J Machuzak J Ramos J Barlett D Costley A E Cripwell P Porte L Smith R Kaita R
American Physical Society Bulletin vol.37 no.6 1992 (Program of 1992 Annual Meeting of APS Division of Plasma Physics, Seattle, 1992) Paper 8R22, p.1575.

434. Fast ECE correlation radiometry for fluctuation measurements in JET and PBX-M.
Zolfaghari A M Luckhardt S Woskov P P Cohn D R Jones S Kesner J Machuzak J Ramos J J Bartlett D V Costley A E Cripwell P Porte L Smith R J Kaita R
Review of Scientific Instruments vol.63 no.101992 (Procs. 9th Topical Conf. on High Temperature Plasma Diagnostics, Santa Fe, New Mexico, 1992) pp.4619-4621.

435. JET Annual Report 1991. JET Joint Undertaking, 1992. Edited by B.E.Keen and G.W.O'Hara.
EUR 14435 en (EUR-JET-AR14).

436. JET Progress Report 1991. JET Joint Undertaking, 1992. 2 vols.
Edited and compiled by B.E.Keen.
EUR 14434 en (EUR-JET-PR9).